Implications of immune landscape in tumor microenvironment

Edited by
Selvarangan Ponnazhagan, Juana Serrano Lopez
and Somchai Chutipongtanate

About Frontiers

Frontiers is more than just an open access publisher of scholarly articles: it is a pioneering approach to the world of academia, radically improving the way scholarly research is managed. The grand vision of Frontiers is a world where all people have an equal opportunity to seek, share and generate knowledge. Frontiers provides immediate and permanent online open access to all its publications, but this alone is not enough to realize our grand goals.

Frontiers journal series

The Frontiers journal series is a multi-tier and interdisciplinary set of open-access, online journals, promising a paradigm shift from the current review, selection and dissemination processes in academic publishing. All Frontiers journals are driven by researchers for researchers; therefore, they constitute a service to the scholarly community. At the same time, the *Frontiers journal series* operates on a revolutionary invention, the tiered publishing system, initially addressing specific communities of scholars, and gradually climbing up to broader public understanding, thus serving the interests of the lay society, too.

Dedication to quality

Each Frontiers article is a landmark of the highest quality, thanks to genuinely collaborative interactions between authors and review editors, who include some of the world's best academicians. Research must be certified by peers before entering a stream of knowledge that may eventually reach the public – and shape society; therefore, Frontiers only applies the most rigorous and unbiased reviews. Frontiers revolutionizes research publishing by freely delivering the most outstanding research, evaluated with no bias from both the academic and social point of view. By applying the most advanced information technologies, Frontiers is catapulting scholarly publishing into a new generation.

What are Frontiers Research Topics?

Frontiers Research Topics are very popular trademarks of the *Frontiers journals series*: they are collections of at least ten articles, all centered on a particular subject. With their unique mix of varied contributions from Original Research to Review Articles, Frontiers Research Topics unify the most influential researchers, the latest key findings and historical advances in a hot research area.

Find out more on how to host your own Frontiers Research Topic or contribute to one as an author by contacting the Frontiers editorial office: frontiersin.org/about/contact

Implications of immune landscape in tumor microenvironment

Topic editors

Selvarangan Ponnazhagan — University of Alabama at Birmingham, United States
Juana Serrano Lopez — Health Research Institute Foundation Jimenez Diaz (IIS-FJD), Spain
Somchai Chutipongtanate — University of Cincinnati, United States

Citation

Table of contents

Editorial: Implications of immune landscape in tumor microenvironment

Somchai Chutipongtanate[1,2], Selvarangan Ponnazhagan[3,4] and Juana Serrano-López[5]*

[1]Milk, Microbiome, Immunity and Lactation Research for Child Health (MILCH) and Novel Therapeutics Lab, Division of Epidemiology, Department of Environmental and Public Health Sciences, University of Cincinnati College of Medicine, Cincinnati, OH, United States, [2]Department of Environmental and Public Health Sciences, University of Cincinnati College of Medicine, Cincinnati, OH, United States, [3]O'Neal Comprehensive Cancer Center, University of Alabama at Birmingham, Birmingham, AL, United States, [4]Department of Pathology, University of Alabama at Birmingham, Birmingham, AL, United States, [5]Experimental Hematology Lab, IIS-Fundación Jiménez Díaz, Universidad Autónoma de Madrid (UAM), Madrid, Spain

Editorial on the Research Topic
Implications of immune landscape in tumor microenvironment

The tumor microenvironment (TME) plays an essential role in cancer development, acting as a complex ecosystem where interactions between tumor cells and the neighboring stromal and immune components critically influence tumor progression, immune evasion, and therapeutic resistance. High-throughput technologies based on RNA sequencing are facilitating a picture of the tumor-derived oncotranscriptomes. That massive information is being used to generate new hypothesis for *in silico* screening of small molecules by for example, integrative LINCs (iLINCs) connectivity map or DREIMT platforms (1, 2). This Research Topic compiles a series of cutting-edge studies that provide detailed insights into the cellular and molecular mechanisms governing these interactions within the TME in several solid tumors. This Research Topic underscores the importance of targeting the TME in the development of next-generation cancer therapies. Firstly, Molina et al. underscores prognostic significance of tumor-infiltrating lymphocytes (TILs) in prostate cancer. By analyzing the density and phenotype of regulatory T cells (Tregs; CD3$^+$Foxp3$^+$) and memory T cells (Tmem; CD3$^+$CD45RO$^+$) within different tumor localizations, the study reveals that high Treg infiltration correlates with poor outcomes, while high Tmem infiltration is protective. Furthermore, they found that Foxp3 expression is highly associated with CTLA-4 and TIM-3 gene expression suggesting a potential immunosuppressive network at play. This finding highlighted the therapeutic promise of targeting Tregs in prostate cancer. Similarly, myeloid cells with immune suppressive functions, have also been involved in prostate cancer progression. Kobayashi et al. underscores the prognostic significance of myeloid-derived suppressor cell (MDSC) subtypes in prostate cancer. Elevated levels of PMN-MDSCs (CD33$^+$HLA-DR$^-$CD14$^-$CD15$^+$) subtype instead M-MDSC (CD33$^+$HLA-DR$^+$CD14$^+$CD15$^-$) correlate with poorer

survival outcomes in the metastatic Castration-resistant prostate cancer (mCRPC) patients, making them potential biomarkers for prognosis and as therapeutic targets. This study emphasizes the need for further research into MDSCs and their role in cancer progression, particularly in identifying biomarkers for patient stratification and therapeutic interventions. Another myeloid cells affected by TME are Dendritic Cells (DCs), characterized by their crucial role in anti-tumor immunity. In blood cancers, the function of DCs is impaired due to the influence of the TME, leading them to remain in an immature state. However, isolating these cells and maturing them *in vitro* for use in vaccines may enhance treatment outcomes for cancer patients (3). In this topic Xiao et al. elucidate mechanisms by which the TME disrupts DC function and the potential therapeutic strategies to restore DC activity. Combining DC-based vaccines with immune checkpoint inhibitors and targeting the immunosuppressive TME could enhance the effectiveness of immunotherapies. Shifting focus to Pancreatic Ductal Adenocarcinoma (PDAC), one of the most lethal cancers due to its "immunologically cold" TME, the review by Joseph et al. provides a comprehensive analysis of the TME in PDAC. They emphasize the roles of Tumor Associated Macrophages (TAMs), MDSCs, and Tregs. Therapeutic strategies that target the stroma and modulate the immune response, such as combining immune checkpoint inhibitors with stroma-targeting agents, hold promise for improving outcomes in PDAC. Building on this, Freeman et al. have found that blocking Insulin-like Growth Factors (IGF) signaling increases production of CXCL9/10 by down-regulating AKT/phosphoSTAT3 in TAMs and Fibroblasts, thereby facilitating CD8^{+} Cytotoxic T Cell recruitment into Pancreatic Tumors. However, despite the increased infiltration, these CD8^{+} T cells remain functionally inactive, as shown by a GZMB assay. This study opens new avenues for combining IGF inhibitors with therapies that activate T cells, offering hope for overcoming the immunosuppressive TME in PDAC. The challenges of treating cancer are further complicated when it metastasizes to the bone, where a unique interplay between immune cells, bone cells, and tumor cells creates a complex therapeutic landscape. Chen et al. discusses how tumor-infiltrating cells, particularly from breast cancer, lung or prostate cancer, disarm cytotoxic T lymphocytes (CTL) and natural killer (NK) cells by upregulating programmed death-ligand 1 (PD-L1) expression or reprogramming bone cell toward osteoclastogenesis and consequently tumor progression. The study also highlights the importance of understanding tumor dormancy and the need for combination therapies to address the multifaceted nature of bone metastasis. In children, adolescents and young adults, osteosarcoma is the most common bone tumor. Orrapin et al. provides an in-depth review of the complex tumor-immune microenvironment (TIME) in osteosarcoma and the complex interactions within the TIME that drive tumor progression and resistance to therapy. Glioblastoma (GBM), a highly aggressive brain tumor with limited treatment options, presents another formidable challenge. Kushihara et al. investigates the immune microenvironment of GBM, revealing that tumors with high expression of O6-methylguanine-DNA

(MGMT-H) exhibit a more active immune microenvironment. Despite this, immune evasion mechanisms remain a challenge, suggesting that combination therapies targeting both immune activation and suppression are necessary. Future research should focus on validating these findings and elucidating the role of tertiary lymphoid structures (TLS) in GBM. In contrast to adult brain tumors, pediatric brain tumors exhibit significant differences in immune composition, as highlighted by the study of Cao et al. This study uses single-cell RNA-sequencing (scRNA-seq) and bulk RNA-sequencing to comprehensively map the immune ecosystem in pediatric brain tumors, providing a deeper understanding of the TME and identifying potential therapeutic targets. The study suggests that targeting myeloid cells, rather than T cells, may be a more effective strategy for immunotherapy in these young patients. Importantly, the variability of the TME across different mouse models has been highlighted in the review by Carretta et al. Their work underscores the heterogeneity of cancer-associated fibroblasts (CAF) across various syngeneic mouse models, further illustrating the complexity of the TME. This variability suggests that selecting appropriate preclinical models and thoroughly understanding the specific characteristics of the TME are crucial for predicting therapeutic outcomes more accurately. Thus, researchers can develop more effective cancer treatments. Future research should focus on devising strategies to target CAFs and modulate the extracellular matrix (ECM), thereby enhancing the efficacy of immunotherapies in cancer treatment. Finally, the identification of predictive biomarkers could significantly enhance the precision of future studies, enabling us to identify patients who are most likely to benefit from the novel therapeutic strategies discussed above. The oncogene MYC, known as a central regulator of both cancer metabolism and immune evasion, plays a pivotal role in driving metabolic reprogramming that supports tumor growth and immune escape. Despite the challenges in directly targeting MYC, Venkatraman et al. focus on MYC interactome to uncover alternative targets and develop biomarkers that could predict responses to MYC-targeted therapies. Notably, they highlight the development of the MYC inhibitor OMO-103, which is currently in phase I clinical trials. The recently published results from this trial suggest that OMO-103 is a promising new therapy for targeting the MYC oncogene in solid tumors, demonstrating a favorable safety profile, preliminary efficacy, and the ability to inhibit MYC transcriptional activity (4). Future research should continue to explore the intricate interactions within the TME, develop personalized therapeutic strategies, and identify biomarkers that predict treatment response. This editorial brings together the significant findings from recent studies and outlines the future directions necessary to advance our understanding of the TME and its implications for cancer therapy.

Author contributions

SC: Writing – review & editing. SP: Writing – review & editing. JS: Writing – review & editing, Writing – original draft.

Funding

Conflict of interest

The authors declare that the research was conducted in the absence of any commercial or financial relationships that could be construed as a potential conflict of interest.

The authors declare that they were an editorial board members in Frontiers at the time of submission. This had no impact on the review process and the final decision.

Publisher's note

References

1. Serrano Lopez J, Jimenez-Jimenez C, Chutipongtanate S, Serrano J, Rodriguez-Moreno M, Jimenez A, et al. High-throughput RNA sequencing transcriptome analysis of ABC-DLBCL reveals several tumor evasion strategies. *Leuk Lymphoma*. (2022) 63:1861–70. doi: 10.1080/10428194.2022.2056173

2. Troule K, Lopez-Fernandez H, Garcia-Martin S, Reboiro-Jato M, Carretero-Puche C, Martorell-Marugan J, et al. DREIMT: a drug repositioning database and prioritization tool for immunomodulation. *Bioinformatics*. (2021) 37:578–9. doi: 10.1093/bioinformatics/btaa727

3. Serrano-Lopez J, Sanchez-Garcia J, Serrano J, Alvarez-Rivas MA, Garcia-Castellano JM, Roman-Gomez J, et al. Nonleukemic myeloid dendritic cells obtained from autologous stem cell products elicit antileukemia responses in patients with acute myeloid leukemia. *Transfusion*. (2011) 51:1546–55. doi: 10.1111/j.1537-2995.2010.03042.x

4. Garralda E, Beaulieu ME, Moreno V, Casacuberta-Serra S, Martinez-Martin S, Foradada L, et al. MYC targeting by OMO-103 in solid tumors: a phase 1 trial. *Nat Med*. (2024) 30:762–71. doi: 10.1038/s41591-024-02805-1

Impaired function of dendritic cells within the tumor microenvironment

Zhihua Xiao[1,2†], Ruiqi Wang[1†], Xuyan Wang[1], Haikui Yang[1],
Jiamei Dong[1], Xin He[1], Yang Yang[1], Jiahao Guo[1,2],
Jiawen Cui[1,2] and Zhiling Zhou[1*]

[1]Department of Pharmacy, Zhuhai People's Hospital (Zhuhai Hospital Affiliated with Jinan University),
Zhuhai, China, [2]College of Pharmacy, Jinan University, Guangzhou, China

Dendritic cells (DCs), a class of professional antigen-presenting cells, are considered key factors in the initiation and maintenance of anti-tumor immunity due to their powerful ability to present antigen and stimulate T-cell responses. The important role of DCs in controlling tumor growth and mediating potent anti-tumor immunity has been demonstrated in various cancer models. Accordingly, the infiltration of stimulatory DCs positively correlates with the prognosis and response to immunotherapy in a variety of solid tumors. However, accumulating evidence indicates that DCs exhibit a significantly dysfunctional state, ultimately leading to an impaired anti-tumor immune response due to the effects of the immunosuppressive tumor microenvironment (TME). Currently, numerous preclinical and clinical studies are exploring immunotherapeutic strategies to better control tumors by restoring or enhancing the activity of DCs in tumors, such as the popular DC-based vaccines. In this review, an overview of the role of DCs in controlling tumor progression is provided, followed by a summary of the current advances in understanding the mechanisms by which the TME affects the normal function of DCs, and concluding with a brief discussion of current strategies for DC-based tumor immunotherapy.

KEYWORDS

dendritic cell, tumor microenvironment, immune tolerance, immunosuppressive populations, DC-based vaccine

1 Introduction

Dendritic cells (DCs), first discovered by Steinman and Cohn in 1973 ([1]), serve as a bridge between innate and adaptive immunity in the host immune response. Based on differences in the expression of cell surface markers, DCs can be divided into two main subgroups: conventional DCs (cDCs) and plasmacytoid DCs (pDCs), each with a unique function in immune activity ([2]). cDCs have powerful antigen capture and presentation capacities and are one of the mainstays of T-cell activation in the body. In contrast, pDCs

can present antigens to T-cells, although not as efficiently as cDCs. The main characteristic of pDCs is that they can direct the immune response by secreting high levels of type I interferons (IFN-I) (3, 4). Furthermore, DCs have been extensively studied, and their central role in initiating and maintaining anti-tumor immune responses to hinder tumor progression has been well established. However, the tumor microenvironment (TME) shows characteristics that are different from those of normal tissues, including the infiltration of a large population of immunosuppressive cells and a unique environment of hypoxia and lactate accumulation (5–7), rendering DCs incompetent by impairing their maturation, limiting their antigen capture, and downregulating the expression of costimulatory molecules in a variety of ways (8, 9). In this review, the essential role of DCs in tumor immunosurveillance is discussed, and the mechanisms by which the TME affects the function of DCs in tumors are summarized. Finally, we evaluated the improvement in DC-based tumor immunotherapy strategies, particularly DC-based vaccines.

2 The role of dendritic cells in tumor immunosurveillance

Effective anti-tumor immune responses involve a series of stepwise events. Chen et al. summarized the complex anti-tumor immune process as the "Cancer-Immunity Cycle" (reviewed in (10)), which provides an important framework for understanding the overall picture of the anti-tumor immune process. Furthermore, DCs are pivotal in the overall anti-tumor immune response due to their key role in T cell activation and immune response initiation (Figure 1). Briefly, immature DCs that infiltrate the tumor tissue recognize and phagocytose apoptotic or necrotic tumor cells and thus tumor cell antigens. They subsequently enter an activation/maturation process triggered by an intrinsic program and migrate from the tumor tissue via the lymphatic vessels or blood circulation to tumor-draining lymph nodes (TDLNs). During migration, DCs mature and acquire new characteristics, including the upregulation of CC-chemokine receptor 7 (CCR7) for improved motility, the upregulation of major histocompatibility complex (MHC) class I and class II molecules for antigen presentation, upregulation of costimulatory molecules such as CD80, CD86, and CD40, and increased cytokine secretion for enhanced T-cell stimulation. Mature DCs load endo-processed antigenic peptides onto MHC class I or MHC class II molecules for presentation to naïve T-cells, and at the same time, the costimulatory molecules interact with the ligands on T cells, which synergistically stimulate the activation and differentiation of T-cells in TDLNs (3, 11–17). Tertiary lymphoid structures (TLS), which are crucial in the anti-tumor immune response, may also be the destination for the migration of mature DCs (18, 19). The TLS may represent a privileged site for the local presentation of neighboring tumor antigens to T-cells by DCs and the activation, proliferation, and differentiation of T-cells (19, 20). This is also supported by a single-cell analysis of human non-small cell lung cancer lesions, which showed that mature DCs enriched in
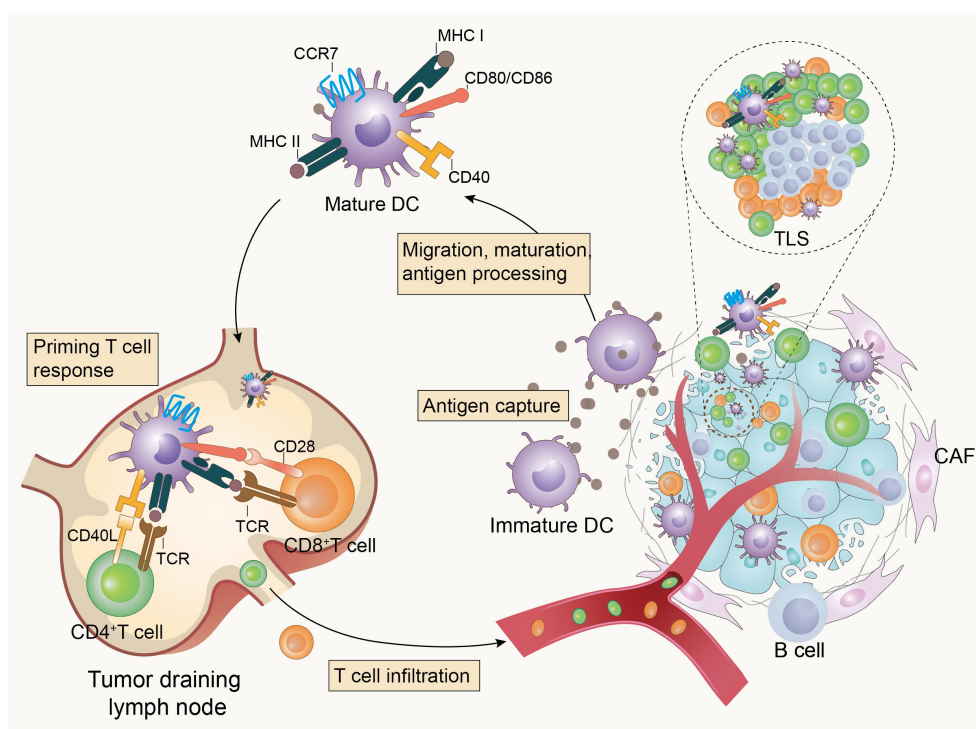
FIGURE 1

Dendritic cells initiate anti-tumor immunity. Tumor-infiltrating dendritic cells recognize and capture tumor-associated antigens, then become mature and homing to tumor-draining lymph nodes (TDLNs) or tertiary lymphoid structures (TLS) to activate T-cells and initiate anti-tumor immunity in response to the presence of tumors.

immunoregulatory molecules (mregDCs) accumulated in the TLS in close proximity to T-cells (21). MregDCs are a new cluster of DCs identified by Maier et al. in human and mouse non-small cell cancers and are characterized by the expression of both maturation markers and regulatory molecules (22). MregDCs have also been described in various human cancers, including hepatocellular carcinoma (23), breast cancer (24), colon cancer (25), and gastric cancer (26). Li et al. summarized the basic characteristics of mregDCs and suggested that lysosomal-associated membrane protein 3 (LAMP3) may be a fundamental recognition marker for them (27). Ginhoux et al. proposed that mregDCs can refer to a distinct molecular state induced in cDC1s, cDC2s, and potentially inflammatory DC3s upon sensing or capturing cell-associated materials that have a distinct ability to interact with antigen-specific T-cells (28). Analysis of tumors and metastatic lymph nodes from patients with head and neck lymphoma revealed that mregDCs may contribute to the prognosis by balancing regulatory and effector T-cells (29).

It is well established that DCs play a key role in stimulating cytotoxic T-cells and driving immune responses against cancer and that the levels of intratumoral stimulatory DCs in human tumors are associated with increased overall survival (30–32). Hegde et al. suggested that different scales of infiltration of cDCs would induce different levels of T-cell responses and that increased infiltration and activation of cDCs enhanced the activity of CD8$^+$ T and T$_H$1 cells in a pancreatic cancer mouse model (33). In addition, further evidence for the role of DCs in controlling tumor development is derived from the fact that the absence and dysfunction of DCs in tumor-bearing mouse models lead to poorer outcomes and insensitivity to anti-tumor treatment. Batf3-deficient mice (Batf3$^{-/-}$) lack cross-presenting DCs and fail to trigger cytotoxic T lymphocyte-mediated immune responses to tumor-associated antigens (34–36), and Mittal et al. observed increased tumor metastasis and poorer survival in Batf3$^{-/-}$ mouse models of breast cancer and melanoma than in wild-type mice (37). Furthermore, it has been observed in several Batf3$^{-/-}$ mouse models that activated DCs are required to promote the anti-tumor efficacy of immunostimulatory antibodies, such as anti-PD-1, anti-PD-L1, and anti-CD137, and deficiencies in DCs limit the efficacy (35, 38). This suggests that the functional status of DCs is closely related to the efficacy of tumor immunotherapy. pDCs have a weak antigen-presenting capacity but can participate in the tumor immune response in other ways, such as by secreting IFN-I (39) and cross-priming naïve CD8$^+$ T-cells by transferring antigens to cDCs via exosomes (40). However, the function of pDCs in TME remains controversial. In patients with colon cancer, an increased density of infiltrating pDCs was significantly correlated with increased progression-free and overall survival (41). In addition, a naturally occurring pDCs subset expressing high levels of OX40 with a unique immunostimulatory phenotype was identified in the TME of patients with head and neck squamous cell carcinoma, which, when synergized with cDCs, generated potent tumor antigen-specific CD8$^+$ T-cell responses (42). However, as reported by Sisirak and partners, tumor-infiltrating pDCs in patients with breast and ovarian cancer are associated with poor outcomes (43, 44), and this may be linked to tumor cell-derived cytokines such as TGF-β and TNF-α, which limit the ability of pDCs to produce IFN-I and induce them to

be tolerogenic (45, 46). The specific microenvironmental context and functional status of pDCs appear to determine their effects on cancer immunity and patient outcomes.

Overall, the evidence indicates that DCs, although representing a relatively rare subset of immune cells, are an essential part of anti-tumor immunogenesis. Moreover, when functionally activated, they are associated with stalled tumor progression and improved therapeutic responsiveness. However, the prognostic role of DCs in patients with cancer cannot be generalized and is largely dependent on the density, maturation, and activity of DCs. In general, tumor infiltration by activated, well-functioning DCs tends to predict a better prognosis, whereas DCs with impaired functional status in the TME may have the opposite effect on tumor progression (47–50). The TME causes the loss of antigen presentation and T-cell stimulatory capacity by inhibiting the maturation and migration of DCs, altering their ability to secrete cytokines. This can even induce tolerogenic or immunosuppressive DCs, allowing the tumor to escape surveillance and extermination by the immune system.

3 Immunosuppressive effects of the TME on dendritic cells

The conditions for tumor development, metastasis, and invasion are provided by the TME, a complex and dynamically evolving system composed of numerous components, including tumor cells, immune cells, the extracellular matrix, and soluble cytokines. Accumulating evidence indicates that immunosuppressive populations and stromal cells, as well as the unique metabolic environment of the TME, negatively regulate the maturation, migration, and effector functions of DCs (Figure 2).

3.1 Inhibition of dendritic cells by immunosuppressive populations

One of the most prominent features of the TME is the progressive accumulation of tumor-associated immunosuppressive cell populations, such as regulatory T-cells (Tregs), myeloid-derived suppressor cells (MDSCs), and tumor-associated macrophages (TAMs) (51, 52).

Aberrant chemokine alterations in the TME are important in the tumor recruitment of immunosuppressive cells (53). Tumor cells can induce the migration of Tregs to the TME by upregulating the expression of several chemokines, including the C-C motif chemokine ligand (CCL) 17/22 (54), CCL20 (55), and CCL28 (56, 57). Moreover, the ability of Tregs to use free fatty acids and lactate allows them to survive and maintain their suppressive identity, particularly in a harsh nutrient TME (58, 59). Tregs are a major suppressor group that induce DCs dysfunction and limit tumor immunogenesis (60). One important mechanism by which Tregs cause DCs dysfunction is through cytotoxic T-lymphocyte-associated antigen 4 (CTLA-4). Tregs expressing CTLA-4 compete with CD28 on conventional T-cells for the co-stimulatory molecules CD80 and CD86 on the surface of DCs,
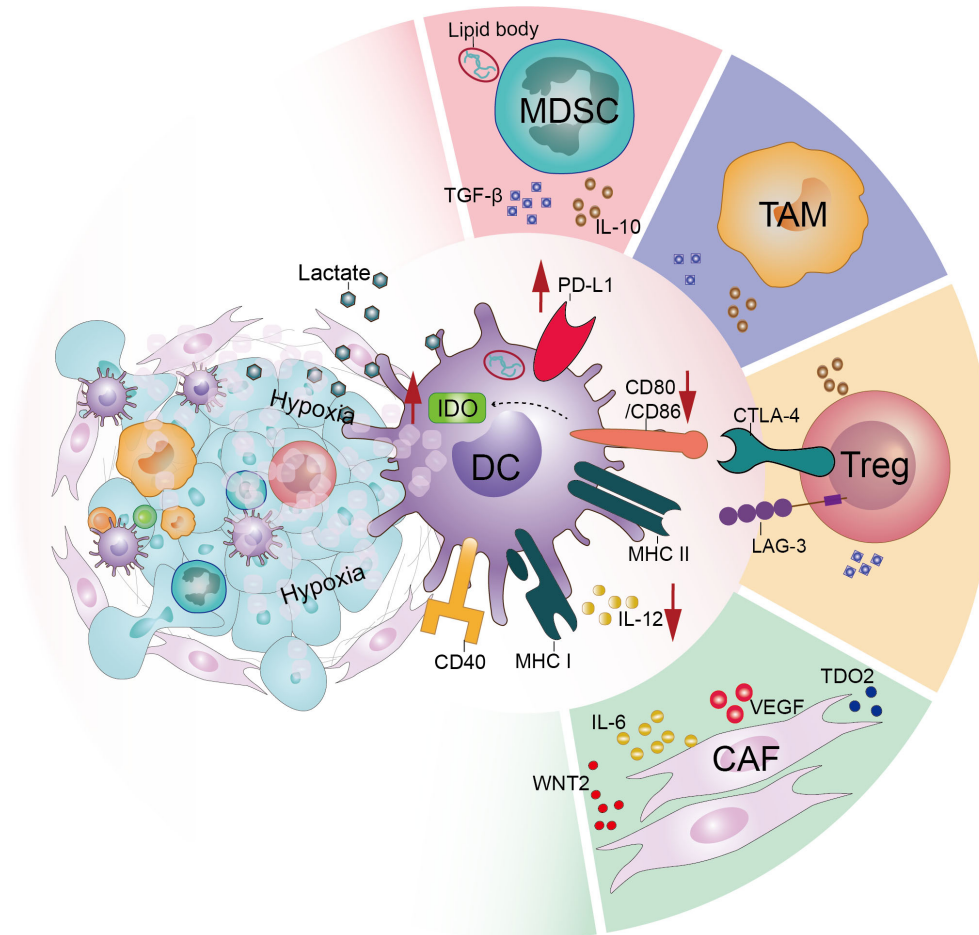
FIGURE 2
Tumor microenvironment acts on dendritic cells and downregulates their function. In the tumor microenvironment, various factors interact directly or indirectly with dendritic cells to dysfunction them. These include the large number of immunosuppressive populations such as regulatory T-cells (Tregs), tumor-associated macrophages (TAMs) and myeloid-derived suppressor cells (MDSCs) infiltrating the tumor microenvironment. In addition, the effects of stromal cells such as cancer-associated fibroblasts (CAFs) and the particular hypoxic and acidic microenvironment of the tumor microenvironment cannot be ignored.

with CTLA-4 having a greater affinity and avidity than CD28 (61). In addition, Tregs are able to downregulate CD80/CD86 molecules expressed by DCs in a CTLA-4-dependent manner (62–65), and depletion of CD80/86 in mice was also found to cause upregulation of PD-L1 in DCs (66), resulting in multiple inhibitory effects on DC-mediated T-cell immune responses. Furthermore, the interaction of CTLA-4 with CD80/CD86 induces the production of indoleamine-2,3-dioxygenase (IDO) in DCs, which can induce tryptophan catabolism to pro-apoptotic metabolites, leading to the suppression of effector T-cell activation (67–69). In addition to CTLA-4, lymphocyte activation gene-3 (LAG-3), an immune checkpoint molecule that has recently received considerable attention, is constitutively expressed on Tregs and can limit the T cell stimulatory capacity of DCs by interacting with MHC class II molecules (70, 71). A number of other interactions, including the secretion of inhibitory cytokines such as IL-10 and TGF-β (72), delivery of miRNAs to DCs by secreted extracellular vesicles, thereby inducing a tolerogenic phenotype in DCs (73), expression of CD27 molecules that interfere with CD70/CD27 stimulatory signaling between DCs and effector T-cells (74), and direct

induction of death through mutual contact with DCs (75), are also important means for Tregs to impede the onset of DCs-mediated tumor immunity. Consistently, enhanced anti-tumor immune responses induced by DCs have been observed after reducing the infiltration of tumor-associated Tregs and the secretion of their immunosuppressive molecules in various tumor-bearing mouse models (67, 76–78). Thus, Tregs appear to be an important cell subpopulation in the TME that acts directly on DCs and mediates their dysfunction, so the depletion of Tregs may be beneficial for DCs to mediate anti-tumor immunity.

MDSCs are a heterogeneous population of immature myeloid cells with immunosuppressive properties. Under the stimulation of the pathological conditions of cancer, the maturation and differentiation of bone marrow-derived progenitor cells are blocked, resulting in the accumulation of immunosuppressive MDSCs. MDSCs are recruited to the TME *via* multiple chemokine signals such as CCL2, CCL5, CCL26, C-X-C motif chemokine ligand (CXCL) 8, CXCL12, and other mediators such as granulocyte-macrophage colony-stimulating factor (GM-CSF), IL-6, or prostaglandin E2 (PGE2) that participate in expanding MDSCs

(79). Previous studies have shown that activated MDSCs impede anti-tumor immunity and promote tumor progression through a series of actions, and that DCs are negatively affected (80). Hu et al. observed that upregulated MDSCs were associated with higher IL-10 expression, lower IL-12 production by DCs, and lower T-cell stimulatory activity in mice with hepatocellular carcinoma (81). Furthermore, it has been reported that tumor-associated DCs accumulate large amounts of lipid bodies (LB) containing oxidized lipids, impeding cross-presentation in DCs by covalently binding to heat shock protein 70 and preventing the translocation of peptide-MHC I complexes (pMHC) to the cell surface (82–84). Ugolini et al. found that in tumor-bearing mice, polymorphonuclear (PMN)-MDSCs are able to transfer lipid bodies to DCs, causing them to exhibit impaired antigen cross-presentation. Consistently, in MDSCs depleted or myeloperoxidase (MPO, a key enzyme for the production of oxidized lipids in MDSCs) deficient mice, DCs showed improved activity for tumor antigens cross-presentation (85). Thus, it appears that the abnormally large accumulation of lipids and impaired antigen cross-presentation in DCs are at least partially related to MDSCs and that selective depletion of MDSCs may be a potential option for restoring the function of DCs in tumor conditions.

In many solid tumor types, TAMs are among the most abundant populations of tumor-infiltrating immune cells in the TME (86). TAMs may localize to the TME either by traveling *via* chemotactic gradients regulated by factors such as CCL2, IL-1β, and macrophage colony-stimulating factor 1 (CSF1), differentiating from monocytes in the TME or by repolarization of tissue-resident macrophages (87). In addition, TAMs in the TME are more inclined to polarize into an anti-inflammatory phenotype due to the influence of cytokines such as PGE2 (88–90). TAMs are involved in multiple aspects of immunosuppression, and a high infiltration of TAMs into solid tumors is usually associated with a poor prognosis (86, 91–93). Unlike Tregs, which interact directly with DCs, TAMs mediate the recruitment of other immunosuppressive cells and secrete inhibitory cytokines that influence the maturation and function of DCs (94). Ruffell et al. described that in the TME of breast cancer mice, TAMs inhibit the production of IL-12 by DCs through the secretion of IL-10, attenuating the cytotoxic CD8+ T-cell response (95). Several preclinical studies have also suggested that TAM depletion in the TME can reshape the link between DCs and T-cells. For example, in a study based on a murine model of lung cancer, after targeting macrophages with a CSF1R inhibitor (CSF1Ri), the authors observed increased crosstalk between immunostimulatory populations, including DCs, NK cells, and T-cells, and increased levels of IL-12 expressed by DCs and T-cells, respectively (96). TAMs were consistently targeted by CSF1Ri (PLX3397) in a mouse model of mesothelioma. When combined with a DC-based vaccine, a robust and durable anti-tumor immune response was observed (97).

3.2 The function of dendritic cells is limited by stromal cells

Tumor progression and immune tolerance cannot be achieved without the involvement of tumor stromal components (98). Cancer-associated fibroblasts (CAFs), a complex and heterogeneous cell population, are the most abundant components of a tumor stroma. Tissue-resident fibroblasts are the major sources of CAFs (99), which can be activated by stimulation of various factors of TME such as TGF-β, TNF, fibroblast growth factor, and platelet-derived growth factor (100, 101). Additionally, mesenchymal stem cells, epithelial cells, and endothelial cells adjacent to cancer cells and fibroblasts recruited from the bone marrow are potential sources of CAFs (102, 103). The interaction of CAFs with immune cells has been identified as a key contributor to tumor progression. Several recent studies have revealed that CAFs can drive the immune escape of tumor cells by impeding the maturation, migration, and antigen presentation of DCs. Berzaghi et al. reported that the co-incubation of CAFs obtained from surgically resected fresh tumor tissue from lung cancer patients with mature DCs results in impaired migration and antigen uptake (104). In another study, it was proposed that human lung cancer cell-stimulated CAFs impair the differentiation and function of DCs by upregulating tryptophan-2,3-dioxygenase (TDO2) (105). Cheng et al. found that *in vitro* hepatocellular carcinoma patient-derived CAFs can recruit normal DCs and mediate STAT3 pathway activation by expressing IL-6, inducing their transformation into regulatory DCs (106). Furthermore, CAFs secrete abundant active factors such as vascular endothelial growth factor (VEGF), which promote angiogenesis while mediating damage to the migratory and T-cell stimulatory capacities of DCs (107, 108). Excellent work was reported by Huang et al., who found that CAF-secreted WNT2 was involved in the differentiation and immunostimulatory activity of DCs *in vitro*, and accordingly, anti-WNT2 was observed to increase the level of intratumoral activated DCs and significantly improve the anti-tumor responses of DC-mediated antigen-specific CD8+ T cells in murine tumor models (109). This suggests that in the TME, both stromal cells and immunosuppressive cells influence anti-tumor immunity. Therefore, for effective tumor therapy, it is essential to consider targeting stromal cells.

3.3 Environmental factors that regulate dendritic cell function in the TME

Compared with normal tissues, the TME exhibits a significantly hypoxic and acidic environment and is an important mediator of tumor progression.

Hypoxia is a central player in shaping the immune context of the TME, which results from an imbalance between increased oxygen consumption and inadequate oxygen supply owing to the rapid proliferation of tumor cells (110). Many physiological functions of DCs, including migration and maturation, are regulated by hypoxia. Hypoxic immature DCs exhibit upregulated motility/migration ability (111), while their antigen uptake ability is seemingly downregulated (112, 113). Consistently, Suthen et al. observed significant enrichment of Tregs and cDC2 in hypoxic regions of tumor samples from patients with HCC, as well as lower CD8+ T-cells, and found a significant downregulation of HLA-DR expression by cDC2 under hypoxic conditions, which may be related to the increased intercontact between Tregs and cDC2 during hypoxia (114). Besides, it is well known that hypoxia-inducible factor-1alpha (HIF-1α) plays a key role

in the cellular response to hypoxia (115, 116), yet the effects of HIF-1α on DCs appear to be controversial. On the one hand, several scholars have demonstrated that the increase in HIF-1α in DCs under hypoxia is accompanied by an increase in the expression of HIF-1α target genes, including those involved in glycolysis, and that the increase in glycolysis will promote the maturation and migration of DCs (117–119). On the other hand, however, it has been proposed that constitutive expression of HIF-1α impairs the immunostimulatory capacity of DCs *in vivo* by inducing DCs to upregulate the expression of immunosuppressive mediators such as IL-10, iNOS, and VEGF (120, 121). Additionally, prolonged exposure to hypoxia induces cell death in DCs, which can be prevented by HIF-1α inhibition, suggesting that HIF-1α may be involved in this process (122). It was observed in human glioma cells that hypoxia induces PD-L1 upregulation in an HIF-1α-dependent manner, and it was further found in a murine glioma model that the combination of HIF-1α inhibitor and anti-PD-L1 antibody can improve the activation of DCs and CD8^{+} T-cells (123). Notably, hypoxic conditions recruit more immunosuppressive Tregs (56, 114) and TAMs (124), thereby indirectly curbing the function of DCs. Overall, hypoxia appears to facilitate the migration and maturation of DCs and compromise their normal functions. The exact changes in the behavior of DCs under hypoxic conditions need to be further elucidated.

Tumor cells exhibit altered metabolism, preferentially converting glucose to lactate through glycolysis even under oxygen-rich conditions. This results in a large accumulation of lactate and increases the acidity of the TME (125–127). Numerous studies have shown that lactate accumulation in the TME adversely affects the DC function. For example, tumor-derived lactate restricts the presentation of tumor-specific antigens by DCs to other immune cells (128). Lactate is also involved in regulating the phenotype of DCs, resulting in increased production of anti-inflammatory cytokines and decreased production of pro-inflammatory cytokines (129, 130). In patients with melanoma, the function of pDCs is impaired by lactic acidosis (131), with the same phenomenon observed in patients with breast cancer and murine models (132). Some researchers have suggested that in mice, the migratory capacity of DCs is significantly diminished in acidic environments and does not recover after removal of the acidic microenvironment, suggesting that extracellular acidosis may cause irreversible DCs dysfunction (133). In addition, exposure of mesothelioma cells to acidosis promotes the secretion of TGF-β2, which in turn leads to the accumulation of lipid droplets in DCs, resulting in a reduction in DC migratory capacity (134). These findings support the view that an acidic environment is not conducive to the proper functioning of DCs. However, Geffner et al. argued that extracellular acidosis stimulates antigen capture, promotes the expression of MHC class II molecules CD86 and CD40, and induces the maturation and secretion of IL-12 in mouse (135) and human DCs (136). Notably, the maintenance of an acidic environment and the accumulation of lactate in the TME complement each other. In tumors, an acidic environment can promote the accumulation of lactate and thus impair the function of DCs.

In general, owing to the combination of many factors in the TME, DCs are significantly dysfunctional. An accurate understanding of the role of each component in DC dysfunction will help to better understand the tumor state and to accurately explore ways to restore the activity of DCs. However, the TME is a complex and interconnected whole, and ultimately, all factors need to be linked for a systematic and comprehensive understanding of the causes and processes of the dysfunction of DCs.

4 Dendritic cell-based strategies for cancer immunotherapy

As the key activators of the immune response, the immune activation potential of DCs can be used to induce anti-tumor responses in patients with cancer, which is a promising development. Primary strategies based on DCs include the creation of immunoenhancers that promote the generation and activation of DCs, or the preparation of autologous DC-based vaccines for patient administration. Flt3L, GM-CSF, and Toll-like receptor (TLR) ligands are common immunoenhancers. The development and maintenance of DCs depend on the Flt/Flt3L axis (137), and attempts have been made in clinical studies to enhance the immune response induced by tumor vaccines by administering Flt3L (NCT02129075) (138). GM-CSF stimulates the differentiation, activation, and migration of DCs (139, 140), and consistently, administration of the CpG ODN/GM-CSF combination in melanoma patients results in enhanced mutation of all identifiable DC subpopulations and the recruitment of T-cell-stimulating and cross-presenting DCs to support protective melanoma immunity (141). When combined with TLRs in DCs, TLR ligands can activate signal transduction pathways and induce the expression of genes involved in the maturation of DCs (142). Therefore, some immunostimulatory ligands for TLRs, such as poly (I:C), are often used as immunoadjuvants in DC-based therapies and have shown promising results (143, 144). DEC205, also known as CD205 or LY75, is an endocytic receptor expressed at high levels by CD8^{+} DCs and is involved in antigen uptake and cross-presentation (145). The fusion of tumor antigens with targeted antibodies against DEC205 to enhance DC-induced immune responses has been well studied and explored in clinical trials (138, 146). Recently, a pioneering study provided new insights into the application of DEC205 as a therapeutic target. Martinek et al. analyzed the transcriptome of T-cells and macrophages *in situ* in melanoma patient samples using immunofluorescence-guided laser capture microdissection and observed that stromal macrophages contained a gene expression signature linked to antigen capture and presentation (*CD14^{+}LY75^{+}*). This can distinguish patients with significantly better long-term survival and includes a gene module of monocyte-derived DCs (147). This study provides valuable insights into the reprogramming of stromal macrophages to upregulate gene features related to antigen capture and presentation to acquire DCs function and could be a potential option for cancer therapy.

DC-based therapeutic cancer vaccines are a popular strategy for stimulating an effective tumor immune response as they return autologous activated DCs loaded with tumor-associated antigens to patients (148). In April 2010, the FDA approved the marketing of the first DCs vaccine, sipuleucel-T, for the treatment of prostate cancer (149). Furthermore, in the NCCN Clinical Practice Guidelines in

Oncology (NCCN Guidelines®): Prostate Cancer (version 1.2023), sipuleucel-T is recommended for the treatment of metastatic castration-resistant prostate cancer (CRPC) and is a category 1 option for certain patients who have not received previous treatment with docetaxel or novel hormone therapy. Sipuleucel-T is also an option for patients with metastatic CRPC who have received prior treatment with docetaxel or a novel hormone therapy, but not for patients who have already received both (150). In recent years, DC-based vaccines have undergone extensive clinical trials for the treatment of various cancers, including liver cancer (151), melanoma (152), lung cancer (153), ovarian cancer (154), and pancreatic cancer (155). Although the safety of DC-based vaccines has been proven over the past few decades, their clinical efficacy requires improvement. Consequently, DC-based vaccines are undergoing a great deal of technical innovation, including the selection of DC subpopulations, methods of induction maturation, and choice of loading antigens (148, 156), with the aim of exploiting the anti-tumor potential of DCs more effectively.

The key to cancer immunotherapy is the manipulation of the immune system to achieve cancer control and the desired treatment.

The efficacy of immune checkpoint inhibitors, which have shown some success, depends largely on the present baseline immune response, and DC-based vaccines are highly effective at rescuing the baseline anti-tumor immune response. Therefore, there has been considerable interest in combining DC-based vaccines with immune checkpoint inhibitors (ICIs), and several such studies have been conducted in recent years (Table 1). Recently, Guo et al. reported a case of a patient with metastatic gastric cancer whose tumor progressed after the first two months of receiving personalized neoantigen-loaded monocyte-derived dendritic cell (Neo-MoDC) vaccine alone, despite the observed T-cell response against the tumor neoantigen and the fact that upregulated PD-1 levels in T-cells were observed after Neo-MoDC vaccine administration. Subsequently, the patient received a combination treatment of the Neo-MoDC vaccine and nivolumab; promisingly, the combination triggered a stronger immune response and mediated complete regression of all tumors for over 25 months (157). Furthermore, anti-PD-1/PD-L1 antibodies in combination with DC-based vaccines have been extensively explored in a variety of murine tumor models (158–164) and, without exception, combination treatment has shown

TABLE 1 Active clinical trials combining DC-based vaccine with immune checkpoint inhibitors (ICIs) therapy (clinicaltrials.gov, April 28, 2023).

Intervention		Tumor	Phase	N	Trial identifier	Status
ICIs	DC-based vaccine used					
Pembrolizumab	Anti-HER2/HER3 DC vaccine	Breast cancer	II	23	NCT04348747	Recruiting
	CCL21-gene modified autologous DC vaccine	Non-small cell lung cancer	I	24	NCT03546361	Recruiting
	Autologous DC loaded with autologous tumor homogenate	Mesothelioma	I	18	NCT03546426	Recruiting
	Autologous tumor lysate-pulsed DC vaccine	Glioblastoma	I	40	NCT04201873	Recruiting
	Intra-tumor injection of autologous DC	Non-Hodgkin lymphoma	I/II	11	NCT03035331	Active, not recruiting
	Therapeutic autologous DC	Melanoma	I/II	7	NCT03325101	Active, not recruiting
	Autologous DC pulsed with melanoma tumor-specific peptides	Melanoma	I	12	NCT03092453	Active, not recruiting
Nivolumab	Autologous neoantigen pulsed autologous DC vaccine	Hepatocellular carcinoma and liver metastases from colorectal carcinoma	II	60	NCT04912765	Recruiting
Camrelizumab	Glioblastoma stem-like cell antigens- pulsed DC vaccine (GSC-DCV)	Glioblastoma	II	40	NCT04888611	Recruiting
Atezolizumab	Autologous DC vaccine	Small cell lung cancer	I/II	20	NCT04487756	Recruiting
	DC loaded with the mesothelioma-associated tumor antigen WT1	Pleural mesothelioma	I/II	15	NCT05765084	Recruiting
Nivolumab/ Ipilimumab	DC-based p53 Vaccine	Small cell lung cancer	II	14	NCT03406715	Active, not recruiting
	Tumor-lysate loaded autologous dendritic cells	Glioblastoma	I/II	25	NCT03879512	Recruiting
Anti-PD-1 antibody	Autologous EphA2-targeting CAR-DC vaccine loaded with KRAS mutant peptide (KRAS-EphA-2-CAR-DC)	Solid tumors	I	10	NCT05631899	Recruiting
	Autologous EphA2-targeting CAR-DC vaccine loaded with TP53 mutant peptide (TP53-EphA-2-CAR-DC)	Solid tumors or lymphomas	I	10	NCT05631886	Recruiting
Anti-PD-1/PD-L1 antibody	Alpha-type-1 polarized dendritic cell (αDC1) vaccine	Melanoma	II	24	NCT04093323	Recruiting

superior efficacy compared to monotherapy, with stronger anti-tumor-specific T-cell responses and lower immunosuppressive cell infiltration. Additionally, the combination of anti-CTLA-4 and DC-based vaccines could lead to more effective cancer treatments. For example, in a clinical trial (NCT01302496), researchers enrolled 39 patients with pretreated advanced melanoma who received a DC-based mRNA vaccination plus ipilimumab. The results showed that a strong tumor-associated antigen-specific immune response was observed in patients treated with the combination of a DC-based vaccine and ipilimumab, with an encouraging 6-month overall response rate of 38%. Subsequent long-term follow-up after more than 5 years indicates that 7/39 patients, who all achieved a complete response, were still disease-free (165). Similarly, in the exploration of multiple preclinical experimental models of pancreatic cancer (166), breast cancer (167), colorectal cancer (168), and melanoma (169), the silencing of CTLA-4 can induce a more effective anti-tumor immune response together with DC-based vaccines by reducing the infiltration of immunosuppressive cells and increasing the Teff/Treg ratio. In summary, combining DC-based vaccines with immune checkpoint inhibitors is a promising option for treating tumors.

Combining a personalized DC-based vaccine with chemotherapeutic agents and targeted drugs is also an effective way

to improve the efficacy of tumor vaccines, and we have compiled active relevant clinical trials in Tables 2, 3. It is already clear that chemotherapy can enhance the efficacy of DC-based vaccines by enhancing antigen production and eliminating suppressive immune cells. Some specific chemotherapeutic drugs, such as cyclophosphamide (170), have been shown to directly deplete suppressive immune cells in patients with cancer at low doses. A phase I clinical study suggested that cyclophosphamide with a DC-based vaccine treatment downregulated tumor infiltration of immunosuppressed cells and demonstrated excellent anticancer effects (NCT01241682) (171). In glioblastoma, a combination of Temozolomide- and DC-based vaccines has been favored, and recently, the publication of the results of a phase III prospective externally controlled cohort trial has gained widespread attention (NCT00045968). The results show that the median overall survival for patients with newly diagnosed glioblastoma assigned to the DCVax-L cohort (232 patients, 222 of whom received autologous tumor lysate-loaded dendritic cell vaccine "DCVax-L" plus temozolomide) at enrollment was 19.3 months from the time of randomization compared with 16.5 months from randomization for the 1366-patient external control populations. In addition, in patients with recurrent glioblastoma, the combination of DCVax-L with standard treatment showed a survival benefit (172). Currently,

TABLE 2 Active clinical trials combining DC-based vaccine with chemotherapy drugs (clinicaltrials.gov, May 28, 2023).

Intervention		Tumor	Phase	N	Trial identifier	Status
Chemotherapy drug(s)	DC-based vaccine used					
Temozolomide	Autologous dendritic cells loaded with autologous tumor homogenate in glioblastoma	Glioblastoma	II	28	NCT04523688	Recruiting
	Malignant glioma tumor lysate-pulsed autologous dendritic cell vaccine	Glioblastoma	I	21	NCT01957956	Active, not recruiting
	Autologous Wilms' tumor 1 (WT1) messenger (m)RNA-loaded dendritic cell (DC) vaccine	Glioblastoma	I/II	20	NCT02649582	Recruiting
	Dendritic and glioma cells fusion vaccine	Glioblastoma	I/II	10	NCT04388033	Recruiting
	Human CMV pp65-LAMP mRNA-pulsed autologous DCs	Glioblastoma	II	80	NCT03688178	Recruiting
	Autologous dendritic cells pulsed with multiple neoantigen peptides	Glioblastoma	I	10	NCT04968366	Recruiting
Cyclophosphamide/ Fludarabine	NY-ESO-1-157-165 peptide pulsed dendritic cell vaccine	Malignant neoplasm	II	6	NCT01697527	Active, not recruiting
	Autologous dendritic cells loaded with autologous tumor-lysate	Melanoma	I	20	NCT01946373	Recruiting
	MART-1 peptide-pulsed dendritic cells	Melanoma	II	1230	NCT00338377	Active, not recruiting
Cyclophosphamide	Autologous dendritic cell vaccine loaded with personalized peptides	Non-small cell lung cancer	I	16	NCT05195619	Recruiting
Gemcitabine	Autologous DC vaccine	Sarcoma	I	19	NCT01803152	Active, not recruiting
Platinum/ Pemetrexed	Dendritic cells loaded with the mesothelioma-associated tumor antigen Wilms' tumor protein 1	Malignant pleural mesothelioma	I/II	28	NCT02649829	Active, not recruiting
Decitabine	Dendritic cell/acute myelogenous leukemia fusion cell vaccine	Acute myelogenous leukemia	I	45	NCT03679650	Recruiting

TABLE 3 Active clinical trials combining DC-based vaccine with targeted drugs (clinicaltrials.gov, May 28, 2023).

Intervention		Tumor	Phase	N	Trial identifier	Status
Targeted drug(s)	DC-based vaccine used					
Trastuzumab/Pepinemab	Dendritic cell (DC1) vaccine	Breast cancer	I	28	NCT05378464	Recruiting
Trastuzumab/Pertuzumab	HER-2 pulsed DC1	Breast cancer	II	53	NCT05325632	Recruiting

chemotherapy remains the primary treatment for most cancers, and the combination of chemotherapy and DC-based vaccines has promising prospects owing to their cooperative effect. Furthermore, the combination of DC-based vaccines and targeted drugs has been explored. In a phase II clinical trial, Storkus et al. proposed that DC-based vaccines targeting tumor blood vessel antigens combined with dasatinib could induce therapeutic immune responses in patients with checkpoint-refractory advanced melanoma (NCT01876212) (173). Trastuzumab can enhance the uptake and cross-presentation of HER-2 derived peptides by DCs to improve the generation of peptide-specific CTLs (174), which provides a theoretical reference for the combination of Trastuzumab with a DC-based vaccine.

5 Conclusion

DCs play an indispensable role in triggering anti-tumor immune responses. However, under tumor conditions, immunosuppressive TME weakens their function. The defective function of DCs is an important reason why tumors evade immune surveillance and is closely associated with the poor efficacy of some immunotherapies, such as immune checkpoint inhibitors. Based on the pivotal role of DCs in the immune response, which determines their importance in anti-tumor therapy, many studies have been undertaken to improve the function of DCs, and some protocols, such as DC-based vaccines, have become available options for the treatment of tumors. In addition, the use of DC-based vaccines in combination with ICIs has good application prospects because they can induce a more effective baseline immune response, which is necessary for ICIs to exert their anticancer effects. However, several issues remain unaddressed. The complex composition of the TME and the close and diverse interactions among its components ultimately result in the inhibition of the normal function of multiple immunostimulatory cells, including DCs, and the induction of immune escape. How to effectively and selectively target the immunosuppressive effects of the TME on DCs needs to be further explored.

Author contributions

ZZ designed the study. ZX and RW wrote the manuscript and generated the figures. XW and HY revised and reviewed the manuscript. JD, XH, YY, JG, and JC contributed to the conceptualization and critically edited the manuscript. All authors contributed to the article and approved the submitted version.

Funding

Conflict of interest

The authors declare that the research was conducted in the absence of any commercial or financial relationships that could be construed as a potential conflict of interest.

Publisher's note

All claims expressed in this article are solely those of the authors and do not necessarily represent those of their affiliated organizations, or those of the publisher, the editors and the reviewers. Any product that may be evaluated in this article, or claim that may be made by its manufacturer, is not guaranteed or endorsed by the publisher.

References

1. Steinman RM, Cohn ZA. Identification of a novel cell type in peripheral lymphoid organs of mice. i. morphology, quantitation, tissue distribution. *J Exp Med* (1973) 137 (5):1142–62. doi: 10.1084/jem.137.5.1142

2. Guilliams M, Ginhoux F, Jakubzick C, Naik SH, Onai N, Schraml BU, et al. Dendritic cells, monocytes and macrophages: a unified nomenclature based on ontogeny. *Nat Rev Immunol* (2014) 14(8):571–8. doi: 10.1038/nri3712

3. Wculek SK, Cueto FJ, Mujal AM, Melero I, Krummel MF, Sancho D. Dendritic cells in cancer immunology and immunotherapy. *Nat Rev Immunol* (2020) 20(1):7–24. doi: 10.1038/s41577-019-0210-z

4. Kvedaraite E, Ginhoux F. Human dendritic cells in cancer. *Sci Immunol* (2022) 7 (70):eabm9409. doi: 10.1126/sciimmunol.abm9409

5. Anderson NM, Simon MC. The tumor microenvironment. *Curr Biol CB.* (2020) 30(16):R921–r5. doi: 10.1016/j.cub.2020.06.081

6. Boedtkjer E, Pedersen SF. The acidic tumor microenvironment as a driver of cancer. *Annu Rev Physiol* (2020) 82:103–26. doi: 10.1146/annurev-physiol-021119-034627

7. Huber V, Camisaschi C, Berzi A, Ferro S, Lugini L, Triulzi T, et al. Cancer acidity: an ultimate frontier of tumor immune escape and a novel target of

immunomodulation. *Semin Cancer Biol* (2017) 43:74–89. doi: 10.1016/j.semcancer.2017.03.001

8. Nakamura K, Smyth MJ. Myeloid immunosuppression and immune checkpoints in the tumor microenvironment. *Cell Mol Immunol* (2020) 17(1):1–12. doi: 10.1038/s41423-019-0306-1

9. Pitt JM, Marabelle A, Eggermont A, Soria JC, Kroemer G, Zitvogel L. Targeting the tumor microenvironment: removing obstruction to anticancer immune responses and immunotherapy. *Ann Oncol Off J Eur Soc Med Oncol* (2016) 27(8):1482–92. doi: 10.1093/annonc/mdw168

10. Chen DS, Mellman I. Oncology meets immunology: the cancer-immunity cycle. *Immunity* (2013) 39(1):1–10. doi: 10.1016/j.immuni.2013.07.012

11. Joffre OP, Segura E, Savina A, Amigorena S. Cross-presentation by dendritic cells. *Nat Rev Immunol* (2012) 12(8):557–69. doi: 10.1038/nri3254

12. Guermonprez P, Valladeau J, Zitvogel L, Théry C, Amigorena S. Antigen presentation and T cell stimulation by dendritic cells. *Annu Rev Immunol* (2002) 20:621–67. doi: 10.1146/annurev.immunol.20.100301.064828

13. Sánchez-Paulete AR, Teijeira A, Cueto FJ, Garasa S, Pérez-Gracia JL, Sánchez-Arráez A, et al. Antigen cross-presentation and T-cell cross-priming in cancer immunology and immunotherapy. *Ann Oncol Off J Eur Soc Med Oncol* (2017) 28 (suppl_12):xii44–55. doi: 10.1093/annonc/mdx237

14. Dunn GP, Old LJ, Schreiber RD. The three Es of cancer immunoediting. *Annu Rev Immunol* (2004) 22:329–60. doi: 10.1146/annurev.immunol.22.012703.104803

15. Worbs T, Hammerschmidt SI, Förster R. Dendritic cell migration in health and disease. *Nat Rev Immunol* (2017) 17(1):30–48. doi: 10.1038/nri.2016.116

16. Veglia F, Gabrilovich DI. Dendritic cells in cancer: the role revisited. *Curr Opin Immunol* (2017) 45:43–51. doi: 10.1016/j.coi.2017.01.002

17. Borst J, Ahrends T, Bąbała N, Melief CJM, Kastenmüller W. CD4(+) T cell help in cancer immunology and immunotherapy. *Nat Rev Immunol* (2018) 18(10):635–47. doi: 10.1038/s41577-018-0044-0

18. Schumacher TN, Thommen DS. Tertiary lymphoid structures in cancer. *Sci (New York NY)* (2022) 375(6576):eabf9419. doi: 10.1126/science.abf9419

19. Sautès-Fridman C, Petitprez F, Calderaro J, Fridman WH. Tertiary lymphoid structures in the era of cancer immunotherapy. *Nat Rev Cancer.* (2019) 19(6):307–25. doi: 10.1038/s41568-019-0144-6

20. Goc J, Germain C, Vo-Bourgais TK, Lupo A, Klein C, Knockaert S, et al. Dendritic cells in tumor-associated tertiary lymphoid structures signal a Th1 cytotoxic immune contexture and license the positive prognostic value of infiltrating CD8+ T cells. *Cancer Res* (2014) 74(3):705–15. doi: 10.1158/0008-5472.Can-13-1342

21. Leader AM, Grout JA, Maier BB, Nabet BY, Park MD, Tabachnikova A, et al. Single-cell analysis of human non-small cell lung cancer lesions refines tumor classification and patient stratification. *Cancer Cell* (2021) 39(12):1594–609.e12. doi: 10.1016/j.ccell.2021.10.009

22. Maier B, Leader AM, Chen ST, Tung N, Chang C, LeBerichel J, et al. A conserved dendritic-cell regulatory program limits antitumour immunity. *Nature* (2020) 580(7802):257–62. doi: 10.1038/s41586-020-2134-y

23. Zhang Q, He Y, Luo N, Patel SJ, Han Y, Gao R, et al. Landscape and dynamics of single immune cells in hepatocellular carcinoma. *Cell* (2019) 179(4):829–45.e20. doi: 10.1016/j.cell.2019.10.003

24. Bassez A, Vos H, Van Dyck L, Floris G, Arijs I, Desmedt C, et al. A single-cell map of intratumoral changes during anti-PD1 treatment of patients with breast cancer. *Nat Med* (2021) 27(5):820–32. doi: 10.1038/s41591-021-01323-8

25. Zhang L, Li Z, Skrzypczynska KM, Fang Q, Zhang W, O'Brien SA, et al. Single-cell analyses inform mechanisms of myeloid-targeted therapies in colon cancer. *Cell* (2020) 181(2):442–59.e29. doi: 10.1016/j.cell.2020.03.048

26. Li Y, Hu X, Lin R, Zhou G, Zhao L, Zhao D, et al. Single-cell landscape reveals active cell subtypes and their interaction in the tumor microenvironment of gastric cancer. *Theranostics* (2022) 12(8):3818–33. doi: 10.7150/thno.71833

27. Li J, Zhou J, Huang H, Jiang J, Zhang T, Ni C. Mature dendritic cells enriched in immunoregulatory molecules (mregDCs): a novel population in the tumour microenvironment and immunotherapy target. *Clin Trans Med* (2023) 13(2):e1199. doi: 10.1002/ctm2.1199

28. Ginhoux F, Guilliams M, Merad M. Expanding dendritic cell nomenclature in the single-cell era. *Nat Rev Immunol* (2022) 22(2):67–8. doi: 10.1038/s41577-022-00675-7

29. Minohara K, Imai M, Matoba T, Wing JB, Shime H, Odanaka M, et al. Mature dendritic cells enriched in regulatory molecules may control regulatory T cells and the prognosis of head and neck cancer. *Cancer Sci* (2023) 114(4):1256–69. doi: 10.1111/cas.15698

30. Barry KC, Hsu J, Broz ML, Cueto FJ, Binnewies M, Combes AJ, et al. A natural killer-dendritic cell axis defines checkpoint therapy-responsive tumor microenvironments. *Nat Med* (2018) 24(8):1178–91. doi: 10.1038/s41591-018-0085-8

31. Böttcher JP, Bonavita E, Chakravarty P, Blees H, Cabeza-Cabrerizo M, Sammicheli S, et al. NK cells stimulate recruitment of cDC1 into the tumor microenvironment promoting cancer immune control. *Cell* (2018) 172(5):1022–37.e14. doi: 10.1016/j.cell.2018.01.004

32. Broz ML, Binnewies M, Boldajipour B, Nelson AE, Pollack JL, Erle DJ, et al. Dissecting the tumor myeloid compartment reveals rare activating antigen-presenting

cells critical for T cell immunity. *Cancer Cell* (2014) 26(5):638–52. doi: 10.1016/j.ccell.2014.09.007

33. Hegde S, Krisnawan VE, Herzog BH, Zuo C, Breden MA, Knolhoff BL, et al. Dendritic cell paucity leads to dysfunctional immune surveillance in pancreatic cancer. *Cancer Cell* (2020) 37(3):289–307.e9. doi: 10.1016/j.ccell.2020.02.008

34. Tussiwand R, Lee WL, Murphy TL, Mashayekhi M, Kc W, Albring JC, et al. Compensatory dendritic cell development mediated by BATF-IRF interactions. *Nature* (2012) 490(7421):502–7. doi: 10.1038/nature11531

35. Sánchez-Paulete AR, Cueto FJ, Martínez-López M, Labiano S, Morales-Kastresana A, Rodríguez-Ruiz ME, et al. Cancer immunotherapy with immunomodulatory anti-CD137 and anti-PD-1 monoclonal antibodies requires BATF3-dependent dendritic cells. *Cancer discovery.* (2016) 6(1):71–9. doi: 10.1158/2159-8290.Cd-15-0510

36. Spranger S, Dai D, Horton B, Gajewski TF. Tumor-residing Batf3 dendritic cells are required for effector T cell trafficking and adoptive T cell therapy. *Cancer Cell* (2017) 31(5):711–23.e4. doi: 10.1016/j.ccell.2017.04.003

37. Mittal D, Vijayan D, Putz EM, Aguilera AR, Markey KA, Straube J, et al. Interleukin-12 from CD103(+) Batf3-dependent dendritic cells required for NK-cell suppression of metastasis. *Cancer Immunol Res* (2017) 5(12):1098–108. doi: 10.1158/2326-6066.Cir-17-0341

38. Salmon H, Idoyaga J, Rahman A, Leboeuf M, Remark R, Jordan S, et al. Expansion and activation of CD103(+) dendritic cell progenitors at the tumor site enhances tumor responses to therapeutic PD-L1 and BRAF inhibition. *Immunity* (2016) 44(4):924–38. doi: 10.1016/j.immuni.2016.03.012

39. Zitvogel L, Galluzzi L, Kepp O, Smyth MJ, Kroemer G. Type I interferons in anticancer immunity. *Nat Rev Immunol* (2015) 15(7):405–14. doi: 10.1038/nri3845

40. Fu C, Peng P, Loschko J, Feng L, Pham P, Cui W, et al. Plasmacytoid dendritic cells cross-prime naive CD8 T cells by transferring antigen to conventional dendritic cells through exosomes. *Proc Natl Acad Sci United States America.* (2020) 117 (38):23730–41. doi: 10.1073/pnas.2002345117

41. Kießler M, Plesca I, Sommer U, Wehner R, Wilczkowski F, Müller L, et al. Tumor-infiltrating plasmacytoid dendritic cells are associated with survival in human colon cancer. *J immunother Cancer* (2021) 9(3):e001813. doi: 10.1136/jitc-2020-001813

42. Poropatich K, Dominguez D, Chan WC, Andrade J, Zha Y, Wray B, et al. OX40 + plasmacytoid dendritic cells in the tumor microenvironment promote antitumor immunity. *J Clin Invest* (2020) 130(7):3528–42. doi: 10.1172/jci131992

43. Labidi-Galy SI, Sisirak V, Meeus P, Gobert M, Treilleux I, Bajard A, et al. Quantitative and functional alterations of plasmacytoid dendritic cells contribute to immune tolerance in ovarian cancer. *Cancer Res* (2011) 71(16):5423–34. doi: 10.1158/0008-5472.Can-11-0367

44. Sisirak V, Faget J, Gobert M, Goutagny N, Vey N, Treilleux I, et al. Impaired IFN-α production by plasmacytoid dendritic cells favors regulatory T-cell expansion that may contribute to breast cancer progression. *Cancer Res* (2012) 72(20):5188–97. doi: 10.1158/0008-5472.Can-11-3468

45. Sisirak V, Vey N, Goutagny N, Renaudineau S, Malfroy M, Thys S, et al. Breast cancer-derived transforming growth factor-β and tumor necrosis factor-α compromise interferon-α production by tumor-associated plasmacytoid dendritic cells. *Int J cancer.* (2013) 133(3):771–8. doi: 10.1002/ijc.28072

46. Terra M, Oberkampf M, Fayolle C, Rosenbaum P, Guillerey C, Dadaglio G, et al. Tumor-derived TGFβ alters the ability of plasmacytoid dendritic cells to respond to innate immune signaling. *Cancer Res* (2018) 78(11):3014–26. doi: 10.1158/0008-5472.Can-17-2719

47. Meyer MA, Baer JM, Knolhoff BL, Nywening TM, Panni RZ, Su X, et al. Breast and pancreatic cancer interrupt IRF8-dependent dendritic cell development to overcome immune surveillance. *Nat Commun* (2018) 9(1):1250. doi: 10.1038/s41467-018-03600-6

48. Zhu S, Yang N, Wu J, Wang X, Wang W, Liu YJ, et al. Tumor microenvironment-related dendritic cell deficiency: a target to enhance tumor immunotherapy. *Pharmacol Res* (2020) 159:104980. doi: 10.1016/j.phrs.2020.104980

49. Laoui D, Keirsse J, Morias Y, Van Overmeire E, Geeraerts X, Elkrim Y, et al. The tumour microenvironment harbours ontogenically distinct dendritic cell populations with opposing effects on tumour immunity. *Nat Commun* (2016) 7:13720. doi: 10.1038/ncomms13720

50. Verneau J, Sautés-Fridman C, Sun CM. Dendritic cells in the tumor microenvironment: prognostic and theranostic impact. *Semin Immunol* (2020) 48:101410. doi: 10.1016/j.smim.2020.101410

51. Gajewski TF, Schreiber H, Fu YX. Innate and adaptive immune cells in the tumor microenvironment. *Nat Immunol* (2013) 14(10):1014–22. doi: 10.1038/ni.2703

52. Tie Y, Tang F, Wei YQ, Wei XW. Immunosuppressive cells in cancer: mechanisms and potential therapeutic targets. *J Hematol Oncol* (2022) 15(1):61. doi: 10.1186/s13045-022-01282-8

53. Bule P, Aguiar SI, Aires-Da-Silva F, Dias JNR. Chemokine-directed tumor microenvironment modulation in cancer immunotherapy. *Int J Mol Sci* (2021) 22 (18):9804. doi: 10.3390/ijms22189804

54. Mizukami Y, Kono K, Kawaguchi Y, Akaike H, Kamimura K, Sugai H, et al. CCL17 and CCL22 chemokines within tumor microenvironment are related to accumulation of Foxp3+ regulatory T cells in gastric cancer. *Int J cancer.* (2008) 122 (10):2286–93. doi: 10.1002/ijc.23392

55. Wang D, Yang L, Yu W, Wu Q, Lian J, Li F, et al. Colorectal cancer cell-derived CCL20 recruits regulatory T cells to promote chemoresistance *via* FOXO1/CEBPB/NF-κB signaling. *J immunother cancer.* (2019) 7(1):215. doi: 10.1186/s40425-019-0701-2

56. Facciabene A, Peng X, Hagemann IS, Balint K, Barchetti A, Wang LP, et al. Tumour hypoxia promotes tolerance and angiogenesis *via* CCL28 and t(reg) cells. *Nature* (2011) 475(7355):226–30. doi: 10.1038/nature10169

57. Ren L, Yu Y, Wang L, Zhu Z, Lu R, Yao Z. Hypoxia-induced CCL28 promotes recruitment of regulatory T cells and tumor growth in liver cancer. *Oncotarget* (2016) 7 (46):75763–73. doi: 10.18632/oncotarget.12409

58. Watson MJ, Vignali PDA, Mullett SJ, Overacre-Delgoffe AE, Peralta RM, Grebinoski S, et al. Metabolic support of tumour-infiltrating regulatory T cells by lactic acid. *Nature* (2021) 591(7851):645–51. doi: 10.1038/s41586-020-03045-2

59. Angelin A, Gil-de-Gómez L, Dahiya S, Jiao J, Guo L, Levine MH, et al. Foxp3 reprograms T cell metabolism to function in low-glucose, high-lactate environments. *Cell Metab* (2017) 25(6):1282–93.e7. doi: 10.1016/j.cmet.2016.12.018

60. Togashi Y, Shitara K, Nishikawa H. Regulatory T cells in cancer immunosuppression - implications for anticancer therapy. *Nat Rev Clin Oncol* (2019) 16(6):356–71. doi: 10.1038/s41571-019-0175-7

61. Chen L, Flies DB. Molecular mechanisms of T cell co-stimulation and co-inhibition. *Nat Rev Immunol* (2013) 13(4):227–42. doi: 10.1038/nri3405

62. Qureshi OS, Zheng Y, Nakamura K, Attridge K, Manzotti C, Schmidt EM, et al. Trans-endocytosis of CD80 and CD86: a molecular basis for the cell-extrinsic function of CTLA-4. *Sci (New York NY).* (2011) 332(6029):600–3. doi: 10.1126/science.1202947

63. Hou TZ, Qureshi OS, Wang CJ, Baker J, Young SP, Walker LS, et al. A transendocytosis model of CTLA-4 function predicts its suppressive behavior on regulatory T cells. *J Immunol (Baltimore Md 1950).* (2015) 194(5):2148–59. doi: 10.4049/jimmunol.1401876

64. Ovcinnikovs V, Ross EM, Petersone L, Edner NM, Heuts F, Ntavli E, et al. CTLA-4-mediated transendocytosis of costimulatory molecules primarily targets migratory dendritic cells. *Sci Immunol* (2019) 4(35):eaaw0902. doi: 10.1126/sciimmunol.aaw0902

65. Gu P, Gao JF, D'Souza CA, Kowalczyk A, Chou KY, Zhang L. Trogocytosis of CD80 and CD86 by induced regulatory T cells. *Cell Mol Immunol* (2012) 9(2):136–46. doi: 10.1038/cmi.2011.62

66. Tekguc M, Wing JB, Osaki M, Long J, Sakaguchi S. Treg-expressed CTLA-4 depletes CD80/CD86 by trogocytosis, releasing free PD-L1 on antigen-presenting cells. *Proc Natl Acad Sci United States America.* (2021) 118(30):e2023739118. doi: 10.1073/pnas.2023739118

67. Liu Y, Xu P, Liu H, Fang C, Guo H, Chen X, et al. Silencing IDO2 in dendritic cells: a novel strategy to strengthen cancer immunotherapy in a murine lung cancer model. *Int J Oncol* (2020) 57(2):587–97. doi: 10.3892/ijo.2020.5073

68. Shevach EM. Mechanisms of foxp3+ T regulatory cell-mediated suppression. *Immunity* (2009) 30(5):636–45. doi: 10.1016/j.immuni.2009.04.010

69. Grohmann U, Orabona C, Fallarino F, Vacca C, Calcinaro F, Falorni A, et al. CTLA-4-Ig regulates tryptophan catabolism in vivo. *Nat Immunol* (2002) 3(11):1097–101. doi: 10.1038/ni846

70. Huang CT, Workman CJ, Flies D, Pan X, Marson AL, Zhou G, et al. Role of LAG-3 in regulatory T cells. *Immunity* (2004) 21(4):503–13. doi: 10.1016/j.immuni.2004.08.010

71. Liang B, Workman C, Lee J, Chew C, Dale BM, Colonna L, et al. Regulatory T cells inhibit dendritic cells by lymphocyte activation gene-3 engagement of MHC class II. *J Immunol (Baltimore Md 1950).* (2008) 180(9):5916–26. doi: 10.4049/jimmunol.180.9.5916

72. Li C, Jiang P, Wei S, Xu X, Wang J. Regulatory T cells in tumor microenvironment: new mechanisms, potential therapeutic strategies and future prospects. *Mol Cancer.* (2020) 19(1):116. doi: 10.1186/s12943-020-01234-1

73. Tung SL, Boardman DA, Sen M, Letizia M, Peng Q, Cianci N, et al. Regulatory T cell-derived extracellular vesicles modify dendritic cell function. *Sci Rep* (2018) 8 (1):6065. doi: 10.1038/s41598-018-24531-8

74. Muth S, Klaric A, Radsak M, Schild H, Probst HC. CD27 expression on treg cells limits immune responses against tumors. *J Mol Med (Berlin Germany).* (2022) 100 (3):439–49. doi: 10.1007/s00109-021-02116-9

75. Boissonnas A, Scholer-Dahirel A, Simon-Blancal V, Pace L, Valet F, Kissenpfennig A, et al. Foxp3+ T cells induce perforin-dependent dendritic cell death in tumor-draining lymph nodes. *Immunity* (2010) 32(2):266–78. doi: 10.1016/j.immuni.2009.11.015

76. Galvin KC, Dyck L, Marshall NA, Stefanska AM, Walsh KP, Moran B, et al. Blocking retinoic acid receptor-α enhances the efficacy of a dendritic cell vaccine against tumours by suppressing the induction of regulatory T cells. *Cancer immunology immunother CII.* (2013) 62(7):1273–82. doi: 10.1007/s00262-013-1432-8

77. Rossowska J, Anger N, Szczygieł A, Mierzejewska J, Pajtasz-Piasecka E. Intratumoral lentivector-mediated TGF-β1 gene downregulation as a potent strategy for enhancing the antitumor effect of therapy composed of cyclophosphamide and dendritic cells. *Front Immunol* (2017) 8:713. doi: 10.3389/fimmu.2017.00713

78. Conroy H, Galvin KC, Higgins SC, Mills KH. Gene silencing of TGF-β1 enhances antitumor immunity induced with a dendritic cell vaccine by reducing tumor-associated regulatory T cells. *Cancer immunology immunother CII.* (2012) 61 (3):425–31. doi: 10.1007/s00262-011-1188-y

79. Groth C, Hu X, Weber R, Fleming V, Altevogt P, Utikal J, et al. Immunosuppression mediated by myeloid-derived suppressor cells (MDSCs) during tumour progression. *Br J cancer.* (2019) 120(1):16–25. doi: 10.1038/s41416-018-0333-1

80. Yaseen MM, Abuharfeil NM, Darmani H, Daoud A. Mechanisms of immune suppression by myeloid-derived suppressor cells: the role of interleukin-10 as a key immunoregulatory cytokine. *Open Biol* (2020) 10(9):200111. doi: 10.1098/rsob.200111

81. Hu CE, Gan J, Zhang RD, Cheng YR, Huang GJ. Up-regulated myeloid-derived suppressor cell contributes to hepatocellular carcinoma development by impairing dendritic cell function. *Scandinavian J gastroenterology.* (2011) 46(2):156–64. doi: 10.3109/00365521.2010.516450

82. Ramakrishnan R, Tyurin VA, Veglia F, Condamine T, Amoscato A, Mohammadyani D, et al. Oxidized lipids block antigen cross-presentation by dendritic cells in cancer. *J Immunol (Baltimore Md 1950).* (2014) 192(6):2920–31. doi: 10.4049/jimmunol.1302801

83. Herber DL, Cao W, Nefedova Y, Novitskiy SV, Nagaraj S , Tyurin VA, et al. Lipid accumulation and dendritic cell dysfunction in cancer. *Nat Med* (2010) 16 (8):880–6. doi: 10.1038./nm.2172

84. Veglia F, Tyurin VA, Mohammadyani D, Blasi M, Duperret EK, Donthireddy L, et al. Lipid bodies containing oxidatively truncated lipids block antigen cross-presentation by dendritic cells in cancer. *Nat Commun* (2017) 8(1):2122. doi: 10.1038/s41467-017-02186-9

85. Ugolini A, Tyurin VA, Tyurina YY, Tcyganov EN, Donthireddy L, Kagan VE, et al. Polymor-phonuclear myeloid-derived suppressor cells limit antigen cross-presentation by dendritic cells in cancer. *JCI Insight* (2020) 5(15):e138581. doi: 10.1172/jci.insight.138581

86. Chen Y, Song Y, Du W, Gong L, Chang H, Zou Z. Tumor-associated macrophages: an accomplice in solid tumor progression. *J Biomed Sci* (2019) 26 (1):78. doi: 10.1186/s12929-019-0568-z

87. Pathria P, Louis TL, Varner JA. Targeting tumor-associated macrophages in cancer. *Trends Immunol* (2019) 40(4):310–27. doi: 10.1016/j.it.2019.02.003

88. Mazzoni M, Mauro G, Erreni M, Romeo P, Minna E, Vizioli MG, et al. Senescent thyrocytes and thyroid tumor cells induce M2-like macrophage polarization of human monocytes *via* a PGE2-dependent mechanism. *J Exp Clin Cancer Res* (2019) 38(1):208. doi: 10.1186/s13046-019-1198-8

89. Boutilier AJ, Elsawa SF. Macrophage polarization states in the tumor microenvironment. *Int J Mol Sci* (2021) 22(13):6995. doi: 10.3390/ijms22136995

90. Mantovani A, Sozzani S, Locati M, Allavena P, Sica A. Macrophage polarization: tumor-associated macrophages as a paradigm for polarized M2 mononuclear phagocytes. *Trends Immunol* (2002) 23(11):549–55. doi: 10.1016/s1471-4906(02)02302-5

91. Pan Y, Yu Y, Wang X, Zhang T. Tumor-associated macrophages in tumor immunity. *Front Immunol* (2020) 11:583084. doi: 10.3389/fimmu.2020.583084

92. DeNardo DG, Ruffell B. Macrophages as regulators of tumour immunity and immunotherapy. *Nat Rev Immunol* (2019) 19(6):369–82. doi: 10.1038/s41577-019-0127-6

93. Hinshaw DC, Shevde LA. The tumor microenvironment innately modulates cancer progression. *Cancer Res* (2019) 79(18):4557–66. doi: 10.1158/0008-5472.Can-18-3962

94. Beury DW, Parker KH, Nyandjo M, Sinha P, Carter KA, Ostrand-Rosenberg S. Cross-talk among myeloid-derived suppressor cells, macrophages, and tumor cells impacts the inflammatory milieu of solid tumors. *J Leukoc Biol* (2014) 96(6):1109–18. doi: 10.1189/jlb.3A0414-210R

95. Ruffell B, Chang-Strachan D, Chan V, Rosenbusch A, Ho CM, Pryer N, et al. Macrophage IL-10 blocks CD8+ T cell-dependent responses to chemotherapy by suppressing IL-12 expression in intratumoral dendritic cells. *Cancer Cell* (2014) 26 (5):623–37. doi: 10.1016/j.ccell.2014.09.006

96. Pfirschke C, Zilionis R, Engblom C, Messemaker M, Zou AE, Rickelt S, et al. Macrophage-targeted therapy unlocks antitumoral cross-talk between IFNγ-secreting lymphocytes and IL12-producing dendritic cells. *Cancer Immunol Res* (2022) 10(1):40–55. doi: 10.1158/2326-6066.Cir-21-0326

97. Dammeijer F, Lievense LA, Kaijen-Lambers ME, van Nimwegen M, Bezemer K, Hegmans JP, et al. Depletion of tumor-associated macrophages with a CSF-1R kinase inhibitor enhances antitumor immunity and survival induced by DC immunotherapy. *Cancer Immunol Res* (2017) 5(7):535–46. doi: 10.1158/2326-6066.Cir-16-0309

98. Turley SJ, Cremasco V, Astarita JL. Immunological hallmarks of stromal cells in the tumour microenvironment. *Nat Rev Immunol* (2015) 15(11):669–82. doi: 10.1038/nri3902

99. Arina A, Idel C, Hyjek EM, Alegre ML, Wang Y, Bindokas VP, et al. Tumor-associated fibroblasts predominantly come from local and not circulating precursors. *Proc Natl Acad Sci United States America.* (2016) 113(27):7551–6. doi: 10.1073/pnas.1600363113

100. Park D, Sahai E, Rullan A. SnapShot: cancer-associated fibroblasts. *Cell* (2020) 181(2):486–.e1. doi: 10.1016/j.cell.2020.03.013

101. Hawinkels LJ, Paauwe M, Verspaget HW, Wiercinska E, van der Zon JM, van der Ploeg K, et al. Interaction with colon cancer cells hyperactivates TGF-β signaling in cancer-associated fibroblasts. *Oncogene* (2014) 33(1):97–107. doi: 10.1038/onc.2012.536

102. Chen X, Song E. Turning foes to friends: targeting cancer-associated fibroblasts. *Nat Rev Drug discovery*. (2019) 18(2):99–115. doi: 10.1038/s41573-018-0004-1

103. Mao X, Xu J, Wang W, Liang C, Hua J, Liu J, et al. Crosstalk between cancer-associated fibroblasts and immune cells in the tumor microenvironment: new findings and future perspectives. *Mol Cancer*. (2021) 20(1):131. doi: 10.1186/s12943-021-01428-1

104. Berzaghi R, Tornaas S, Lode K, Hellevik T, Martinez-Zubiaurre I. Ionizing radiation curtails immunosuppressive effects from cancer-associated fibroblasts on dendritic cells. *Front Immunol* (2021) 12:662594. doi: 10.3389/fimmu.2021.662594

105. Hsu YL, Hung JY, Chiang SY, Jian SF, Wu CY , Lin YS, et al. Lung cancer-derived galectin-1 contributes to cancer associated fibroblast-mediated cancer progression and immune suppression through TDO2/kynurenine axis. *Oncotarget* (2016) 7(19):27584–98. doi: 10.18632/oncotarget.8488

106. Cheng JT, Deng YN, Yi HM, Wang GY, Fu BS, Chen WJ, et al. Hepatic carcinoma-associated fibroblasts induce IDO-producing regulatory dendritic cells through IL-6-mediated STAT3 activation. *Oncogenesis* (2016) 5(2):e198. doi: 10.1038/oncsis.2016.7

107. Long J, Hu Z, Xue H, Wang Y, Chen J, Tang F, et al. Vascular endothelial growth factor (VEGF) impairs the motility and immune function of human mature dendritic cells through the VEGF receptor 2-RhoA-cofilin1 pathway. *Cancer Sci* (2019) 110(8):2357–67. doi: 10.1111/cas.14091

108. Kugeratski FG, Atkinson SJ, Neilson LJ, Lilla S, Knight JRP, Serneels J, et al. Hypoxic cancer-associated fibroblasts increase NCBP2-AS2/HIAR to promote endothelial sprouting through enhanced VEGF signaling. *Sci Signaling* (2019) 12(567):eaan8247. doi: 10.1126/scisignal.aan8247

109. Huang TX, Tan XY, Huang HS, Li YT, Liu BL, Liu KS, et al. Targeting cancer-associated fibroblast-secreted WNT2 restores dendritic cell-mediated antitumour immunity. *Gut* (2022) 71(2):333–44. doi: 10.1136/gutjnl-2020-322924

110. Jing X, Yang F, Shao C, Wei K, Xie M, Shen H, et al. Role of hypoxia in cancer therapy by regulating the tumor microenvironment. *Mol Cancer*. (2019) 18(1):157. doi: 10.1186/s12943-019-1089-9

111. Ricciardi A, Elia AR, Cappello P, Puppo M, Vanni C, Fardin P, et al. Transcriptome of hypoxic immature dendritic cells: modulation of chemokine/receptor expression. *Mol Cancer Res MCR*. (2008) 6(2):175–85. doi: 10.1158/1541-7786.Mcr-07-0391

112. Elia AR, Cappello P, Puppo M, Fraone T, Vanni C, Eva A, et al. Human dendritic cells differentiated in hypoxia down-modulate antigen uptake and change their chemokine expression profile. *J Leukoc Biol* (2008) 84(6):1472–82. doi: 10.1189/jlb.0208082

113. Yang M, Ma C, Liu S, Sun J, Shao Q, Gao W, et al. Hypoxia skews dendritic cells to a T helper type 2-stimulating phenotype and promotes tumour cell migration by dendritic cell-derived osteopontin. *Immunology* (2009) 128(1 Suppl):e237–49. doi: 10.1111/j.1365-2567.2008.02954.x

114. Suthen S, Lim CJ, Nguyen PHD, Dutertre CA, Lai HLH, Wasser M, et al. Hypoxia-driven immunosuppression by treg and type-2 conventional dendritic cells in HCC. *Hepatol (Baltimore Md)*. (2022) 76(5):1329–44. doi: 10.1002/hep.32419

115. McGettrick AF, O'Neill LAJ. The role of HIF in immunity and inflammation. *Cell Metab* (2020) 32(4):524–36. doi: 10.1016/j.cmet.2020.08.002

116. Kierans SJ, Taylor CT. Regulation of glycolysis by the hypoxia-inducible factor (HIF): implications for cellular physiology. *J Physiol* (2021) 599(1):23–37. doi: 10.1113/jp280572

117. Liu J, Zhang X, Chen K, Cheng Y, Liu S, Xia M, et al. CCR7 chemokine receptor-inducible lnc-Dpf3 restrains dendritic cell migration by inhibiting HIF-1α-Mediated glycolysis. *Immunity* (2019) 50(3):600–15.e15. doi: 10.1016/j.immuni.2019.01.021

118. Guak H, Al Habyan S, Ma EH, Aldossary H, Al-Masri M, Won SY, et al. Glycolytic metabolism is essential for CCR7 oligomerization and dendritic cell migration. *Nat Commun* (2018) 9(1):2463. doi: 10.1038/s41467-018-04804-6

119. Filippi I, Morena E, Aldinucci C, Carraro F, Sozzani S, Naldini A. Short-term hypoxia enhances the migratory capability of dendritic cell through HIF-1α and PI3K/Akt pathway. *J Cell Physiol* (2014) 229(12):2067–76. doi: 10.1002/jcp.24666

120. Han Z, Dong Y, Lu J, Yang F, Zheng Y, Yang H. Role of hypoxia in inhibiting dendritic cells by VEGF signaling in tumor microenvironments: mechanism and application. *Am J Cancer Res* (2021) 11(8):3777–93. Available at: https://pubmed.ncbi.nlm.nih.gov/34522449/.

121. Tran CW, Gold MJ, Garcia-Batres C, Tai K, Elford AR, Himmel ME, et al. Hypoxia-inducible factor 1 alpha limits dendritic cell stimulation of CD8 T cell immunity. *PloS One* (2020) 15(12):e0244366. doi: 10.1371/journal.pone.0244366

122. Naldini A, Morena E, Pucci A, Miglietta D, Riboldi E, Sozzani S, et al. Hypoxia affects dendritic cell survival: role of the hypoxia-inducible factor-1α and lipopolysaccharide. *J Cell Physiol* (2012) 227(2):587–95. doi: 10.1002/jcp.22761

123. Ding XC, Wang LL, Zhang XD, Xu JL, Li PF, Liang H, et al. The relationship between expression of PD-L1 and HIF-1α in glioma cells under hypoxia. *J Hematol Oncol* (2021) 14(1):92. doi: 10.1186/s13045-021-01102-5

124. Leblond MM, Gérault AN, Corroyer-Dulmont A, MacKenzie ET, Petit E, Bernaudin M, et al. Hypoxia induces macrophage polarization and re-education toward an M2 phenotype in U87 and U251 glioblastoma models. *Oncoimmunology* (2016) 5(1):e1056442. doi: 10.1080/2162402x.2015.1056442

125. Vander Heiden MG, Cantley LC, Thompson CB. Understanding the warburg effect: the metabolic requirements of cell proliferation. *Sci (New York NY)*. (2009) 324(5930):1029–33. doi: 10.1126/science.1160809

126. Manoharan I, Prasad PD, Thangaraju M, Manicassamy S. Lactate-dependent regulation of immune responses by dendritic cells and macrophages. *Front Immunol* (2021) 12:691134. doi: 10.3389/fimmu.2021.691134

127. Hayes C, Donohoe CL, Davern M, Donlon NE. The oncogenic and clinical implications of lactate induced immunosuppression in the tumour microenvironment. *Cancer letters*. (2021) 500:75–86. doi: 10.1016/j.canlet.2020.12.021

128. Brown TP, Bhattacharjee P, Ramachandran S, Sivaprakasam S, Ristic B, Sikder MOF, et al. The lactate receptor GPR81 promotes breast cancer growth *via* a paracrine mechanism involving antigen-presenting cells in the tumor microenvironment. *Oncogene* (2020) 39(16):3292–304. doi: 10.1038/s41388-020-1216-5

129. Gottfried E, Kunz-Schughart LA, Ebner S, Mueller-Klieser W, Hoves S, Andreesen R, et al. Tumor-derived lactic acid modulates dendritic cell activation and antigen expression. *Blood* (2006) 107(5):2013–21. doi: 10.1182/blood-2005-05-1795

130. Nasi A, Fekete T, Krishnamurthy A, Snowden S, Rajnavölgyi E, Catrina AI, et al. Dendritic cell reprogramming by endogenously produced lactic acid. *J Immunol (Baltimore Md 1950)*. (2013) 191(6):3090–9. doi: 10.4049/jimmunol.1300772

131. Monti M, Vescovi R, Consoli F, Farina D, Moratto D, Berruti A, et al. Plasmacytoid dendritic cell impairment in metastatic melanoma by lactic acidosis. *Cancers* (2020) 12(8):2085. doi: 10.3390/cancers12082085

132. Raychaudhuri D, Bhattacharya R, Sinha BP, Liu CSC, Ghosh AR, Rahaman O, et al. Lactate induces pro-tumor reprogramming in intratumoral plasmacytoid dendritic cells. *Front Immunol* (2019) 10:1878. doi: 10.3389/fimmu.2019.01878

133. Tong L, Yue P, Yang Y, Huang J, Zeng Z, Qiu W. Motility and mechanical properties of dendritic cells deteriorated by extracellular acidosis. *Inflammation* (2021) 44(2):737–45. doi: 10.1007/s10753-020-01373-z

134. Trempolec N, Degavre C, Doix B, Brusa D, Corbet C, Feron O. Acidosis-induced TGF-β2 production promotes lipid droplet formation in dendritic cells and alters their potential to support anti-mesothelioma T cell response. *Cancers* (2020) 12(5):1284. doi: 10.3390/cancers12051284

135. Vermeulen M, Giordano M, Trevani AS, Sedlik C, Gamberale R, Fernández-Calotti P, et al. Acidosis improves uptake of antigens and MHC class I-restricted presentation by dendritic cells. *J Immunol (Baltimore Md 1950)*. (2004) 172(5):3196–204. doi: 10.4049/jimmunol.172.5.3196

136. Martínez D, Vermeulen M, von Euw E, Sabatté J, Maggíni J, Ceballos A, et al. Extracellular acidosis triggers the maturation of human dendritic cells and the production of IL-12. *J Immunol (Baltimore Md 1950)*. (2007) 179(3):1950–9. doi: 10.4049/jimmunol.179.3.1950

137. Cueto FJ, Sancho D. The Flt3L/Flt3 axis in dendritic cell biology and cancer immunotherapy. *Cancers* (2021) 13(7):1525. doi: 10.3390/cancers13071525

138. Bhardwaj N, Friedlander PA, Pavlick AC, Ernstoff MS, Gastman BR, Hanks BA, et al. Flt3 ligand augments immune responses to anti-DEC-205-NY-ESO-1 vaccine through expansion of dendritic cell subsets. *Nat cancer*. (2020) 1(12):1204–17. doi: 10.1038/s43018-020-00143-y

139. van de Laar L, Coffer PJ, Woltman AM. Regulation of dendritic cell development by GM-CSF: molecular control and implications for immune homeostasis and therapy. *Blood* (2012) 119(15):3383–93. doi: 10.1182/blood-2011-11-370130

140. Oosterling SJ, Mels AK, Geijtenbeek TB, van der Bij GJ, Tuk CW, Vuylsteke RJ, et al. Preoperative granulocyte/macrophage colony-stimulating factor (GM-CSF) increases hepatic dendritic cell numbers and clustering with lymphocytes in colorectal cancer patients. *Immunobiology* (2006) 211(6-8):641–9. doi: 10.1016/j.imbio.2006.06.010

141. Sluijter BJ, van den Hout MF, Koster BD, van Leeuwen PA, Schneiders FL, van de Ven R, et al. Arming the melanoma sentinel lymph node through local administration of CpG-b and GM-CSF: recruitment and activation of BDCA3/CD141(+) dendritic cells and enhanced cross-presentation. *Cancer Immunol Res* (2015) 3(5):495–505. doi: 10.1158/2326-6066.Cir-14-0165

142. Duan T, Du Y, Xing C, Wang HY, Wang RF. Toll-like receptor signaling and its role in cell-mediated immunity. *Front Immunol* (2022) 13:812774. doi: 10.3389/fimmu.2022.812774

143. Mehrotra S, Britten CD, Chin S, Garrett-Mayer E, Cloud CA, Li M, et al. Vaccination with poly(IC:LC) and peptide-pulsed autologous dendritic cells in patients with pancreatic cancer. *J Hematol Oncol* (2017) 10(1):82. doi: 10.1186/s13045-017-0459-2

144. Anfray C, Mainini F, Digifico E, Maeda A, Sironi M, Erreni M, et al. Intratumoral combination therapy with poly(I:C) and resiquimod synergistically triggers tumor-associated macrophages for effective systemic antitumoral immunity. *J immunother Cancer* (2021) 9(9):e002408. doi: 10.1136/jitc-2021-002408

145. Shrimpton RE, Butler M, Morel AS, Eren E, Hue SS, Ritter MA. CD205 (DEC-205): a recognition receptor for apoptotic and necrotic self. *Mol Immunol* (2009) 46(6):1229–39. doi: 10.1016/j.molimm.2008.11.016

146. Dhodapkar MV, Sznol M, Zhao B, Wang D, Carvajal RD, Keohan ML, et al. Induction of antigen-specific immunity with a vaccine targeting NY-ESO-1 to the

dendritic cell receptor DEC-205. *Sci Trans Med* (2014) 6(232):232ra51. doi: 10.1126/scitranslmed.3008068

147. Martinek J, Lin J, Kim KI, Wang VG, Wu TC, Chiorazzi M, et al. Transcriptional profiling of macrophages *in situ* in metastatic melanoma reveals localization-dependent phenotypes and function. *Cell Rep Med* (2022) 3(5):100621. doi: 10.1016/j.xcrm.2022.100621

148. van Willigen WW, Bloemendal M, Gerritsen WR, Schreibelt G, de Vries IJM, Bol KF. Dendritic cell cancer therapy: vaccinating the right patient at the right time. *Front Immunol* (2018) 9:2265. doi: 10.3389/fimmu.2018.02265

149. National Cancer Institute. Drugs approved for prostate cancer . Available at: https://www.cancer.gov/ about-cancer/treatment/drugs/sipuleucel-t (Accessed 9 April 2023).

150. National Comprehensive Cancer Network. NCCN clinical practice guidelines in oncology: prostate cancer (Version 1.2023) . Available at: https://www.nccn.org/guidelines.

151. Peng S, Chen S, Hu W, Mei J, Zeng X, Su T, et al. Combination neoantigen-based dendritic cell vaccination and adoptive T-cell transfer induces antitumor responses against recurrence of hepatocellular carcinoma. *Cancer Immunol Res* (2022) 10(6):728–44. doi: 10.1158/2326-6066.Cir-21-0931

152. Carreno BM, Magrini V, Becker-Hapak M, Kaabinejadian S, Hundal J, Petti AA, et al. Cancer immunotherapy. a dendritic cell vaccine increases the breadth and diversity of melanoma neoantigen-specific T cells. *Sci (New York NY).* (2015) 348 (6236):803–8. doi: 10.1126/science.aaa3828

153. Ding Z, Li Q, Zhang R, Xie L, Shu Y, Gao S, et al. Personalized neoantigen pulsed dendritic cell vaccine for advanced lung cancer. *Signal transduction targeted Ther* (2021) 6(1):26. doi: 10.1038/s41392-020-00448-5

154. Fucikova J, Hensler M, Kasikova L, Lanickova T, Pasulka J, Rakova J, et al. An autologous dendritic cell vaccine promotes anticancer immunity in patients with ovarian cancer with low mutational burden and cold tumors. *Clin Cancer Res an Off J Am Assoc Cancer Res* (2022) 28(14):3053–65. doi: 10.1158/1078-0432.Ccr-21-4413

155. Lau SP, Klaase L, Vink M, Dumas J, Bezemer K, van Krimpen A, et al. Autologous dendritic cells pulsed with allogeneic tumour cell lysate induce tumour-reactive T-cell responses in patients with pancreatic cancer: a phase I study. *Eur J Cancer (Oxford Engl 1990).* (2022) 169:20–31. doi: 10.1016/j.ejca.2022.03.015

156. Saxena M, Bhardwaj N. Re-emergence of dendritic cell vaccines for cancer treatment. *Trends cancer.* (2018) 4(2):119–37. doi: 10.1016/j.trecan.2017.12.007

157. Guo Z, Yuan Y, Chen C, Lin J, Ma Q, Liu G, et al. Durable complete response to neoantigen-loaded dendritic-cell vaccine following anti-PD-1 therapy in metastatic gastric cancer. *NPJ Precis Oncol* (2022) 6(1):34. doi: 10.1038/s41698-022-00279-3

158. Teng CF, Wang T, Shih FY, Shyu WC, Jeng LB. Therapeutic efficacy of dendritic cell vaccine combined with programmed death 1 inhibitor for hepatocellular carcinoma. *J Gastroenterol hepatology.* (2021) 36(7):1988–96. doi: 10.1111/jgh.15398

159. Barshidi A, Karpisheh V, Noukabadi FK, Kiani FK, Mohammadi M, Afsharimanesh N, et al. Dual blockade of PD-1 and LAG3 immune checkpoints increases dendritic cell vaccine mediated T cell responses in breast cancer model. *Pharm Res* (2022) 39(8):1851–66. doi: 10.1007/s11095-022-03297-9

160. Chu TH, Vo MC, Park HS, Lakshmi TJ, Jung SH, Kim HJ, et al. Potent anti-myeloma efficacy of dendritic cell therapy in combination with pomalidomide and programmed death-ligand 1 blockade in a preclinical model of multiple myeloma. *Cancer immunology immunother CII.* (2021) 70(1):31–45. doi: 10.1007/s00262-020-02654-0

161. Vo MC, Jung SH, Chu TH, Lee HJ, Lakshmi TJ, Park HS, et al. Lenalidomide and programmed death-1 blockade synergistically enhances the effects of dendritic cell

vaccination in a model of murine myeloma. *Front Immunol* (2018) 9:1370. doi: 10.3389/fimmu.2018.01370

162. Shi W, Yang X, Xie S, Zhong D, Lin X, Ding Z, et al. A new PD-1-specific nanobody enhances the antitumor activity of T-cells in synergy with dendritic cell vaccine. *Cancer letters.* (2021) 522:184–97. doi: 10.1016/j.canlet.2021.09.028

163. Yazdani M, Gholizadeh Z, Nikpoor AR, Mohamadian Roshan N, Jaafari MR, Badiee A. Ex vivo dendritic cell-based (DC) vaccine pulsed with a low dose of liposomal antigen and CpG-ODN improved PD-1 blockade immunotherapy. *Sci Rep* (2021) 11 (1):14661. doi: 10.1038/s41598-021-94250-0

164. Teng CF, Wang T, Wu TH, Lin JH, Shih FY, Shyu WC, et al. Combination therapy with dendritic cell vaccine and programmed death ligand 1 immune checkpoint inhibitor for hepatocellular carcinoma in an orthotopic mouse model. *Ther Adv Med Oncol* (2020) 12:1758835920922034. doi: 10.1177/1758835920922034

165. De Keersmaecker B, Claerhout S, Carrasco J, Bar I, Corthals J, Wilgenhof S, et al. TriMix and tumor antigen mRNA electroporated dendritic cell vaccination plus ipilimumab: link between T-cell activation and clinical responses in advanced melanoma. *J immunother Cancer* (2020) 8(1):e000329. doi: 10.1136/jitc-2019-000329

166. Zaidi N, Quezada SA, Kuroiwa JMY, Zhang L, Jaffee EM, Steinman RM, et al. Anti-CTLA-4 synergizes with dendritic cell-targeted vaccine to promote IL-3-dependent CD4(+) effector T cell infiltration into murine pancreatic tumors. *Ann New York Acad Sci* (2019) 1445(1):62–73. doi: 10.1111/nyas.14049

167. Liu L, Wang Y, Miao L, Liu Q, Musetti S, Li J, et al. Combination immunotherapy of MUC1 mRNA nano-vaccine and CTLA-4 blockade effectively inhibits growth of triple negative breast cancer. *Mol Ther J Am Soc Gene Ther* (2018) 26 (1):45–55. doi: 10.1016/j.ymthe.2017.10.020

168. Esmaily M, Masjedi A, Hallaj S, Nabi Afjadi M, Malakotikhah F, Ghani S, et al. Blockade of CTLA-4 increases anti-tumor response inducing potential of dendritic cell vaccine. *J Controlled release Off J Controlled Release Society.* (2020) 326:63–74. doi: 10.1016/j.jconrel.2020.06.017

169. Sun NY, Chen YL, Lin HW, Chiang YC, Chang CF, Tai YJ, et al. Immune checkpoint ab enhances the antigen-specific anti-tumor effects by modulating both dendritic cells and regulatory T lymphocytes. *Cancer letters.* (2019) 444:20–34. doi: 10.1016/j.canlet.2018.11.039

170. Ghiringhelli F, Menard C, Puig PE, Ladoire S, Roux S, Martin F, et al. Metronomic cyclophosphamide regimen selectively depletes CD4+CD25+ regulatory T cells and restores T and NK effector functions in end stage cancer patients. *Cancer immunology immunother CII.* (2007) 56(5):641–8. doi: 10.1007/s00262-006-0225-8

171. Cornelissen R, Hegmans JP, Maat AP, Kaijen-Lambers ME, Bezemer K, Hendriks RW, et al. Extended tumor control after dendritic cell vaccination with low-dose cyclophosphamide as adjuvant treatment in patients with malignant pleural mesothelioma. *Am J Respir Crit Care Med* (2016) 193(9):1023–31. doi: 10.1164/rccm.201508-1573OC

172. Liau LM, Ashkan K, Brem S, Campian JL, Trusheim JE, Iwamoto FM, et al. Association of autologous tumor lysate-loaded dendritic cell vaccination with extension of survival among patients with newly diagnosed and recurrent glioblastoma: a phase 3 prospective externally controlled cohort trial. *JAMA Oncol* (2023) 9(1):112–21. doi: 10.1001/jamaoncol.2022.5370

173. Storkus WJ, Maurer D, Lin Y, Ding F, Bose A, Lowe D, et al. Dendritic cell vaccines targeting tumor blood vessel antigens in combination with dasatinib induce therapeutic immune responses in patients with checkpoint-refractory advanced melanoma. *J immunother Cancer* (2021) 9(11):e003675. doi: 10.1136/jitc-2021-003675

174. Gall VA, Philips AV, Qiao N, Clise-Dwyer K, Perakis AA, Zhang M, et al. Trastuzumab increases HER2 uptake and cross-presentation by dendritic cells. *Cancer Res* (2017) 77(19):5374–83. doi: 10.1158/0008-5472.Can-16-2774

The unique immune ecosystems in pediatric brain tumors: integrating single-cell and bulk RNA-sequencing

Liangliang Cao†, Wanqun Xie†, Wenkun Ma†, Heng Zhao, Jiajia Wang, Zhuangzhuang Liang, Shuaiwei Tian*, Baocheng Wang* and Jie Ma*

Department of Pediatric Neurosurgery, Xinhua Hospital Affiliated to Shanghai Jiao Tong University School of Medicine, Shanghai, China

Background: The significant progress of immune therapy in non-central nervous system tumors has sparked interest in employing the same strategy for adult brain tumors. However, the advancement of immunotherapy in pediatric central nervous system (CNS) tumors is not yet on par. Currently, there is a lack of comprehensive comparative studies investigating the immune ecosystem in pediatric and adult CNS tumors at a high-resolution single-cell level.

Methods: In this study, we comprehensively analyzed over 0.3 million cells from 171 samples, encompassing adult gliomas (IDH wild type and IDH mutation) as well as four major types of pediatric brain tumors (medulloblastoma (MB), ependymoma (EPN), H3K27M-mutation (DIPG), and pediatric IDH-mutation glioma (P-IDH-M)). Our approach involved integrating publicly available and newly generated single-cell datasets. We compared the immune landscapes in different brain tumors, as well as the detailed functional phenotypes of T-cell and myeloid subpopulations. Through single-cell analysis, we identified gene sets associated with major cell types in the tumor microenvironment (gene features from single-cell data, scFes) and compared them with existing gene sets such as GSEA and xCell. The CBTTC and external GEO cohort was used to analyze and validate the immune-stromal-tumor patterns in pediatric brain tumors which might potentially respond to the immunotherapy.

Results: From the perspective of single-cell analysis, it was observed that major pediatric brain tumors (MB, EPN, P-IDH-M, DIPG) exhibited lower immune contents compared with adult gliomas. Additionally, these pediatric brain tumors displayed diverse immunophenotypes, particularly in regard to myeloid cells. Notably, the presence of HLA-enriched myeloid cells in MB was found to be independently associated with prognosis. Moreover, the scFes, when compared with commonly used gene features, demonstrated superior performance in independent single-cell datasets across various tumor types. Furthermore, our study revealed the existence of heterogeneous immune ecosystems at the bulk-RNA sequencing level among different brain tumor types. In addition, we

identified several immune-stromal-tumor patterns that could potentially exhibit significant responses to conventional immune checkpoint inhibitors.

Conclusion: The single-cell technique provides a rational path to deeply understand the unique immune ecosystem of pediatric brain tumors. In spite of the traditional attitudes of "cold" tumor towards pediatric brain tumor, the immune-stroma-tumor patterns identified in this study suggest the feasibility of immune checkpoint inhibitors and pave the way for the upcoming tide of immunotherapy in pediatric brain tumors.

1 Introduction

The therapeutic strategy targeting the specific component in the immune ecosystem has achieved remarkable advances in recent years (1, 2). Considering the distinct immune microenvironment and the molecular and immunological characters of pediatric brain tumors, it should be more rigorous to apply the scientific findings of their adult counterparts in them (3–5). Recent studies have shown that there are significant differences in immune compositions between children and adults at the levels of bulk RNA and DNA methylation. However, these deconvolution-based methods are unable to directly measure and achieve a high-resolution depiction of the immune composition landscape (6). The direct and systematic mapping of immune ecosystems in pediatric brain tumors, including the detailed immunophenotypes of immune cells, is still lacking. Therefore, a full understanding of the tumor microenvironment (TME) compositions of the CNS at the single-cell level is the essential precondition of the successful application of immunotherapy.

As the major immune components infiltrating into the TME, myeloid cells play important roles in modulating the antitumor functions (7). Some therapeutic strategies redirecting them are ongoing. In order to clearly understand their various functional phenotypes among different cancer types, Zhang et al. systematically investigated the unique and recurrent phenotypes of myeloid across 15 tumor types and identified some potential targets, for example, LAPM3 cDCs and TNF+ mast cells. The CNS hosts the heterogeneous populations of myeloid cells, including microglia and border-associated macrophage. It is conceivable that the functions of microglia are distinct and highly diverse in different ages and pathological conditions (8–10). Klemm et al. found that microglial (MG) and bone marrow-derived myeloid (BMDM) exhibited a multifaceted polarization phenotype and diverse transcriptional programming in adult gliomas and brain metastases (4) and acquired tumor-associated signatures with the dysregulations of hypoxia and inflammatory molecules (9, 11). Recently, the mystery of the TME in pediatric brain tumors was unveiled. The TME of medulloblastoma (MB) was analyzed

systematically, and several myeloid clusters were identified (12). In addition, the polarization characters (M1/M2) and prognostic value in MB were investigated by multiple fluorescence immunohistochemistry (13). However, the identification of recurrent functional phenotypes spanning multiple pediatric brain tumor types is still lacking, which will undoubtedly affect the fully understanding of heterogeneity and evolution of the TME.

Different from depicting the state of certain cell type, the systematical identification of constant and specific immune cell pairings of immune, stromal, and tumor cells across the diverse tumor types will provide priori knowledge for cancer immunity before immunotherapy (14). Krummel et al. identified 12 immune archetypes in over 10 tumor types with 10 immune cell features, mainly focusing on non-CNS cancer types (15). Considering the unique immune characteristics of the central nervous system (CNS), phenotypic differences between children and adults, the predominance of malignant cells in CNS tumors, and the potential benefits of immunotherapy in treating pediatric brain tumors, it remains unknown whether a distinct immune-stromal-tumor ecosystem exists.

In this study, combining with the published and newly generated scRNA-seq data, we mapped the landscapes of the TME across six major brain tumor types and comprehensively analyzed the immunophenotypes of T cells and myeloid cells in different cancer types. Different from the definitions of myeloid cells using a single gene in previous studies, we combined the marker genes with mostly affected pathways to discover the recurrent function phenotypes across different brain tumors. In addition, considering the unique stromal composition and predominance of malignant cells in pediatric brain tumors, we constructed the gene features of different cell types (namely, scFes) including the tumor-related features based on single-cell analysis and finally identified 12 immune-stromal-tumor patterns. We believe this study will provide a comprehensive compendium to understand the complexity of the TME and potential strategies for the upcoming tide of immunotherapy in pediatric brain tumors.

2 Materials and methods

2.1 Single-cell RNA-seq datasets collected in this study

We collected published scRNA-seq data covering four pediatric brain tumor types (ependymoma (EPN), medulloblastoma (MB), IDH-mutation glioma (P-IDH-M), and H3K27M-mutation glioma (DIPG)) and two adult gliomas [IDH-wild glioma (adult-IDH-W) and IDH-mutation glioma (adult-IDH-M)] (Figure 1A).

To supplement the publicly available data and study the immune components in the "cold" tumors (16, 17), we collected five specimens of MB (including three unpublished datasets generated previously and two newly produced) (18) and obtained the snRNA-seq data using the 10x Genomics platform (19) (Table S1). The study protocol was approved by the Ethics Committee of Xinhua Hospital Affiliated to Shanghai Jiao Tong University School of Medicine, and the written informed consents were obtained from all patients.

2.2 Primary scRNA-seq data preprocessing

2.2.1 Data qualification and transformation

For the newly generated snRNA-seq data from 10x Genomics, the Cell Ranger (version 3.0, 10x Genomics Inc.) was used for the alignment and quantification of sequencing reads against the GRCh38 human reference genome. The cells with fewer than 2,000 UMI counts, less than 200 detected genes and >10% mitochondrial gene count, were filtered out. DoubletFinder with default parameters was applied to remove the potential doublets (20).

For previously published scRNA-Seq data, the quality-passed cells from the original publications were used for downstream analysis. Count data generated based on 10x Genomics Chromium were normalized by the NormalizeData function from the Seurat packages (version 4.1.1) (21). The TPM data generated based on Smart-seq2 were log2-transformed.

2.2.2 Comparing two methods identifying known cell types

The Cluster-based method was based on the Seurat pipeline, and two or more marker genes were used to annotate the cell types (for example, MBP, MOG, and PLP1 were combinedly to mark the mature oligodendrocytes). Another method named "positive selection" (cells with positive expression of known markers) were performed according to the expression of single marker gene (for example, oligodendrocytes were annotated if the expression level of "MBP" was higher than the average level). Then, the cell numbers, mean expression level of markers, and mean enrichment scores of mark pathway were compared.

2.2.3 Clustering per dataset

Two-run clustering was performed on every dataset to reduce the technical noise. The first-run clustering was to obtain the coarse cell types. The percentages of mitochondrial genes and heat shock protein genes were calculated and added using the AddMetaData function. The cell-cycle score of each cell was scored by the CellCycleScoring function for the G2/M and S cell-cycle phases. The 10x Genomics-based dataset was renormalized by the SCTransform function, and the donor effect, number of UMIs, percentage of mitochondrial transcripts, percentage of heat shock protein genes, and cell-cycle scores were regressed out. The top 2000 genes were identified as highly variable genes (HVG) and used for principal component analysis (PCA). The Shared Nearest Neighbor (SNN) graph was built with the top 15 principal components, and the cells were clustered using the Louvain algorithm with default parameters. The primary cell types were annotated according to the marker genes. Then, the second-run clustering was performed on each cell type as the pipeline of first-run clustering. The resolution parameter of clustering was set to 50 to construct the mini-clusters to find out and exclude the contaminant cells or doublets. The reminding cells were kept for the downstream analysis.

2.3 Ro/e analysis for the tissue abundance of T-cell subpopulations

To characterize the tissue distribution of a specific T subpopulation, odds ratios (ORs) were calculated and used to indicate preferences. We constructed a 2×2 contingency table. This table included the number of cells belonging to the target T-cell subpopulation i in tissue j, the number of cells of T cell i in other tissues, the number of cells of non-i T cells in tissue j, and the number of cells of non-i T cells in other tissues. To determine the significance, Fisher's exact test was applied to this contingency table, allowing us to obtain the OR and corresponding p-value. The p-values were then adjusted using the BH method implemented in the R function p.adjust. Consequently, a higher OR with a value above 1.5 indicated a preference for the target T-cell subpopulation i to distribute in tissue j. Conversely, a lower OR with a value below 0.5 indicated a preference for T cell i not to distribute in tissue j.

2.4 Conduction of two independent RNA-seq cohorts of pediatric brain tumors

2.4.1 RNA-seq cohorts of pediatric brain tumors from the Children's Brain Tumor Tissue Consortium

Transcriptomic data and clinical data were downloaded from the USCS XENA portal https://xena.ucsc.edu/as FPKM units. Overall, 11 pediatric brain tumor types, namely, anaplastic astrocytoma (AA), astrocytoma (AS), atypical teratoid rhabdoid tumor (ATRT), choroid plexus papilloma (CPP), craniopharyngioma (CPG), diffuse intrinsic pontine glioma (DIPG), ependymoma (EPN), ganglioglioma (GG), medulloblastoma (MB), oligodendroglioma (OG), and primitive neuroectodermal tumor (PNET), were used in this study. In total, 679 pediatric samples were included for further analysis.
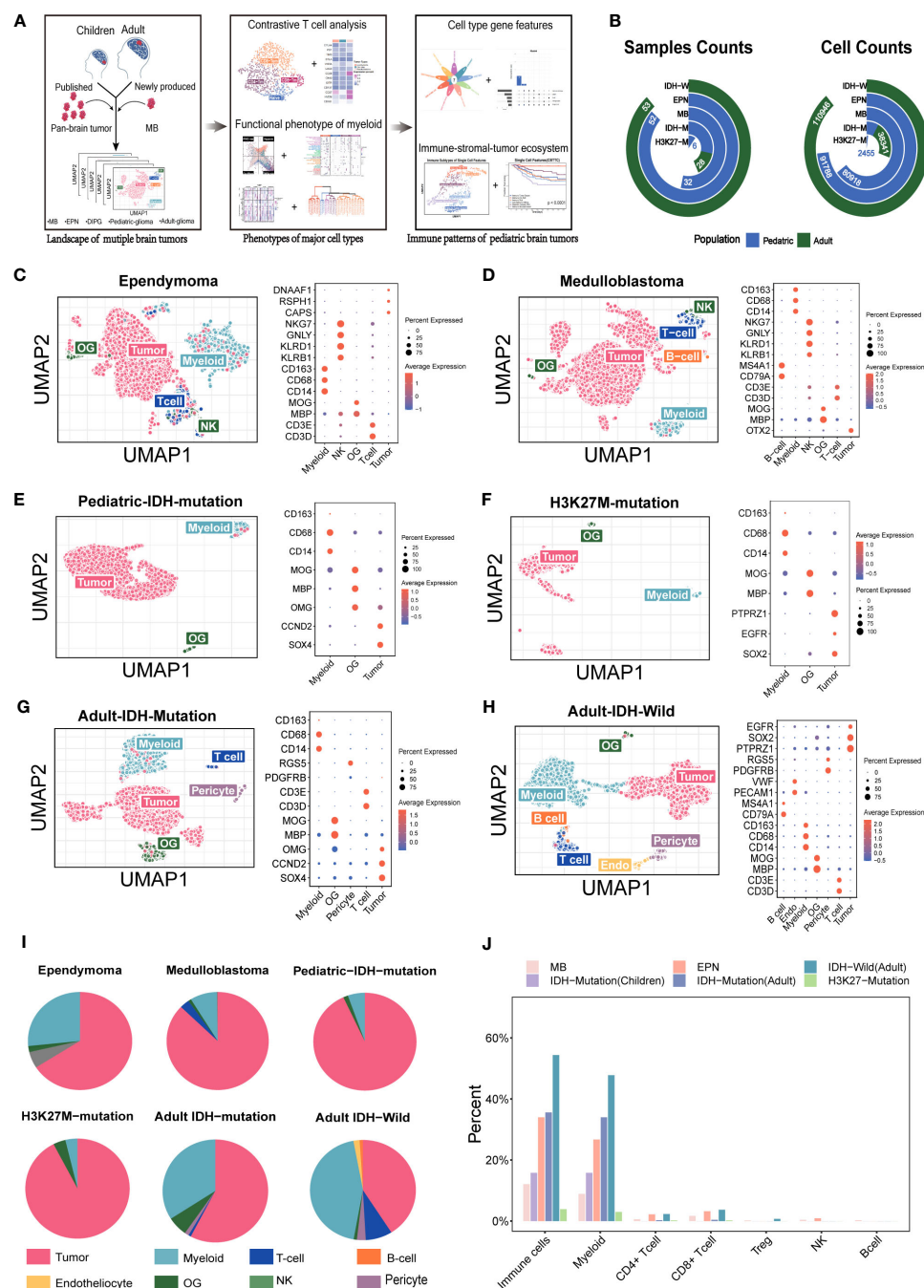
FIGURE 1

Overview of the single cells from the major pediatric brain tumors and adult gliomas. **(A)** Summary of the workflow used to analyze the immune components and functional phenotypes of myeloid and T cells, construct gene features, and identify the immune. **(B)** The included sample numbers and cell counts. **(C−H)** (Ependymoma, medulloblastoma, pediatric IDH-mutation glioma, H3K27M-mutation glioma, adult IDH-wild glioma, adult IDH-mutation glioma) Uniform Manifold Approximation and Projection (UMAP) plot of the analyzed single cells and dot plot of marker genes for each cell type. Each color represents one cell type. **(I)** Pie chart showing the relative size of each cell type. **(J)** The comparison of immune components among the major pediatric brain tumors and adult gliomas.

2.4.2 Independent external cohort of pediatric brain tumors from GEO

We collected 44 public datasets using Affymetrix protocol (U133 Plus 2.0 Array) from the GEO (total samples number = 2,331). The adult patients were excluded. CEL files were processed using the gcRMA package and log2 transformation for consistent normalization. The criteria of quality control were set as low correlation (<0.8) and similarity (outlier distribution *via* k-means analysis) with each tumor type. Finally, out of 2,331 samples, 1,245 were retained for further analysis. The batch effect was removed with the preservation of tumor characters using the combat function of the sva package.

2.5 Purified cell type compendium including immune, stromal, and tumor cell lines

We collected 76 RNA-seq gene expression datasets (1911 samples) based on the GPL570 platform from GEO to create a cell compendium, including sorted T cells, B cells, NK cells, granulocytes, endotheliocytes, oligodendrocytes, pericytes, medulloblastoma cells, glioma cells, and ependymoma cells. CEL files were downloaded and processed using the gcRMA package and log2 transformation for consistent normalization.

2.6 Discrimination of MG and BMDM in 10× datasets based on machine-learning method

Due to the low expression rates of classical MG and BMDM in 10× datasets, a pipeline based on random forest was constructed. Previous studies reported that MG and BMDM in the gliomas and brain metastases always increased the other core gene set signals but still maintained their cell type specificity. Therefore, we hypothesized that some stable core genes maintaining the specificity of MG and BMDM might exist across different brain tumors and could be detected by different platforms. Then, we constructed a machine-learning pipeline based on random forest to discriminate the MG and MBDM in MB (Figure 3A). For EPN, the IDH wild glioma which had paired 10× and Smart-seq2 data, the Smart-seq2 datasets were used to identify the MG and BMDM through the Seurat pipeline with the classical markers. First, the cells of IDH wild glioma and ependymoma from Smart-seq2 were clustered *via* the Seurat pipeline. The resolution parameters were set at 0.3 and were defined as MGs and BMDMs according to their respective markers (Figures S3A-C). Then, the classifications based on the random forest of IDH wild and ependymoma were conducted, and their ability of discriminating the MG and BMDM in the smart-seq datasets were validated (Figures S3B, C). Then, the classifications were applied to the pared 10× data of EPN and IDH-wild gliomas. After that, the classifications based on the annotated Smart-seq2 datasets were constructed using the randomForest function from the randomForest package with default parameters. The classifications were evaluated with the cmdscale functions. Then, the classifications were used to predict the cell types in the 10x Genomics datasets of corresponding tumor types (EPN the IDH wild glioma).

The differential expression genes (DEGs) between MG and BMDM of EPN the IDH wild glioma were analyzed respectively with the FindMarker function (logFC >0.25, adjust p value <0.01). Moreover, the intersection of DEGs was regarded as the conserved DEGs of MG and BMDM fit on the 10x Genomics platform. The Seurat object of MB and IDH-mutation glioma based on the 10x Genomics platform, only containing the conserved DEGs, was

conducted and analyzed with the Seurat pipeline. All the conserved DEGs were used as HVGs when the PCA was performed. The resolution parameters were set at 0.2.

2.7 Identification of immunophenotypes of myeloid cells in different tumor types

2.7.1 Clustering myeloid cells

To reduce the noises from different platforms and studies, a five-step procedure was applied (22). First, after extracting myeloid and clustering with default parameters, respectively, the aov package was used to perform the analysis of variance (ANOVA) and obtain the F values of every gene. The percentile ranks of F values was calculated. Second, genes were ordered ascendingly by the median of percentile ranks across different datasets. Third, excluding the ribosome genes, cell-cycle genes, and heat shock protein genes, the top 2000 genes detected in over half of datasets were identified as informative genes. Fourth, in order to comprehensively analyze the myeloid subsets of the major brain tumors, we integrated two independent datasets by Seurat for each tumor type (MB, EPN, P-DH-M glioma, and adult IDH mutation glioma) to obtain a larger cell number (16, 17) (Figures S4A-E). Due to the large samples of adult IDH wild gliomas a recent study provided, we just selected the primary samples for the analysis of the myeloid subset (23). We integrated the myeloid compartments by the PrepSCTIntegration function from the Seurat package to obtain a large cell number in these "cold" tumors. The parameters of k.weigh and k.filter were set according to the cell counts. Fifth, the informative genes were used as HVGs when the PCA was performed and the resolution parameter was set from 0.1 to 2 to obtain the different cluster numbers. The Davies–Bouldin index (DBI) was to determine the best number of clusters.

2.7.2 Functional annotation of myeloid cells with marker genes and pathways

For the purpose of functional comparison of myeloid subsets among different brain tumors, we use the marker genes and most affected pathways to define their functional phenotypes. Marker genes combined with most affected pathways were used to comprehensively annotate the myeloid cells from different tumor types. First, the FindAllMarkers function from the Seurat package was used to find out the marker genes, and the gene ontology (GO) analysis was performed with the clusterProfile package (version: 4.2.2) based on marker genes to determine the affected pathways (24). In addition, the gsva function from the GSVA package (Version:1.42.0) was performed on the expression data to obtain the matrix of cells and pathways (25). Then, the differential pathways of each clusters were analyzed with the limma package (3.50.3) (logFC >0, adjust p value <0.05) (26). Then, the intersected pathways of GO analysis and differential pathways from GSVA were ranked according to the enrichment
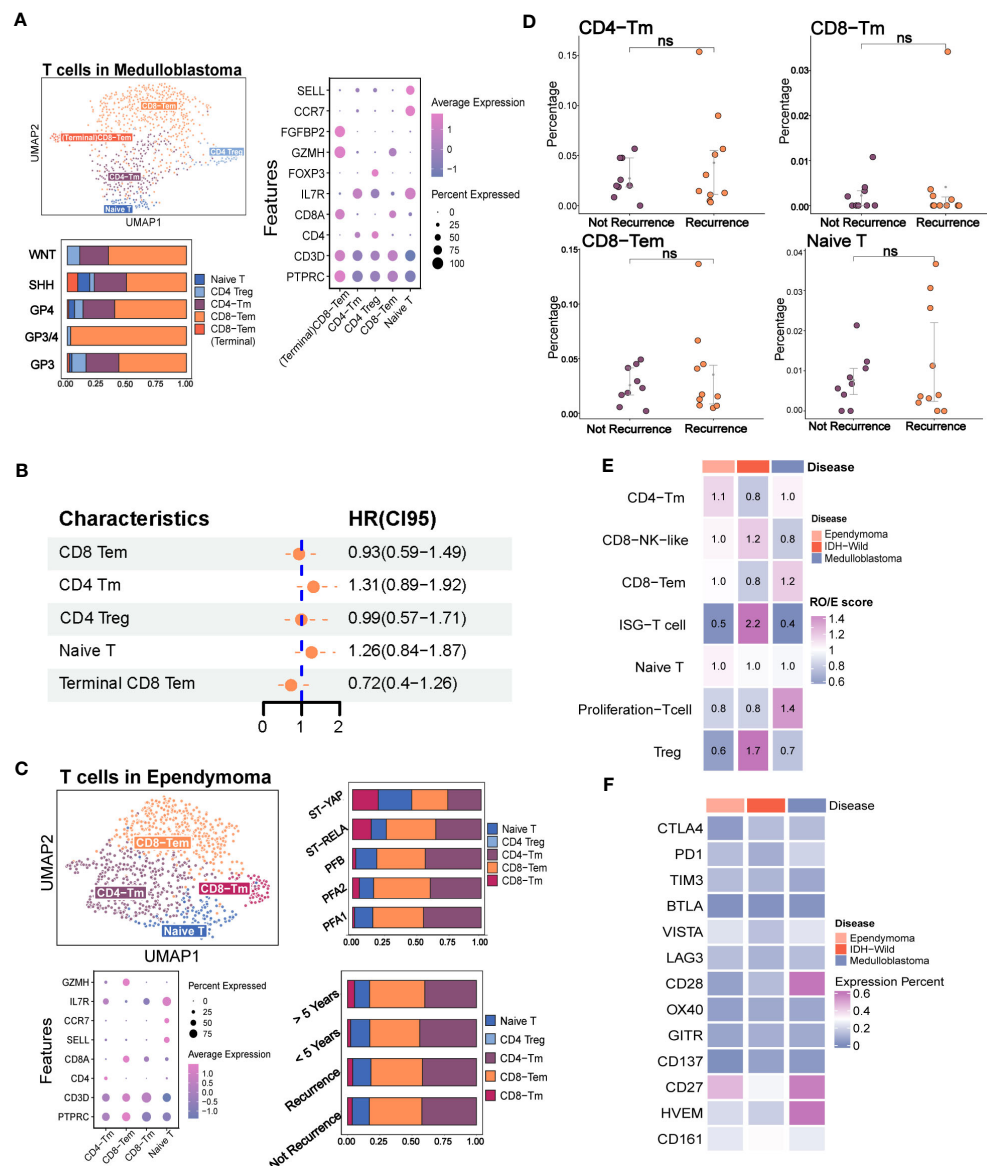
FIGURE 2

The immune phenotypes of T cells in the major pediatric brain tumors. **(A)** The evaluation of T-cell subpopulation in medulloblastoma including the UMAP plot of the identified T-cell subsets, dot plot of marker genes for each cell type, histogram for the relative size of each subset among different molecular subtypes, and Kaplan–Meier plot for terminal CD8 effector memory T cells. **(B)** Forest plot shows none of the T-cell subpopulations are independent factors of prognosis. **(C)** Evaluation of the T-cell subpopulation in ependymoma including the UMAP plot of the analyzed single cells, dot plot of marker genes for each cell type and histogram for the relative size of each subset among different molecular subtypes and prognosis groups. **(D)** Point plot shows that none of the T-cell subpopulations have significant changes between recurrence and non-recurrence groups. **(E)** Heatmap reveals the tissue prevalence of each T-cell subpopulation by Ro/e score. **(F)** Heatmap shows the expression percentage of immune checkpoint molecules in T cells of ependymoma, medulloblastoma, and adult IDH wild gliomas. The "ns" represents "not significant".

score and the marker genes in the top intersected pathway were ranked by logFC. The intersected pathway with maximal enrichment score and containing top10 marker genes was determined as the marker pathway. The corresponding marker genes with the maximal logFC were used as the marker genes. A bubble plot was made to compare the median −log10 of q value and median gene counts of specific pathway in different clusters. A heat map was to compare the mean of z-score-transformed expression value of the marker genes determined in this study and those previously reported.

2.8 Similarity analysis of clusters from different tumor types

The integrated gene expression matrices were z-score-transformed averaged per cluster. Thus, the original gene by cell expression matrix was converted to the gene by cluster expression matrix. Matrices of EPN, MB, pediatric IDH mutation, adult IDH wild, and adult IDH mutation were combined by column, and only genes present in all datasets were retained. The combined matrix was used for hierarchical clustering with the hclust function, and

the dendrograms were created by as.ggdend from the dendextend package (27).

2.9 Construction of gene features (scFes) describing TME properties

In order to obtain the gene features of classical cell types that could be applied to different tumor types and different platforms, a five-step procedure was applied. First, the common adult and pediatric tumor types including adult IDH-W and adult IDH-M gliomas, EPN, MB, DIPG, and P-IDH-M were incorporated in, and most tumor types contained two types of datasets based on 10x Genomics and Smart-seq2 platforms. Second, the gene features of specific cell type were identified per dataset using the FindMarkers function. The threshold values were determined according to the cell types. The rigorous parameters were chosen for the common cell types, such as myeloid cells, T cells, CD4, CD8, B cells, NK cells, oligodendroglia cells, endothelial cells, and pericytes (adjust p value <10e-20, min.pct >0.3, and logFC >1 for Smart-seq2; adjust p value <10e-10, min.pct>0.1, and logFC >0.25 for 10x Genomics). The relatively loose threshold values were chosen for the subpopulations of major cell types, such as MG, BMDM, naïve T cells, CD4 memory cells, CD8 memory cells, and CD8 effector cells (adjust p value <10e-10, min.pct >0.3, and logFC>1 for Smart-seq2; adjust p value <10e-10, min.pct >0.1, and logFC >0.25 for 10x Genomics). Third, the intersected gene features of every cell type from each dataset were obtained. The gene features of cytotoxic CD8 T cells were chosen from the genes existed in three quarters of datasets containing this cell type. Due to the heterogeneity of tumor components in different tumor types, genes meeting the threshold values of common cell types in more than one tumor types were selected as the conserved tumor features.

2.10 Construction of gene features of immune-stromal patterns

In order to extend the immune-stromal-tumor patterns in the external dataset (GEO), the gene signatures were generated by DEG analysis between the specific archetype and each of the other 11 archetypes, using limma and Voom (p value <0.05, logFC >1)(15). The intersection between the top 3,000 genes by logFC of each of 11 DEGs per archetype was assigned as an initial gene features. If the initial gene features had more than 20 genes, coefficients of variation (CV) were calculated and the top 20 genes with the lowest CV and detected in at least 80% of cells of corresponding archetype were defined as the archetype gene features. If the initial gene features were less than 20 genes, the initial gene features were defined as archetype gene features.

2.11 Multiplex immunohistochemistry

For multiplex immunohistochemistry (mIHC) staining (CD11b, HLA-DQA1, and CD1E for cluster 2 in medulloblastoma, and CD11b,

CD3, and MAG for immune patterns), co-staining of the selected markers was performed using a Four-Color Fluorescence Kit (Recordbio Biological Technology, Shanghai, China) based on the tyramide signal amplification (TSA) technology according to the manufacturer's instruction. All the slides were scanned using a Pannoramic P-MIDI (3DHISTECH, Hungary). The positive cell numbers were calculated by HALO 3.3 software (Indica Labs, USA).

3 Results

3.1 Low immune infiltration of pediatric brain tumors

To dissect the tumor ecosystems in children, in addition to the accessible public data, we collected five medulloblastoma specimens from four patients for snRNA-seq based on 10x Genomics. The predominant functional phenotypes of T cell and myeloid subsets and immune-stomal-tumor patterns in children were investigated (Figure 1A). In total, more than 0.3 million cells from 171 samples covering adult gliomas and four major pediatric brain tumor types were included (Figure 1B).

To analyze the TME components of each tumor type, we evaluated the major current methods identifying known cell types, namely, clustering-based (CB) method and positive expression of marker genes (PEMG) method. We found that the CB method performed better overall (Figure S1). For the datasets based on 10x Genomics or Smart-Seq2, the CB method was able to identify more cells than the PEMG method in most tumor types, which was important for the "cold" tumor types. Our data indicated that the "cold" tumor types like MB and EPN also contained the major classical immune cells, such as T cells (PTPRC, CD3D), B cells (CD79A, IGHG1, MZB1), and NK cells (KLRB1) (Figures 1C–H). In addition, the immune components varied significantly among the different brain tumors (Figure 1I) and were lower in the pediatric brain tumors (MB, EPN, and pediatric IDH-M) than those in the adult brain tumors (IDH-W and adult IDH-M) (Figure 1J). Similar with the previous studies, myeloid cells were predominant among all the immune cells in brain tumors, and MB and EPN held a relatively higher rate of CD8 T cells among all the tumor types (6). However, the functional phenotypes of them in pediatric brain tumors are still unknown.

3.2 Targeting the T cells may not be the optimal strategy for MB and EPN

According to the previous studies on various types of tumors, certain subsets of T cells, including effector T cells, memory T cells, and exhausted T cells, have been found to have specific functions in either eliminating or tolerating tumor cells within the tumor microenvironments (22, 28, 29). Due to the extremely low contents of T cells in IDH mutation glioma and H3K27 mutation glioma, we focused on the characteristics of T cells in the MB, EPN, and adult IDH wild glioma (Figures 2A, B, S2D). In order to explore the phenotypes of T cells in MB and EPN, we defined the

subpopulations of T cells according to the known markers identified in a recent study of T-cell atlas. The results revealed that T cells in MB mainly consisted of CD8 effector memory T cells (CD8 Tem, GZMH), CD8 terminal effector memory T cells (terminal CD8 Tem, FGFBP2), CD4 memory T cells (CD4 Tm, IL7R), regulatory T cells (Treg, FOXP3), and naive T cells (Tn, CCR7, and SELL) (Figures 2A, S1A) (22). Different molecular subtypes of MB held a heterogeneous composition of T-cell subpopulations (Figure 2A). Moreover, CD8 Tem formed the majority of T cells in all of the subtypes (Figure 2A). We also found that the higher scores of CD8 Tem markers were associated with a survival advantage in MB, whereas an opposite effect was observed in CD4 Tm and Tn (Figure S2B). However, the univariate Cox analysis revealed that the T-cell subpopulations did not significantly correlate with prognosis (Figure 2B). Considering that Kaplan–Meier (KM) analysis is a non-parametric method and Cox regression is a semiparametric method that takes multiple factors into account, the results of Cox analysis may indeed be considered to have higher credibility (30). In

EPN, T cells mainly consisted of CD8 Tem, CD8 Tm, CD4 Tm, and Tn. The subpopulations of T cells were evenly distributed in different molecular subtypes (Figures 2C, S2C). Moreover, both the group with a follow-up period of over and less than 5 years, as well as the recurrence and non-recurrence groups, exhibited similar percentages of T-cell subtypes (Figure 2C). There was also no significant difference in the percentages of four subpopulations between the recurrence and not recurrence groups (Figure 2D).

We next quantified the tissue enrichment of T-cell subsets among the different tumor types by integrating the different T-cell data from different datasets (Figures S2E-G). The IFIT3+ T cells and Treg identified within the three tumor types were preferentially enriched in adult IDH-W gliomas (Figure S2H). The Ro/e analysis also demonstrated the preferences (Figure 2E). Based on the comparison of expression percentage of immune checkpoints, we observed that classical molecules like PD1, CTLA4, TIM3, and LAG3 and newly reported molecules like CD161 were extremely low in these brain tumors, which might partly explain the difficulty
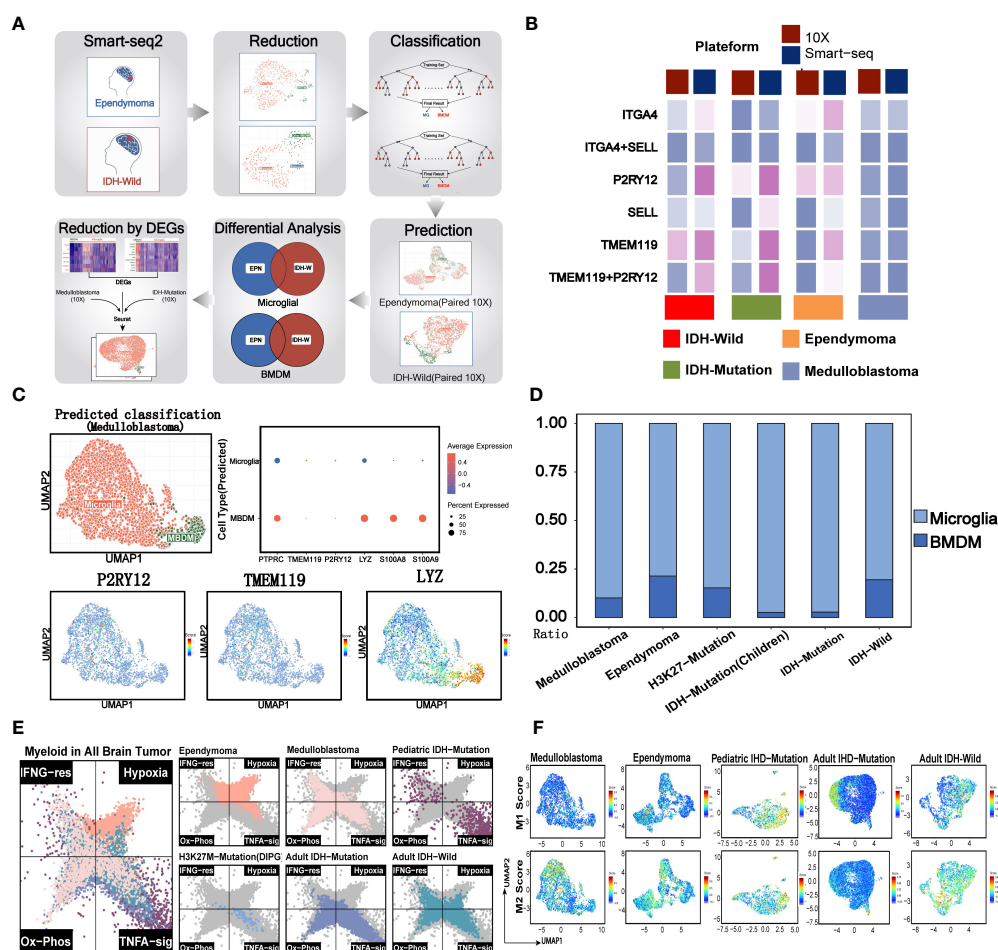
FIGURE 3

Evaluation of traditional immune phenotypes of myeloid cells in pediatric and adult brain tumors. **(A)** Summary of the workflow used to discriminate the microglial and BMDM in the 10x data. **(B)** The comparison of 10x and Smart-Seq2 platforms across the different brain tumors. **(C)** Evaluation of MG and BMDM in 10x data of medulloblastoma. The UMAP plot displays the consistency between the predicted MG and BMDM and the clusters. The dot plot shows the expression of classical markers in the MG and BMDM. UMAP plots of marker genes show the expression of classical markers in the cells. **(D)** The relative size of MG and BMDM across the different brain tumors. **(E)** Two-dimensional butterfly plot visualization of classical tumor-related pathway scores in pediatric and adult brain tumors. Colors represent different tumors. **(F)** The M1 and M2 scores of the different clusters across the different brain tumors.

for their clinical transformation in brain tumors (Figure 2F) (31). Overall, the low contents of T cells and low expression rates of immune checkpoints indicated that the traditional immunotherapy strategies targeting the local T cells in the tumor microenvironment, such as immune checkpoint blockade, may not be the optimal treatment strategy for pediatric MB and EPN.

3.3 Assessment of known functional phenotypes of myeloid cells

Tumor-associated macrophages (TAM) were regarded as a potential target in the future immunotherapy. We next accessed the characteristics of known phenotypes of myeloid cells, such as MG, BMDM, M1, and M2, in the major pediatric brain tumors. The previous studies reported that the MG and BMDM in brain tumors showed distinct transcriptomic profiles and inflammatory polarization tendency, which are additionally influenced by the underlying disease type (4). However, it was apparent from Figure 3B that the expression percentages of classical MG and BMDM markers (P2RY12 and TMEM119 for MG, and ITGA4 and SELL for BMDM) from the 10x platform were significantly lower when compared with those from the Smart-Seq2 technique (4, 9, 23). The results revealed that identified MGs and BMDMs were largely consistent with clusters obtained from the Seurat pipeline, indicating that the internal characteristics of MG and BMDM were basically preserved across different conditions (Figures S3A–C). When evaluating the classical markers in MG and BMDM, predominance in the expression levels and percentages of markers remained in the corresponding cell types (Figures S3D, E). Similarly, they were also highly consistent with the cluster results of Seurat (Figures 3C, S3F). The results showed that the ratio of MG and BMDM varied among brain tumors, and MG comprised the vast majority of myeloid cells (4), especially for the pediatric and adult IDH mutation gliomas (Figure 3D). However, the rough classification of MG and BMDM still lacks guidance for the functional phenotypes.

Previous studies reported that myeloid subsets on glioblastoma (GBM) were significantly enriched in classical inflammatory signals and metabolic pathways (4, 9, 23). The butterfly plot revealed a significant enrichment of hypoxia in myeloid cells of ependymoma, when compared with other brain tumors (Figure 3E). Similar with the myeloid cells of adult brain tumors, myeloid cells of medulloblastoma were significantly enriched in oxidative phosphorylation and TNFα pathways while deficient in hypoxia signals. Classical inflammatory hallmarks (IFNα response and TNFα-signaling) were enriched in myeloid cells of pediatric IDH mutation gliomas, indicating the anti-tumorigenic phenotypes of these cells in the microenvironment.

Then, we investigated the M1 and M2 signature scores in the clusters of all the tumor types (Figure S3G). We found the co-expression of both M1 and M2 gene signatures in most of myeloid subsets from EPN, pediatric IDH-M glioma, and IDH-W glioma. Additionally, certain clusters exhibited both lower M1 and M2 gene feature scores, suggesting that the categorization of M1 and M2 may not be entirely applicable for the classification of myeloid brain

tumors (Figure 3F) (23, 32). Therefore, this defective classification of myeloid cells in brain tumors suggested that it was significant to further uncover the function in a specific tumor microenvironment.

3.4 Comparative analysis of functional states of myeloid subsets from pediatric and adult brain tumors

In order to comprehensively analyze the myeloid subsets of the major brain tumors, we integrated two independent datasets. The results revealed that the batch effects were removed (Figures S4A–E). The best number of clusters was evaluated by DBI (Figure S4F). The results showed that the myeloid cells in EPN were the most heterogeneous because of the largest cluster numbers (Figure S4A). Except for the pediatric IDH mutation gliomas which had no significant pathways via ssGSEA, the marker pathways of each myeloid cluster across the pediatric and adult brain tumors uncovered the common perturbation of functional modules, such as leukocyte activation and interferon response, and exclusive pathway perturbation in brain tumors, such as pathways related to cilium organization and endocytosis in ependymoma (Figure 4A). Then, we investigated marker genes in different clusters to find out the myeloid clusters with similar expression levels of marker genes but defined as different myeloid subsets (Figure 4B). For example, similar expression levels of NDRG1, LDHA, MHCII molecules, interferon genes, GPM6A, C9, and SRGAP2 were discovered in different myeloid subpopulations, indicating the similar functional states in different brain tumors. The previously reported markers were also compared among different tumor types, for example, the homeostasis myeloid subpopulation with high expression levels of P2RY12 and CX3CR1 in gliomas and cluster 2 marked with the pathway of "GTPase signal transduction" in ependymoma (9), the activated microglial subsets highly expressing CD83 and TNF in GBM, and the clusters6 marked with pathways of "positive cytokine production" in ependymoma (23) (Figure 4C).

To quantify their similarities, we calculated the correlations between the average transcriptome of each cluster in different tumor types. As expected, the same major lineages from different cancer types, such as cycling, monocyte-like, hypoxia-related, cytokine-stimulated, and interferon-related subpopulations, were clustered together, further demonstrating the shared myeloid lineages between pediatric and adult brain tumors (Figures 5A). Then, we used the angiogenic and phagocytic signatures, a dichotomous functional phenotype, to access the functional phenotypes of each cluster across the different tumor types (33). As expected, some clusters exhibited significantly preferential signature scores. However, most clusters in pediatric brain tumors had a similar score in the two phenotype signatures (Figure S5A). Using the public clinical data, we investigated the relationship of the different myeloid lineages with patient prognosis. The clusters highly expressing HLA genes were negatively associated with prognosis in multiple tumors except for EPN (Figures 5B–D, S5C, D). Furthermore, the HLA gene-enriched cluster in MB was the independent factor of prognosis (Figure 5E) and it had better

performance than molecular subtypes and traditional histology when predicting the 5-year survival (Figure 5F). Then, we determined three markers to define this cluster (Figure S5B). By conducting subtyping analysis on medulloblastoma, it was found that this cluster exhibited significant subtyping preferences, primarily existing in the G3 and SHH subtypes (Figure 5G). The mIHC staining of tumor sections further confirmed the existence of this subset (Figure 5H).

3.5 Establishment of TME gene expression signatures

To analyze TMEs using the transcriptomic data, the gene expression signatures (scFes) of immune and stromal components were constructed via combining multiple datasets of different tumor types from 10x and Smartseq2 platforms to find out the conserved gene signatures (Methods, Figure S6A, Table S2). We compared the

scFes with the previously reported gene sets and found only small overlap among them (Figures S6B–I). To confirm the cell type-specific expression patterns of scFes, 1,891 RNA-seq profiles of sorted cell subpopulations across multiple GEO datasets were conducted and the final scFes were highly cell type specific and showed effective segregation, with high expression scores for cell types associated with each signature (Figures 6A, B). In addition, we evaluated scFes in the averaged expression data of cell line (34) and found that scFes performed better when marking CD8 T cells and Treg (Figures S6J, K). Furthermore, we conducted validation and comparison of scFes with published counterparts in independent scRNA datasets of various tumor types at the single-cell level. Our analysis revealed that scFes effectively identified cell types annotated by classical markers and outperformed gene features of certain cell types from GSEA (35), xCell (36), and recently published studies (15) (Figures 6C, D, S7A, B).

Considering the important roles of tumor cells and the unique role of OG in the cell networks of the brain TME depicted by the
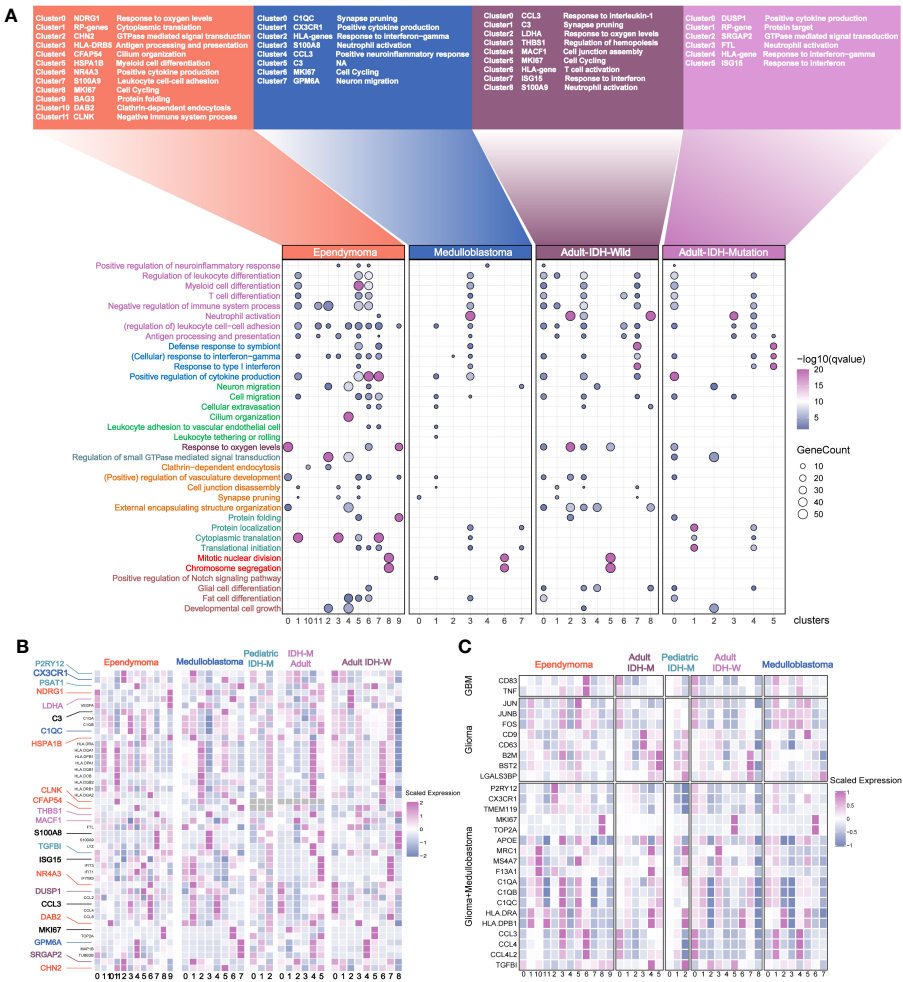
FIGURE 4

Annotation of the myeloid subsets from the major pediatric and adult brain tumors. **(A)** The names of the different clusters. The most affected terms in each cluster are represented in a dot plot, with the size of the dot corresponding to the number of genes per term and the color of the dots corresponding to the q value of enrichment after −log10 transformation. **(B)** The selected genes with different colors are used as the marker genes. Color-coding is consistent with the tumor types. **(C)** The previously reported marker genes of myeloid subpopulations in the different clusters across the different brain tumors.
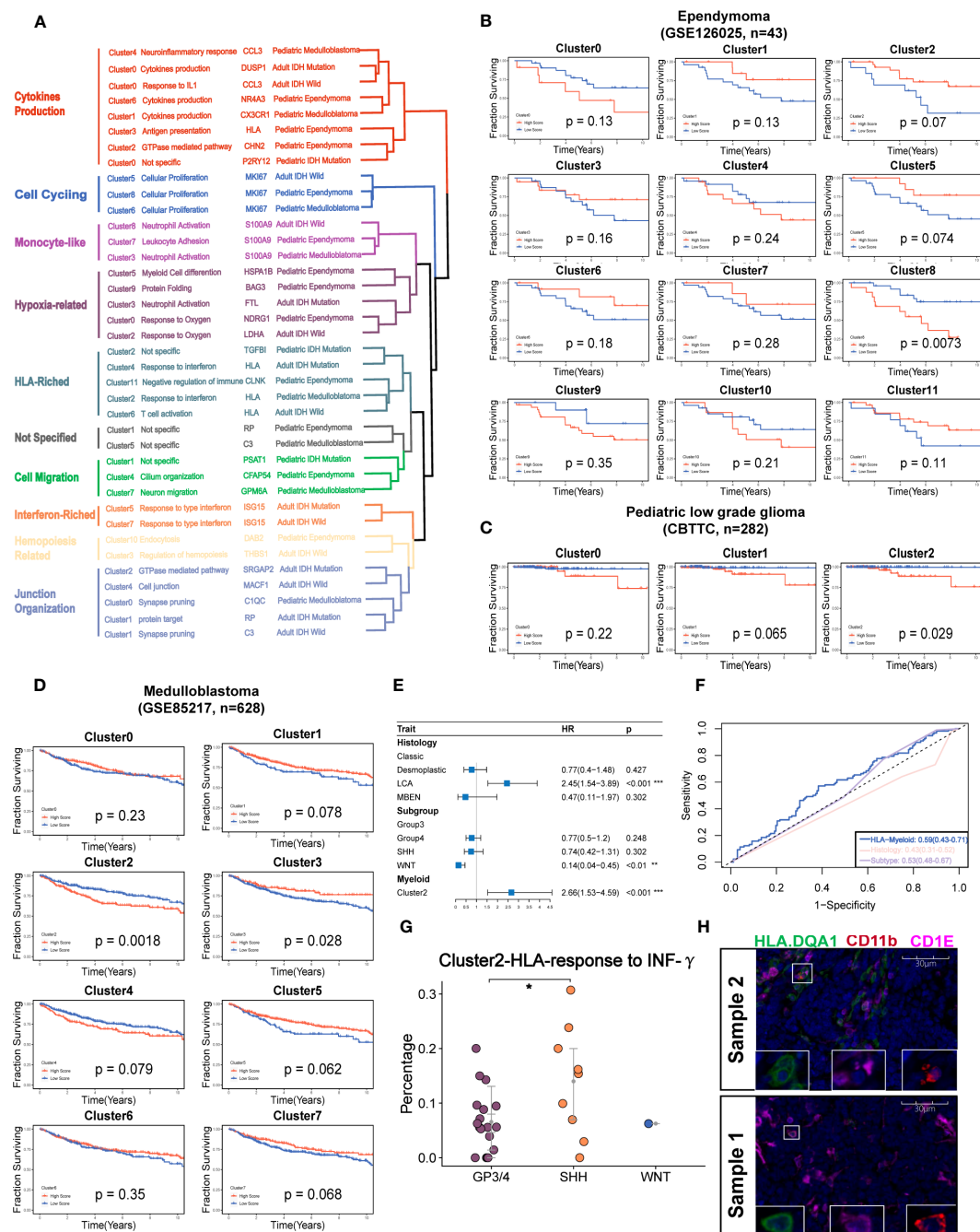
FIGURE 5

Identification of the potential targeted myeloid subsets. **(A)** Hierarchical clustering shows the similarity of clusters across the different brain tumors. **(B)** Kaplan−Meier survival curves generated with each cluster signature score of EPN using GSE126025. **(C)**. v. **(D)**. Kaplan−Meier survival curves generated with each cluster signature score of the medulloblastoma using GSE85217. **(E)** The forest plot reveals that the cluster 2 of medulloblastoma is the independent factor of prognosis. **(F)** The ROC curve shows a higher AUC value of cluster 2 of medulloblastoma than classical histology and molecular subtypes. **(G)** The percent of Cluster2 in medulloblastoma was significantly higher in SHH subgroup. **(H)** The mIHC demonstrates the existence of cluster 2 in the two samples of MB.The "*" represents "P value < 0.05".

single-cell datasets, the gene signatures of tumor components correlated with the recruitment of immune cells (named as "positive immune recruitment" (positive-IR) and "negative immune recruitment" (negative-IR) which were positively and negatively correlated with the expression level of CD45, respectively) and OG were also explored to create a holistic approach describing the TME of brain tumors. We accessed the two tumor features in a newly produced dataset of medulloblastoma, which was a kind of well-known "cold" tumor, and found that they were predominantly existed in the specific

tumor clusters, and the negative-IR score was significantly higher, indicating the tumor components might contribute to the deficiency of immune components in medulloblastoma (Figures 6D, E, S8A).

Furthermore, we accessed the two tumor features and OG features in two independent bulk RNA datasets of pan-cancer (Figures 6F–H). The results revealed that the positive-IR score was significantly higher in the tumor group and might be associated with better prognosis (Figures 6F, S8B) whereas the negative-IR score was significantly lower in the tumor group (Figure 6G), according to the fact of the activated immune system in brain tumors compared with immune-privileged normal brain (Figure 6H). OG scores were significantly associated with prognosis (Figure S8D), but whether this correlation was influenced by clinical parameters such as WHO classification, metastasis state, and the history of radiotherapy and chemotherapy still required data with more comprehensive clinical information. In addition, the relatively higher positive-IR score in EPM, MB, and pediatric IDH-mutation gliomas might partially account for the lower immune content when compared with adult brain tumors (Figures 1J, 6I). Moreover, the paradox between the higher positive-IR and lowest immune content in DIPG, and some exceptions of the correlations between immune recruitment feature scores and immune cell feature scores, indicated the existence of other factors affecting the immune recruitment in addition to the tumor cells (Figures 6I–J). The OG feature score was higher in the normal brain, suggesting that the developmental program promoting the formation of mature oligodendrocytes was blocked in tumors (37, 38). Furthermore, the higher OG feature score was associated with better prognosis (Figure 6H). However, the tumor-related features and this exclusive stromal component of CNS were always ignored in the current studies of the TME and deserved further study.

3.6 Coarse classification of immune patterns in pediatric brain tumors

A recent study identified 12 immune archetypes across multiple cancers types but only including one pediatric brain tumor type (15). A holistic survey of the immune archetypes in pediatric brain tumors is still lacking. As expected, the cell types varied among the different tumor types (Figure 7A). We next explored the primary archetypes by following the same pipeline but including the unique stromal component—the OG feature. The three markers (ITGAM for myeloid, CD3 for T cell, and MAG for OG) were used for primary classification, and the DBI was used to determine the optimal cluster number. The primary classification contained eight clusters (Figures 7B, S9A, Table S3), including the six previously reported immune archetypes and two new small clusters (named myeloid stromal centric and T-cell stromal centric archetypes). The expression level of the three markers varied significantly among the eight clusters (Figures S9B–D). The immune archetypes were highly tumor specific (Figure 7C) and significantly associated with prognosis (Figure 7D).

Based on this, we next investigated the characteristics of tumor biology among the eight clusters. The immune stromal-rich and

immune-rich clusters were characterized by the elevated expression scores of antitumor cytokines, M1, MHC molecules, and costimulatory molecules, demonstrating an immune-active TME compared with the immune stromal desert and immune desert clusters. However, the coexistence of the highest score of protumor factors, such as protumor cytokines, M2, and checkpoint molecules, indicated the reprogramming of the immune microenvironment in these two clusters (Figure 7E). The transcriptomic programs of interferon-stimulated genes (ISGs) and immune escape and chemokines also demonstrated the lasting but exhausted tumor immunology in them (Figures S9E, F). Conversely, the enrichment with transcriptomic programs of the cell cycle in the immune stromal desert and immune desert clusters was consistent with the increased capacity of tumor proliferation (Figures S9F, 7E). In addition, the GSEA and PROGENy analysis also revealed the differential enrichment of tumor-related pathways among the eight clusters (Figures S9G, 7F). The increased PI3K pathway activation in the immune desert cluster calculated with PROGENy analysis suggested the potential targeted therapy for this subset (Figure 7F). The differential sensitivity to the vinblastine and cisplatin, which were used as the traditional chemotherapy, might provide the possibility to the individualized treatment (Figures 7G, H) (39). Finally, we further confirmed the eight clusters via mIHC assays in the tumor tissues including five MBs, three EPNs, five CPGs, two CPPs, five ASs, three DIPGs, and two GGs (Figure 7I).

3.7 Immune archetypes based on 9-features

Unlike in the non-CNS tumor types, no CD4-biased or CD8-biased tumors existed in the pediatric brain tumors when analyzed with gene sets from scFes and Combes et al. (Figures S10A, B). Considering the fact that coarse classification of stromal components (CD44 and CD90) used in the previous study might contain malignant cells (15) and the malignant cells might negatively or positively affect the immune recruitment, the tumor-related features (positive IR and negative IR) were also included. MG is the exclusive cellular components in the brain, and their phenotypes might be highly diverse in different pathological conditions, Therefore, the BMDM and MG features were also included for further classification. Similarly, the DBI was used to determine the optimal cluster number (Figure S10C). Finally, 12 immune-stromal-tumor patterns (namely, 12 clusters) were identified with nine features (Figures 8A, S10D, Table S3). The marker genes and gene features from scFes demonstrated predominant cell types in each cluster (Figures 8B, C). Furthermore, we obtained the DEGs of 12 clusters and conducted an external cohort including 1,245 children and a similar composition of tumor type with Children's Brain Tumor Tissue Consortium (CBTTC) to validate the 12 clusters (Table S4). After removing the batch effect, the similar archetypes were validated in the external dataset (Figures S10E, F). Similar with the coarse classification based on the 9-feature, the predominant archetypes varied among the major pediatric brain tumors, and
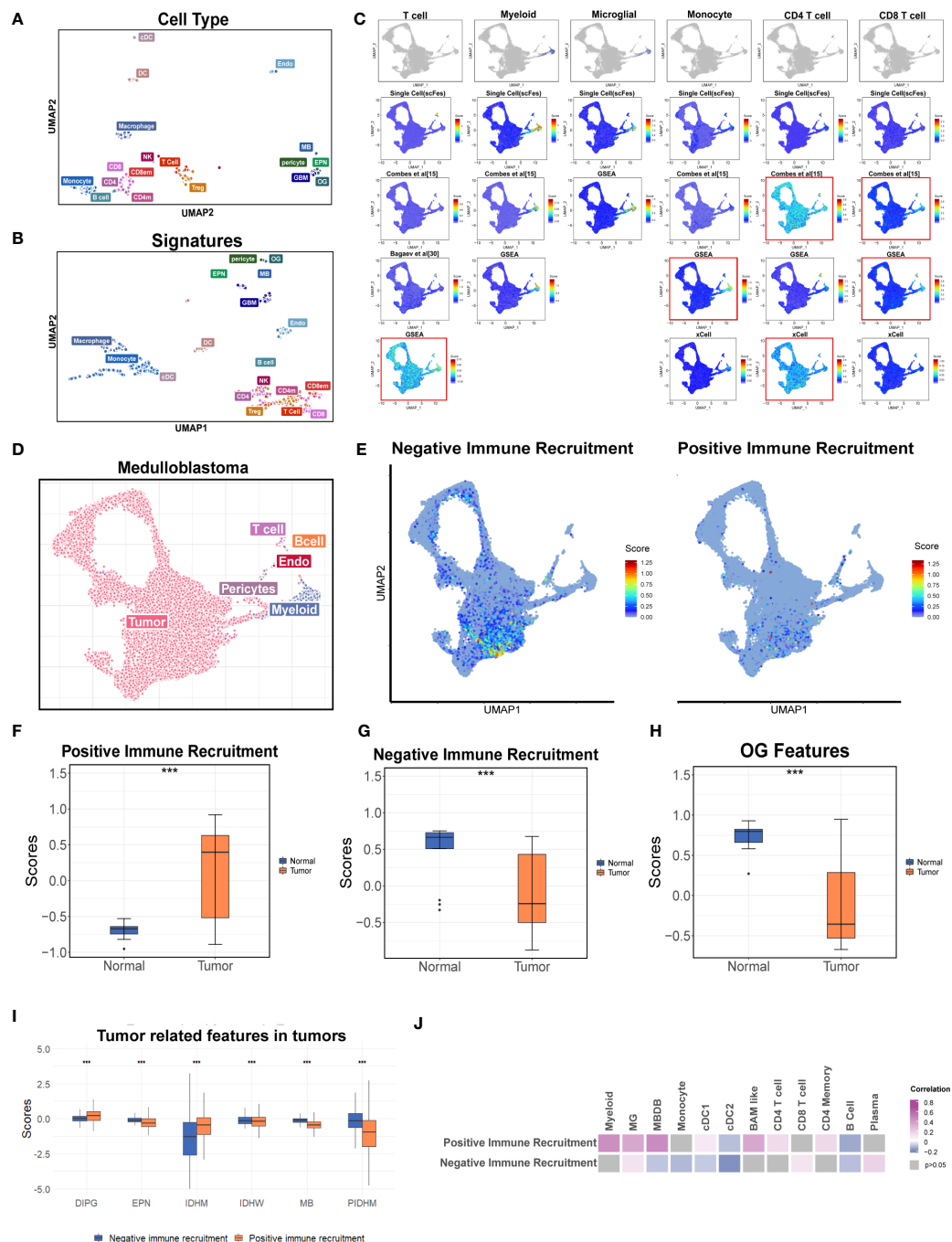
FIGURE 6

Construction the gene features of different cell types in the TME. **(A)** UMAP of the purified cell samples marked with the original cell annotation. **(B)** UMAP of purified cell samples in the space of the scFes scores. **(C)** UMAP overlays of the feature scores of major cell types in the single-cell dataset of MB (newly produced). **(D)** UMAP plot of the newly produced single cell data. Each color represents one cell type. **(E)** UMAP overlays of the tumor-related features. **(F)** Box plot shows the signature score-positive immune recruitment in GSE50161 including the medulloblastoma, ependymoma, glioblastoma multiforme, pilocytic astrocytoma, and normal brain. **(G)** Box plot shows the signature score-negative immune recruitment in GSE50161 including the medulloblastoma, ependymoma, glioblastoma multiforme, pilocytic astrocytoma, and normal brain **(H)** Box plot shows the OG signature score in GSE50161 including the medulloblastoma, ependymoma, glioblastoma multiforme, pilocytic astrocytoma, and normal brain. **(I)** Box plot shows the comparison of tumor-related signature scores across the different brain tumors. **(J)** Heatmap reveals the correlations between the tumor-related signature score and scFeg scores of different immune cell types. "***" represents the "P value <0.001".

the relative composition of archetypes by tumor types was similar in CBTTC and GEO (Figure 8D). The inconsistency of individual archetypes between the two datasets, such as IR-tumor rich in high-grade glioma and tumor recruitment BMDM bias in

ependymoma, might come from the discrepant composition of pathological or molecular subtypes. Compared with the interaction pair of some cell types in the non-CNS tumors (15), the immune component tended to synchronous change maybe
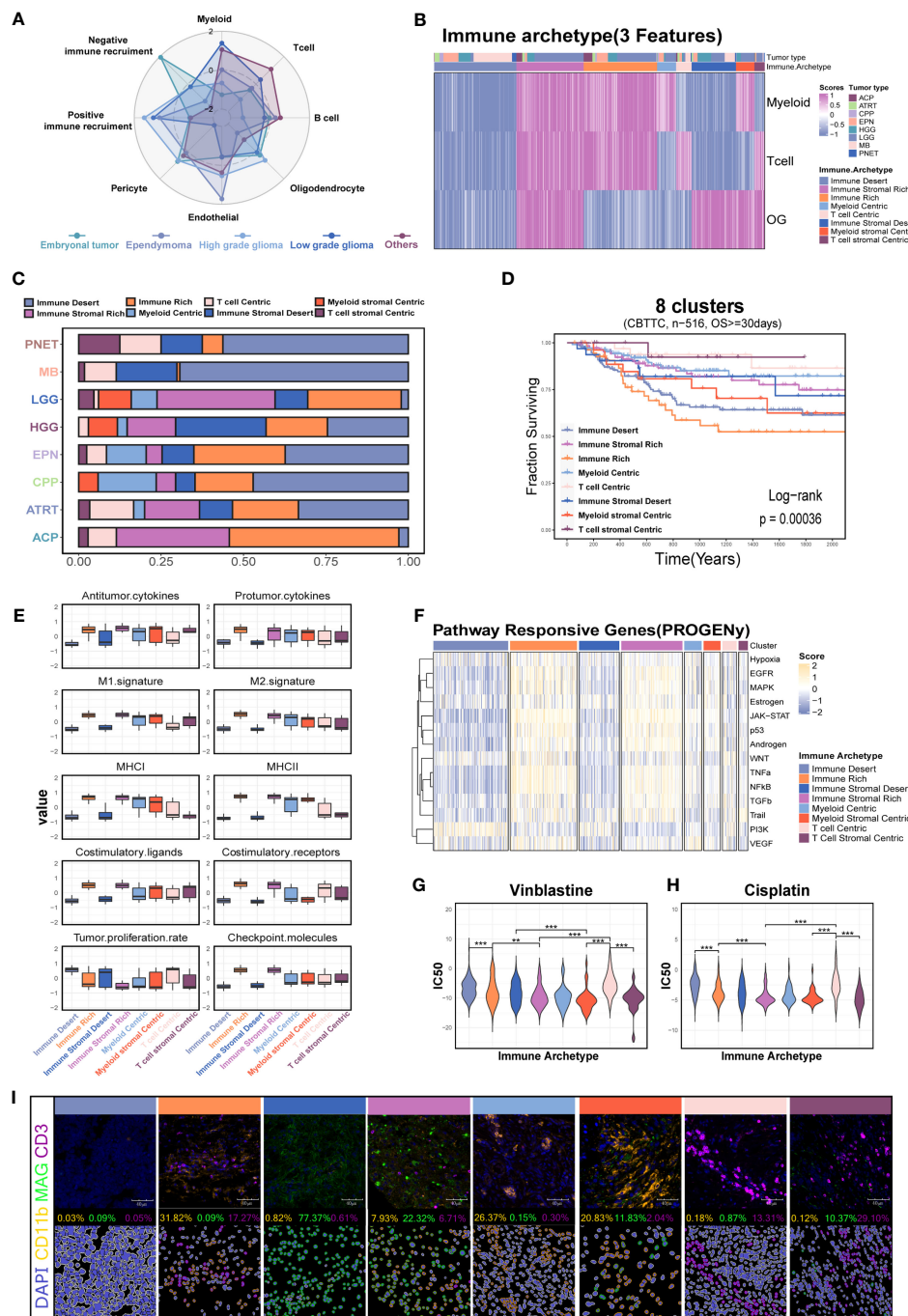
FIGURE 7

Investigation of the immune patterns based on the myeloid, T-cell, and oligodendrocyte features (3-feaure) in the CBTTC dataset. **(A)** Radar plot shows the signature score of major cell types across the major pediatric brain tumors. **(B)** The eight clusters based on the 3-feature. **(C)** Histogram for the relative size of each immune patterns among the different pediatric brain tumors. **(D)** Kaplan−Meier survival curves generated with signature scores of eight clusters (34). **(E)** Box plot shows the differences in the major immune-related processes across the eight immune patterns. **(F)** Relative signaling pathway activity scores in tumor cells measured from RNA-seq by PROGENy. **(G)** The drug sensitivity analysis of vinblastine and cisplatin among the different immune patterns. **(H)** Kaplan−Meier survival curves generated with the OG signature score using the CBTTC dataset. Box plot shows the OG signature score in GSE50161 including the medulloblastoma, ependymoma, glioblastoma multiforme, pilocytic astrocytoma, and normal brain. **(I)** mIHC demonstrated the eight immune patterns across the different brain tumors. "**" and "***" respectively represent the "P value <0.01" and "P value <0.001".

due to the unique immune recruitment mechanism (Figure 8E). Finally, we used the TIDE score to evaluate the immune response of immune archetypes. Immune-rich and immune stromal-rich clusters had a high response rate over 50% (Figure S10G), whereas

the further classification, namely, 12 clusters, obviously had better ability to discriminate the responsive and non-responsive subsets. Surprisingly, immune-rich, immune-rich tumor recruitment, and immune stromal tumor recruitment with a high TIDE score had a

high response rate over 75% and immune desert nearly did not respond to immune checkpoint inhibitors (40). Moreover, all the craniopharyngioma (CPG) might respond to PD-1 or CTLA inhibitors (Figure S10H; Figures 8F–G). Therefore, pediatric brain tumors exhibit a distinct immune ecosystem, suggesting that CPG could potentially serve as a candidate for traditional immune therapy, such as immune checkpoint inhibitors.

4 Discussion

Pediatric brain tumors are the leading cause of cancer-related deaths in children, and the prognosis of certain tumor type remains abysmal, for example, the survival time of DIPG is always measured in just months. In spite of the advances in the combination of multidisciplinary diagnosis and treatment, surgery, and systemic

FIGURE 8
Further investigation of the immune patterns (12 clusters) based on the nine features in the CBTTC dataset. **(A)** UMAP displays the 12 immune patters in the CBTTC cohorts. Each dot represents a single cluster. **(B)** The heatmap shows the mean expression levels of the marker genes of predominant cell type in each cluster using the integrated CBTTC dataset. **(C)** Box plot shows the differences in the major cell types across the different immune patterns. **(D)** Pie charts display the relative size of immune patterns in the major tumor types. Color-coding is consistent with A. **(E)** Bubble plot reveals the signature scores of multiple cell types and immune related molecules in the 12 clusters. **(F, G)** The prediction of response rates in each cluster and tumor type.

therapy, the therapy-related long-term adverse events, such as hearing loss and neurodevelopment and neurocognitive disorders, are still the troubling complications. The extensive immunotherapy using cytokines, certain immune cells (T cell, DC, NK) and immune checkpoint inhibitors (ICIs) in the non-CNS cancers spurred the interest in pediatric brain tumors to minimize long-term morbidities (41–43). In this study, we firstly presented a holistic survey of major pediatric brain tumors from the single-cell perspective, including the immune cell abundances, identification of functional phenotypes of T cells and myeloid cells, and the immune-stromal-tumor patterns. In this study, we evaluated CB and PEMG to identify known cell types. Although the expression levels of myeloid marker gene (ITGAM) in all the tumor types were relatively lower in the CB method, the enrichment scores of the mark pathway were even higher when comparing with those of the PEMG method. The PEMG method seemed to identify more OG cells probably because of the relatively rigorous criterion of OG identification in the CB method—high expression of three marker genes (MBP, MOG, PLP1)—whereas the PEMG method just identified the cells expressing single marker genes. To construct a global tumor niche atlas of different tumor types, we performed cell clustering and marker gene identification using Seurat. In our study, we primarily utilize the marker genes employed in the original research to annotate the cells in the public datasets. The identification of malignant cells is determined by the deficient expression of established stromal marker genes or marker genes associated with mature neural or OG cells within the non-immune cell population. As we know, some tumors, like medulloblastoma, have typical copy number variations; the malignant cells were mainly inferred based on overall copy number variations in the bioinformatics analysis process. Since pediatric brain tumors generally have lower copy number variations compared with adult tumors (44), and existing copy number variation algorithms developed for single-cell data, such as inferCNV (45) and copyKAT (44), may not be suitable for identifying malignant cells with low copy number variations, we did not use a copy number variation-based strategy in our study. Moreover, we included a wide range of brain tumors in our analysis. To ensure consistent analysis strategies for each tumor type and dataset, and to avoid discrepancies caused by different analysis approaches, we employed the clustering analysis combined with feature genes which demonstrated higher universality and achieved effective clustering. Our study provides an essential step towards fully understanding the TME in the major pediatric brain tumors before mechanically applying the current immunotherapy strategy on them.

Here, we revealed the distinct characteristics of the TME in the major tumor types (MB, EPN, IDH-mutation, and H3K27M-mutation) in children, which contained fewer immune cells than those in adults. Consistent with the previous study investigating the immunophenotypes of pediatric brain tumors via multicolor FACS, the EPN held higher infiltrating myeloid and T cells than MB (Figure 1J) (46). The strategy targeting the T cells has demonstrated non-persistent clinical responses in adult IDH-wild gliomas (47, 48). Although another study reported that Group 3 MB might respond better than SHH MB when applied with the PD-1 inhibitor

in murine, the extremely low contents of T cells and expression percentage of PD-1 in MB and EPN suggested that the current strategy targeting the T cells in pediatric brain tumors should be more cautious (Figures 1J, 3F) (49).

In spite of tremendous challenges of immunotherapy in pediatric brain tumors, some opportunities still exist. An unprecedented number of studies have demonstrated the myeloid lineage-associated resistance mechanisms in the resistance to therapy (50, 51). Developing the therapeutic strategies targeting myeloid subpopulations, as the dominated immune cells in the TME, is of enormous potential to complement the current immunotherapy strategies (52). For example, depleting CD73 in mice could decrease the immunosuppressive macrophage subset but increase the immunostimulatory subpopulations to enhance the anti-PD1 effectiveness (53). However, the diverse functions of myeloid cells are highly dependent on the different neuropathological conditions. Our study showed that classical cancer-related hallmarks in the myeloid of children and adult were highly heterogenous. The cytokine-enriched clusters were the shared myeloid type among the different tumors, indicating the common response to pathological conditions (Figure 5A) (9, 12, 54). Unlike those in adult brain, the myeloid subsets highly expressing interferon-related genes were not detected in children. Although we did not detect the clusters significantly highly expressing CD73, we uncovered a DC-like subpopulation highly expressing HLA genes and CD1E, which was associated with worse prognosis, and was an independent prognostic indicator of MB patient survival. This observation suggested that this myeloid subset was a potential target, but the strategy of targeting the myeloid subpopulation should be tailored according to their functional phenotypes in different tumor types.

Malignant cells are the major component of brain tumors. Parsing the relations among the immune and stromal components and tumor cells is essential to clearly understanding the feasibility of immunotherapy in pediatric brain tumors. In this study, we identified the common tumor-related features across the different tumor types which were correlated with the expression level of CD45 and found that they were significantly correlated with multiple immune cell types (Figure 6J). Interestingly, the negative immune recruitment and positive immune recruitment labeled the same tumor clusters (Figure 6E). Previous studies reported that cells often presented a dynamic equilibrium state of promoting or inhibiting a certain pathway or function, rather than simply promoting or inhibiting it (55, 56). In this study, we hope to quantify the immunosuppressive and immune recruitment ability of tumor cells in different tumor types through the gene feature scores. These tumor clusters exhibited synchronous immune recruitment and immune rejection features, indicating a close association between these tumor cells and the formation of the immune microenvironment. This association may have different effects on various types of immune cells, such as TAMs (57), T cells (58), and B cells (59).

The coarse classification-8 clusters, with distinct characteristics of myeloid, T-cell, and oligodendrocyte infiltration, indicated that the different traditional chemotherapy and immunotherapy strategies should be applied (Figures 7G, S10G). Interestingly, the integration of tumor-related features and myeloid subpopulation features helped to further discriminate the subsets potentially responding to the

immune checkpoint inhibitors. Moreover, immune components including the cells, co-stimulators, and MHC molecules were extremely low in the clusters enriching tumor-rejected features (Figure 8E), suggesting the essentiality of fully considering the negative effect on the antitumor immunity and the potential roles of the malignant cells and myeloid subsets in the process of cancer immunology (60–62). Consistent with the previous studies, immunophenotypes of pediatric brain tumors may be less immunosuppressive than those of adult brain tumors, such as craniopharyngiomas and low-grade gliomas, which might light the path to the immunotherapy in pediatric brain tumors, especially for those tumors with high recurrence (Figure 8G) (46, 63, 64).

4.1 Limitations

While our research involved various single-cell datasets of pediatric brain tumors and conducted a thorough analysis of the tumor microenvironment, we regret that a more comprehensive subgroup analysis cannot be performed. This limitation stems from insufficient biological samples, limited size of single-cell data samples, and the absence of molecular subtyping labels for specific tumor types in publicly available datasets. In addition, unlike adult tumors, pediatric brain tumors have a wide variety but low incidence rates. Whether based on public databases or newly generated data from our own samples, the sample size is small. Furthermore, according to the previous studies, scRNA was able to identify higher percentages of immune cells (19). Therefore, the integration analysis was performed in order to maximize the sample size and neutralize the inconsistency of the two different sequencing platforms. However, the potential error caused by sequencing technology and algorithm factors is still unavoidable in our study. It is still worth further in-depth study.

5 Conclusions

In this study, we systematically compared the immunophenotypes of immune cells in the major pediatric brain tumors with those in adult gliomas by integrating the public and newly produced single-cell data and depicted the immune patterns in pediatric brain tumors. These results revealed that specific immune patterns might respond to the PD-1 or CTLA inhibitors. For the relative "cold" tumors, such as MB and EPN, targeting the myeloid subpopulations might also be a potential method.

Data availability statement

The datasets presented in this study can be found in online repositories. The names of the repository/repositories and accession number(s) can be found in the article/Supplementary Material.

Ethics statement

The studies involving humans were approved by Ethic committee of Xinhua Hospital Affiliated to Shanghai Jiao Tong University School of Medicine. The studies were conducted in accordance with the local legislation and institutional requirements. Written informed consent for participation in this study was provided by the participants' legal guardians/next of kin. Written informed consent was obtained from the minor(s)' legal guardian/next of kin for the publication of any potentially identifiable images or data included in this article.

Author contributions

Funding

Conflict of interest

The authors declare that the research was conducted in the absence of any commercial or financial relationships that could be construed as a potential conflict of interest.

The reviewer XD declared a past co-authorship with the author JM to the handling editor.

Publisher's note

Supplementary material

The Supplementary Material for this article can be found online at:
https://www.frontiersin.org/articles/10.3389/fimmu.2023.1238684/full#supplementary-material

SUPPLEMENTARY FIGURE 1

The comparison of two methods-clustering-based (CB) method and positive expression of marker genes (PEMG) method. X axis represents the parameters of marker genes, cell types and corresponding marker pathways, and the y axis represents the ratio of the parameters between the two methods. The red line represents the mean ratio of all parameters.

SUPPLEMENTARY FIGURE 2

(A). UMAP overlays of the feature scores and marker genes expression level of T cell subpopulations in the single cell dataset of Medulloblastoma. (B). Kaplan−Meier survival curves generated with signature score of each T cell subpopulation in the medulloblastoma. (C). UMAP overlays of the feature scores and marker genes expression level of T cell subpopulations in the single cell dataset of ependymoma. (D). Identification of T cell subpopulations in the adult IDH-wild glioma. UMAP shows the identified T cell subsets, and dotplot shows the marker genes of each subpopulations. (E). The integration of T cells from the different datasets GSE155446 (medulloblastoma), GSE125969 (ependymoma) and GSE182109 (adult IDH-wild glioma). (F). The T cell subpopulations identified in the integrated T cell dataset. (G). The marker genes of each identified subpopulation of T cell. (H). The comparison of percentages of T cell subpopulations among the different tumors.

SUPPLEMENTARY FIGURE 3

(A).The UMAP plot shows the clusters of myeloid compartments from the H3K27M-mutation based on smart-seq2. The dotplot displays the classical marker genes of MG and BMDM in each cluster. (B). The UMAP plots respectively show the clusters of myeloid compartments from the adult IDH-wild gliomas based on smart-seq2 and displays the discrimination between MG and BMDM. The dotplot displays the classical marker genes of MG and BMDM in each cluster. (C). The UMAP plots respectively show the clusters of myeloid compartments from the ependymoma based on smart-seq2 and displays the discrimination between MG and BMDM. The dotplot displays the classical marker genes of MG and BMDM in each cluster. (D−F). Evaluation of MG and BMDM in the 10X data of medulloblastoma, adult IDH-wild glioma and IDH-mutation glioma. The UMAP plot displays the consistency between the predicted MG and BMDM and the clusters. The dotplot shows the expression of classical markers in the MG and BMDM. UMAP plots of marker genes shows the expression of classical markers in the cells. (G). The UMAP plots shows the clusters of myeloid cells from the ependymoma, medulloblastoma, pediatric IDH-mutation glioma, adult IDH-mutation glioma and adult IDH-wild gliomas.

SUPPLEMENTARY FIGURE 4

(A−D). The evaluation of myeloid subpopulations in ependymoma, medulloblastoma, pediatric IDH-mutation and adult IDH-mutation. The UMAP plots show the integration of the single cells from the different sources and the clusters of integrated myeloid datasets. The dotplots display the marker genes of each cluster. (E). The UMAP plots shows the clusters of myeloid cells from the adult IDH-wild gliomas. (F). The line charts show the optimal cluster number (dotted line) and the minimum value of

Davies-Bouldin index (DBI) of different integrated myeloid datasets of each tumor type. X axis represents the cluster number, and Y axis represents the DBI.

SUPPLEMENTARY FIGURE 5

(A). Heatmap display the phagocytosis and angiogenesis scores in each cluster across the different tumors. (B). Dotplot shows the marker genes (HLA-DQA1 and CD1E) in the cluster2 of medulloblastoma. (C). Kaplan−Meier survival curves generated with each clusters signature score of adult IDH-mutation glioma using the CGGA dataset. (D). Kaplan−Meier survival curves generated with each clusters signature score of adult IDH-wild glioma using the CGGA dataset.

SUPPLEMENTARY FIGURE 6

(A).The intersections of marker genes of major cell types across the different datasets. (B−I). Upset plot reveals the intersections of gene features from scFes and other gene features from different sources. (J, K) Heatmap and hierarchical clustering of mean expression levels in the purified cell lines collected by previous study (34).

SUPPLEMENTARY FIGURE 7

(A). UMAP overlays of the feature scores of major cell types in the independent single cell dataset of ependymoma. (B). UMAP overlays of the feature scores of major cell types in the independent single cell dataset of adult IDH-wild glioma.

SUPPLEMENTARY FIGURE 8

(A).The tumor cells in the medulloblastoma were sampled and the heatmap shows that the expression levels of negative-IR genes in the most of tumor cells are higher those of positive-IR genes. (B−D). The positive-IP scores(B), the negative-IR scores(C) and OG(D) scores were associated with the better prognosis.

SUPPLEMENTARY FIGURE 9

(A). The line chart shows optimal cluster number (dotted line) and the minimum value of DBI. X axis represents the cluster number, and Y axis represents the DBI. (B−D). The violin plots respectively show the expression levels of three markers among the 8 clusters. (E). Heatmap and hierarchical clustering of median chemokine gene expression per cluster in the CBTTC cohort. (F). Dotplot shows the median chemokine gene expression per cluster of tumor related processes in the CBTTC cohort. (G). A heatmap showing top and bottom Hallmark Pathways with the top 20 variances among the 8 clusters.

SUPPLEMENTARY FIGURE 10

(A). Heatmap and hierarchical clustering of CD4 and CD8 features from scFes. (B). Heatmap and hierarchical clustering of CD4 and CD8 features from the recently published article(引文). (C). The line chart shows optimal cluster number (dotted line) and the minimum value of DBI. X axis represents the cluster number, and Y axis represents the DBI. (D). The heatmap shows the 12 clusters based on the 9 features via hierarchical clustering. (E). The PCA plot reveals the batch effect among the different RNA-seq datasets from GEO and the removal of batch effect with the preservation of corresponding tumor characters. (F). The heatmap shows the mean expression levels of the marker genes of predominant cell type in each cluster using the integrated GEO dataset (G). The prediction of response rates in each cluster (8 clusters). (H). The TIDE score among the different clusters (12 clusters).

References

1. Weller M, Butowski N, Tran DD, Recht LD, Lim M, Hirte H, et al. Rindopepimut with temozolomide for patients with newly diagnosed, EGFRvIII-expressing glioblastoma (ACT IV): a randomised, double-blind, international phase 3 trial. *Lancet Oncol* (2017) 18(10):1373–85. doi: 10.1016/s1470-2045(17)30517-x

2. Hilf N, Kuttruff-Coqui S, Frenzel K, Bukur V, Stevanovic S, Gouttefangeas C, et al. Actively personalized vaccination trial for newly diagnosed glioblastoma. *Nature* (2019) 565(7738):240–5. doi: 10.1038/s41586-018-0810-y

3. Friebel E, Kapolou K, Unger S, Núñez NG, Utz S, Rushing EJ, et al. Single-Cell mapping of human brain cancer reveals tumor-specific instruction of tissue-invading leukocytes. *Cell* (2020) 181(7):1626–1642.e1620. doi: 10.1016/j.cell.2020.04.055

4. Klemm F, Maas RR, Bowman RL, Kornete M, Soukup K, Nassiri S, et al. Interrogation of the microenvironmental landscape in brain tumors reveals disease-Specific alterations of immune cells. *Cell* (2020) 181(7):1643–1660.E17. doi: 10.1016/j.cell.2020.05.007

5. Mathewson ND, Ashenberg O, Tirosh I, Gritsch S, Perez EM, Marx S, et al. Inhibitory CD161 receptor identified in glioma-infiltrating T cells by single-cell analysis. *Cell* (2021) 184(5):1281–1298.e1226. doi: 10.1016/j.cell.2021.01.022

6. Grabovska Y, Mackay A, O'Hare P, Crosier S, Finetti M, Schwalbe EC, et al. Pediatric pan-central nervous system tumor analysis of immune-cell infiltration identifies correlates of antitumor immunity. *Nat Commun* (2020) 11(1):4324. doi: 10.1038/s41467-020-18070-y

7. Engblom C, Pfirschke C, Pittet MJ. The role of myeloid cells in cancer therapies. *Nat Rev Cancer* (2016) 16(7):447–62. doi: 10.1038/nrc.2016.54

8. Masuda T, Sankowski R, Staszewski O, Bottcher C, Amann L, Sagar, et al. Spatial and temporal heterogeneity of mouse and human microglia at single-cell resolution. *Nature* (2019) 566(7744):388–92. doi: 10.1038/s41586-019-0924-x

9. Sankowski R, Bottcher C, Masuda T, Geirsdottir L, Sindram E, Prinz M. Mapping microglia states in the human brain through the integration of high-dimensional techniques. *Nat Neurosci* (2019) 22(12):2098–110. doi: 10.1038/s41593-019-0532-y

10. Masuda T, Sankowski R, Staszewski O, Prinz M. Microglia heterogeneity in the single-cell era. *Cell Rep* (2020) 30(5):1271–81. doi: 10.1016/j.celrep.2020.01.010

11. Ochocka N, Segit P, Walentynowicz KA, Wojnicki K, Cyranowski S, Swatler J, et al. Single-cell RNA sequencing reveals functional heterogeneity of glioma-associated brain macrophages. *Nat Commun* (2021) 12(1):1151. doi: 10.1038/s41467-021-21407-w

12. Riemondy KA, Venkataraman S, Willard N, Nellan A, Sanford B, Griesinger AM, et al. Neoplastic and immune single-cell transcriptomics define subgroup-specific intra-tumoral heterogeneity of childhood medulloblastoma. *Neuro Oncol* (2022) 24 (2):273–86. doi: 10.1093/neuonc/noab135

13. Zhang J, Yuan X, Wang Y, Liu J, Li Z, Li S, et al. Tumor-Associated macrophages correlate with prognosis in medulloblastoma. *Front Oncol* (2022) 12:893132. doi: 10.3389/fonc.2022.893132

14. Mujal AM, Krummel MF. Immunity as a continuum of archetypes. *Science* (2019) 364(6435):28–9. doi: 10.1126/science.aau8694

15. Combes AJ, Samad B, Tsui J, Chew NW, Yan P, Reeder GC, et al. Discovering dominant tumor immune archetypes in a pan-cancer census. *Cell* (2022) 185(1):184–203.e119. doi: 10.1016/j.cell.2021.12.004

16. Alvarez M, Benhammou JN, Maher ND, French SW, Han SB, Sinsheimer JS, et al. Human liver single nucleus and single cell RNA sequencing identify a hepatocellular carcinoma-associated cell-type affecting survival. *Genome Med* (2022) 14(1):50. doi: 10.1186/s13073-022-01055-5

17. Gupta A, Shamsi F, Altemose N, Dorlhiac GF, Cypess AM, White AP, et al. Characterization of transcript enrichment and detection bias in single-nucleus RNA-seq for mapping of distinct human adipocyte lineages. *Genome Res* (2022) 32(2):242–57. doi: 10.1101/gr.275509.121

18. Luo Z, Xia M, Shi W, Zhao C, Wang J, Xin D, et al. Human fetal cerebellar cell atlas informs medulloblastoma origin and oncogenesis. *Nature* (2022) 612(7941):787–94. doi: 10.1038/s41586-022-05487-2

19. Slyper M, Porter CBM, Ashenberg O, Waldman J, Drokhlyansky E, Wakiro I, et al. A single-cell and single-nucleus RNA-Seq toolbox for fresh and frozen human tumors. *Nat Med* (2020) 26(5):792–802. doi: 10.1038/s41591-020-0844-1

20. McGinnis CS, Murrow LM, Gartner ZJ. DoubletFinder: Doublet detection in single-cell RNA sequencing data using artificial nearest neighbors. *Cell Syst* (2019) 8 (4):329–337.e324. doi: 10.1016/j.cels.2019.03.003

21. Butler A, Hoffman P, Smibert P, Papalexi E, Satija R. Integrating single-cell transcriptomic data across different conditions, technologies, and species. *Nat Biotechnol* (2018) 36(5):411–20. doi: 10.1038/nbt.4096

22. Zheng L, Qin S, Si W, Wang A, Xing B, Gao R, et al. Pan-cancer single-cell landscape of tumor-infiltrating T cells. *Science* (2021) 374(6574):abe6474. doi: 10.1126/science.abe6474

23. Abdelfattah N, Kumar P, Wang C, Leu JS, Flynn WF, Gao R, et al. Single-cell analysis of human glioma and immune cells identifies S100A4 as an immunotherapy target. *Nat Commun* (2022) 13(1):767. doi: 10.1038/s41467-022-28372-y

24. Wu T, Hu E, Xu S, Chen M, Guo P, Dai Z, et al. clusterProfiler 4.0: A universal enrichment tool for interpreting omics data. *Innovation (Camb)* (2021) 2(3):100141. doi: 10.1016/j.xinn.2021.100141

25. Sonja H, Robert C, Justin G. GSVA:Gene set variation analysis for microarray and RNA-seq data. *BMC Bioinf* (2013) 16:14–7. doi: 10.1186/1471-2105-14-7

26. Ritchie ME, Phipson B, Wu D, Hu Y, Law CW, Shi W, et al. limma powers differential expression analyses for RNA-sequencing and microarray studies. *Nucleic Acids Res* (2015) 43(7):e47. doi: 10.1093/nar/gkv007

27. Galili T. dendextend: An R package for visualizing, adjusting and comparing trees of hierarchical clustering. *Bioinformatics* (2015) 31(22):3718–20. doi: 10.1093/bioinformatics/btv428

28. Liu Z, Zhou Q, Wang Z, Zhang H, Zeng H, Huang Q, et al. Intratumoral TIGIT+ CD8+ T-cell infiltration determines poor prognosis and immune evasion in patients with muscle-invasive bladder cancer. *J Immunother Cancer* (2020) 8(2):e000978. doi: 10.1136/jitc-2020-000978

29. Dai S, Zeng H, Liu Z, Jin K, Jiang W, Wang Z, et al. Intratumoral CXCL13+CD8 +T cell infiltration determines poor clinical outcomes and immunoevasive contexture in patients with clear cell renal cell carcinoma. *J Immunother Cancer* (2021) 9(2): e001823. doi: 10.1136/jitc-2020-001823

30. Li K. *Medical statistics (7th ed).* People's Medical Publishing House (2022) p. pp 152–158.

31. Reardon DA, Brandes AA, Omuro A, Mulholland P, Lim M, Wick A, et al. Effect of nivolumab vs bevacizumab in patients with recurrent glioblastoma: The checkMate 143 phase 3 randomized clinical trial. *JAMA Oncol* (2020) 6(7):1003–10. doi: 10.1001/jamaoncol.2020.1024

32. Aran D, Looney AP, Liu L, Wu E, Fong V, Hsu A, et al. Reference-based analysis of lung single-cell sequencing reveals a transitional profibrotic macrophage. *Nat Immunol* (2019) 20(2):163–72. doi: 10.1038/s41590-018-0276-y

33. Zhang L, Li Z, Skrzypczynska KM, Fang Q, Zhang W, O'Brien SA, et al. Single-Cell analyses inform mechanisms of myeloid-Targeted therapies in colon cancer. *Cell* (2020) 181(2):442–459.e429. doi: 10.1016/j.cell.2020.03.048

34. Bagaev A, Kotlov N, Nomie K, Svekolkin V, Gafurov A, Isaeva O, et al. Conserved pan-cancer microenvironment subtypes predict response to immunotherapy. *Cancer Cell* (2021) 39(6):845–865.e847. doi: 10.1016/j.ccell.2021.04.014

35. Subramanian A, Tamayo P, Mootha VK, Mukherjee S, Ebert BL, Gillette MA, et al. Gene set enrichment analysis_ A knowledge-based approach for interpreting genome-wide expression profiles. *Proc Natl Acad Sci U.S.A.* (2005) 102(43):15545–50. doi: 10.1073/pnas.0506580102

36. Aran D, Hu Z, Butte AJ. xCell: digitally portraying the tissue cellular heterogeneity landscape. *Genome Biol* (2017) 18(1):220. doi: 10.1186/s13059-017-1349-1

37. Tirosh I, Venteicher AS, Hebert C, Escalante LE, Patel AP, Yizhak K, et al. Single-cell RNA-seq supports a developmental hierarchy in human oligodendroglioma. *Nature* (2016) 539(7628):309–13. doi: 10.1038/nature20123

38. Hovestadt V, Smith KS, Bihannic L, Filbin MG, Shaw ML, Baumgartner A, et al. Resolving medulloblastoma cellular architecture by single-cell genomics. *Nature* (2019) 572(7767):74–9. doi: 10.1038/s41586-019-1434-6

39. Geeleher P, Cox N, Huang RS. pRRophetic: An R package for prediction of clinical chemotherapeutic response from tumor gene expression levels. *PLoS One* (2014) 9(9):e107468. doi: 10.1371/journal.pone.0107468

40. Jiang P, Gu S, Pan D, Fu J, Sahu A, Hu X, et al. Signatures of T cell dysfunction and exclusion predict cancer immunotherapy response. *Nat Med* (2018) 24(10):1550–8. doi: 10.1038/s41591-018-0136-1

41. Gholamin S, Mitra SS, Feroze AH, Liu J, Kahn SA, Zhang M, et al. Disrupting the CD47–SIRPα anti-phagocytic axis by a humanized anti-CD47 antibody is an efficacious treatment for Malignant pediatric brain tumors. *Sci Transl Med* (2017) 9 (381). doi: 10.1126/scitranslmed.aaf2968

42. Foster JB, Madsen PJ, Hegde M, Ahmed N, Cole KA, Maris JM, et al. Immunotherapy for pediatric brain tumors: past and present. *Neuro Oncol* (2019) 21 (10):1226–38. doi: 10.1093/neuonc/noz077

43. Majzner RG, Ramakrishna S, Yeom KW, Patel S, Chinnasamy H, Schultz LM, et al. GD2-CAR T cell therapy for H3K27M-mutated diffuse midline gliomas. *Nature* (2022) 603(7903):934–41. doi: 10.1038/s41586-022-04489-4

44. Gröbner SN, Worst BC, Weischenfeldt J, Buchhalter I, Kleinheinz K, Rudneva VA, et al. The landscape of genomic alterations across childhood cancers. *Nature* (2018) 555(7696):321–7. doi: 10.1038/nature25480

45. Patel AP, Tirosh I, Trombetta JJ, Shalek AK, Gillespie SM, Wakimoto H. Single-cell RNA-seq highlights intratumoral heterogeneity in primary glioblastoma. *Science* (2014) 344(6190):1396–401. doi: 10.1126/science.1254257

46. Griesinger AM, Birks DK, Donson AM, Amani V, Hoffman LM, Waziri A, et al. Characterization of distinct immunophenotypes across pediatric brain tumor types. *J Immunol* (2013) 191(9):4880–8. doi: 10.4049/jimmunol.1301966

47. Filley AC, Henriquez M, Dey M. Recurrent glioma clinical trial, CheckMate-143: the game is not over yet. *Oncotarget* (2017) 8:91779. doi: 10.18632/oncotarget.21586

48. Zhao J, Chen AX, Gartrell RD, Silverman AM, Aparicio L, Chu T, et al. Immune and genomic correlates of response to anti-PD-1 immunotherapy in glioblastoma. *Nat Med* (2019) 25(3):462–9. doi: 10.1038/s41591-019-0349-y

49. Pham CD, Flores C, Yang C, Pinheiro EM, Yearley JH, Sayour EJ, et al. Differential immune microenvironments and response to immune checkpoint blockade among molecular subtypes of murine medulloblastoma. *Clin Cancer Res* (2016) 22(3):582–95. doi: 10.1158/1078-0432.CCR-15-0713

50. DeNardo DG, Ruffell B. Macrophages as regulators of tumour immunity and immunotherapy. *Nat Rev Immunol* (2019) 19(6):369–82. doi: 10.1038/s41577-019-0127-6

51. Goswami S, Anandhan S, Raychaudhuri D, Sharma P. Myeloid cell-targeted therapies for solid tumours. *Nat Rev Immunol* (2022) 23(2):106–20. doi: 10.1038/s41577-022-00737-w

52. Pang L, Khan F, Heimberger AB, Chen P. Mechanism and therapeutic potential of tumor-immune symbiosis in glioblastoma. *Trends Cancer* (2022) S2405-8033 (22):00097–8. doi: 10.1016/j.trecan.2022.04.010

53. Panagioti E, Kurokawa C, Viker K, Ammayappan A, Anderson SK, Sotiriou S, et al. Immunostimulatory bacterial antigen-armed oncolytic measles virotherapy significantly increases the potency of anti-PD1 checkpoint therapy. *J Clin Invest* (2021) 131(13). doi: 10.1172/JCI141614

54. Hammond TR, Dufort C, Dissing-Olesen L, Giera S, Young A, Wysoker A, et al. Single-Cell RNA sequencing of microglia throughout the mouse lifespan and in the injured brain reveals complex cell-State changes. *Immunity* (2019) 50(1):253–271.e256. doi: 10.1016/j.immuni.2018.11.004

55. Xiang W, Shi R, Kang X, Zhang X, Chen P, Zhang L. Monoacylglycerol lipase regulates cannabinoid receptor 2-dependent macrophage activation and cancer progression. *Nat Commun* (2018) 9(1):2574. doi: 10.1038/s41467-018-04999-8

56. He L, Yuan L, Yu W, Sun Y, Jiang D, Wang X, et al. A regulation loop between YAP and NR4A1 balances cell proliferation and apoptosis. *Cell Rep* (2020) 33 (3):108284. doi: 10.1016/j.celrep.2020.108284

57. Wolfsberger J, Sakil HAM, Zhou L, Bree N, Baldisseri E, Ferreira S, et al. TAp73 represses NF-κB-mediated recruitment of tumor-associated macrophages in breast cancer. *Proc Natl Acad Sci USA* (2021) 118(10):e2017089118. doi: 10.1073/pnas.2017089118

58. Moreno Ayala MA, Campbell TF, Zhang C, Dahan N, Bockman A, Prakash V, et al. CXCR3 expression in regulatory T cells drives interactions with type I dendritic cells in tumors to restrict CD8+ T cell antitumor immunity. *Immunity* (2023) 56 (7):1613–1630.e5. doi: 10.1016/j.immuni.2023.06.003

59. Lu Y, Zhao Q, Liao JY, Song E, Xia Q, Pan J, et al. Complement signals determine opposite effects of B cells in chemotherapy-induced immunity. *Cell* (2020) 180 (6):1081–1097.e24. doi: 10.1016/j.cell.2020.02.015

60. Gordon SR, Maute RL, Dulken BW, Hutter G, George BM, McCracken MN, et al. PD-1 expression by tumour-associated macrophages inhibits

phagocytosis and tumour immunity. *Nature* (2017) 545(7655):495–9. doi: 10.1038/nature22396

61. Garris CS, Arlauckas SP, Kohler RH, Trefny MP, Garren S, Piot C, et al. Successful anti-PD-1 cancer immunotherapy requires T cell-Dendritic cell crosstalk involving the cytokines IFN-gamma and IL-12. *Immunity* (2018) 49(6):1148–1161.e1147. doi: 10.1016/j.immuni.2018.09.024

62. Hou J, Zhao R, Xia W, Chang CW, You Y, Hsu JM, et al. PD-L1-mediated gasdermin C expression switches apoptosis to pyroptosis in cancer cells and facilitates tumour necrosis. *Nat Cell Biol* (2020) 22(10):1264–75. doi: 10.1038/s41556-020-0575-z

63. Majzner RG, Simon JS, Grosso JF, Martinez D, Pawel BR, Santi M, et al. Assessment of programmed death-ligand 1 expression and tumor-associated immune cells in pediatric cancer tissues. *Cancer* (2017) 123(19):3807–15. doi: 10.1002/cncr.30724

64. Lieberman NAP, DeGolier K, Kovar HM, Davis A, Hoglund V, Stevens J, et al. Characterization of the immune microenvironment of diffuse intrinsic pontine glioma: implications for development of immunotherapy. *Neuro Oncol* (2019) 21(1):83–94. doi: 10.1093/neuonc/noy145

Glossary

TME	tumor microenvironment
CNS	center nervous system
scRNA-seq	single-cell RNA sequencing
MG	microglial
BMDM	bone marrow-derived myeloid
scFes	gene features based on single-cell data
BBB	blood–brain barrier
TAM	tumor-associated macrophage
P-IDH-M	pediatric IDH-mutation
IDH-W	IDH-wild
HVG	highly variable genes
PCA	principal component analysis
SNN	shared nearest neighbor
AA	anaplastic astrocytoma
MB	medulloblastoma
EPN	ependymoma
AS	astrocytoma
ATRT	atypical teratoid rhabdoid tumor
CPP	choroid plexus papilloma
CPG	craniopharyngioma
DIPG	diffuse intrinsic pontine glioma
EPN	ependymoma
GG	ganglioglioma
OG	oligodendrocyte
PNET	primitive neuroectodermal tumor
DEGs	differential expression genes
DBI	Davies–Bouldin Index
logFC	log fold change
CV	coefficient of variation
CB	clustering-based
PEMG	positive expression of marker genes
GBM	glioblastoma
mIHC	multiple immunohistochemistry
negative-PR	negative immune recruitment
positive-PR	positive immune recruitment
CD8 Tem	CD8 effector memory T cells
terminal CD8 Tem	CD8 terminal effector memory T cells
CD4 Tm	CD4 memory T cells

(Continued)

Continued

Treg	regulatory T cell
Tn	naive T cell
ISG	interferon-stimulated gene

![frontiers | Frontiers in Immunology]

Dissecting tumor microenvironment heterogeneity in syngeneic mouse models: insights on cancer-associated fibroblast phenotypes shaped by infiltrating T cells

Marco Carretta[1†], Marie-Louise Thorseth[1†], Aimilia Schina[1],
Dennis Alexander Agardy[1], Astrid Zedlitz Johansen[1],
Kevin James Baker[1], Shawez Khan[1],
Anne Mette Askehøj Rømer[1], Klaire Yixin Fjæstad[1],
Hannes Linder[1], Dorota Ewa Kuczek[1], Marco Donia[1],
Lars Grøntved[2] and Daniel Hargbøl Madsen[1,3*]

[1]National Center for Cancer Immune Therapy (CCIT-DK), Department of Oncology, Copenhagen
University Hospital - Herlev and Gentofte, Herlev, Denmark, [2]Department of Biochemistry and
Molecular Biology, University of Southern Denmark, Odense, Denmark, [3]Department of Immunology
and Microbiology, University of Copenhagen, Copenhagen, Denmark

Murine syngeneic tumor models have been used extensively for cancer research for several decades and have been instrumental in driving the discovery and development of cancer immunotherapies. These tumor models are very simplistic cancer models, but recent reports have, however, indicated that the different inoculated cancer cell lines can lead to the formation of unique tumor microenvironments (TMEs). To gain more knowledge from studies based on syngeneic tumor models, it is essential to obtain an in-depth understanding of the cellular and molecular composition of the TME in the different models. Additionally, other parameters that are important for cancer progression, such as collagen content and mechanical tissue stiffness across syngeneic tumor models have not previously been reported. Here, we compare the TME of tumors derived from six common syngeneic tumor models. Using flow cytometry and transcriptomic analyses, we show that strikingly unique TMEs are formed by the different cancer cell lines. The differences are reflected as changes in abundance and phenotype of myeloid, lymphoid, and stromal cells in the tumors. Gene expression analyses support the different cellular composition of the TMEs and indicate that distinct immunosuppressive mechanisms are employed depending on the tumor model. Cancer-associated fibroblasts (CAFs) also acquire very different phenotypes across the tumor models. These differences include differential expression of genes encoding extracellular matrix (ECM) proteins, matrix metalloproteinases (MMPs), and immunosuppressive factors. The gene expression profiles suggest that CAFs can contribute to the formation of an immunosuppressive TME, and flow cytometry analyses show increased PD-L1 expression by CAFs in the immunogenic tumor models, MC38 and CT26. Comparison with CAF subsets identified in other studies shows that

CAFs are skewed towards specific subsets depending on the model. In athymic mice lacking tumor-infiltrating cytotoxic T cells, CAFs express lower levels of PD-L1 and lower levels of fibroblast activation markers. Our data underscores that CAFs can be involved in the formation of an immunosuppressive TME.

1 Introduction

The past two decades have seen the rapid development of cancer therapies that directly involve the patient's immune system (1, 2). The therapies are collectively termed immunotherapy and comprise a range of immunomodulating therapies that target different steps within the cancer immunity cycle with the goal of generating an anti-cancer response (3). These new immunotherapeutic approaches, such as immune checkpoint inhibitors (ICIs) targeting CTLA-4 or PD-1/PD-L1, have demonstrated clinical efficacy in a wide variety of solid tumors (4, 5) and have highlighted the critical role that the immune system plays in fighting cancer. However, only a minority of patients respond to these therapies and display long-term responses, while most patients do not respond or may develop resistance to the treatment (6, 7). The formation of an immunosuppressive tumor microenvironment (TME) has been suggested as a major obstacle to the successful outcome of immunotherapy and understanding how the TME influences anti-tumor immune activity currently represents a central theme in cancer immunotherapy research.

Studies of the immune composition of human tumors, have identified great heterogeneity between cancer types and between tumors of the same cancer type (8). A high level of tumor-infiltrating $CD8^+$ T cells and Th1 cytokine expression, commonly defined as an immunogenic or 'hot' tumor, is generally associated with a good prognosis (9). Conversely, low T cell infiltration and the presence of suppressive myeloid cells contribute to the establishment of an immunologically 'cold' tumor, which is associated with poor prognosis (8). Some tumors display a third immune profile known as "immune-excluded", characterized by the presence of immune cells confined to the stroma and lack of infiltration into the tumor nests (10). Immunosuppressive myeloid cells such as M2-like macrophages and myeloid-derived suppressor cells (MDSCs) have been shown to play major roles in the immune evasion of cancer cells (11, 12) and are also involved in remodeling of the surrounding extracellular matrix (ECM) (13–15).

Other mechanisms contributing to an immunosuppressive TME involve stromal cells such as cancer-associated fibroblasts (CAFs) (16, 17). These cells are the most abundant non-hematopoietic cells in the TME and cover a range of subsets and

activation states rather than being a uniform cell type (18, 19). Several studies indicate that CAFs may have different origins, which might contribute to their dynamic heterogeneity and explain why common CAF-markers such as fibroblast-activation protein (FAP), α-smooth muscle actin (α-SMA), PDGF receptor (PDGFR), or CD90/THY1, are not always expressed at the same time (19, 20).

During cancer progression, CAFs are centrally engaged in remodeling the surrounding ECM through the secretion of ECM components such as collagens or ECM-remodeling enzymes like matrix metalloproteinases (MMPs) (18, 21, 22). This can lead to the formation of a tumor-specific ECM, which is often associated with increased tissue stiffness (23). The ECM can stimulate cancer growth and metastasis (24–26), whilst also regulating the motility and activity of tumor-infiltrating T cells (23, 27–29). Moreover, the ECM also influences the activity of other types of immune cells, including NK cells and macrophages (30–32). In addition to the CAF-mediated ECM alterations, CAFs have many other pro-tumorigenic functions, such as promotion of tumor formation, progression, and metastasis (19, 20). CAFs are involved in immunosuppression and T cell exclusion through the secretion of a variety of chemokines and cytokines, including CXCL12, CCL2, IL-6, IL-10, and TGF-β (19, 33–36) or through the upregulation of PD-L2 and FasL (37). CAFs can also secrete vascular endothelial growth factor (VEGF), which not only promotes angiogenesis, but also exerts immunomodulatory functions by inhibiting the development of dendritic cells (DCs) and downregulating their antigen-presentation abilities (38, 39).

Recently, CAFs have been shown to comprise a heterogeneous and functionally diverse cell population, with multiple CAF subsets identified (18, 20, 40). The high plasticity within the CAF population has been observed in human cancers as well as in mouse cancer models (41–43). The number of identified subsets varies between studies, but many of these describe a subset involved in ECM remodeling often termed myofibroblastic CAFs (myCAFs) and a subset with immune modulatory functions often termed inflammatory CAFs (iCAFs) (42–44).

A common tool for cancer research is the use of *in vivo* mouse tumor models. Human patient-derived xenograft (PDX) models, in which human tumor material is engrafted in mice, have become a central part of research in tumor biology and conventional cancer

therapies (45). These models involve the transplantation of human cancer tissue into immune-deficient mice to avoid graft rejection. The lack of a functional immune system in these mice is not optimal for the research of immunotherapies. Genetically engineered mouse models (GEMMs) are excellent models to recapitulate the native tumor niches and provide useful insights into the interaction between malignant cells and immune effectors (46). However, GEMMs are often poorly immunogenic, and few of these models have proven to be responsive to immunotherapy (47). Syngeneic mouse tumor models, some of which were developed over 60 years ago, are economical and accessible models. The inoculated cancer cells lead to short latency periods and very fast tumor growth, which might not accurately mimic the human disease. In most cases, cells are injected subcutaneously instead of orthotopically, which could also result in differences from the human situation. Nevertheless, syngeneic tumor models have recently regained attention as reliable models for immunotherapy research since they retain a fully intact immune system and native stromal components. Consequently, syngeneic mouse models are an important approach for preclinical testing of immunotherapies, and major discoveries in the field of immunotherapy were made with the use of these mouse tumor models (48, 49).

Although developed decades ago, the immunological and molecular characteristics of syngeneic tumor mouse models and their TME have not been fully elucidated. In this work, we set out to thoroughly characterize the TME in a panel of common syngeneic mouse tumor models. Using flow cytometry and RNA sequencing (RNAseq), we characterize the tumor immune infiltrate in the different tumor models. Furthermore, we evaluate the stromal components of these models by investigating the relative tumor stiffness, collagen abundance, and the transcriptome of the CAFs. The study reveals large differences between CAFs in the different models. Comparison to established CAF subsets reveals that CAFs from the different models have similarities to specific subsets. The obtained data can contribute to improved preclinical model selection for target validation and immunotherapy drug development in future studies. Additionally, a thorough analysis of the CAFs indicates a significant contribution to the formation of an immunosuppressive TME from these cells. We show that activation of CAFs and acquisition of an immunosuppressive phenotype is driven by the tumor-infiltrating T cells.

2 Materials and methods

2.1 Cell culture of murine cancer cell lines

The murine cancer cell lines B16-F10 (melanoma), Pan02 (pancreatic ductal carcinoma), MC38 (colon carcinoma), LL2 (lung carcinoma), and CT26 (colon carcinoma) were obtained from the CCIT-DK cell biobank. EO771.LMB (breast carcinoma) was kindly gifted by Prof. Robin L. Anderson (Olivia Newton-John Cancer Research Institute, Heidelberg, Australia). The CT26 cell line is derived from a BALB/c mouse whereas the remaining cell lines are derived from C57BL/6 mice. All cell lines were tested mycoplasma-negative. Cell lines were cultured in cell culture-treated flasks (Corning,

NY, USA) at 37°C and 5% CO_2. CT26 was cultured in RPMI 1640 + GlutaMAX^{TM}, 10% fetal bovine serum (FBS), and 1% penicillin/streptomycin (P/S) (all from Gibco, Thermo Fisher, Waltham, MA, USA). B16-F10, LL2, and Pan02 were cultured in DMEM + GlutaMAX^{TM} (Gibco, Thermo Fisher, Waltham, MA, USA), 10% FBS, and 1% P/S. EO771.LMB was cultured in DMEM, 20% FBS, 1% P/S, and 20 mM HEPES (Gibco, Thermo Fisher, Waltham, MA, USA). MC38 was cultured in DMEM + GlutaMAX^{TM}, 10% FBS, 1% P/S, 1% HEPES, 1% non-essential amino acid (NEAA) supplement, and 1% sodium pyruvate (all from Gibco, Thermo Fisher, Waltham, MA, USA). At approximately 90% confluency, the supernatant was removed, and the cells were washed twice with phosphate-buffered saline (PBS; Gibco, Thermo Fisher, Waltham, MA, USA). After washing, cells were detached by trypsinization using 0.25% Trypsin-EDTA (Gibco, Thermo Fisher, Waltham, MA, USA), and detached cells were resuspended in respective media and seeded in new culture flasks.

2.2 Animal experiments

Animal experiments were performed at the animal facility of the Department of Oncology, Herlev Hospital. All experiments were approved by the Danish Animal Experiment Council (license registration number 2016-15-0201-01020 and 2021-15-0201-00999). Daily care and breeding of C57BL/6 mice (C57BL/6JBomTac) and NMRI nude mice (BomTac : NMRI-*Foxn1$^{nu/nu}$*) were performed by animal caretakers. BALB/c mice (BALB/cAnNRJ) and BALB/c nude mice (BALB/cAnNRJ-*Foxn1$^{nu/nu}$*) were purchased from Janvier Labs (Janvier, Labs, Le Genest-Saint-Isle, France). Harvested cancer cells were counted using a hemocytometer (Hausser Scientific, Horsham, PA, USA), centrifuged at 300 g for 5 minutes at room temperature (RT) and resuspended in respective cell culture medium without supplements in the concentration of 5×10^5 cells per 100 µL. Cells were placed on ice and directly before injection agitated using a pipette to ensure a homogenous cell suspension. A total of 5×10^5 cells were inoculated subcutaneously using a 1 ml syringe and 25 G needle in the right flank or in both flanks of adult female mice (10-15 weeks old). Injected cells had been cultured for a maximum of 20 passages after acquisition of the cell lines. Tumor dimensions were measured three times weekly with a digital caliper, and the tumor volume was calculated using the formula volume $(mm^3) = (length) \times (width)^2/2$. Mice were regularly examined for formation of ulcers on the surface of the tumors and excluded from further analysis at the presence of ulcers. The experimental endpoint was defined as tumor volume reaching 1200mm^3. The mice were euthanized by cervical dislocation, and the tumor tissue was harvested. The excised tumors were divided into fragments and placed in digestion buffer (2.1 mg/ml collagenase type 1 (Worthington Biochemical Corporation, Lakewood, NJ, USA), 75 µg/ml DNase I (Worthington Biochemical Corporation), 5 mM CaCl$_2$, and 1% P/S in RPMI 1640 medium) for flow cytometry analysis, in RNAlater (Thermo Fisher Scientific, Waltham, MA, USA) for RNA isolation, or in 4% formaldehyde for histological staining. For shear rheology, whole tumors were placed in cold PBS and analyzed the same day.

2.3 Flow cytometry

Tumor fragments were placed in digestion buffer and chopped into small pieces using surgical scissors. The suspension was placed at 4°C in the dark overnight in an end-over-end rotator. The next day, the tumor digest was incubated at 37°C for 10 to 60 minutes and then homogenized by pipetting. The tumor digest was passed through a 70 μm cell strainer (Corning, NY, USA) together with PBS to obtain a single cell suspension. Erythrocytes were lysed using 2 mL red blood cell lysis buffer (Qiagen, Venlo, The Netherlands) and incubated up to 5 minutes at RT. The lysis was stopped by adding 30 mL of cell culture media. The single-cell suspension was centrifuged for 5 minutes at 300 g, the supernatant was discarded, and cells were resuspended in FACS buffer (5% bovine serum albumin (Sigma-Aldrich, St. Louis, MO), 5 mM EDTA (Sigma-Aldrich, St. Louis, MO) in PBS).

Whole tumor single-cell suspensions or purified CD45$^+$ cell fractions were counted using a hemocytometer, and 5 x 10^5 cells per sample were transferred to Falcon$^®$ FACS tubes (Corning, NY, USA), resuspended in 100 μL FACS buffer containing 0.5 μL FcR blocking reagent (Miltenyi Biotec, Bergisch Gladbach, Germany), and incubated for 10 minutes at 4°C in the dark. Afterwards, samples were stained with an antibody cocktail of either the general, myeloid, or lymphoid panel (Supplementary Table 3). Cells were incubated with antibodies for 20 minutes at 4°C in the dark and subsequently washed with 2 mL PBS and centrifuged for 5 minutes at 300 g. A live-dead staining was included in all analyses. The supernatant was discarded, and cell suspensions were resuspended in 500 μL FACS buffer. Samples stained with the general panel underwent secondary staining with streptavidin-APC (BioLegend, San Diego, CA, USA) for 10 minutes at 4°C in the dark prior to resuspension. The samples were analyzed using the flow cytometers LSR II or FACS Canto II (BD Biosciences, San Jose, CA, USA). 50000 total events per analysis were typically recorded. For the myeloid and lymphoid panel, where a preceding CD45+ enrichment had been performed, the numbers were occasionally lower although always at least 10000 events. Time plots were inspected to ensure the flow had been stable during the analyses. Data analysis was performed with FlowJo version 10.7.1 (FlowJo LLC, Ashland, OR, USA). Gating strategies are found in Supplementary Figures 2–4. Fluorescence minus one (FMO) staining was performed for FAP, CD11b, CD3, CD4, CD8 and CD25. For CD206, a control staining similar to an FMO was performed but with the inclusion of an isotype control antibody conjugated with the same fluorophore as the anti-CD206 antibody. To avoid spillover of emission signals from other channels, all panels underwent a compensation procedure prior to running samples, using the BD FACS Diva software version 8.0.1 (BD Biosciences, San Jose, CA, USA). A list of antibodies can be found in Supplementary Table 3.

2.4 Purification of CD45$^+$ cells

To enrich the leukocyte population of whole tumor suspensions for flow cytometry analysis or FACS sorting, the CD45$^+$ population was enriched by magnetic-activated cell sorting. Single-cell suspensions were counted, centrifuged at 300 g for 5 minutes at RT, and then resuspended in 90 μL of FACS buffer with 10 μL FcR blocking reagent (Miltenyi Biotec) per 10^7 cells. Cells were incubated for 10 minutes at 4°C and subsequently labeled with 10 μL CD45 MicroBeads (Miltenyi Biotec, Bergisch Gladbach, Germany) per 10^7 cells and incubated for 20 minutes at 4°C. After incubation, cells were washed once with FACS buffer and loaded onto LS columns (Miltenyi Biotec, Bergisch Gladbach, Germany) placed in a magnetic MACS MultiStand (Miltenyi Biotec, Bergisch Gladbach, Germany). The column was washed once with 2 mL FACS buffer, and subsequently the CD45$^+$ fraction was eluted from the column.

2.5 Fluorescence activated cell sorting

The CD45$^-$ fraction left after CD45$^+$ purification was used to sort FAP$^+$ CAFs from the tumors. CD45$^-$ cell suspensions were stained with a live/dead marker and FAP-Biotin (R&D Systems, Minneapolis, MN, USA) followed by secondary staining with streptavidin as described above. Up to 3 x 10^5 cells were sorted into PBS. The samples were sorted using a FACS Aria I cell sorter (BD Biosciences, San Jose, CA, USA). Immediately after sorting, cells were processed for RNA isolation.

2.6 Shear rheology

The relative stiffness of tumors was measured by shear rheology using a DHR-2 rotational rheometer (TA Instruments, New Castle, DE, USA). After excision, tumors were kept in PBS on ice and measurements were taken the same day. Tumors were cut using a scalpel, and disks of 8-mm diameter were obtained using a biopsy punch. Measurements were performed using an 8-mm parallel plate geometry at 21°C, at a fixed angular frequency of 1 rad/s, and an increasing strain from 0.1 to 2%. Storage modulus (G′) was extracted at 0.3% strain (shown to be within the linear viscoelastic response range).

2.7 RNA isolation

RNA was isolated from sorted cells or tumor fragments using the RNeasy$^®$ Mini Kit (Qiagen, Venlo, The Netherlands) according to the manufacturer's protocol. When isolating RNA from sorted cells, the cells were centrifuged for 5 minutes at 300 g and lysed by resuspension in 350 μL RLT lysis buffer. When isolating RNA from tumor tissue, a tumor fragment of approximately 30 mg was placed in a 2 mL microcentrifuge tube with 500 μL RLT buffer containing 1:100 β-mercaptoethanol and a 5 mm stainless steel bead. The tumor fragment was homogenized with a TissueLyser (Qiagen, Venlo, The Netherlands) for 3 minutes at a frequency of 25/s. The bead was removed, and the samples were spun down at top

speed (21,000 *g*) for 3 minutes. A volume of 350 μL lysate was used for RNA isolation. Isolated RNA was stored at -80°C until further analysis. Concentration, purity, and integrity of RNA extracts were measured using the Agilent RNA 6000 Nano Kit and the Agilent 2100 Bioanalyzer (both from Agilent Technologies, Santa Clara, CA, USA) according to manufacturer's instructions.

2.8 qRT-PCR

Reverse transcription of RNA was done using the iScript cDNA Synthesis Kit (Bio-Rad Laboratories, Hercules, CA, USA) according to the manufacturer's instructions to obtain complementary DNA (cDNA). Controls without reverse transcriptase and controls without template were included. The quantitative real-time PCR (qRT-PCR) was done using the Brilliant III Ultra-Fast SYBR Green QPCR Master Mix (Agilent Technologies, Santa Clara, CA, USA) according to the manufacturer's instructions. The program used was: 3 minutes at 95°C, 40 cycles of 5 seconds at 95°C, 40 cycles of 20 seconds at 60°C, and a melting curve analysis of 65-95°C with 0.5°C increment, 5 seconds per step. qRT-PCR was performed using an AriaMX Real-Time PCR System (G8830A, Agilent Technologies, Santa Clara, CA, USA). Samples were run in triplicates and normalized to the internal reference gene, *Actb*. Relative fold changes were calculated using the comparative cycle threshold (ΔΔCT) method. Primers were designed using the Primer-BLAST tool ((National Center for Biotechnology Information, National Institutes of Health, Bethesda, MD, USA). Primer sequences are listed in Supplementary Table 4.

2.9 RNA sequencing and analysis

A total of 1000 ng RNA from tumor fragments and 400 ng RNA from sorted CAFs was prepared for sequencing using polydT enrichment according to the manufacturer's protocol (Illumina, San Diego, CA, USA). Library preparation was performed using the NEBNext RNA library prep kit (Illumina, San Diego, CA, USA). The library quality was assessed using a Fragment Analyzer (Agilent, Santa Clara, CA, USA) followed by library quantification using the Illumina library quantification kit. Sequencing was done on a NovaSeq 6000 platform (Illumina, San Diego, CA, USA). Sequenced reads were aligned to the mouse reference mm10 genome using STAR, version 2.5.0 (50). The gene expression count matrix was generated using HOMER (51).

All analyses were performed with R. Differential expression analysis was performed using the DESeq2 package. Principal component analysis was performed using the prcomp package. z-score normalized RPKM values of selected genes were used to generate heatmaps using the pheatmap package. Fuzzy clustering was performed using VSClust (52). The gene lists used for illustrating myeloid factors, lymphoid factors, and stromal factors were based on gene lists by NanoString Technologies. The gene lists used for illustrating collagens and core matrisome genes were from

the matrisomeDB (53, 54). The gene lists used for illustrating immunosuppressive factors and MMPs were self-generated.

2.10 CIBERSORT analysis

The computational framework of the CIBERSORT analytical tool (55), along with the developed ImmuCC signature matrix (non-tissue specific) (56), suitable for the deconvolution of mouse bulk RNA-Seq data, were used to characterize and quantify 25 immune cell subtypes. The ImmuCC signature matrix consists of 511 genes and 489 genes from our bulk RNAseq data were mapped (22 missing).

For deconvolution of the bulk RNAseq samples with CIBERSORT, RPKM pre-normalized data were used to produce the input mixture matrix. Additionally, the analysis included both CIBERSORT-Relative and CIBERSORT-Absolute modes. While CIBERSORT-Relative represents immune cell fractions, which are relative to the total immune content, therefore suitable for intra-sample comparisons, CIBERSORT-Absolute produces a score that quantifies the abundance of each cell type, making it appropriate for intra-sample comparisons between cell types as well as inter-sample comparisons of the same cell type. The CIBERSORT outputs were generated by performing 1000 permutations and by disabling the quantile normalization parameter.

For the purposes of this study, three population schemes were defined, resulting in the aggregation of some of the 25 immune sub-populations. Furthermore, the CIBERSORT estimates were averaged across cell line replicates, to generate one estimate/score per cell line.

Total absolute scores for sub-populations merged were calculated as the sum of the sub-populations. The relative fractions were re-calculated based on the new total immune content of each scheme. The CIBERSORT software source code in R was obtained from the website: https://cibersort.stanford.edu/, after registration and request for access and download.

2.11 Histology

Tumors were fixed in 4% formaldehyde overnight at 4°C. Samples were transferred to 70% ethanol and stored at 4°C until paraffin embedding. Tissues were embedded in paraffin and cut into 3.5 μm tissue sections. Sections were deparaffinized with xylene and hydrated through ethanol/water dilutions. For the detection of fibrillar collagen, sections were stained with 0.1% Sirius red diluted in saturated picric acid (Ampliqon, Odense, Denmark) and counterstained with Weigert's hematoxylin. Images of stained sections were acquired using a light microscope with polarization filters. Picrosirius red (PSR) positive areas were quantified with Qupath software (ver. 0.2.3) (57) using the Qupath Pixel Classifier with full resolution. Positive and negative areas were manually assigned on several sections, and these were used to train the Pixel Classifier until it could reliably detect positive areas. Ten squares were randomly distributed across each section and the trained Pixel

Classifier was run on these. The average of the 10 squares was determined for each section.

2.12 Statistics

Data analyses, statistical analyses, and graph generations were performed with Prism 8 (GraphPad) unless otherwise stated. Correlations between percentage collagen positive area and storage modulus and percentage FAP$^+$ CAFs were assessed by Pearson rank correlations. Asterisks in the graphs indicate

significance as described in respective figure legends. Differences were considered statistically significant at $p < 0.05$.

3 Results

3.1 Murine tumor models display distinct gene expression profiles indicative of differences in the tumor microenvironment

To study the TME formed in different mouse tumor models, we selected a panel of commonly used syngeneic mouse models

FIGURE 1

Six commonly used murine syngeneic tumor models show distinct gene expression profiles. **(A)** Table summarizing the tumor models, cancer type, origin, and rate of ulceration. **(B)** Principal component analysis (PCA) plot of RNA isolated from tumor fragments derived from the indicated cell lines. C-F) Heatmaps of normalized (Z-score) RNAseq read counts of genes encoding myeloid factors **(C)**, lymphoid factors **(D)**, stromal factors **(E)**, and immunorsuppressive factors **(F)**.

representative of some of the most common human cancer types (Figure 1A). Five of the murine cell lines (EO771.LMB, B16-F10, LL/2, Pan02, and MC38) are derived from C57BL/6 mice, while CT26 is derived from BALB/c mice (Figure 1A). B16-F10 will be referred to hereafter as B16, EO771.LMB as EO771, and LL/2 as LL2. The inoculated B16, LL2, MC38 and CT26 cells all formed fast growing tumors, whereas EO771 and Pan02 displayed slower growth kinetics (not shown). Pan02 tumors grew particularly slowly and had a strong tendency to develop severe tumor ulceration. When tumor volumes exceeded 150 mm^3, 50% of mice with Pan02 tumors had developed ulcers compared to maximum 23% of other tumor-bearing mice (Figure 1A). Ulcerating tumors were excluded from subsequent analyses of the TME.

For a detailed comparison of the six tumor models, we initially analyzed the tumors by RNAseq (full gene expression dataset in Supplementary Table 1). A principal component analysis (PCA) highlights the profound differences in the gene expression pattern between the tumor models (Figure 1B). The transcriptomic differences were expected since the used cancer cell lines originate from different tissues, but analysis of the expression of genes related to myeloid cells (Figure 1C) and lymphoid cells (Figure 1D) indicated that formation of distinct TMEs also contributed to the observed global gene expression differences. All tumor models have discrete expression profiles of genes related to both myeloid and lymphoid cells, with B16 and EO771 tumors having gene expression profiles indicative of low immune infiltration. Expression analysis of genes encoding stromal factors also showed large differences in the stromal compartment between the tumor models (Figure 1E). To investigate the influence of tumor-infiltrating T cells on tumor growth, B16, Pan02, MC38, and CT26 cells were subcutaneously injected into athymic nude mice that lack functional T cells and at the same time into immunocompetent wildtype mice. MC38 and CT26 cancer cells harbor many mutations and are considered immunogenic tumor models (58). As expected, MC38 and CT26 grew substantially faster in nude mice, suggesting high immunogenicity of these tumor models (Supplementary Figures 1A, B). B16 and Pan02 tumor growth were not different in nude mice compared to wildtype mice (Supplementary Figures 1C, D). Interestingly, gene expression analysis of a panel of immunosuppressive factors showed obvious differences between the tumor models, indicating that they depend on different mechanisms for immune escape (Figure 1F). Even between the two immunogenic colorectal cancer models MC38 and CT26, clear differences were observed. MC38 tumors have a particularly high expression of *Ido1* and *Ido2*, whereas CT26 tumors express high levels of *Arg2*, *Ptgs1*, and *Ptgs2* encoding arginase-2, COX-1, and COX-2, respectively.

3.2 Flow cytometry analysis of the TME unveil different immune cell compositions between tumor models

To further characterize the distinct TME of the six tumor models, we analyzed the cellular composition of single cell suspensions of tumors by flow cytometry. The TME was characterized with a special focus on immune cell populations but also on the presence of other cell types such as CAFs and endothelial cells (for gating strategy see Supplementary Figures 2–4).

First, the overall immune infiltrate defined as CD45$^+$ cells was quantified as well as non-immune cells such as CAFs (Figure 2A). The tumor models showed large variations in CD45$^+$ cell infiltration, extending from poorly immune-infiltrated tumor models (EO771, CT26, and B16) to highly immune-infiltrated models such as MC38 and Pan02 (Figure 2A). The percentage of CAFs varied greatly between tumor models with the breast cancer model EO771 displaying the highest amount of CAFs (Figure 2A). Upregulation of PD-L1 by cancer cells or myeloid cells including tumor-associated macrophages (TAMs) is a common mechanism employed by tumors for evading immune-mediated elimination (2). Our analysis showed that PD-L1 expression was generally lower on cancer cells (CD45$^-$FAP$^-$CD31$^-$) compared to immune cells (CD45$^+$) (Figures 2B, C), but with some tumor models such as CT26 having a relatively high level of PD-L1 expression on cancer cells (Figure 2B). The expression of PD-L1 on immune cells followed a similar pattern with highest expression in MC38 and CT26 tumors (Figure 2C). Moreover, we observed expression of PD-L1 by CAFs, with a particularly high expression of PD-L1 on CAFs from CT26 and MC38 tumors (Figure 2D).

To expand our characterization of the TME, we analyzed the composition of tumor-infiltrating immune cells. Myeloid cells were divided into monocytic myeloid-derived suppressor cells (M-MDSCs) (CD11b$^+$F4/80$^-$Ly6C^{hi}Ly6G$^-$), polymorphonuclear (PMN)-MDSCs (CD11b$^+$F4/80$^-$Ly6C^{lo}Ly6G$^+$), dendritic cells (F4/80$^-$CD11c$^+$), and TAMs (CD11b$^+$F4/80$^+$). The M-MDSCs comprised a large fraction of the total number of cells in MC38 tumors and a low fraction in B16 and CT26 tumors (Figure 2E). In contrast, PMN-MDSCs made up a small fraction of cells in MC38 tumors and instead a larger fraction in the Pan02 and LL2 tumor model (Figure 2F). Dendritic cells made up a large fraction of cells in LL2 and MC38 tumors (Figure 2G). CD103$^+$ dendritic cells are critical for the generation of anti-tumor immune responses (59). We therefore analyzed the fraction of dendritic cells that belonged to this subset across the tumor models. In EO771, LL2, and MC38 tumors, CD103+ dendritic cells comprised a large fraction of dendritic cells, whereas this fraction was slightly smaller in the B16, Pan02, and CT26 tumors (Figure 2H).

TAMs made up a comparable proportion of cells across most of the tumor models, with a slightly larger fraction in B16 and MC38 tumors (Figure 2I). The fraction of TAMs that were CD206$^+$, which is an indicator of M2 polarization, was smallest in B16 tumors followed by LL2 tumors and equally large in the other models (Figure 2J).

The infiltration of lymphoid cells in the TME was also assessed. Notably, the largest amount of CD8$^+$ T cells was observed in Pan02, MC38, and CT26 tumors (Figure 2K). Within the CD8$^+$ T cell population, the proportion of PD-1$^+$ cells was highest in CT26 tumors and lowest in B16 and LL2 tumors (Figure 2L). CD4$^+$ T cells were most abundant in EO771, Pan02, and MC38 tumors (Figure 2M). The fraction of PD-1$^+$CD4$^+$ T cells was largest in
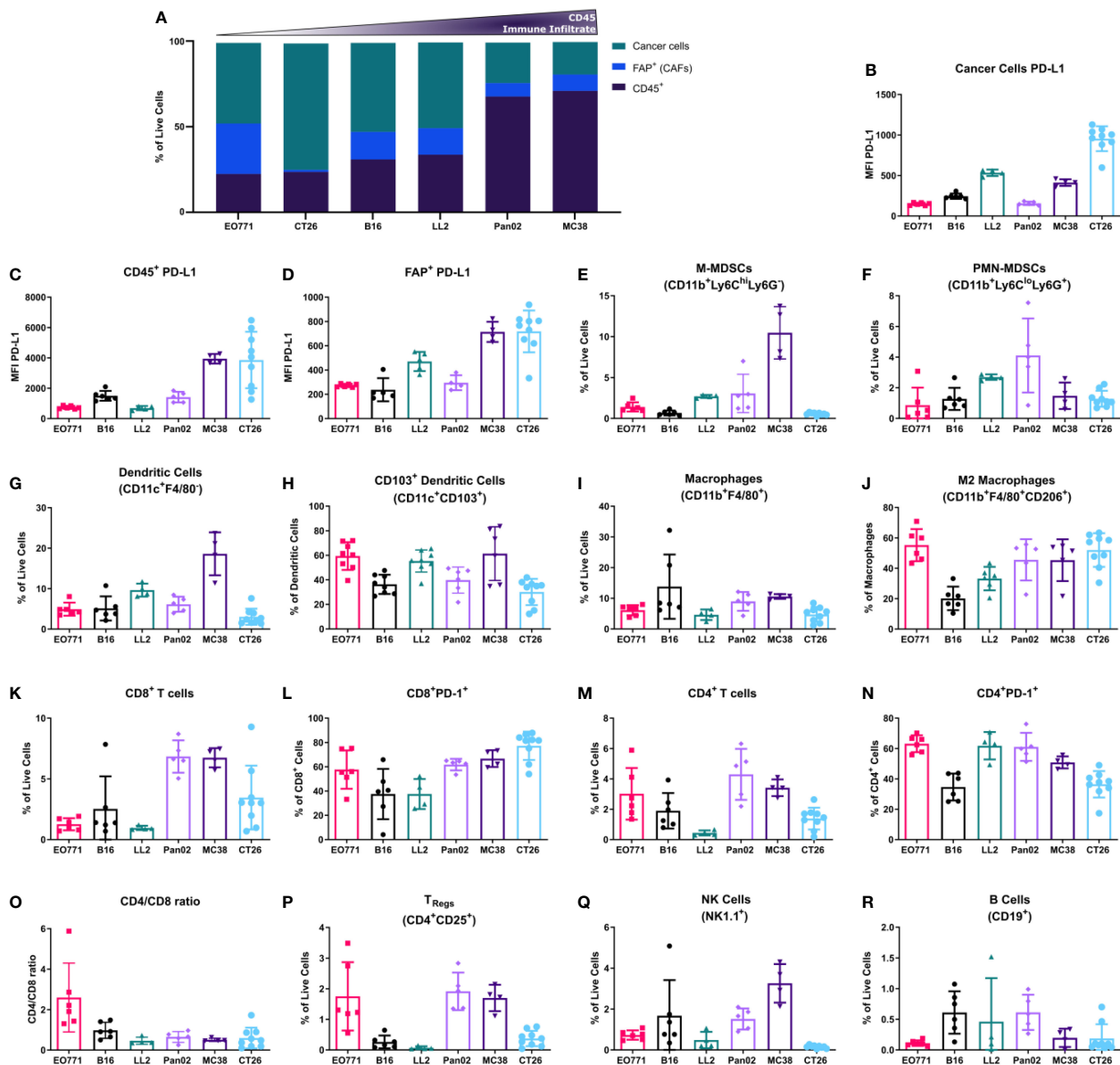
FIGURE 2

Flow cytometry analysis of the tumor microenvironment unveils different composition of immune populations across tumor models. **(A)** Histogram summarizing the median abundance (% of live cells) of cancer cells, CAFs, and immune cells; **(B-R)** PD-L1 median fluorescence intensity (MFI) expression on cancer cells **(B)**, CD45+ cells **(C)**, and FAP+ CAFs **(D)**; percentage of M-MDSCs **(E)**, PMN-MDSCs **(F)**, and dendritic cells **(G)** out of living cells; percentage of CD103+ dendritic cells out of all dendritic cells **(H)**; percentage of macrophages out of living cells **(I)**; percentage of M2-like macrophages out of all macrophages **(J)**; percentage of CD8+ T cells out of living cells **(K)**; percentage of PD-1+ CD8+ T cells out of all CD8+ T cells **(L)**; percentage of CD4+ T cells out of living cells **(M)**; percentage of PD-1+ CD4+ T cells out of all CD4+ T cells **(N)**; CD4/CD8 ratio **(O)**; percentage of TRegs **(P)**, NK cells **(Q)**, and B cells **(R)** out of living cells. **(A-D)** are based on the general flow cytometry panel, **(E-J)** are based on the myeloid flow cytometry panel, and **(K-R)** are based on the lymphoid flow cytometry panel.

EO771, LL2, and Pan02 tumors (Figure 2N). The differences in infiltration of CD8+ and CD4+ T cells led to a CD4/CD8 ratio that was high in EO771 tumors, intermediate in B16 tumors, and low in the other tumor models (Figure 2O). The highest numbers of CD25+CD4+ T cells, which in mice primarily represent regulatory T cells (Tregs) (60), were observed in EO771, Pan02, and MC38 tumors (Figure 2P). NK cells were most abundant in B16, Pan02, and MC38 tumors and almost completely absent in CT26 tumors (Figure 2Q). The number of tumor-infiltrating B cells was very low

in all models although slightly higher in B16, LL2, and Pan02 tumors (Figure 2R).

3.3 Transcriptomic analyses uncover clear immunological diversity between tumor models

To further analyze the immune composition of the TME, we took advantage of the ability to estimate the relative abundance of different

cellular components based on RNAseq data. Using the CIBERSORT tool (55), which allows for quantifications of cell fractions from bulk tissue gene expression profiles, we first compared the cell type abundances obtained from RNAseq and flow cytometry.

The absolute amount of immune infiltration in the tumors estimated using CIBERSORT was largely in line with the CD45$^+$ quantification by flow cytometry with the only exception of CT26 that based on the RNAseq data appeared more immune infiltrated compared to the flow cytometry-based analysis (Figure 3A, compare to Figure 2A). The estimated ratio of lymphoid to myeloid cells was also comparable to the flow cytometry data (Figure 3B). Additionally, we observed that the composition of the myeloid compartment differed quite a lot with for instance macrophage infiltration estimated substantially higher by CIBERSORT compared to the quantification by flow cytometry in all the models, except for the B16 tumors (Figure 3C). The composition of the lymphoid compartment was similar, although the number of NK cells was generally estimated to be higher compared to our flow cytometry data (Figure 3C).

Next, we utilized CIBERSORT to analyze T cell subsets. Notable differences in the composition of T cell subsets were observed between the tumor models (Figure 3D). The highest fractions of activated CD8$^+$ T cells were found in B16 and MC38 tumors, while CT26 tumors had the largest fraction of naïve CD8$^+$ cells (Figure 3D). Across all models, CT26 tumors contained the lowest fraction of T$_{regs}$, while this population accounted for larger proportions in Pan02, LL2, and EO771 tumors (Figure 3D). The predicted ratio of CD8$^+$ T cells to T$_{regs}$ was particularly high in CT26 and B16 tumors (Figure 3E).

3.4 Collagen content and tissue stiffness vary profoundly between tumor models

The ECM constitutes an important component of the TME with multiple tumor-promoting properties (61), including the suppression of immune-mediated killing of cancer cells (23, 27–
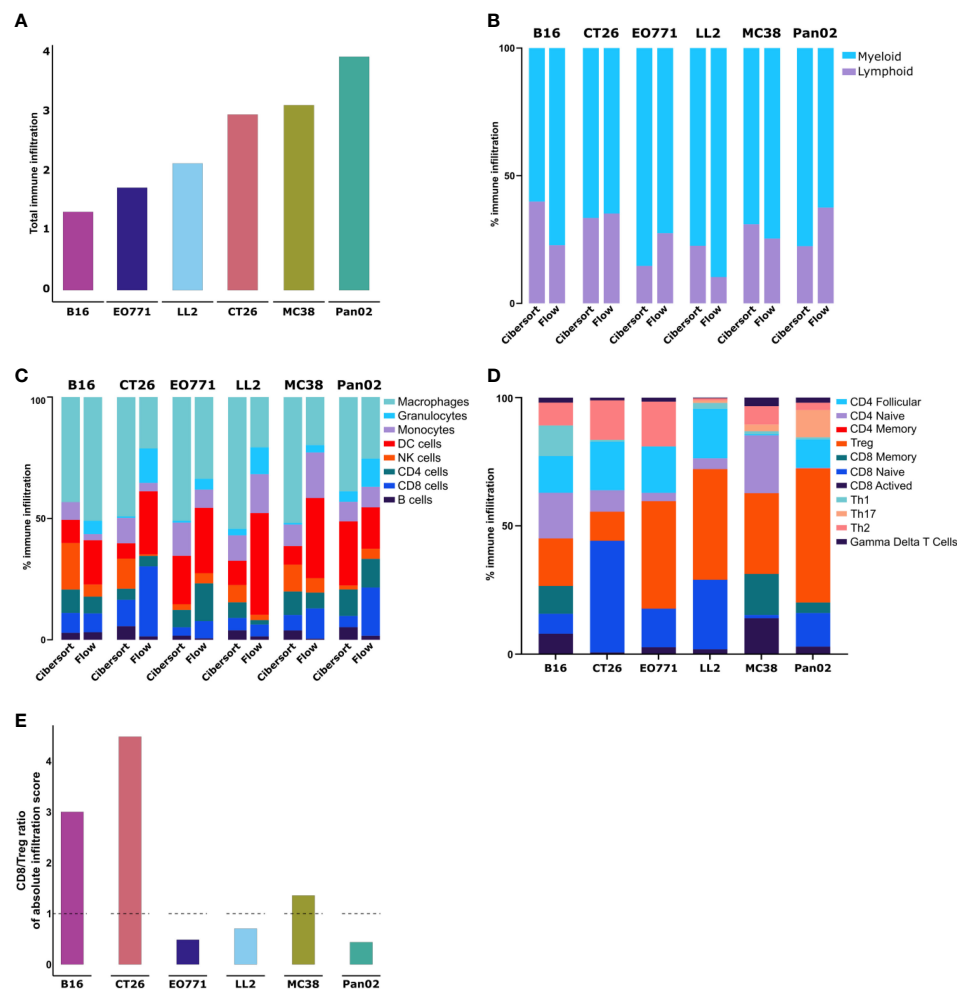
FIGURE 3

Transcriptomic analysis of whole tumors shows differences in immune cell composition between models. **(A)** Absolute amount of immune infiltration across six tumor models based on RNA isolated from tumor fragments analyzed using the CIBERSORT tool. **(B)** Ratio of lymphoid to myeloid cells based on RNAseq data analyzed using the CIBERSORT tool. **(C)** Comparison of immune cell population abundancies estimated from CIBERSORT and flow cytometry. **(D)** Abundancies of specific T cell subsets across the tumor models. **(E)** Ratio of CD8 to T^{regs} based on absolute infiltration score.

30). The quantitatively dominant ECM component is collagen type I, which is also an important contributor to increased tissue stiffness of solid tumors.

The mechanical stiffness of excised tumors was measured using shear rheology. Pan02 tumors had the highest tissue stiffness, while B16 tumors had the lowest stiffness (Figure 4A). All the other models displayed intermediate levels of stiffness (Figure 4A). Picrosirius red (PSR) staining was used to visualize and quantify fibrillar collagen-positive areas in paraffin-embedded tissue sections (Figures 4B, C). Pan02 tumors also had the highest levels of intratumorally deposited fibrillar collagen, and B16 tumors had the lowest levels (Figures 4B, C). In alignment with these quantifications, a positive correlation between the collagen-

positive area and tumor stiffness was observed (Figure 4D). CAFs are the main producers of collagen type I in the TME, but the collagen-positive area did not correlate with the number of tumor-infiltrating FAP⁺ CAFs (Figure 4E). This suggests that CAFs in the different models can acquire distinct phenotypes, which contribute to collagen deposition and tumor stiffness to various degrees.

3.5 Cancer-associated fibroblasts display model-specific transcriptional programs

The cell-surface serine protease FAP is a commonly used CAF-marker that is expressed on the majority of identified CAF subsets
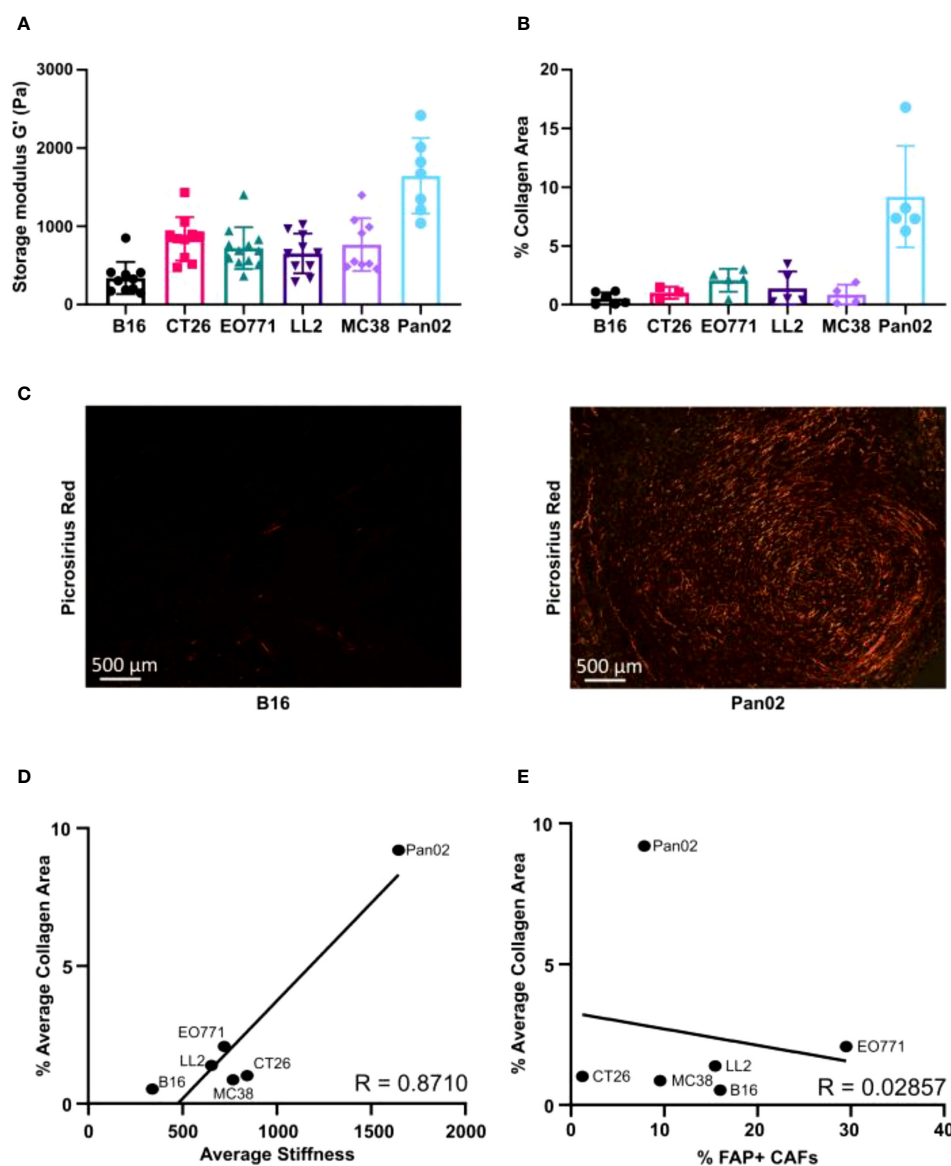
FIGURE 4
Relative extracellular matrix stiffness measurements by shear rheology varies profoundly between models. **(A)** Measurements of mechanical stiffness (storage modulus) for all the tumor models (n = 7-12). **(B)** Quantification of collagen based on picrosirius red (PSR) staining of paraffin-embedded tissue sections (n = 3-6). **(C)** Representative images of PSR staining in B16 (left) and Pan02 (right) tumor sections. **(D)** Correlation between storage modules (stiffness) and percentage of collagen positive area, analyzed by Pearson rank correlation (R = 0.8710). **(E)** Correlation between percentage of FAP+ CAFs and percentage of collagen positive area analyzed by Pearson rank correlation (R = 0.02857).

(43). To examine if CAFs acquire distinct phenotypes in the different tumor models, FAP+ CAFs were FACS-sorted for whole transcriptome analyses. For each tumor model, RNA was successfully obtained from two individual rounds of cell sorting, with the exception of B16 tumors from which we were unable to obtain RNA of sufficiently high quality. The gene expression dataset can be found in Supplementary Table 2. Based on a scree plot (Supplementary Figure 5), it was apparent that 3 principal components were describing most of the variation between samples. Therefore, we created a 3D PCA plot, which showed that the transcriptional program of CAFs varies between the different tumor models (Figure 5A). Fuzzy clustering analysis confirmed that the CAFs have distinct tumor model-specific gene expression profiles (Figure 5B). CAFs are centrally engaged in ECM remodeling associated with cancer progression (19). To investigate the tumor model-specific role of CAFs in these processes, the gene expression profiles of collagens and core matrisome genes were examined (Figures 5C, D). The analysis clearly showed that CAFs contribute to ECM production in solid tumors in unique ways depending on the tumor model. Moreover, the gene expression profile of genes encoding MMPs, which are critical enzymes for the cancer-associated degradation of ECM components, differed dramatically between tumor models (Figure 5E). In addition to the well-established role of CAFs in ECM remodeling, a growing body of evidence indicates that CAFs can also acquire an immunosuppressive phenotype and thereby promote tumor growth. Interestingly, a comparison of the expression of genes known to be involved in immunosuppression in the TME showed that CAFs had very different patterns of expression of these genes depending on the tumor model (Figure 5F). In the CT26 tumor model, CAFs expressed high levels of a range of transcripts encoding immunosuppressive molecules, including *Cd274*, *Tgfb1*, *Nos2*, *Arg1*, and *Lgals9*. This indicates that these CAFs could be important for inhibiting T cell activity in the TME.

To investigate how CAFs from the individual tumor models relate to CAF subsets described by others, we compared our RNAseq data to gene signatures based on single cell sequencing of murine 4T1 breast cancer (43) or murine KPC pancreatic cancer (42). The comparison did not show a perfect overlap between CAFs from the tumor models and the specific subsets but nevertheless indicated a tumor model-dependent skewing toward certain subsets (Figures 5G, H). CAFs from MC38 tumors showed similarities with vascular CAFs (vCAFs) and proliferating CAFs (prCAFs) identified in murine 4T1 breast tumors (Figure 5G). CAFs from Pan02 tumors showed similarities with antigen-presenting CAFs (apCAFs) identified in KPC tumors (Figure 5H). CAFs from CT26 tumors appeared very similar to the myofibroblastic CAFs (myCAFs) and inflammatory CAFs (iCAFs) identified in both 4T1 and KPC tumors (Figures 5G, H).

3.6 Tumor-infiltrating T cells promote an immunosuppressive CAF phenotype

CAFs from CT26 tumors had a distinct gene expression profile indicative of high immunosuppressive activity (Figures 5F–H) and

expressed higher levels of cell surface PD-L1 (Figure 2B). To investigate the importance of T cell infiltration for acquisition of the specific CAF phenotype in CT26 tumors, we compared tumors established in immunocompetent BALB/c mice and in T cell-deficient athymic BALB/c nude mice. Flow cytometry analysis of the TME confirmed that CD8+ T cells were absent in the nude mice (Figure 6A). The absence of CD8+ T cells was accompanied by a reduction in TAM infiltration (Figure 6B), whereas the abundance of other cell populations was unaffected (Figure 6C). The number of CAFs was similar between tumors from immunocompetent and nude mice (Figure 6D), but PD-L1 expression on CAFs was lower in the absence of CD8+ T cells (Figure 6E).

To further characterize the CAFs, FAP+ cells were FACS-isolated from CT26 tumors from immunocompetent mice and from nude mice (Supplementary Figure 6) and analyzed by qRT-PCR. There was a trend towards upregulation of genes encoding fibroblast activation markers (*Col1a1, Mrc2, Acta2*) in the presence of tumor-infiltrating CD8+ T cells (Figure 6F). We also assessed the expression of five genes implicated in CAF-mediated immune suppression. Among these, *Cxcl12* was significantly upregulated in the immunocompetent tumors, and there was a clear trend towards an upregulation of *Il6* and *Cd274* (PD-L1) (Figure 6F). These results suggest that tumor-infiltrating T cells could be critically involved in promoting activation of CAFs as well as an immunosuppressive CAF phenotype in the immunogenic CT26 tumor model.

4 Discussion

In this study, we compared the TMEs of six commonly used syngeneic mouse tumor models. For optimal comparison of the tumor models we exclusively used female mice, which are also easier than males to keep in harmonious groups. We cannot exclude that gender-dependent differences between the models could exist. Although several of the models have comparably fast tumor growth kinetics and appear macroscopically similar, we observed striking differences in the formed TME. RNAseq of dissected tumor tissue showed distinct gene expression profiles of each of the six tumor models. This information can potentially be utilized for the rational selection of appropriate tumor models for future studies. The distinct gene expression profiles could in part be due to the diversity in the cancer cell lines' tissue origins. However, further analysis of genes related to myeloid, lymphoid, and stromal cells indicated that distinct cellular composition of the TMEs also contributed to the observed differences. We also identified large differences in the expression of immunosuppressive genes, suggesting the acquisition of tumor model-specific mechanisms of immune escape. For instance, *Ido1* and *Ido2* are highly expressed in MC38 tumors, whereas Pan02 tumors have a strong TGF-β signature. Among the tumor models in our panel, MC38 and CT26 tumors, which are the most immunogenic, displayed the highest levels of PD-L1 gene expression.

Analysis of the cell composition of the TME using flow cytometry confirmed that the tumor models were infiltrated with highly varying numbers of immune and stromal cells. Even the two
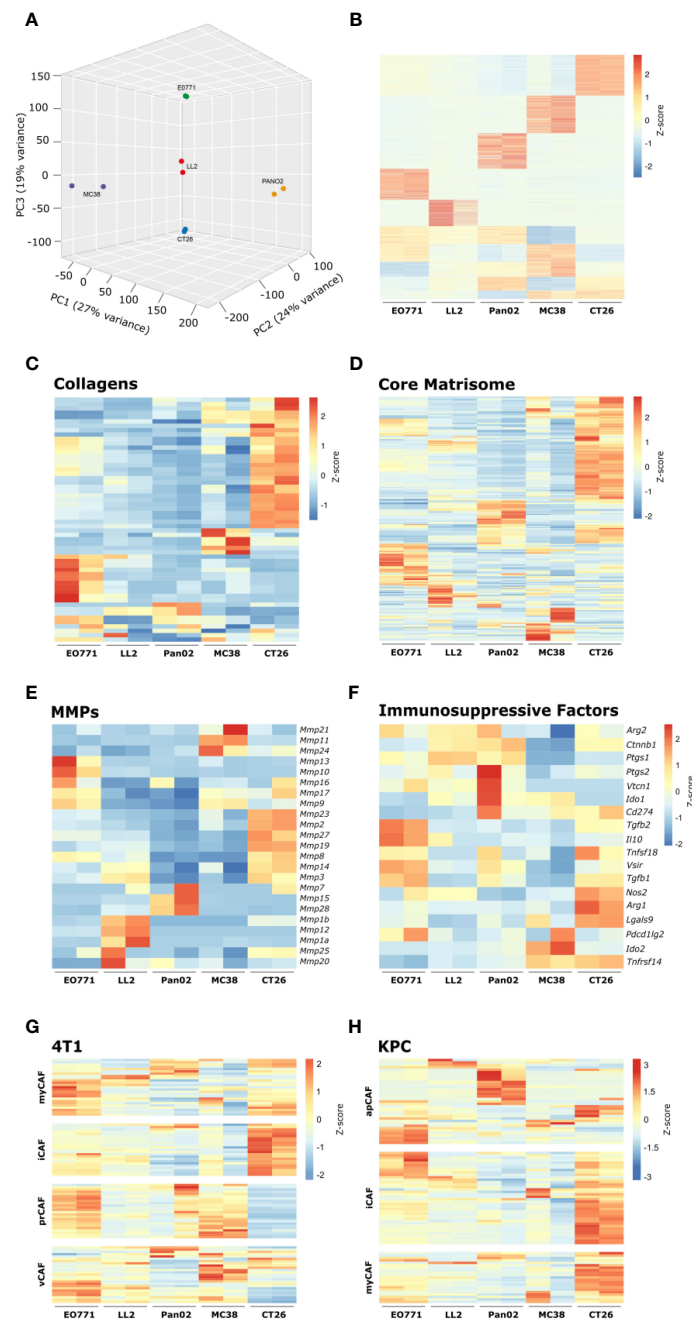
FIGURE 5

Transcriptomic analysis of isolated CAFs reveal model-specific transcriptional programs. **(A)** 3D PCA analysis based on RNAseq of FACS-isolated CAFs from tumors from five tumor models. **(B)** Fuzzy clustering analysis of RNA from isolated CAFs. **(C-F)** Heatmaps of normalized (Z-score) RNAseq read counts of genes encoding collagens **(C)**, core matrisome proteins **(D)**, MMPs **(E)**, and immunosuppressive factors **(F)**. **(G, H)** Comparison of RNAseq data from isolated CAFs from the indicated models with previously described CAF subsets from murine 4T1 breast cancer42 **(G)** and murine pancreatic cancer41 **(H)**.

colon cancer models, CT26 and MC38, were dramatically different, with MC38 tumors being much more immune infiltrated than CT26 tumors. The MC38 and CT26 tumor models are commonly used for immunotherapy research and knowledge about the distinct TMEs of these two models should be taken into account since different strategies could be required for successful immunotherapeutic efficacy in the two colorectal tumor models. It should be noted that the different strains of mice used for the

MC38 (C57BL/6) and CT26 tumors (BALB/c) could contribute to some of the observed differences. In addition to the overall level of immune infiltration, large differences in the composition of immune cells in the individual tumor models were observed. For instance, MC38 tumors contained high numbers of M-MDSCs whereas PMN-MDSCs were most abundant in LL2 and Pan02 tumors. It should be noted that we quantified PMN-MDSCs and M-MDSCs based solely on surface markers that would also identify
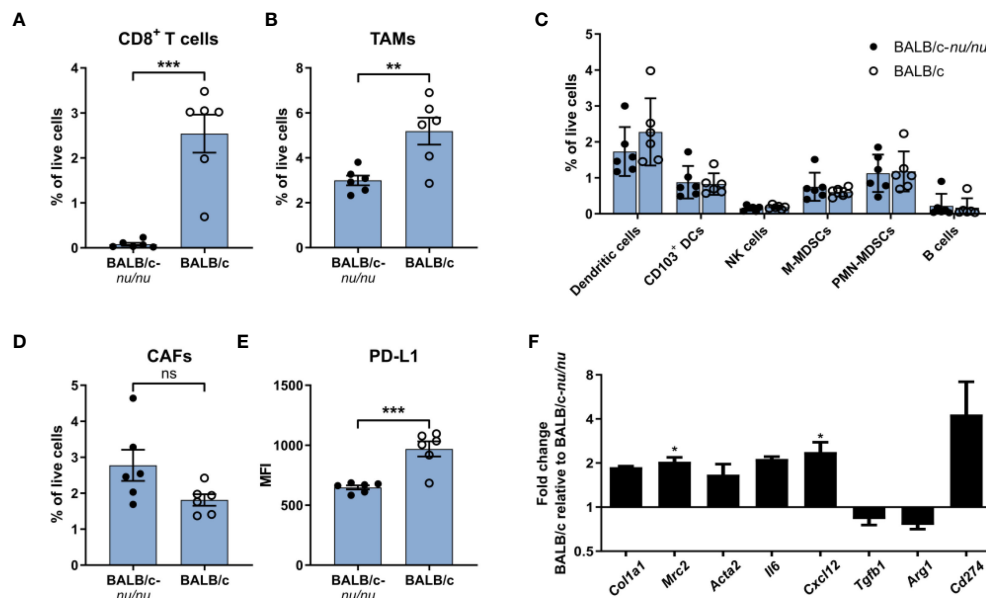
FIGURE 6
The immunosuppressive phenotype of CAFs is induced by tumor-infiltrating T cells. Flow cytometry analysis of CT26 tumors from athymic BALB/c nude (BALB/c nu/nu) mice (filled circles) and BALB/c mice (empty circles). **(A)** Percentage of CD8+ T cells out of live cells. **(B)** Percentage of TAMs (CD11b+F4/80+) out of live cells. **(C)** Percentage of six immune cell populations out of live cells. **(D)** Percentage of CAFs (CD45-FAP+) out of live cells. **(E)** PD-L1 MFI expression of CAFs. n = 6. **(F)** qRT-PCR analysis of a panel of genes associated with activation or immunosuppression in sorted FAP+ CAFs. Error bars indicate SEM. Statistical analysis was performed by two-tailed Student's t-test. *** = p ≤ 0.001, ** = p ≤ 0.01, * = p ≤ 0.05, not significant when p > 0.05. In review

granulocytes and monocytes, respectively (62). Further analyses would be needed to characterize and confirm the immunosuppressive activity of these cells.

As an alternative to flow cytometry-based profiling of the tumors, we also estimated the immune composition from bulk RNAseq data using the CIBERSORT tool. In regard to the overall infiltration of myeloid and lymphoid cells, the results were well in line with the flow cytometry-based profiling. However, the RNAseq-based estimation of the relative abundance of different myeloid cell types showed some discrepancies with the flow cytometry analysis. Although the flow cytometry analyses were limited by a relatively low number of surface markers to distinguish the individual cell populations, we speculate that a main reason for the discrepancy between the flow cytometry- and RNAseq-based analyses is that the gene signatures used to estimate cell type abundancies still require refinement. The tool is, however, extremely valuable in the absence of the possibility of flow cytometry analysis. In this study, the CIBERSORT tool enabled us to estimate the abundance of lymphocyte subsets for which required markers were not included in the flow cytometry analysis.

Our characterization of the TME complements previous reports investigating the immune cell composition in various tumor models based on flow cytometry or RNA sequencing (58, 63–65). Although some variations between the different studies are seen, our data is largely in line with these reports. Collectively, these studies form an excellent framework for the rational selection of appropriate tumor models for future cancer immunotherapy research. In addition to a characterization of the immune cell composition in tumors, we have in our study also examined the number and phenotype of

infiltrating CAFs as well as the tissue stiffness of the tumor models. These are components of the TME that can influence invasive tumor growth directly and modulate immune activity in the tumors.

An increased matrix stiffness, which is also reflected in increased tissue stiffness, has been strongly associated with aggressive tumor growth and poor prognosis in patients with gastrointestinal and breast cancer (66–69). Although the pro-tumorigenic role of increased matrix stiffness has been studied extensively, surprisingly little is known about the relative tissue stiffness of common syngeneic tumor models. Here, we showed that Pan02 tumors had the highest fibrillar collagen content and tissue stiffness, whereas B16 tumors had very low collagen content and tissue stiffness. The collagen content did not correlate with the number of CAFs, and indeed the CAFs in the different tumor models also displayed very distinct phenotypes. CAFs appeared to differ dramatically in their ECM remodeling abilities based on gene expression profiles.

Whole-transcriptome analysis of CAFs from the characterized tumor models suggested that they can acquire very different immunosuppressive functions. A comparison to CAF subset gene signatures obtained from studies of murine breast and pancreatic cancer showed some similarities to these subsets depending on the tumor model. The model-dependent skewing towards specific CAF subsets did, however, not give any further insight into the different collagen-levels observed in the tumor models. CAFs from CT26 tumors showed resemblance to myCAFs and iCAFs, which was in accordance with the high expression of matrisome genes and genes involved in immunosuppression, including *Cd274* encoding PD-L1.

It is still not well understood how large a role PD-L1 expressed by CAFs plays for the suppression of T cell activity within the TME. By comparing CAFs from CT26 tumors formed in immunocompetent or T cell-deficient athymic BALB/c mice, we observed that the presence of tumor-infiltrating T cells led to the upregulation of PD-L1 expression. The presence of T cells also led to increased expression of *Mrc2* (70, 71), which is associated with fibroblast activation, and *Cxcl12*, which is associated with the formation of an immunosuppressive and T cell-excluding TME (36, 41). Altogether, our data underscores that CAFs are highly plastic cells that are affected by cues from the TME and the observed gene expression profiles suggest that they can contribute to immunosuppression.

Data availability statement

The datasets presented in this study can be found in online repositories. The names of the repository/repositories and accession number(s) can be found below: The data has been uploaded to GEO (accession number GSE245293).

Ethics statement

The animal study was approved by the Danish Animal Experiment Council. The study was conducted in accordance with the local legislation and institutional requirements.

Author contributions

MC: Formal Analysis, Investigation, Validation, Visualization, Writing – original draft, Writing – review & editing. M-LT: Formal Analysis, Investigation, Validation, Visualization, Writing – original draft, Writing – review & editing. AS: Formal Analysis, Investigation, Validation, Visualization, Writing – review & editing. DA: Formal Analysis, Investigation, Validation, Visualization, Writing – review & editing. AJ: Investigation, Validation, Visualization, Writing – review & editing, Formal Analysis. KB: Formal Analysis, Investigation, Validation, Visualization, Writing – review & editing. SK: Formal Analysis, Investigation, Validation, Visualization, Writing – review & editing. AR: Formal Analysis, Investigation, Validation, Visualization, Writing – review & editing. KF: Formal Analysis, Investigation, Validation, Visualization, Writing – review & editing. DK: Formal Analysis, Investigation, Validation, Visualization, Writing – review & editing. MD: Methodology, Project administration, Resources, Writing – review & editing. LG: Formal Analysis, Methodology, Resources, Validation, Visualization, Writing – review & editing. DM: Conceptualization, Funding acquisition, Methodology, Project administration, Resources, Supervision, Validation, Visualization, Writing – original draft, Writing – review & editing. HL: Formal analysis, Visualization, Writing – review & editing.

Funding

Acknowledgments

Conflict of interest

The authors declare that the research was conducted in the absence of any commercial or financial relationships that could be construed as a potential conflict of interest.

Publisher's note

All claims expressed in this article are solely those of the authors and do not necessarily represent those of their affiliated organizations, or those of the publisher, the editors and the reviewers. Any product that may be evaluated in this article, or claim that may be made by its manufacturer, is not guaranteed or endorsed by the publisher.

Supplementary material

The Supplementary Material for this article can be found online at: https://www.frontiersin.org/articles/10.3389/fimmu.2023.1320614/full#supplementary-material

References

1. Sharma P, Allison J. The future of immune checkpoint therapy. *Science* (2015) 348 (6230):56–61. doi: 10.1126/science.aaa8172

2. Sharma P, Goswami S, Raychaudhuri D, Siddiqui BA, Singh P, Nagarajan A, et al. Immune checkpoint therapy—current perspectives and future directions. *Cell* (2023) 186(8):1652–69. doi: 10.1016/j.cell.2023.03.006

3. Vesely MD, Kershaw MH, Schreiber RD, Smyth MJ. Natural innate and adaptive immunity to cancer. *Annu Rev Immunol* (2011) 29:235–71. doi: 10.1146/annurev-immunol-031210-101324

4. Hodi FS, O'Day SJ, McDermott DF, Weber RW, Sosman JA, Haanen JB, et al. Improved survival with ipilimumab in patients with metastatic melanoma. *N Engl J Med* (2010) 363(8):711–23. doi: 10.1056/NEJMoa1003466

5. Larkin J, Chiarion-Sileni V, Gonzalez R, Grob JJ, Cowey CL, Lao CD, et al. Combined nivolumab and ipilimumab or monotherapy in untreated melanoma. *N Engl J Med* (2015) 373(1):23–34. doi: 10.1056/NEJMoa1504030

6. Restifo NP, Smyth MJ, Snyder A. Acquired resistance to immunotherapy and future challenges. *Nat Rev Cancer.* (2016) 16(2):121–6. doi: 10.1038/nrc.2016.2

7. Draghi A, Chamberlain CA, Furness A, Donia M. Acquired resistance to cancer immunotherapy. Seminars in Immunopathology. *Semin Immunopathology* (2019) 41:31–40. doi: 10.1007/s00281-018-0692-y

8. Fridman WH, Pagès F, Sautès-Fridman C, Galon J. The immune contexture in human tumours: Impact on clinical outcome. *Nat Rev Cancer.* (2012) 12(4):298–306. doi: 10.1038/nrc3245

9. Chen DS, Mellman I. Elements of cancer immunity and the cancer-immune set point. *Nature* (2017) 541(7637):321–30. doi: 10.1038/nature21349

10. Mellman I, Chen DS, Powles T, Turley SJ. The cancer-immunity cycle: Indication, genotype, and immunotype. *Immunity* (2023) 56(10):2188–205. doi: 10.1016/j.immuni.2023.09.011

11. Solito S, Marigo I, Pinton L, Damuzzo V, Mandruzzato S, Bronte V. Myeloid-derived suppressor cell heterogeneity in human cancers. *Ann N Y Acad Sci* (2014) 1319 (1):47–65. doi: 10.1111/nyas.12469

12. Ugel S, Canegrave S, De Sanctis F, Bronte V. Monocytes in the tumor microenvironment. *Annu Rev Pathol Mech Dis* (2021) 16:93–122. doi: 10.1146/annurev-pathmechdis-012418-013058

13. Madsen DH, Jürgensen HJ, Siersbæk MS, Kuczek DE, Grey Cloud L, Liu S, et al. Tumor-associated macrophages derived from circulating inflammatory monocytes degrade collagen through cellular uptake. *Cell Rep* (2017) 21(13):3662–71. doi: 10.1016/j.celrep.2017.12.011

14. Madsen DH, Leonard D, Masedunskas A, Moyer A, Jürgensen HJ, Peters DE, et al. M2-like macrophages are responsible for collagen degradation through a mannose receptor-mediated pathway. *J Cell Biol* (2013) 202(6):951–66. doi: 10.1083/jcb.201301081

15. Madsen DH, Bugge TH. Imaging collagen degradation in *vivo* highlights a key role for M2-polarized macrophages in extracellular matrix degradation. *Oncoimmunology* (2013) 2(12):e27127. doi: 10.4161/onci.27127

16. Barrett RL, Pure E. Cancer-associated fibroblasts and their influence on tumor immunity and immunotherapy. *Elife* (2020) 9:1–20. doi: 10.7554/eLife.57243

17. Davidson S, Coles M, Thomas T, Kollias G, Ludewig B, Turley S, et al. Fibroblasts as immune regulators in infection, inflammation and cancer. *Nat Rev Immunol* (2021) 21(11):704–17. doi: 10.1038/s41577-021-00540-z

18. Sahai E, Astsaturov I, Cukierman E, DeNardo DG, Egeblad M, Evans RM, et al. A framework for advancing our understanding of cancer-associated fibroblasts. *Nat Rev Cancer* (2020) 20(3):174–86. doi: 10.1038/s41568-019-0238-1

19. Chhabra Y, Weeraratna AT. Fibroblasts in cancer: Unity in heterogeneity. *Cell* (2023) 86(8):1580–609. doi: 10.1016/j.cell.2023.03.016

20. Mhaidly R, Mechta-Grigoriou F. Role of cancer-associated fibroblast subpopulations in immune infiltration, as a new means of treatment in cancer. *Immunol Rev* (2021) 302(1):259–72. doi: 10.1111/imr.12978

21. Thorseth M-L, Carretta M, Jensen C, Mølgaard K, Jürgensen HJ, Engelholm LH, et al. Uncovering mediators of collagen degradation in the tumor microenvironment. *Matrix Biol Plus* (2022) 13:100101. doi: 10.1016/j.mbplus.2022.100101

22. Madsen DH, Bugge TH. The source of matrix-degrading enzymes in human cancer: Problems of research reproducibility and possible solutions. *J Cell Biol* (2015) 209(2):195–8. doi: 10.1083/jcb.201501034

23. Rømer AMA, Thorseth M, Hargbøl DH, Madsen DH. Immune modulatory properties of collagen in cancer. *Front Immunol* (2021) 12:1–15. doi: 10.3389/fimmu.2021.791453

24. Levental KR, Yu H, Kass L, Lakins JN, Egeblad M, Erler JT, et al. Matrix crosslinking forces tumor progression by enhancing integrin signaling. *Cell* (2009) 139 (5):891–906. doi: 10.1016/j.cell.2009.10.027

25. Winkler J, Abisoye-Ogunniyan A, Metcalf KJ, Werb Z. Concepts of extracellular matrix remodelling in tumour progression and metastasis. *Nat Commun* (2020) 11 (1):5120. doi: 10.1038/s41467-020-18794-x

26. Acerbi I, Cassereau ID, Au A, Park C, Chen YY, Liphardt J, et al. Human breast cancer invasion and aggression correlates with ECM stiffness and immune cell infiltration. *Integr Biol* (2015) 7(10):1120–34. doi: 10.1039/c5ib00040h

27. Kuczek DE, Larsen AMH, Thorseth M-L, Carretta M, Kalvisa A, Siersbæk MS, et al. Collagen density regulates the activity of tumor-infiltrating T cells. *J Immunother Cancer* (2019) 7(1):68. doi: 10.1186/s40425-019-0556-6

28. Gordon-Weeks A, Yuzhalin AE. Cancer extracellular matrix proteins regulate tumour immunity. *Cancers (Basel).* (2020) 12(11):1–25. doi: 10.3390/cancers12113331

29. Salmon H, Franciszkiewicz K, Damotte D, Dieu-Nosjean M-CC, Validire P, Trautmann A, et al. Matrix architecture defines the preferential localization and migration of T cells into the stroma of human lung tumors. *J Clin Invest* (2012) 122 (3):899–910. doi: 10.1172/JCI45817

30. Larsen AMH, Kuczek DE, Kalvisa A, Siersbæk MS, Thorseth M, Johansen AZ, et al. Collagen density modulates the immunosuppressive functions of macrophages. *J Immunol* (2020) 205(5):1461–72. doi: 10.4049/jimmunol.1900789

31. Bunting MD, Vyas M, Requesens M, Langenbucher A, Schiferle EB, Manguso RT, et al. Extracellular matrix proteins regulate NK cell function in peripheral tissues. *Sci Adv* (2022) 8(11):1–20. doi: 10.1126/sciadv.abk3327

32. Sangaletti S, Chiodoni C, Tripodo C, Colombo MP. Common extracellular matrix regulation of myeloid cell activity in the bone marrow and tumor microenvironments. *Cancer Immunol Immunother* (2017) 66(8):1059–67. doi: 10.1007/s00262-017-2014-y

33. Feig C, Jones JO, Kraman M, Wells RJB, Deonarine A, Chan DS, et al. Targeting CXCL12 from FAP-expressing carcinoma-associated fibroblasts synergizes with anti-PD-L1 immunotherapy in pancreatic cancer. *Proc Natl Acad Sci U S A* (2013) 110(50):20212–7. doi: 10.1073/pnas.1320318110

34. Kato T, Noma K, Ohara T, Kashima H, Katsura Y, Sato H, et al. Cancer-associated fibroblasts affect intratumoral CD8β and Foxp3β T cells *via* IL6 in the tumor microenvironment. *Clin Cancer Res* (2018) 24(19):4820–33. doi: 10.1158/1078-0432.CCR-18-0205

35. Perez-Penco M, Weis-Banke SE, SChina A, Siersbæk M, Hübbe ML, Jørgensen MA, et al. TGFβ-derived immune modulatory vaccine: targeting the immunosuppressive and fibrotic tumor microenvironment in a murine model of pancreatic cancer. *J Immunother Cancer* (2022) 10(12):1–15. doi: 10.1136/jitc-2022-005491

36. Wang Z, Moresco P, Yan R, Li J, Gao Y, Biasci D, et al. Carcinomas assemble a filamentous CXCL12–keratin-19 coating that suppresses T cell–mediated immune attack. *Proc Natl Acad Sci* (2022) 119(4):1–11. doi: 10.1073/pnas.2119463119

37. Lakins MA, Ghorani E, Munir H, Martins CP, Shields JD. Cancer-associated fibroblasts induce antigen-specific deletion of CD8 + T Cells to protect tumour cells. *Nat Commun* (2018) 1):948. doi: 10.1038/s41467-018-03347-0

38. Li YL, Zhao H, Ren XB. Relationship of VEGF/VEGFR with immune and cancer cells: staggering or forward? *Cancer Biol Med* (2016) 13(2):206–14. doi: 10.20892/j.issn.2095-3941.2015.0070

39. Laxmanan S, Robertson SW, Wang E, Lau JS, Briscoe DM, Mukhopadhyay D. Vascular endothelial growth factor impairs the functional ability of dendritic cells through Id pathways. *Biochem Biophys Res Commun* (2005) 334(1):193–8. doi: 10.1016/j.bbrc.2005.06.065

40. Kanzaki R, Pietras K. Heterogeneity of cancer-associated fibroblasts: Opportunities for precision medicine. *Cancer Sci* (2020) 111(8):2708–17. doi: 10.1111/cas.14537

41. Costa A, Kieffer Y, Scholer-Dahirel A, Pelon F, Bourachot B, Cardon M, et al. Fibroblast heterogeneity and immunosuppressive environment in human breast cancer. *Cancer Cell* (2018) 33(3):463–479.e10. doi: 10.1016/j.ccell.2018.01.011

42. Elyada E, Bolisetty M, Laise P, Flynn WF, Courtois ET, Burkhart RA, et al. Cross-species single-cell analysis of pancreatic ductal adenocarcinoma reveals antigen-presenting cancer-associated fibroblasts. *Cancer Discovery* (2019) 9(8):1102–23. doi: 10.1158/2159-8290.CD-19-0094

43. Bartoschek M, Oskolkov N, Bocci M, Lövrot J, Larsson C, Sommarin M, et al. Spatially and functionally distinct subclasses of breast cancer-associated fibroblasts revealed by single cell RNA sequencing. *Nat Commun* (2018) 9(1):5150. doi: 10.1038/s41467-018-07582-3

44. Affo S, Nair A, Brundu F, Ravichandra A, Bhattacharjee S, Matsuda M, et al. Promotion of cholangiocarcinoma growth by diverse cancer-associated fibroblast subpopulations. *Cancer Cell* (2021) 39(6):866–882.e11. doi: 10.1016/j.ccell.2021.03.012

45. Li Q-X, Feuer G, Ouyang X, An X. Experimental animal modeling for immuno-oncology. *Pharmacol Ther* (2017) 173:34–46. doi: 10.1016/j.pharmthera.2017.02.002

46. Zitvogel L, Pitt JM, Daillère R, Smyth MJ, Kroemer G. Mouse models in oncoimmunology. *Nat Rev Cancer* (2016) 16(12):759–73. doi: 10.1038/nrc.2016.91

47. Bareham B, Georgakopoulos N, Matas-Céspedes A, Curran M, Saeb-Parsy K. Modeling human tumor-immune environments in *vivo* for the preclinical assessment of immunotherapies. *Cancer Immunol Immunother* (2021) 70(10):2737–50. doi: 10.1007/s00262-021-02897-5

48. Leach DR, Krummel MF, Allison JP. Enhancement of antitumor immunity by CTLA-4 blockade. *Science* (1996) 271(5256):1734–6. doi: 10.1126/science.271.5256.1734

49. Iwai Y, Terawaki S, Honjo T. PD-1 blockade inhibits hematogenous spread of poorly immunogenic tumor cells by enhanced recruitment of effector T cells. *Int Immunol* (2005) 17(2):133–44. doi: 10.1093/intimm/dxh194

50. Dobin A, Davis CA, Schlesinger F, Drenkow J, Zaleski C, Jha S, et al. STAR: Ultrafast universal RNA-seq aligner. *Bioinformatics* (2013) 29(1):15–21. doi: 10.1093/bioinformatics/bts635

51. Heinz S, Benner C, Spann N, Bertolino E, Lin YC, Laslo P, et al. Simple combinations of lineage-determining transcription factors prime cis-regulatory elements required for macrophage and B cell identities. *Mol Cell* (2010) 8(4):576–89. doi: 10.1016/j.molcel.2010.05.004

52. Schwämmle V, Jensen ON. VSClust: feature-based variance-sensitive clustering of omics data. *Bioinformatics* (2018) 34(17):2965–72. doi: 10.1093/bioinformatics/bty224

53. Naba A, Clauser KR, Ding H, Whittaker CA, Carr SA, Hynes RO. The extracellular matrix: Tools and insights for the "omics" era. *Matrix Biol* (2016) 49:10–24. doi: 10.1016/j.matbio.2015.06.003

54. Shao X, Gomez CD, Kapoor N, Considine JM, Grams C, Gao Y, et al. MatrisomeDB 2.0: 2023 updates to the ECM-protein knowledge database. *Nucleic Acids Res* (2023) 51(1 D):D1519–30. doi: 10.1093/nar/gkac1009

55. Newman AM, Liu CL, Green MR, Gentles AJ, Feng W, Xu Y, et al. Robust enumeration of cell subsets from tissue expression profiles. *Nat Methods* (2015) 12 (5):453–7. doi: 10.1038/nmeth.3337

56. Chen Z, Huang A, Sun J, Jiang T, Qin FXF, Wu A. Inference of immune cell composition on the expression profiles of mouse tissue. *Sci Rep* (2017) 7:1–11. doi: 10.1038/srep40508

57. Bankhead P, Loughrey MB, Fernández JA, Dombrowski Y, McArt DG, Dunne PD, et al. QuPath: Open source software for digital pathology image analysis. *Sci Rep* (2017) 7(1):1–7. doi: 10.1038/s41598-017-17204-5

58. Zhong W, Myers JS, Wang F, Wang K, Lucas J, Rosfjord E, et al. Comparison of the molecular and cellular phenotypes of common mouse syngeneic models with human tumors. *BMC Genomics* (2020) 21(1):1–17. doi: 10.1186/s12864-019-6344-3

59. Roberts EW, Broz ML, Binnewies M, Headley MB, Nelson AE, Wolf DM, et al. Critical role for CD103+/CD141+ Dendritic cells bearing CCR7 for tumor antigen trafficking and priming of T cell immunity in melanoma. *Cancer Cell* (2016) 0(2):324–36. doi: 10.1016/j.ccell.2016.06.003

60. Solomon I, Amann M, Goubier A, Arce Vargas F, Zervas D, Qing C, et al. CD25-Treg-depleting antibodies preserving IL-2 signaling on effector T cells enhance effector activation and antitumor immunity. *Nat Cancer* (2020) 1(12):1153–66. doi: 10.1038/s43018-020-00133-0

61. Pickup MW, Mouw JK, Weaver VM. The extracellular matrix modulates the hallmarks of cancer. *EMBO Rep* (2014) 15(12):1243–53. doi: 10.15252/embr.201439246

62. Veglia F, Sanseviero E, Gabrilovich DI. Myeloid-derived suppressor cells in the era of increasing myeloid cell diversity. *Nat Rev Immunol* (2021) 21(8):485–98. doi: 10.1038/s41577-020-00490-y

63. Mosely SIS, Prime JE, Sainson RCA, Koopmann J-O, Wang DYQ, Greenawalt DM, et al. Rational selection of syngeneic preclinical tumor models for immunotherapeutic drug discovery. *Cancer Immunol Res* (2017) 5(1):29–41. doi: 10.1158/2326-6066.CIR-16-0114

64. Yu JW, Bhattacharya S, Yanamandra N, Kilian D, Shi H, Yadavilli S, et al. Tumor-immune profiling of murine syngeneic tumor models as a framework to guide mechanistic studies and predict therapy response in distinct tumor microenvironments. *PLoS One* (2018) 13(11):1–27. doi: 10.1371/journal.pone.0206223

65. van Elsas M, Kleinovink JW, Moerland M, Feiss G, Beyrend G, Arens R, et al. Host genetics and tumor environment determine the functional impact of neutrophils in mouse tumor models. *J Immunother Cancer* (2020) 8(2):e000877. doi: 10.1136/jitc-2020-000877

66. Ohno S, Tachibana M, Fujii T, Ueda S, Kubota H, Nagasue N. Role of stromal collagen in immunomodulation and prognosis of advanced gastric carcinoma. *Int J Cancer* (2002) 97(6):770–4. doi: 10.1002/ijc.10144

67. Li C, Zheng Z, Wu X, Xie Q, Liu P, Hu Y, et al. Stiff matrix induced srGAP2 tension gradients control migration direction in triple-negative breast cancer. *Theranostics* (2023) 13(1):59–76. doi: 10.7150/thno.77313

68. Conklin MW, Eickhoff JC, Riching KM, Pehlke CA, Eliceiri KW, Provenzano PP, et al. Aligned collagen is a prognostic signature for survival in human breast carcinoma. *Am J Pathol* (2011) 178(3):1221–32. doi: 10.1016/j.ajpath.2010.11.076

69. Drifka CR, Loeffler AG, Mathewson K, Keikhosravi A, Eickhoff JC, Liu Y, et al. Highly aligned stromal collagen is a negative prognostic factor following pancreatic ductal adenocarcinoma resection. *Oncotarget* (2016) 7(46):76197–213. doi: 10.18632/oncotarget.12772

70. Madsen DH, Jürgensen HJ, Ingvarsen S, Melander MC, Vainer B, Egerod KL, et al. Endocytic collagen degradation: A novel mechanism involved in protection against liver fibrosis. *J Pathol* (2012) 227(1):94–105. doi: 10.1002/path.3981

71. Jürgensen HJ, van Putten S, Nørregaard KS, Bugge TH, Engelholm LH, Behrendt N, et al. Cellular uptake of collagens and implications for immune cell regulation in disease. *Cell Mol Life Sci* (2020) 77(16):3161–76. doi: 10.1007/s00018-020-03481-3

Glioblastoma with high O6-methyl-guanine DNA methyltransferase expression are more immunologically active than tumors with low *MGMT* expression

Yoshihiro Kushihara[1,2], Shota Tanaka[1], Yukari Kobayashi[2], Koji Nagaoka[2], Miyu Kikuchi[1], Takahide Nejo[1], Erika Yamazawa[1,3], Shohei Nambu[1], Kazuha Kugasawa[1], Hirokazu Takami[1], Shunsaku Takayanagi[1], Nobuhito Saito[1] and Kazuhiro Kakimi[2,4]*

[1]Department of Neurosurgery, Graduate School of Medicine, The University of Tokyo, Tokyo, Japan, [2]Department of Immunotherapeutics, The University of Tokyo Hospital, Tokyo, Japan, [3]Genome Science and Medicine, Research center for Advanced Science and technology, The University of Tokyo, Tokyo, Japan, [4]Department of Immunology, Kindai University Faculty of Medicine, Osakasayama, Osaka, Japan

Background: Glioblastoma (GBM) is a highly lethal brain tumor. The effectiveness of temozolomide (TMZ) treatment in GBM is linked to the methylation status of O6-methyl-guanine DNA methyltransferase (*MGMT*) promoter. Patients with unmethylated *MGMT* promoter have limited treatment options available. Consequently, there is a pressing need for alternative therapeutic strategies for such patients.

Methods: Data, including transcriptomic and clinical information, as well as information on *MGMT* promoter methylation status in primary GBM, were obtained from The Cancer Genome Atlas (TCGA) (n=121) and Chinese Glioma Genome Atlas (CGGA) (n=83) datasets. Samples were categorized into high and low *MGMT* expression groups, MGMT-high (MGMT-H) and MGMT-low (MGMT-L) tumors. A comprehensive transcriptome analysis was conducted to explore the tumor-immune microenvironment. Furthermore, we integrated transcriptome data from 13 GBM patients operated at our institution with findings from tumor-infiltrating lymphocyte (TIL) cultures, specifically investigating their response to autologous tumors.

Results: Gene signatures associated with various immune cells, including CD8 T cells, helper T cells, B cells, and macrophages, were noted in MGMT-H tumors. Pathway analysis confirmed the enrichment of immune cell-related pathways. Additionally, biological processes involved in the activation of monocytes and lymphocytes were observed in MGMT-H tumors. Furthermore, TIL culture experiments showed a greater presence of tumor-reactive T cells in MGMT-H tumors compared to MGMT-L tumors. These findings suggest that MGMT-H

tumors has a potential for enhanced immune response against tumors mediated by CD8 T cells.

Conclusion: Our study provides novel insights into the immune cell composition of MGMT-H tumors, which is characterized by the infiltration of type 1 helper T cells and activated B cells, and also the presence of tumor-reactive T cells evidenced by TIL culture. These findings contribute to a better understanding of the immune response in MGMT-H tumors, emphasizing their potential for immunotherapy. Further studies are warranted to investigate on the mechanisms of *MGMT* expression and antitumor immunity.

1 Introduction

Glioblastoma (GBM) is the most common and lethal malignant brain tumor. Despite its standard-of-care treatments, consisting of maximal safe surgical resection, radiotherapy and chemotherapy with temozolomide (TMZ), the median overall survival (OS) is approximately 16 months (1). It has been widely accepted that O6-methyl-guanine DNA methyltransferase (*MGMT*) promoter methylation in GBM is associated with a benefit from TMZ treatment (1, 2). The cytotoxic effects of TMZ are exerted by the induction of O6-methylguanine (O6mG), leading to the inhibition of DNA replication. MGMT is a DNA repair protein that removes the cytotoxic O6mG DNA lesions generated by TMZ; thereby, MGMT expression, which is suppressed by methylation of *MGMT* promoter, is mechanistically linked to TMZ resistance (3, 4). Patients with unmethylated *MGMT* promoter and high MGMT expression lack effective treatment options and have a poor prognosis. Therefore, there is an urgent need for a new treatment approach, especially for those patients.

Given the ongoing need for innovative treatment methods to enhance outcomes for glioblastoma patients and the proven effectiveness of immune checkpoint inhibitors (ICI) in different types of tumors, researchers are now exploring the potential of ICI in treating glioblastoma. However, thus far, all tested immunotherapies for glioblastoma (GBM) have been unsuccessful in improving clinical outcomes for unselected patient groups. Notably, trials using nivolumab (NIVO), an anti-PD-1 therapy, have failed to show a survival advantage in GBM patients. For instance, in the CheckMate 143 trial, NIVO did not outperform bevacizumab in unselected patients (5), and in the CheckMate 498 study, the combination of PD-1 blockade with radiotherapy did not improve survival compared to the cohort receiving temozolomide plus radiotherapy in patients with an unmethylated MGMT promoter (6). In another trial, CheckMate 548 found that NIVO, combined with temozolomide and radiotherapy, was not superior

to temozolomide, radiotherapy, and placebo in newly diagnosed GBM patients with a methylated MGMT promoter (7). It is necessary to consider treatment options based on the characteristics of the intratumoral immune response in GBM.

A recent study analyzed the association between the main molecular profile of GBM and specific immunological markers (8). It found that the expression of CD8 and CD68, assessed by immunohistochemistry, was higher in GBM cases with unmethylated *MGMT* promoter than those with the methylated counterpart (9). This suggests that the difference in MGMT status contributes to the formation of a unique tumor microenvironment. The importance of *MGMT* methylation status is widely recognized and has been incorporated into clinical trials as well as decision-making for actual treatment for patients. However, among studies, various methodologies are leveraged, such as methylation-specific PCR (MSP), pyrosequencing, or more high-throughput genome-wide methylation arrays, which makes direct comparisons challenging. On the other hand, strong inverse correlations between *MGMT* methylation and its mRNA expression status have been reported. Therefore, in this study, we chose to focus on the transcript-level expression of *MGMT*, instead of its methylation status (4). Our study aimed to define further the immunological tumor microenvironment of GBM with low *MGMT* expression and elucidate its immunological features. We, for the first time, integrated transcriptome data with data from tumor-infiltrating lymphocyte (TIL) cultures to assess the actual contribution of the immunological tumor microenvironment.

2 Materials and methods

2.1 Patients

The discovery cohort for this study consisted of GBM data obtained from The Cancer Genome Atlas (TCGA). Transcriptomic

and clinical data, along with information on *MGMT* promoter methylation status in primary GBM, were acquired from the TCGA Genome Data Commons Data portal (https://portal.gdc.cancer.gov) (download date; 2019/11/11) and cBioportal for Cancer Genomics (https://www.cbioportal.org)(download date; 2019/11/27), respectively. The TCGA-GBM dataset contained 155 cases of primary GBM, of which 121 cases had available information on *MGMT* promoter methylation. Consequently, the analysis was performed on this subset of 121 cases with known *MGMT* promoter methylation status.

The Chinese Glioma Genome Atlas (CGGA) dataset, specifically the mRNAseq_325 series, was employed as the validation cohort. Transcriptomic and clinical data, including information on *MGMT* promoter methylation status in primary GBM, were obtained from the CGGA database (http://www.cgga.org.cn/) (download date; 2019/09/09). Within the mRNAseq_325 series, a total of 85cases of primary GBM were identified, out of which 83 cases had available information on *MGMT* promoter methylation. Accordingly, the analysis focused on this subset.

Furthermore, an additional validation cohort, referred to as the University of Tokyo Hospital (UTH) cohort, was included in the analysis. This cohort comprised 13 consecutive primary GBM patients who underwent surgical resection at The University of Tokyo Hospital between November 2017 and December 2020. RNA samples were extracted from the resected tissues and subjected to RNA-sequencing (RNA-Seq) analysis. All procedures involving human participants were conducted in compliance with the institution's ethical standards, following the guidelines outlined in the 1964 Helsinki Declaration and its subsequent revisions or comparable ethical standards. The study received approval from the research ethics committees of the University of Tokyo (Approval No. G3545), and written informed consent was obtained from all individual participants included in the study. Detailed patient characteristics for the three data cohorts are presented in Table 1 and Supplementary Table 1.

2.2 Clinical sample processing

GBM tumors were collected immediately after surgical resection and frozen in liquid nitrogen for subsequent RNA extraction. The tumor tissue was also processed using the Tumor Dissociation Kit, human (Miltenyi Biotec, Bergisch Gladbach, Germany) and the gentleMACS Octo Dissociator (Miltenyi) to ensure efficient dissociation. The resulting tissue suspensions were then filtered through a 70 μm filter. These suspensions, referred to as fresh tumor digest (FTD), were frozen and stored in a 1:1 mixture of CP-1 (Kyokuto Pharmaceutical Industrial Co. Ltd., Tokyo, Japan) and RPMI-1640 medium (Nacalai Tesque, Kyoto, Japan). FTD was stored in liquid nitrogen to maintain viability for future use in TIL culture.

2.3 RNA extraction

Total RNA samples from the fresh frozen tissues were extracted using the AllPrep DNA/RNA/miRNA Universal Kits (Qiagen, Hilden, Germany), following the manufacturer's instructions. The extracted RNAs were then evaluated for quality and quantity. For next-generation sequencing (NGS), RNA samples meeting the following criteria were selected: a concentration of ≥ 20.0 ng/μL, a total amount of ≥ 0.4 μg, and a RNA integrity number (RIN) of ≥ 7.0, as assessed using the Agilent 2200 TapeStation (Agilent Technologies, Santa Clara, CA, USA).

2.4 RNA-sequencing (RNA-seq)

For RNA-Seq library preparation, the NEBNext[®] UltraTM RNA Library Prep Kit for Illumina[®] (Agilent Technologies) was utilized, following the manufacturer's protocols. The prepared libraries were subjected to sequencing as 150-bp paired-end reads using the NovaSeq platform (Illumina, San Diego, CA, USA) at

TABLE 1 Patient characteristics of the three data cohorts.

		Discovery Cohort	Validation Cohort	Experimental Cohort	
		TCGA_GBM Primary Tumor (n=121)	CGGA_mRNAseq325 GBM Primary Tumor (n=83)	TheUTH GBM Primary Tumor (n=13)	p
Age at diagnosis, mean ± s.d.		60.8 ± 14.1	48.9 ± 12.3	63.3 ± 13.6	< 0.0001
Gender, n(%)	Male	73(60)	51(61)	7(54)	0.873
	Female	48(40)	32(39)	6(46)	
MGMT promoter methylation, n(%)	Methylated	55(45)	32(39)	7(54)	0.454
	Unmethylated	66(55)	51(61)	6(46)	
IDH1 mutation, n(%)	Wild type	113(93)	72(87)	13(100)	0.132
	Mutant type	8(7)	11(13)	0(0)	

VERITAS (Danvers, MA, USA). Each sample yielded approximately 35.1 million reads of 150 base pairs in length on average. The obtained reads were then aligned to the reference genome (GRCh38/hg38) using STAR (v.2.5.2b) (10). Expression values were calculated as fragments per kilobase of exon per million fragments mapped (FPKM) using HTSeq (v.0.6.1) (11) and the R programming language (version 3.4.3; https://www.r-project.org/).

2.5 Differentially expressed genes (DEGs)

Samples were binarily classified into high and low expression groups, MGMT-high (MGMT-H) and MGMT-low (MGMT-L) tumors, according to the median value of *MGMT* mRNA expression. The raw counts obtained from RNA-Seq data were subjected to normalization. Subsequently, the differential expression analysis between MGMT-H tumors and MGMT-L tumors was performed using R version 3.6.2, utilizing the TCC (12) and edgeR (13) packages. Genes showing statistically significant differential expression were identified as differentially expressed genes (DEGs) based on the criteria of a p-value less than 0.05 and a False Discovery Rate (FDR) q-value less than 0.05.

2.6 Gene ontology (GO) functions enrichment analysis

We conducted a gene ontology (GO) functions enrichment analysis using Metascape (http://metascape.org) to elucidate the differences in the main activation processes associated with MGMT status. This comprehensive web resource facilitates data management and analysis (14). We obtained GO terms for the biological process (BP) category from the Molecular Signature Database v7.1 (MSigDB; https://www.gsea-msigdb.org/gsea/msigdb). The enrichment analysis of GO terms for biological processes was performed on the DEGs obtained from the TCC analysis using Metascape. Results were deemed significant if the p-value was less than 0.05 and the FDR q-value was less than 0.05.

2.7 Ingenuity pathway analysis (IPA)

DEGs obtained from the TCC analysis were analyzed using the Ingenuity Pathway Analysis (IPA) software (QIAGEN, Redwood City, CA, USA), accessible at https://www.qiagen.com/ingenuity. The core analysis in IPA encompassed various components, including canonical pathways, upstream regulators, regulator effects, and diseases and biological functions. Advanced algorithms incorporating machine learning techniques were utilized during the analysis (https://qiagen.my.salesforce-sites.com/KnowledgeBase/articles/Knowledge/Graphical-Summary). A Graphical Summary, consolidating the outcomes of the core analysis into a single network diagram, was generated to provide a concise representation of the results.

2.8 Gene set enrichment analysis (GSEA)

Gene set enrichment analysis (GSEA) was conducted to compare the expression levels between the MGMT-H and MGMT-L groups. Specifically, we employed GSEA version 4.1.0 to assess the differential expression of gene sets related to GO terms for BPs associated with characteristic functions in MGMT status. Additionally, we calculated a single-sample GSEA (ssGSEA) (15) score using R version 3.6.2 with the GSVA (16) package version 1.38.2. Results were deemed significant if the p-value was less than 0.05 and the FDR q-value was less than 0.05.

2.9 Calculation of tumor-infiltrating immune cell (TIC) fractions by transcriptome

To determine the proportions of tumor-infiltrating immune cell (TIC) fractions in MGMT-H and MGMT-L tumors, we employed CIBERSORTx and ssGSEA. For CIBERSORTx analysis, we utilized the absolute-mode algorithm based on the LM22 gene signature. The LM22 gene signature was obtained from https://CIBERSORTx.stanford.edu/. The algorithm was executed with 1000 permutations to estimate the proportions of TICs. This allowed us to quantify specific immune cell types within the tumor microenvironment. In parallel, we performed ssGSEA (15) using R version 3.6.2 with the GSVA (16) package version 1.38.2. The ssGSEA analysis was conducted using 28 subpopulations of TILs gene sets (17), referred to as "Charoentong_TIL_28 immunophenotype" in this study. This method enabled the assessment of the enrichment scores for each TIC subpopulation, providing insights into the immune landscape of the tumors. Furthermore, we calculated the "Tumor Immune and Dysfunction and Exclusion (TIDE) score," "Dysfunction" score, and "Exclusion" scores using the TIDE web application (http://tide.dfci.harvard.edu/) (18). These scores measure tumor immune response, immune dysfunction, and immune exclusion, respectively.

2.10 Hierarchical clustering

We utilized an unsupervised hierarchical clustering algorithm for the transcriptome analysis data, which included GO terms BP process ssGSEA scores and TIC fractions. This analysis used R version 3.6.2 with the pheatmap package version 1.0.12. To generate the hierarchical clustering, we calculated the squared Euclidean distance between the samples. This distance measure quantifies the dissimilarity between samples based on their transcriptome profiles. We then applied an agglomerative algorithm with Ward's method, which iteratively merges clusters to minimize the within-cluster variance.

2.11 Molecular diagnosis

Regarding the IDH mutations observed in GBM, they were identified using the Sanger method. Polymerase chain reaction (PCR) was performed using tumor DNA from 13 cases in the UTH cohort. For IDH1 mutations, KOD FX Neo (Toyobo, Osaka, Japan) DNA polymerase was utilized, while for IDH2 mutations, AmpliTaq GoldTM DNA Polymerase with Buffer I (Applied Biosystems, Waltham, MA) was employed. Supplementary Table 2A presents the primer sequences, annealing temperatures, and lengths of the amplified PCR fragments for IDH mutation analysis. Sequence analysis of the PCR product was performed by FASMAC Corporation (Kanagawa, Japan). Mutation analysis was performed with DNADynamo software (BLUE TRACTOR SOFTWARE Ltd, North Wales, UK).

For the assessment of *MGMT* promoter methylation, MSP was employed. Tumor DNA was subjected to bisulfite conversion using the EZ DNA Methylation-Gold Kit (Zymo Research, Irvine, CA) following the provided protocol. The primers were designed to amplify the CpG-rich region of the *MGMT* promoter region based on a previous publication (19). Supplementary Table 2B provides the primer sequences, annealing temperatures, and lengths of the resulting PCR fragments for *MGMT* promoter methylation analysis. Following PCR, electrophoresis was performed to determine the presence or absence of methylation in the *MGMT* promoter region. Episcope® Methylated GCT116 gDNA (Takara Bio Inc., Shiga, Japan) was used as a methylation control, and Episcope® Unmethylated GCT116 DKO gDNA (Takara Bio Inc., Shiga, Japan) was used as an unmethylated control for methylation determination.

2.12 Immunohistochemistry

Immunohistochemistry (IHC) was performed on 4µm-thick sections prepared from formalin-fixed paraffin-embedded (FFPE) samples. Automated IHC staining was conducted at Kyodo Byori Co., Ltd. (Kobe, Japan), using specific antibodies diluted with BOND Polymer Refine Detection (Leica Biosystems, Newcastle, UK) on the Leica Bond-MAX automated immunohistochemistry staining system, following the manufacturer's instructions. The antibodies used were targeted against CD4, CD8, CD20, CD68, and CD163. Each section was digitally imaged using the BIOREVO-9000 fluorescence microscope (Keyence, Osaka, Japan), and the BZ-II Analyzer image analysis software (Keyence, Osaka, Japan) was utilized to quantify the area of IHC positive staining and calculate the IHC positive staining area per unit tumor area (µm2).

2.13 TIL culture

Under sterile conditions, surgically resected tumor specimens from the UTH cohort were divided into three parts: one for RNA-Seq, one for FTD and one for TIL culture. For TIL culture, tumors were minced using scalpels immediately after resection. The minced tumor tissues were then incubated for 2-3 weeks at 37°C in RPMI 1640 medium (Nacalai Tesque) supplemented with CTS™ Immune Cell Serum Replacement (5%, Gibco, NY, USA), HEPES buffer solution (10mM, Dojindo, Kumamoto, Japan), MEM Non-essential Amino Acids Solution (Wako, Osaka, Japan), Sodium Pyruvate (1mM, Wako, Osaka, Japan), 2-mercaptoethanol (Invitrogen, CA, USA), penicillin/streptomycin (Nacalai Tesque), Interleukin-2 (IL-2) (6000U/mL, PeproTech, NJ, USA), and an Indoleamine 2,3-dioxygenase inhibitor (IDOi) called 1-methyl-L-tryptophan (100uM, Sigma-Aldrich, MO, USA). The tissue and culture medium were placed in a 24-well plate (Corning, Corning, NY). The cultivation period for TIL was set to 2-3week. The lymphocyte count in the TIL culture medium was determined using flow cytometry. Live cells were identified with 7-AAD Viability Staining Solution (BioLegend, #420404), and mononuclear cells within that subset were gated and counted using flow-count beads, Flow-Count Fluorospheres (Beckman Coulter, #7547053). Stained cells were analyzed on a Gallios flow cytometer (Beckman Coulter), and data were processed using Kaluza (Beckman Coulter). Positive TIL proliferation was defined as obtaining 3.0×10^5 or more TILs per well (Supplementary Figure 1A). The TIL culture rate was calculated as the ratio of the number of wells with positive TIL proliferation to the total number of cultured wells. This measure assessed TIL culture's success rate in terms of obtaining viable and proliferating TILs.

2.14 Interferonγ (IFNγ) Enzyme-Linked Immuno-Sorbent Assay (ELISA)

To aassess the tumor reactivity of cultured TIL, FTD was thawed and examined for the viability of the tumor cells. Only FTD with satisfactory viability of tumor cells was utilized. Subsequently, the FTD was co-cultured with TIL for 20-24 hours. TIL and FTD were also independently cultured for 20-24 hours as background controls. At the time of thawing, FTD was evaluated for viability. After incubation, the culture supernatant was collected, and the levels of IFNγ were measured using an ELISA kit (Thermo Fisher Scientific, Waltham, MA, USA) following the manufacturer's protocols.

The tumor-reactive IFNγ was calculated using the following formula:

$$\text{Tumor} - \text{reactive IFN}\gamma$$

$$= \text{IFN}\gamma\,(\text{TIL} + \text{FTD}) - [\text{IFN}\gamma\,(\text{TIL}) + \text{IFN}\gamma\,(\text{FTD})]$$

Here, IFNγ (TIL+FTD) represents the amount of IFNγ in the supernatant of the TIL+FTD co-culture, IFNγ (TIL) represents the amount of IFNγ in the supernatant of TIL alone, and IFNγ (FTD) represents the amount of IFNγ in the supernatant of FTD alone.

The tumor-specific immune response was considered positive if the amount of tumor-reactive IFNγ exceeded 100 pg/ml (Supplementary Figure 1B). Each patient's tumor-reactive immune response rate was defined as the ratio of the number of wells exhibiting a tumor-reactive immune response to the total number of cultured wells.

2.15 Statistics

The statistical analyses for continuous variables were performed with the Wilcoxon rank-sum test. In the comparison of three groups for continuous variables, the Kruskal-Wallis test was performed. The analyses for nominal variables were performed with Fisher's exact test. Statistical significance was set at P < 0.05 and FDR < 0.05 except for the differential gene expression and gene set enrichment analysis. All statistical analyses and plotting were performed using R 3.6.2. or JMP Pro 16 (SAS Institute Japan, Tokyo, Japan).

3 Results

3.1 DEGs in MGMT-H and MGMT-L tumors

The *MGMT* gene is epigenetically silenced through its promoter methylation, leading to decreased MGMT expression. However, factors other than *MGMT* promoter methylation, such as p53, SP-1, and NF-κB, are also known to regulate MGMT expression (3). Interestingly, some cases with *MGMT* promoter methylation exhibit high MGMT expression (Figure 1A). Given the lack of standardized methodology for methylation analysis (3), we classified the samples into two groups based on *MGMT* mRNA expression levels: MGMT-H (high expression) and MGMT-L (low expression). The classification used the median value of *MGMT* mRNA expression as the threshold (Figure 1B; Supplementary Table 1). This binary classification approach allows us to compare the characteristics and outcomes between the high and low *MGMT* expression groups across different cohorts.

In our comprehensive gene expression analysis of the TCGA-GBM cohort, we compared the RNA-seq data of MGMT-H and MGMT-L tumors. Our analysis revealed 3761 DEGs between them. Among these DEGs, 2637 were up-regulated, and 1124 were down-regulated in MGMT-H tumors (Figure 1C). We performed pathway and process enrichment analysis using the GO Biological Process in the Metascape database to gain insights into the biological functions associated with these DEGs. The DEGs up-regulated in MGMT-H tumors were found to be closely related to immune response processes, including "adaptive immune response," "complement activation," and "response to chemokine" (Figure 1D). On the other hand, the DEGs up-regulated in MGMT-L tumors were primarily involved in gene replication, expression, and regulation processes, such as "brain development," "covalent chromatin modification," and "mRNA metabolic process" (Figure 1E). Furthermore, we conducted IPA to gain further insights into the underlying mechanisms and downstream effects of the observed gene expression changes (Figure 1F). The IPA analysis indicated that factors such as IFNG, TNF, IL21, CCL2, and CCL11 are expected to be up-regulated in the MGMT-H group. This suggests enhanced lymphocyte migration through activating these factors in MGMT-H tumors. Our findings highlight the distinct biological functions and pathways associated with MGMT-H and MGMT-L tumors, particularly in immune response and gene regulation processes.

3.2 GSEA analysis of MGMT-H and MGMT-L tumors

In the Metascape analysis, each DEG's gene expression levels were not considered. To conduct a more comprehensive analysis, we performed GSEA, which incorporates gene expression levels. GSEA analysis was conducted on MGMT-H and MGMT-L tumors using the MSigDB Biological Process category. Among the top 30 activated processes in MGMT-H tumors (Supplementary Table 3A), immune-related processes were predominant. Conversely, the top 30 activated processes in MGMT-L tumors were primarily associated with gene replication, expression, and regulation (Supplementary Table 3B).

To further investigate these top 30 biological processes, we performed ssGSEA on each patient. The ssGSEA scores of these biological processes were compared between MGMT-H and MGMT-L tumors (Figure 2). T cell-related immune processes, such as "T cell-mediated cytotoxicity" and "lymphocyte chemotaxis," were found to be activated in MGMT-H tumors (Figure 2A). These findings suggest that MGMT-H tumors exhibit a more potent anti-tumor immunity induction against GBM cells than MGMT-L tumors. Additionally, B cell-related immune processes, including "complement activation," "regulation of humoral immune response," "positive regulation of B cell activation," and "regulation of complement activation," were also activated in MGMT-H tumors. These results indicate a potential connection between B cell immunity and anti-tumor immunity in MGMT-H tumors or suggest the formation of tertiary lymphoid structure in the tumor. Furthermore, the process of monocyte migration ("monocyte chemotaxis") and the process associated with antigen recognition for phagocytosis by macrophages and antigen-presenting cells ("phagocytosis recognition") were activated. These results suggest the activation of T cell-mediated anti-tumor immunity in MGMT-H tumors. In line with the Metascape analysis, immune-related processes were not found to be activated in MGMT-L tumors. Instead, processes associated with GBM tumor characteristics, such as cell division, gene expression, and histone modification, were found to be activated (Figure 2B).

3.3 Immune cell profiling and phenotyping of MGMT-H and MGMT-L tumors

Subsequently, we conducted immune cell profiling to quantify the abundance and identify the specific types of immune cells infiltrating the tumors. We utilized the LM22 signature matrix within the CIBERSORTx platform for this analysis, which covers 22 immune cell types (Figure 3A). However, it is important to note that the LM22 immune subsets do not provide information regarding the phenotype, activation, or differentiation status of the immune cells. To overcome this limitation, we implemented the ssGSEA method using a set of 28 subpopulations of TILs gene sets, referred to as the "Charoentong TIL 28 immunophenotype" (17) (Figure 3B). This approach allowed us to examine T cell

FIGURE 1

Gene expression patterns characteristic of MGMT-H/L groups. **(A)** The relationship between the methylation of the *MGMT* promoter region and gene transcription is depicted in panel. **(B)** The samples were classified into two groups, namely low expression and high expression, based on the median value of *MGMT* expression. **(C)** The M-A plot illustrates the differential expression of genes (DEGs) that are either up-regulated or down-regulated in the TCGA GBM dataset. This plot shows the relationship between the average concentration (log mean expression) and fold-change (log fold change) across the genes. Genes with dots located above 0 on the y-axis indicate lower expression in MGMT-H patients compared to MGMT-L patients, while genes with dots located below 0 on the y-axis indicate higher expression in MGMT-H patients compared to MGMT-L patients. Each gene is represented by a black dot on the plot. The magenta dots indicate significant DEGs that meet the criteria for a significant adjusted P value of less than 0.05 and an FDR q-value of less than 0.05. A Metascape enrichment analysis was conducted to identify statistically enriched ontology terms (specifically, Gene Ontology Biological Process terms) using the set of DEGs. A bar graph was generated to display the enriched terms associated with the upregulated gene set in MGMT-H **(D)** and MGMT-L **(E)**. Each term is represented by a bar, and the color of each bar corresponds to the p-value associated with the enrichment. The color gradient reflects the significance of the enrichment, with darker shades indicating more significant p-values. **(F)** The Ingenuity Pathway Analysis (IPA) was utilized to generate graphical pathways based on the DEGs. In the graphical pathways, factors expected to be highly expressed in MGMT-H are represented by a black legend, while factors expected to be highly expressed in MGMT-L are represented by a blue legend. The network analysis revealed that genes related to adaptive immune reactions, such as IFNG and TNF, were highly upregulated in MGMT-H. Consequently, this led to an upregulation of lymphocyte chemotaxis in MGMT-H. In contrast, genes such as IL37, RICTOR, NR1H2 were highly expressed in MGMT-L.

FIGURE 2

The ssGSEA values in the top 30 most highly expressed gene sets in each of the MGMT-H/L groups in MSigDB C5 Biological Process gene sets. ssGSEA was performed using gene sets associated with the top 30 most highly expressed genes in MGMT-H **(A)** and MGMT-L **(B)** tumors. Wilcoxon test, *: P <0.05; **: P <0.01; ***: P <0.001; n.s.: P ≧0.05.

phenotypes and functional states more comprehensively by incorporating these gene sets. By leveraging these specific gene sets, we gained insights into T cells' phenotypic and functional characteristics within the tumor microenvironment. This methodology provides a more detailed understanding of the diverse T cell populations and their functional states in the tumors under investigation.

In the CIBERSORTx analysis, we observed that the scores for CD8 T cells were significantly higher (p = 0.015), while the scores

for naive CD4 T cells were significantly lower (p = 0.028) in MGMT-H tumors compared to MGMT-L tumors (Figure 3A). However, there were no significant differences in other immune cell populations between MGMT-H and MGMT-L tumors. Furthermore, when utilizing the Charoentong 28 TIL immunophenotype gene set analysis, we found that the ssGSEA scores for activated CD8 T cells (p = 0.040), type 1 T helper cells (p = 0.026), activated B cells (p = 0.015), and macrophages (p = 0.017) were significantly higher in MGMT-H tumors compared to

MGMT-L tumors (Figure 3B). These findings reinforce the notion that immune responses are actively engaged and enhanced in MGMT-H tumors. Taken together, these results support the notion that MGMT-H tumors exhibit heightened immune activation and potentially more robust anti-tumor immune responses compared to MGMT-L tumors.

Furthermore, we utilized the TIDE web application (http://tide.dfci.harvard.edu) (18) to assess immune evasion signatures (Figure 3C). The dysfunction scores, which reflect the degree of T cell dysfunction, were slightly higher in MGMT-H tumors compared to MGMT-L tumors, although the difference did not reach statistical significance (p = 0.405). These findings indicate that MGMT-H tumors exhibit a higher level of T cell infiltration that may have undergone functional impairment or dysfunction.

3.4 Validation with the CGGA GBM cohort

We extended our analysis to validate the pathways enriched in MGMT-H or MGMT-L tumors and the highly expressed infiltrating immune cell phenotypes using the CGGA GBM cohort. We observed that *MGMT* expression was generally higher in *MGMT* promoter unmethylated tumors compared to methylated tumors. However, it is worth noting that some *MGMT* promoter methylated tumors still exhibited high levels of *MGMT* expression (Figure 4A). Therefore, similar to the discovery cohort, we classified samples into low and high groups based on the median value of *MGMT* expression (Figure 4B).

Using the MSigDB C5 BP gene sets that are highly expressed in each of the MGMT-H/L groups identified in the comparison
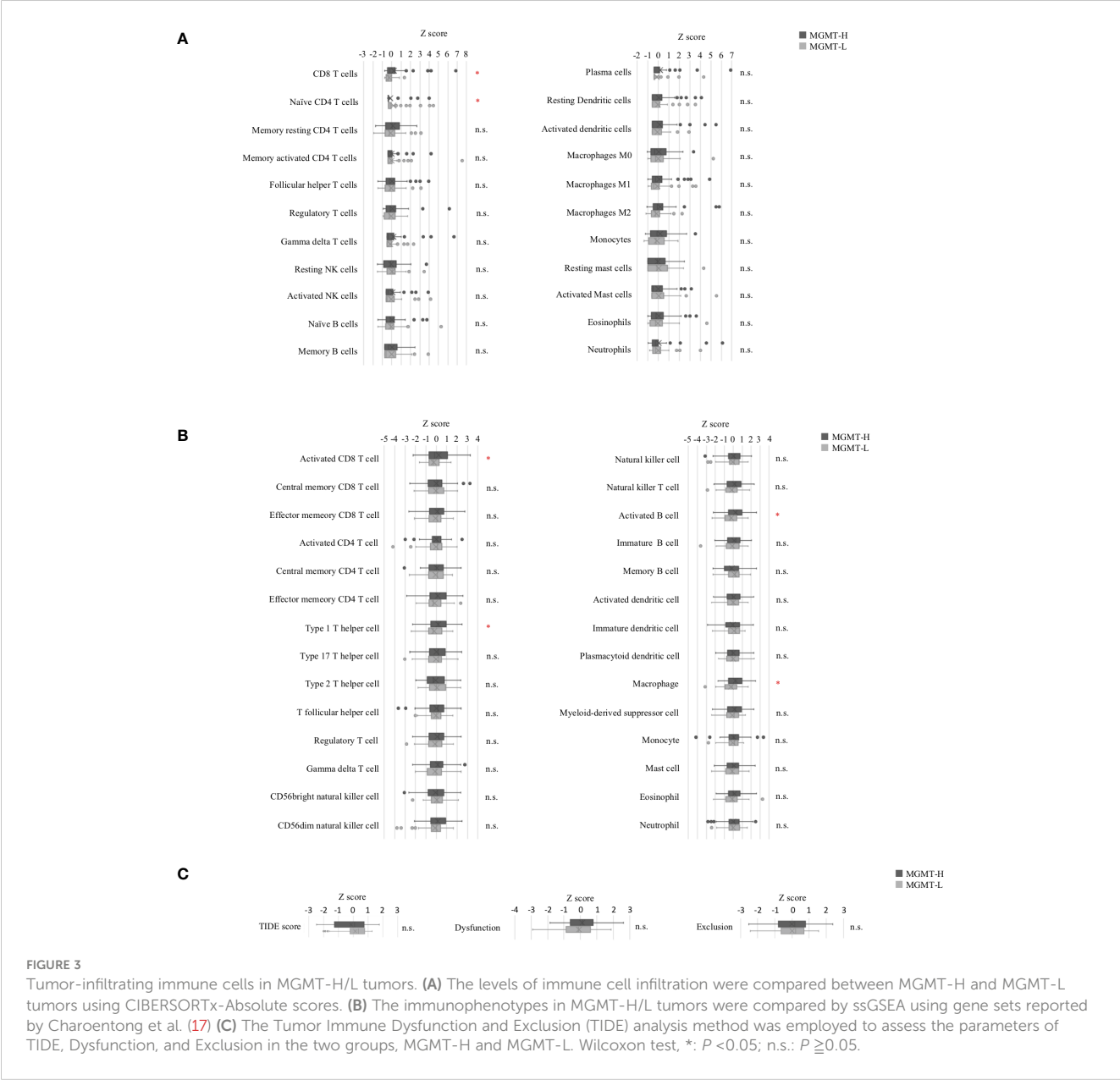
FIGURE 3

Tumor-infiltrating immune cells in MGMT-H/L tumors. **(A)** The levels of immune cell infiltration were compared between MGMT-H and MGMT-L tumors using CIBERSORTx-Absolute scores. **(B)** The immunophenotypes in MGMT-H/L tumors were compared by ssGSEA using gene sets reported by Charoentong et al. (17) **(C)** The Tumor Immune Dysfunction and Exclusion (TIDE) analysis method was employed to assess the parameters of TIDE, Dysfunction, and Exclusion in the two groups, MGMT-H and MGMT-L. Wilcoxon test, *: $P <0.05$; n.s.: $P \geq 0.05$.
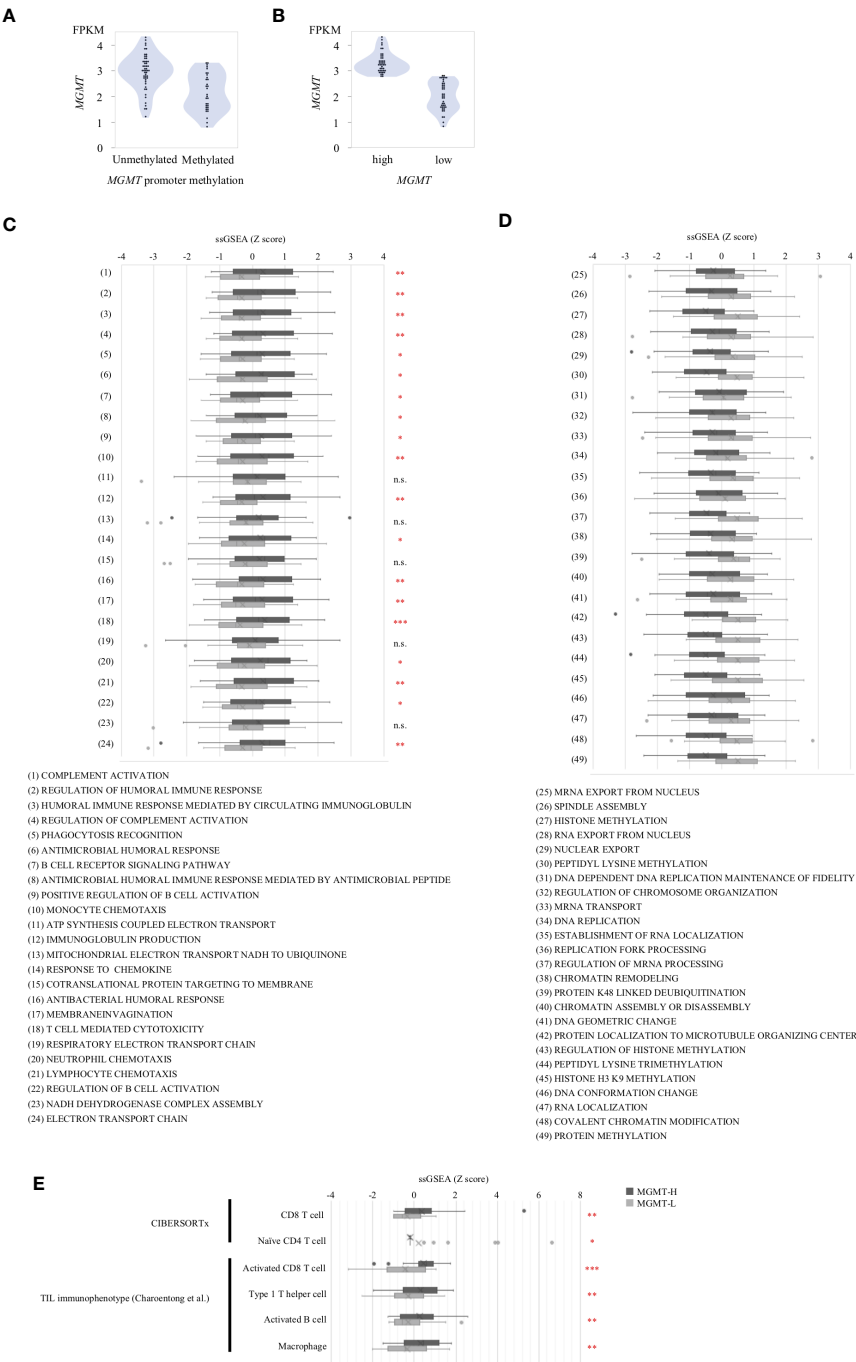
FIGURE 4

Validation Analysis in CGGA cohort. **(A)** *MGMT* mRNA expression in CGGA human GBM correlated with the methylation of *MGMT* promoter region. **(B)** The samples were classified into two groups, namely low expression and high expression, based on the median value of *MGMT* expression. Gene sets from the MSigDB Biological Process category that significantly different between MGMT-H and MGMT-L tumors in TCGA cohort were applied to CGGA cohort. **(C)** The set of genes within MSigDB C5 BP that were highly expressed in the MGMT-H group detected in the TCGA database were validated in CGGA. **(D)** The set of genes within MSigDB C5 BP that were highly expressed in the MGMT-L group detected in the TCGA database were validated in CGGA. **(E)** Immunophenotypes highly expressed in the MGMT-H group detected in the TCGA database were validated in CGGA. Wilcoxon test, *: P <0.05; **: P <0.01; ***: P <0.001; n.s.: P ≥0.05.

between the MGMT-H/L groups in the TCGA GBM cohort, we also performed ssGSEA analysis in the CGGA GBM cohort. ssGSEA values of those gene sets were used to compare the two MGMT-H/L groups in the CGGA GBM cohort (Figures 4C, D). Consistent with the findings in the TCGA cohort, 19 out of 24 gene sets enriched in

MGMT-H tumors displayed higher ssGSEA scores in MGMT-H tumors compared to MGMT-L tumors in the CGGA GBM cohort (Figure 4C). Similarly, 22 out of 25 gene sets enriched in MGMT-L tumors showed higher ssGSEA scores in MGMT-L tumors compared to MGMT-H tumors (Figure 4D). Furthermore, Digital

cytometry results in the TCGA GBM cohort were also validated in the CGGA GBM cohort. Specifically, we calculated the absolute scores of T cell CD8 and T cell CD4 naive using CIBERSORTx and the ssGSEA scores of activated CD8 T cell, type 1 T helper cell, activated B cell, and macrophage using the Charoentong TIL 28 immunophenotype gene set. These values were used for MGMT-H/L intergroup comparisons (Figure 4E). Notably, we obtained similar results in the CGGA GBM cohort, further supporting the consistency of our findings across different datasets. Overall, the validation in the CGGA GBM cohort provides robustness to our results, confirming the enriched pathways and immune cell phenotypes characteristic of MGMT-H and MGMT-L tumors identified in the discovery cohort.

3.5 Immunophenotyping of GBM using selected gene sets

The distinct gene sets are summarized in Table 2 that characterize MGMT-H and MGMT-L GBM tumors by analyzing the TCGA cohort and validating the findings using the CGGA cohort. Based on the gene sets enriched in MGMT-H and MGMT-L tumors, we immunophenotyped the GBM tumor microenvironment through hierarchical clustering (Figure 5). In Figure 5A, we observed a subgroup of cases with higher scores for immune-related gene sets, including activated CD8 T cell, type 1 T helper cell, activated B cell, and macrophage. The TIDE and Dysfunction scores were high in these cases, while the Exclusion scores were low. These results suggest an increased immune

response and infiltration of immune cells into the tumor microenvironment in these cases. Conversely, there was another subgroup of cases with higher scores for GBM tumor-related processes, such as cell division, gene expression, and histone modification. These results indicate a dominance of tumor-specific processes in these cases. Consistent with the TCGA cohort, we observed a similar pattern in the CGGA GBM cohort (Figure 5B). Immune-related gene sets were more activated in MGMT-H tumors compared to MGMT-L tumors, while GBM tumor-related process gene sets were more activated in MGMT-L tumors compared to MGMT-H tumors. Overall, these findings demonstrate the distinct immunophenotypes and gene expression profiles associated with MGMT-H and MGMT-L GBM tumors, highlighting the complex interplay between the tumor microenvironment and tumor-specific processes.

3.6 Molecular diagnosis and immunohistochemical analysis

The results of the analysis in the TCGA and CGGA cohorts were also validated in the UTH cohort.

In the UTH cohort, consisting of 13 GBM patients, all cases were IDH wild-type, with MGMT promoter methylation observed in 6 cases and unmethylation in 7cases (Supplementary Table 4). We divided them into MGMT-H group (6 patients) and MGMT-L group (7 patients) based on their MGMT expression levels (Figures 6A, B). First, the results of the digital cytometry analysis were also validated in the UTH cohort. Consistent with the findings

TABLE 2 The distinct gene sets that characterize MGMT-H and MGMT-L GBM tumors.

	High expression gene sets in MGMT-H	High expression gene sets in MGMT-L
MSigDB C5 Biological Process	COMPLEMENT ACTIVATION REGULATION OF HUMORAL IMMUNE RESPONSE HUMORAL IMMUNE RESPONSE MEDIATED BY CIRCULATING IMMUNOGLOBULIN REGULATION OF COMPLEMENT ACTIVATION PHAGOCYTOSIS RECOGNITION ANTIMICROBIAL HUMORAL RESPONSE B CELL RECEPTOR SIGNALING PATHWAY ANTIMICROBIAL HUMORAL IMMUNE RESPONSE MEDIATED BY ANTIMICROBIAL PEPTIDE POSITIVE REGULATION OF B CELL ACTIVATION MONOCYTE CHEMOTAXIS IMMUNOGLOBULIN PRODUCTION RESPONSE TO CHEMOKINE ANTIBACTERIAL HUMORAL RESPONSE MEMBRANE INVAGINATION T CELL MEDIATED CYTOTOXICITY NEUTROPHIL CHEMOTAXIS LYMPHOCYTE CHEMOTAXIS REGULATION OF B CELL ACTIVATION GOBP_ELECTRON_TRANSPORT_CHAIN	MRNA EXPORT FROM NUCLEUS SPINDLE ASSEMBLY HISTONE METHYLATION RNA EXPORT FROM NUCLEUS NUCLEAR EXPORT PEPTIDYL LYSINE METHYLATION REGULATION OF CHROMOSOME ORGANIZATION MRNA TRANSPORT ESTABLISHMENT OF RNA LOCALIZATION REGULATION OF MRNA PROCESSING CHROMATIN REMODELING GPROTEIN K48 LINKED DEUBIQUITINATION CHROMATIN ASSEMBLY OR DISASSEMBLY DNA GEOMETRIC CHANGE PROTEIN LOCALIZATION TO MICROTUBULE ORGANIZING CENTER REGULATION OF HISTONE METHYLATION PEPTIDYL LYSINE TRIMETHYLATION HISTONE H3 K9 METHYLATION DNA CONFORMATION CHANGE RNA LOCALIZATION COVALENT CHROMATIN MODIFICATION PROTEIN METHYLATION
CIBERSORTx	CD8 T cell	Naïve CD4 T cell
Charoentong TIL 28 immunophenotype	Activated CD8 T cell Type 1 T helper cell Activated B cell Macrophage	

FIGURE 5
Heat map analysis using factors that have been selected from the TCGA-GBM and CGGA cohorts' analysis. **(A)** TCGA primary GBM cohort. **(B)** CGGA primary GBM cohort.

in the TCGA cohort, the CIBERSORTx analysis revealed a higher abundance of CD8 T cells in MGMT-H tumors compared to MGMT-L tumors (p = 0.015) (Figure 6C). Otherwise, there were no significant differences between MGMT-H/L groups in naive CD4 T cell, activated CD8 T cell, type 1 helper T cell, activated B cell, and macrophage. However, in activated CD8 T cell, type 1 helper T cell, activated B cell, and macrophage, numbers tended to be higher in the MGMT-H group. Validation was then performed on the results of the gene set in the MSigDB C5 Biological Process. Although statistical significance was not reached, GSEA analysis also showed

a trend of more activated immunological phenotypes in MGMT-H tumors (Figures 6D, E). To further investigate the infiltration of immune cells into the tumors, we performed immunohistochemical analysis on FFPE tissues from the UTH cohort. Specifically, we examined the presence of CD4^{+}, CD8^{+}, CD20^{+}, CD68^{+}, and CD163^{+} cells within the tumor microenvironment (Figure 7A; Supplementary Table 4). As anticipated, the immunohistochemical analysis revealed a higher infiltration of CD8^{+} (p = 0.012) and CD4^{+} (p = 0.039) cells in MGMT-H tumors compared to MGMT-L tumors (Figure 7B). No significant difference was observed

FIGURE 6

The gene expression profiles of MGMT-H/L tumors in UTH dataset. **(A)** *MGMT* mRNA expression in human GBM correlated with the methylation of *MGMT* promoter region. **(B)** Samples were divided into two groups, low and high, according to *MGMT* median expression level. **(C)** CIBERSORTx and ssGSEA analysis using gene sets that were significantly different in the TCGA-GBM cohort. ssGSEA value were compared between MGMT-H/L tumors using MSigDB C5 Biological Process Gene sets that were significantly different between MGMT-H **(D)** and MGMT-L **(E)** in the TCGA-GBM cohort. Wilcoxon test, *: $P < 0.05$; **: $P < 0.01$; n.s.: $P \geq 0.05$.

between the two groups for CD20, CD68, and CD163 (p = 1.000, p = 0.927, p = 0.523). These results from the UTH cohort corroborate the findings from the TCGA cohort, indicating a consistent pattern of increased infiltration of $CD8^+$ and $CD4^+$ cells in MGMT-H tumors. These results suggest a potential association between *MGMT* expression levels and the immune cell composition within the tumor microenvironment.

3.7 Tumor-specific immune response

To investigate tumor-specific T cells within the tumors, we conducted TIL culture experiments in UTH cohort. Tumor samples were finely minced into small 2-3 mm pieces using a surgical scalpel and then cultured with IL-2 for 2 to 3 weeks in a 24-well plate. The proliferation of TILs was observed in 11 out of 13 cases, with 6 out
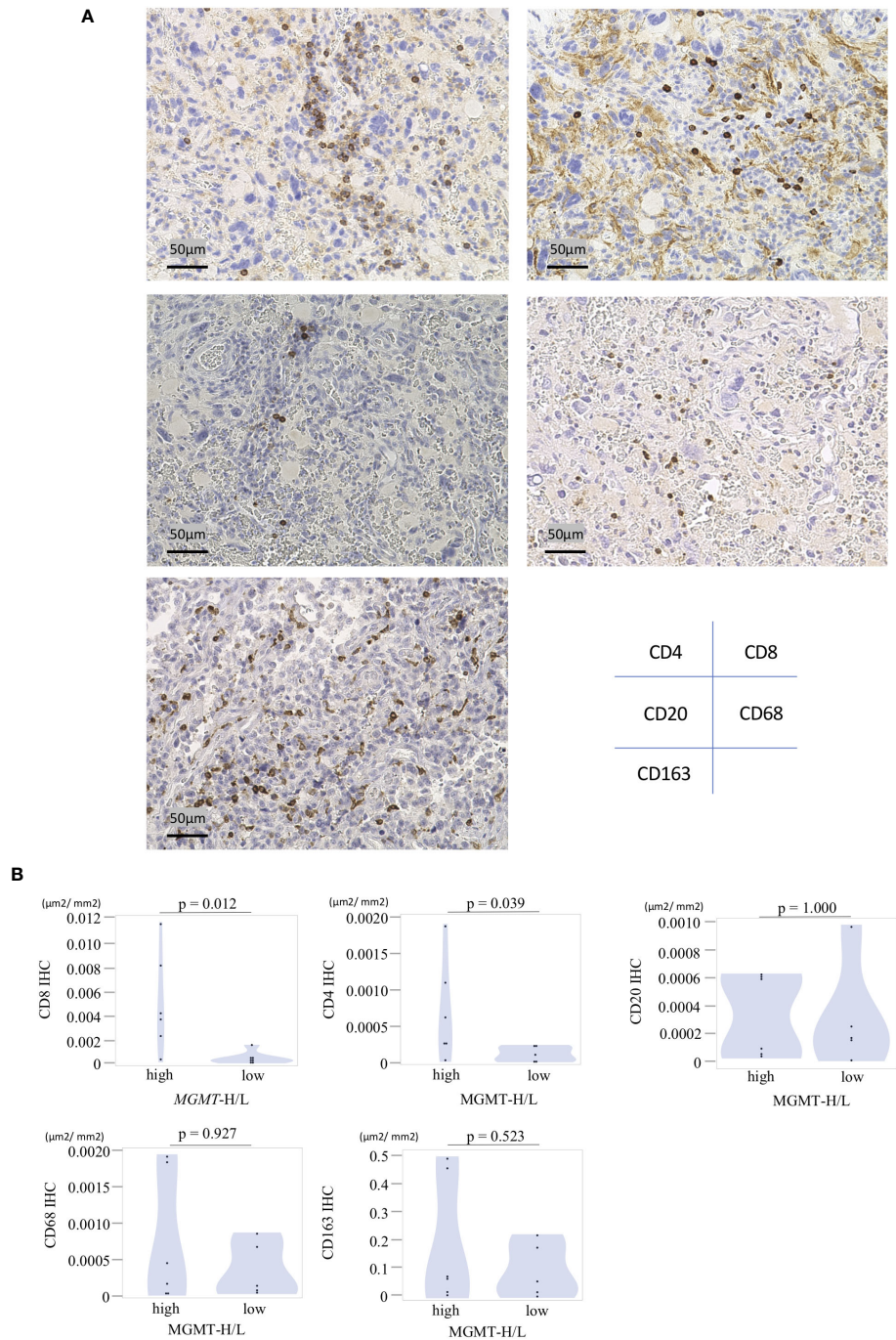
FIGURE 7
Immunohistochemical analysis of MGMT-H/L tumors. **(A)** FFPE slides were subjected to immunostaining for CD4^{+}, CD8^{+}, CD20^{+}, CD68^{+}, and CD163^{+} cells within the tumor. Representative examples of each marker were presented at a magnification of x200. **(B)**The area of positive signals was automatically measured by the BIOREVO-9000 fluorescence microscope (Keyence, Osaka, Japan), and the BZ-II Analyzer image analysis software (Keyence) was utilized to quantify the area of IHC positive staining and calculate the IHC positive staining area per unit tumor area(μm2). The ratio of positive cell area to GBM tumor area was calculated and compared between the MGMT-H/L groups.

of 6 MGMT-H tumors and 5 out of 7 MGMT-L tumors showing successful TIL expansion. From a total of 407 wells used for TIL cultures, we achieved the expansion of TILs to reach a cell count of 3×10^5 or more per well in 150 wells (Supplementary Table 4). Consequently, the overall TIL culture rate was determined to be 36.9%. When considering the MGMT-H and MGMT-L tumors separately, the TIL culture rate was 47.5% and 26.1%, respectively

(Figure 8A). However, the difference between these two groups did not reach statistical significance (p=0.098).

Following the expansion of TILs, we examined their reactivity to autologous tumors by assessing their production of IFNγ during co-culture with tumors cryopreserved as FTD (Supplementary Table 4). Out of the 150 wells with TIL proliferation, co-culture experiments with tumors could not be conducted in 6 wells from 2
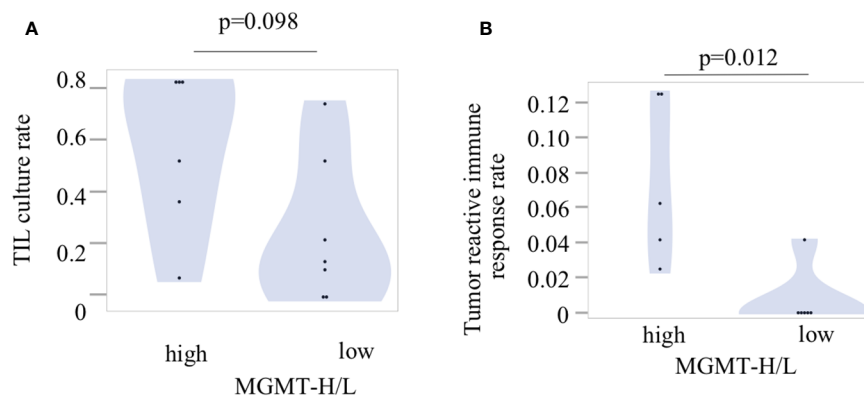
FIGURE 8
Tumor-infiltrating lymphocytes and their reactivity to the tumors. **(A)** The TIL culture rate was calculated as the ratio of the number of wells with positive TIL proliferation to the total number of cultured wells. **(B)** The tumor reactivity of cultured TILs was determined by IFNγ production after incubation of TILs and fresh tumor digest (FTD). The culture supernatant was collected, and the levels of IFNγ were measured using an ELISA. Each patient's tumor-reactive immune response rate was defined as the ratio of the number of wells exhibiting a tumor-reactive immune response to the total number of cultured wells.

cases due to insufficient cryopreserved tumor specimens. Therefore, co-culturing with the tumor was performed in 144 wells, including 94 wells from 5 cases of MGMT-H tumors and 50 wells from 4 cases of MGMT-L tumors (Supplementary Table 4). The concentration of IFNγ in the culture supernatant was measured using ELISA, and wells exhibiting IFNγ levels of 100 pg/ml or higher were considered to indicate a tumor-specific immune response. We observed the production of IFNγ in 12 wells from 6 cases, including 11 wells from 5 cases of MGMT-H tumors and 1 well from 1 case of MGMT-L tumor (Supplementary Table 4). These results demonstrate that tumor-specific immune responses were significantly higher in MGMT-H tumors than in MGMT-L tumors (p = 0.012) (Figure 8B).

To provide a comprehensive view of the findings, we integrated the transcriptome data, immunohistochemical analysis, and TIL culture data into a heat map comparing MGMT-H and MGMT-L tumors (Figure 9). The heat map illustrates the co-expression of activated CD8 T cells, type 1 helper cells, activated B cells, and macrophages in specific cases within the MGMT-H tumors. Notably, these MGMT-H tumors also tended to elicit a tumor-specific immune response.

In summary, our study revealed that MGMT-H tumors displayed activation of adaptive immunity, particularly involving CD8 cells and type 1 helper T cells, which contributed to the induction of a tumor-specific immune response. These findings highlight the importance of understanding the immunological landscape of MGMT-H tumors and suggest potential targets for immunotherapy interventions to enhance tumor-specific immune responses in GBM.

4 Discussion

Understanding the interaction between the tumor and the immune system is crucial for developing effective treatments for GBM, particularly for patients with an unmethylated MGMT

promoter and high MGMT expression, who face limited treatment options and a poor prognosis. This study investigated the relationship between MGMT expression or MGMT promoter methylation and tumor immunity. Consistent with a recent analysis of GBM's molecular profile and specific immunological markers, which revealed higher expression of CD8 and CD68 in GBM cases with an unmethylated MGMT promoter compared to the methylated counterpart (9), our comprehensive genetic analysis consistently demonstrated enhanced immune responses in GBM with MGMT-H tumors. This was evident through the up-regulation of gene signatures associated with tumor-infiltrating immune cells. Significantly, TIL culture experiments indicated a greater presence of tumor-reactive T cells in MGMT-H tumors compared to MGMT-L tumors. These findings suggest that MGMT-H tumors have the potential for antitumor immune responses mediated by CD8 T cells.

Based on our study results, Supplementary Figure 2 presents a schematic diagram illustrating the expected tumor immune status in MGMT-H/L, respectively. Our study contributes to the field in two novel aspects. Firstly, we demonstrate for the first time that MGMT-H tumors exhibit a more significant infiltration of type 1 helper T cells and activated B cells. These immune cell subtypes are crucial in orchestrating effective immune responses against tumors (20–22). Identifying these cell types in MGMT-H tumors adds to our understanding of the immune landscape and highlights potential targets for immunotherapeutic interventions. Secondly, our *in vitro* TIL culture experiments provide novel insights by demonstrating that MGMT-H tumors harbor more tumor-reactive T cells. This observation extends beyond the mere abundance of T cells in MGMT-H tumors and confirms the functional reactivity of the existing T cells toward the tumor. Our results were consistent with the previous report that the combination of neoantigen quality and T lymphocyte infiltrates was associated with the longest survival of GBM patients (23).These findings hold significant implications for developing immunotherapies tailored to exploit the existing immune response in MGMT-H tumors.
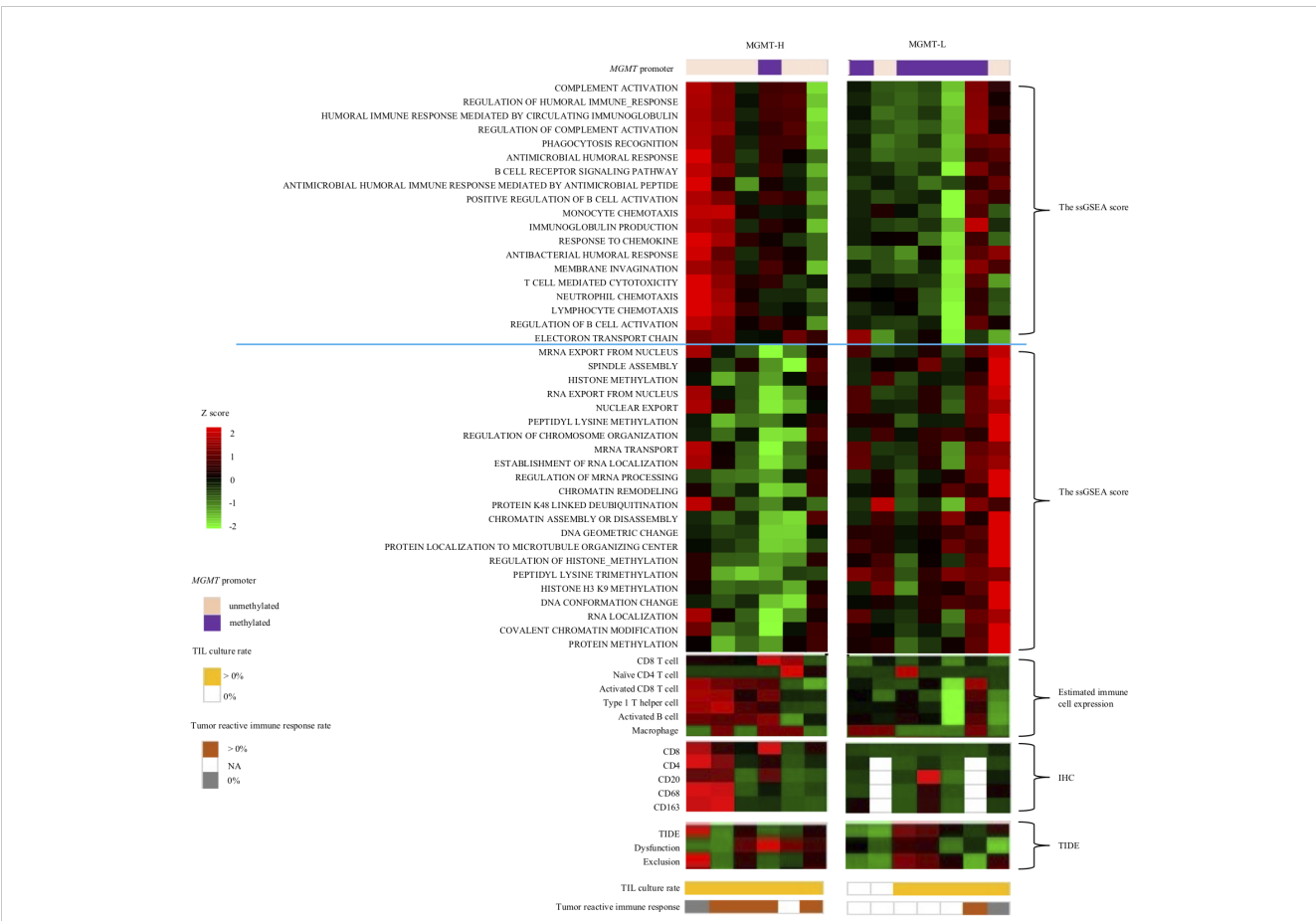
FIGURE 9

Integrated analysis of tumor microenvironment of MGMT-H/L GBM. In the UTH cohort, a heat map analysis using factors that have been selected from the TCGA-GBM and CGGA cohorts' analysis, IHC result and TIL culture result. Patients in the MGMT-H group had higher expression of immune-related genes and higher expression of activated CD8 T cell, type 1 helper cell and activated B cell. In addition, such patients tended to have a higher incidence of tumor reactive immune response.

One notable finding in this study is the up-regulated signature of activated B cells detected in MGMT-H tumors (Figure 3B; Table 2). Antigen presentation is critical in activating naïve CD8 T cells, and antigen-presenting cells, including B cells, are instrumental in this process (24). The emerging research has highlighted the involvement of B cells in antigen presentation within the tumor microenvironment (22). Furthermore, the presence of tertiary lymphoid structures (TLS) has been identified within tumors, including GBM (25, 26). TLS is an organized immune cell structure that resembles to secondary lymphoid organs and contributes to local immune responses. TLS formation has been associated with improved responsiveness to immunotherapy in various cancer types, such as melanoma (27). Considering these findings, the increased signature of activated B cells in MGMT-H tumors suggests their potential role in antigen presentation and the formation of TLS within the tumor microenvironment. Zhou et al. stratified glioma into three distinct tumor subtypes with the gene expression profile of TLS genes (28). The C subtype glioma with high immune infiltration was poor prognosis without immune checkpoint blockade therapy. These findings may have implications for understanding the immune response and potential immunotherapeutic strategies in GBM. Further research is needed to investigate the precise mechanisms

and functional significance of activated B cells and TLS in MGMT-H tumors and their potential impact on the efficacy of immunotherapy.

Despite CD8 T cells showing activation of anti-tumor immunity in MGMT-H tumors, previous studies have indicated that the achieved immune response is insufficient to control the growth of GBM based on clinical data (1, 29). Past reports indicate that even in cases presenting MGMT-H with MGMT-unmethylated status, efficacy with Nivo alone cannot be anticipated (6). It is speculated that MGMT-H tumors may contain immunosuppressive factors that hinder the cytotoxicity of CD8 T cells. One such factor is the presence of highly expressed macrophages in MGMT-H tumors, known as tumor-associated macrophages (TAMs) (30–32). TAMs have different functional classifications, with anti-inflammatory TAMs being predominant in GBM (33). These anti-inflammatory TAMs suppress T cell function and pro-inflammatory TAM activities, contributing to the immunosuppressive microenvironment (33, 34). Targeting anti-inflammatory TAMs is a reasonable strategy to modulate the immunosuppressive environment and enhance the therapeutic effect and CSF-1R may be one such example. Inhibiting CSF-1R signaling can reduce anti-inflammatory TAMs and promote a pro-inflammatory phenotype, improving anti-tumor immune responses (30, 31). However, further research is needed to

determine the safety, efficacy, and optimal treatment combinations for CSF-1R-targeted therapy in GBM. The complex tumor microenvironment and interactions between immune cell populations present challenges in developing effective immunotherapies. Nonetheless, targeting TAMs may hold promise for immunotherapy in GBM.

To clarify the relationship between *MGMT* expression or *MGMT* promoter methylation and tumor immunity, further investigations are needed. One approach could be creating an orthotopic murine model by injecting GBM cell lines with MGMT knockout or overexpression. This model would allow quantification of intratumoral immune cell infiltration, for example, by assessing TIL expression levels through techniques such as flow cytometry, IHC or RNA-Seq. By comparing the degree of *MGMT* expression or promoter methylation, with the level of immune cell infiltration, we can gain insights into the association between *MGMT* and tumor immunity.

This study has several limitations that should be acknowledged. Firstly, the cases included in the experiment were obtained from a single institution, resulting in a relatively small sample size. Including a larger number of cases from multiple institutions in future studies is imperative. Secondly, the transcriptome analysis conducted in this study focused on tumor bulk samples, limiting the ability to analyze individual immune cells' specific functions and interactions. Although TAMs originate from brain-resident microglia and blood-derived monocytes, deconvolution of immune cells from bulk RNA-Seq data cannot discriminate between microglia and monocytes, nor can it identify astrocytes that are enriched in GBM with microglia. Incorporating single-cell analysis techniques would be valuable in evaluating the detailed expression levels and functions of each immune cell. Thirdly, the immunohistochemical staining method employed in this study only targeted specific markers, such as CD8 T cells. Multi-color analysis for type 1 helper T cells, activated B cells, and macrophages are necessary. Furthermore, analyzing the three-dimensional spatial relationship between these immune cells within the tumor microenvironment would provide insights into their cell-cell interactions. Lastly, the analysis in this study was limited to transcriptome analysis, and it is important to supplement the findings with whole exome sequencing data and methylome analysis. This will allow us to explore the relationship between MGMT status and factors such as neoantigens, gene mutations, and methylation patterns. Addressing these limitations in future studies will provide a more comprehensive understanding of the relationship between *MGMT* and the immune landscape in GBM.

5 Conclusions

Our study presents novel findings by characterizing the immune cell composition of MGMT-H tumors, highlighting the infiltration of activated CD8 T cells, type 1 helper T cells, activated B cells, and macrophages and revealing the presence of tumor-reactive T cells by TIL culture experiments. These results offer valuable insights into future immunotherapeutic strategies specifically targeting MGMT-H tumors.

Data availability statement

The raw RNA-Seq data were deposited in the DNA Data Bank of Japan (DDBJ) under the accession number DRA016557. The original contributions presented in the study are included in the article/Supplementary Material, further inquiries can be directed to the corresponding author.

Ethics statement

The studies involving humans were approved by the research ethics committees of the University of Tokyo. The studies were conducted in accordance with the local legislation and institutional requirements. The participants provided their written informed consent to participate in this study.

Author contributions

Funding

Acknowledgments

Conflict of interest

Dr. KKa reports grants from TAKARA BIO Inc. outside the submitted work. The Department of Immunotherapeutics, The

University of Tokyo Hospital, is an endowed department by TAKARA BIO Inc.

The remaining authors declare that the research was conducted in the absence of any commercial or financial relationships that could be construed as a potential conflict of interest.

Publisher's note

All claims expressed in this article are solely those of the authors and do not necessarily represent those of their affiliated organizations, or those of the publisher, the editors and the reviewers. Any product that may be evaluated in this article, or claim that may be made by its manufacturer, is not guaranteed or endorsed by the publisher.

Supplementary material

The Supplementary Material for this article can be found online at: https://www.frontiersin.org/articles/10.3389/fimmu.2024.1328375/full#supplementary-material

References

1. Stupp R, Mason WP, Van Den Bent MJ, Weller M, Fisher B, Taphoorn MJB, et al. Radiotherapy plus concomitant and adjuvant temozolomide for glioblastoma. *New Engl J Med* (2005) 352(10):987–96. doi: 10.1056/NEJMoa043330

2. Shah N, Lin B, Sibenaller Z, Ryken T, Lee H, Yoon JG, et al. Comprehensive analysis of MGMT promoter methylation: correlation with MGMT expression and clinical response in GBM. *PloS One* (2011) 6(1):e16146. doi: 10.1371/journal.pone.0016146

3. Wick W, Weller M, Van Den Bent M, Sanson M, Weiler M, Von Deimling A, et al. MGMT testing—the challenges for biomarker-based glioma treatment. *Nat Rev Neurology* (2014) 10(7):372–85. doi: 10.1038/nrneurol.2014.100

4. Butler M, Pongor L, Su YT, Xi L, Raffeld M, Quezado M, et al. MGMT status as a clinical biomarker in glioblastoma. *Trends Cancer* (2020) 6(5):380–91. doi: 10.1016/j.trecan.2020.02.010

5. Reardon DA, Brandes AA, Omuro A, Mulholland P, Lim M, Wick A, et al. Effect of nivolumab vs bevacizumab in patients with recurrent glioblastoma: the checkMate 143 phase 3 randomized clinical trial. *JAMA Oncol* (2020) 6(7):1003–10. doi: 10.1001/jamaoncol.2020.1024

6. Omuro A, Brandes AA, Carpentier AF, Idbaih A, Reardon DA, Cloughesy T, et al. Radiotherapy combined with nivolumab or temozolomide for newly diagnosed glioblastoma with unmethylated MGMT promoter: An international randomized phase III trial. *Neuro Oncol* (2023) 25(1):123–34. doi: 10.1093/neuonc/noac099

7. Lim M, Weller M, Idbaih A, Steinbach J, Finocchiaro G, Raval RR, et al. Phase III trial of chemoradiotherapy with temozolomide plus nivolumab or placebo for newly diagnosed glioblastoma with methylated MGMT promoter. *Neuro Oncol* (2022) 24(11):1935–49. doi: 10.1093/neuonc/noac116

8. Ott M, Prins RM, Heimberger AB. The immune landscape of common CNS Malignancies: implications for immunotherapy. *Nat Rev Clin Oncol* (2021) 18(11):729–744. doi: 10.1038/s41571-021-00518-9

9. Rahman M, Kresak J, Yang C, Huang J, Hiser W, Kubilis P, et al. Analysis of immunobiologic markers in primary and recurrent glioblastoma. *J Neurooncol* (2018) 137(2):249–57. doi: 10.1007/s11060-017-2732-1

10. Dobin A, Davis CA, Schlesinger F, Drenkow J, Zaleski C, Jha S, et al. STAR: ultrafast universal RNA-seq aligner. *Bioinformatics* (2013) 29(1):15–21. doi: 10.1093/bioinformatics/bts635

11. Anders S, Pyl PT, Huber W. HTSeq–a Python framework to work with high-throughput sequencing data. *Bioinformatics* (2015) 31(2):166–9. doi: 10.1093/bioinformatics/btu638

12. Sun J, Nishiyama T, Shimizu K, Kadota K. TCC: an R package for comparing tag count data with robust normalization strategies. *BMC Bioinf* (2013) 14:219. doi: 10.1186/1471-2105-14-219

13. Robinson MD, McCarthy DJ, Smyth GK. edgeR: a Bioconductor package for differential expression analysis of digital gene expression data. *Bioinformatics* (2010) 26(1):139–40. doi: 10.1093/bioinformatics/btp616

14. Zhou Y, Zhou B, Pache L, Chang M, Khodabakhshi AH, Tanaseichuk O, et al. Metascape provides a biologist-oriented resource for the analysis of systems-level datasets. *Nat Commun* (2019) 10(1):1523. doi: 10.1038/s41467-019-09234-6

15. Barbie DA, Tamayo P, Boehm JS, Kim SY, Moody SE, Dunn IF, et al. Systematic RNA interference reveals that oncogenic KRAS-driven cancers require TBK1. *Nature* (2009) 462(7269):108–12. doi: 10.1038/nature08460

16. Hänzelmann S, Castelo R, Guinney J. GSVA: gene set variation analysis for microarray and RNA-Seq data. *BMC Bioinf* (2013) 14(1):7. doi: 10.1186/1471-2105-14-7

17. Charoentong P, Finotello F, Angelova M, Mayer C, Efremova M, Rieder D, et al. Pan-cancer immunogenomic analyses reveal genotype-immunophenotype

relationships and predictors of response to checkpoint blockade. *Cell Rep* (2017) 18(1):248–62. doi: 10.1016/j.celrep.2016.12.019

18. Jiang P, Gu S, Pan D, Fu J, Sahu A, Hu X, et al. Signatures of T cell dysfunction and exclusion predict cancer immunotherapy response. *Nat Med* (2018) 24(10):1550–8. doi: 10.1038/s41591-018-0136-1

19. Esteller M, Garcia-Foncillas J, Andion E, Goodman SN, Hidalgo OF, Vanaclocha V, et al. Inactivation of the DNA-repair geneMGMTand the clinical response of gliomas to alkylating agents. *New Engl J Med* (2000) 343(19):1350–4. doi: 10.1056/NEJM200011093431901

20. Engel MA, Neurath MF. Anticancer properties of the IL-12 family–focus on colorectal cancer. *Curr Med Chem* (2010) 17(29):3303–8. doi: 10.2174/092986710793176366

21. Melssen M, Slingluff CL. Vaccines targeting helper T cells for cancer immunotherapy. *Curr Opin Immunol* (2017) 47:85–92. doi: 10.1016/j.coi.2017.07.004

22. Sautès-Fridman C, Petitprez F, Calderaro J, Fridman WH. Tertiary lymphoid structures in the era of cancer immunotherapy. *Nat Rev Cancer* (2019) 19(6):307–25. doi: 10.1038/s41568-019-0144-6

23. Zhang J, Caruso FP, Sa JK, Justesen S, Nam D-H, Sims P, et al. The combination of neoantigen quality and T lymphocyte infiltrates identifies glioblastomas with the longest survival. *Commun Biol* (2019) 2:135. doi: 10.1038/s42003-019-0369-7

24. Chen DS, Mellman I. Oncology meets immunology: the cancer-immunity cycle. *Immunity* (2013) 39(1):1–10. doi: 10.1016/j.immuni.2013.07.012

25. van de Walle T, Vaccaro A, Ramachandran M, Pietilä I, Essand M, Dimberg A. Tertiary lymphoid structures in the central nervous system: implications for glioblastoma. *Front Immunol* (2021) 12:724739. doi: 10.3389/fimmu.2021.724739

26. Helmink BA, Reddy SM, Gao J, Zhang S, Basar R, Thakur R, et al. B cells and tertiary lymphoid structures promote immunotherapy response. *Nature* (2020) 577(7791):549–55. doi: 10.1038/s41586-019-1922-8

27. Cabrita R, Lauss M, Sanna A, Donia M, Skaarup Larsen M, Mitra S, et al. Tertiary lymphoid structures improve immunotherapy and survival in melanoma. *Nature* (2020) 577(7791):561–5. doi: 10.1038/s41586-019-1914-8

28. Zhou X, Li W, Yang J, Qi X, Chen Y, Yang H, et al. Tertiary lymphoid structure stratifies glioma into three distinct tumor subtypes. *Aging* (2021) 13(24):26063–94. doi: 10.18632/aging.203798

29. Gomes I, Moreno DA, Dos Reis MB, da Silva LS, Leal LF, Gonçalves GM, et al. Low MGMT digital expression is associated with a better outcome of IDH1 wildtype glioblastomas treated with temozolomide. *J Neurooncol* (2021) 151(2):135–44. doi: 10.1007/s11060-020-03675-6

30. Sampson JH, Gunn MD, Fecci PE, Ashley DM. Brain immunology and immunotherapy in brain tumours. *Nat Rev Cancer* (2020) 20(1):12–25. doi: 10.1038/s41568-019-0224-7

31. Jackson CM, Choi J, Lim M. Mechanisms of immunotherapy resistance: lessons from glioblastoma. *Nat Immunol* (2019) 20(9):1100–9. doi: 10.1038/s41590-019-0433-y

32. Nduom EK, Weller M, Heimberger AB. Immunosuppressive mechanisms in glioblastoma. *Neuro Oncol* (2015) 17(Suppl 7):vii9–vii14. doi: 10.1093/neuonc/nov151

33. Andersen RS, Anand A, Harwood DSL, Kristensen BW. Tumor-associated microglia and macrophages in the glioblastoma microenvironment and their implications for therapy. *Cancers* (2021) 13(17):4255. doi: 10.3390/cancers13174255

34. Wainwright DA, Balyasnikova IV, Chang AL, Ahmed AU, Moon K-S, Auffinger B, et al. IDO expression in brain tumors increases the recruitment of regulatory T cells and negatively impacts survival. *Clin Cancer Res* (2012) 18(22):6110–21. doi: 10.1158/1078-0432.CCR-12-2130

Innate and adaptive immune-directed tumour microenvironment in pancreatic ductal adenocarcinoma

Ann Mary Joseph[1], Ahmad Al Aiyan[1], Basel Al-Ramadi[2,3,4], Shiv K. Singh[5] and Uday Kishore[1,3]*

[1]Department of Veterinary Medicine (CAVM), United Arab Emirates University, Al Ain, United Arab Emirates, [2]Department of Medical Microbiology and Immunology, College of Medicine and Health Sciences, United Arab Emirates University, Al Ain, United Arab Emirates, [3]Zayed Center for Health Sciences, United Arab Emirates University, Al Ain, United Arab Emirates, [4]ASPIRE Precision Medicine Research Institute Abu Dhabi, United Arab Emirates University, Al Ain, United Arab Emirates, [5]Department of Gastroenterology and Gastrointestinal Oncology, University Medical Center, Goettingen, Germany

One of the most deadly and aggressive cancers in the world, pancreatic ductal adenocarcinoma (PDAC), typically manifests at an advanced stage. PDAC is becoming more common, and by the year 2030, it is expected to overtake lung cancer as the second greatest cause of cancer-related death. The poor prognosis can be attributed to a number of factors, including difficulties in early identification, a poor probability of curative radical resection, limited response to chemotherapy and radiotherapy, and its immunotherapy resistance. Furthermore, an extensive desmoplastic stroma that surrounds PDAC forms a mechanical barrier that prevents vascularization and promotes poor immune cell penetration. Phenotypic heterogeneity, drug resistance, and immunosuppressive tumor microenvironment are the main causes of PDAC aggressiveness. There is a complex and dynamic interaction between tumor cells in PDAC with stromal cells within the tumour immune microenvironment. The immune suppressive microenvironment that promotes PDAC aggressiveness is contributed by a range of cellular and humoral factors, which itself are modulated by the cancer. In this review, we describe the role of innate and adaptive immune cells, complex tumor microenvironment in PDAC, humoral factors, innate immune-mediated therapeutic advances, and recent clinical trials in PDAC.

Abbreviations: PDAC, Pancreatic Ductal Adenocarcinoma; TME, Tumor microenvironment; ADM, acinar-to-ductal metaplasia; IL, Interleukin; CAF, Cancer Associated Fibroblast; TAMs, Tumor associated Macrophages; TANs, Tumor associated Neutrophils; ECM, Extracellular Matrix; Tregs, Regulatory T cells; Bregs, Regulatory B cells; MDSCs, Myeloid derived suppressor cells; TP53, Tumor Protein P53; CDKN2A, Cyclin-dependent kinase inhibitor 2A; SMAD4, Mothers against decapentaplegic homolog 4, or DPC4; BRCA2, BReast CAncer gene 2; EMT, Epithelial-to-Mesenchymal Transition; mPDAC, metastatic PDAC.

1 Introduction

Pancreatic ductal adenocarcinoma (PDAC) is one of the deadliest solid tumours in humans. It is the most frequent form of pancreatic cancer, 90% of all pancreas neoplasms, which is characterised by tubular adenocarcinoma of the ductal glands (1, 2). Pancreatic cancer and pancreatic ductal adenocarcinoma are sometimes used interchangeably. Only 11% of patients with PDAC survive for at least 5 years (3). Over 400,000 people die from PDAC every year, the seventh most common cancer-related cause of death worldwide (4). A usually poor prognosis is projected for the more than 450,000 patients who receive annual diagnosis (5). It is predicted that pancreatic cancer-related death will overtake lung cancer as the second most prevalent cause of cancer-related death in the United States by 2030 (6). Along with the aggressive tumour biology, the pancreas' central placement within the abdominal cavity, the lack of a distinct organ capsule, and the abundance of nearby blood and lymphatic arteries all contribute to the tumor's ability to spread locally and elsewhere such as liver, lung, bone and brain (7). The pancreas, a comparatively clean organ, with very few lymphocytes, is located in the retroperitoneum and has no direct contact with the outside world; instead, it communicates with the digestive tract solely through the pancreatic duct. Therefore, very few lymphocytes can be seen in healthy pancreatic tissue (8, 9). In contrast to other malignancies, the incidence of pancreatic cancer is still rising while survival rates are barely improving.

A few recent reviews in the field describe the immunosuppressive TiME in PDAC and the TME targeted therapeutic approaches (10), pro- and anti-tumour properties of immune cells (11), the effector immune cells with potential biomarkers and targets (12), and the need for reprogramming of the stroma for the development of new therapeutic strategies (13). In this review, we have examined the immune landscape in human PDAC more holistically and how that affects survival and treatment for PDAC patients. This review also includes some of the important areas such as humoral immune factors, its significance, and the coexistence of classical and basal-like phenotypes.

1.1 Therapy

The main therapeutic modalities for PDAC are surgical resection, chemotherapy, and radiotherapy. In most cases, the only form of treatment that has a chance of being curative is radical surgical resection (14, 15). Less than 25–30% of all PDAC patients are considered candidates for partial pancreatectomy at the time of diagnosis (16). Nearly 80% of PDAC patients cannot have a curative resection due to the stromal microenvironment which plays a role in malignant transformation, local invasion, and distant metastasis (17, 18). The development of immune checkpoint blockade (ICB) therapy has revolutionized cancer treatment, but the PDAC immunotherapy regimen, whether used alone or in combination with chemotherapy, has not shown encouraging results in patients with metastatic PDAC (mPDAC) (19). Borderline resectable or locally advanced PDAC patients, have significantly better survival rates in those patients who received

neoadjuvant therapy (20, 21). The neoadjuvant therapy regimen includes chemotherapy with 5-fluorouracil (FOLFIRINOX/FOLFOX), gemcitabine (gemcitabine/nab-paclitaxel) or chemoradiotherapy before surgery. The CA19-9 level is considered a specific biomarker for tumor resectability and overall survival (22).

Conventional cytotoxic therapies such as chemotherapy and radiation therapy have not increased the chances of survival for patients with pancreatic cancer. Since 2011, 5-fluorouracil/leucovorin with irinotecan and oxaliplatin (FOLFIRINOX) and nab-paclitaxel with gemcitabine have been the preferred treatments for mPDAC. Response rates for these treatments range between 23% and 31%, progression-free survival time ranges from 5.5 to 6.6 months, and overall survival times range from 8.5 to 11 months. The only targeted treatment for PDAC that the US Food and Drug Administration (FDA) has approved is erlotinib, an epidermal growth factor receptor (EGFR) inhibitor, in combination with gemcitabine hydrochloride in patients with metastatic, locally advanced, or unresectable PDAC. The absolute benefit of gemcitabine and erlotinib, however, is also negligible for up to 2 weeks (23).

Despite advancements in pancreatic cancer research, screening, and treatment strategies, PDAC has a poor prognosis and resistance to many treatments, including immunotherapy (24). A large matrix of stromal cells is strongly connected with the poor prognosis of PDAC (25). PDAC is characterised by a desmoplastic stroma, a fibrotic TME with respect to normal pancreatic tissue as illustrated in Figure 1. Additionally, different epigenetic modifications as well as mutations in protooncogenes and tumour suppressor genes are seen in the stromal cells surrounding the tumour as well as the tumour epithelium (26, 27). The compact dysplastic stroma of PDAC is a significant barrier to chemotherapeutic agents. Thus, stroma-targeting therapy has been recognised as a prospective approach to enhance the effectiveness of chemotherapy, and hence, patient survival rates (28).

A major component of the stroma in PDAC, hyaluronic acid (HA), interacts with cell surface receptors CD44 and receptor for HA-mediated motility (RHAMM) to promote tumour cell survival and to initiate signalling pathways associated with tumour cell proliferation, migration, and invasion (29–32). Hence, the targeting of HA is regarded as a promising therapeutic approach in the context of PDAC. PEGylated hyaluronidase (PEGPH20) refers to a PEGylated nanoscale complex that consists of recombinant human hyaluronidase (33, 34). Several studies have demonstrated that PEGPH20 has the ability to degrade HA, remodel tumour vasculature, and enhance the effectiveness of chemotherapeutic drugs (33, 35, 36). The study HALO-109-202, a phase II clinical trial, examined the effects of combining PEGPH20 with Abraxane (an albumin-bound paclitaxel nanocomplex) and gemcitabine in 279 patients diagnosed with mPDAC. The results demonstrated a significant increase in progression-free survival and overall survival among patients with elevated levels of HA (37). However, the phase III clinical study failed to considerably improve the PDAC patients' overall survival.

Collagen represents another significant constituent within the extracellular matrix (ECM) of tumours. High levels of fibrillar collagens found in the stroma of PDAC play a critical role in promoting tumour cell survival and tumour progression. This
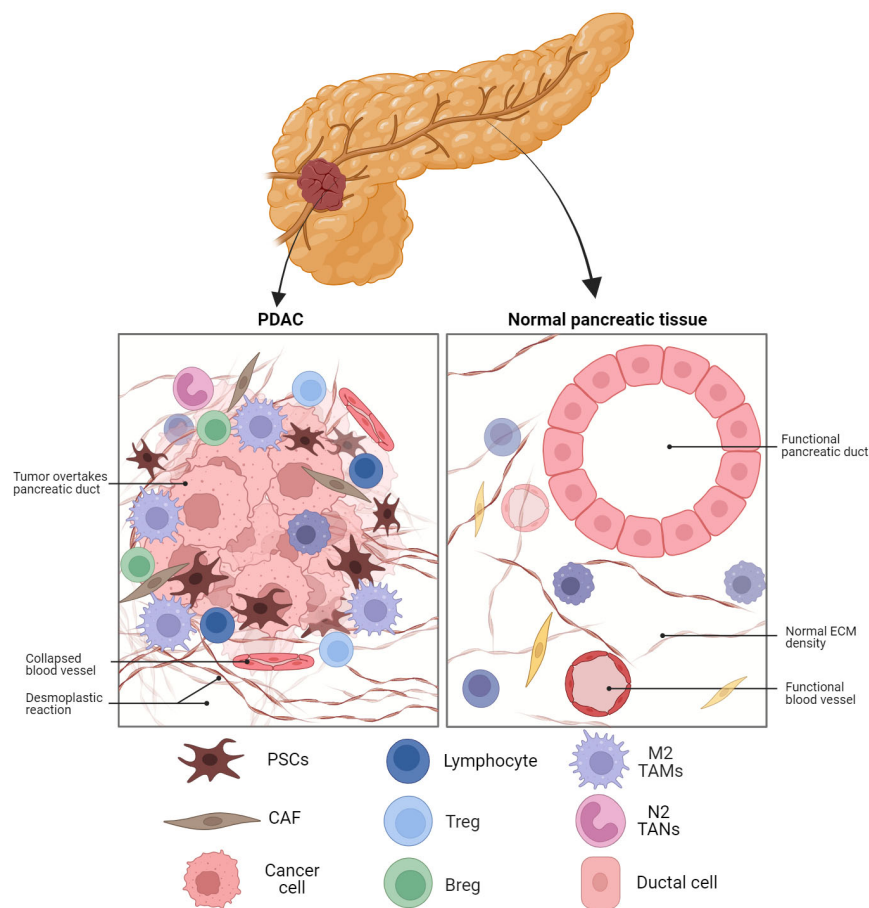
FIGURE 1
Schematic representation of the PDAC TME compared to normal pancreatic tissue. Fibroblast activated in the tissue to CAFs are the dominant cell type in PDAC along with M2 TAMs and MDSC. The dense desmoplastic reaction and collapsed blood vessels provide barriers to cytotoxic T cell infiltration. PDAC, pancreatic ductal adenocarcinoma; ECM, extracellular matrix; PSC, pancreatic stellate cell; CAF, cancer-associated fibroblast;Treg, regulatory T cell; Breg, regulatory B cell; TAM, tumour-associated macrophage; TAN, tumour-associated neutrophil.

process is mediated by the involvement of discoidin domain receptor 1 and 2 (DDR1 and DDR2). Huo et al. revealed that there was a significant correlation between elevated expression levels of DDR1 and an increased risk of unfavourable prognosis in PDAC patients (38). A small molecule inhibitor targeting DDR1 resulted in a decrease in fibrillar collagen deposition and an enhancement in the efficacy of chemotherapy in orthotopic mouse models of PDAC (39). KI-301690, a small molecule that disrupts DDR1 signaling, is a selective DDR1 inhibitor. A combination treatment with gemcitabine significantly inhibited the growth of pancreatic cancer cells (40).

Hedgehog (Hh) signalling pathway is typically characterised by an increased activity in PDAC via the activation of pancreatic stellate cells (41). This pathway has been shown to play a role in the regulation of stroma deposition (42). Multiple strategies have been developed with the aim of treating PDAC through the inhibition of the Hh signalling pathway, with the ultimate goal of eradicating the tumour stroma (43). Cyclopamine, a steroidal alkaloid of natural origin, has been found to effectively inhibit the Hh signalling pathway by binding to the Smoothened (SMO) protein (44). In the PDAC

xenograft mouse model, it was found that the fibronectin content was decreased and tumour vascularization was increased. Co-administration of cyclopamine with paclitaxel-loaded nanoparticles resulted in a significant enhancement of tumour growth inhibition (45). The anti-tumor efficacy was mediated by increased tumor infiltration of CD8$^+$ T cells without concomitant infiltration of immune suppressive cells, and by the coordinated action of Paclitaxel and IFN-γ (46). Another polymeric conjugate of docetaxel and cyclopamine has been examined for its anti-cancer effect in murine PDAC (47). This combination therapy resulted in greater inhibition of orthotopic pancreatic tumor growth.

The majority of PDAC patients have non-resectable tumours by the time they develop symptoms such as weight loss, abdominal pain and jaundice (48). Early detection of PDAC improves survival rates, but its low prevalence makes screening the general population impractical. Screening subgroups may include people with germline mutations, pancreatitis, mucinous pancreatic cysts, and elderly new-onset diabetics (49). For accurate diagnosis, high-resolution ultrasound, endoscopic ultrasound (EUS), computed tomography (CT), and magnetic resonance imaging (MRI) are needed.

1.2 Biomarkers and oncogenic mutations

Advanced PDAC has few treatment options, making early detection crucial for prognosis. Thus, developing diagnostic biomarkers for high-risk populations is important. CA19-9, the only FDA-approved biomarker for the diagnosis and monitoring of PDAC, is probably the most extensively validated biomarker that has diagnostic, prognostic and surveillance value (50, 51). CA125, CA72-4, CA50, CA199, and CA242 are other antigens used as biomarkers (52, 53). A single diagnostic potential for any of these biomarkers could not be established; however, when used along with CA 19-9, they may help distinguish between benign and malignant pancreatic lesions. Similarly, CA19-9, when combined with CEA, appears to have a better prognostic value, particularly in advanced PDAC (54).

Typically, PDAC is characterised by the presence of oncogenic mutations in genes such as KRAS and loss-of-function mutations in tumour suppressors such as TP53, CDNK2A, SMAD4, and BRCA2. These biomarkers and genomic mutations have the potential to function as targets or prognostic indicators, depending on the expression. PDAC originates from a series of precursor lesions, such as pancreatic intraepithelial neoplasia (PanIN), intraductal papillary mucinous neoplasm (IPMN), and mucinous cystic neoplasm (MCN) (55). In most cases, KRAS mutations emerge in PanIN-1 lesions and drive the initiation process, while CDKN2A mutations emerge in PanIN-2 and drive the disease forward. Mutations in TP53 and SMAD4, are frequently found in PanIN-3 and invasive tumours (56, 57). Approximately 95% of pancreatic tumours exhibit RAS mutations, with KRAS alterations being the most prevalent, accounting for 85% of cases. Additionally, KRAS stimulates the nuclear factor κB (NF-κB) pathway, which is linked to the development of a strong inflammatory response (58). Besides mutations in KRAS, inactivation of CDKN2A is observed in approximately 90% of PDAC cases, while SMAD4/DPC4 alterations are present in approximately 55% of cases (59). Also, a significant proportion of PDAC cases, ranging from approximately 50% to 70%, exhibit mutations in the TP53 gene (60). The SMAD4 gene is deactivated in approximately 60% of cases of PDAC (61). This gene plays a crucial role as an effector in the transforming growth factor β (TGF-β) signalling, which is also disrupted in 47% of PDAC cases (62, 63). Dysregulation of various critical processes-related signalling pathways, such as apoptosis and cell proliferation, occurs because of these mutations.

1.3 Classification of PDAC subtypes

Genomic profiling at a large scale has shown that PDAC has two different histological types: "classical" and "basal-like". As shown in Figure 2, the "Classical" or progenitor subtype was distinguished by the expression of epithelial markers and a good prognosis, while the "Basal-like," squamous or quasi-mesenchymal subtype was characterised by the expression of mesenchymal markers and aggressive/metastatic properties. There is still disagreement over how to actually use the subtype classification for clinical decision-making in PDAC, despite the fact that these molecular subtypes of

PDAC may offer new avenues for precision medicine approaches (65). Collisson et al. conducted transcriptome analyses on tissue samples of PDAC, as well as human and murine PDAC cell lines, and identified three distinct molecular subtypes of PDAC, namely the classical, quasi-mesenchymal, and exocrine-like subtypes (66). The classical subtype is distinguished by the activation of genes associated with epithelial and adhesion functions. In contrast, the quasi-mesenchymal subtype predominantly exhibits the expression of genes related to mesenchymal characteristics. Additionally, the exocrine-like subtype is characterised by the upregulation of genes associated with digestive enzymes. It is noteworthy that these subtypes exhibit relevance in terms of survival, as the classical subtype is associated with the most favorable prognosis, while the quasi-mesenchymal subtype is linked with the poorest prognosis (66). Moreover, it has been observed that PDAC cell lines belonging to the classical subtype exhibit resistance to gemcitabine therapy but show sensitivity to erlotinib.

Moffitt et al. later achieved successful molecular subtyping of both the epithelial cells and stroma of PDAC, leading to the identification of two distinct subtypes: normal and activated PDAC stroma. Notably, the activated subtype was associated with a poorer prognosis. The two subtypes specific to tumour were denoted as Classical and Basal-Like (67). The classical subtype is distinguished by the presence of overlapping genetic signatures, such as GATA6. The Basal-like subtype is correlated with a more unfavorable prognosis compared to the Classical subtype. However, it exhibits a more favorable response to adjuvant therapy.

In 2018, Puleo et al. examined the influence of the tumor microenvironment (TME) in PDAC. They categorised PDAC into five distinct clinical subtypes: Pure-basal-like, Stroma-activated, Desmoplastic, Pure-classical, and Immune-classical. Yet another classification distinguishes PDAC into Basal-like A/B, Classical A/B and Hybrids. Basal-like tumors are more aggressive; Basal-like A is associated with metastatic disease, and Basal-like B with resectable disease. Classical A/B tumors are frequently found in the early stage while Hybrids reveal the presence of multiple expression signatures (68).

Recent studies observed the coexistence of basal-like and classical subtype in PDAC. The intratumoral coexistence, which is increased during disease progression, inversely affects the prognosis and treatment based on subtypes. A comprehensive study of the dichotomous role of AP1 transcription factors (JUNB/AP1 versus cJUN/AP1) in PDAC subtype heterogeneity sheds light on the plasticity and stability of classical and basal-like neoplastic cells (69). It also highlights the importance of anti-tumor necrosis factor α (TNF-α) with gemcitabine chemotherapy which may provide a valuable strategy for a better treatment response in PDAC. The co-expression of tumor subtypes has been observed in approximately 90% of tumors using a multiplex immunofluorescence pipeline, based on the protein expression of PDAC subtype markers (70). The extensive intratumoral heterogeneity needs further characterisation in terms of intrinsic and extrinsic factors that dictate subtype heterogeneity. This will open up new prognosis and treatment options for PDAC patients (71).
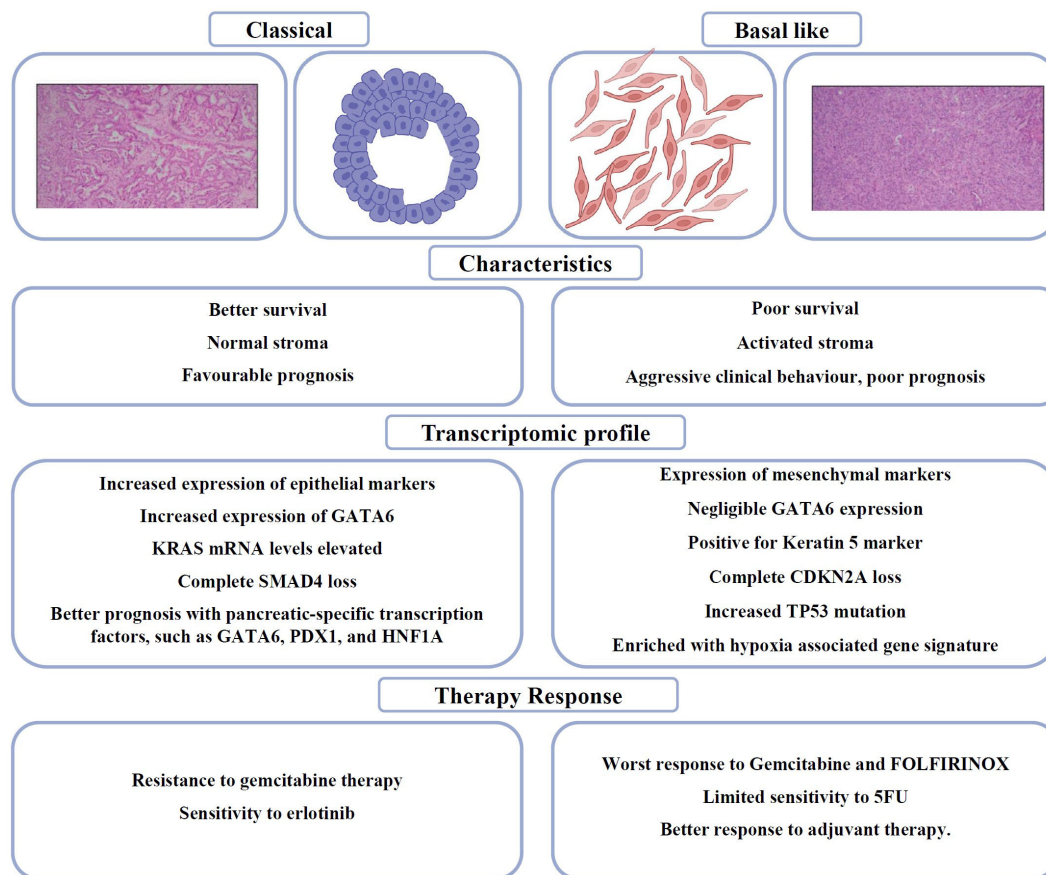
FIGURE 2
Schematic and H&E sections PDAC (Scale: 200 µm) to distinguish between Classical and Basal like subtypes in PDAC (64), summarising the clinicopathological differences, genetic signatures and therapy responses.

2 TME complexity in PDAC

2.1 PDAC heterogeneity and plasticity

The cellular and humoural components make up the heterogeneous PDAC TME. In the cellular component, there are immune cells, endothelial cells, pancreatic stellate cells (PSCs), cancer-associated fibroblasts (CAFs) and myofibroblasts (Figure 3; Table 1). The humoural component is made up of collagen, fibronectin, and multiple soluble factors, including cytokines, chemokines, growth factors and complement components residing in the ECM (94–97). The interaction between these two components is essential for promoting tumour growth and the emergence of therapeutic intervention resistance. The development of an immunosuppressive TME, which allows the tumour to elude immune surveillance, is a feature frequently observed in PDAC.

The human pancreas is comprised of exocrine (acinar), epithelial (ductal), and endocrine (α, β, δ, ϵ) cells. The plasticity of the pancreas is believed to be responsible for maintaining its homeostasis and promoting regeneration. Both acinar and ductal cells in the healthy pancreas can give rise to PDAC, though acinar cells appear to be more prone to oncogenic transformation (98). Acinar cells undergo a plastic trans-differentiation process known as acinar to ductal metaplasia (ADM), which can progress to PanINs, and eventually, adenocarcinoma (99), in response to specific macro- and microenvironmental stimuli, such as tissue damage, inflammatory factors, or stress conditions (98, 100), and become more vulnerable to activating mutations in the proto-oncogene KRAS. PanINs are the most frequent precursor lesions that are linked to the development of invasive PDAC among premalignant lesions with distinct histopathological features such as microscopic mucinous pancreatic ductal lesions with flat to papillary, micropapillary, or cribriform formation with severe nuclear atypia, loss of polarity, macronucleoli, and abnormal mitotic figures (86).

2.2 Inflammatory signatures

The etiology of PDAC would not be complete without highlighting the importance of inflammatory signals for initiation and progression of tumorigenesis. Inflammation and increased immune cell infiltration are common risk factors for human pancreatic cancer. Tumor-promoting inflammation, (101) is an integral part of neoplastic progression in PDAC. Chronic inflammation of the pancreas, known
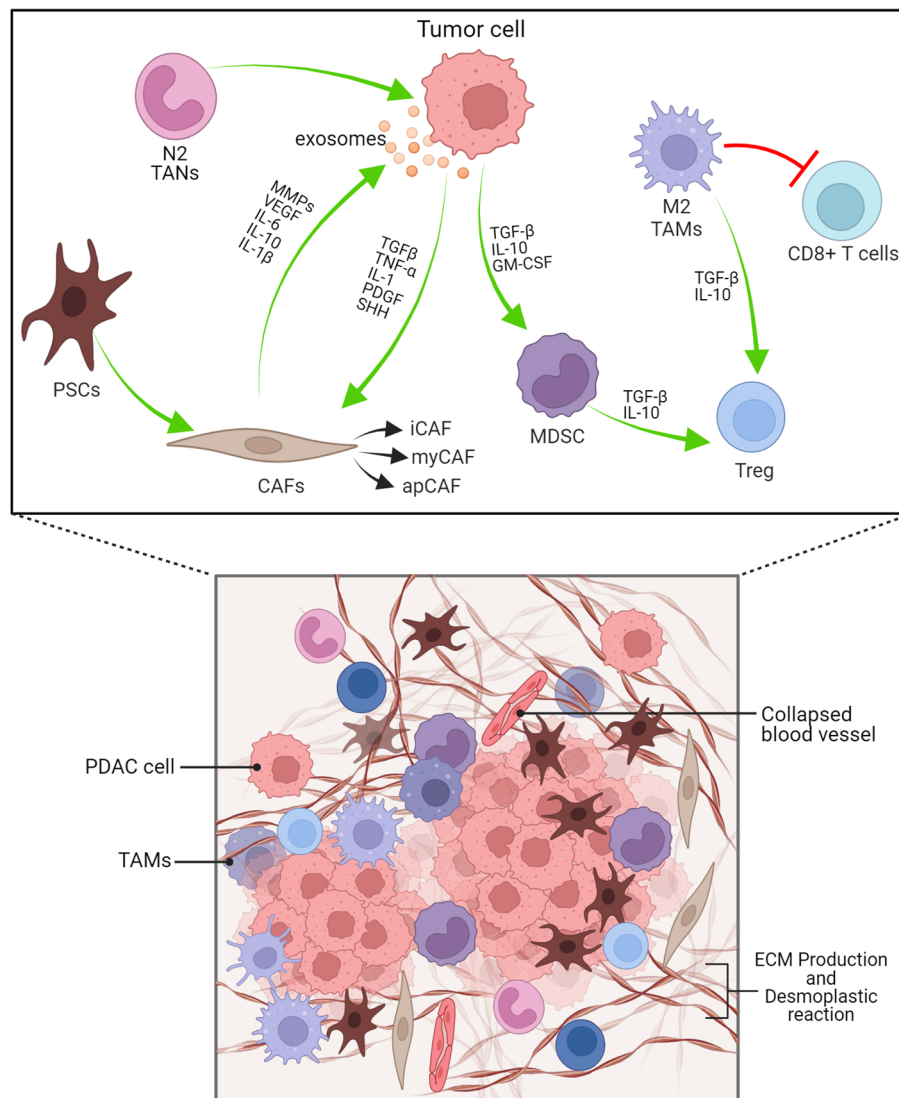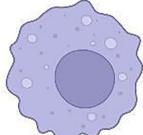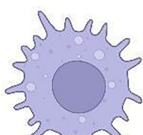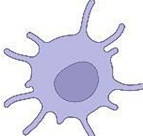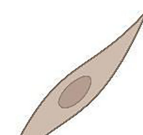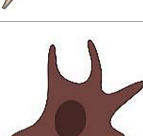
FIGURE 3
PDAC's dense desmoplastic stroma and tumour microenvironment are depicted schematically here. The PDAC stroma is largely made up of CAFs, Macrophages, MDSCs and other immune cells. Exosomes produced from PDAC cells recruits and activates CAFs. Cytokines, TGF-β, IL-1, PDGF, SHH are cruicial for CAF activation. N2 TANs, myCAF, Tregs and Bregs have protumourigenic role. iCAF–inflammatory CAF, myCAF–myofibroblastic CAF, apCAF–antigen presenting CAF.

as pancreatitis, is a significant risk factor for the development of PDAC (102); the importance of environmental factors that cause chronic inflammation (e.g., smoking, heavy alcohol consumption, diet, and obesity) in pancreatic cancer is well established (103, 104). Inflammation promotes tumour formation, growth, progression, and metastasis (105).

The TME inflammatory cells and cancer cells are known to secrete several cytokines, such as IL-6, IL-10, IL-13, VEGF, and TGF-β (106). The anti-inflammatory TGF-β and IL-10, as well as the pro-inflammatory IL-1, IL-6, IL-17, and TNF-α, play a significant role in PDAC. Depending on the cross-talk between cancer cells and inflammatory cells, the ratio of pro- to anti-inflammatory cytokines in the TME constantly changes. Ling et al. demonstrated in a genetically engineered mouse model that oncogenic KRAS leads to
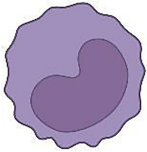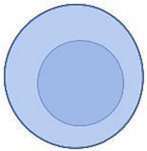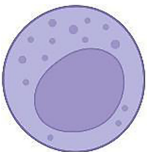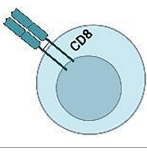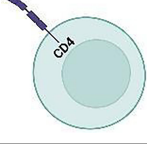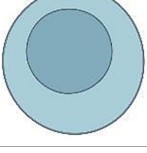
a constitutive activation of NF-κB through IL-1α and p62 (107). Consequently, cancer cell-intrinsic inflammatory signalling networks generate a protumorigenic TME via the expression of cytokines that promote angiogenesis and the recruitment of immune and stromal cells. Several interleukins, including IL-6, were among those dysregulated by the depletion of NF-κB signalling. IL-6 class cytokines (e.g., IL-6, LIF, OSM, IL-11) are among the few regarded as master regulators of inflammation associated with cancer (108). Blocking the inflammatory cytokine IL-6 may improve the efficacy of anti-PD-L1 therapy by modulating immunological features of PDAC in murine models (109). It may enhance T cell trafficking and alter the tumor's T cell population, as the ability of a patient to respond to checkpoint inhibitors is significantly impacted by T cell infiltration into tumours (110).

TABLE 1   The immune cells in the tumor microenvironment of pancreatic ductal adenocarcinoma.

Phenotype	Cell type	Action	Effect	Reference
	TAMs	Release various growth factors, cytokines; promote tumor cell invasion, induce angiogenesis, suppress antitumor immunity, and facilitate tumor cell metastasis Classified into two subtypes: M1 and M2	promote ADM and PanIN	(72) (73) (74) (75)
	M1	Enhanced expression and release of IL-1β, TNF-α, IL-6, or IL-12	Antitumor and pro-inflammatory phenotype	(75)
	M2	IL-10, TGF-β, IL-6, PGE, CCL2, CCL17, CCL20	Protumor and anti-inflammatory properties, Inhibit CD8^{+} T cells activity, increases nodal lymphangiogenesis and poor prognosis	(75) (76) (77)
	TANs	IFN-β, TGF-β signalling	Differentiates into N1 or N2	(78)
	N1	IL-12, CXCL9, CXCL10, and CCL3	Recruitment and activation of CD8^{+} T cells, tumour suppressing	(79)
	N2	VEGF, MMP-9	Tumour promoting by suppressing CTL	(80)
	DC	Antigen presentation DCs infiltrating PDAC increases with TILs infiltration (CD4^{+} and CD8^{+})	Located in stroma and rarely in PDAC TME, improve overall survival	(81)
	CAFs	IL-6, IL-11, TGF-β signaling ECM proteins include collagen, laminin, fibronectin IL-6, CXCL2, CXCL12, and CXCL8	Immune evasion by recruitment of Tregs Inhibitory TiME	(82) (83)
	PSCs	Expressing alpha-smooth actin and produce growth factors, cytokines and ECM components	leads to desmoplastic reaction	(84)

(Continued)

TABLE 1 Continued

Phenotype	Cell type	Action	Effect	Reference
	MDSC	Production of ROS, secretion of peroxynitrite and Arginase-1 Induction of Tregs Depletion of cysteine	inhibit the antitumor functions of T cells and NK cells	(85)
	Tregs	Secrete immunosuppressive cytokines such as IL-10 and TGF-β FOXP3 protein expression and high levels of IL-2 receptor alpha chain CD25	immune evasion barrier for successful tumor immunotherapy	(86) (87)
	NK cells	Exhibit impaired killing of autologous PDAC cells due to NKG2D and DNAM-1 deficiency Increased percentage of NK cells in peripheral blood	Leads to recurrence-free survival	(88) (89)
	CD8+ T cells	IFN-γ, TNF-α, granzymes, FasL	Immunogenically hot tumor, which can respond better to immune checkpoint inhibitors	(81) (90) (91)
	CD4+ T cells	IFN-γ, IL-2, increase CTL activity and IL-4, IL-5, IL-13, decrease CTL activity	Anti-tumor immunity and tumour tolerance	(91)
	B cells	Infiltration of CD20+ B lymphocytes	Prognostic value diverged according to their spatial distribution in the tissue	(92)
	Bregs	IL-10, IL-35, IL-18	Enhance immunological tolerance	(93)

3 Immune suppressive microenvironment in PDAC

3.1 Myeloid cells

The immunosuppressive TME and cell types, a hallmark of pancreatic cancer, are thought to promote tumour invasion and growth. Myeloid cells develop from hematopoietic stem cells in the bone marrow through myelopoiesis. They are characterised by the expression of CD45 and CD11b surface markers. Subsequently, they undergo differentiation into discrete subpopulations, namely macrophages, granulocytes, mast cells, and dendritic cells, all of which are integral constituents of the innate immune system. Myeloid cell abundance in tumours correlates with worse clinical outcomes (111, 112).

The macrophages present within the tumour are commonly known as tumor-associated macrophages (TAMs). Two main

phenotypes of macrophages, known as M1 and M2, are known for their ability to display plasticity. M2 polarised macrophages display immunosuppressive traits and a restricted adaptive immune response. Induction of an M1-like phenotype is typically seen to enable adaptive immunosurveillance. TAMs inhibit T-lymphocyte responses (113) and secrete cytokines that promote the tumor phenotype and metastasis (73, 114). In addition to their ability to directly induce T-lymphocyte apoptosis (115), TAMs produce arginase-1(72), a metalloenzyme that metabolizes and depletes the environment of arginine, an essential compound for T-lymphocyte proliferation (116, 117). Another major TAM subpopulation includes SPP1+ and C1QC+ TAMs, which on further characterization, showed enrichment for epithelial-to-mesenchymal transition (EMT) and a high angiogenesis score in SPP1+ TAMs, while C1QC+ TAMs were enriched for antigen presentation and phagocytosis (118). Granulocytes can be further categorised into three subtypes: eosinophils, basophils, and neutrophils. In the context of the TME,

it is common for neutrophils and monocytes to exist in an immature state, which is commonly referred to as immature myeloid cells or myeloid-derived suppressor cells (MDSCs).

Myeloid cells and other immune cells infiltrate the PDAC TME, resulting in a state of local inflammation (119) in which tumour cells interact with infiltrating immune cells. However, for a transformed cell to survive, it must attain an immunosuppressive phenotype, such as downregulation of MHC class I expression and upregulation of programmed cell death receptor ligand-1 (PD-L1) and CD47, which hinder the anti-tumor immune response by engaging and suppressing the activated T cells and relaying 'don't eat me' signal to the phagocytic macrophages, respectively (120, 121). Constitutively active KRasG12D regulates autophagy-induced MHC class I downregulation, which is a major mechanism that PDAC cells employ to escape immune surveillance (122, 123). Table 1 provides the immune cell composition and its effect in the PDAC TME.

3.2 Cancer-associated fibroblasts

In addition to myeloid immune cells, fibroblasts in stromal components, known as Cancer-associated fibroblasts (CAFs), are an important TME component, including myofibroblastic CAFs (myCAFs), immunogenic CAFs (iCAFs), and antigen-presenting CAFs (apCAFs). PDAC has a unique fibrotic TME with desmoplastic stroma, abundant in ECM proteins produced by CAFs that represent a significant proportion of the cellular composition in the PDAC stroma, ranging from 15% to 85% of stromal cells (124) (Figure 3). CAFs, immune cells, cytokines and chemokines accumulate in the TME of primary and metastatic PDAC, exacerbating the development of an immunosuppressive phenotype (86, 125). CAFs create a physical and metabolic barrier via ECM proteins, thereby diminishing the effectiveness of therapeutic interventions against PDAC by increasing the interstitial tumor pressure that impairs vascular function (126–128). Additionally, CAFs facilitate tumour growth and invasion (129–132) and contribute to chemotherapy resistance by the presence of hyaluronan (18, 33, 127). The role of CAFs in immunosuppression (133), tumour metabolism (134), and secretion of inflammatory factors such as IL-1β, potential initiator of NF-κB signalling (135), have been studied. Therefore, the elimination of CAFs from the TME has the potential to serve as a possible therapeutic approach for the treatment of PDAC (131, 136).

3.3 Extracellular matrix

Increasing desmoplasia, which frequently matches or exceeds the tumor's epithelial component, is a hallmark of PDAC progression. The ECM provides physiological signals to neighboring cells in all tissues. The accumulation of ECM proteins is prevalent in solid tumours including PDAC and is referred to as a desmoplastic reaction (137). TME can modulate interstitial fluid pressure (33, 126) and reduce the density of blood vessels within tumours (33). Collagens, integrins, proteoglycans, glycoproteins, and proteases dominate the ECM of PDAC. These components interact with

cancer cells through a variety of mechanisms (138, 139). Collagens Type I, III and IV are the most prevalent of these constituents. Collagens are active components in PDAC stroma with not for just structural support, but have a direct effect on the growth, survival, and spread of cancer cells (140); patients with higher level of fibrillar collagen have lower overall survival rate (141). $\alpha_v\beta_6$, an epithelial integrin, is upregulated in PDAC (142). Galectin-1 (GAL1), along with other glycoproteins such as periostin and fibulin, has been found to be upregulated in the PDAC TME and is poorly expressed in long-term (10 years) PDAC survivors (143).

CAFs, which originate primarily from PSCs and bone-marrow derived mesenchymal stem cells, are a major regulator of the ECM (144). PSCs are primarily located in the vicinity of pancreatic glands and possess the capability to produce ECM proteins, matrix metalloproteinases (MMPs), and MMP inhibitors, which play a crucial role in regulating ECM turnover (145). PSCs can be activated by pro-inflammatory cytokines, oxidative stress, hypoxia, hyperglycemia, and heightened interstitial pressure (146). Activated PSCs can secrete growth factors such as TGF-β1, PDGF and VEGF (147) to promote pancreatic cancer cell growth, decrease apoptosis, and increase invasion (148). PSCs are the primary source of collagen in tumour stroma, secreting ECM proteins such as α-smooth muscle actin and collagen. Reducing myofibroblasts and ECM in PDAC in vivo can inhibit tumour growth and improve chemotherapy sensitivity.

4 Interplay between innate and adaptive immune mechanisms in PDAC

PDAC is immunologically heterogeneous; this heterogeneity exists between cells within PDAC. CD8^{+} cytotoxic T lymphocytes (CTL) and CD4^{+} T cells are the effector tumor infiltrating lymphocytes (TILs) observed in resected cancer tissue and are believed to participate in the host immune response against cancer which is considered a positive prognostic marker (149). Out of the total T lymphocytes (CD3), >80% are CD8^{+} T and CD4^{+} T Cells (150). The immune cells that target tumors are CTLs. CTLs use the Fas-FasL and perforin–granzyme pathways as major effector mechanisms of cytotoxicity; loss of Fas expression in PDAC tumours result in cancer immune evasion (151). PSCs produce elevated amounts of ECM, driving a fibrotic tissue that entraps infiltrated T cells, alongside immunosuppressive cytokines and expression of PDL-1. Pancreatic cancer cells avoid T cell killing by downregulating Fas, exhibiting low tumour mutational burden, expressing PDL-1 and secreting growth factors and cytokines that recruit immunosuppressive cells. CTLs are localised along the invasive margin of the tumour border or trapped in the surrounding fibrotic tissue but are not present within the tumour core. Moreover, infiltrated CD8^{+} T cells in PDAC tumours often display minimal signs of activation (152). MDSCs express PDL-1 and suppress T cells functions by several mechanisms, including depletion of arginase 1, the release of reactive oxygen species, and secretion of cytokines. Tregs directly suppress T cells, express cytotoxic T-

lymphocyte-associated protein 4 (CTLA-4) and secrete cytokines such as TGF-β and IL-10. TAMs play a role in sequestering T cells at the periphery and secrete immunosuppressive cytokines (91). Tumour-derived cytokines and chemokines drive recruitment of myeloid cells to the TME. These cells, which include TAMs and MDSCs, block the recruitment and priming of T cells, resulting in T cell exclusion within the TME (153).

There is considerable infiltration of CD20+ B lymphocytes in the TME of human PDAC, unlike normal pancreatic tissue (92). There is a distinct spatial heterogeneity for B cells either in ectopic lymph nodes like tertiary lymphoid structures, or interspersed at the tumour–stroma interface. In addition, B cells produce anti-tumor antibodies and present tumor antigens to T cells to improve the cancer immunosurveillance. B cells in the TME respond to tumor-associated antigens by secreting IgG1 antibodies to activate the complement system, and phagocytosis by NK cells and macrophages (154). Alternatively, regulatory B cells (Bregs), dispersed inside the TME, contribute to the dampening of anti-tumor immune responses by secreting anti-inflammatory cytokines (IL-10 and IL-35), which promote tumor growth and metastasis (93). It appears that innate immune cells such as macrophages and neutrophils have a larger role to play in PDAC than the adaptive immune mechanisms.

4.1 Regulatory T cells

In PDAC, regulatory T cells (Tregs) play a major role in tumour immune suppression. Through immunohistochemistry, they can be identified based on forkhead box protein 3 (FOXP3) expression and high levels of IL-2 receptor α chain CD25 in tumour tissues. There is sufficient evidence that Tregs are the primary barrier to an effective tumour immunotherapy (87). In fact, Tregs are significantly increased in the blood of PDAC patients as well as in the pancreatic tissue (155). They are recruited to tumour sites, where they inhibit antitumour cytotoxic response by binding to DCs and preventing DCs from activating CD8+T cells (156). From the premalignant to the invasive stages of PDAC, Tregs aid in suppressing the immune response against PDAC cells (157). In addition, it appears that a high Treg prevalence in PDAC is linked to a poor prognosis and weak PDAC differentiation (158). Single cell RNA seq studies revealed that activated TME is defined by the presence of Tregs, FGF, TAMs (SPP1+, GRN+), M2 like macrophages; in contrast, patients with normal stroma show M1-like macrophages, increased effector and exhausted T-cells (159).

Using the KC mouse model, a model where KRAS genetic changes are brought in for the development of pancreatic cancer, the immune cell infiltration at different stages of PDAC, including normal pancreas, PanINs, and invasive carcinoma, were examined (160, 161). Tregs and MDSCs predominated the immune infiltrate in the early PanIN stages. When the disease reached the PDAC stage, CD4+ and CD8+ cells were infrequently found and the existing CD8+ cells were not activated, suggesting an immunosuppressed TME (160). Strong inverse correlations between MDSCs and CD8+ T-lymphocytes at

all disease stages imply that MDSCs are a key player in tumour immunosuppression (160).

Clinically, pancreatic cancer frequently contains T lymphocytes which surround the pancreatic lesion; CD8+ cells are elevated in the circulation of PDAC patients (162). PDAC has a high percentage of CD4+ Tregs, which support an immunosuppressive phenotype. They are typically found in the stromal regions of the tumour and rarely in conjunction with tumour epithelial cells (157). Treg accumulation is correlated with the progression of both the major preoplastic lesions, PanINs and IPMN, in clinical samples of pre-malignant lesions (157). In murine models of PDAC, an association between Treg infiltration and the growth of pancreatic cancer is established. When syngeneic C57BL/6 mice are subcutaneously injected with mouse pancreatic tumour cells from Pan02, the spleen and tumour-draining lymph nodes of these mice exhibit a marked increase in Tregs (163). The CCR5 receptor, which is preferentially expressed by Tregs, is ligated by tumour cells in murine as well as human PDAC (164). Growth of PDAC is inhibited by CCR5 mediated blockade of Treg accumulation.

4.2 Regulatory B cells

Tumor-infiltrating B lymphocytes in PDAC differentiate into Regulatory B cells (Bregs) that produce IL-10 or IL-35 with the help of other immune cells such as Tregs and MDSCs, cytokines IL-18, CAFs, tumor-associated antigens, damage-associated molecular patterns, hypoxia, pancreatic microbiota, and metabolites in the TME (165, 166). A high number of IL-10/IL-35-producing Bregs are observed in the PDAC stroma of KPC and KC murine models and PDAC patient samples (93). IL-18 promotes Breg differentiation and enhances immunological tolerance, leading to the development and metastasis of PDAC (46). In addition to IL-18, other chemokines such as CXCL13 and CCL21, are responsible for B-cell migration and accumulation within tumors (93).

5 How tumour cells shape innate immune response in PDAC progression

5.1 Tumour intrinsic chemokines and cytokines

Cancer stem cells (CSCs) in PDAC have the ability to self-renew, differentiate into numerous lineages, initiate tumourigenesis, and resist conventional cancer therapy. CSCs are characterized by specific cell surface markers, CD44+CD24+ESA+ (167). Pro-inflammatory cytokines are involved in the CSC self-renewal process (168). Following the development of pancreatitis, the number of CSCs in the circulation greatly increased. However, treatment with the anti-inflammatory drug, dexamethasone, lowers the level of CSCs in the circulation. Thus, inflammation plays an important role in the spread of pancreatic CSCs and perhaps even in PDAC metastasis.

Tumour-derived cytokines and chemokines in PDAC set up the immunosuppressive cellular network by attracting myeloid cells to the TME. TAMs and MDSCs contribute to T cell exclusion from the TME by inhibiting their recruitment and priming. By secreting cytokines, chemokines, and other factors such as GM-CSF, CSF-1, IL-3, CXCL12, and CCL2, TAMs and MDSCs can shape the TME in ways that promote or inhibit tumour growth and survival.

Acinar cell trans-differentiation into duct-like cells, known as acinar to ductal metaplasia (ADM), is the first histologically distinct event during PDAC pathogenesis (98, 99, 169). ADM is required for pancreatic regeneration by the acinar cells and is accompanied by a loss of polarity or contact between cells or with the ECM. However, pro-inflammatory cytokines prevent the acinar reversibility in the presence of oncogenic Kras and advance ADM to lesions PanIN (99). TNF-α and RANTES (Regulated on Activation Normal T Cell Expressed and Secreted) are two pro-inflammatory cytokines secreted by TAMs that cause ADM by triggering NF- κB signalling and the expression of MMPs (170, 171).

The functional relevance of the chemokines in PDAC and their association with the NF-κB pathway has been studied (172). TAMs also secrete IL-6 and promote STAT signaling resulting in tumour growth and progression (173, 174). The initial secretion of cytokines such as PDGF and TGF-β, recruits additional lymphoid and myeloid subsets into the TME, which then secrete more TGF-ß1, CTGF, high mobility group box protein 1 (HMGB1), IL-10, IL-1α, IL-1β, IL-8, TNF-α, and CCL18 depending upon their activation status (175), resulting in chronically inflamed tissues. Signaling through a family of G-protein coupled receptors is an additional important stimulus for the infiltration of these immune cells into the PDAC tissue (176).

Numerous chemokines are described in relation to PDAC pathogenesis and therapy resistance. PDAC cells produce chemokine CCL2 or monocyte chemotactic protein 1 (MCP1), a proinflammatory chemokine that binds to CCR2 and CCR4 under normal conditions (177). CCL2 is found to be highly expressed in Basal like subtype compared to Classical subtype and recruits TAMs to the TME (178). This basal expression is further increased when the cells are stimulated with IL-1, TNF-α or FAS ligand (179). Furthermore, the regulation of CCL2 expression in PDAC cells are attributed to the NF-κB pathway (177, 179, 180). CXCL8, or IL-8, is a chemokine produced by many cell types. IL-8 also binds to CXCR1 and CXCR2, with a higher affinity for CXCR1. In addition to angiogenic functions, IL-8 mediates phagocytosis and chemotaxis.

6 PDAC aggressiveness and immune suppression

6.1 Innate immune-driven PDAC aggressiveness

Immune cell fractionation in PDAC revealed a higher proportion of innate immune cells than adaptive immune cells (8). PDAC tissue contains an abundance of macrophages, MDSCs, DCs, and neutrophils. Single-cell RNA sequencing (RNA-seq) data revealed that macrophages are the predominant immune cells

among the CD45$^+$ population in PDAC (8). Neutrophils also contribute to significant portion of the immune cell infiltrate observed in PDAC (181). Neutrophils are transformed into tumour-associated neutrophils (TANs) after migrating into tumour tissues. TANs were identified as Ly6G$^+$CD11b$^+$ cells (182), and further classified as N1 (tumour suppressing) or N2 (tumour promoting) phenotype (100) and are associated with poor prognoses in PDAC (183). Neutrophils are recruited to the PDAC TME via multiple tumour-secreted chemokines including CXCL1, CXCL2, CXCL5, and CXCL8. They respond to these chemokines by the expression of the CXCR1 and CXCR2 CXC receptors. Tumour size in PDAC correlates with the level of CXCR2 expression (184). Myeloperoxidase$^+$ (MPO$^+$) neutrophils and CD11b$^+$Ly6G$^+$ MDSCs infiltration into tumours is reduced in CXCR2 knockout PKF [mice with conditional Kras^{G12D} mutation and knockout of TGF-β receptor type II (Tgfbr2), (LSL-KrasG12D/+; Tgfbr2flox/flox, Ptf1a-Cre] mice compared to control animals (185). CXCL1, CXCL2, and CXCL5 secretion from tumour cells is elevated in the KPC (LSL-KrasG12D/+; LSL-Trp53R172H/+; Pdx1-Cre) mouse model, in comparison to the normal pancreas (186). Another study demonstrated that CXCL5 has the greatest increase in human PDAC and correlated with both tumour-infiltrating CD15$^+$ granulocytes and neutrophil elastase$^+$ (NE$^+$) granulocytes (187). Neutrophil depletion has been shown in multiple PDAC studies to reduce tumour growth and metastasis. Importantly, in wound healing and transwell assays *in vitro*, neutrophils derived from PDAC patients significantly promoted the migration and invasion of pancreatic cancer cells, whereas neutrophils derived from healthy individuals did not (188). In addition, Neutrophil to Lymphocyte Ratio correlates with a poor prognosis in patients with resectable and unresectable pancreatic cancer (187, 189–191). PDAC patient outcomes also correlate with the presence of neutrophils within the tumour. Neutrophil marker CD177 is inversely associated with overall survival in patients with PDAC (192). Patients with PDAC who have tumour-infiltrating neutrophils with high levels of CD66b$^+$ have significantly lower survival rates (181). In human PDAC tissues, TAN-derived TGF-β induces EMT in human lung cancer tissues through the TGF-β/Smad pathway, contributing to carcinogenesis (193, 194). Another study indicates that inhibition of CXCR2 decreases TAN accumulation, and inhibits PDAC metastasis in mice (186, 195).

DCs are uncommon in the TME of pancreatic cancers and are located at the tumour's periphery (196). Systemically, PDAC patients have decreased levels of blood DCs (197). Notably, higher levels of circulating DCs are associated with improved survival in PDAC patients (197, 198). In addition, surgical removal of the pancreatic tumour improved blood DC function, supporting a tumour-derived effect on immune function of DCs (199). During disease progression, the immune response of the host to pancreatic cancer is reported to shift from immune surveillance to immune tolerance. CXCL17 and intercellular adhesion molecule 2 (ICAM2) appear to mediate this polarisation (200). In addition, tumour-derived cytokines such as TGF-β, IL-10 and IL-6 have been shown to inhibit DC survival and proliferation (201). The proliferation of immature myeloid cells in the bloodstream and spleen may further compromise the immune response. The level of

circulating MDSCs is increased in PDAC, which may promote tumour progression (202, 203). MDSCs inhibit DC activation in pancreatic cancer by producing nitric oxide (NO) (204).

Innate lymphoid cells (ILCs) are innate immune cells that bridge between innate and adaptive immune system. Group 2 ILCs (ILC2s) are activated by IL-33, which have differential roles in PDAC development and progression; ILC2 activation recruits T cells to boost anti-cancer immunity in PDAC tissues via recruitment of CD103+ DCs (205). However, yet another study demonstrated that IL-33-treated ILC2s produced IL-10 and played a protective role in islet allograft survival (206). These results indicate that ILC2s are a highly dynamic cell type and their phenotypes and functions are controlled by the TME. In the TME, immunosuppression is observed where hypoxia converts ILC2s to IL-10+ ILCregs, helping to form a tolerogenic state in pancreatic cancer (9). ILCs recruit CD8+ T and memory T cells in PDAC; ILCs are also able to help CD108+ B cells migrate to tumour locations (207).

6.2 Innate-immune driven immune suppression in PDAC

PDAC is notoriously resistant to immunotherapy, such as cytokine therapy, adoptive T cell therapy, and checkpoint blockade strategies (208–210) Failure of these therapies has been attributed to a lack of CD8+ T cells and severe immunosuppression in the TME of PDAC (45, 211, 212). The presence of excessive fibrosis in the TME hinders the infiltration of adaptive immune cells (127).

At the early PanIN stages, Tregs and MDSCs dominate the immune infiltrate. As the disease progresses, CD4+ and CD8+ cells are inconsistently found; existing CD8+ cells display a lack of activation, suggesting an immune suppressed TME (160). At all stages of disease, there is a strong inverse correlation between MDSCs and CD8+ T-lymphocytes, suggesting that MDSCs are a mediator of tumour immunosuppression (160).

Conventional DCs (cDCs) have been identified as important mediators of antigen priming and T cell activity, with Batf3/Irf8-dependent CD103+ CD24+ cDC1s responsible for CD8+ CTL cross-priming. Moreover, Irf4-dependent CD11b+ CD172a+ cDC2s are implicated in the priming of CD4+ T helper cells (Th) (213). cDCs have also been implicated in T cell-dependent tumour killing and immunotherapy response (214–218). Nonetheless, it has been reported that the levels of circulating MDSCs are elevated in pancreatic cancer, which may promote tumour progression (202, 203); MDSCs produce NO, which inhibits DC activation (204). Depending on microenvironmental stimuli, DC can differentiate into distinct subpopulations, leading to proliferation of myeloid DCs that induce Th1 cell activation, or plasmacytoid DCs that facilitate immunosuppressive T cell development. Tumour-derived cytokines have been reported to induce a tolerogenic plasmacytoid DC phenotype (201). Furthermore, recent data suggest the existence of a specific subset CD11b+ DCs that foster an immunosuppressive TME, which favors metastatic progression through the expansion of Tregs and suppression of CD8+ T cells (219). These findings

indicate that PDAC is characterized not only by a reduced number of DCs, but also by complex modulation of DC subpopulations, which affects tumour development.

6.3 Complement system

The complement system is a crucial mechanism that connects innate immunity to adaptive immunity and aids the body in combating foreign pathogens and abnormal host cells (220). The complement system can be activated by three distinct pathways: classical, alternative, and lectin. The three pathways converge on the cleavage of complement component C3 into subunits C3a and C3b (C3 convertase) and C5 into fragments C5a and C5b (C5 convertase). As inflammatory mediators or anaphylatoxins, C3a and C5a, cause inflammation by causing histamine release and by activating immune cells such as neutrophils, eosinophils, and macrophages (221). Malignant tumours have increased complement protein expression (222). Activation of the complement system in the TME promotes tumourigenesis (222). PDAC tissue shows an upregulation of C3 and C5, producing more anaphylatoxins (223, 224), C3a and C5a, which upregulate inflammatory mediators and cytokines and cause direct stimulation of TNF-α and IL-1 (220). In addition, these anaphylatoxins increase the recruitment of macrophages in the TME (225).

The complement system has an important role to play in PDAC. The expression of complement regulatory proteins/receptors, CD46, CD55, and CD59, is well established in PDAC cell lines (226). Properdin, the only known up-regulator of the alternative pathway, is highly expressed in the early stages of PDAC; its decreased expression in samples from patients with late-stage PDAC has been reported (227). Neutrophils are known to secrete properdin, which is stored in their granules (228). Elevated properdin expression in PDAC patients with increased neutrophil infiltration is more likely to associate with classical subtype and higher overall and disease-free survival. Properdin induces apoptosis in basal-like pancreatic cancer cell lines, suggesting its anti-tumourigenic role in PDAC (229). Studies have also reported that properdin can recognize cancer cells and play a protective role during tumourigenesis (230). Alternatively, properdin level is strongly down-regulated in PDAC serum (231). The inhibition of complement activation promotes cancer cell immune evasion and seems to hamper the efficacy of cancer immunotherapy.

7 Targeting innate immunity in PDAC

Existing therapies for patients with PDAC include surgical resection, chemoradiation therapy, and immunotherapy; however, only a small percentage of patients benefit from these treatments. Single-cell RNA-seq studies on the PDAC TME show innate immune cell dominance, which can be directly activated by many cytokines without antigen presentation, unlike adaptive immunity. Given the predominant infiltration, decreased antigenicity, and instant activation, innate immunity may be more important than adaptive immunity in the PDAC immune TME.

On the basis of a growing comprehension of the role of TME in PDAC, neutrophils have emerged as a possible therapeutic target. Targeting neutrophils in PDAC has shown encouraging results in a number of preclinical studies that utilised CXCR2 inhibitors or Ly6G antibodies (187). The preference for CXCR2 as a target may possibly arise from the fact that blocking CXCR2 affects not just the CXCL5/CXCR2 axis but also additional CXCR2 ligands, such as CXCL1-3 and CXCL6-8.

TAMs are one of the most important regulators in the PDAC TME. Depletion of TAMs could dramatically decrease tumourigenesis (232); inhibiting M2 macrophage polarisation is essential for preventing PDAC development, enhancing antitumour immunity, and even clinical treatment (233). New developments in macrophage adjustment have been put forth, such as blocking CSF-1/CSF-1R, CD40 agonists, and other agents, which are helpful in re-educating TAMs from their M2 state to M1. It is currently possible to effectively halt tumour growth and cure tumours owing to an expanding variety of macrophage-targeting strategies. When combined with standard therapy and immunotherapeutic drugs, the blocking of CSF-1/CSF-1R activation can be a potential strategy for treating PDAC by decreasing the TAM population (234). Reprogramming the M2 phenotype of TAMs can significantly change the immunological status of the TME and reactivate the immune system's antitumour activity.

The phase II clinical testing of multiple antibodies against CSF1/1R in PDAC patients has been undertaken (235). The efficacy of cabiralizumab (Five Prime), a humanized IgG4 mAb against CSF1R, together with the anti-PD1 antibody, nivolumab, in patients with advanced/metastatic PDAC who progressed after first-line chemotherapy (NCT03336216) was evaluated (236). Similarly, another phase Ib/II trial evaluated a fully humanised IgG2 monoclonal anti–CSF1R antibody, AMG 820 (Amgen), in combination with pembrolizumab, on patients with metastatic PDAC (NCT02713529). Both trials failed to reach their effectiveness goals despite exhibiting target-specific alterations, such as the decrease in monocytes. The failure may have been related to the normal stroma association of the CSF1/CSF1R signaling and non-specific targeting based on the expression of CSF1R seen across all myeloid cells. In another phase Ib/II trial that included patients with metastatic PDAC, limited activity was observed with the anti–CSF1 antibody, lacnotuzumab (Novartis), given in combination with anti-PD1 spartalizumab (NCT02807844) (237).

HA is highly overexpressed by tumour cells and CAFs in PDAC; enzymatic depletion of HA using PEGylated hyaluronidase improves therapeutic effectiveness (37). Based on the expression levels of HA, clinical phase I/II study (NCT01839487) revealed robust response rates for patients. However, when combined together, nab-paclitaxel and gemcitabine failed to prolong progression free survival (238).

High levels of integrin molecule CD11b/CD18 on myeloid, cell surface, which is essential for their trafficking and cellular activities within inflammatory tissues, make them amenable to therapeutic targeting. ADH-503 is a small-molecule agonist that partially activates CD11b, causing TAMs to repolarize, fewer immunosuppressive myeloid cells to infiltrate the tumour, and improve DC responses. As a result, checkpoint inhibitors are now effective in PDAC models that were previously resistant to their effects and antitumour T cell immunity is improved. These results show that molecular inhibition of CD11b alters immunosuppressive myeloid cell responses and may overcome the limitations of existing clinical approaches to immunotherapy resistance (239).

DC vaccination has emerged as a novel strategy to prime host anti-tumour immunity (240). Specifically, the combination of a DC vaccine with gemcitabine led to eradication of orthotopic tumours and provided durable protection against PDAC in mouse models (241).

ECM plays a significant role in PDAC tumour growth, metastasis, and resistance to therapy. Accumulating preclinical studies with patient-derived specimens suggest that targeting the dense desmoplastic ECM proteins of PDAC may offer the potential for clinically useful treatments. In clinical practice, it has not yet been possible to successfully target the ECM to improve overall survival.

8 Recent clinical trials

Antibodies against immune checkpoints, such as anti-PD-1/PD-L1 and anti-CTLA-4, brought transformation in the treatment of several malignancies, but failed to elicit effective anti-tumour response in PDAC patients (19). A phase II clinical trial (NCT02879318) assessed the safety and efficacy of combination chemotherapy (Gemcitabine and nab-paclitaxel) with immune checkpoint inhibitors (durvalumab; PD-L1 inhibitor) and tremelimumab (CTLA-4 inhibitor), which did not improve survival rate significantly (242). Modified FOLFIRINOX (Folinic acid, fluorouracil, irinotecan, and oxaliplatin) with Sintilimab (human IgG4 monoclonal antibody for PD-1) used in a clinical trial (NCT03977272) did not show any survival benefit (243). Another phase II trial (NCT032124250) evaluated the efficacy of nivolumab (anti-PD-1) and/or sotigalimab (CD40 agonistic antibody) with gemcitabine/nab-paclitaxel (chemotherapy) in patients with first-line metastatic PDAC (244). The overall survival rate was 57.7% in nivolumab/chemotherapy group compared to 48.1% observed in sotigalimab/chemotherapy and 41.3% in nivolumab/sotigalimab/chemotherapy treatment regimen. Granulocyte-macrophage colony-stimulating factor (GM-CSF)-secreting allogeneic pancreatic tumour cell (GVAX) immunotherapy and ipilimumab did not improve overall survival, but clear biologic effects on peripheral and intratumoural immune cells were observed, such as increase in T cell activation markers, peripheral T helper and cytotoxic effector memory cells, and decrease in naïve cytotoxic T cells and increase in M1 macrophage content (245). A Phase Ib/II study (NCT02331251) using gemcitabine, nab-paclitaxel, and pembrolizumab to evaluate the safety and efficacy in mPDAC improved the overall survival rate in naive chemotherapy patients (246).

A phase 1b clinical trial (NCT03307148) targeting PSCs with all-trans-retinoic-acid (ATRA) can reprogram pancreatic stroma to suppress PDAC growth (247). ATRA as a stromal-targeting agent with gemcitabine-nab-paclitaxel is safe and tolerable and will be

evaluated in a phase II randomized controlled trial for locally advanced PDAC.

The clinicaltrials.gov registry provided with recent clinical trial data on PDAC having interventional therapy (Table 2). NCT02993731 is the largest cohort of patients with mPDAC administered nab-paclitaxel with gemcitabine. The addition of napabucasin to nab-paclitaxel with gemcitabine did not improve efficacy in patients with previously untreated mPDAC (248). CXCR2 antagonist that blocks neutrophil migration and reduces circulating neutrophil counts was studied in a clinical trial, (NCT02583477). In NCT02501902, the tolerability and antitumor activity of palbociclib plus nab-paclitaxel treatment in patients with PDAC did not meet the prespecified efficacy (249). The safety and efficacy of LMB-100, an immunotoxin that targets mesothelin with and without nab-paclitaxel was studied in NCT02810418 (250). This study resulted in increased numbers of active circulating CD4 and CD8 T cells, and identified specific changes in serum cytokines and peripheral CD4 T cell subsets associated with capillary leak syndrome, the major toxicity of immunotoxin therapies. NCT03611556 showed similar safety but a trend towards improved outcome (251). In NCT02289898, addition of demcizumab did not improve the efficacy in comparison with

placebo (252). NCT01893801, provided encouraging results with high response rate and improved median survival (253). In NCT01658943, selumetinib plus MK-2206 did not improve overall survival in patients with mPDAC for whom gemcitabine-based chemotherapy had failed (254). The baseline immune status predicts PDAC disease course and overall survival in NCT01280058 (255). Tremelimumab monotherapy is ineffective for metastatic PDAC (NCT02527434) (256). New therapeutic options are being studied in the clinical trials: NCT02981342, NCT02558894, NCT02178709. The availability of these results and other ongoing research will help improve the future trials in PDAC patients.

9 Conclusions and perspectives

The abundant desmoplastic stroma is inextricably linked to the immune landscape of human PDAC. This dense extracellular matrix contributes to the low immunogenicity of PDAC, thereby impeding the infiltration of effector T cells and fostering an immunosuppressive TME. There exists an urgent demand to enhance our understanding of the intricate interplay among tumour cells, immune cells and stromal components within the

TABLE 2 The clinical trial data collected from clinicaltrials.gov with keywords as pancreatic ductal adenocarcinoma and interventional study.

Study Phase	Clinical trial ID	Intervention/Treatment	Number of patients analysed	Overall survival 95% CI (Months)	Progression free survival 95% CI (Months)
Phase III	NCT02993731	Napabucasin Plus Nab-paclitaxel With Gemcitabine	565	11.43	6.70
		Nab-paclitaxel With Gemcitabine	569	11.73	6.08
Phase II	NCT02981342	Abemaciclib	33	2.71	1.68
		Abemaciclib LY3023414	33	3.29	1.81
		Gemcitabine Capecitabine	33	Data not estimable	3.25
Phase II	NCT02558894	Durvalumab (MEDI4736) monotherapy	33	3.1	1.5
		tremelimumab+MEDI4736	32	3.6	1.5
Phase II	NCT02178709	Folfirinox	43	15.7	*
Phase I- Phase II	NCT02583477	MEDI4736 in combination with nab-paclitaxel and gemcitabine	3	*	*
		MEDI4736 in combination with AZD5069	18	2.8	1.6
Phase I	NCT02501902	Palbociclib Nab-Paclitaxel	Approx 30-60 patients	**	**
Phase I- Phase II	NCT02810418	Immunotoxin (LMB-100) Nab-Paclitaxel	Approx 35-40 patients	**	**
Phase I- Phase II	NCT03611556	Oleclumab Durvalumab Gemcitabine Nab-paclitaxel Oxaliplatin Folinic acid 5-FU	213	***	***

(Continued)

TABLE 2 Continued

Study Phase	Clinical trial ID	Intervention/Treatment	Number of patients analysed	Overall survival 95% CI (Months)	Progression free survival 95% CI (Months)
Phase II	NCT02289898	Demcizumab Abraxane gemcitabine Placebo	207	*	*
Phase I-Phase II	NCT01893801	nab-paclitaxel Cisplatin gemcitabine	25	16.4	10.1
Phase II	NCT01658943	Akt Inhibitor MK2206 Selumetinib	58	3.9	1.9
		mFOLFOX	62	6.7	2.0
Phase II	NCT01280058	WT Reo virus Carboplatin Paclitaxel	36	7.3	4.9
		Carboplatin Paclitaxel	37	8.8	5.2
Phase II	NCT02527434	Tremelimumab monotherapy MEDI4736 monotherapy MEDI4736 + tremelimumab combination therapy	20	3.98	*

* Data not available.
** Sequential assessment.
*** Dose escalation study.
The overall survival (OS) and progression free survival of these clinical trials are given in the table.

context of pancreatic cancer. Enhancing our understanding of these interactions will be essential for improving therapeutic approaches for human PDAC.

The communication between the tumour cells and the TME is mediated by many factors including extracellular vesicles (EVs). Exosomes which are EVs with a diameter of 30-150 nm are secreted by tumour cells as well as the stromal cells in the TiME during tumour progression (257). PDAC-derived EVs distinctly regulate angiogenesis by inducing cell proliferation, mobility and secretion of pro-angiogenic factors. Cancer-associated thrombosis is yet another complication in PDAC via the expression of tissue factors. PDAC derived exosomes regulate pancreatic functions including lipidosis and glucose intake inhibition. The immunosuppressive Treg expansion is also mediated by EVs in PDAC through upregulation of the expression of FOXO transcription factors and nuclear translocation in FOXP3^{+} Tregs (258). The chemoresistant cells produce exosomal cargos that aggravate chemoresistance in sensitive cells leading to anti-apoptotic effect. Advanced PDAC patient serum has exosomes that can enhance liver and lung metastasis (259). There exists a crosstalk between tumour cells and TME mediated by EVs. PDAC-derived small EVs induce the polarisation towards M2 macrophages and inhibit effector T-cell response that promote immunosuppression and anti-tumour immunity. The potential of exosomes to stimulate the immune system of PDAC patients can be used as nanocarriers of immunotherapeutic agents (260). Therefore, understanding about this crosstalk can help develop targeted immunotherapy (261).

The immunosuppression in PDAC is multi-factorial. PDAC is characterized by an abundance of MDSCs and M2 TAMs. In contrast, the presence of CD8^{+} T cells is significantly low. The varied role of TME in PDAC can be treated by a multi-modal strategy that targets tumour promoting properties and improve the survival rate (262). The chemotherapy with immunotherapy combination tried thus far did not improve survival in mPDAC. Hence, site specific delivery of immunotherapeutics is currently under development. The ongoing clinical trials that evaluate the combination immunotherapy may elucidate mechanisms to bring down the immune suppression by TiME. The clinical trials may be evaluated further for the infiltration of adaptive immune cells like effector T cells. Patient specific biomarker identification and targeted therapy may improve the clinical outcomes. More clinical studies targeting the TiME in PDAC can enhance the potency of chemotherapy/immunotherapy treatment regimen. In general, it is thought that conceptual breakthroughs in understanding the overall TME of PDAC could facilitate the development of novel therapeutic approaches that target numerous processes simultaneously, resulting in combined benefits.

Author contributions

AJ: Data curation, Formal analysis, Investigation, Visualization, Writing – original draft. AA: Software, Visualization, Writing – original draft, Writing – review & editing. BA-R: Funding acquisition, Writing – review & editing. SS: Conceptualization, Formal analysis, Investigation, Supervision, Writing – review & editing. UK: Conceptualization, Funding acquisition, Project administration, Supervision, Writing – review & editing.

Funding

Conflict of interest

The authors declare that the research was conducted in the absence of any commercial or financial relationships that could be construed as a potential conflict of interest.

The author(s) declared that they were an editorial board member of Frontiers, at the time of submission. This had no impact on the peer review process and the final decision.

Publisher's note

All claims expressed in this article are solely those of the authors and do not necessarily represent those of their affiliated organizations, or those of the publisher, the editors and the reviewers. Any product that may be evaluated in this article, or claim that may be made by its manufacturer, is not guaranteed or endorsed by the publisher.

References

1. Cascinu S, Falconi M, Valentini V, Jelic S. ESMO Guidelines Working Group. Pancreatic cancer: ESMO Clinical Practice Guidelines for diagnosis, treatment and follow-up. *Ann Oncol* (2010) 21(Suppl 5):v55–8. doi: 10.1093/annonc/mdq165

2. Haeberle L, Esposito I. Pathology of pancreatic cancer. *Transl Gastroenterol Hepatol* (2019) 4:50. doi: 10.21037/tgh.2019.06.02

3. Siegel RL, Miller KD, Fuchs HE, Jemal A. Cancer statistic. *CA: A Cancer J Clin* (2022) 72(1):7–33. doi: 10.3322/caac.21708

4. Sung H, Ferlay J, Siegel RL, Laversanne M, Soerjomataram I, Jemal A, et al. Global cancer statistics 2020: GLOBOCAN estimates of incidence and mortality worldwide for 36 cancers in 185 countries. *CA Cancer J Clin* (2021) 71(3):209–49. doi: 10.3322/caac.21660

5. Khalaf N, El-Serag HB, Abrams HR, Thrift AP. Burden of pancreatic cancer: from epidemiology to practice. *Clin Gastroenterol Hepatol* (2021) 19(5):876–84. doi: 10.1016/j.cgh.2020.02.054

6. Rahib L, Wehner MR, Matrisian LM, Nead KT. Estimated projection of US cancer incidence and death to 2040. *JAMA Network Open* (2021) 4(4):e214708. doi: 10.1001/jamanetworkopen.2021.4708

7. Zhang L, Jin R, Yang X, Ying D. A population-based study of synchronous distant metastases and prognosis in patients with PDAC at initial diagnosis. *Front Oncol* (2023) 13:1087700. doi: 10.3389/fonc.2023.1087700

8. Steele NG, Carpenter ES, Kemp SB, Sirihorachai VR, The S, Delrosario L, et al. Multimodal mapping of the tumor and peripheral blood immune landscape in human pancreatic cancer. *Nat Cancer* (2020) 1(11):1097–112. doi: 10.1038/s43018-020-00121-4

9. Ye L, Jin K, Liao Z, Xiao Z, Xu H, Lin X, et al. Hypoxia-reprogrammed regulatory group 2 innate lymphoid cells promote immunosuppression in pancreatic cancer. *EBioMedicine* (2022) 79:104016. doi: 10.1016/j.ebiom.2022.104016

10. Guo J, Wang S, Gao Q. An integrated overview of the immunosuppression features in the tumor microenvironment of pancreatic cancer. *Front Immunol* (2023) 14:1258538. doi: 10.3389/fimmu.2023.1258538

11. Rubin SJS, Sojwal RS, Gubatan J, Rogalla S. The tumor immune microenvironment in pancreatic ductal adenocarcinoma: neither hot nor cold. *Cancers (Basel)* (2022) 14(17):4236. doi: 10.3390/cancers14174236

12. Muller M, Haghnejad V, Schaefer M, Gauchotte G, Caron B, Peyrin-Biroulet L, et al. The immune landscape of human pancreatic ductal carcinoma: key players, clinical implications, and challenges. *Cancers (Basel)* (2022) 14(4):995. doi: 10.3390/cancers14040995

13. Wang K, He H. Pancreatic tumor microenvironment. *Adv Exp Med Biol* (2020) 1296:243–57. doi: 10.1007/978-3-030-59038-3_15

14. Nitecki SS, Sarr MG, Colby TV, van Heerden JA. Long-term survival after resection for ductal adenocarcinoma of the pancreas Is it really improving?. *Ann Surg* (1995) 221(1):59–66. doi: 10.1097/00000658-199501000-00007

15. Vera R, Díez L, Martín Pérez E, Plaza JC, Sanjuanbenito A, Carrato A. Surgery for pancreatic ductal adenocarcinoma. *Clin Transl Oncol* (2017) 19(11):1303–11. doi: 10.1007/s12094-017-1688-0

16. Stathis A, Moore MJ. Advanced pancreatic carcinoma: current treatment and future challenges. *Nat Rev Clin Oncol* (2010) 7(3):163–72. doi: 10.1038/nrclinonc.2009.236

17. Bhowmick NA, Neilson EG, Moses HL. Stromal fibroblasts in cancer initiation and progression. *Nature* (2004) 432(7015):332–7. doi: 10.1038/nature03096

18. Hwang RF, Moore T, Arumugam T, Ramachandran V, Amos KD, Rivera A, et al. Cancer-associated stromal fibroblasts promote pancreatic tumor progression. *Cancer Res* (2008) 68(3):918–26. doi: 10.1158/0008-5472.CAN-07-5714

19. O'Reilly EM, Oh DY, Dhani N, Renouf DJ, Lee MA, Sun W, et al. Durvalumab with or without tremelimumab for patients with metastatic pancreatic ductal adenocarcinoma: A phase 2 randomized clinical trial. *JAMA Oncol* (2019) 5 (10):1431–8. doi: 10.1001/jamaoncol.2019.1588

20. Pan L, Fang J, Tong C, Chen M, Zhang B, Juengpanich S, et al. Survival benefits of neoadjuvant chemo(radio)therapy versus surgery first in patients with resectable or borderline resectable pancreatic cancer: a systematic review and meta-analysis. *World J Surg Onc* (2019) 18(1):1. doi: 10.1186/s12957-019-1767-5

21. Chawla A, Molina G, Pak LM, Rosenthal M, Mancias JD, Clancy TE, et al. Neoadjuvant Therapy is Associated with Improved Survival in Borderline-Resectable Pancreatic Cancer. *Ann Surg Oncol* (2020) 27(4):1191–1200. doi: 10.1245/s10434-019-08087-z

22. Nasief H, Hall W, Zheng C, Tsai S, Wang L, Erickson B, et al. Improving treatment response prediction for chemoradiation therapy of pancreatic cancer using a combination of delta-radiomics and the clinical biomarker CA19-9. *Front Oncol* (2020) 9:1464. doi: 10.3389/fonc.2019.01464

23. Moore MJ, Goldstein D, Hamm J, Figer A, Hecht JR, Gallinger S, et al. Erlotinib plus gemcitabine compared with gemcitabine alone in patients with advanced pancreatic cancer: a phase III trial of the National Cancer Institute of Canada Clinical Trials Group. *J Clin Oncol* (2007) 25(15):1960–6. doi: 10.1200/JCO.2006.07.9525

24. Nsingwane Z, Elebo N, Mhlambi N, Devar J, Omoshoro-jones J, Smith M, et al. Complement protein levels decrease with tumour severity in pancreatic ductal adenocarcinoma. *HPB* (2022) 24:S266. doi: 10.1016/j.hpb.2022.05.562

25. Beatty GL, Chiorean EG, Fishman MP, Saboury B, Teitelbaum UR, Sun W, et al. CD40 agonists alter tumor stroma and show efficacy against pancreatic carcinoma in mice and humans. *Science* (2011) 331(6024):1612–6. doi: 10.1126/science.1198443

26. Moinfar F, Man YG, Arnould L, Bratthauer GL, Ratschek M, Tavassoli FA. Concurrent and independent genetic alterations in the stromal and epithelial cells of mammary carcinoma: implications for tumorigenesis1. *Cancer Res* (2000) 60(9):2562–6.

27. Hu M, Yao J, Cai L, Bachman KE, van den Brûle F, Velculescu V, et al. Distinct epigenetic changes in the stromal cells of breast cancers. *Nat Genet* (2005) 37(8):899–905. doi: 10.1038/ng1596

28. Jiang B, Zhou L, Lu J, Wang Y, Liu C, You L, et al. Stroma-targeting therapy in pancreatic cancer: one coin with two sides? *Front Oncol* (2020) 10. doi: 10.3389/fonc.2020.576399

29. Minchinton AI, Tannock IF. Drug penetration in solid tumours. *Nat Rev Cancer* (2006) 6(8):583–92. doi: 10.1038/nrc1893

30. Sohr S, Engeland K. RHAMM is differentially expressed in the cell cycle and downregulated by the tumor suppressor p53. *Cell Cycle* (2008) 7(21):3448–60. doi: 10.4161/cc.7.21.7014

31. Toole BP, Slomiany MG. Hyaluronan: a constitutive regulator of chemoresistance and Malignancy in cancer cells. *Semin Cancer Biol* (2008) 18(4):244–50. doi: 10.1016/j.semcancer.2008.03.009

32. Misra S, Hascall VC, Markwald RR, Ghatak S. Interactions between hyaluronan and its receptors (CD44, RHAMM) regulate the activities of inflammation and cancer. *Front Immunol* (2015) 6:201. doi: 10.3389/fimmu.2015.00201

33. Jacobetz MA, Chan DS, Neesse A, Bapiro TE, Cook N, Frese KK, et al. Hyaluronan impairs vascular function and drug delivery in a mouse model of pancreatic cancer. *Gut* (2013) 62(1):112–20. doi: 10.1136/gutjnl-2012-302529

34. Singha NC, Nekoroski T, Zhao C, Symons R, Jiang P, Frost GI, et al. Tumor-associated hyaluronan limits efficacy of monoclonal antibody therapy. *Mol Cancer Ther* (2015) 14(2):523–32. doi: 10.1158/1535-7163.MCT-14-0580

35. Thompson CB, Shepard HM, O'Connor PM, Kadhim S, Jiang P, Osgood RJ, et al. Enzymatic depletion of tumor hyaluronan induces antitumor responses in preclinical animal models. *Mol Cancer Ther* (2010) 9(11):3052–64. doi: 10.1158/1535-7163.MCT-10-0470

36. Whatcott CJ, Han H, Von Hoff DD. Orchestrating the tumor microenvironment to improve survival for patients with pancreatic cancer: normalization, not destruction. *Cancer J* (2015) 21(4):299–306. doi: 10.1097/PPO.0000000000000140

37. Hingorani SR, Zheng L, Bullock AJ, Seery TE, Harris WP, Sigal DS, et al. HALO 202: randomized phase II study of PEGPH20 plus nab-paclitaxel/gemcitabine versus nab-paclitaxel/gemcitabine in patients with untreated, metastatic pancreatic ductal adenocarcinoma. *J Clin Oncol* (2018) 36(4):359–66. doi: 10.1200/JCO.2017.74.9564

38. Huo Y, Yang M, Liu W, Yang J, Fu X, Liu D, et al. High expression of DDR1 is associated with the poor prognosis in Chinese patients with pancreatic ductal adenocarcinoma. *J Exp Clin Cancer Res* (2015) 34(1):88. doi: 10.1186/s13046-015-0202-1

39. Aguilera KY, Huang H, Du W, Hagopian MM, Wang Z, Hinz S, et al. Inhibition of discoidin domain receptor 1 reduces collagen-mediated tumorigenicity in pancreatic ductal adenocarcinoma. *Mol Cancer Ther* (2017) 16(11):2473–85. doi: 10.1158/1535-7163.MCT-16-0834

40. Ko S, Jung KH, Yoon YC, Han BS, Park MS, Lee YJ, et al. A novel DDR1 inhibitor enhances the anticancer activity of gemcitabine in pancreatic cancer. *Am J Cancer Res* (2022) 12(9):4326–42.

41. Rucki AA, Zheng L. Pancreatic cancer stroma: understanding biology leads to new therapeutic strategies. *World J Gastroenterol* (2014) 20(9):2237–46. doi: 10.3748/wjg.v20.i9.2237

42. Yauch RL, Gould SE, Scales SJ, Tang T, Tian H, Ahn CP, et al. A paracrine requirement for hedgehog signalling in cancer. *Nature* (2008) 455(7211):406–10. doi: 10.1038/nature07275

43. Onishi H, Katano M. Hedgehog signaling pathway as a new therapeutic target in pancreatic cancer. *World J Gastroenterol* (2014) 20(9):2335–42. doi: 10.3748/wjg.v20.i9.2335

44. Heretsch P, Tzagkaroulaki L, Giannis A. Cyclopamine and hedgehog signaling: chemistry, biology, medical perspectives. *Angew Chem Int Ed Engl* (2010) 49(20):3418–27. doi: 10.1002/anie.200906967

45. Zhang B, Jiang T, Shen S, She X, Tuo Y, Hu Y, et al. Cyclopamine disrupts tumor extracellular matrix and improves the distribution and efficacy of nanotherapeutics in pancreatic cancer. *Biomaterials* (2016) 103:12–21. doi: 10.1016/j.biomaterials.2016.06.048

46. Zhao Y, Shen M, Feng Y, He R, Xu X, Xie Y, et al. Regulatory B cells induced by pancreatic cancer cell-derived interleukin-18 promote immune tolerance *via* the PD-1/PD-L1 pathway. *Oncotarget* (2018) 9(19):14803–14. doi: 10.18632/oncotarget.22976

47. Almawash SA, Mondal G, Mahato RI. Coadministration of polymeric conjugates of docetaxel and cyclopamine synergistically inhibits orthotopic pancreatic cancer growth and metastasis. *Pharm Res* (2018) 35(1):17. doi: 10.1007/s11095-017-2303-3

48. Porta M, Fabregat X, Malats N, Guarner L, Carrato A, de Miguel A, et al. Exocrine pancreatic cancer: symptoms at presentation and their relation to tumour site and stage. *Clin Transl Oncol* (2005) 7(5):189–97. doi: 10.1007/BF02712816

49. Singhi AD, Koay EJ, Chari ST, Maitra A. Early detection of pancreatic cancer: opportunities and challenges. *Gastroenterology* (2019) 156(7):2024–40. doi: 10.1053/j.gastro.2019.01.259

50. Goonetilleke KS, Siriwardena AK. Systematic review of carbohydrate antigen (CA 19-9) as a biochemical marker in the diagnosis of pancreatic cancer. *Eur J Surg Oncol* (2007) 33(3):266–70. doi: 10.1016/j.ejso.2006.10.004

51. Ballehaninna UK, Chamberlain RS. Serum CA 19-9 as a biomarker for pancreatic cancer-A comprehensive review. *Indian J Surg Oncol* (2011) 2(2):88–100. doi: 10.1007/s13193-011-0042-1

52. Wang Z, Tian YP. Clinical value of serum tumor markers CA19-9, CA125 and CA72-4 in the diagnosis of pancreatic carcinoma. *Mol Clin Oncol* (2014) 2(2):265–8. doi: 10.3892/mco.2013.226

53. Lei XF, Jia SZ, Ye J, Qiao YL, Zhao GM, Li XH, et al. Application values of detection of serum CA199, CA242 and CA50 in the diagnosis of pancreatic cancer. *J Biol Regul Homeost Agents* (2017) 31(2):383–8.

54. van Manen L, Groen JV, Putter H, Vahrmeijer AL, Swijnenburg RJ, Bonsing BA, et al. Elevated CEA and CA19-9 serum levels independently predict advanced pancreatic cancer at diagnosis. *Biomarkers* (2020) 25(2):186–93. doi: 10.1080/1354750X.2020.1725786

55. Maitra A, Fukushima N, Takaori K, Hruban RH. Precursors to invasive pancreatic cancer. *Adv Anat Pathol* (2005) 12(2):81–91. doi: 10.1097/01.pap.0000155055.14238.25

56. Hruban RH, Goggins M, Parsons J, Kern SE. Progression model for pancreatic cancer. *Clin Cancer Res* (2000) 6(8):2969–72.

57. Makohon-Moore A, Iacobuzio-Donahue CA. Pancreatic cancer biology and genetics from an evolutionary perspective. *Nat Rev Cancer* (2016) 16(9):553–65. doi: 10.1038/nrc.2016.66

58. Sclabas GM, Fujioka S, Schmidt C, Evans DB, Chiao PJ. NF-kappaB in pancreatic cancer. *Int J Gastrointest Cancer* (2003) 33(1):15–26. doi: 10.1385/IJGC:33:1:15

59. Löhr M, Klöppel G, Maisonneuve P, Lowenfels AB, Lüttges J. Frequency of K-ras mutations in pancreatic intraductal neoplasias associated with pancreatic ductal adenocarcinoma and chronic pancreatitis: a meta-analysis. *Neoplasia* (2005) 7(1):17–23. doi: 10.1593/neo.04445

60. Scarpa A, Capelli P, Mukai K, Zamboni G, Oda T, Iacono C, et al. Pancreatic adenocarcinomas frequently show p53 gene mutations. *Am J Pathol* (1993) 142 (5):1534–43.

61. Hahn SA, Schutte M, Hoque AT, Moskaluk CA, da Costa LT, Rozenblum E, et al. DPC4, a candidate tumor suppressor gene at human chromosome 18q21.1. *Science* (1996) 271(5247):350–3. doi: 10.1126/science.271.5247.350

62. Bailey P, Chang DK, Nones K, Johns AL, Patch AM, Gingras MC, et al. Genomic analyses identify molecular subtypes of pancreatic cancer. *Nature* (2016) 531(7592):47–52. doi: 10.1038/nature16965

63. Dardare J, Witz A, Merlin JL, Gilson P, Harlé A. SMAD4 and the TGFβ Pathway in patients with pancreatic ductal adenocarcinoma. *Int J Mol Sci* (2020) 21(10):3534. doi: 10.3390/ijms21103534

64. Low RRJ, Lim WW, Nguyen PM, Lee B, Christie M, Burgess AW, et al. The diverse applications of pancreatic ductal adenocarcinoma organoids. *Cancers* (2021) 13 (19):4979. doi: 10.3390/cancers13194979

65. Miyabayashi K, Baker LA, Deschênes A, Traub B, Caligiuri G, Plenker D, et al. Intraductal transplantation models of human pancreatic ductal adenocarcinoma reveal progressive transition of molecular subtypes. *Cancer Discov* (2020) 10(10):1566–89. doi: 10.1158/2159-8290.CD-20-0133

66. Collisson EA, Sadanandam A, Olson P, Gibb WJ, Truitt M, Gu S, et al. Subtypes of pancreatic ductal adenocarcinoma and their differing responses to therapy. *Nat Med* (2011) 17(4):500–3. doi: 10.1038/nm.2344

67. Moffitt RA, Marayati R, Flate EL, Volmar KE, Loeza SGH, Hoadley KA, et al. Virtual microdissection identifies distinct tumor- and stroma-specific subtypes of pancreatic ductal adenocarcinoma. *Nat Genet* (2015) 47(10):1168–78. doi: 10.1038/ng.3398

68. Chan-Seng-Yue M, Kim JC, Wilson GW, Ng K, Figueroa EF, O'Kane GM, et al. Transcription phenotypes of pancreatic cancer are driven by genomic events during tumor evolution. *Nat Genet* (2020) 52(2):231–40. doi: 10.1038/s41588-019-0566-9

69. Klein L, Tu M, Krebs N, Urbach L, Grimm D, Latif MU, et al. Spatial tumor immune heterogeneity facilitates subtype co-existence and therapy response *via* AP1 dichotomy in pancreatic cancer. *bioRxiv* (2023) 173. doi: 10.1101/2023.10.30.563552

70. Williams HL, Dias Costa A, Zhang J, Raghavan S, Winter PS, Kapner KS, et al. Spatially resolved single-cell assessment of pancreatic cancer expression subtypes reveals co-expressor phenotypes and extensive intratumoral heterogeneity. *Cancer Res* (2023) 83(3):441–55. doi: 10.1158/0008-5472.CAN-22-3050

71. Espinet E, Klein L, Puré E, Singh SK. Mechanisms of PDAC subtype heterogeneity and therapy response. *Trends Cancer* (2022) 8(12):1060–71. doi: 10.1016/j.trecan.2022.08.005

72. Rodriguez PC, Quiceno DG, Zabaleta J, Ortiz B, Zea AH, Piazuelo MB, et al. Arginase I production in the tumor microenvironment by mature myeloid cells inhibits T-cell receptor expression and antigen-specific T-cell responses. *Cancer Res* (2004) 64 (16):5839–49. doi: 10.1158/0008-5472.CAN-04-0465

73. Qian B, Deng Y, Im JH, Muschel RJ, Zou Y, Li J, et al. A distinct macrophage population mediates metastatic breast cancer cell extravasation, establishment and growth. *PLoS One* (2009) 4(8):e6562. doi: 10.1371/journal.pone.0006562

74. Kamisawa T, Wood LD, Itoi T, Takaori K. Pancreatic cancer. *Lancet* (2016) 388 (10039):73–85. doi: 10.1016/S0140-6736(16)00141-0

75. Helm O, Held-Feindt J, Grage-Griebenow E, Reiling N, Ungefroren H, Vogel I, et al. Tumor-associated macrophages exhibit pro- and anti-inflammatory properties by which they impact on pancreatic tumorigenesis. *Int J Cancer* (2014) 135(4):843–61. doi: 10.1002/ijc.28736

76. Eriksson E, Milenova I, Wenthe J, Moreno R, Alemany R, Loskog A. IL-6 signaling blockade during CD40-mediated immune activation favors antitumor factors by reducing TGF-β, collagen type I, and PD-L1/PD-1. *J Immunol* (2019) 202(3):787–98. doi: 10.4049/jimmunol.1800717

77. Kurahara H, Shinchi H, Mataki Y, Maemura K, Noma H, Kubo F, et al. Significance of M2-polarized tumor-associated macrophage in pancreatic cancer. *J Surg Res* (2011) 167(2):e211–219. doi: 10.1016/j.jss.2009.05.026

78. Yin H, Gao S, Chen Q, Liu S, Shoucair S, Ji Y, et al. Tumor-associated N1 and N2 neutrophils predict prognosis in patients with resected pancreatic ductal adenocarcinoma: A preliminary study. *MedComm (2020)* (2022) 3(4):e183. doi: 10.1002/mco2.183

79. Wang X, Qiu L, Li Z, Wang XY, Yi H. Understanding the multifaceted role of neutrophils in cancer and autoimmune diseases. *Front Immunol* (2018) 9:2456. doi: 10.3389/fimmu.2018.02456

80. Jaillon S, Ponzetta A, Di Mitri D, Santoni A, Bonecchi R, Mantovani A. Neutrophil diversity and plasticity in tumour progression and therapy. *Nat Rev Cancer* (2020) 20(9):485–503. doi: 10.1038/s41568-020-0281-y

81. Fukunaga A, Miyamoto M, Cho Y, Murakami S, Kawarada Y, Oshikiri T, et al. CD8+ tumor-infiltrating lymphocytes together with CD4+ tumor-infiltrating lymphocytes and dendritic cells improve the prognosis of patients with pancreatic adenocarcinoma. *Pancreas* (2004) 28(1):e26–31. doi: 10.1097/00006676-200401000-00023

82. Gorchs L, Fernández Moro C, Bankhead P, Kern KP, Sadeak I, Meng Q, et al. Human pancreatic carcinoma-associated fibroblasts promote expression of co-inhibitory markers on CD4+ and CD8+ T-cells. *Front Immunol* (2019) 10:847. doi: 10.3389/fimmu.2019.00847

83. Zhang T, Ren Y, Yang P, Wang J, Zhou H. Cancer-associated fibroblasts in pancreatic ductal adenocarcinoma. *Cell Death Dis* (2022) 13(10):1–11. doi: 10.1038/s41419-022-05351-1

84. Apte MV, Park S, Phillips PA, Santucci N, Goldstein D, Kumar RK, et al. Desmoplastic reaction in pancreatic cancer: role of pancreatic stellate cells. *Pancreas* (2004) 29(3):179–87.

85. Thyagarajan A, Alshehri MSA, Miller KLR, Sherwin CM, Travers JB, Sahu RP. Myeloid-derived suppressor cells and pancreatic cancer: implications in novel therapeutic approaches. *Cancers (Basel)* (2019) 11(11):1627. doi: 10.3390/cancers11111627

86. Ren B, Cui M, Yang G, Wang H, Feng M, You L, et al. Tumor microenvironment participates in metastasis of pancreatic cancer. *Mol Cancer* (2018) 17:108. doi: 10.1186/s12943-018-0858-1

87. Curiel TJ. Tregs and rethinking cancer immunotherapy. *J Clin Invest* (2007) 117 (5):1167–74. doi: 10.1172/JCI31202

88. Lim SA, Kim J, Jeon S, Shin MH, Kwon J, Kim TJ, et al. Defective localization with impaired tumor cytotoxicity contributes to the immune escape of NK cells in pancreatic cancer patients. *Front Immunol* (2019) 10. doi: 10.3389/fimmu.2019.00496

89. Hoshikawa M, Aoki T, Matsushita H, Karasaki T, Hosoi A, Odaira K, et al. NK cell and IFN signatures are positive prognostic biomarkers for resectable pancreatic cancer. *Biochem Biophys Res Commun* (2018) 495(2):2058–65. doi: 10.1016/j.bbrc.2017.12.083

90. van der Leun AM, Thommen DS, Schumacher TN. CD8+ T cell states in human cancer: insights from single-cell analysis. *Nat Rev Cancer* (2020) 20(4):218–32. doi: 10.1038/s41568-019-0235-4

91. Goulart MR, Stasinos K, Fincham REA, Delvecchio FR, Kocher HM. T cells in pancreatic cancer stroma. *World J Gastroenterol* (2021) 27(46):7956–68. doi: 10.3748/wjg.v27.i46.7956

92. Castino GF, Cortese N, Capretti G, Serio S, Di Caro G, Mineri R, et al. Spatial distribution of B cells predicts prognosis in human pancreatic adenocarcinoma. *Oncoimmunology* (2016) 5(4):e1085147. doi: 10.1080/2162402X.2015.1085147

93. Senturk ZN, Akdag I, Deniz B, Sayi-Yazgan A. Pancreatic cancer: Emerging field of regulatory B-cell-targeted immunotherapies. *Front Immunol* (2023) 14:1152551. doi: 10.3389/fimmu.2023.1152551

94. Chu GC, Kimmelman AC, Hezel AF, DePinho RA. Stromal biology of pancreatic cancer. *J Cell Biochem* (2007) 101(4):887–907. doi: 10.1002/jcb.21209

95. Korc M. Pancreatic cancer–associated stroma production. *Am J Surg* (2007) 194 (4, Supplement):S84–6. doi: 10.1016/j.amjsurg.2007.05.004

96. Feig C, Gopinathan A, Neesse A, Chan DS, Cook N, Tuveson DA. The pancreas cancer microenvironment. *Clin Cancer Res* (2012) 18(16):4266–76. doi: 10.1158/1078-0432.CCR-11-3114

97. Kota J, Hancock J, Kwon J, Korc M. Pancreatic cancer: Stroma and its current and emerging targeted therapies. *Cancer Letters* (2017) 391:38–49. doi: 10.1016/j.canlet.2016.12.035

98. Kopp JL, von Figura G, Mayes E, Liu FF, Dubois CL, Morris JP, et al. Identification of sox9-dependent acinar-to-ductal reprogramming as the principal mechanism for initiation of pancreatic ductal adenocarcinoma. *Cancer Cell* (2012) 22 (6):737–50. doi: 10.1016/j.ccr.2012.10.025

99. Storz P. Acinar cell plasticity and development of pancreatic ductal adenocarcinoma. *Nat Rev Gastroenterol Hepatol* (2017) 14(5):296–304. doi: 10.1038/nrgastro.2017.12

100. Fridlender ZG, Sun J, Kim S, Kapoor V, Cheng G, Ling L, et al. Polarization of tumor-associated neutrophil phenotype by TGF-beta: "N1" versus "N2" TAN. *Cancer Cell* (2009) 16(3):183–94. doi: 10.1016/j.ccr.2009.06.017

101. Hanahan D, Weinberg RA. Hallmarks of cancer: the next generation. *Cell* (2011) 144(5):646–74. doi: 10.1016/j.cell.2011.02.013

102. Lowenfels AB, Maisonneuve P, Cavallini G, Ammann RW, Lankisch PG, Andersen JR, et al. Pancreatitis and the risk of pancreatic cancer. *New Engl J Med* (1993) 328(20):1433–7. doi: 10.1056/NEJM199305203282001

103. Xu M, Jung X, Hines OJ, Eibl G, Chen Y. Obesity and pancreatic cancer: overview of epidemiology and potential prevention by weight loss. *Pancreas* (2018) 47 (2):158. doi: 10.1097/MPA.0000000000000974

104. Weissman S, Takakura K, Eibl G, Pandol SJ, Saruta M. The diverse involvement of cigarette smoking in pancreatic cancer development and prognosis. *Pancreas* (2020) 49(5):612. doi: 10.1097/MPA.0000000000001550

105. Grivennikov SI, Greten FR, Karin M. Immunity, inflammation, and cancer. *Cell* (2010) 140(6):883–99. doi: 10.1016/j.cell.2010.01.025

106. Yako YY, Kruger D, Smith M, Brand M. Cytokines as biomarkers of pancreatic ductal adenocarcinoma: A systematic review. *PloS One* (2016) 11(5):e0154016. doi: 10.1371/journal.pone.0154016

107. Ling J, Kang Y, Zhao R, Xia Q, Lee DF, Chang Z, et al. KrasG12D-induced IKK2/β/NF-κB activation by IL-1α and p62 feedforward loops is required for development of pancreatic ductal adenocarcinoma. *Cancer Cell* (2012) 21(1):105–20. doi: 10.1016/j.ccr.2011.12.006

108. Grivennikov SI, Karin M. Inflammatory cytokines in cancer: tumour necrosis factor and interleukin 6 take the stage. *Ann Rheumatic Dis* (2011) 70(Suppl 1):i104–8. doi: 10.1136/ard.2010.140145

109. Mace TA, Shakya R, Pitarresi JR, Swanson B, McQuinn CW, Loftus S, et al. IL-6 and PD-L1 antibody blockade combination therapy reduces tumour progression in murine models of pancreatic cancer. *Gut* (2018) 67(2):320–32. doi: 10.1136/gutjnl-2016-311585

110. Herbst RS, Soria JC, Kowanetz M, Fine GD, Hamid O, Gordon MS, et al. Predictive correlates of response to the anti-PD-L1 antibody MPDL3280A in cancer patients. *Nature* (2014) 515(7528):563–7. doi: 10.1038/nature14011

111. Sanford DE, Belt BA, Panni RZ, Mayer A, Deshpande AD, Carpenter D, et al. Inflammatory monocyte mobilization decreases patient survival in pancreatic cancer: A role for targeting the CCL2/CCR2 axis. *Clin Cancer Res* (2013) 19(13):3404–15. doi: 10.1158/1078-0432.CCR-13-0525

112. Tsujikawa T, Kumar S, Borkar RN, Azimi V, Thibault G, Chang YH, et al. Quantitative multiplex immunohistochemistry reveals myeloid-inflamed tumor-immune complexity associated with poor prognosis. *Cell Rep* (2017) 19(1):203–17. doi: 10.1016/j.celrep.2017.03.037

113. Gabrilovich DI, Velders MP, Sotomayor EM, Kast WM. Mechanism of immune dysfunction in cancer mediated by immature Gr-1+ myeloid cells. *J Immunol* (2001) 166(9):5398–406. doi: 10.4049/jimmunol.166.9.5398

114. Lin EY, Li JF, Gnatovskiy L, Deng Y, Zhu L, Grzesik DA, et al. Macrophages regulate the angiogenic switch in a mouse model of breast cancer. *Cancer Res* (2006) 66 (23):11238–46. doi: 10.1158/0008-5472.CAN-06-1278

115. Saio M, Radoja S, Marino M, Frey AB. Tumor-infiltrating macrophages induce apoptosis in activated CD8(+) T cells by a mechanism requiring cell contact and mediated by both the cell-associated form of TNF and nitric oxide. *J Immunol* (2001) 167(10):5583–93. doi: 10.4049/jimmunol.167.10.5583

116. Rodriguez PC, Quiceno DG, Ochoa AC. L-arginine availability regulates T-lymphocyte cell-cycle progression. *Blood* (2007) 109(4):1568–73. doi: 10.1182/blood-2006-06-031856

117. Munder M, Choi BS, Rogers M, Kropf P. L-arginine deprivation impairs Leishmania major-specific T-cell responses. *Eur J Immunol* (2009) 39(8):2161–72. doi: 10.1002/eji.200839041

118. Werba G, Weissinger D, Kawaler EA, Zhao E, Kalfakakou D, Dhara S, et al. Single-cell RNA sequencing reveals the effects of chemotherapy on human pancreatic adenocarcinoma and its tumor microenvironment. *Nat Commun* (2023) 14(1):797. doi: 10.1038/s41467-023-36296-4

119. Komura T, Sakai Y, Harada K, Kawaguchi K, Takabatake H, Kitagawa H, et al. Inflammatory features of pancreatic cancer highlighted by monocytes/macrophages and CD4+ T cells with clinical impact. *Cancer Sci* (2015) 106(6):672–86. doi: 10.1111/cas.12663

120. Casey SC, Tong L, Li Y, Do R, Walz S, Fitzgerald KN, et al. MYC regulates the antitumor immune response through CD47 and PD-L1. *Science* (2016) 352(6282):227–31. doi: 10.1126/science.aac9935

121. Coelho MA, de Carné Trécesson S, Rana S, Zecchin D, Moore C, Molina-Arcas M, et al. Oncogenic RAS signaling promotes tumor immunoresistance by stabilizing PD-L1 mRNA. *Immunity* (2017) 47(6):1083–1099.e6. doi: 10.1016/j.immuni.2017.11.016

122. El-Jawhari JJ, El-Sherbiny YM, Scott GB, Morgan RSM, Prestwich R, Bowles PA, et al. Blocking oncogenic RAS enhances tumour cell surface MHC class I expression but does not alter susceptibility to cytotoxic lymphocytes. *Mol Immunol* (2014) 58(2):160–8. doi: 10.1016/j.molimm.2013.11.020

123. Yamamoto K, Venida A, Yano J, Biancur DE, Kakiuchi M, Gupta S, et al. Autophagy promotes immune evasion of pancreatic cancer by degrading MHC-I. *Nature* (2020) 581(7806):100–5. doi: 10.1038/s41586-020-2229-5

124. Lafaro KJ, Melstrom LG. The paradoxical web of pancreatic cancer tumor microenvironment. *Am J Pathology* (2019) 189(1):44–57. doi: 10.1016/j.ajpath.2018.09.009

125. Diab M, El-Rayes BF. The heterogeneity of CAFs and immune cell populations in the tumor microenvironment of pancreatic adenocarcinoma. *J Cancer Metastasis Treat* (2022) 8:42. doi: 10.20517/2394-4722.2022.60

126. Olive KP, Jacobetz MA, Davidson CJ, Gopinathan A, McIntyre D, Honess D, et al. Inhibition of Hedgehog signaling enhances delivery of chemotherapy in a mouse model of pancreatic cancer. *Science* (2009) 324(5933):1457–61. doi: 10.1126/science.1171362

127. Provenzano PP, Cuevas C, Chang AE, Goel VK, Von Hoff DD, Hingorani SR. Enzymatic targeting of the stroma ablates physical barriers to treatment of pancreatic ductal adenocarcinoma. *Cancer Cell* (2012) 21(3):418–29. doi: 10.1016/j.ccr.2012.01.007

128. Steins A, van Mackelenbergh MG, van der Zalm AP, Klaassen R, Serrels B, Goris SG, et al. High-grade mesenchymal pancreatic ductal adenocarcinoma drives stromal deactivation through CSF-1. *EMBO Rep* (2020) 21(5):e48780. doi: 10.15252/embr.201948780

129. Ohuchida K, Mizumoto K, Murakami M, Qian LW, Sato N, Nagai E, et al. Radiation to stromal fibroblasts increases invasiveness of pancreatic cancer cells through tumor-stromal interactions. *Cancer Res* (2004) 64(9):3215–22. doi: 10.1158/0008-5472.CAN-03-2464

130. Sada M, Ohuchida K, Horioka K, Okumura T, Moriyama T, Miyasaka Y, et al. Hypoxic stellate cells of pancreatic cancer stroma regulate extracellular matrix fiber organization and cancer cell motility. *Cancer Lett* (2016) 372(2):210–8. doi: 10.1016/j.canlet.2016.01.016

131. Endo S, Nakata K, Ohuchida K, Takesue S, Nakayama H, Abe T, et al. Autophagy is required for activation of pancreatic stellate cells, associated with pancreatic cancer progression and promotes growth of pancreatic tumors in mice. *Gastroenterology* (2017) 152(6):1492–1506.e24. doi: 10.1053/j.gastro.2017.01.010

132. Koikawa K, Ohuchida K, Ando Y, Kibe S, Nakayama H, Takesue S, et al. Basement membrane destruction by pancreatic stellate cells leads to local invasion in

pancreatic ductal adenocarcinoma. *Cancer Lett* (2018) 425:65–77. doi: 10.1016/j.canlet.2018.03.031

133. Feig C, Jones JO, Kraman M, Wells RJB, Deonarine A, Chan DS, et al. Targeting CXCL12 from FAP-expressing carcinoma-associated fibroblasts synergizes with anti-PD-L1 immunotherapy in pancreatic cancer. *Proc Natl Acad Sci USA* (2013) 110 (50):20212–7. doi: 10.1073/pnas.1320318110

134. Halbrook CJ, Lyssiotis CA. Employing metabolism to improve the diagnosis and treatment of pancreatic cancer. *Cancer Cell* (2017) 31(1):5–19. doi: 10.1016/j.ccell.2016.12.006

135. Kalluri R. The biology and function of fibroblasts in cancer. *Nat Rev Cancer* (2016) 16(9):582–98. doi: 10.1038/nrc.2016.73

136. Kozono S, Ohuchida K, Eguchi D, Ikenaga N, Fujiwara K, Cui L, et al. Pirfenidone inhibits pancreatic cancer desmoplasia by regulating stellate cells. *Cancer Res* (2013) 73(7):2345–56. doi: 10.1158/0008-5472.CAN-12-3180

137. Pandol S, Edderkaoui M, Gukovsky I, Lugea A, Gukovskaya A. Desmoplasia of pancreatic ductal adenocarcinoma. *Clin Gastroenterol Hepatol* (2009) 7(11 Suppl):S44–47. doi: 10.1016/j.cgh.2009.07.039

138. Weniger M, Honselmann KC, Liss AS. The extracellular matrix and pancreatic cancer: A complex relationship. *Cancers* (2018) 10(9):316. doi: 10.3390/cancers10090316

139. Tian C, Clauser KR, Öhlund D, Rickelt S, Huang Y, Gupta M, et al. Proteomic analyses of ECM during pancreatic ductal adenocarcinoma progression reveal different contributions by tumor and stromal cells. *Proc Natl Acad Sci USA* (2019) 116 (39):19609–18. doi: 10.1073/pnas.1908626116

140. Öhlund D, Franklin O, Lundberg E, Lundin C, Sund M. Type IV collagen stimulates pancreatic cancer cell proliferation, migration, and inhibits apoptosis through an autocrine loop. *BMC Cancer* (2013) 13:154. doi: 10.1186/1471-2407-13-154

141. Laklai H, Miroshnikova YA, Pickup MW, Collisson EA, Kim GE, Barrett AS, et al. Genotype tunes pancreatic ductal adenocarcinoma tissue tension to induce matricellular fibrosis and tumor progression. *Nat Med* (2016) 22(5):497–505. doi: 10.1038/nm.4082

142. Sipos B, Hahn D, Carceller A, Piulats J, Hedderich J, Kalthoff H, et al. Immunohistochemical screening for beta6-integrin subunit expression in adenocarcinomas using a novel monoclonal antibody reveals strong up-regulation in pancreatic ductal adenocarcinomas in vivo and in vitro. *Histopathology* (2004) 45 (3):226–36. doi: 10.1111/j.1365-2559.2004.01919.x

143. Pan S, Chen R, Tamura Y, Crispin DA, Lai LA, May DH, et al. Quantitative glycoproteomics analysis reveals changes in N-glycosylation level associated with pancreatic ductal adenocarcinoma. *J Proteome Res* (2014) 13(3):1293–306. doi: 10.1021/pr4010184

144. Sahai E, Astsaturov I, Cukierman E, DeNardo DG, Egeblad M, Evans RM, et al. A framework for advancing our understanding of cancer-associated fibroblasts. *Nat Rev Cancer* (2020) 20(3):174–86. doi: 10.1038/s41568-019-0238-1

145. Ferdek PE, Jakubowska MA. Biology of pancreatic stellate cells-more than just pancreatic cancer. *Pflugers Arch* (2017) 469(9):1039–50. doi: 10.1007/s00424-017-1968-0

146. Apte MV, Pirola RC, Wilson JS. Pancreatic stellate cells: a starring role in normal and diseased pancreas. *Front Physiol* (2012) 3:344. doi: 10.3389/fphys.2012.00344

147. Korc M, Chandrasekar B, Shah GN. Differential binding and biological activities of epidermal growth factor and transforming growth factor alpha in a human pancreatic cancer cell line. *Cancer Res* (1991) 51(23 Pt 1):6243–9.

148. Kikuta K, Masamune A, Watanabe T, Ariga H, Itoh H, Hamada S, et al. Pancreatic stellate cells promote epithelial-mesenchymal transition in pancreatic cancer cells. *Biochem Biophys Res Commun* (2010) 403(3–4):380–4. doi: 10.1016/j.bbrc.2010.11.040

149. Peng J, Sun BF, Chen CY, Zhou JY, Chen YS, Chen H, et al. Single-cell RNA-seq highlights intra-tumoral heterogeneity and malignant progression in pancreatic ductal adenocarcinoma. *Cell Res* (2019) 29(9):725–38. doi: 10.1038/s41422-019-0195-y

150. Carstens JL, Correa de Sampaio P, Yang D, Barua S, Wang H, Rao A, et al. Spatial computation of intratumoral T cells correlates with survival of patients with pancreatic cancer. *Nat Commun* (2017) 8(1):15095. doi: 10.1038/ncomms15095

151. Tesfaye AA, Kamgar M, Azmi A, Philip PA. The evolution into personalized therapies in pancreatic ductal adenocarcinoma: challenges and opportunities. *Expert Rev Anticancer Ther* (2018) 18(2):131–48. doi: 10.1080/14737140.2018.1417844

152. Stone ML, Beatty GL. Cellular determinants and therapeutic implications of inflammation in pancreatic cancer. *Pharmacol Ther* (2019) 201:202–13. doi: 10.1016/j.pharmthera.2019.05.012

153. Vonderheide RH, Bear AS. Tumor-derived myeloid cell chemoattractants and T cell exclusion in pancreatic cancer. *Front Immunol* (2020) 11:605619. doi: 10.3389/fimmu.2020.605619

154. Pylayeva-Gupta Y, Das S, Handler JS, Hajdu CH, Coffre M, Koralov SB, et al. IL35-producing B cells promote the development of pancreatic neoplasia. *Cancer Discovery* (2016) 6(3):247–55. doi: 10.1158/2159-8290.CD-15-0843

155. Liyanage UK, Moore TT, Joo HG, Tanaka Y, Herrmann V, Doherty G, et al. Prevalence of regulatory T cells is increased in peripheral blood and tumor microenvironment of patients with pancreas or breast adenocarcinoma. *J Immunol* (2002) 169(5):2756–61. doi: 10.4049/jimmunol.169.5.2756

156. Krishnamoorthy M, Lenehan JG, Burton JP, Maleki Vareki S. Immunomodulation in pancreatic cancer. *Cancers* (2020) 12(11):3340. doi: 10.3390/cancers12113340

157. Hiraoka N, Onozato K, Kosuge T, Hirohashi S. Prevalence of FOXP3+ regulatory T cells increases during the progression of pancreatic ductal adenocarcinoma and its premalignant lesions. *Clin Cancer Res* (2006) 12(18):5423–34. doi: 10.1158/1078-0432.CCR-06-0369

158. Tang Y, Xu X, Guo S, Zhang C, Tang Y, Tian Y, et al. An increased abundance of tumor-infiltrating regulatory T cells is correlated with the progression and prognosis of pancreatic ductal adenocarcinoma. *PloS One* (2014) 9(3):e91551. doi: 10.1371/journal.pone.0091551

159. Oh K, Yoo YJ, Torre-Healy LA, Rao M, Fassler D, Wang P, et al. Coordinated single-cell tumor microenvironment dynamics reinforce pancreatic cancer subtype. *Nat Commun* (2023) 14(1):5226. doi: 10.1038/s41467-023-40895-6

160. Clark CE, Hingorani SR, Mick R, Combs C, Tuveson DA, Vonderheide RH. Dynamics of the immune reaction to pancreatic cancer from inception to invasion. *Cancer Res* (2007) 67(19):9518–27. doi: 10.1158/0008-5472.CAN-07-0175

161. Hackeng WM, Hruban RH, Offerhaus GJA, Brosens LAA. Surgical and molecular pathology of pancreatic neoplasms. *Diagn Pathol* (2016) 11(1):47. doi: 10.1186/s13000-016-0497-z

162. Fogar P, Sperti C, Basso D, Sanzari MC, Greco E, Davoli C, et al. Decreased total lymphocyte counts in pancreatic cancer: an index of adverse outcome. *Pancreas* (2006) 32(1):22. doi: 10.1097/01.mpa.0000188305.90290.50

163. Linehan DC, Goedegebuure PS. CD25+ CD4+ regulatory T-cells in cancer. *Immunol Res* (2005) 32(1–3):155–68. doi: 10.1385/IR:32:1-3:155

164. Tan MCB, Goedegebuure PS, Belt BA, Flaherty B, Sankpal N, Gillanders WE, et al. Disruption of CCR5-dependent homing of regulatory T cells inhibits tumor growth in a murine model of pancreatic cancer. *J Immunol* (2009) 182(3):1746–55. doi: 10.4049/jimmunol.182.3.1746

165. Lindner S, Dahlke K, Sontheimer K, Hagn M, Kaltenmeier C, Barth TFE, et al. Interleukin 21-induced granzyme B-expressing B cells infiltrate tumors and regulate T cells. *Cancer Res* (2013) 73(8):2468–79. doi: 10.1158/0008-5472.CAN-12-3450

166. Arsenijevic T, Nicolle R, Bouchart C, D'Haene N, Demetter P, Puleo F, et al. Pancreatic cancer meets human microbiota: close encounters of the third kind. *Cancers (Basel)* (2021) 13(6):1231. doi: 10.3390/cancers13061231

167. Li C, Heidt DG, Dalerba P, Burant CF, Zhang L, Adsay V, et al. Identification of pancreatic cancer stem cells. *Cancer Res* (2007) 67(3):1030–7. doi: 10.1158/0008-5472.CAN-06-2030

168. Korkaya H, Liu S, Wicha MS. Regulation of cancer stem cells by cytokine networks: attacking cancers inflammatory roots. *Clin Cancer Res* (2011) 17(19):6125–9. doi: 10.1158/1078-0432.CCR-10-2743

169. Parte S, Nimmakayala RK, Batra SK, Ponnusamy MP. Acinar to ductal cell trans-differentiation: A prelude to dysplasia and pancreatic ductal adenocarcinoma. *Biochim Biophys Acta (BBA) - Rev Cancer* (2022) 1877(1):188669. doi: 10.1016/j.bbcan.2021.188669

170. Liou GY, Döppler H, Necela B, Krishna M, Crawford HC, Raimondo M, et al. Macrophage-secreted cytokines drive pancreatic acinar-to-ductal metaplasia through NF-κB and MMPs. *J Cell Biol* (2013) 202(3):563–77. doi: 10.1083/jcb.201301001

171. Poh AR, Ernst M. Tumor-associated macrophages in pancreatic ductal adenocarcinoma: therapeutic opportunities and clinical challenges. *Cancers* (2021) 13 (12):2860. doi: 10.3390/cancers13122860

172. Geismann C, Schäfer H, Gundlach JP, Hauser C, Egberts JH, Schneider G, et al. NF-κB dependent chemokine signaling in pancreatic cancer. *Cancers* (2019) 11 (10):1445. doi: 10.3390/cancers11101445

173. Lesina M, Kurkowski MU, Ludes K, Rose-John S, Treiber M, Klöppel G, et al. Stat3/socs3 activation by IL-6 transsignaling promotes progression of pancreatic intraepithelial neoplasia and development of pancreatic cancer. *Cancer Cell* (2011) 19(4):456–69. doi: 10.1016/j.ccr.2011.03.009

174. Deschênes-Simard X, Mizukami Y, Bardeesy N. Macrophages in pancreatic cancer: Starting things off on the wrong track. *J Cell Biol* (2013) 202(3):403–5. doi: 10.1083/jcb.201307066

175. Chen Q, Wang J, Zhang Q, Zhang J, Lou Y, Yang J, et al. Tumour cell-derived debris and IgG synergistically promote metastasis of pancreatic cancer by inducing inflammation *via* tumour-associated macrophages. *Br J Cancer* (2019) 121(9):786–95. doi: 10.1038/s41416-019-0595-2

176. Sriram K, Salmerón C, Wiley SZ, Insel PA. GPCRs in pancreatic adenocarcinoma: Contributors to tumor biology and novel therapeutic targets. *Br J Pharmacol* (2020) 177(11):2434–55. doi: 10.1111/bph.15028

177. Takaya H, Andoh A, Shimada M, Hata K, Fujiyama Y, Bamba T. The expression of chemokine genes correlates with nuclear factor-kappaB activation in human pancreatic cancer cell lines. *Pancreas* (2000) 21(1):32–40. doi: 10.1097/00006676-200007000-00049

178. Tu M, Klein L, Spinet E, Georgomanolis T, Wegwitz F, Li X, et al. TNF-α-producing macrophages determine subtype identity and prognosis *via* AP1 enhancer reprogramming in pancreatic cancer. *Nat Cancer* (2021) 2(11):1185–203. doi: 10.1038/s43018-021-00258-w

179. Shimada M, Andoh A, Araki Y, Fujiyama Y, Bamba T. Ligation of the Fas antigen stimulates chemokine secretion in pancreatic cancer cell line PANC-1. *J Gastroenterol Hepatol* (2001) 16(9):1060–7. doi: 10.1046/j.1440-1746.2001.02583.x

180. Sun H, Zhao L, Pan K, Zhang Z, Zhou M, Cao G. "Integrated analysis of mRNA and miRNA expression profiles in pancreatic ductal adenocarcinoma". *Oncology Reports 37, no. 5* (2017), 2779–86. doi: 10.3892/or.2017.5526

181. Ino Y, Yamazaki-Itoh R, Shimada K, Iwasaki M, Kosuge T, Kanai Y, et al. Immune cell infiltration as an indicator of the immune microenvironment of pancreatic cancer. *Br J Cancer* (2013) 108(4):914–23. doi: 10.1038/bjc.2013.32

182. Sagiv JY, Michaeli J, Assi S, Mishalian I, Kisos H, Levy L, et al. Phenotypic diversity and plasticity in circulating neutrophil subpopulations in cancer. *Cell Rep* (2015) 10(4):562–73. doi: 10.1016/j.celrep.2014.12.039

183. Wang WQ, Liu L, Xu HX, Wu CT, Xiang JF, Xu J, et al. Infiltrating immune cells and gene mutations in pancreatic ductal adenocarcinoma. *Br J Surg* (2016) 103 (9):1189–99. doi: 10.1002/bjs.10187

184. Qiao B, Luo W, Liu Y, Wang J, Liu C, Liu Z, et al. The prognostic value of CXC chemokine receptor 2 (CXCR2) in cancers: a meta-analysis. *Oncotarget* (2018) 9 (19):15068–76. doi: 10.18632/oncotarget.23492

185. Sano M, Ijichi H, Takahashi R, Miyabayashi K, Fujiwara H, Yamada T, et al. Blocking CXCLs-CXCR2 axis in tumor-stromal interactions contributes to survival in a mouse model of pancreatic ductal adenocarcinoma through reduced cell invasion/migration and a shift of immune-inflammatory microenvironment. *Oncogenesis* (2019) 8(2):8. doi: 10.1038/s41389-018-0117-8

186. Steele CW, Karim SA, Leach JDG, Bailey P, Upstill-Goddard R, Rishi L, et al. CXCR2 inhibition profoundly suppresses metastases and augments immunotherapy in pancreatic ductal adenocarcinoma. *Cancer Cell* (2016) 29(6):832–45. doi: 10.1016/j.ccell.2016.04.014

187. Nywening TM, Belt BA, Cullinan DR, Panni RZ, Han BJ, Sanford DE, et al. Targeting both tumour-associated CXCR2+ neutrophils and CCR2+ macrophages disrupts myeloid recruitment and improves chemotherapeutic responses in pancreatic ductal adenocarcinoma. *Gut* (2018) 67(6):1112–23. doi: 10.1136/gutjnl-2017-313738

188. Jin W, Yin H, Li H, Yu XJ, Xu HX, Liu L. Neutrophil extracellular DNA traps promote pancreatic cancer cells migration and invasion by activating EGFR/ERK pathway. *J Cell Mol Med* (2021) 25(12):5443–56. doi: 10.1111/jcmm.16555

189. Garcea G, Ladwa N, Neal CP, Metcalfe MS, Dennison AR, Berry DP. Preoperative neutrophil-to-lymphocyte ratio (NLR) is associated with reduced disease-free survival following curative resection of pancreatic adenocarcinoma. *World J Surg* (2011) 35(4):868–72. doi: 10.1007/s00268-011-0984-z

190. Stotz M, Gerger A, Eisner F, Szkandera J, Loibner H, Ress AL, et al. Increased neutrophil-lymphocyte ratio is a poor prognostic factor in patients with primary operable and inoperable pancreatic cancer. *Br J Cancer* (2013) 109(2):416–21. doi: 10.1038/bjc.2013.332

191. Suzuki R, Takagi T, Hikichi T, Konno N, Sugimoto M, Watanabe KO, et al. Derived neutrophil/lymphocyte ratio predicts gemcitabine therapy outcome in unresectable pancreatic cancer. *Oncol Lett* (2016) 11(5):3441–5. doi: 10.3892/ol.2016.4381

192. Wang Y, Fang T, Huang L, Wang H, Zhang L, Wang Z, et al. Neutrophils infiltrating pancreatic ductal adenocarcinoma indicate higher Malignancy and worse prognosis. *Biochem Biophys Res Commun* (2018) 501(1):313–9. doi: 10.1016/j.bbrc.2018.05.024

193. Aoyagi Y, Oda T, Kinoshita T, Nakahashi C, Hasebe T, Ohkochi N, et al. Overexpression of TGF-beta by infiltrated granulocytes correlates with the expression of collagen mRNA in pancreatic cancer. *Br J Cancer* (2004) 91(7):1316–26. doi: 10.1038/sj.bjc.6602141

194. Hu P, Shen M, Zhang P, Zheng C, Pang Z, Zhu L, et al. Intratumoral neutrophil granulocytes contribute to epithelial-mesenchymal transition in lung adenocarcinoma cells. *Tumour Biol* (2015) 36(10):7789–96. doi: 10.1007/s13277-015-3484-1

195. Gong L, Cumpian AM, Caetano MS, Ochoa CE, de la Garza MM, Lapid DJ, et al. Promoting effect of neutrophils on lung tumorigenesis is mediated by CXCR2 and neutrophil elastase. *Mol Cancer* (2013) 12(1):154. doi: 10.1186/1476-4598-12-154

196. Dallal RM, Christakos P, Lee K, Egawa S, Son YI, Lotze MT. Paucity of dendritic cells in pancreatic cancer. *Surgery* (2002) 131(2):135–8. doi: 10.1067/msy.2002.119937

197. Tjomsland V, Sandström P, Spångeus A, Messmer D, Emilsson J, Falkmer U, et al. Pancreatic adenocarcinoma exerts systemic effects on the peripheral blood myeloid and plasmacytoid dendritic cells: an indicator of disease severity? *BMC Cancer* (2010) 10:87. doi: 10.1186/1471-2407-10-87

198. Yamamoto T, Yanagimoto H, Satoi S, Toyokawa H, Yamao J, Kim S, et al. Circulating myeloid dendritic cells as prognostic factors in patients with pancreatic cancer who have undergone surgical resection. *J Surg Res* (2012) 173(2):299–308. doi: 10.1016/j.jss.2010.09.027

199. Takahashi K, Toyokawa H, Takai S, Satoi S, Yanagimoto H, Terakawa N, et al. Surgical influence of pancreatectomy on the function and count of circulating dendritic cells in patients with pancreatic cancer. *Cancer Immunol Immunother* (2006) 55 (7):775–84. doi: 10.1007/s00262-005-0079-5

200. Hiraoka N, Yamazaki-Itoh R, Ino Y, Mizuguchi Y, Yamada T, Hirohashi S, et al. CXCL17 and ICAM2 are associated with a potential anti-tumor immune response in early intraepithelial stages of human pancreatic carcinogenesis. *Gastroenterology* (2011) 140(1):310–21. doi: 10.1053/j.gastro.2010.10.009

201. Bellone G, Carbone A, Smirne C, Scirelli T, Buffolino A, Novarino A, et al. Cooperative induction of a tolerogenic dendritic cell phenotype by cytokines secreted by pancreatic carcinoma cells. *J Immunol* (2006) 177(5):3448–60. doi: 10.4049/jimmunol.177.5.3448

202. Basso D, Fogar P, Falconi M, Fadi E, Sperti C, Frasson C, et al. Pancreatic tumors and immature immunosuppressive myeloid cells in blood and spleen: role of inhibitory co-stimulatory molecules PDL1 and CTLA4. An *in vivo* and *in vitro* study. *PloS One* (2013) 8(1):e54824. doi: 10.1371/journal.pone.0054824

203. Karakhanova S, Link J, Heinrich M, Shevchenko I, Yang Y, Hassenpflug M, et al. Characterization of myeloid leukocytes and soluble mediators in pancreatic cancer: importance of myeloid-derived suppressor cells. *Oncoimmunology* (2015) 4(4):e998519. doi: 10.1080/2162402X.2014.998519

204. Markowitz J, Wang J, Vangundy Z, You J, Yildiz V, Yu L, et al. Nitric oxide mediated inhibition of antigen presentation from DCs to CD4+ T cells in cancer and measurement of STAT1 nitration. *Sci Rep* (2017) 7(1):15424. doi: 10.1038/s41598-017-14970-0

205. Moral JA, Leung J, Rojas LA, Ruan J, Zhao J, Sethna Z, et al. ILC2s amplify PD-1 blockade by activating tissue-specific cancer immunity. *Nature* (2020) 579 (7797):130–5. doi: 10.1038/s41586-020-2015-4

206. Huang Q, Ma X, Wang Y, Niu Z, Wang R, Yang F, et al. IL-10 producing type 2 innate lymphoid cells prolong islet allograft survival. *EMBO Mol Med* (2020) 12(11):e12305. doi: 10.15252/emmm.202012305

207. Sugimura R, Wang CY. The role of innate lymphoid cells in cancer development and immunotherapy. *Front Cell Dev Biol* (2022) 10:803563. doi: 10.3389/fcell.2022.803563

208. Royal RE, Levy C, Turner K, Mathur A, Hughes M, Kammula US, et al. Phase 2 trial of single agent Ipilimumab (anti-CTLA-4) for locally advanced or metastatic pancreatic adenocarcinoma. *J Immunother* (2010) 33(8):828–33. doi: 10.1097/CJI.0b013e3181eec14c

209. Brahmer JR, Tykodi SS, Chow LQM, Hwu WJ, Topalian SL, Hwu P, et al. Safety and activity of anti-PD-L1 antibody in patients with advanced cancer. *N Engl J Med* (2012) 366(26):2455–65. doi: 10.1056/NEJMoa1200694

210. Kunk PR, Bauer TW, Slingluff CL, Rahma OE. From bench to bedside a comprehensive review of pancreatic cancer immunotherapy. *J Immunother Cancer* (2016) 4:14. doi: 10.1186/s40425-016-0119-z

211. Stromnes IM, Brockenbrough JS, Izeradjene K, Carlson MA, Cuevas C, Simmons RM, et al. Targeted depletion of an MDSC subset unmasks pancreatic ductal adenocarcinoma to adaptive immunity. *Gut* (2014) 63(11):1769–81. doi: 10.1136/gutjnl-2013-306271

212. Beatty GL, Winograd R, Evans RA, Long KB, Luque SL, Lee JW, et al. Exclusion of T cells from pancreatic carcinomas in mice is regulated by ly6C(low) F4/80(+) extratumoral macrophages. *Gastroenterology* (2015) 149(1):201–10. doi: 10.1053/j.gastro.2015.04.010

213. Gardner A, Ruffell B. Dendritic cells and cancer immunity. *Trends Immunol* (2016) 37(12):855–65. doi: 10.1016/j.it.2016.09.006

214. Roberts EW, Broz ML, Binnewies M, Headley MB, Nelson AE, Wolf DM, et al. Critical role for CD103(+)/CD141(+) dendritic cells bearing CCR7 for tumor antigen trafficking and priming of T cell immunity in melanoma. *Cancer Cell* (2016) 30(2):324–36. doi: 10.1016/j.ccell.2016.06.003

215. Salmon H, Idoyaga J, Rahman A, Leboeuf M, Remark R, Jordan S, et al. Expansion and activation of CD103(+) dendritic cell progenitors at the tumor site enhances tumor responses to therapeutic PD-L1 and BRAF inhibition. *Immunity* (2016) 44(4):924–38. doi: 10.1016/j.immuni.2016.03.012

216. Spranger S, Dai D, Horton B, Gajewski TF. Tumor-residing batf3 dendritic cells are required for effector T cell trafficking and adoptive T cell therapy. *Cancer Cell* (2017) 31(5):711–723.e4. doi: 10.1016/j.ccell.2017.04.003

217. de Mingo Pulido Á, Gardner A, Hiebler S, Soliman H, Rugo HS, Krummel MF, et al. TIM-3 regulates CD103+ Dendritic cell function and response to chemotherapy in breast cancer. *Cancer Cell* (2018) 33(1):60–74.e6. doi: 10.1016/j.ccell.2017.11.019

218. Binnewies M, Mujal AM, Pollack JL, Combes AJ, Hardison EA, Barry KC, et al. Unleashing type-2 dendritic cells to drive protective antitumor CD4+ T cell immunity. *Cell* (2019) 177(3):556–71. doi: 10.1016/j.cell.2019.02.005

219. Kenkel JA, Tseng WW, Davidson MG, Tolentino LL, Choi O, Bhattacharya N, et al. An immunosuppressive dendritic cell subset accumulates at secondary sites and promotes metastasis in pancreatic cancer. *Cancer Res* (2017) 77(15):4158–70. doi: 10.1158/0008-5472.CAN-16-2212

220. Merle NS, Noe R, Halbwachs-Mecarelli L, Fremeaux-Bacchi V, Roumenina LT. Complement system part II: role in immunity. *Front Immunol* (2015) 6:257. doi: 10.3389/fimmu.2015.00257

221. Merle NS, Church SE, Fremeaux-Bacchi V, Roumenina LT. Complement system part I - molecular mechanisms of activation and regulation. *Front Immunol* (2015) 6:262. doi: 10.3389/fimmu.2015.00262

222. Zhang R, Liu Q, Li T, Liao Q, Zhao Y. Role of the complement system in the tumor microenvironment. *Cancer Cell Int* (2019) 19:300. doi: 10.1186/s12935-019-1027-3

223. Bettac L, Denk S, Seufferlein T, Huber-Lang M. Complement in pancreatic disease-perpetrator or savior? *Front Immunol* (2017) 8:15. doi: 10.3389/fimmu.2017.00015

224. Hussain N, Das D, Pramanik A, Pandey MK, Joshi V, Pramanik KC. Targeting the complement system in pancreatic cancer drug resistance: a novel therapeutic approach. *Cancer Drug Resist* (2022) 5(2):317–27. doi: 10.20517/cdr.2021.150

225. Ajona D, Ortiz-Espinosa S, Pio R. Complement anaphylatoxins C3a and C5a: Emerging roles in cancer progression and treatment. *Semin Cell Dev Biol* (2019) 85:153–63. doi: 10.1016/j.semcdb.2017.11.023

226. Ravindranath NMH, Shuler C. Cell-surface density of complement restriction factors (CD46, CD55, and CD59): oral squamous cell carcinoma versus other solid tumors. *Oral Surg Oral Med Oral Pathol Oral Radiol Endod* (2007) 103(2):231–9. doi: 10.1016/j.tripleo.2006.05.028

227. Mellby LD, Nyberg AP, Johansen JS, Wingren C, Nordestgaard BG, Bojesen SE, et al. Serum biomarker signature-based liquid biopsy for diagnosis of early-stage pancreatic cancer. *J Clin Oncol* (2018) 36(28):2887–94. doi: 10.1200/JCO.2017.77.6658

228. Varghese PM, Mukherjee S, Al-Mohanna FA, Saleh SM, Almajhdi FN, Beirag N, et al. Human properdin released by infiltrating neutrophils can modulate influenza A virus infection. *Front Immunol* (2021) 12:747654. doi: 10.3389/fimmu.2021.747654

229. Kishore U, Varghese PM, Mangogna A, Klein L, Tu M, Urbach L, et al. Neutrophil-derived complement factor P induces cytotoxicity in basal-like cells *via* caspase 3/7 activation in pancreatic cancer. *bioRxiv* (2023) 10:28. doi: 10.1101/2023.10.28.564512v1

230. Fuster MM, Esko JD. The sweet and sour of cancer: glycans as novel therapeutic targets. *Nat Rev Cancer* (2005) 5(7):526–42. doi: 10.1038/nrc1649

231. Wingren C, Sandström A, Segersvärd R, Carlsson A, Andersson R, Löhr M, et al. Identification of serum biomarker signatures associated with pancreatic cancer. *Cancer Res* (2012) 72(10):2481–90. doi: 10.1158/0008-5472.CAN-11-2883

232. Zhang Y, Velez-Delgado A, Mathew E, Li D, Mendez FM, Flannagan K, et al. Myeloid cells are required for PD-1/PD-L1 checkpoint activation and the establishment of an immunosuppressive environment in pancreatic cancer. *Gut* (2017) 66(1):124–36. doi: 10.1136/gutjnl-2016-312078

233. Yang S, Liu Q, Liao Q. Tumor-associated macrophages in pancreatic ductal adenocarcinoma: origin, polarization, function, and reprogramming. *Front Cell Dev Biol* (2021) 8:607209. doi: 10.3389/fcell.2020.607209

234. Cannarile MA, Weisser M, Jacob W, Jegg AM, Ries CH, Rüttinger D. Colony-stimulating factor 1 receptor (CSF1R) inhibitors in cancer therapy. *J Immunother Cancer* (2017) 5(1):53. doi: 10.1186/s40425-017-0257-y

235. Zhu Y, Knolhoff BL, Meyer MA, Nywening TM, West BL, Luo J, et al. CSF1/CSF1R blockade reprograms tumor-infiltrating macrophages and improves response to T-cell checkpoint immunotherapy in pancreatic cancer models. *Cancer Res* (2014) 74 (18):5057–69. doi: 10.1158/0008-5472.CAN-13-3723

236. Wang-Gillam A, O'Reilly EM, Bendell JC, Wainberg ZA, Borazanci EH, Bahary N, et al. A randomized phase II study of cabiralizumab (cabira) + nivolumab (nivo) ± chemotherapy (chemo) in advanced pancreatic ductal adenocarcinoma (PDAC). *JCO* (2019) 37(4_suppl):TPS465–5. doi: 10.1200/JCO.2019.37.4_suppl.TPS465

237. Ho WJ, Jaffee EM. Macrophage-targeting by CSF1/1R blockade in pancreatic cancers. *Cancer Res* (2021) 81(24):6071–3. doi: 10.1158/0008-5472.CAN-21-3603

238. Van Cutsem E, Tempero MA, Sigal D, Oh DY, Fazio N, Macarulla T, et al. Randomized phase III trial of pegvorhyaluronidase alfa with nab-paclitaxel plus gemcitabine for patients with hyaluronan-high metastatic pancreatic adenocarcinoma. *J Clin Oncol* (2020) 38(27):3185–94. doi: 10.1200/JCO.20.00590

239. Panni RZ, Herndon JM, Zuo C, Hegde S, Hogg GD, Knolhoff BL, et al. Agonism of CD11b reprograms innate immunity to sensitize pancreatic cancer to immunotherapies. *Sci Trans Med* (2019) 11(499):eaau9240. doi: 10.1126/scitranslmed.aau9240

240. Lamberti MJ, Nigro A, Mentucci FM, Rumie Vittar NB, Casolaro V, Dal Col J. Dendritic cells and immunogenic cancer cell death: A combination for improving antitumor immunity. *Pharmaceutics* (2020) 12(3):256. doi: 10.3390/pharmaceutics12030256

241. Konduri V, Li D, Halpert MM, Liang D, Liang Z, Chen Y, et al. Chemo-immunotherapy mediates durable cure of orthotopic KrasG12D/p53−/− pancreatic ductal adenocarcinoma. *Oncoimmunology* (2016) 5(9):e1213933. doi: 10.1080/2162402X.2016.1213933

242. Renouf DJ, Loree JM, Knox JJ, Topham JT, Kavan P, Jonker D, et al. The CCTG PA.7 phase II trial of gemcitabine and nab-paclitaxel with or without durvalumab and tremelimumab as initial therapy in metastatic pancreatic ductal adenocarcinoma. *Nat Commun* (2022) 13:5020. doi: 10.1038/s41467-022-32591-8

243. Fu Q, Chen Y, Huang D, Guo C, Zhang X, Xiao W, et al. Sintilimab plus modified FOLFIRINOX in metastatic or recurrent pancreatic cancer: the randomized phase ii cispd3 trial. *Ann Surg Oncol* (2023) 30(8):5071–80. doi: 10.1245/s10434-023-13383-w

244. Padrón LJ, Maurer DM, O'Hara MH, O'Reilly EM, Wolff RA, Wainberg ZA, et al. Sotigalimab and/or nivolumab with chemotherapy in first-line metastatic pancreatic cancer: clinical and immunologic analyses from the randomized phase 2 PRINCE trial. *Nat Med* (2022) 28(6):1167–77. doi: 10.1038/s41591-022-01829-9

245. Wu AA, Bever KM, Ho WJ, Fertig EJ, Niu N, Zheng L, et al. A phase 2 study of allogeneic GM-CSF transfected pancreatic tumor vaccine (GVAX) with ipilimumab as maintenance treatment for metastatic pancreatic cancer. *Clin Cancer Res* (2020) 26 (19):5129–39. doi: 10.1158/1078-0432.CCR-20-1025

246. Weiss GJ, Blaydorn L, Beck J, Bornemann-Kolatzki K, Urnovitz H, Schütz E, et al. Phase Ib/II study of gemcitabine, nab-paclitaxel, and pembrolizumab in metastatic pancreatic adenocarcinoma. *Invest New Drugs* (2018) 36(1):96–102. doi: 10.1007/s10637-017-0525-1

247. Kocher HM, Basu B, Froeling FEM, Sarker D, Slater S, Carlin D, et al. Phase I clinical trial repurposing all-trans retinoic acid as a stromal targeting agent for pancreatic cancer. *Nat Commun* (2020) 11(1):4841. doi: 10.1038/s41467-020-18636-w

248. Bekaii-Saab T, Okusaka T, Goldstein D, Oh DY, Ueno M, Ioka T, et al. Napabucasin plus nab-paclitaxel versus gemcitabine plus nab-paclitaxel with gemcitabine in previously untreated metastatic pancreatic adenocarcinoma: an adaptive multicentre, randomised, open-label, phase 3, superiority trial. *eClinicalMedicine* (2023) 58:101897. doi: 10.1016/j.eclinm.2023.101897

249. Hidalgo M, Garcia-Carbonero R, Lim KH, Messersmith WA, Garrido-Laguna I, Borazanci E, et al. A preclinical and phase ib study of palbociclib plus nab-paclitaxel in patients with metastatic adenocarcinoma of the pancreas. *Cancer Res Commun* (2022) 2(11):1326–33. doi: 10.1158/2767-9764.CRC-22-0072

250. Pegna GJ, Lee M, Peer CJ, Ahmad MI, Venzon DJ, Yu Y, et al. Systemic immune changes accompany combination treatment with immunotoxin LMB-100 and nab-paclitaxel. *Cancer Med* (2022) 12(4):4236–49. doi: 10.1002/cam4.5290

251. Coveler AL, Reilley M, Zalupski M, Macarulla T, Fountzilas C, Castanon Alvarez E, et al. Safety and clinical activity of oleclumab (O) ± durvalumab (D) + chemotherapy (CT) in patients (pts) with metastatic pancreatic ductal adenocarcinoma (mPDAC): A phase 1b/2 randomized study. *JCO* (2023) 41(16_suppl):4136–6. doi: 10.1200/JCO.2023.41.16_suppl.4136

252. Gracian AC, Dean A, Muñoz A, Hidalgo M, Pazo-Cid R, Martin M, et al. YOSEMITE: A 3 arm double-blind randomized phase 2 study of gemcitabine, paclitaxel protein-bound particles for injectable suspension, and placebo (GAP) versus gemcitabine, paclitaxel protein-bound particles for injectable suspension and either 1 or 2 truncated courses of demcizumab (GAD). *Ann Oncol* (2017) 28:v211. doi: 10.1093/annonc/mdx369.004

253. Jameson GS, Borazanci EH, Babiker HM, Poplin E, Niewiarowska AA, Gordon MS, et al. A phase Ib/II pilot trial with nab-paclitaxel plus gemcitabine plus cisplatin in patients (pts) with stage IV pancreatic cancer. *JCO* (2017) 35(4_suppl):341–1. doi: 10.1200/JCO.2017.35.4_suppl.341

254. Chung V, McDonough S, Philip PA, Cardin D, Wang-Gillam A, Hui L, et al. Effect of selumetinib and MK-2206 vs oxaliplatin and fluorouracil in patients with metastatic pancreatic cancer after prior therapy: SWOG S1115 study randomized clinical trial. *JAMA Oncol* (2017) 3(4):516–22. doi: 10.1001/jamaoncol.2016.5383

255. Farren MR, Mace TA, Geyer S, Mikhail S, Wu C, Ciombor K, et al. Systemic immune activity predicts overall survival in treatment-naïve patients with metastatic pancreatic cancer. *Clin Cancer Res* (2016) 22(10):2565–74. doi: 10.1158/1078-0432.CCR-15-1732

256. Smith C, Zheng W, Dong J, Wang Y, Lai J, Liu X, et al. Tumor microenvironment in pancreatic ductal adenocarcinoma: Implications in immunotherapy. *World J Gastroenterol* (2022) 28(27):3297–313. doi: 10.3748/wjg.v28.i27.3297

257. Théry C, Witwer KW, Aikawa E, Alcaraz MJ, Anderson JD, Andriantsitohaina R, et al. Minimal information for studies of extracellular vesicles 2018 (MISEV2018): a position statement of the International Society for Extracellular Vesicles and update of the MISEV2014 guidelines. *J Extracell Vesicles* (2018) 7(1):1535750. doi: 10.1080/20013078.2018.1535750

258. Shen T, Huang Z, Shi C, Pu X, Xu X, Wu Z, et al. Pancreatic cancer-derived exosomes induce apoptosis of T lymphocytes through the p38 MAPK-mediated endoplasmic reticulum stress. *FASEB J* (2020) 34(6):8442–58. doi: 10.1096/fj.201902186R

259. Chang CH, Pauklin S. Extracellular vesicles in pancreatic cancer progression and therapies. *Cell Death Dis* (2021) 12(11):1–12. doi: 10.1038/s41419-021-04258-7

260. Batista IA, Melo SA. Exosomes and the future of immunotherapy in pancreatic cancer. *Int J Mol Sci* (2019) 20(3):567. doi: 10.3390/ijms20030567

261. Fyfe J, Dye D, Razak NBA, Metharom P, Falasca M. Immune evasion on the nanoscale: Small extracellular vesicles in pancreatic ductal adenocarcinoma immunity. *Semin Cancer Biol* (2023) 96:36–47. doi: 10.1016/j.semcancer.2023.09.004

262. Ho WJ, Jaffee EM, Zheng L. The tumour microenvironment in pancreatic cancer — clinical challenges and opportunities. *Nat Rev Clin Oncol* (2020) 17(9):527–40. doi: 10.1038/s41571-020-0363-5

frontiers | Frontiers in Immunology

Targeting MYC at the intersection between cancer metabolism and oncoimmunology

Simran Venkatraman[1], Brinda Balasubramanian[2],
Chanitra Thuwajit[3], Jaroslaw Meller[4,5,6], Rutaiwan Tohtong[1]*
and Somchai Chutipongtanate[4,7]*

[1]Department of Biochemistry, Faculty of Science, Mahidol University, Bangkok, Thailand, [2]Division of Cancer and Stem Cells, Biodiscovery Institute, School of Medicine, University of Nottingham, Nottingham, United Kingdom, [3]Department of Immunology, Faculty of Medicine Siriraj Hospital, Mahidol University, Bangkok, Thailand, [4]Department of Environmental and Public Health Sciences, University of Cincinnati College of Medicine, Cincinnati, OH, United States, [5]Department of Biomedical Informatics, University of Cincinnati College of Medicine, Cincinnati, OH, United States, [6]Division of Biomedical Informatics, Cincinnati Children's Hospital Medical Center, Cincinnati, OH, United States, [7]Milk, microbiome, Immunity and Lactation research for Child Health (MILCH) and Novel Therapeutics Lab, Division of Epidemiology, Department of Environmental and Public Health Sciences, University of Cincinnati College of Medicine, Cincinnati, OH, United States

MYC activation is a known hallmark of cancer as it governs the gene targets involved in various facets of cancer progression. Of interest, MYC governs oncometabolism through the interactions with its partners and cofactors, as well as cancer immunity via its gene targets. Recent investigations have taken interest in characterizing these interactions through multi-Omic approaches, to better understand the vastness of the MYC network. Of the several gene targets of MYC involved in either oncometabolism or oncoimmunology, few of them overlap in function. Prominent interactions have been observed with MYC and HIF-1α, in promoting glucose and glutamine metabolism and activation of antigen presentation on regulatory T cells, and its subsequent metabolic reprogramming. This review explores existing knowledge of the role of MYC in oncometabolism and oncoimmunology. It also unravels how MYC governs transcription and influences cellular metabolism to facilitate the induction of pro- or anti-tumoral immunity. Moreover, considering the significant roles MYC holds in cancer development, the present study discusses effective direct or indirect therapeutic strategies to combat MYC-driven cancer progression.

1 Introduction

MYC is a proto-oncogenic transcription factor that governs a myriad of cellular processes including cell proliferation, survival, DNA damage repairs, histone modifications, and cellular metabolism (1). MYC is a family of transcription factors, i.e., MYC(c-MYC), MYCN (N-Myc) and MYCL (L-Myc), all of these contain a basic helix-loop-helix structure (bHLH) and leucine zipper (LZ) structural motifs with 6 conserved regions known as the MYC homology boxes (2). MYC family shares similar functions but has distinct tissue specificity; c-MYC is ubiquitously expressed in a broad variety of tissue development, n-MYC in neural and hematopoietic tissues, and L-MYC in lungs. The bHLH structure allows the interaction of MYC with DNA, while the LZ structure allows interaction with its partner transcription factor MAX. This MYC-MAX heterodimer interacts with numerous elements to either promote or repress transcription of gene targets (3).

Dysregulation of MYC implicates a wide array of diseases including neurodegenerative diseases (4), immune disorders (5), and cancers (6). Of the known hallmarks of cancer, MYC dysregulation has been reported to result in angiogenesis (7), cell replicative immortality (8), cell invasion and migration (8), alterations in cellular energetics (9), insensitivity to growth signals (10), and evading immune recognition and programmed cell death (6, 11). Because of its multifaceted dysregulation, MYC-driven cancers are often associated with poor prognosis (12–14). The involvement of MYC in both metabolism and immune evasion is highly concerning, especially in the context of malignant transformation. MYC promotes cell proliferation under conditions that would typically prove fatal for normal cells by manipulating glucose metabolism and eluding immunosurveillance by releasing metabolites within the tumor microenvironment (TME) (15, 16). While this facet has great implications for tumor progression, it also poses a particular threat in both tumorigenesis and potential tumor recurrence (17, 18).

Estimating up to 70% of cancers are affected by MYC aberration (19, 20), MYC therefore has been perceived as one of the most valuable targets for cancer therapy. However, direct pharmacological inhibition of MYC has remained challenging due to its lack of enzymatic activity or binding sites. Hence, this has raised interest in exploring the interactome of MYC to identify druggable targets, thereby modulating MYC-dependent transcriptome. A prototype of this approach is Omomyc, a MAX-interfering peptide. Omomyc was found to halt breast cancer progression, and regressed lung cancer in preclinical models (21). Currently, clinical trials are underway to determine the safety and efficacy of this drug in non-small cell lung cancer and colorectal cancer (ClinicalTrials.gov identifier NCT04808362). The success of this proof-of-concept inhibition of protein-protein interactions of MYC encourages the development of many such small molecules in therapeutically targeting MYC.

In this review, we enumerate the recent studies that characterize the targets and partners of MYC involved in cancer metabolism and immunology. Further, we discuss current evidence of the overlap between cellular functions governed by MYC and how one function may influence another. This guides us to further unravel how MYC orchestrates cancer growth by mediating metabolism and oncoimmunology. Lastly, in the growing interest of mitigating the 'undruggable' nature of MYC, we discuss currently available therapeutic strategies to combat MYC, a central target in the grand scheme of cancer.

2 Key MYC partners and targets

MYC structure consists of several domains that allow binding interactions of coactivators, heterodimers, or ligases. Each of these interactors facilitates the function of MYC in carrying out various biological processes. Its organization begins with a transcription activation site, which is a conserved region known as the MYC homology box (MBI and II), followed by a proline, glutamine, threonine-rich region, two more MYC homology boxes (MBIII and IV), and lastly, a basic HLH-LZ, at the carboxy-terminal (22). Because of the various regions available for interactions, and the implication of MYC in various cellular processes and molecular functions, there is a growing interest in unraveling the vast network of MYC and its interactome. In Figure 1, we summarized the text-mined sources of MYC protein-protein interactions with key partners.

Investigating the mechanisms of action revealed crucial insights into MYC functions; MYC utilizes its transcription activation domain to recruit cofactors containing chromatin modifiers, specifically histone acetyltransferases (HATs). One such cofactor, p300 (EP300) HAT, was identified as having a novel functional interaction with MYC (3). Moreover, p300 was also found to interact with N-MYC in regulating cell proliferation in MYCN-amplified neuroblastoma cell lines (23). Conversely, MYC transcriptionally represses gene expression of its targets by interacting with transcription factors such as MIZ-1 and NFY-B, which facilitates the recruitment of histone deacetylases (HDACs) (24). This finding highlights the multifaceted role of MYC, whereby it acts as a regulator by binding to the promoter region of target genes and modulates DNA methylation through the recruitment of HATs and HDACs.

MYC is considered a systemic regulator of diverse functions, because of the multidomain structure and the requirement of chromatin-modulating cofactors. MYC functions as a molecular switch of activating and/or repressing the transcription of its gene targets, depending on the position at which specific cofactors bind. The transactivation domain spans the MB1 and MB2 regions (22). Within this domain, cofactors that are shown to bind and activate gene transcription include FBW7 (25, 26), TAF1 (27), TBP (27), p-TEFb (28) TRRAP (3, McMahon et al., 1998), GCN5 (29), TIP60 (30), TIP48 (31), p400 (32), and SKP2 (33). These transactivating cofactors promote the transcription of target genes related to cell proliferation and survival, including CDK4 (34), CDC25A (35), and E2F1. Moreover, beyond sustained proliferative signaling, MYC has roles in various other hallmarks of cancer mediated by its gene targets. For instance, in promoting angiogenesis, MYC binds to the promoter region of VEGFA, thereby increasing its production (36).
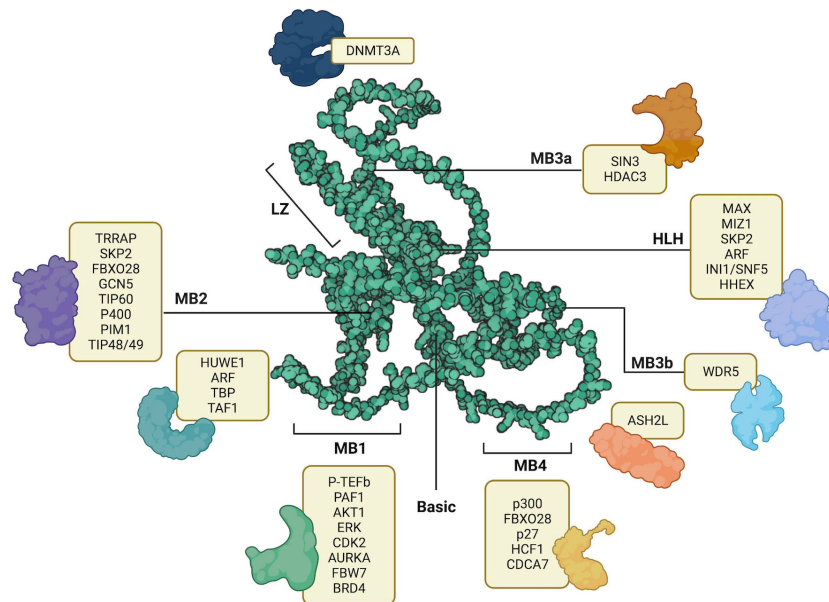
FIGURE 1
AlphaFold predicted structure of MYC (AF- P01106-F1) its annotated structural domains and their respective interactors. LZ – Leucine Zipper, HLH – Helix-Loop-Helix, MB1-MB4 – MYC binding boxes. Created with BioRender.com.

Moreover, MYC regulates invasion and migration by inducing the transcriptional activation of LGALS1 (37).

Conversely, the repression of MYC gene targets is triggered by cofactors binding in and between the regions of MB2 and MB3, and the bHLHLZ region. Cofactors that contribute to transrepression of MYC gene targets include TIP48/49, DNMT3a (38), PRC2 (39), HDAC1 (40), HDAC3 (41), KDM4B (42), and MIZ-1 (43, 44). In the initiation and progression of cancer, the expression of tumor-suppressing genes is usually repressed. Likewise, the expression of NDRG2 (45), PTEN (46), CDKN2C (46), CDKN1A (46), p21 (47, 48), p15 (48, 49), N-cadherin (48), is repressed by MYC, and therefore suppresses tumor suppressing functions, leading to cancer progression (50). Another key determinant of MYC global transcriptional amplification and systemic activity is its abundance and regulation (2). Patange et al's investigation reveals that the overexpression of MYC results in prolonged bursts of transcriptional activation by altering the binding affinity of transcription factors involved in the pre-initiation complex to RNA polymerase II (51). Together, the abundance of MYC and a balance of these transactivators or transrepressors, dictate the fate of cancer progression.

Of these hallmarks, cancer metabolism and oncoimmunology have garnered interest from several researchers due to the rising opportunities in therapeutic development. In this direction, MYC is a systemic regulator of diverse functions by employing various interactors. The MYC interactome extends further into oncoimmunology and oncometabolism by transcribing or repressing specific gene targets. Key interacting partners, stability partners, cofactors, and gene targets of MYC involved in tumor progression illustrated in Figure 2, in which their details are summarized in Table 1. Some of these key partners are discussed in the contexts of oncometabolism and oncoimmunology in the next section.

3 MYC roles in oncometabolism and oncoimmunology

The regulatory network of MYC is extensive, spanning across gene targets and cofactors involved in various aspects of cancer development, including cellular metabolism and immunology. Aberrant cell proliferation not only requires altered energy metabolism but also evasion from immunosurveillance. Recent evidence suggests that metabolism is a key element that controls immune evasion (84–86). The following sections summarize the role of MYC in regulating key elements of oncometabolism and oncoimmunology.

3.1 MYC and cancer metabolic reprogramming

In the case of regulated cell growth and proliferation, nutrient availability is essential. Hence, there needs to be a system in place to "sense" the level of available nutrients, to regulate the metabolism of available resources and maintain the balance of homeostasis. In mammals, systemically, this regulation occurs with the storage of glucose as glycogen in the liver, and the metabolism of fat by lipolysis, in response to starvation. At a cellular level, the availability of nutrients affects the activation of mTOR, and subsequently MYC expression. In the availability of nutrients, mTOR is activated in cells, which phosphorylates PI3K-AKT and therefore inhibits FOXO, a MYC antagonist (65). The activated mTOR also enhances MYC translation and function in transcribing genes favoring cancer progression (87). However, nutrient shortage inhibits mTOR

FIGURE 2

Protein-protein interaction network analysis of MYC and its interacting partners reveal several key regulatory processes including cellular metabolism, immune system, cell cycle and cell death. FDR, false discovery rate.
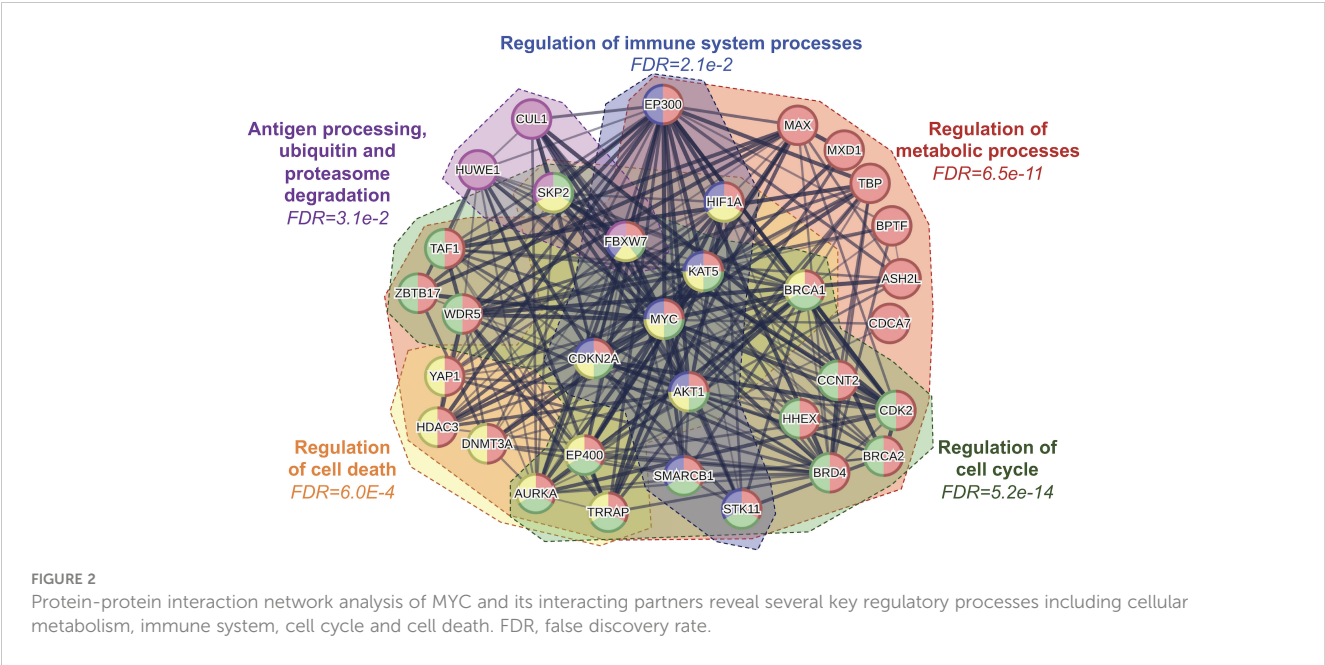
TABLE 1 Key partners and interactors of MYC involved in cancer.

Interactor	Interaction Type	Interaction Site	Role in Cancer	Reference
AKT1	Interaction partner	MB1	Energetic and Metabolic Pathways and Developmental Signaling	(52)
ARF	Interaction partner	Between MB1 and MB2, HLH	Tumor suppressor that inhibits MYC transactivation, proliferation, and transformation.	(53)
ASH2L	Interaction partner	Between MB3b and MB4	Epigenetic regulation	(54)
AURKA	Stability partner	MB1	Promotes tumor invasion, migration, proliferation. Protects MYC from proteasomal degradation	(55)
BPTF	Cofactors	NK[†]	Cancer cell proliferation, cell cycle progression	(56)
BRCA1	Gene Target/Antagonist	–	Tumor suppressor, DNA repair activity	(57, 58)
BRCA2	Gene Target	–	Genomic Instability/DNA repair activity	(59)
BRD4	Cofactors	MB1	Promotes MYC-activated gene transcription.	(60)
CDCA7	Interaction partner	C-Terminus	Tumorigenesis	(61)
CDK2	Stability partner	MB1	Regulates MYC-mediated suppression of senescence.	(62)
CUL1	Gene target	–	Ubiquitin mediated proteolysis and cell cycle progression	(63)
DNMT3a	Transrepression partner	Between MB2 and MB3a	Represses the transcription of cell cycle dependent kinase inhibitors, promoting tumor cell proliferation.	(38)
FOXO	Antagonist	–	Metabolism, adapting to Hypoxia	(64, 65)
FBW7	Stability partner	MB1	Regulates Ubiquitin mediated degradation of MYC. Prevents MYC-activated tumor progression.	(25, 26)
FBX028	Stability partner	MB2, MB4	Promotes Ubiquitination of MYC	(66)
HDAC3	Transrepression partner	MB3a	Binds to MYC to repress *FOXA2* gene transcription, leading to tumorigenesis.	(41)
HHEX	Interaction partner	HLH	Regulates tumor hyperproliferation, metabolism, and transformation.	(67)
HIF1A	Antagonist	–	Metabolism and Proliferation	(68)

(Continued)

TABLE 1 Continued

Interactor	Interaction Type	Interaction Site	Role in Cancer	Reference
HUWE1	Stability partner	Between MB1 and MB2	Promotes Ubiquitination of MYC	(69)
KAT5	Stability partner	Indirect interaction via Ubiquitin-mediated proteolysis	Invasion and Migration	(70)
LKB1	Interaction partner	NK†	Energetic and Metabolic Pathways and Developmental Signaling	(52)
MAD	Cofactors	bHLHLZ	Cell Proliferation, Differentiation, Tumorigenesis	(71)
MAX	Heterodimerization partner	bHLHLZ	Proliferation and Tumor Progression	(72, 73)
MIZ1	Interaction partner	bHLHLZ	Tumorigenesis	(44)
p27	Cofactors/ Antagonist	MB4	Proliferation and Tumor Progression	(74, 75)
p300	Cofactors	MB4	Proliferation, Invasion and Migration	(23)
p400	Cofactors	MB2	Facilitates Gene Expression of MYC targets	(32)
P65	Antagonist/ Transactivation	–	Immune Checkpoint expression, Inhibiting Apoptosis	(76, 77)
p-TEFb	Transactivation partner	MB1	Facilitates Gene Expression of MYC targets.	(28)
SIN3	Stability partner	MB3a	Recruits HDAC1 to exert deacetylase activity. Induces the degradation of MYC.	(78)
SKP2	Stability partner	MB2, HLH	Ubiquitin mediated proteolysis and cell cycle progression	(33)
SNF5	Transactivation	HLH	Facilitates Gene Expression of MYC targets. The protein itself has tumor suppressor roles by suppressing tumorigenesis.	(79, 80)
TAF1	Transactivation partner	Between MB1 and MB2	Essential for forming the transcription initiation complex TFIID, to activate MYC-activated gene transcription.	(27)
TBP	Transactivation partner	Between MB1 and MB2	Essential for forming the transcription initiation complex TFIID, to activate MYC-activated gene transcription.	(27)
TIP48/49	Cofactor	MB2	Essential cofactor for oncogenic transformation induced by MYC activation.	(31)
TIP60	Transactivation partner	MB2	Mediator to recruit Histone Acetyltransferases to MYC to facilitate gene expression of MYC targets.	(30)
TRRAP	Cofactors	MB2	Facilitates Gene expression of MYC targets	(3, 81)
VEGFA	Gene Target	–	Angiogenesis	(82)
WDR5	Interaction partner	MB3b	Tumorigenesis	(83)
YAP1	Interaction partner	NK†	Energetic and Metabolic Pathways and Developmental Signaling	(52)

NK† - Interaction Site Not Known; (-) No Physical Interaction.

activation, which thereby yields active FOXO, that limits MYC expression and function (65).

In the process of neoplastic transformation, cancer cells require an increase in glucose uptake to energize their rapid proliferation. Interestingly, this glucose is fermented to produce lactate in the presence of oxygen in a process called the Warburg Effect to yield energy in the form of adenosine triphosphate (ATP). Several investigators revealed that this increased consumption of glucose is due to the oncogenic levels of MYC, as evidenced in Burkitt's lymphoma (88) and MYC-driven liver carcinoma (89). This occurs by MYC upregulating various elements of the glycolytic cycle, such as the expression of glucose transporter, GLUT1 (90), glycolytic

enzymes hexokinase 2 (HK2), phosphofructokinase-M1 (PFKM-1) (91), enolase-1 (ENO1) and lactate dehydrogenase A (LDHA) (92). As a result, the increased glucose uptake and metabolic glycolysis driven by MYC, leads to an accumulation of lactate. While often misconstrued as a waste product, tumors take advantage of the lactate produced by the Warburg Effect to promote various pro-oncogenic functions such as immunomodulation and angiogenesis (93). Consequently, a plausible alternative strategy is to inhibit MYC-driven metabolic reprogramming. For instance, Cargill et al. (94) reported the therapeutic potential of a small molecule inhibitor of a glycolytic enzyme, PFKFB3, in inhibiting the downstream effects of MYC in small cell lung cancer. Moreover, Zuo et al.

(95), explored the use of vitamin D activated-long noncoding RNA *MEG3* to suppress glycolysis by promoting c-MYC degradation in colorectal cancer. As mentioned earlier, MYC exerts control over multiple targets within the glycolytic process, these findings support a potential therapeutic approach by targeting specific components

that abate MYC-driven glycolysis. The role of MYC in cancer metabolism is depicted in Figure 3.

In promoting glucose uptake and metabolism, NAD$^+$ ions are produced as metabolites, which are utilized in amino acid synthesis. Cancer cells exhibit a reliance on amino acids, which promote their
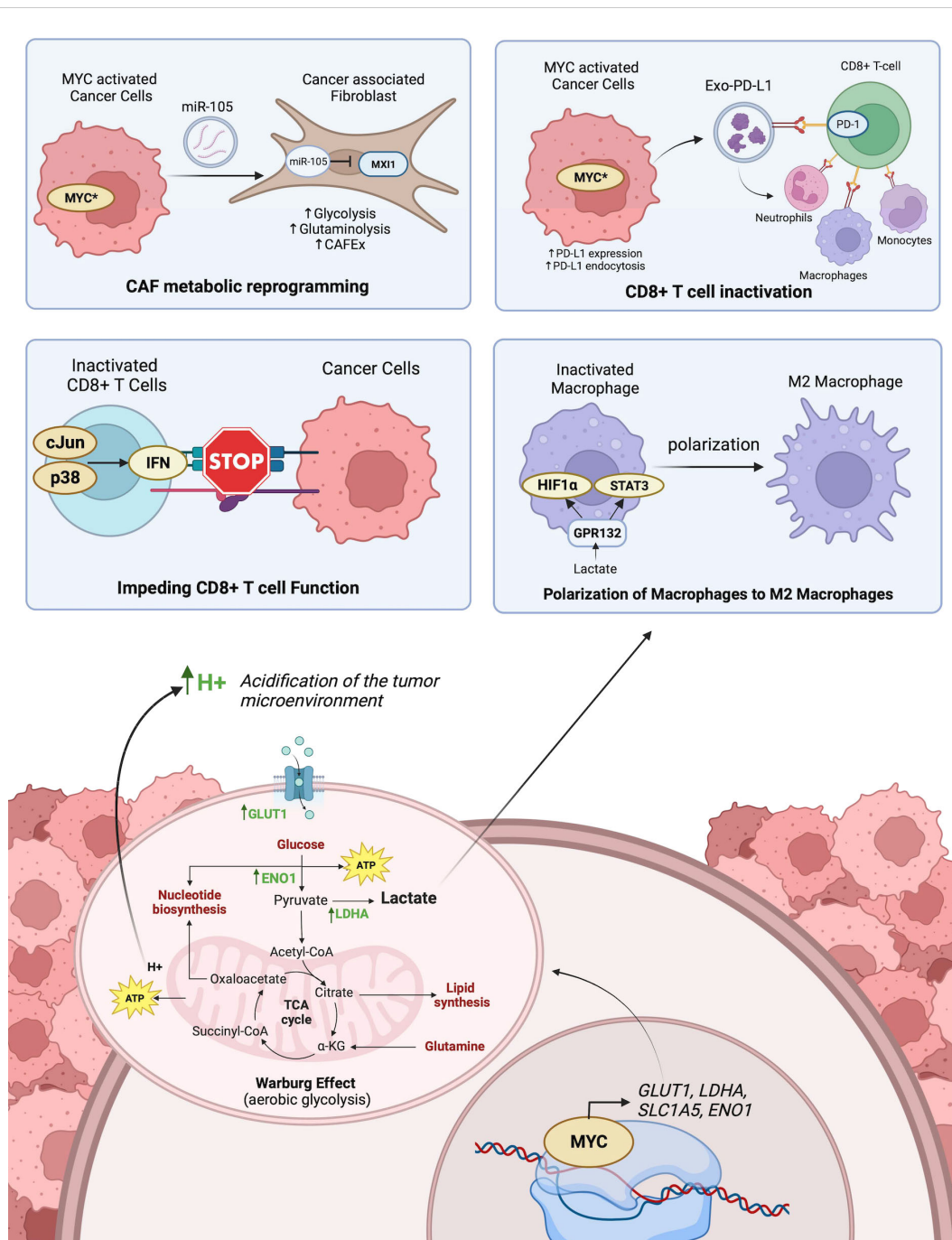
FIGURE 3
The role of MYC-driven transcriptional activation on cancer and immune cell metabolism and its influence on anti-tumor immunity. Top-left panel shows CAF metabolic reprogramming as a result of activated MYC in tumors exporting miR-105 which is imported into CAFs and inhibits MXI1. Top-right panel shows the inactivation of CD8$^+$ T cells by MYC activated export of PD-L1 from tumor cells bound to PD-1 receptors on CD8$^+$ T cells. Middle left panel shows how the acidification of the microenvironment triggers p38 and c-Jun signaling pathways in CD8$^+$ T cells which promotes interferon-mediated inactivation of CD8$^+$ T cell function. Middle right panel shows lactate released in the tumor microenvironment from tumor cells polarizes the differentiation of M1 macrophages to M2 macrophages. The bottom panel shows how MYC activated transcription of key enzymes promotes Warburg Effect within tumor cells. Created with BioRender.com.

survival and proliferation, especially under nutritional constraints. Therefore, malignant cells hijack mechanisms to upregulate amino acid production (96).

Just as MYC is a key driver of the metabolic switch in the presence of oxygen (normoxia), HIF1A is a key driver of the metabolic switch in the absence of oxygen (hypoxia) (97). In hypoxic conditions, MYC activity is usually inhibited by HIF1a by impeding the heterodimerization of MYC/MAX complex. HIF1a and MXI1 bind to MAX, thereby yielding unbound MYC destined for degradation (68). This impediment to MYC activity subsequently affects MYC target genes involved in mitochondrial biogenesis, apoptosis, and metabolic reprogramming (98). HIF1A also impedes MYC activity by upregulating the expression of FOXO3a which binds to MYC gene target promoters (99). Notably, however, when MYC is overexpressed, it overcomes the inhibitory effects of HIF1A. Although MYC and HIF1A antagonize each other functions, they share common gene targets in glycolysis, including HK2, PFK1, ENO1, and LDHA. Additionally, when both MYC and HIF1A are overexpressed, they collaborate in promoting angiogenesis and activating the expression of their gene targets (100). Thus, both HIF1A and MYC are key therapeutic targets for cancer progression.

MYC reprograms amino acid metabolism by activating the serine and glutamine synthesis pathways. Under nutrient-deprived conditions, MYC upregulates the expression of five major enzymes in serine biosynthesis, i.e., phosphoglycerate dehydrogenase (PHGDH), phosphoserine aminotransferase 1 (PSAT1), phosphoserine phosphatase (PSPH), serine hydroxymethyltransferases 1 and 2 (SHMT1 and SHMT2). The transcriptional upregulation of these genes facilitates nucleic acid production and cell cycle progression (101, 102). Another amino acid in high demand during tumor development is glutamine. MYC upregulates glutamine synthetase (GS) to promote glutamine anabolism (103), and paradoxically, it enhances glutamine catabolism by upregulating SLC1A5 and SLC7A5 amino acid transporters (104). To facilitate the conversion of glutamine to glutamate, MYC upregulates the expression of glutaminase (GLS) (105) and represses the expression of miR-23 which interrupts GLS translation (106). The availability of amino acids has emerged as a promising therapeutic target. As a result, there has been a significant focus on developing inhibitors that specifically target enzymes involved in amino acid synthesis. For example, pharmacological inhibition of MYC-driven GLS by CB-839 has recently shown encouraging results in suppressing various cancers in vitro and in vivo (107–109), and currently examined in a phase 1 clinical trial of solid tumors (NCT02071862).

3.2 MYC and cancer immune evasion

The immune system is a highly regulated defense mechanism instated to recognize and eliminate pathogens, or dysregulated cells, to maintain a healthy body. As cancer cells propagate uncontrollably, they acquire traits to evade immune recognition. This happens by downregulating self-antigen presentation, promoting an immunosuppressive TME through the release of cytokines, recruiting pro-tumoral immune cells, and increasing the expression of inhibitory immune checkpoint molecules. MYC is reportedly a grand orchestrator of cancer growth and immune evasion, as it regulates most of these traits by modulating its gene targets (110).

In establishing a tumor-proliferative environment beneath the surveillance of anti-tumor immune cells, tumor cells must recruit and modulate regulatory immune cells. In a lung adenoma model in vivo, Kortlever et al. (72) revealed that MYC cooperated with KRAS to reprogram stromal cells via epithelial-derived CCL9 and IL-23, resulting in CCL9-mediated macrophage recruitment, PD-L1-dependent discrimination of T and B cells, and IL-23 mediated exclusion of adaptive T and B cells and innate immune NK cells. Deactivating MYC was found to reverse this reprogramming and reinstate normal anti-tumor immune function (111). Noted that MYC is upregulated in tumor-associated macrophages (TAMs), which is involved in suppressing immunosurveillance (112). Moreover, in head and neck squamous cell carcinoma (HNSCC), therapeutic inhibition of MYC promoted intrinsic anti-tumor immune responses through the cGAS-STING signaling pathway, and CD8^{+} T-cell infiltration of HNSCC in vivo (113). Together, this evidence shows how MYC creates the TME through the release of cytokines or modulating gene expression to promote pro-tumoral immune cell infiltration and suppress immunosurveillance.

Importantly, MYC also governs the expression of immune checkpoint molecules and self-antigens to switch off immune cell recognition of tumors. Particularly in osteosarcoma, Jiang et al. (114), observed that pharmacological inhibition of MYC resulted in reprogramming the tumor immune microenvironment through the release of T-cell recruiting chemokines and crosstalk of co-stimulatory immune checkpoint molecules CD40 and CD40L. Moreover, a recent study by Dhanasekaran et al. (115), reported that MYC transcriptionally repressed MHC-1 antigen presentation and therefore repressed T-cell immune response in MYC-driven hepatocellular carcinoma. This phenomenon was pharmacologically reversible by the dual-inhibition of immune checkpoint molecules, PD-L1 and CTLA-4. MYC directly regulates the expression of CD47 and PD-L1 through transcriptional activation (116). Other than upregulating the expression of PD-L1 as cell surface receptors, expressed PD-L1 is also packaged into vesicles for export into exo-PD-L1 (117). This exo-PD-L1 promotes immune escape by PD-1/PD-L1 mediated cytotoxic T-cell inactivation through direct interaction or indirectly by exo-PD-L1 uptake in tumor-promoting immune cells (Figure 3). Recent investigations have reported evidence of exo-PD-L1 in various cancers including prostate, breast, melanoma, and pancreatic cancer (118). Besides the regulation of immune checkpoint molecule expression, MYC is also involved in post-translational modification of immunosuppressive glycans. Smith et al. (119), recently demonstrated that MYC regulates Siglec ligands through the transcriptional regulation of ST6GALNAC4 and the induction of a glycan so-called disialylated Galβ1-3GalNAc (disialyl-T antigen). Disialyl-T functions as an inhibitory glyco-immune checkpoint molecule that "switches off" immune response in T-cells by engaging pro-tumoral macrophages. This shows that MYC systemically extends itself in creating an immunosuppressive

environment by recruiting pro-tumoral macrophages, repelling anti-tumor immune cells, releasing cytokines, and modulating immune checkpoint molecules, by transcriptionally activating key gene targets.

Cumulatively, MYC systemically extends itself in creating an immunosuppressive environment by recruiting pro-tumoral macrophages, repelling anti-tumor immune cells, releasing cytokines, and modulating immune checkpoint molecules, by transcriptionally activating key gene targets.

3.3 MYC at the intersection between oncometabolism and oncoimmunology

Since MYC plays an essential role in regulating key targets involved in both metabolic reprogramming and immune evasion, it is likely that MYC induces one hallmark to influence the activation of another. Studies to date support this notion. Figure 3 summarizes the role of MYC at the interplay between cancer metabolism and oncoimmunology.

MYC promotes the Warburg Effect by upregulating glucose transporters and key glycolytic enzymes, the yield of H^+ ions from NADH reduction influences the microenvironment by lowering the pH. This acidic environment facilitates cancer cells to invade the tumor stroma (120). This acidification of the microenvironment also suppresses $CD8^+$ T lymphocyte functions, thereby promoting an immunosuppressive microenvironment. More specifically, this is mediated by activation of the p38, JNK/c-Jun signaling pathways, which promotes interferon production (121). Moreover, the lactate produced from tumors polarizes M2-tumor-associated macrophages (122). This is facilitated by the recognition of extracellular lactate levels with GPR132, and the subsequent upregulation of HIF-1α and activation of STAT3 signaling (123, 124). HIF-1α and MYC reciprocally regulate the expression of each. MYC is often seen to interact with HIF-1α in regulating T-cell metabolism by transcriptionally regulating genes involved in glucose and glutamine transport. Moreover, HIF-1α cooperates with MYC to shape the tumor immune microenvironment (100, 125). Similarly, Marchingo et al. (126), unraveled metabolic proteome changes including SLC7A5 and SLC1A5 during T cell activation governed by MYC. These are some of the ways MYC influences oncoimmunology by promoting glucose or amino acid metabolisms.

Conversely, modulating the tumor immune microenvironment also influences cellular energetics. This is particularly evidenced in the metabolic reprogramming of T lymphocytes after antigen activation. Wang et al. (127), reported the antigen activation of T lymphocytes drove the upregulation of genes encoding enzymes and transporters involved in glycolysis and glutaminolysis as governed by MYC. This antigen-activated MYC-driven metabolic reprogramming is responsible for T cell proliferation. Another investigation by Tsai et al. (128) focused on how immunoediting of the TME in early-stage tumorigenesis reprograms cancer metabolism in a way that supports immune evasion. The results suggested that interferon-gamma (IFNγ) released from T cell immunosurveillance stimulated STAT3-dependent MYC

upregulation in melanoma cells, which subsequently activated genes involved in glycolysis and oxidative phosphorylation while suppressing IFNγ-induced cellular senescence (128). Besides T cells, cancer-associated fibroblasts (CAFs) are known to play an important role in regulating antitumoral immunity by recruiting the infiltration of effector T cells and modifying immunosuppressive cells (129, 130). CAFs also influence the metabolism of cancer cells through the secretion of various metabolites that fuel cancer proliferation (131). In breast cancer, MYC promotes this interaction through extracellular vesicles (EVs) containing miR-105 transported from cancer cells to CAFs (132). MiR-105 suppresses the expression of endogenous MYC inhibitor MXI1, thereby sustaining MYC activation in CAFs and subsequently facilitating glucose and glutamine metabolisms (132). Increased metabolism in CAFs yields increased lactate levels in the TME which offers an advantage for cancer cells and impedes effector T-cell function (133). While the influence of cancer metabolism on the immunosuppressive TME is well characterized, there are fewer studies exploring the reciprocal communication between cancer and stromal cells through EV molecular cargos.

Besides the dynamic abundance of MYC effecting global transcriptional changes involved in oncometabolism and oncoimmunology, MYC can modulate gene targets that induce metabolic changes influencing cancer immunity and possess dual roles in cancer development. We have compiled the summarized information in Table 2, highlighting a few notable gene targets of the exhaustive list of MYC-regulated genes involved in both oncometabolism and oncoimmunology. Further studies focusing on the gene targets and MYC-regulated gene network at the immune-metabolic crossroad shall offer novel alternative strategies to attenuate tumor invasiveness and treatment resistance caused by MYC aberration.

4 Targeting MYC to tackle oncometabolism and oncoimmunology: 2 birds 1 stone?

MYC has previously been labeled "undruggable" due to its lack of an enzymatic active site and inaccessibility to its nuclear localization (20, 159). Various approaches have been employed to address the undruggable MYC through its actionable interacting partners and gene targets as illustrated in Figure 4.

Investigators exploited the heterodimerization between MYC and MAX to inactivate MYC-activated transcription. One study showed that pharmacological inhibition of MYC by 10058-F4 resulted in changes in lipid and amino acid metabolism in neuroblastoma cell lines (160). Additionally, another MYC-MAX perturbagen, Mycro3 resulted in enhanced $CD8^+$T cell function in surveilling cancer cells and inducing anti-tumor immune response (161). Another approach is the inhibition of MYC transcription by bromodomain-containing 4 (BRD4), using inhibitors such as JQ1 and OTX-015 (162). In medulloblastoma, the transcriptional inhibition of MYC by OTX-015 alters cancer glycolysis and amino acid metabolism (163). Moreover, the use of JQ1 in

TABLE 2 Key gene targets of MYC in cancer metabolism and oncoimmunology.

Gene Target	Main Hallmark	Role in Oncometabolism	Role in Oncoimmunology	Reference
LDHA	Metabolism	Required in the production of lactate in anaerobic glycolysis.	Inhibits immune killing and promotes immunosuppression by increasing lactate production and influencing the microenvironment. Negatively regulates immune infiltration.	(92) (134, 135)
GLUT1	Metabolism	A glucose transporter responsible for the uptake of glucose into cells.	Associated with increases in neutrophil, platelet, monocytes, and lymphocyte count. Negatively correlates with tumor-infiltrating T -cells but positively correlates with neutrophils and dendritic cells	(90, 136, 137)
ENO1	Metabolism	Responsible for converting 3' biphosphoglycerate to 3'biphosphopyruvate	Promotes anti-tumor immunity by promoting PD-L1 proteolysis.	(90, 138)
SLC1A5	Metabolism	Glutamine Transporter	Overexpression is associated with the presence of immunosuppressive immune cells such as CD68+ macrophage, FOXP3+ regulatory T cells, CD20+ B cells, and PD1+ lymphocytes. SLC1A5 is also required for MYC induction of cytokine-stimulated NK cells.	(84) (139)
SLC38A5	Metabolism	Glutamine Transporter and amino acid coupled Na+/H+ exchanger	Maintains extracellular acidification while maintaining intracellular pH. Acidification of the microenvironment turns off? anti-tumor lymphocyte function.	(140, 141)
IL-23	Immunology	When secreted by tumor-associated macrophages it Interlinks glutamine addiction and immune evasion in kidney cancer.	Cytokine that recruits pro-tumoral macrophages	(111, 142)
CD47	Immunology	Tumor intrinsic CD47 regulates glycolysis in colorectal cancer cells by stabilizing ENO1.	Inhibitory Immune Checkpoint Molecule which turns off immune response in NK and T cells	(143, 144)
PD-L1	Immunology	Regulates glycolysis by improving PFKFB3 expression in renal cell carcinoma cells.	Inhibitory Immune Checkpoint Molecule which turns off immune response in NK and T cells	(143, 145)
VEGF	Immunology	Exogenous VEGF alters metabolism of triple negative breast cancer cells by modulating MAPK-ERK and PI3K-AKT pathways	An immunosuppressive growth factor that impedes the development of T cells and impairs maturation of dendritic cells.	(146–149)
HIF1A	Immunology	Transcribes genes that encode glycolytic enzymes (such as HK2, TPI, ENO1, and PKM) and glutamine metabolism.	Produces IL-9 during TH9 differentiation involved in pro-inflammatory signaling and anti-tumor immunity. HIF1A also partners with mTOR to promote CD8 memory T cell generation. HIF1A also upregulates PD-L1 on tumor cells.	(125, 150–152)
STING	Immunology	STING driven interferon signaling drives metabolic reprogramming of pancreatic cancer cells.	STING induced interferon signaling is crucial in inducing anti-cancer immune response. STING activation enhances antigen presentation and therefore activation of T cells.	(153–155)
TGFB	Immunology	Canonical signaling of TGF-β modulates metabolic reprogramming by upregulating genes involved in glycolysis and oxidative phosphorylation.	TGF-β is a cytokine that promotes cancer progression by impairing T cell proliferation and expansion. TGF-β in cancer associated fibroblasts also promotes immune evasion through ECM signaling.	(156–158)

neuroblastoma, melanoma cells promoted tumor immunogenicity and potentiated immune checkpoint blockade therapy (164). However, over the decades, MYC-targeted strategies against cancers have yet to see success in clinical trials due to the half-life of MYC and the rapid metabolism of the small-molecule inhibitors (20, 165). One significant challenge has been translating in vitro findings in vivo (166), until recently.

In the advent of overcoming the limitations of current MYC inhibitor designs, Omomyc, a 90 amino acid mutant MYC peptide that disrupts the MYC-MAX dimerization, rose to clinical development (167). Omomyc has exuded various pro-apoptotic effects in various cancers, and the potential of immune reprogramming of tumors (168). However, the effect of Omomyc

treatment on the metabolic reprogramming of cancers is yet to be determined. Because of its potent reduction of tumor burden, Omomyc stands as the first direct MYC inhibitor to ascend in dose-escalated phase 1 and phase 2 clinical trials of patients with non-small cell lung, colorectal, and breast cancer (NCT04808362). More recently, another phase 1 clinical trial (NCT06059001) has been initiated in metastatic pancreatic cancer. This success should encourage further improvements in this design to effectively target MYC and systemically shut down MYC-driven oncogenic pathways.

The growing body of evidence of the vastness of the "onco-MYC network" and its grave implications on cancer progression point to MYC being an ideal therapeutic target. Considering the
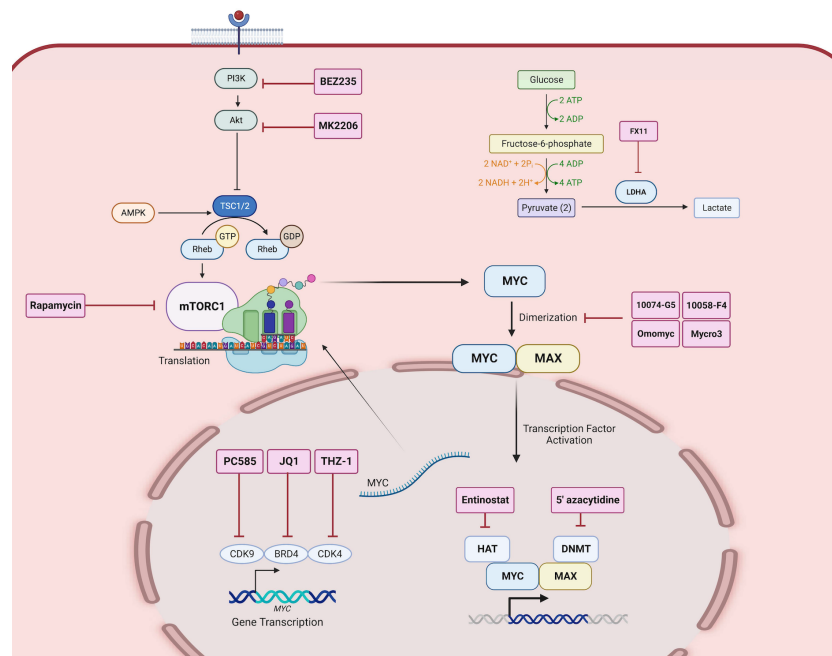
FIGURE 4
Direct and indirect MYC-targeted therapeutic strategies. Therapeutic inhibitors are depicted as labeled red boxes. PC585 inhibits CDK9, JQ1 inhibits BRD4, and THZ-1 inhibits CDK4, which together are key transcription factors that regulate MYC gene expression. BEZ235 is a PI3K inhibitor, MK2206 is an Akt inhibitor, and Rapamycin is a mTOR inhibitor, which together inhibit the translation of MYC. 10074-G5, 10058-F4, Omomyc, and Mycro3 inhibits the heterodimerization of MYC and MAX. Entinostat inhibits HAT and 5'azacytidine inhibits DNMT which are co-factors that aid in MYC activated transcription of gene targets. FX11 inhibits LDHA, a gene target of MYC, and thus inhibits the downstream function of MYC activation. Created with BioRender.com.

overlap in function of the gene targets of MYC between oncometabolism and oncoimmunology, we believe that targeting MYC directly or indirectly may systemically impact both hallmarks. Several investigators have untangled the MYC network to identify indirect putative targets to combat MYC-driven effects. For example, the inhibition of LDHA, a direct gene target of MYC, by FX11, not only suppresses MYC but also inhibits MYC-induced metabolic changes (169). Moreover, inhibition of MYC-regulated glutaminase (GLS) by CB-839 also has a similar effect in reversing MYC-driven metabolic changes such as nucleotide metabolism in ovarian and glioblastoma (109, 170). Moreover, this has shown promise for clinical development in various cancers including colorectal and leukemic cancers (NCT02861300; NCT02071927).

The approach of tackling MYC gene targets has also been successful in modulating the immune evasive nature of tumors. For instance, dual inhibition of MYC targets PD-L1 and CTLA-4 reverses MYC-driven immunosuppression through pro-inflammatory macrophages in hepatocellular carcinoma (115). Moreover, MYC partners with epigenetic modulators such as histone acetylases (HAT) and DNA methylases (DNMT), in the transcriptional activation of immunosuppressive gene targets of MYC (171). Targeting, MYC-epigenetic modulators may reverse this phenomenon and exude anticancer effects. In this direction, Topper et al. (172), tested this hypothesis by combining epigenetic modulators including 5'-azacytidine and entinostat to assess its effect on tumor burden. As a result, this combination increased the number CD8^{+}T and natural killer cells in the TME, promoted immunosurveillance of tumors, and reduced MYC-driven interferon signaling. These indirect pharmacological inhibitions are effective in modulating the downstream effects of MYC-driven tumors (172). These indirect pharmacological inhibitions are effective in modulating the downstream effects of MYC aberration as aforementioned, the therapeutic potentials of targeting gene targets at the crossroad between oncometabolism and oncoimmunology (Table 2) warrants further investigations.

5 Challenges and perspectives

Despite the success of Omomyc in preclinical models, the development of MYC-targeted therapy has miles to go until we reach the growing demand of patients who require effective treatment. The main challenge posed against all small molecule inhibitors against MYC is the rapid metabolism of the drug, and the quick half-life of MYC regeneration. One reported limitation of Omomyc is the fast distribution and catabolism, thereby limiting its use in preclinical and *in vivo* models (173). Other challenges include the multiple disordered conformations of the putative binding regions of MYC (174). Thus, this warrants further development in the design of MYC inhibition. Recent investigations approach this issue by using *in silico* tools to facilitate drug design. Using *in silico* tools offers a wealth of information to guide the development of a MYC-targeted therapeutic strategy. This ranges from identifying potential binding sites on MYC and predicting

different drug binding conformations using molecular docking to identifying close targets or partners upstream or downstream of MYC. For instance, Yu et al. employed conformational simulation of intrinsically disordered MYC to identify binding sites and "multi-conformational" molecular docking. This guided the identification of seven compounds that bind to MYC *in vitro* and inhibited cell proliferation in *c-MYC* overexpressing cell lines (175). Moreover, in 2018, a novel inhibitor, 7594-0035 was reported to specifically target MYC indicated for the treatment of refractory multiple myeloma. The novel inhibitor was identified using the drug database ChemDiv and molecularly docked to the crystallized structure of the MYC-MAX heterodimer complexed with DNA (PDB ID: 1NKP) (176). This evidence shows promise in unmasking the elusive binding pockets of MYC by simulating the interaction between the MYC-MAX heterodimer and small molecule structures, to develop better direct inhibitors of the MYC oncoprotein.

The advent of machine learning and artificial intelligence opens opportunities for investigators to design novel peptides, predict novel binding sites on MYC, and explore indirect key partners or regulators of MYC that may be therapeutically targeted alternatively. One successful example of this approach is the discovery of novel inhibitors by Xing et al. (177). that target BRD4 which regulates the transcription of the *MYC* gene (Figure 4). In their investigation, a structure-based virtual screening approach with machine-learning algorithms was performed to learn the structure of the BRD4 protein and predict the likelihood of the compound inhibiting BRD4 based on its binding pattern. This led to the discovery of 15 new BRD4 inhibitors which were experimentally validated (177). This approach could be extended by integrating machine learning and molecular docking to identify binding pockets within MYC at which predicted inhibitor structures may bind. Another approach utilizes novel *in silico* tools to predict miRNAs capable of regulating MYC and its partners; nonetheless, only a few miRNA regulators of MYC expression, such as miR-19, have been validated (178). This presents an avenue of research yet to be claimed to expand the available therapeutic options for inhibiting MYC.

A promising approach in employing *in silico* tools to discover pharmacological inhibition of MYC is using pharmacogenomic connectivity analysis of cancer transcriptomes and drug sensitivity data. To this effect, the iLINCS consortium facilitates "pharmaco-multi-Omics" analysis by integrating data from transcriptomic, proteomic, phospho-proteomic, and genomic sources to drug sensitivity data from chemical perturbation or gene knockdown signatures (179). This approach may not only supplement our understanding of the potential interactors of MYC, but also of the potential mechanism of action of these small molecules against MYC. An example of this approach being successful is seen in an excellent investigation led by Howard et al. (180). In the interest of repositioning pharmacological inhibitors toward the inhibition of eIF4A1 against triple-negative breast cancer, Howard et al. (180) surveyed and screened the Prestwick Chemical Library for potential therapeutics against eIF4A1, where iLINCS pharmacogenomics was implemented to elucidate the mechanism of action of these candidate molecules.

They identified that in the inhibition of eIF4A1, c-MYC is also suppressed, thus warranting further exploration of the interaction between eIF4A1 and c-MYC (180). While this investigation showed how c-MYC itself is an indirect target of some small molecules, future investigations may build on this information and identify other small molecules that impede c-MYC activity.

6 Conclusion

MYC activation is characteristic of various aggressive tumor types. This aggression is typically mediated by the crosstalk of cancer metabolism and cancer immunity. MYC is central to both hallmarks by partnering with various cofactors or transcription factors and by its gene targets. This thus presents MYC as a promising therapeutic target for cancer therapy. This review explores how MYC bridges these hallmarks by inducing metabolic reprogramming that influences an immunosuppressive microenvironment, and conversely, promoting immune evasive markers to influence immune cell and cancer cell metabolism. Moreover, the gene targets of MYC are often seen to be involved in both hallmarks and would therefore present as ideal alternative targets to combat MYC-driven effects. Direct inhibition of MYC has been challenging due to the short half-life of MYC oncoprotein and the high metabolism of the small molecule inhibitors, which has impeded the development of MYC inhibitors in clinical trials. However, Omomyc overcame these limitations, exuded potent anti-cancer effects, and has ascended toward clinical development for multiple cancers. This review surmises that MYC inhibition would be beneficial in systemically combating metabolic reprogramming and immune evasion in various cancers. Thus, we encourage more pharmacological strategies should be centered around MYC inhibition. Moreover, future investigation attention should be drawn toward elucidating the molecular mechanism behind MYC inhibition in both oncometabolism and oncoimmunology.

Author contributions

SV: Data curation, Methodology, Visualization, Writing – original draft. BB: Data curation, Methodology, Writing – review & editing. CT: Resources, Supervision, Writing – review & editing. JM: Resources, Supervision, Writing – review & editing. RT: Funding acquisition, Resources, Supervision, Writing – review & editing. SC: Conceptualization, Methodology, Supervision, Visualization, Writing – review & editing.

Conflict of interest

The authors declare that the research was conducted in the
absence of any commercial or financial relationships that could be
construed as a potential conflict of interest.

The author(s) declared that they were an editorial board
member of Frontiers, at the time of submission. This had no
impact on the peer review process and the final decision.

Publisher's note

All claims expressed in this article are solely those of the authors
and do not necessarily represent those of their affiliated
organizations, or those of the publisher, the editors and the
reviewers. Any product that may be evaluated in this article, or
claim that may be made by its manufacturer, is not guaranteed or
endorsed by the publisher.

References

1. Stine ZE, Walton ZE, Altman BJ, Hsieh AL, Dang CV. MYC, metabolism, and cancer. *Cancer Discovery* (2015) 5:1024–39. doi: 10.1158/2159-8290.CD-15-0507

2. Das SK, Lewis BA, Levens D. MYC: a complex problem. *Trends Cell Biol* (2022) 33:235–46. doi: 10.1016/j.tcb.2022.07.006

3. Kalkat M, Resetca D, Lourenco C, Chan PK, Wei Y, Shiah YJ, et al. MYC protein interactome profiling reveals functionally distinct regions that cooperate to drive tumorigenesis. *Mol Cell* (2018) 72:836–848 e7. doi: 10.1016/j.molcel.2018.09.031

4. Marinkovic T, Marinkovic D. Obscure involvement of MYC in neurodegenerative diseases and neuronal repair. *Mol Neurobiol* (2021) 58:4169–77. doi: 10.1007/s12035-021-02406-w

5. Trop-Steinberg S, Azar Y. Is myc an important biomarker? Myc expression in immune disorders and cancer. *Am J Med Sci* (2018) 355:67–75. doi: 10.1016/j.amjms.2017.06.007

6. Gabay M, Li Y, Felsher DW. MYC activation is a hallmark of cancer initiation and maintenance. *Cold Spring Harb Perspect Med* (2014) 4:a014241. doi: 10.1101/cshperspect.a014241

7. Wilson A, Murphy MJ, Oskarsson T, Kaloulis K, Bettess MD, Oser GM, et al. c-Myc controls the balance between hematopoietic stem cell self-renewal and differentiation. *Genes Dev* (2004) 18:2747–63. doi: 10.1101/gad.313104

8. Liu H, Radisky DC, Yang D, Xu R, Radisky ES, Bissell MJ, et al. MYC suppresses cancer metastasis by direct transcriptional silencing of alphav and beta3 integrin subunits. *Nat Cell Biol* (2012) 14:567–74. doi: 10.1038/ncb2491

9. Eberlin LS, Gabay M, Fan AC, Gouw AM, Tibshirani RJ, Felsher DW, et al. Alteration of the lipid profile in lymphomas induced by MYC overexpression. *Proc Natl Acad Sci USA* (2014) 111:10450–5. doi: 10.1073/pnas.1409778111

10. Hanahan D, Weinberg RA. The hallmarks of cancer. *Cell* (2000) 100:57–70. doi: 10.1016/S0092-8674(00)81683-9

11. Casey SC, Baylot V, Felsher DW. MYC: master regulator of immune privilege. *Trends Immunol* (2017) 38:298–305. doi: 10.1016/j.it.2017.01.002

12. Mossafa H, Damotte D, Jenabian A, Delarue R, Vincenneau A, Amouroux I, et al. Non-Hodgkin's lymphomas with Burkitt-like cells are associated with c-Myc amplification and poor prognosis. *Leuk Lymp* (2006) 47:1885–93. doi: 10.1080/10428190600687547

13. Vita M, Henriksson M. The myc oncoprotein as A therapeutic target for human cancer. *Semin Cancer Biol* (2006) 16:318–30. doi: 10.1016/j.semcancer.2006.07.015

14. Qu J, Zhao X, Wang J, Liu X, Yan Y, Liu L, et al. MYC overexpression with its prognostic and clinicopathological significance in breast cancer. *Oncotarget* (2017) 8:93998–4008. doi: 10.18632/oncotarget.21501

15. De Jonge AV, Mutis T, Roemer MGM, Scheijen B, Chamuleau MED. Impact of MYC on anti-tumor immune responses in aggressive B cell non-hodgkin lymphomas: consequences for cancer immunotherapy. *Cancers (Basel)* (2020) 12:3052. doi: 10.3390/cancers12103052

16. Dong Y, Tu R, Liu H, Qing G. Regulation of cancer cell metabolism: oncogenic MYC in the driver's seat. *Signal Transduct Target Ther* (2020) 5:124. doi: 10.1038/s41392-020-00235-2

17. Podsypanina K, Politi K, Beverly LJ, Varmus HE. Oncogene cooperation in tumor maintenance and tumor recurrence in mouse mammary tumors induced by Myc and mutant Kras. *Proc Natl Acad Sci USA* (2008) 105:5242–7. doi: 10.1073/pnas.0801197105

18. Tang HY, Goldman AR, Zhang X, Speicher DW, Dang CV. Measuring MYC-mediated metabolism in tumorigenesis. *Methods Mol Biol* (2021) 2318:231–9. doi: 10.1007/978-1-0716-1476-1_11

19. Carabet LA, Rennie PS, Cherkasov A. Therapeutic inhibition of myc in cancer. Structural bases and computer-aided drug discovery approaches. *Int J Mol Sci* (2018) 20:120. doi: 10.3390/ijms20010120

20. Llombart V, Mansour MR. Therapeutic targeting of "undruggable". *MYC. EBioMed* (2022) 75:103756. doi: 10.1016/j.ebiom.2021.103756

21. Soucek L, Whitfield JR, Sodir NM, Masso-Valles D, Serrano E, Karnezis AN, et al. Inhibition of Myc family proteins eradicates KRas-driven lung cancer in mice. *Genes Dev* (2013) 27:504–13. doi: 10.1101/gad.205542.112

22. Conacci-Sorrell M, Mcferrin L, Eisenman RN. An overview of MYC and its interactome. *Cold Spring Harb Perspect Med* (2014) 4:a014357. doi: 10.1101/cshperspect.a014357

23. Cheng C, He T, Chen K, Cai Y, Gu Y, Pan L, et al. P300 interacted with N-myc and regulated its protein stability via altering its post-translational modifications in neuroblastoma. *Mol Cell Proteomics* (2023) 22:100504. doi: 10.1016/j.mcpro.2023.100504

24. Hann SR. MYC cofactors: molecular switches controlling diverse biological outcomes. *Cold Spring Harb Perspect Med* (2014) 4:a014399. doi: 10.1101/cshperspect.a014399

25. Welcker M, Orian A, Jin J, Grim JE, Harper JW, Eisenman RN, et al. The Fbw7 tumor suppressor regulates glycogen synthase kinase 3 phosphorylation-dependent c-Myc protein degradation. *Proc Natl Acad Sci USA* (2004) 101:9085–90. doi: 10.1073/pnas.0402770101

26. Yada M, Hatakeyama S, Kamura T, Nishiyama M, Tsunematsu R, Imaki H, et al. Phosphorylation-dependent degradation of c-Myc is mediated by the F-box protein Fbw7. *EMBO J* (2004) 23:2116–25. doi: 10.1038/sj.emboj.7600217

27. Wei Y, Resetca D, Li Z, Johansson-Akhe I, Ahlner A, Helander S, et al. Multiple direct interactions of TBP with the MYC oncoprotein. *Nat Struct Mol Biol* (2019) 26:1035–43. doi: 10.1038/s41594-019-0321-z

28. Gargano B, Amente S, Majello B, Lania L. P-TEFb is a crucial co-factor for Myc transactivation. *Cell Cycle* (2007) 6:2031–7. doi: 10.4161/cc.6.16.4554

29. Kenneth NS, Ramsbottom BA, Gomez-Roman N, Marshall L, Cole PA, White RJ. TRRAP and GCN5 are used by c-Myc to activate RNA polymerase III transcription. *Proc Natl Acad Sci USA* (2007) 104:14917–22. doi: 10.1073/pnas.0702909104

30. Frank SR, Parisi T, Taubert S, Fernandez P, Fuchs M, Chan HM, et al. MYC recruits the TIP60 histone acetyltransferase complex to chromatin. *EMBO Rep* (2003) 4:575–80. doi: 10.1038/sj.embor.embor861

31. Wood MA, Mcmahon SB, Cole MD. An ATPase/helicase complex is an essential cofactor for oncogenic transformation by c-Myc. *Mol Cell* (2000) 5:321–30. doi: 10.1016/S1097-2765(00)80427-X

32. Tworkowski KA, Chakraborty AA, Samuelson AV, Seger YR, Narita M, Hannon GJ, et al. Adenovirus E1A targets p400 to induce the cellular oncoprotein Myc. *Proc Natl Acad Sci USA* (2008) 105:6103–8. doi: 10.1073/pnas.0802095105

33. Kim SY, Herbst A, Tworkowski KA, Salghetti SE, Tansey WP. Skp2 regulates Myc protein stability and activity. *Mol Cell* (2003) 11:1177–88. doi: 10.1016/S1097-2765(03)00173-4

34. Hermeking H, Rago C, Schuhmacher M, Li Q, Barrett JF, Obaya AJ, et al. Identification of CDK4 as a target of c-MYC. *Proc Natl Acad Sci USA* (2000) 97:2229–34. doi: 10.1073/pnas.050586197

35. Galaktionov K, Chen X, Beach D. Cdc25 cell-cycle phosphatase as a target of c-myc. *Nature* (1996) 382:511–7. doi: 10.1038/382511a0

36. Shi Y, Xu X, Zhang Q, Fu G, Mo Z, Wang GS, et al. tRNA synthetase counteracts c-Myc to develop functional vasculature. *Elife* (2014) 3:e02349. doi: 10.7554/eLife.02349

37. Yan S, Zhou C, Lou X, Xiao Z, Zhu H, Wang Q, et al. PTTG overexpression promotes lymph node metastasis in human esophageal squamous cell carcinoma. *Cancer Res* (2009) 69:3283–90. doi: 10.1158/0008-5472.CAN-08-0367

38. Brenner C, Deplus R, Didelot C, Loriot A, Vire E, De Smet C, et al. Myc represses transcription through recruitment of DNA methyltransferase corepressor. *EMBO J* (2005) 24:336–46. doi: 10.1038/sj.emboj.7600509

39. Tian X, Pelton A, Shahsafaei A, Dorfman DM. Differential expression of enhancer of zeste homolog 2 (EZH2) protein in small cell and aggressive B-cell non-Hodgkin lymphomas and differential regulation of EZH2 expression by p-ERK1/2 and MYC in aggressive B-cell lymphomas. *Mod Pathol* (2016) 29:1050–7. doi: 10.1038/modpathol.2016.114

40. Satou A, Taira T, Iguchi-Ariga SM, Ariga H. A novel transrepression pathway of c-Myc. Recruitment of a transcriptional corepressor complex to c-Myc by MM-1, a c-Myc-binding protein. *J Biol Chem* (2001) 276:46562–7. doi: 10.1074/jbc.M104937200

41. Kurland JF, Tansey WP. Myc-mediated transcriptional repression by recruitment of histone deacetylase. *Cancer Res* (2008) 68:3624–9. doi: 10.1158/0008-5472.CAN-07-6552

42. Yang J, Altahan AM, Hu D, Wang Y, Cheng PH, Morton CL, et al. The role of histone demethylase KDM4B in Myc signaling in neuroblastoma. *J Natl Cancer Inst* (2015) 107:djv080. doi: 10.1093/jnci/djv080

43. Staller P, Peukert K, Kiermaier A, Seoane J, Lukas J, Karsunky H, et al. Repression of p15INK4b expression by Myc through association with Miz-1. *Nat Cell Biol* (2001) 3:392–9. doi: 10.1038/35070076

44. Van Riggelen J, Muller J, Otto T, Beuger V, Yetil A, Choi PS, et al. The interaction between Myc and Miz1 is required to antagonize TGFbeta-dependent autocrine signaling during lymphoma formation and maintenance. *Genes Dev* (2010) 24:1281–94. doi: 10.1101/gad.585710

45. Yao L, Zhang J, Liu X. NDRG2: a Myc-repressed gene involved in cancer and cell stress. *Acta Biochim Biophys Sin (Shanghai)* (2008) 40:625–35. doi: 10.1111/j.1745-7270.2008.00434.x

46. Liu M, Yao B, Gui T, Guo C, Wu X, Li J, et al. PRMT5-dependent transcriptional repression of c-Myc target genes promotes gastric cancer progression. *Theranostics* (2020) 10:4437–52. doi: 10.7150/thno.42047

47. Wu S, Cetinkaya C, Munoz-Alonso MJ, Von Der Lehr N, Bahram F, Beuger V, et al. Myc represses differentiation-induced p21CIP1 expression via Miz-1-dependent interaction with the p21 core promoter. *Oncogene* (2003) 22:351–60. doi: 10.1038/sj.onc.1206145

48. Zeller KI, Jegga AG, Aronow BJ, O'donnell KA, Dang CV. An integrated database of genes responsive to the Myc oncogenic transcription factor: identification of direct genomic targets. *Genome Biol* (2003) 4:R69. doi: 10.1186/gb-2003-4-10-r69

49. Seoane J, Le HV, Massague J. Myc suppression of the p21(Cip1) Cdk inhibitor influences the outcome of the p53 response to DNA damage. *Nature* (2002) 419:729–34. doi: 10.1038/nature01119

50. Adhikary S, Eilers M. Transcriptional regulation and transformation by Myc proteins. *Nat Rev Mol Cell Biol* (2005) 6:635–45. doi: 10.1038/nrm1703

51. Patange S, Ball DA, Wan Y, Karpova TS, Girvan M, Levens D, et al. Myc amplifies gene expression through global changes in transcription factor dynamics. *Cell Rep* (2022) 38:110292. doi: 10.1016/j.celrep.2021.110292

52. Mo X, Qi Q, Ivanov AA, Niu Q, Luo Y, Havel J, et al. AKT1, LKB1, and YAP1 revealed as MYC interactors with nanoLuc-based protein-fragment complementation assay. *Mol Pharmacol* (2017) 91:339–47. doi: 10.1124/mol.116.107623

53. Zhang Q, Spears E, Boone DN, Li Z, Gregory MA, Hann SR. Domain-specific c-Myc ubiquitylation controls c-Myc transcriptional and apoptotic activity. *Proc Natl Acad Sci USA* (2013) 110:978–83. doi: 10.1073/pnas.1208334110

54. Ullius A, Luscher-Firzlaff J, Costa IG, Walsemann G, Forst AH, Gusmao EG, et al. The interaction of MYC with the trithorax protein ASH2L promotes gene transcription by regulating H3K27 modification. *Nucleic Acids Res* (2014) 42:6901–20. doi: 10.1093/nar/gku312

55. Richards MW, Burgess SG, Poon E, Carstensen A, Eilers M, Chesler L, et al. Structural basis of N-Myc binding by Aurora-A and its destabilization by kinase inhibitors. *Proc Natl Acad Sci USA* (2016) 113:13726–31. doi: 10.1073/pnas.1610626113

56. Richart L, Carrillo-De Santa Pau E, Rio-Machin A, De Andres MP, Cigudosa JC, Lobo VJS, et al. BPTF is required for c-MYC transcriptional activity and *in vivo* tumorigenesis. *Nat Commun* (2016) 7:10153. doi: 10.1038/ncomms10153

57. Wang Q, Zhang H, Kajino K, Greene MI. BRCA1 binds c-Myc and inhibits its transcriptional and transforming activity in cells. *Oncogene* (1998) 17:1939–48. doi: 10.1038/sj.onc.1202403

58. Chen Y, Xu J, Borowicz S, Collins C, Huo D, Olopade OI. c-Myc activates BRCA1 gene expression through distal promoter elements in breast cancer cells. *BMC Cancer* (2011) 11:246. doi: 10.1186/1471-2407-11-246

59. Luoto KR, Meng AX, Wasylishen AR, Zhao H, Coackley CL, Penn LZ, et al. Tumor cell kill by c-MYC depletion: role of MYC-regulated genes that control DNA double-strand break repair. *Cancer Res* (2010) 70:8748–59. doi: 10.1158/0008-5472.CAN-10-0944

60. Devaiah BN, Mu J, Akman B, Uppal S, Weissman JD, Cheng D, et al. MYC protein stability is negatively regulated by BRD4. *Proc Natl Acad Sci USA* (2020) 117:13457–67. doi: 10.1073/pnas.1919507117

61. Gill RM, Gabor TV, Couzens AL, Scheid MP. The MYC-associated protein CDCA7 is phosphorylated by AKT to regulate MYC-dependent apoptosis and transformation. *Mol Cell Biol* (2013) 33:498–513. doi: 10.1128/MCB.00276-12

62. Sears R, Nuckolls F, Haura E, Taya Y, Tamai K, Nevins JR. Multiple Ras-dependent phosphorylation pathways regulate Myc protein stability. *Genes Dev* (2000) 14:2501–14. doi: 10.1101/gad.836800

63. O'hagan RC, Ohh M, David G, De Alboran IM, Alt FW, Kaelin WG, et al. Myc-enhanced expression of Cul1 promotes ubiquitin-dependent proteolysis and cell cycle progression. *Genes Dev* (2000) 14:2185–91. doi: 10.1101/gad.827200

64. Bouchard C, Lee S, Paulus-Hock V, Loddenkemper C, Eilers M, Schmitt CA. FoxO transcription factors suppress Myc-driven lymphomagenesis via direct activation of Arf. *Genes Dev* (2007) 21:2775–87. doi: 10.1101/gad.453107

65. Peck B, Ferber EC, Schulze A. Antagonism between FOXO and MYC regulates cellular powerhouse. *Front Oncol* (2013) 3:96. doi: 10.3389/fonc.2013.00096

66. Cepeda D, Ng HF, Sharifi HR, Mahmoudi S, Cerrato VS, Fredlund E, et al. CDK-mediated activation of the SCF(FBXO) (28) ubiquitin ligase promotes MYC-driven transcription and tumourigenesis and predicts poor survival in breast cancer. *EMBO Mol Med* (2013) 5:1067–86. doi: 10.1002/emmm.201202341

67. Marfil V, Blazquez M, Serrano F, Castell JV, Bort R. Growth-promoting and tumourigenic activity of c-Myc is suppressed by Hhex. *Oncogene* (2015) 34:3011–22. doi: 10.1038/onc.2014.240

68. Koshiji M, Kageyama Y, Pete EA, Horikawa I, Barrett JC, Huang LE. HIF-1alpha induces cell cycle arrest by functionally counteracting Myc. *EMBO J* (2004) 23:1949–56. doi: 10.1038/sj.emboj.7600196

69. Adhikary S, Marinoni F, Hock A, Hulleman E, Popov N, Beier R, et al. The ubiquitin ligase HectH9 regulates transcriptional activation by Myc and is essential for tumor cell proliferation. *Cell* (2005) 123:409–21. doi: 10.1016/j.cell.2005.08.016

70. Wei X, Cai S, Boohaker RJ, Fried J, Li Y, Hu L, et al. KAT5 promotes invasion and metastasis through C-MYC stabilization in ATC. *Endocr Relat Cancer* (2019) 26:141–51. doi: 10.1530/ERC-18-0193

71. Amati B, Land H. Myc-Max-Mad: a transcription factor network controlling cell cycle progression, differentiation and death. *Curr Opin Genet Dev* (1994) 4:102–8. doi: 10.1016/0959-437X(94)90098-1

72. Blackwood EM, Eisenman RN. Max: a helix-loop-helix zipper protein that forms a sequence-specific DNA-binding complex with Myc. *Science* (1991) 251:1211–7. doi: 10.1126/science.2006410

73. Castell A, Yan Q, Fawkner K, Hydbring P, Zhang F, Verschut V, et al. A selective high affinity MYC-binding compound inhibits MYC : MAX interaction and MYC-dependent tumor cell proliferation. *Sci Rep* (2018) 8:10064. doi: 10.1038/s41598-018-28107-4

74. Bouchard C, Thieke K, Maier A, Saffrich R, Hanley-Hyde J, Ansorge W, et al. Direct induction of cyclin D2 by Myc contributes to cell cycle progression and sequestration of p27. *EMBO J* (1999) 18:5321–33. doi: 10.1093/emboj/18.19.5321

75. Garcia-Gutierrez L, Bretones G, Molina E, Arechaga I, Symonds C, Acosta JC, et al. Myc stimulates cell cycle progression through the activation of Cdk1 and phosphorylation of p27. *Sci Rep* (2019) 9:18693. doi: 10.1038/s41598-019-54917-1

76. La Rosa FA, Pierce JW, Sonenshein GE. Differential regulation of the c-myc oncogene promoter by the NF-kappa B rel family of transcription factors. *Mol Cell Biol* (1994) 14:1039–44. doi: 10.1128/MCB.14.2.1039

77. Huang H, Ma L, Li J, Yu Y, Zhang D, Wei J, et al. NF-kappaB1 inhibits c-Myc protein degradation through suppression of FBW7 expression. *Oncotarget* (2014) 5:493–505. doi: 10.18632/oncotarget.1643

78. Garcia-Sanz P, Quintanilla A, Lafita MC, Moreno-Bueno G, Garcia-Gutierrez L, Tabor V, et al. Sin3b interacts with Myc and decreases Myc levels. *J Biol Chem* (2014) 289:22221–36. doi: 10.1074/jbc.M113.538744

79. Cheng SW, Davies KP, Yung E, Beltran RJ, Yu J, Kalpana GV. c-MYC interacts with INI1/hSNF5 and requires the SWI/SNF complex for transactivation function. *Nat Genet* (1999) 22:102–5. doi: 10.1038/8811

80. Weissmiller AM, Wang J, Lorey SL, Howard GC, Martinez E, Liu Q, et al. Inhibition of MYC by the SMARCB1 tumor suppressor. *Nat Commun* (2019) 10:2014. doi: 10.1038/s41467-019-10022-5

81. Mcmahon SB, Van Buskirk HA, Dugan KA, Copeland TD, Cole MD. The novel ATM-related protein TRRAP is an essential cofactor for the c-Myc and E2F oncoproteins. *Cell* (1998) 94:363–74. doi: 10.1016/S0092-8674(00)81479-8

82. Baudino TA, Mckay C, Pendeville-Samain H, Nilsson JA, Maclean KH, White EL, et al. c-Myc is essential for vasculogenesis and angiogenesis during development and tumor progression. *Genes Dev* (2002) 16:2530–43. doi: 10.1101/gad.1024602

83. Thomas LR, Wang Q, Grieb BC, Phan J, Foshage AM, Sun Q, et al. Interaction with WDR5 promotes target gene recognition and tumorigenesis by MYC. *Mol Cell* (2015) 58:440–52. doi: 10.1016/j.molcel.2015.02.028

84. Loftus RM, Assmann N, Kedia-Mehta N, O'brien KL, Garcia A, Gillespie C, et al. Amino acid-dependent cMyc expression is essential for NK cell metabolic and functional responses in mice. *Nat Commun* (2018) 9:2341. doi: 10.1038/s41467-018-04719-2

85. Kim S, Jang JY, Koh J, Kwon D, Kim YA, Paeng JC, et al. Programmed cell death ligand-1-mediated enhancement of hexokinase 2 expression is inversely related to T-cell effector gene expression in non-small-cell lung cancer. *J Exp Clin Cancer Res* (2019) 38:462. doi: 10.1186/s13046-019-1407-5

86. Cruz-Bermudez A, Laza-Briviesca R, Casarrubios M, Sierra-Rodero B, Provencio M. The role of metabolism in tumor immune evasion: novel approaches to improve immunotherapy. *Biomedicines* (2021) 9:361. doi: 10.3390/biomedicines9040361

87. Csibi A, Lee G, Yoon SO, Tong H, Ilter D, Elia I, et al. The mTORC1/S6K1 pathway regulates glutamine metabolism through the eIF4B-dependent control of c-Myc translation. *Curr Biol* (2014) 24:2274–80. doi: 10.1016/j.cub.2014.08.007

88. Le A, Lane AN, Hamaker M, Bose S, Gouw A, Barbi J, et al. Glucose-independent glutamine metabolism via TCA cycling for proliferation and survival in B cells. *Cell Metab* (2012) 15:110–21. doi: 10.1016/j.cmet.2011.12.009

89. Yuneva MO, Fan TW, Allen TD, Higashi RM, Ferraris DV, Tsukamoto T, et al. The metabolic profile of tumors depends on both the responsible genetic lesion and tissue type. *Cell Metab* (2012) 15:157–70. doi: 10.1016/j.cmet.2011.12.015

90. Osthus RC, Shim H, Kim S, Li Q, Reddy R, Mukherjee M, et al. Deregulation of glucose transporter 1 and glycolytic gene expression by c-Myc. *J Biol Chem* (2000) 275:21797–800. doi: 10.1074/jbc.C000023200

91. Kim JW, Gao P, Liu YC, Semenza GL, Dang CV. Hypoxia-inducible factor 1 and dysregulated c-Myc cooperatively induce vascular endothelial growth factor and metabolic switches hexokinase 2 and pyruvate dehydrogenase kinase 1. *Mol Cell Biol* (2007) 27:7381–93. doi: 10.1128/MCB.00440-07

92. Shim H, Dolde C, Lewis BC, Wu CS, Dang G, Jungmann RA, et al. c-Myc transactivation of LDH-A: implications for tumor metabolism and growth. *Proc Natl Acad Sci USA* (1997) 94:6658–63. doi: 10.1073/pnas.94.13.6658

93. Perez-Tomas R, Perez-Guillen I. Lactate in the tumor microenvironment: an essential molecule in cancer progression and treatment. *Cancers (Basel)* (2020) 12:3244. doi: 10.3390/cancers12113244

94. Cargill KR, Stewart CA, Park EM, Ramkumar K, Gay CM, Cardnell RJ, et al. Targeting MYC-enhanced glycolysis for the treatment of small cell lung cancer. *Cancer Metab* (2021) 9:33. doi: 10.1186/s40170-021-00270-9

95. Zuo S, Wu L, Wang Y, Yuan X. Long Non-coding RNA MEG3 Activated by Vitamin D Suppresses Glycolysis in Colorectal Cancer via Promoting c-Myc Degradation. *Front Oncol* (2020) 10:274. doi: 10.3389/fonc.2020.00274

96. Wei Z, Liu X, Cheng C, Yu W, Yi P. Metabolism of amino acids in cancer. *Front Cell Dev Biol* (2020) 8:603837. doi: 10.3389/fcell.2020.603837

97. Lee P, Chandel NS, Simon MC. Cellular adaptation to hypoxia through hypoxia inducible factors and beyond. *Nat Rev Mol Cell Biol* (2020) 21:268–83. doi: 10.1038/s41580-020-0227-y

98. Zhang H, Gao P, Fukuda R, Kumar G, Krishnamachary B, Zeller KI, et al. HIF-1 inhibits mitochondrial biogenesis and cellular respiration in VHL-deficient renal cell carcinoma by repression of C-MYC activity. *Cancer Cell* (2007) 11:407–20. doi: 10.1016/j.ccr.2007.04.001

99. Jensen KS, Binderup T, Jensen KT, Therkelsen I, Borup R, Nilsson E, et al. FoxO3A promotes metabolic adaptation to hypoxia by antagonizing Myc function. *EMBO J* (2011) 30:4554–70. doi: 10.1038/emboj.2011.323

100. Li Y, Sun XX, Qian DZ, Dai MS. Molecular crosstalk between MYC and HIF in cancer. *Front Cell Dev Biol* (2020) 8:590576. doi: 10.3389/fcell.2020.590576

101. Haggerty TJ, Zeller KI, Osthus RC, Wonsey DR, Dang CV. A strategy for identifying transcription factor binding sites reveals two classes of genomic c-Myc target sites. *Proc Natl Acad Sci USA* (2003) 100:5313–8. doi: 10.1073/pnas.0931346100

102. Sun L, Song L, Wan Q, Wu G, Li X, Wang Y, et al. cMyc-mediated activation of serine biosynthesis pathway is critical for cancer progression under nutrient deprivation conditions. *Cell Res* (2015) 25:429–44. doi: 10.1038/cr.2015.33

103. Bott AJ, Peng IC, Fan Y, Faubert B, Zhao L, Li J, et al. Oncogenic myc induces expression of glutamine synthetase through promoter demethylation. *Cell Metab* (2015) 22:1068–77. doi: 10.1016/j.cmet.2015.09.025

104. Nicklin P, Bergman P, Zhang B, Triantafellow E, Wang H, Nyfeler B, et al. Bidirectional transport of amino acids regulates mTOR and autophagy. *Cell* (2009) 136:521–34. doi: 10.1016/j.cell.2008.11.044

105. Wise DR, Deberardinis RJ, Mancuso A, Sayed N, Zhang XY, Pfeiffer HK, et al. Myc regulates a transcriptional program that stimulates mitochondrial glutaminolysis and leads to glutamine addiction. *Proc Natl Acad Sci USA* (2008) 105:18782–7. doi: 10.1073/pnas.0810199105

106. Gao P, Tchernyshyov I, Chang TC, Lee YS, Kita K, Ochi T, et al. c-Myc suppression of miR-23a/b enhances mitochondrial glutaminase expression and glutamine metabolism. *Nature* (2009) 458:762–5. doi: 10.1038/nature07823

107. Jacque N, Ronchetti AM, Larrue C, Meunier G, Birsen R, Willems L, et al. Targeting glutaminolysis has antileukemic activity in acute myeloid leukemia and synergizes with BCL-2 inhibition. *Blood* (2015) 126:1346–56. doi: 10.1182/blood-2015-01-621870

108. Luengo A, Gui DY, Vander Heiden MG. Targeting metabolism for cancer therapy. *Cell Chem Biol* (2017) 24:1161–80. doi: 10.1016/j.chembiol.2017.08.028

109. Shen YA, Hong J, Asaka R, Asaka S, Hsu FC, Suryo Rahmanto Y, et al. Inhibition of the MYC-regulated glutaminase metabolic axis is an effective synthetic lethal approach for treating chemoresistant ovarian cancers. *Cancer Res* (2020) 80:4514–26. doi: 10.1158/0008-5472.CAN-19-3971

110. Dhanasekaran R, Deutzmann A, Mahauad-Fernandez WD, Hansen AS, Gouw AM, Felsher DW. The MYC oncogene - the grand orchestrator of cancer growth and immune evasion. *Nat Rev Clin Oncol* (2022) 19:23–36. doi: 10.1038/s41571-021-00549-2

111. Kortlever RM, Sodir NM, Wilson CH, Burkhart DL, Pellegrinet L, Brown Swigart L, et al. Myc cooperates with ras by programming inflammation and immune suppression. *Cell* (2017) 171:1301–1315 e14. doi: 10.1016/j.cell.2017.11.013

112. Gao FY, Li XT, Xu K, Wang RT, Guan XX. c-MYC mediates the crosstalk between breast cancer cells and tumor microenvironment. *Cell Commun Signal* (2023) 21:28. doi: 10.1186/s12964-023-01043-1

113. Liu S, Qin Z, Mao Y, Zhang W, Wang Y, Jia L, et al. Therapeutic targeting of MYC in head and neck squamous cell carcinoma. *Oncoimmunology* (2022) 11:2130583. doi: 10.1080/2162402X.2022.2130583

114. Jiang K, Zhang Q, Fan Y, Li J, Zhang J, Wang W, et al. MYC inhibition reprograms tumor immune microenvironment by recruiting T lymphocytes and activating the CD40/CD40L system in osteosarcoma. *Cell Death Discovery* (2022) 8:117. doi: 10.1038/s41420-022-00923-8

115. Dhanasekaran R, Hansen AS, Park J, Lemaitre L, Lai I, Adeniji N, et al. MYC overexpression drives immune evasion in hepatocellular carcinoma that is reversible through restoration of proinflammatory macrophages. *Cancer Res* (2023) 83:626–40. doi: 10.1158/0008-5472.CAN-22-0232

116. Marinkovic D, Marinkovic T. The new role for an old guy: MYC as an immunoplayer. *J Cell Physiol* (2021) 236:3234–43. doi: 10.1002/jcp.30123

117. Chen G, Huang AC, Zhang W, Zhang G, Wu M, Xu W, et al. Exosomal PD-L1 contributes to immunosuppression and is associated with anti-PD-1 response. *Nature* (2018) 560:382–6. doi: 10.1038/s41586-018-0392-8

118. Liu J, Peng X, Yang S, Li X, Huang M, Wei S, et al. Extracellular vesicle PD-L1 in reshaping tumor immune microenvironment: biological function and potential therapy strategies. *Cell Commun Signal* (2022) 20:14. doi: 10.1186/s12964-021-00816-w

119. Smith BAH, Deutzmann A, Correa KM, Delaveris CS, Dhanasekaran R, Dove CG, et al. MYC-driven synthesis of Siglec ligands is a glycoimmune checkpoint. *Proc Natl Acad Sci USA* (2023) 120:e2215376120. doi: 10.1073/pnas.2215376120

120. Estrella V, Chen T, Lloyd M, Wojtkowiak J, Cornnell HH, Ibrahim-Hashim A, et al. Acidity generated by the tumor microenvironment drives local invasion. *Cancer Res* (2013) 73:1524–35. doi: 10.1158/0008-5472.CAN-12-2796

121. Ippolito L, Morandi A, Giannoni E, Chiarugi P. Lactate: A metabolic driver in the tumour landscape. *Trends Biochem Sci* (2019) 44:153–66. doi: 10.1016/j.tibs.2018.10.011

122. Colegio OR, Chu NQ, Szabo AL, Chu T, Rhebergen AM, Jairam V, et al. Functional polarization of tumour-associated macrophages by tumour-derived lactic acid. *Nature* (2014) 513:559–63. doi: 10.1038/nature13490

123. Chen P, Zuo H, Xiong H, Kolar MJ, Chu Q, Saghatelian A, et al. Gpr132 sensing of lactate mediates tumor-macrophage interplay to promote breast cancer metastasis. *Proc Natl Acad Sci USA* (2017) 114:580–5. doi: 10.1073/pnas.1614035114

124. Wang L, Sun L, Sun H, Xing Y, Zhou S, An G, et al. GPR65 as a potential immune checkpoint regulates the immune microenvironment according to pan-cancer analysis. *Heliyon* (2023) 9:e13617. doi: 10.1016/j.heliyon.2023.e13617

125. Gnanaprakasam JNR, Sherman JW, Wang R. MYC and HIF in shaping immune response and immune metabolism. *Cytokine Growth Factor Rev* (2017) 35:63–70. doi: 10.1016/j.cytogfr.2017.03.004

126. Marchingo JM, Sinclair LV, Howden AJ, Cantrell DA. Quantitative analysis of how Myc controls T cell proteomes and metabolic pathways during T cell activation. *Elife* (2020) 9:e53725. doi: 10.7554/eLife.53725

127. Wang R, Dillon CP, Shi LZ, Milasta S, Carter R, Finkelstein D, et al. The transcription factor Myc controls metabolic reprogramming upon T lymphocyte activation. *Immunity* (2011) 35:871–82. doi: 10.1016/j.immuni.2011.09.021

128. Tsai CH, Chuang YM, Li X, Yu YR, Tzeng SF, Teoh ST, et al. Immunoediting instructs tumor metabolic reprogramming to support immune evasion. *Cell Metab* (2023) 35:118–133 e7. doi: 10.1016/j.cmet.2022.12.003

129. Liu T, Han C, Wang S, Fang P, Ma Z, Xu L, et al. Cancer-associated fibroblasts: an emerging target of anti-cancer immunotherapy. *J Hematol Oncol* (2019) 12:86. doi: 10.1186/s13045-019-0770-1

130. Mao X, Xu J, Wang W, Liang C, Hua J, Liu J, et al. Crosstalk between cancer-associated fibroblasts and immune cells in the tumor microenvironment: new findings and future perspectives. *Mol Cancer* (2021) 20:131. doi: 10.1186/s12943-021-01428-1

131. Martinez-Outschoorn UE, Lisanti MP, Sotgia F. Catabolic cancer-associated fibroblasts transfer energy and biomass to anabolic cancer cells, fueling tumor growth. *Semin Cancer Biol* (2014) 25:47–60. doi: 10.1016/j.semcancer.2014.01.005

132. Yan W, Wu X, Zhou W, Fong MY, Cao M, Liu J, et al. Cancer-cell-secreted exosomal miR-105 promotes tumour growth through the MYC-dependent metabolic reprogramming of stromal cells. *Nat Cell Biol* (2018) 20:597–609. doi: 10.1038/s41556-018-0083-6

133. Comito G, Iscaro A, Bacci M, Morandi A, Ippolito L, Parri M, et al. Lactate modulates CD4(+) T-cell polarization and induces an immunosuppressive environment, which sustains prostate carcinoma progression via TLR8/miR21 axis. *Oncogene* (2019) 38:3681–95. doi: 10.1038/s41388-019-0688-7

134. Serganova I, Cohen IJ, Vemuri K, Shindo M, Maeda M, Mane M, et al. LDH-A regulates the tumor microenvironment via HIF-signaling and modulates the immune response. *PLoS One* (2018) 13:e0203965. doi: 10.1371/journal.pone.0203965

135. Van Wilpe S, Koornstra R, Den Brok M, De Groot JW, Blank C, De Vries J, et al. Lactate dehydrogenase: A marker of diminished antitumor immunity. *Oncoimmunology* (2020) 9:1731942. doi: 10.1080/2162402X.2020.1731942

136. Li F, He C, Yao H, Liang W, Ye X, Ruan J, et al. GLUT1 Regulates the Tumor Immune Microenvironment and Promotes Tumor Metastasis in Pancreatic Adenocarcinoma via ncRNA-mediated Network. *J Cancer* (2022) 13:2540–58. doi: 10.7150/jca.72161

137. Park SY, Cho DG, Shim BY, Cho U. Relationship between systemic inflammatory markers, GLUT1 expression, and maximum 18F-fluorodeoxyglucose uptake in non-small cell lung carcinoma and their prognostic significance. *Diagn (Basel)* (2023) 13:1013. doi: 10.3390/diagnostics13061013

138. Zhang C, Zhang K, Gu J, Ge D. ENO1 promotes antitumor immunity by destabilizing PD-L1 in NSCLC. *Cell Mol Immunol* (2021) 18:2045–7. doi: 10.1038/s41423-021-00710-y

139. Ansari RE, Craze ML, Althobiti M, Alfarsi L, Ellis IO, Rakha EA, et al. Enhanced glutamine uptake influences composition of immune cell infiltrates in breast cancer. *Br J Cancer* (2020) 122:94–101. doi: 10.1038/s41416-019-0626-z

140. Flinck M, Kramer SH, Pedersen SF. Roles of pH in control of cell proliferation. *Acta Physiol (Oxf)* (2018) 223:e13068. doi: 10.1111/apha.13068

141. Wang ZH, Peng WB, Zhang P, Yang XP, Zhou Q. Lactate in the tumour microenvironment: From immune modulation to therapy. *EBioMedicine* (2021) 73:103627. doi: 10.1016/j.ebiom.2021.103627

142. Fu Q, Xu L, Wang Y, Jiang Q, Liu Z, Zhang J, et al. Tumor-associated macrophage-derived interleukin-23 interlinks kidney cancer glutamine addiction with immune evasion. *Eur Urol* (2019) 75:752–63. doi: 10.1016/j.eururo.2018.09.030

143. Casey SC, Tong L, Li Y, Do R, Walz S, Fitzgerald KN, et al. MYC regulates the antitumor immune response through CD47 and PD-L1. *Science* (2016) 352:227–31. doi: 10.1126/science.aac9935

144. Hu T, Liu H, Liang Z, Wang F, Zhou C, Zheng X, et al. Tumor-intrinsic CD47 signal regulates glycolysis and promotes colorectal cancer cell growth and metastasis. *Theranostics* (2020) 10:4056–72. doi: 10.7150/thno.40860

145. Yu Y, Liang Y, Li D, Wang L, Liang Z, Chen Y, et al. Glucose metabolism involved in PD-L1-mediated immune escape in the Malignant kidney tumour microenvironment. *Cell Death Discovery* (2021) 7:15. doi: 10.1038/s41420-021-00401-7

146. Ohm JE, Gabrilovich DI, Sempowski GD, Kisseleva E, Parman KS, Nadaf S, et al. VEGF inhibits T-cell development and may contribute to tumor-induced immune suppression. *Blood* (2003) 101:4878–86. doi: 10.1182/blood-2002-07-1956

147. Yang J, Yan J, Liu B. Targeting VEGF/VEGFR to modulate antitumor immunity. *Front Immunol* (2018) 9:978. doi: 10.3389/fimmu.2018.00978

148. Bose D, Banerjee S, Singh RK, Wise LM, Robertson ES. Vascular endothelial growth factor encoded by Parapoxviruses can regulate metabolism and survival of triple negative breast cancer cells. *Cell Death Dis* (2020) 11:996. doi: 10.1038/s41419-020-03203-4

149. Zalpoor H, Aziziyan F, Liaghat M, Bakhtiyari M, Akbari A, Nabi-Afjadi M, et al. The roles of metabolic profiles and intracellular signaling pathways of tumor microenvironment cells in angiogenesis of solid tumors. *Cell Commun Signal* (2022) 20:186. doi: 10.1186/s12964-022-00951-y

150. Pearce EL, Walsh MC, Cejas PJ, Harms GM, Shen H, Wang LS, et al. Enhancing cd8 T-cell memory by modulating fatty acid metabolism. *Nature* (2009) 460:103–7. doi: 10.1038/nature08097

151. Shi LZ, Wang R, Huang G, Vogel P, Neale G, Green DR, et al. HIF1alpha-dependent glycolytic pathway orchestrates a metabolic checkpoint for the differentiation of TH17 and Treg cells. *J Exp Med* (2011) 208:1367–76. doi: 10.1084/jem.20110278

152. Wang Y, Bi Y, Chen X, Li C, Li Y, Zhang Z, et al. Histone deacetylase SIRT1 negatively regulates the differentiation of interleukin-9-producing CD4(+) T cells. *Immunity* (2016) 44:1337–49. doi: 10.1016/j.immuni.2016.05.009

153. Zhu Y, An X, Zhang X, Qiao Y, Zheng T, Li X. STING: a master regulator in the cancer-immunity cycle. *Mol Cancer* (2019) 18:152. doi: 10.1186/s12943-019-1087-y

154. Liang K, Abt ER, Le TM, Cho A, Dann AM, Cui J, et al. STING-driven interferon signaling triggers metabolic alterations in pancreas cancer cells visualized by [(18)F]FLT PET imaging. *Proc Natl Acad Sci USA* (2021) 118:e2105390118. doi: 10.1073/pnas.2105390118

155. Wu SY, Xiao Y, Wei JL, Xu XE, Jin X, Hu X, et al. MYC suppresses STING-dependent innate immunity by transcriptionally upregulating DNMT1 in triple-negative breast cancer. *J Immunother Cancer* (2021) 9:e002528. doi: 10.1136/jitc-2021-002528

156. Chakravarthy A, Khan L, Bensler NP, Bose P, De Carvalho DD. TGF-beta-associated extracellular matrix genes link cancer-associated fibroblasts to immune evasion and immunotherapy failure. *Nat Commun* (2018) 9:4692. doi: 10.1038/s41467-018-06654-8

157. Xue VW, Chung JY, Cordoba CAG, Cheung AH, Kang W, Lam EW, et al. Transforming growth factor-beta: A multifunctional regulator of cancer immunity. *Cancers (Basel)* (2020) 12:3099. doi: 10.3390/cancers12113099

158. Angioni R, Sanchez-Rodriguez R, Viola A, Molon B. TGF-beta in cancer: metabolic driver of the tolerogenic crosstalk in the tumor microenvironment. *Cancers (Basel)* (2021) 13:401. doi: 10.3390/cancers13030401

159. Wang C, Zhang J, Yin J, Gan Y, Xu S, Gu Y, et al. Alternative approaches to target Myc for cancer treatment. *Signal Transduct Target Ther* (2021) 6:117. doi: 10.1038/s41392-021-00500-y

160. Zirath H, Frenzel A, Oliynyk G, Segerstrom L, Westermark UK, Larsson K, et al. MYC inhibition induces metabolic changes leading to accumulation of lipid droplets in tumor cells. *Proc Natl Acad Sci USA* (2013) 110:10258–63. doi: 10.1073/pnas.1222404110

161. Yang C, Liu Y, Hu Y, Fang L, Huang Z, Cui H, et al. Myc inhibition tips the immune balance to promote antitumor immunity. *Cell Mol Immunol* (2022) 19:1030–41. doi: 10.1038/s41423-022-00898-7

162. Chen H, Liu H, Qing G. Targeting oncogenic Myc as a strategy for cancer treatment. *Signal Transduct Target Ther* (2018) 3:5. doi: 10.1038/s41392-018-0008-7

163. Graziani V, Garcia AR, Alcolado LS, Le Guennec A, Henriksson MA, Conte MR. Metabolic rewiring in MYC-driven medulloblastoma by BET-bromodomain inhibition. *Sci Rep* (2023) 13:1273. doi: 10.1038/s41598-023-27375-z

164. Wu X, Nelson M, Basu M, Srinivasan P, Lazarski C, Zhang P, et al. MYC oncogene is associated with suppression of tumor immunity and targeting Myc induces tumor cell immunogenicity for therapeutic whole cell vaccination. *J Immunother Cancer* (2021) 9:e001388. doi: 10.1136/jitc-2020-001388

165. Clausen DM, Guo J, Parise RA, Beumer JH, Egorin MJ, Lazo JS, et al. *In vitro* cytotoxicity and *in vivo* efficacy, pharmacokinetics, and metabolism of 10074-G5, a novel small-molecule inhibitor of c-Myc/Max dimerization. *J Pharmacol Exp Ther* (2010) 335:715–27. doi: 10.1124/jpet.110.170555

166. Camarda R, Williams J, Goga A. *In vivo* reprogramming of cancer metabolism by MYC. *Front Cell Dev Biol* (2017) 5:35. doi: 10.3389/fcell.2017.00035

167. Masso-Valles D, Soucek L. Blocking myc to treat cancer: reflecting on two decades of omomyc. *Cells* (2020) 9:883. doi: 10.3390/cells9040883

168. Beaulieu ME, Jauset T, Masso-Valles D, Martinez-Martin S, Rahl P, Maltais L, et al. Intrinsic cell-penetrating activity propels Omomyc from proof of concept to viable anti-MYC therapy. *Sci Transl Med* (2019) 11:eaar5012. doi: 10.1126/scitranslmed.aar5012

169. Le A, Cooper CR, Gouw AM, Dinavahi R, Maitra A, Deck LM, et al. Inhibition of lactate dehydrogenase A induces oxidative stress and inhibits tumor progression. *Proc Natl Acad Sci USA* (2010) 107:2037–42. doi: 10.1073/pnas.0914433107

170. De Los Santos-Jimenez J, Rosales T, Ko B, Campos-Sandoval JA, Alonso FJ, Marquez J, et al. Metabolic adjustments following glutaminase inhibition by CB-839 in glioblastoma cell lines. *Cancers (Basel)* (2023) 15:531. doi: 10.3390/cancers15020531

171. Poole CJ, Van Riggelen J. MYC-master regulator of the cancer epigenome and transcriptome. *Genes (Basel)* (2017) 8:142. doi: 10.3390/genes8050142

172. Topper MJ, Vaz M, Chiappinelli KB, Destefano Shields CE, Niknafs N, Yen RC, et al. Epigenetic therapy ties MYC depletion to reversing immune evasion and treating lung cancer. *Cell* (2017) 171:1284–1300 e21. doi: 10.1016/j.cell.2017.10.022

173. Demma MJ, Mapelli C, Sun A, Bodea S, Ruprecht B, Javaid S, et al. Omomyc reveals new mechanisms to inhibit the MYC oncogene. *Mol Cell Biol* (2019) 39:e00248-19. doi: 10.1128/MCB.00248-19

174. Michel J, Cuchillo R. The impact of small molecule binding on the energy landscape of the intrinsically disordered protein C-myc. *PloS One* (2012) 7:e41070. doi: 10.1371/journal.pone.0041070

175. Yu C, Niu X, Jin F, Liu Z, Jin C, Lai L. Structure-based inhibitor design for the intrinsically disordered protein c-myc. *Sci Rep* (2016) 6:22298. doi: 10.1038/srep22298

176. Yao R, Sun X, Xie Y, Sun X, Yao Y, Li H, et al. Identification of a novel c-Myc inhibitor with antitumor effects on multiple myeloma cells. *Biosci Rep* (2018) 38:BSR20181027. doi: 10.1042/BSR20181027

177. Xing J, Lu W, Liu R, Wang Y, Xie Y, Zhang H, et al. Machine-learning-assisted approach for discovering novel inhibitors targeting bromodomain-containing protein 4. *J Chem Inf Model* (2017) 57:1677–90. doi: 10.1021/acs.jcim.7b00098

178. Mu P, Han YC, Betel D, Yao E, Squatrito M, Ogrodowski P, et al. Genetic dissection of the miR-17~92 cluster of microRNAs in Myc-induced B-cell lymphomas. *Genes Dev* (2009) 23:2806–11. doi: 10.1101/gad.1872909

179. Pilarczyk M, Fazel-Najafabadi M, Kouril M, Shamsaei B, Vasiliauskas J, Niu W, et al. Connecting omics signatures and revealing biological mechanisms with iLINCS. *Nat Commun* (2022) 13:4678. doi: 10.1038/s41467-022-32205-3

180. Howard CM, Estrada M, Terrero D, Tiwari AK, Raman D. Identification of cardiac glycosides as novel inhibitors of eIF4A1-mediated translation in triple-negative breast cancer cells. *Cancers (Basel)* (2020) 12:2169. doi: 10.3390/cancers12082169

Multiple influence of immune cells in the bone metastatic cancer microenvironment on tumors

Shixin Chen[1,2,3,4†], Jiangchu Lei[1,2,3,4†], Haochen Mou[1,2,3,4†], Wenkan Zhang[1,2,3,4], Lingxiao Jin[1,2,3,4], Senxu Lu[1,2,3,4], Eloy Yinwang[1,2,3,4], Yucheng Xue[1,2,3,4], Zhenxuan Shao[1,2,3,4], Tao Chen[1,2,3,4], Fangqian Wang[1,2,3,4], Shenzhi Zhao[1,2,3,4], Xupeng Chai[1,2,3,4], Zenan Wang[1,2,3,4], Jiahao Zhang[1,2,3,4], Zengjie Zhang[1,2,3,4*], Zhaoming Ye[1,2,3,4*] and Binghao Li[1,2,3,4*]

[1]Department of Orthopedic Surgery, The Second Affiliated Hospital, Zhejiang University School of Medicine, Hangzhou, China, [2]Orthopedics Research Institute of Zhejiang University, Hangzhou, Zhejiang, China, [3]Key Laboratory of Motor System Disease Research and Precision Therapy of Zhejiang Province, Hangzhou, Zhejiang, China, [4]Clinical Research Center of Motor System Disease of Zhejiang Province, Hangzhou, Zhejiang, China

Bone is a common organ for solid tumor metastasis. Malignant bone tumor becomes insensitive to systemic therapy after colonization, followed by poor prognosis and high relapse rate. Immune and bone cells *in situ* constitute a unique immune microenvironment, which plays a crucial role in the context of bone metastasis. This review firstly focuses on lymphatic cells in bone metastatic cancer, including their function in tumor dissemination, invasion, growth and possible cytotoxicity-induced eradication. Subsequently, we examine myeloid cells, namely macrophages, myeloid-derived suppressor cells, dendritic cells, and megakaryocytes, evaluating their interaction with cytotoxic T lymphocytes and contribution to bone metastasis. As important components of skeletal tissue, osteoclasts and osteoblasts derived from bone marrow stromal cells, engaging in 'vicious cycle' accelerate osteolytic bone metastasis. We also explain the concept tumor dormancy and investigate underlying role of immune microenvironment on it. Additionally, a thorough review of emerging treatments for bone metastatic malignancy in clinical research, especially immunotherapy, is presented, indicating current challenges and opportunities in research and development of bone metastasis therapies.

1 Introduction

Bone metastasis is a common target organ of metastasis for several solid tumor types, including lung, breast, prostate, colorectal, thyroid, and gynecological tumors, and melanoma. Statistically, approximately 70% of patients with metastatic prostate and breast cancer develop bone metastases (1). Once cancer has spread to the bone, it is usually difficult to cure and is accompanied by a variety of accompanying complications such as pain, increased risk of fractures, and hypercalcemia (2).

Early studies of bone metastatic cancer present a phenomenon known as the "vicious cycle," in which interactions between tumor cells and bone cells exacerbate the development of bone metastatic cancer (3). Tumor cells release substances such as parathyroid hormone-related protein (PTHrP), which stimulates osteoblasts to produce nuclear factor B receptor-activated ligand (RANKL), which further activates osteoclasts and leads to osteolysis. In turn, the multiple factors produced by osteolysis further promote tumor growth and more bone loss (4). This study reveals the impact of the bone microenvironment on the interactions between tumor cells.

The tumor microenvironment (TME) is a composite of various components (5), including the immune microenvironment. Meanwhile, the bone plays an important role as an immune organ in the body. The immune microenvironment of bone metastatic cancer is characterized by immune cells, such as T cells, macrophages, dendritic cells (DC), megakaryocytes, and myeloid-derived suppressor cells (MDSCs) (6). MDSCs are derived from immature myeloid progenitor cells and inhibit the immune function of T cells and NK cells in the TME (7). In addition, the bone microenvironment contains two key cell types: osteoblasts and osteoclasts. Osteoblasts are derived from multiple potential mesenchymal stem cells in the bone marrow stroma (8). Most prostate cancer bone metastases are osteogenic, with tumor cells tending to promote osteogenic activation of osteoblasts, whereas osteoclasts are derived from monocytes and are responsible for bone resorption (9). In osteolytic tumors such as bone metastases of the breast, lung, and kidney, tumor cells tend to promote the osteolytic function of osteoclasts.

Key factors in the immune microenvironment may include the local cytokine environment, the presence of helper stromal cells, specific types of immune cells, all of which play an important role in tumor-specific interactions (10). Different types of immune cells exert different functions in the immune microenvironment of metastatic bone cancer. Immune cells, such as NK cells and cytotoxic T cells, are capable of directly killing tumor cells using different mechanisms, whereas other immune cell subtypes, such as regulatory T cells (Tregs), a subtypes of CD4+ T helper cells, M2-type macrophages, tolerogenic DC, and MDSCs, inhibit adaptive immune responses to tumors, thereby promoting tumor progression and metastasis (11).

In metastatic cancer of the bone, specific cells in the bone and immune cells share a common environment (12), therefore this paper reviews the different types of cells and their effects in the immune microenvironment, and discusses areas for future development in this field.

2 Lymphatic immune cells

2.1 T cells

T cells originate from hematopoietic stem cells and lymphoid progenitors stored in the bone marrow and differentiate into primary lymphoid organs waiting to be activated by antigens. Partial tumor-infiltrating lymphocytes (TIL) in tumors have tumor cell-killing function (13). However, in the immunosuppressive microenvironment of bone metastatic cancer, T cells can be suppressed, leading to depletion or inactivation of T cells (14). Furthermore, the microenvironment of bone metastatic cancer also attracts other T cell subtypes, such as Tregs and other CD4+ T cells, which can support tumor growth and metastasis (11). For example, T cells can promote the development and maturation of osteoclasts, which can lead to the malignant cycle of bone metastatic cancer. In bone metastatic cancer, T cells are recruited and activated by tumor secreted factors such as PTHrP, interleukin (IL)-7, and IL-8, and recruited T cells can secrete tumor necrosis factor-α (TNF-α) or RANKL to induce bone resorption (15), which allows T cells to also participate in the vicious cycle process. Of course, this osteoclast-promoting effect is unique to nonactivated T cells (16).

T cells can be classified according to their function as cytotoxic T lymphocytes (CTL) and helper T cells (Th), where Th cells can be further classified as Th1, Th2, Th9, Th17, Th22, Tfh, and Tregs, depending on their function. Recent studies have shown that Th1, Th2, Th17, and Tregs are involved in the occurrence and development of tumor cells in bone metastases (17–21).

2.1.1 Cytotoxic T lymphocytes

CTLs are closely associated with the anticancer immune response, as these cells expresses a CD8 glycoprotein on its surface, and are also known as CD8+ T cells (22). They are activated to kill tumor cells by interacting with DC that present tumor-specific antigens (23).

Interferon-γ (IFN-γ) produced by CTL plays a key role in determining the antitumor ability of CTLs. Production of IFN-γ contributes to the tumor expression of MHC-I, making them more easily recognizable by CTLs (24), and directly inhibits tumor cell proliferation and induces apoptosis, thus exerts a direct role in the fight against cancer (25). IFN-γ from other sources also plays an important role in CTLs. PD-L1 deficiency in myeloid cells in bone metastatic cancers upregulates immunostimulatory genes, thereby contributing to macrophage polarization towards the M1 type and enhances IFN-γ signaling, which promotes the recruitment and activation of CTLs (26). Additionally, the presence of IFN-γ reduces tumor-associated bone loss and inhibits osteoblast development (27). However, IFN-γ also inhibits tumor cell killing by immune cells. Specifically, IFN-γ inhibits CTL function by upregulating the expression of programmed death ligand 1 (PD-L1) on the surface of tumor cells; thus, increasing its binding to the programmed cell death-1 (PD-1) receptor on the surface of CTL cells (28). IFN-γ can also activate interferon regulatory factor 2 (IRF2), a CTL transcription factor in the TME, thus changing CTL from an

activated state to a depleted state and forcing tumor cells to evade immune surveillance (29).

CTLs are also affected by osteoclasts in bone metastatic cancer. Osteoclasts have been shown to undergo apoptosis and produce apoptotic vesicles during cyclic bone remodeling in bone metastatic cancer, thus inhibiting the infiltration and activity of CTLS (30). Conversely, osteoclasts exert a positive regulatory effect on CTLs. Lyn(-/-) mice, with more numerous osteoclasts, had reduced bone tumor growth despite enhanced osteolysis, due to the increased tumor-killing function of CTLs as a result of the increase in osteoclasts (31).

Furthermore, in addition to playing an important role in tumor metastasis to bone, CTLs also exert multiple critical functions in different types of bone metastatic cancers. Overexpression of estrogen-related receptor alpha (ERRα) in breast cancer bone metastases activates the tumor-killing effect of CTLs, through the production of chemokines C-C chemokine receptor type 17 (CCL17) and C-C chemokine receptor type 20 (CCL20), which allows CTLs to evade the control of transforming growth factor-β (TGF-β) (32). The up-regulation of IL-27 in bone metastasis of prostate cancer can lead to up-regulation of genes related to T-cell activation (33). The signal transducer and activator of the transcription 6 (STAT6) pathway is important in CTL immune suppression, which can be independent of Tregs (34). Snail(+) tumor cells can secrete Human follistatin-like protein 1 (FSTL1) not only to directly promote tumor bone metastasis, but also to generate CD45(-) activated leukocyte cell adhesion molecule (ALCAM)(+) cells, which can be surrounded by CD8+ T cells with weak CTL activity that contribute to the development of bone metastatic cancer (35).

2.1.2 Th cells

Th cells are immune T cells that produce cytokines involved in the adaptive immune response (36). Th cells play an important role in the mechanisms regulating of entry tumors into the bone environment and subsequent adaptive immune processes. Activated Th cells also release a variety of factors, such as IL-6, IL-11, IL-15, RANKL, and TNF-α, which promote osteoclastogenesis and bone resorption and provide a favorable environment for tumor bone metastasis (37, 38) (Figure 1). IL-7 is involved in T-cell proliferation and activation and can prompt CD8 + and CD4+ T cells to produce factors such as RANKL and TNF-α (39). These factors play a role in bone metastasis in the bone environment. However, activated CD4+ T cells also produce IFN-γ, which can inhibit osteoclast activity (40). Thus, Th cells influence the bone environment by releasing multiple factors and are also involved in regulating immune infiltration of tumors. Some studies have also implicated Th cells in the process of bone metastasis (41). Of particular note, in breast cancer, inhibition of poly ADP-ribose polymerase 2 (PARP2) increases the risk of bone metastasis, as this leads to an increase in immature myeloid cells in the bone marrow, which inhibits Th cell recruitment and creates an immunosuppressive microenvironment (42).

As mentioned previously, naïve Th cells can differentiate into different subtypes, including Th1, Th2, Th17, and Tregs, which exert different in the tumor immune response. This further highlights the importance of Th cells in bone metastatic cancer. Th1 cells in bone metastases of melanoma are affected by intestinal microbes, and when intestinal microbes are depleted, Th1 cell growth is inhibited, accelerating tumor growth and osteolysis (17). Despite the increase in CD4+ T cells within prostate cancer
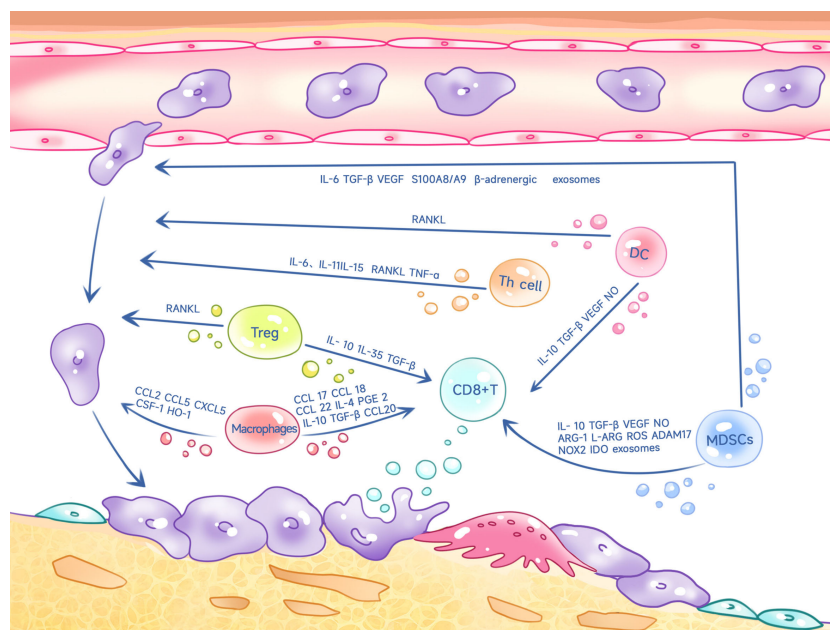

FIGURE 1
Th cells, Tregs, macrophages, MDSCs, DC cells inhibit CD8+ T cell killing on tumors and promote tumor cell metastasis to bone through multiple factors.

bone metastases, they are insensitive to immune checkpoint therapy, because CD4+ T cells differentiate into the Th17 rather than the Th1 line, mechanically because bone tumors promote osteoclast-mediated bone resorption, releasing TGF-β, which inhibits the development of the Th1 line (18). Wang et al. used genetically engineered hematopoietic stem cells (HSC) to deliver a small molecule inhibitor of TGF-β to the bone marrow, which resulted in the differentiation of CD4+T into Th1 and Th2 cells (19). LysM(Cre)/Tgfbr2 knockdown significantly inhibits the proliferation, angiogenesis, and osteoclast activation of metastatic cancer (43).

2.1.3 Tregs

Regulatory T cells (Tregs) are an important subpopulation of CD4+ T cells that are essential for the induction and maintenance of normal peripheral tolerance and the prevention of autoimmunity (20). Tregs can inhibit the function of many cells in bone metastatic cancers, including CD8+ T cells and Th1 cells, thus generating an immunosuppressive microenvironment (21). The specific mechanism is exerted through IL-10, IL-35, and TGF-β activity (44, 45) (Figure 1). Additionally, Tregs significantly inhibited the proliferation of CD4+CD25- T cells by directly contacting and thus blocking the delivery of costimulatory signals (46).

Increased Treg infiltration in prostate cancer often leads to a poor prognosis. In the immune microenvironment of bone metastasis from prostate cancer, Tregs can translocate to the bone marrow through C-X-C chemokine receptor 4 (CXCR4)/C-X-C Motif Chemokine 12 (CXCL12) (47). In addition to its immunosuppressive effects, Forkhead box protein P3 (Foxp3)+ Tregs are a key source of RANKL (48). As mentioned previously, RANKL produced by T cells can promote osteolysis to bone metastasis (37) (Figure 1). Bone marrow DC, in turn, promote the proliferation of Tregs through the receptor activator of NF-KappaB (RANK)-RANKL axis (47, 49). Thus, Tregs form a positive feedback axis for tumor bone metastasis and osteolysis through the RANK-RANKL axis.

Expression of CD73 on the surface of Tregs can also promote tumor metastasis (50). During the immune response, Th17 cells can be transformed into Tregs, which results from activation of the aromatic hydrocarbon receptor (AHR) by TGF-β (51). Activation of TNFR2 in Tregs by TNF can promote the expansion of immunosuppressive Tregs (52). The Tregs bone metastatic cancer microenvironment also interacts with osteoblasts and osteoclasts. For instance, osteoblasts can inhibit the function of CTLs by creating a suitable environment for Tregs through aerobic glycolysis (53). Tregs regulate osteoclast differentiation through cytotoxic T lymphocyte antigen (CTLA-4) in cell-to-cell contacts (54), thus altering the immune microenvironment of bone metastatic cancer.

2.2 Natural killer cells

Natural killer cells (NK cells) rapidly recognize and destroy cancer cells (55). For example, NK cells can release perforin and granzyme, mechanisms that lead to apoptosis of cancer cells (56).

However, several factors can influence the function of NK cells. In the early stages of bone metastasis, estrogen receptor (ER)-positive luminal cancers release signal peptide, CUB domain and EGF-like domain containing 2 (SCUBE2), which may help to induce osteoblasts to differentiate into osteoclasts, thereby inhibiting NK cells activity and providing favorable conditions for tumor colonization (57). In breast cancer, overactivation of the Janus kinase (JAK)/STAT signaling pathway has been widely reported (58, 59). However, inhibition of the JAK/STAT signaling pathway decreases the antitumor immune function of NK cells in metastatic tumors (60). Gut microbial deprivation also inhibits the proliferation of NK cells in bone metastatic tumors (17). This phenomenon suggests that intestinal microbes may play a role in modulating the immune response. Furthermore, in the case of neuroblastoma bone metastases, IL-2 therapy has been shown to be effective, suppressing tumors by increasing NK cell activity (61). Overexpression of PTHrP promoted bone metastasis of small-cell lung cancer in a mouse model, which may be related to NK cell depletion, but the exact mechanism needs to be further investigated (62).

3 Myeloid immune cells

3.1 Macrophages

Macrophages are an important component of the mononuclear phagocyte system (MPS) and are key cells in the tumor immune system (63). The main immune cells that infiltrate tumors are macrophages, also known as tumor-associated macrophages (TAM) (64). There is growing evidence that these macrophages play an important role in the immune microenvironment of bone metastatic cancer and play a key regulatory role in tumor progression, angiogenesis, invasion, and metastasis (65–67).

3.1.1 Impact on adaptive immunity

Macrophages can polarize into M1 and M2 types in the TME (68–70). M1 macrophages can produce reactive oxygen species (ROS), have high antigen presentation potential, and can recruit CTLs (71–73). Although M2 macrophages are usually considered pro-tumorigenic, M2 macrophages can recruit Tregs and Th2 cells by secreting anti-inflammatory factors that induce adaptive immune incompetence of the body against tumors (74, 75).

The chemokine CCL20 is highly expressed in macrophages, as is the homologous C–C chemokine receptor type 6 (CCR6) expressed on T cells. Macrophages in bone metastatic cancers inhibit the immune response of T cells to tumors through regulation of the CCL20-CCR6 axis (76). Furthermore, TAM-derived CCL17, CCL18, CCL22, IL-4, IL-10, TGF-β, and prostaglandin E2 (PGE 2) can inhibit the antitumor function of T cells (77–83). In bone metastases of prostate cancer, fusion of tumor cells with myeloid cells, including macrophages, further suppresses the immune response while promoting tumor growth (84) (Figure 1).

3.1.2 Impact on tumor metastasis

Macrophages can promote the growth of tumor cells in bone in several ways (85), and inhibition of macrophages reduces the incidence of tumor bone metastasis (86). Targeting anti-CD115 antibodies reduces the number of macrophages in tumors and therefore reduces osteolytic lesions in transplanted breast cancer cells (87). The interaction between macrophages and prostate cancer cells contributes to upregulation of cathepsin K expression in macrophages, which promotes tumor progression within metastases (88). CD137, a member of the TNF receptor superfamily, can promote macrophage migration into the TME and stimulate macrophage transformation into osteoclasts by enhancing Fra1 expression, thus promoting tumor bone metastasis (89). Furthermore, CCL5 secreted by TAMs contributes to bone metastasis of prostate cancer (90). CCL2 can help prostate tumor growth and bone metastasis by recruiting macrophages and osteoclasts (91) and macrophages also promote breast cancer bone metastases in an IL-4R-dependent manner, and inhibition of IL-4R effectively reduces the occurrence of bone metastases (92). Furthermore, CXCL5 and colony stimulating factor 1 (CSF-1) are associated with macrophage-driven bone metastasis (87, 93–95) Cyclooxygenase-1 (COX-1) positive macrophages can play an important role in prostate cancer bone metastasis (96) (Figure 1).

These studies highlight the important role of macrophages in immunomodulation and bone metastasis and provide useful information to better understand the onset and progression of bone metastatic cancer.

3.2 Myeloid-derived suppressor cells

Myeloid-derived suppressor cells (MDSC) are distinct immunosuppressive cells in tumors. MDSCs consist of a heterogeneous population of immature myeloid cells (IMCs) with immunosuppressive functions (97). MDSCs have been found to be widely infiltrated in a wide variety of cancers and have a significant ability to suppress T cell responses, leading to a poor prognosis. Such cells have attracted increasing attention in the academic community (81). Furthermore, MDSCs play a crucial role in bone (98).

3.2.1 Impact on adaptive immunity

MDSCs inhibit T cell proliferation by suppressing the immune response of T cells in several ways: (i) by generating arginase-1 (ARG-1)-dependent depletion and chelating L-cysteine depletion of L-arginine to inhibit T cell proliferation; (ii) by interfering with the signaling of the IL-2 receptor and generating ROS and NO to inhibit T-cell function; (iii) by expressing ADAM 17 (which contains structural domains of de-integrins and metalloproteinases17) and galactose lectin 9 that interfere with T-cell metastasis and pro-apoptosis activity; and (iv) by inducing Treg proliferation, which promotes bone metastasis growth (99–101). MDSCs also inhibit NK cell function via TGF-β, and IL-10 (102–104) inhibits dendritic cell differentiation and antigen presentation through IL-10, vascular endothelial growth factor (VEGF), NADPH oxidases (NOX2), and ROS (103, 105–108). Recent studies have shown that MDSC-produced exosomes can overactivate or deplete CD8+ T cells, thus suppressing immune function (109). In bone metastasis of breast cancer, MDSCs express PD-L1, which not only inhibits T cell function, but also promotes osteoclastogenesis, thus facilitating the progression of bone metastatic cancer (16) (Figure 1).

3.2.2 Impact on tumor metastasis

In the metastatic bone cancer microenvironment, MDSCs not only have immunosuppressive effects, but also accelerate bone lysis and destruction. MDSCs can promote bone tumor metastasis through a variety of mechanisms (98, 110). Tumors recruit MDSCs through the CCL2/CCL12-CCR2, CCL3/4/5-CCR5, CCL15-CCR1, CX3CL1/CCL26-CX3CR2, CXCL5/CXCL2/CXCL1-CXCR2, CXCL8 (IL-8)-CXCR1/CXCR2, CCL21-CCR7, CXCL13-CXCR5 pathways, promoting immunosuppression in the TME, while, MDSCs also promote tumor metastasis via the CCL5/CCR5,CCL15-CCR1,CXCL5/CXCL1-CCR2, CXCL8 (IL-8)-CXCR1/CXCR2 pathways (111). MDSCs also secrete TGF-β, S100A8/A9, VEGF and exosomes to interact with the immune system, endothelial cells, fibroblasts, and liver stellate cells, thus making the bone microenvironment suitable for tumor implantation (112). Furthermore, in a 4T1 mouse metastasis model, inhibition of interferon regulatory factor 7 (IRF7) enhanced the prometastatic activity of MDSCs. Conversely, IRF7 overexpression can counteract the effects of MDSCs and restore the activity of CD8+ T cells and NK cells to reduce metastasis (113). MDSCs can also promote tumor metastasis by enhancing β-adrenergic signaling and the IL-6/STAT3 pathway (114). The prometastatic effects of MDSCs are also closely related to osteoclasts. MDSCs derived from bone metastatic cancers can be induced to become osteoclast progenitors and can differentiate into osteoclasts (115). In addition to becoming osteoclasts themselves, they can also induce osteoclastogenesis, and in bone metastatic cancers, MDSC-produced nitric oxide (NO) not only mediates immunosuppression, but also mediates osteoclast generation (98, 99). Due to the fact that bone metastasized tumors express hypoxia-inducible factor (HIF)-1α at a higher level than primary tumors, which plays an important role in osteoclast formation (98, 99), and NO in turn up-regulates HIF-1α through various mechanisms, such as phosphatidylinositol 3-kinase and schizogen-activated protein kinase (116). Tumor cell levels of PTHrP and GL I-Kruppel 2(Gli 2) can be induced by MDSCs, which are also involved in osteoclastogenesis (110) (Figure 1).

3.3 Dendritic cells

DC are a class of immune cells that originate in the bone marrow and are widely distributed in various tissues (117–119). They play a key role in the induction and regulation of innate and adaptive immune responses by antigen presentation (117–120). DC efficiently phagocytose apoptotic cells and cross-present viral,

tumor, and autoantigens to CD8(+) T cells (121, 122). In tumors, the role of DC is crucial, as they are capable of initiating an effective T cell response, attracting T cells to the tumor site, and maintaining the function of effector memory T cells (22, 123). Circulating DC readily migrate to the bone marrow due to the high expression of vascular cell adhesion molecule-1 (VCAM-1) and endothelial selectin in the microvasculature of the bone marrow, which is critical for metastatic bone cancers (124).

3.3.1 Impact on adaptive immunity

DC can differentiate into two subpopulations: myeloid DC (mDC) and plasmacytoid DC (pDC) (123). Although the importance of DC in antitumor immune responses is well known, cancer cells can still promote an immunosuppressive phenotype by affecting DC. In metastatic bone cancer, DC in the TME inhibit the tumor-killing activity of CD8+ T cells by producing cytokines such as IL-10, VEGF, TGF-β, and NO (125). IL-6 produced by tumor cells can contribute to the differentiation of hematopoietic stem and progenitor cells (HSPC) into monocyte-dendritic progenitor cells (MDPs) (126). Furthermore, high expression of CD1a(+) and CD83 (+) has been reported to be negatively correlated with the development of bone metastases (127). In breast cancer bone metastases, pDC can persistently activate Th2, increase infiltration of Tregs and MDSCs, and produce osteolytic cytokines, leading to severe bone destruction (128). Mitochondrial transcription factor A (TFAM) deletion improves the presentation of antigens by DC through the cGAS-STING pathway, reversing immunosuppression in the TME (129). Furthermore, DC can induce the production of the PTHrP-derived peptide, PTR-4, which maintains CTL activation and thus improves tumor killing (130).

3.3.2 Impact on tumor metastasis

DC also play a key role in promoting tumor metastasis. TGF-β produced by tumors inhibits dendritic cell migration from the tumor site to lymphatic drainage, increasing the risk of tumor metastasis (131) (Figure 1).

3.3.3 RANK-RANKL and dendritic cells

The RANK-RANKL axis is closely related to DC. RANKL was first identified in 1997 using human bone marrow-derived DC (132), and RANK signaling in DC leads to immune tolerance in many cases (132–135). For example, RANKL from tumors of the genital tract induces an immature and tolerogenic phenotype in DC (136). DC are critical in antitumor combination therapies with anti-CTLA-4 and anti-RANKL antibodies (137). Thus, RANK signaling in DC may contribute to immune tolerance in bone metastatic cancers. RANKL produced by pDC can directly affect MDSCs by inducing their differentiation into osteoclasts, which promotes bone destruction and growth of breast cancer cells (138) (Figure 1). Furthermore, infiltration of pDC in cancer is associated with elevated levels of chemokines and cytokines that are directly or indirectly related to immunosuppression and osteoclastogenesis (138). These soluble factors also induce RANKL expression, which further stimulates osteoclastogenesis.

In conclusion, the dual role of DC in metastatic bone cancer is important for understanding the dynamic balance of the immune microenvironment and the metastatic mechanism of tumors. These findings are expected to provide new ideas for future immunotherapeutic strategies to improve immune system control of bone metastatic cancer.

3.4 Megakaryocytes

Megakaryocytes (MKs) are a class of cells derived from bone marrow-resident hematopoietic stem cells (HSC), which play a role in platelet production by responding to thrombopoietin (TPO) and exert a regulatory role in platelet production through their response to TPO. In addition to their effects on platelet production, MKs also affect osteoclasts and osteoblasts, thus regulating the bone microenvironment (139–142). Therefore, MKs also play a key role in bone metastatic cancer. MKs can inhibit osteoclast function while promoting osteoblast proliferation (143). In a mouse model, intracardiac injection of TPO-treated prostate cancer cells reduced the formation of bone metastases (144). Furthermore, the number of MKs in the bone marrow increased after intracardiac injection of highly osteogenic breast cancer cells (145, 146), suggesting that MKs play a key role in bone metastasis.

4 Osteoclasts and osteoblasts in bone metastatic cancer

4.1 Osteoclasts

Osteoclasts are a specialized class of cell types derived from monocytic macrophages (147). Their development and function are regulated, in part, by CSF-1 and RANKL (148). RANKL and CSF-1 bind to RANK in mature osteoclasts to induce the process of bone resorption. Furthermore, the balance between RANKL and its osteoprotegerin receptor (OPG) plays a key role in the regulation of osteoclast function. Knockdown of OPG in mice resulted in a decrease in bone density, while overexpression of OPG increased bone density (149).

During osteolytic bone metastasis, tumor cells continuously secrete a variety of osteoclastogenic cytokines in the bone, including CSF-1, PTHrP, RANKL, IL-8, IL-11, prostaglandin E, matrix metalloproteinase 1 (MMP-1), stromal cell communication network (CCN), and TNF-α (150–156). These factors directly stimulate osteoclast-mediated bone resorption and lead to the release of bone-derived tumor growth factors such as TGF-β, insulin-like growth factors (IGF), platelet-derived growth factor (PDGF), and bone morphogenetic protein (BMP) in the bone matrix, which promotes tumor growth in bone metastases (157, 158). TGF-β, a factor released after bone matrix lysis, stimulates the tumor's secretion of PTHrP directly (159). This osteolytic cascade response is driven by the production of PTHrP. PTHrP plays a dual role in bone reconstruction. First, PTHrP upregulates monocyte chemoattractant protein-1(MCP-1) in

osteoblasts, a key mediator of osteoclastogenesis, leading to the formation of osteoblastic lesions (160). Second, PTHrP stimulates osteoclast formation by improving osteoblast production of RANKL and CCL2 (142). Thus, a mutual promotion between tumor cells and osteoblasts, in which tumor cells promote osteolysis, and osteolysis then releases tumor growth factors that promote tumor growth, becomes a key therapeutic challenge. Breast cancer cells secrete an integrin-binding sialoprotein (IBSP) in bone, which attracts osteoclasts and creates an osteoclast-rich bone microenvironment (161). The R-responsive protein 2 (RSPO2) ligand in breast cancer cells interacts with RANK to promote osteoclast-mediated osteolysis (162). Furthermore, an ATP-dependent transporter protein called ABCC5 also mediates osteoclast-mediated bone resorption in breast cancer bone metastases (163). Inhibition of AEPase activity in breast cancer cells reduces osteoclast differentiation while attenuating osteolytic lesions caused by breast cancer bone metastases from breast cancer (164). Furthermore, early growth response-1 (EGR1) plays a direct role in the regulation of angiogenesis and osteoclastogenic factors in prostate cancer bone metastasis (165). Induction of tumor cells stimulates osteoclasts to secrete the IL-20RB ligand IL-19, which activates JAK1/STAT3 signaling and thus promotes proliferation of bone metastatic cancer cells (166). Furthermore, galactose lectin-3 (Gal-3) is located on the surface of osteoclasts and regulates the microenvironment of osteolytic bone metastatic cancer in the presence of RANKL (167). In bone metastatic cancers, CD47 on the surface of multiple cells regulates osteoclasts by modulating nitric oxide synthase activity, thus increasing the risk of tumor bone metastasis (168).

Exosomes secreted by tumor cells promote osteoclast differentiation and activation, leading to bone damage and remodeling of the bone metastasis microenvironment. The exosome miR-21 from SCP28 cells promotes osteoclast formation by regulating the expression of PDCD4 protein (155). In breast cancer bone metastasis, the miR-124/IL-11 axis plays a crucial role in the survival and differentiation of osteoclast progenitor cells (169). Furthermore, osteoblastic tumor exosomes can also induce osteoclast differentiation (170). For prostate cancer cells, extracellular vesicles (EVs) promote osteoclast formation in the presence of RANKL (171). Furthermore, tumor EVs of atypical cancer origin can also promote bone metastasis in hepatocellular carcinoma (172).

The mechanical environment of the bone is also critical for bone metastatic cancer. The activities of osteoblasts and cancer cells are regulated by the mechanical environment. Early changes in the mechanical environment can activate osteoclasts, which can lead to extensive osteolytic bone loss triggered by advanced bone metastatic cancer (173).

However, it is important to note that tumors also exert a dual effect on osteoclasts in the bone environment. In bone metastasis, tumor cell-secreted CST6 enters osteoclasts and inhibits the activity of the cysteine protease cathepsin B (CTSB), leading to the up-regulation of sphingosinekinase1 (SPHK1), which inhibits RANKL-induced activation of p38 and suppresses osteoclast maturation (174) (Figure 2).

To inhibit tumor growth, some clinical strategies can be achieved by breaking this "vicious cycle". For example, procoxacin reduces prostate cancer bone metastasis by disrupting the feedback loop of the TGF-β/C-Raf/MAPK pathway and inhibiting osteoblast and osteoclast activity (175). Denosumab is a fully human IgG2 monoclonal antibody that specifically targets RANKL. It binds to RANKL with high affinity and specificity and inhibits the binding of RANKL to osteoclast precursors and osteoclast surface RANK, thus inhibiting osteoclast differentiation and activity, and disrupting the "vicious cycle" in tumor bone metastasis. This helps to inhibit excessive bone resorption and reduce bone destruction (176).

Bisphosphonates are a class of drugs that are absorbed by bone at sites of active bone metabolism (177). Bisphosphonates inhibit osteoclast activity and survival, reducing osteoclast-mediated bone resorption. Furthermore, they can also cause osteoclast apoptosis and have a direct apoptotic effect on tumor cells (178). Therefore, bisphosphonate therapy is now the standard of care for patients with malignant bone disease in a variety of tumor types, including prostate, breast, lung, and multiple myeloma (179). Furthermore, STING agonists can also modulate osteoclast function in the TME and reduce osteolysis, thus slowing tumor progression (180).

4.2 Osteoblasts

Osteoblasts are derived from mesenchymal stem cells whose primary function is bone formation. The Wnt and Runt-related transcription factor 2 (Runx2) pathways play a key role in the maturation and directed differentiation of osteoblasts (181). A hallmark of osteoblast differentiation is the formation of type 1 collagen, and this process becomes critical when mediated by Shh signaling directed at prostate cancer. The stromal collagen and Shh signaling pathways act synergistically and are essential for osteoblast formation. Although cancer bone metastasis is generally presented as osteolytic metastasis, the main mechanism of cancer bone metastasis is osteogenic metastasis (182).

Prostate cancers secrete a variety of factors, such as BMP and endothelin-1 (ET-1), which promote the maturation of osteogenic precursor cells, PTHrP, which inhibits osteoblast apoptosis, aminoproteinases, which indirectly promote bone formation, and urinary fibrinogen activator (uPA) (183). These conditions contribute to the enhanced deposition of a new bone matrix. Furthermore, prostate cancer secreted CCN3 improves the expression of BMP, Runx2, and osterix in osteoblasts through glycogen synthase kinase3β (GSK3β) and β-catenin signaling pathways (184).

Although cancer bone metastasis is predominantly osteolytic, CD137 has been reported to recruit monocytes/macrophages to migrate into the TME and promote the differentiation of monocytes or macrophages into osteoblasts during bone metastasis (89). Hypoxic conditions activate HIF-1α, a specific signaling factor for osteoblasts. Activation of HIF-1α signaling increases CXCL12 blood levels, which directly activates the CXCR4 receptor and promotes the migration of breast cancer cells to bone (185).
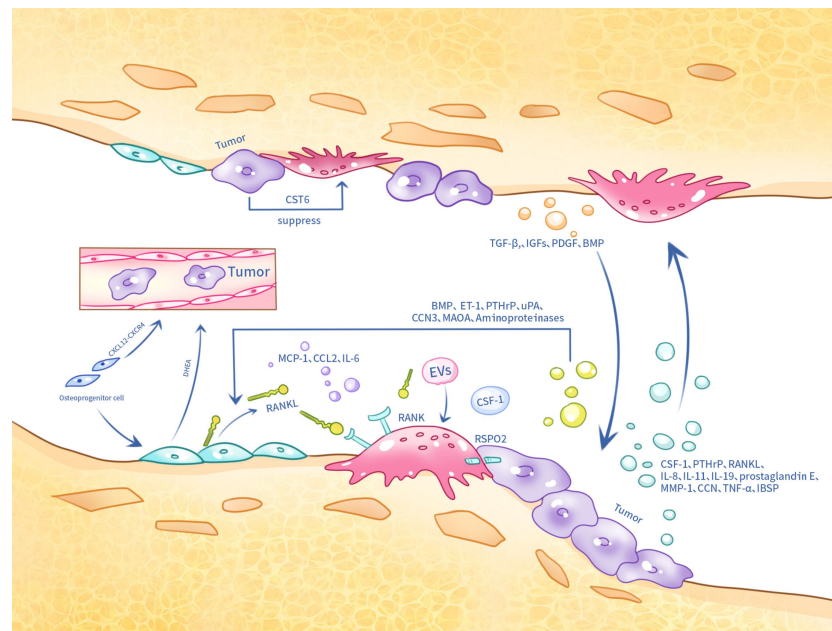
FIGURE 2
Tumor cells, osteoclasts and osteoblasts in metastatic bone cancer interact with each other at the skeletal site by several means.

Furthermore, in clinical practice, the reduction of androgen levels is one of the main approaches in prostate cancer treatment. Osteoblasts have been reported to secrete the adrenal androgen precursor dehydroepiandrosterone (DHEA), which does not induce the androgen receptor (AR), but promotes cancer progression and metastasis (186). Monoamine oxidase A (MAOA) also plays an important role in prostate cancer bone metastasis. MAOA stimulates the release of IL-6 from osteoblasts, which creates a bone microenvironment conducive to the homing, growth and survival of cancer cells, and also activates osteoclastogenesis through the production of RANKL and IL-6 by osteoblasts, which contributes to the development of bone metastases from cancer (187). Furthermore, VCAM1 has been reported to activate painless micrometastases by recruiting osteoblast progenitor cells (188). Studies in animal models have shown that Plumbagin successfully inhibited breast cancer cell metastasis and osteolysis by significantly altering the RANKL/OPG ratio in osteoblasts (189) (Figure 2).

5 Tumor dormancy in tumor metastasis to bone

Tumor metastasis formation is a complex process that includes local invasion and infiltration of tumor cells, survival, and extravasation of tumor cells after entering the circulation, as well as survival and proliferation in target organs (190). After invading the bloodstream, tumor cells are defined circulating tumor cells (CTCs) (191). A small percentage of tumor cells can reach distant organs to colonize (192). Once they reach a distant site, tumor cells remain dormant until that environment can support tumor growth and proliferation (193, 194). Numerous clinical studies have found

that tumors have metastasized to bone early in their development, entering a dormant state in preparation for future growth (195). Clinical observations have found that for tumors that are susceptible to bone metastasis, the number of patients with skeletal lesions is less than the number of patients with diffuse tumor cells (DTC) detectable in the bone marrow, a finding that supports the idea that the bone microenvironment supports tumor dormancy (196, 197). Therefore, understanding the relationship between the bone microenvironment and tumor dormancy can contribute to subsequent treatment and research.

5.1 Metastasis

Perivascular cells highly expressing CXCL12 in vascular microhabitats in bone marrow sinuses can keep breast cancer cells dormant in the vasculature through CXCL-12/CXCR4 interaction (198). Immunohistochemical analysis of bone marrow from breast cancer patients showed that dormant breast cancer cells preferentially localize in CXCL12-rich vascular regions (198). CXCR4/CXCL12 also plays a crucial role in bone metastasis of prostate cancer (199). However, unlike breast cancer, prostate cancer cells may benefit from this supportive environment that maintains dormancy, but does not contribute to tumor growth (193). Furthermore, growth-arrest specific 6 (GAS6) can induce tumor dormancy in cancer (200).

5.2 Influence of immune factors

The bone microenvironment is also an immune-privileged site that protects dormant tumor cells from environmental damage and

resulting immune responses. Tregs in the bone immune microenvironment can create an immune microenvironment that supports the growth of dormant tumor cells, allowing them to evade immune attacks (201). MDSCs in the bone microenvironment can prevent the removal of dormant tumor cells by inhibiting the activity of anti-TME CTLs and NK cells (10); Furthermore, bone marrow mesenchymal stem cells can also protect dormant tumor cells (195).

6 Immunotherapy for metastatic bone cancer

Bone metastatic cancers are resistant to a variety of immunotherapies due to a specific immunosuppressive microenvironment (10, 202). As a result, current treatment for patients with bone metastases has focused primarily on palliative therapies to reduce pain and improve quality of life. Due to the specificity and importance of multiple immune cells in bone metastatic cancer, it is particularly crucial to find effective immunotherapy methods for bone metastatic cancer.

Human PD-1 (CD279), encoded by the PDCD1 gene, is a transmembrane protein that is expressed as an immunosuppressive receptor predominantly on monocytes, B cells, NK cells, macrophages, and activated T-cells (203–206). Its ligands PD-L1 and PD-L2 are expressed in DC, macrophages, and tumor cells (207, 208). PD-1 activation can mediate T cell inactivation and block signaling downstream of T-cell receptor (TCR) activation (209, 210). In immunotherapy, α-PD-1 drugs, such as nivolumab, can bind to immune cells such as T cells, B cells, NK cells, macrophages, and monocytes expressing PD-1, thus blocking PD-1 signaling (203–205). This helps to keep T cells continuously activated to fight off tumors. In patients with bone metastases from non-small cell lung cancer, overall survival increased by 7.9 months in patients with nivolumab (211), suggesting that α-PD-1 therapy may be useful to reduce tumor burden in patients with bone metastases.

Combining a PD-1 blocker (nivolumab) with a CTLA-4 blocker (ipilimumab) is more effective than PD-1 blockers alone and is a standard of care for many different cancers (211). In a study of advanced renal clear cell carcinoma, a lower 12 month OS rate was found in patients with bone metastases treated with ipilimumab/nivolumab (41.7%) compared to patients without bone metastases (82.7%) (212). Another retrospective study of patients with renal cell carcinoma (RCC) bone metastases treated with ipilimumab/nivolumab found relatively low efficacy (21%) and median OS (25.6 months) (213), and, generally, patients with bone metastases responded poorly to the combination of PD-1 and CTLA-4 inhibitors (213, 214). This may be related to the fact that bone metastatic cancers present an immunologically "cold" phenotype (215) and an immunosuppressive microenvironment (including infiltration of multiple immunosuppressive cells such as Tregs). Thus, eliminating Tregs in the bone metastatic microenvironment is a promising aspect of immunotherapy. Furthermore, anti-PD-1 immunotherapy can also produce long-term benefits in preventing

bone destruction and relieving pain in bone cancer by inhibiting osteoclastogenesis (216).

NK cells kill tumors through multiple mechanisms, including granzyme B and perforin-mediated apoptosis or Fas-Fas ligand interactions. When IRF7 levels are restored, the response of host NK cells can be reactivated (113). Furthermore, gut microbial supplementation also helps promote NK cell proliferation in metastatic bone tumors (17). The ability of modified NK cells to produce IL-2 and IL-15, stimulate proliferation, and increase resistance to tumors makes them a new option for the treatment of bone metastatic cancer (217).

Macrophages play a crucial role in the immunotherapy of bone metastatic cancer.M2-type macrophages inhibit CD8+ T-cell resistance to tumors through multiple pathways. The use of anti-CD115 antibodies, trabectedin, clodronic acid, and zoledronic acid reduces the number of macrophages within the tumor (218). Macrophages are recruited to tumor sites primarily through the CCL2/CCR2 axis and CSF-1/CSF-1R signaling, so blocking these two signaling axes also reduces macrophage infiltration (219–221).

MDSCs are extensively infiltrated in metastatic bone cancers and have a significant ability to suppress T cell responses. Based on available evidence, the use of CXCR4 antagonists and indoleamine2,3-dioxygenase1 (IDO1) inhibitors activates CD8+ T cells and suppresses MDSCs, thus delaying bone metastasis in mouse breast cancer disease (222). Dickkopf-1 (Dkk1), a secreted Wnt antagonist, modulates the number and function of MDSCs in bone metastases in mice (223). Furthermore, multiple chemokine axes, such as CCR2/CCL2, CXCR2/CXCL5, and CXCR4/CXCL12, and inhibition of these signaling pathways prevents the entry of MDSCs from the bone marrow into the TME (10).

In immunotherapy, tolerogenic DC or pDC in tumors can affect the killing function of CD8+ T cells. By using PDCA1 antibodies, pDC can be reduced, thus reducing the load of bone metastases in breast cancer (128). Furthermore, microtubule destabilizers (e.g., dolastatin 10 and ansamitocin P3) can convert tolerant DC into activated DC that stimulate the killing effect of CD8+ T cells, which in turn fight the tumor (224). DC vaccines have also been considered a new approach to treating bone metastases by injecting DC-carrying tumor antigens to activate the immune response within the tumor (38). In a model of melanoma metastasis, stimulation of DC with cyclic VHCDR3-derived peptide (Rb9) inhibited melanoma metastasis (225). CD103 +cDC1 vaccine inhibited primary and metastatic tumor growth, and IL-12 produced by CD103+DC was critical for NK cell-mediated tumor control (226, 227) (Table 1).

7 Discussion

Survival of patients with multiple solid tumors that metastasize to the bone is a great challenge. Previous studies have thoroughly explained the "vicious cycle" between tumor cells that metastasize to bone and osteoclasts and osteoblasts, and there are various therapeutic approaches, including the use of deslumab and

TABLE 1 The latest treatment for several immune cells.

Cell Type	Treatment
CD8+T	α-PD-1,α-CTLA-4
NK cell	α-PD-1,IRF7 Agonists,gut microbe,Engineered NK cells(IL-2, IL-15)
macrophage	α-PD-1, anti-CD115 antibodies,trabectedin,clodronic acid, zoledronic acid,CCR2 inhibitors,CSF1R inhibitors
MDSCs	CXCR4 antagonists,CCR2 inhibitors, CXCR2 inhibitors,IDO1 inhibitors,Dickkopf-1
DC	PDCA1 antibodies,DC vaccines,microtubule destabilizers, VHCDR3-derived peptide
osteoclast	Procoxacin anti-RANKL antagonists. Bisphosphonates. STING agonists
osteoblast	Procoxacin. Plumbagin

bisphosphonates, that can break the "vicious cycle". Meanwhile, the role of various types of immune cells and non-immune cells in the bone microenvironment during the transfer of tumor cells from the primary site to the bone has also been well studied. However, the multiple effects of multiple immune cells on adaptive immunity, i.e., on the specific tumor-killing effects of CTLs, after tumor cells colonize the immune microenvironment following bone are still not well reviewed, and thus a better understanding of the immune microenvironment of metastatic bone cancer is crucial for multiple effects. How to balance the immune cell effects on tumor-killing function and tumor growth promotion is a central question for the subsequent exploration of therapeutic approaches for bone metastatic cancer. Breaking the suppressive function of immune cells on adaptive immunity and enhancing the tumor-killing effect of immune cells on promoting CTLs will be the direction of future research on the immune microenvironment of bone metastatic cancer. In this review, we describe the multiple effects of various immune cells in the bone immune microenvironment, including osteoclasts and osteoblasts, on tumor metastasis and on adaptive immunity, highlighting the specific mechanisms by which the various types of immune cells function.

We also discuss tumor dormancy at the skeletal site, including the various types of immune factors that may influence tumor dormancy. Many solid tumors develop bone metastases at an early stage, but the tumor cells are dormant and the bone microenvironment protects the dormant tumor cells. Studying the effects of immune cells in the bone microenvironment on dormant tumor cells can guide clinical treatment for preventing bone metastasis in solid tumors. How to kill dormant tumor cells while avoiding harmful effects on the body's normal bone immune microenvironment is still a question that needs to be explored.

We also reviewed current and future therapeutic approaches for the treatment of bone metastatic cancers. Within conventional immunotherapeutic agents, α-PD-1 agents have been shown to be helpful in reducing the tumor burden in patients with bone metastases from non-small cell lung cancers, and because of the special microenvironment of bone, α-PD-1 immunotherapy also

has an impact on other factors such as osteoclasts, making the future of α-PD-1 in bone metastatic cancers also worthy of explore., as our understanding of the signaling mechanisms between tumor cells and cells in the bone immune microenvironment increases, several emerging therapeutic approaches, such as modification of NK cells, targeting of MDSCs and macrophages, and DC vaccines, can also be effective and efficient in halting the progression of skeletal lesions.

In conclusion, the interplay between the intrinsic cells of the bone, the immune cells, the bone matrix, and the tumor cells is critical for the progression of the tumor. Once the tumor invades the bone, how to prevent the immune cells from being called "accomplices" of tumor progression is still a question. What factors can break the "vicious cycle" between the four also needs to be further investigated. What factors promote tumor dormancy in metastatic bone cancer, and what factors cause dormant tumor cells to awaken and proliferate. Traditional immunotherapy is not effective in metastatic bone cancer, and it is worth exploring how to improve the effectiveness of immunotherapy in metastatic bone cancer by targeting various types of immune cells. The future of many emerging therapies is bright, but further research is needed to exploit the specificities of the bone microenvironment to combat bone tumors.

Author contributions

CS: Writing – original draft, Writing – review & editing. LJ: Writing – original draft, Writing – review & editing. MH: Writing – original draft, Writing – review & editing. ZW: Writing – original draft. JL: Writing – original draft. LS: Writing – review & editing. YE: Writing – review & editing. XY: Writing – original draft, Writing – review & editing. ZS: Writing – review & editing. TC: Writing – review & editing. WF: Writing – review & editing. ZS: Writing – review & editing. CX: Writing – review & editing. WZ: Writing – original draft. ZJ: Writing – original draft. ZZ: Writing – original draft. ZY: Writing – review & editing. LB: Methodology, Resources, Supervision, Writing – original draft, Writing – review & editing.

Funding

Conflict of interest

The authors declare that the research was conducted in the absence of any commercial or financial relationships that could be construed as a potential conflict of interest.

Publisher's note

All claims expressed in this article are solely those of the authors and do not necessarily represent those of their affiliated organizations, or those of the publisher, the editors and the reviewers. Any product that may be evaluated in this article, or claim that may be made by its manufacturer, is not guaranteed or endorsed by the publisher.

References

1. Hernandez RK, Wade SW, Reich A, Pirolli M, Liede A, Lyman GH. Incidence of bone metastases in patients with solid tumors: analysis of oncology electronic medical records in the United States. *BMC Cancer*. (2018) 18:44. doi: 10.1186/s12885-017-3922-0.

2. Fornetti J, Welm AL, Stewart SA. Understanding the bone in cancer metastasis. *J Bone Miner Res*. (2018) 33:2099–113. doi: 10.1002/jbmr.3618.

3. Yoneda T, Sasaki A, Mundy GR. Osteolytic bone metastasis in breast cancer. *Breast Cancer Res Treat*. (1994) 32:73–84. doi: 10.1007/BF00666208.

4. Fidler IJ. The pathogenesis of cancer metastasis: the "seed and soil" hypothesis revisited. *Nat Rev Cancer*. (2003) 3:453–8. doi: 10.1038/nrc1098.

5. Hanahan D, Weinberg RA. Hallmarks of cancer: the next generation. *Cell*. (2011) 144:646–74. doi: 10.1016/j.cell.2011.02.013.

6. Fu T, Dai LJ, Wu SY, Xiao Y, Ma D, Jiang YZ, et al. Spatial architecture of the immune microenvironment orchestrates tumor immunity and therapeutic response. *J Hematol Oncol*. (2021) 14:98. doi: 10.1186/s13045-021-01103-4.

7. Nakamura K, Smyth MJ. Myeloid immunosuppression and immune checkpoints in the tumor microenvironment. *Cell Mol Immunol*. (2020) 17:1–12. doi: 10.1038/s41423-019-0306-1.

8. Suva LJ, Washam C, Nicholas RW, Griffin RJ. Bone metastasis: mechanisms and therapeutic opportunities. *Nat Rev Endocrinol*. (2011) 7:208–18. doi: 10.1038/nrendo.2010.227.

9. Bussard KM, Gay CV, Mastro AM. The bone microenvironment in metastasis; what is special about bone? *Cancer Metastasis Rev*. (2008) 27:41–55. doi: 10.1007/s10555-007-9109-4.

10. Xiang L, Gilkes DM. The contribution of the immune system in bone metastasis pathogenesis. *Int J Mol Sci*. (2019) 20:999. doi: 10.3390/ijms20040999.

11. Smith HA, Kang Y. The metastasis-promoting roles of tumor-associated immune cells. *J Mol Med (Berl)*. (2013) 91:411–29. doi: 10.1007/s00109-013-1021-5.

12. Tsukasaki M, Takayanagi H. Osteoimmunology: evolving concepts in bone-immune interactions in health and disease. *Nat Rev Immunol*. (2019) 19:626–42. doi: 10.1038/s41577-019-0178-8.

13. Pagès F, Galon J, Dieu-Nosjean MC, Tartour E, Sautès-Fridman C, Fridman WH. Immune infiltration in human tumors: a prognostic factor that should not be ignored. *Oncogene*. (2010) 29:1093–102. doi: 10.1038/onc.2009.416.

14. Crespo J, Sun H, Welling TH, Tian Z, Zou W. T cell anergy, exhaustion, senescence, and stemness in the tumor microenvironment. *Curr Opin Immunol*. (2013) 25:214–21. doi: 10.1016/j.coi.2012.12.003.

15. Fournier PGJ, Chirgwin JM, Guise TA. New insights into the role of T cells in the vicious cycle of bone metastases. *Curr Opin Rheumatol*. (2006) 18:396–404. doi: 10.1097/01.bor.0000231909.35043.da.

16. Arellano DL, Juárez P, Verdugo-Meza A, Almeida-Luna PS, Corral-Avila JA, Drescher F, et al. Bone microenvironment-suppressed T cells increase osteoclast formation and osteolytic bone metastases in mice. *J Bone Miner Res*. (2022) 37:1446–63. doi: 10.1002/jbmr.4615.

17. Pal S, Perrien DS, Yumoto T, Faccio R, Stoica A, Adams J, et al. The microbiome restrains melanoma bone growth by promoting intestinal NK and Th1 cell homing to bone. *J Clin Invest*. (2022) 132:e157340. doi: 10.1172/JCI157340.

18. Jiao S, Subudhi SK, Aparicio A, Ge Z, Guan B, Miura Y, et al. Differences in tumor microenvironment dictate T helper lineage polarization and response to immune checkpoint therapy. *Cell*. (2019) 179:1177–1190.e13. doi: 10.1016/j.cell.2019.10.029

19. Wang B, Bai J, Tian B, Chen H, Yang Q, Chen Y, et al. Genetically engineered hematopoietic stem cells deliver TGF-β Inhibitor to enhance bone metastases immunotherapy. *Adv Sci (Weinh)*. (2022) 9:e2201451. doi: 10.1002/advs.202201451.

20. Zou W. Regulatory T cells, tumour immunity and immunotherapy. *Nat Rev Immunol*. (2006) 6:295–307. doi: 10.1038/nri1806.

21. Khazaie K, von Boehmer H. The impact of CD4+CD25+ Treg on tumor specific CD8+ T cell cytotoxicity and cancer. *Semin Cancer Biol*. (2006) 16:124–36. doi: 10.1016/j.semcancer.2005.11.006.

22. Owen KL, Parker BS. Beyond the vicious cycle: The role of innate osteoimmunity, autommicry and tumor-inherent changes in dictating bone metastasis. *Mol Immunol*. (2019) 110:57–68. doi: 10.1016/j.molimm.2017.11.023.

23. Caers J, Deleu S, Belaid Z, De Raeve H, Van Valckenborgh E, De Bruyne E, et al. Neighboring adipocytes participate in the bone marrow microenvironment of multiple myeloma cells. *Leukemia*. (2007) 21:1580–4. doi: 10.1038/sj.leu.2404658.

24. Martini M, Testi MG, Pasetto M, Picchio MC, Innamorati G, Mazzocco M, et al. IFN-gamma-mediated upmodulation of MHC class I expression activates tumor-specific immune response in a mouse model of prostate cancer. *Vaccine*. (2010) 28:3548–57. doi: 10.1016/j.vaccine.2010.03.007.

25. Kakuta S, Tagawa Yi, Shibata S, Nanno M, Iwakura Y. Inhibition of B16 melanoma experimental metastasis by interferon-gamma through direct inhibition of cell proliferation and activation of antitumour host mechanisms. *Immunology*. (2002) 105:92–100. doi: 10.1046/j.0019-2805.2001.01342.x.

26. Zuo H, Wan Y. Inhibition of myeloid PD-L1 suppresses osteoclastogenesis and cancer bone metastasis. *Cancer Gene Ther*. (2022) 29:1342–54. doi: 10.1038/s41417-022-00446-5.

27. Mendoza-Reinoso V, McCauley LK, Fournier PGJ. Contribution of macrophages and T cells in skeletal metastasis. *Cancers (Basel)*. (2020) 12:1014. doi: 10.3390/cancers12041014.

28. Dong H, Strome SE, Salomao DR, Tamura H, Hirano F, Flies DB, et al. Tumor-associated B7-H1 promotes T-cell apoptosis: a potential mechanism of immune evasion. *Nat Med*. (2002) 8:793–800. doi: 10.1038/nm730.

29. Lukhele S, Rabbo DA, Guo M, Shen J, Elsaesser HJ, Quevedo R, et al. The transcription factor IRF2 drives interferon-mediated CD8+ T cell exhaustion to restrict anti-tumor immunity. *Immunity*. (2022) 55:2369–2385.e10. doi: 10.1016/j.immuni.2022.10.020

30. Wu Y, Ai H, Xi Y, Tan J, Qu Y, Xu J, et al. Osteoclast-derived apoptotic bodies inhibit naive CD8+ T cell activation via Siglec15, promoting breast cancer secondary metastasis. *Cell Rep Med*. (2023) 4:101165. doi: 10.1016/j.xcrm.2023.101165.

31. Zhang K, Kim S, Cremasco V, Hirbe AC, Collins L, Piwnica-Worms D, et al. CD8+ T cells regulate bone tumor burden independent of osteoclast resorption. *Cancer Res*. (2011) 71:4799–808. doi: 10.1158/0008-5472.CAN-10-3922.

32. Bouchet M, Lainé A, Boyault C, Proponnet-Guerault M, Meugnier E, Bouazza L, et al. ERRα Expression in bone metastases leads to an exacerbated antitumor immune response. *Cancer Res*. (2020) 80:2914–26. doi: 10.1158/0008-5472.CAN-19-3584.

33. Zolochevska O, Diaz-Quiñones AO, Ellis J, Figueiredo ML. Interleukin-27 expression modifies prostate cancer cell crosstalk with bone and immune cells in vitro. *J Cell Physiol*. (2013) 228:1127–36. doi: 10.1002/jcp.24265.

34. Ostrand-Rosenberg S, Grusby MJ, Clements VK. Cutting edge: STAT6-deficient mice have enhanced tumor immunity to primary and metastatic mammary carcinoma. *J Immunol*. (2000) 165:6015–9. doi: 10.4049/jimmunol.165.11.6015.

35. Kudo-Saito C, Fuwa T, Murakami K, Kawakami Y. Targeting FSTL1 prevents tumor bone metastasis and consequent immune dysfunction. *Cancer Res*. (2013) 73:6185–93. doi: 10.1158/0008-5472.CAN-13-1364.

36. Zhu J. T helper cell differentiation, heterogeneity, and plasticity. *Cold Spring Harb Perspect Biol*. (2018) 10:a030338. doi: 10.1101/cshperspect.a030338.

37. Monteiro AC, Leal AC, Gonçalves-Silva T, Mercadante ACT, Kestelman F, Chaves SB, et al. T cells induce pre-metastatic osteolytic disease and help bone metastases establishment in a mouse model of metastatic breast cancer. *PloS One*. (2013) 8:e68171. doi: 10.1371/journal.pone.0068171.

38. Luo G, He Y, Zhao Q, Yu X. Immune cells act as promising targets for the treatment of bone metastasis. *Recent Pat Anticancer Drug Discovery*. (2017) 12:221–33. doi: 10.2174/1574892812666170606123113.

39. Giuliani N, Colla S, Sala R, Moroni M, Lazzaretti M, La Monica S, et al. Human myeloma cells stimulate the receptor activator of nuclear factor-kappa B ligand (RANKL) in T lymphocytes: a potential role in multiple myeloma bone disease. *Blood*. (2002) 100:4615–21. doi: 10.1182/blood-2002-04-1121.

40. Schoenborn JR, Wilson CB. Regulation of interferon-gamma during innate and adaptive immune responses. *Adv Immunol*. (2007) 96:41–101. doi: 10.1016/S0065-2776(07)96002-2.

41. Meng F, Han X, Min Z, He X, Zhu S. Prognostic signatures associated with high infiltration of Tregs in bone metastatic prostate cancer. *Aging (Albany NY)*. (2021) 13:17442–61. doi: 10.18632/aging.v13i13.

42. Zuo H, Yang D, Yang Q, Tang H, Fu YX, Wan Y. Differential regulation of breast cancer bone metastasis by PARP1 and PARP2. *Nat Commun*. (2020) 11:1578. doi: 10.1038/s41467-020-15429-z.

43. Meng X, Vander Ark A, Lee P, Hostetter G, Bhowmick NA, Matrisian LM, et al. Myeloid-specific TGF-β signaling in bone promotes basic-FGF and breast cancer bone metastasis. *Oncogene*. (2016) 35:2370–8. doi: 10.1038/onc.2015.297.

44. Jarnicki AG, Lysaght J, Todryk S, Mills KHG. Suppression of antitumor immunity by IL-10 and TGF-beta-producing T cells infiltrating the growing tumor: influence of tumor environment on the induction of CD4+ and CD8+ regulatory T cells. *J Immunol*. (2006) 177:896–904. doi: 10.4049/jimmunol.177.2.896.

45. Collison LW, Workman CJ, Kuo TT, Boyd K, Wang Y, Vignali KM, et al. The inhibitory cytokine IL-35 contributes to regulatory T-cell function. *Nature*. (2007) 450:566–9. doi: 10.1038/nature06306.

46. Thornton AM, Shevach EM. CD4+CD25+ immunoregulatory T cells suppress polyclonal T cell activation in *vitro* by inhibiting interleukin 2 production. *J Exp Med*. (1998) 188:287–96. doi: 10.1084/jem.188.2.287.

47. Zou L, Barnett B, Safah H, Larussa VF, Evdemon-Hogan M, Mottram P, et al. Bone marrow is a reservoir for CD4+CD25+ regulatory T cells that traffic through CXCL12/CXCR4 signals. *Cancer Res*. (2004) 64:8451–5. doi: 10.1158/0008-5472.CAN-04-1987.

48. Tan W, Zhang W, Strasner A, Grivennikov S, Cheng JQ, Hoffman RM, et al. Tumour-infiltrating regulatory T cells stimulate mammary cancer metastasis through RANKL-RANK signalling. *Nature*. (2011) 470:548–53. doi: 10.1038/nature09707.

49. Zhao E, Wang L, Dai J, Kryczek I, Wei S, Vatan L, et al. Regulatory T cells in the bone marrow microenvironment in patients with prostate cancer. *Oncoimmunology*. (2012) 1:152–61. doi: 10.4161/onci.1.2.18480.

50. Stagg J, Divisekera U, Duret H, Sparwasser T, Teng MWL, Darcy PK, et al. CD73-deficient mice have increased antitumor immunity and are resistant to experimental metastasis. *Cancer Res*. (2011) 71:2892–900. doi: 10.1158/0008-5472.CAN-10-4246.

51. Gagliani N, Amezcua Vesely MC, Iseppon A, Brockmann L, Xu H, Palm NW, et al. Th17 cells transdifferentiate into regulatory T cells during resolution of inflammation. *Nature*. (2015) 523:221–5. doi: 10.1038/nature14452.

52. Chopra M, Riedel SS, Biehl M, Krieger S, von Krosigk V, Bäuerlein CA, et al. Tumor necrosis factor receptor 2-dependent homeostasis of regulatory T cells as a player in TNF-induced experimental metastasis. *Carcinogenesis*. (2013) 34:1296–303. doi: 10.1093/carcin/bgt038.

53. Muscarella AM, Aguirre S, Hao X, Waldvogel SM, Zhang XHF. Exploiting bone niches: progression of disseminated tumor cells to metastasis. *J Clin Invest*. (2021) 131:e143764. doi: 10.1172/JCI143764.

54. Karavitis J, Hix LM, Shi YH, Schultz RF, Khazaie K, Zhang M. Regulation of COX2 expression in mouse mammary tumor cells controls bone metastasis and PGE2-induction of regulatory T cell migration. *PloS One*. (2012) 7:e46342. doi: 10.1371/journal.pone.0046342.

55. Vivier E, Raulet DH, Moretta A, Caligiuri MA, Zitvogel L, Lanier LL, et al. Innate or adaptive immunity? The example of natural killer cells. *Science*. (2011) 331:44–9. doi: 10.1126/science.1198687.

56. Smyth MJ, Cretney E, Kelly JM, Westwood JA, Street SEA, Yagita H, et al. Activation of NK cell cytotoxicity. *Mol Immunol*. (2005) 42:501–10. doi: 10.1016/j.molimm.2004.07.034.

57. Wu Q, Tian P, He D, Jia Z, He Y, Luo W, et al. SCUBE2 mediates bone metastasis of luminal breast cancer by modulating immune-suppressive osteoblastic niches. *Cell Res*. (2023) 33:464–78. doi: 10.1038/s41422-023-00810-6.

58. Walker SR, Nelson EA, Zou L, Chaudhury M, Signoretti S, Richardson A, et al. Reciprocal effects of STAT5 and STAT3 in breast cancer. *Mol Cancer Res*. (2009) 7:966–76. doi: 10.1158/1541-7786.MCR-08-0238.

59. Marotta LLC, Almendro V, Marusyk A, Shipitsin M, Schemme J, Walker SR, et al. The JAK2/STAT3 signaling pathway is required for growth of CD44+CD24− stem cell-like breast cancer cells in human tumors. *J Clin Invest*. (2011) 121:2723–35. doi: 10.1172/JCI44745.

60. Bottos A, Gotthardt D, Gill JW, Gattelli A, Frei A, Tzankov A, et al. Decreased NK-cell tumour immunosurveillance consequent to JAK inhibition enhances metastasis in breast cancer models. *Nat Commun*. (2016) 7:12258. doi: 10.1038/ncomms12258.

61. Lode HN, Xiang R, Dreier T, Varki NM, Gillies SD, Reisfeld RA. Natural killer cell-mediated eradication of neuroblastoma metastases to bone marrow by targeted interleukin-2 therapy. *Blood*. (1998) 91:1706–15. doi: 10.1182/blood.V91.5.1706.1706_1706_1715.

62. Sone S, Yano S. Molecular pathogenesis and its therapeutic modalities of lung cancer metastasis to bone. *Cancer Metastasis Rev*. (2007) 26:685–9. doi: 10.1007/s10555-007-9081-z.

63. Hume DA. The mononuclear phagocyte system. *Curr Opin Immunol*. (2006) 18:49–53. doi: 10.1016/j.coi.2005.11.008.

64. Pollard JW. Tumour-educated macrophages promote tumour progression and metastasis. *Nat Rev Cancer*. (2004) 4:71–8. doi: 10.1038/nrc1256.

65. Wynn TA, Chawla A, Pollard JW. Macrophage biology in development, homeostasis and disease. *Nature*. (2013) 496:445–55. doi: 10.1038/nature12034.

66. Biswas SK, Mantovani A. Macrophage plasticity and interaction with lymphocyte subsets: cancer as a paradigm. *Nat Immunol*. (2010) 11:889–96. doi: 10.1038/ni.1937.

67. Lin Y, Xu J, Lan H. Tumor-associated macrophages in tumor metastasis: biological roles and clinical therapeutic applications. *J Hematol Oncol*. (2019) 12:76. doi: 10.1186/s13045-019-0760-3.

68. Gordon S, Taylor PR. Monocyte and macrophage heterogeneity. *Nat Rev Immunol*. (2005) 5:953–64. doi: 10.1038/nri1733.

69. Mantovani A, Sozzani S, Locati M, Allavena P, Sica A. Macrophage polarization: tumor-associated macrophages as a paradigm for polarized M2 mononuclear phagocytes. *Trends Immunol*. (2002) 23:549–55. doi: 10.1016/S1471-4906(02)02302-5.

70. Xue J, Schmidt SV, Sander J, Draffehn A, Krebs W, Quester I, et al. Transcriptome-based network analysis reveals a spectrum model of human macrophage activation. *Immunity*. (2014) 40:274–88. doi: 10.1016/j.immuni.2014.01.006.

71. Chávez-Galán L, Olleros ML, Vesin D, Garcia I. Much More than M1 and M2 Macrophages, There are also CD169(+) and TCR(+) Macrophages. *Front Immunol*. (2015) 6:263. doi: 10.3389/fimmu.2015.00263

72. Kapellos TS, Bonaguro L, Gemünd I, Reusch N, Saglam A, Hinkley ER, et al. Human monocyte subsets and phenotypes in major chronic inflammatory diseases. *Front Immunol*. (2019) 10:2035. doi: 10.3389/fimmu.2019.02035.

73. Haloul M, Oliveira ERA, Kader M, Wells JZ, Tominello TR, El Andaloussi A, et al. mTORC1-mediated polarization of M1 macrophages and their accumulation in the liver correlate with immunopathology in fatal ehrlichiosis. *Sci Rep*. (2019) 9:14050. doi: 10.1038/s41598-019-50320-y.

74. Mehta AK, Kadel S, Townsend MG, Oliwa M, Guerriero JL. Macrophage biology and mechanisms of immune suppression in breast cancer. *Front Immunol*. (2021) 12:643771. doi: 10.3389/fimmu.2021.643771.

75. Ugel S, De Sanctis F, Mandruzzato S, Bronte V. Tumor-induced myeloid deviation: when myeloid-derived suppressor cells meet tumor-associated macrophages. *J Clin Invest*. (2015) 125:3365–76. doi: 10.1172/JCI80006.

76. Kfoury Y, Baryawno N, Severe N, Mei S, Gustafsson K, Hirz T, et al. Human prostate cancer bone metastases have an actionable immunosuppressive microenvironment. *Cancer Cell*. (2021) 39:1464–1478.e8. doi: 10.1016/j.ccell.2021.09.005.

77. Chen Y, Song Y, Du W, Gong L, Chang H, Zou Z. Tumor-associated macrophages: an accomplice in solid tumor progression. *J BioMed Sci*. (2019) 26:78. doi: 10.1186/s12929-019-0568-z.

78. Bingle L, Brown NJ, Lewis CE. The role of tumour-associated macrophages in tumour progression: implications for new anticancer therapies. *J Pathol*. (2002) 196:254–65. doi: 10.1002/path.1027.

79. Annacker O, Asseman C, Read S, Powrie F. Interleukin-10 in the regulation of T cell-induced colitis. *J Autoimmun*. (2003) 20:277–9. doi: 10.1016/S0896-8411(03)00045-3.

80. Thomas DA, Massagué J. TGF-beta directly targets cytotoxic T cell functions during tumor evasion of immune surveillance. *Cancer Cell*. (2005) 8:369–80. doi: 10.1016/j.ccr.2005.10.012.

81. Ruffell B, Chang-Strachan D, Chan V, Rosenbusch A, Ho CMT, Pryer N, et al. Macrophage IL-10 blocks CD8+ T cell-dependent responses to chemotherapy by suppressing IL-12 expression in intratumoral dendritic cells. *Cancer Cell*. (2014) 26:623–37. doi: 10.1016/j.ccell.2014.09.006.

82. Kalinski P. Regulation of immune responses by prostaglandin E2. *J Immunol*. (2012) 188:21–8. doi: 10.4049/jimmunol.1101029.

83. Kim OH, Kang GH, Noh H, Cha JY, Lee HJ, Yoon JH, et al. Proangiogenic TIE2 (+)/CD31 (+) macrophages are the predominant population of tumor-associated macrophages infiltrating metastatic lymph nodes. *Mol Cells*. (2013) 36:432–8. doi: 10.1007/s10059-013-0194-7.

84. Ye X, Huang X, Fu X, Zhang X, Lin R, Zhang W, et al. Myeloid-like tumor hybrid cells in bone marrow promote progression of prostate cancer bone metastasis. *J Hematol Oncol*. (2023) 16:46. doi: 10.1186/s13045-023-01442-4.

85. Cho HJ, Jung JI, Lim DY, Kwon GT, Her S, Park JH, et al. Bone marrow-derived, alternatively activated macrophages enhance solid tumor growth and lung metastasis of mammary carcinoma cells in a Balb/C mouse orthotopic model. *Breast Cancer Res*. (2012) 14:R81. doi: 10.1186/bcr3195.

86. Hiraoka K, Zenmyo M, Watari K, Iguchi H, Fotovati A, Kimura YN, et al. Inhibition of bone and muscle metastases of lung cancer cells by a decrease in the number of monocytes/macrophages. *Cancer Sci*. (2008) 99:1595–602. doi: 10.1111/j.1349-7006.2008.00880.x.

87. Fend L, Accart N, Kintz J, Cochin S, Reymann C, Le Pogam F, et al. Therapeutic effects of anti-CD115 monoclonal antibody in mouse cancer models through dual inhibition of tumor-associated macrophages and osteoclasts. *PloS One*. (2013) 8:e73310. doi: 10.1371/journal.pone.0073310.

88. Herroon MK, Rajagurubandara E, Rudy DL, Chalasani A, Hardaway AL, Podgorski I. Macrophage cathepsin K promotes prostate tumor progression in bone. *Oncogene*. (2013) 32:1580–93. doi: 10.1038/onc.2012.166.

89. Jiang P, Gao W, Ma T, Wang R, Piao Y, Dong X, et al. CD137 promotes bone metastasis of breast cancer by enhancing the migration and osteoclast differentiation of monocytes/macrophages. *Theranostics*. (2019) 9:2950–66. doi: 10.7150/thno.29617.

90. Huang R, Wang S, Wang N, Zheng Y, Zhou J, Yang B, et al. CCL5 derived from tumor-associated macrophages promotes prostate cancer stem cells and metastasis via

activating β-catenin/STAT3 signaling. *Cell Death Dis*. (2020) 11:234. doi: 10.1038/s41419-020-2435-y.

91. Mizutani K, Sud S, McGregor NA, Martinovski G, Rice BT, Craig MJ, et al. The chemokine CCL2 increases prostate tumor growth and bone metastasis through macrophage and osteoclast recruitment. *Neoplasia*. (2009) 11:1235–42. doi: 10.1593/neo.09988.

92. Ma RY, Zhang H, Li XF, Zhang CB, Selli C, Tagliavini G, et al. Monocyte-derived macrophages promote breast cancer bone metastasis outgrowth. *J Exp Med*. (2020) 217:e20191820. doi: 10.1084/jem.20191820.

93. Roca H, Jones JD, Purica MC, Weidner S, Koh AJ, Kuo R, et al. Apoptosis-induced CXCL5 accelerates inflammation and growth of prostate tumor metastases in bone. *J Clin Invest*. (2018) 128:248–66. doi: 10.1172/JCI92466.

94. Sullivan AR, Pixley FJ. CSF-1R signaling in health and disease: a focus on the mammary gland. *J Mammary Gland Biol Neoplasia*. (2014) 19:149–59. doi: 10.1007/s10911-014-9320-1.

95. Drapkin BJ, Farago AF. Unexpected synergy reveals new therapeutic strategy in SCLC. *Trends Pharmacol Sci*. (2019) 40:295–7. doi: 10.1016/j.tips.2019.03.005.

96. Halin Bergström S, Nilsson M, Adamo H, Thysell E, Jernberg E, Stattin P, et al. Extratumoral heme oxygenase-1 (HO-1) expressing macrophages likely promote primary and metastatic prostate tumor growth. *PloS One*. (2016) 11:e0157280. doi: 10.1371/journal.pone.0157280.

97. Ling Z, Yang C, Tan J, Dou C, Chen Y. Beyond immunosuppressive effects: dual roles of myeloid-derived suppressor cells in bone-related diseases. *Cell Mol Life Sci*. (2021) 78:7161–83. doi: 10.1007/s00018-021-03966-9.

98. Gabrilovich DI, Nagaraj S. Myeloid-derived suppressor cells as regulators of the immune system. *Nat Rev Immunol*. (2009) 9:162–74. doi: 10.1038/nri2506.

99. Sawant A, Ponnazhagan S. Myeloid-derived suppressor cells as osteoclast progenitors: a novel target for controlling osteolytic bone metastasis. *Cancer Res*. (2013) 73:4606–10. doi: 10.1158/0008-5472.CAN-13-0305.

100. Ryan MR, Shepherd R, Leavey JK, Gao Y, Grassi F, Schnell FJ, et al. An IL-7-dependent rebound in thymic T cell output contributes to the bone loss induced by estrogen deficiency. *Proc Natl Acad Sci U S A*. (2005) 102:16735–40. doi: 10.1073/pnas.0505168102.

101. Keskinov AA, Shurin MR. Myeloid regulatory cells in tumor spreading and metastasis. *Immunobiology*. (2015) 220:236–42. doi: 10.1016/j.imbio.2014.07.017.

102. Wu MY, Li CJ, Yiang GT, Cheng YL, Tsai APY, Hou YT, et al. Molecular regulation of bone metastasis pathogenesis. *Cell Physiol Biochem*. (2018) 46:1423–38. doi: 10.1159/000489184.

103. Hu CE, Gan J, Zhang RD, Cheng YR, Huang GJ. Up-regulated myeloid-derived suppressor cell contributes to hepatocellular carcinoma development by impairing dendritic cell function. *Scand J Gastroenterol*. (2011) 46:156–64. doi: 10.3109/00365521.2010.516450.

104. Li H, Han Y, Guo Q, Zhang M, Cao X. Cancer-expanded myeloid-derived suppressor cells induce anergy of NK cells through membrane-bound TGF-beta 1. *J Immunol*. (2009) 182:240–9. doi: 10.4049/jimmunol.182.1.240.

105. Brimnes MK, Vangsted AJ, Knudsen LM, Gimsing P, Gang AO, Johnsen HE, et al. Increased level of both CD4+FOXP3+ regulatory T cells and CD14+HLA-DR⁻/low myeloid-derived suppressor cells and decreased level of dendritic cells in patients with multiple myeloma. *Scand J Immunol*. (2010) 72:540–7. doi: 10.1111/sji.2010.72.issue-6.

106. Won WJ, Deshane JS, Leavenworth JW, Oliva CR, Griguer CE. Metabolic and functional reprogramming of myeloid-derived suppressor cells and their therapeutic control in glioblastoma. *Cell Stress*. (2019) 3:47–65. doi: 10.15698/cst.

107. Li YL, Zhao H, Ren XB. Relationship of VEGF/VEGFR with immune and cancer cells: staggering or forward? *Cancer Biol Med*. (2016) 13:206–14. doi: 10.20892/j.issn.2095-3941.2015.0070.

108. Wang SH, Lu QY, Guo YH, Song YY, Liu PJ, Wang YC. The blockage of Notch signalling promoted the generation of polymorphonuclear myeloid-derived suppressor cells with lower immunosuppression. *Eur J Cancer*. (2016) 68:90–105. doi: 10.1016/j.ejca.2016.08.019.

109. Rashid MH, Borin TF, Ara R, Piranlioglu R, Achyut BR, Korkaya H, et al. Critical immunosuppressive effect of MDSC−derived exosomes in the tumor microenvironment. *Oncol Rep*. (2021) 45:1171–81. doi: 10.3892/or.

110. Danilin S, Merkel AR, Johnson JR, Johnson RW, Edwards JR, Sterling JA. Myeloid-derived suppressor cells expand during breast cancer progression and promote tumor-induced bone destruction. *Oncoimmunology*. (2012) 1:1484–94. doi: 10.4161/onci.21990.

111. Li BH, Garstka MA, Li ZF. Chemokines and their receptors promoting the recruitment of myeloid-derived suppressor cells into the tumor. *Mol Immunol*. (2020) 117:201–15. doi: 10.1016/j.molimm.2019.11.014.

112. Wang Y, Ding Y, Guo N, Wang S. MDSCs: key criminals of tumor pre-metastatic niche formation. *Front Immunol*. (2019) 10:172. doi: 10.3389/fimmu.2019.00172.

113. Bidwell BN, Slaney CY, Withana NP, Forster S, Cao Y, Loi S, et al. Silencing of Irf7 pathways in breast cancer cells promotes bone metastasis through immune escape. *Nat Med*. (2012) 18:1224–31. doi: 10.1038/nm.2830.

114. An J, Feng L, Ren J, Li Y, Li G, Liu C, et al. Chronic stress promotes breast carcinoma metastasis by accumulating myeloid-derived suppressor cells through

activating β-adrenergic signaling. *Oncoimmunology*. (2021) 10:2004659. doi: 10.1080/2162402X.2021.2004659.

115. Sawant A, Deshane J, Jules J, Lee CM, Harris BA, Feng X, et al. Myeloid-derived suppressor cells function as novel osteoclast progenitors enhancing bone loss in breast cancer. *Cancer Res*. (2013) 73:672–82. doi: 10.1158/0008-5472.CAN-12-2202.

116. Papachristou DJ, Basdra EK, Papavassiliou AG. Bone metastases: molecular mechanisms and novel therapeutic interventions. *Med Res Rev*. (2012) 32:611–36. doi: 10.1002/med.20224.

117. Banchereau J, Steinman RM. Dendritic cells and the control of immunity. *Nature*. (1998) 392:245–52. doi: 10.1038/32588.

118. Steinman RM, Banchereau J. Taking dendritic cells into medicine. *Nature*. (2007) 449:419–26. doi: 10.1038/nature06175.

119. Steinman RM. Decisions about dendritic cells: past, present, and future. *Annu Rev Immunol*. (2012) 30:1–22. doi: 10.1146/annurev-immunol-100311-102839.

120. Steinman RM, Cohn ZA. Identification of a novel cell type in peripheral lymphoid organs of mice. I. Morphology, quantitation, tissue distribution. *J Exp Med*. (1973) 137:1142–62. doi: 10.1084/jem.137.5.1142.

121. Albert ML, Pearce SF, Francisco LM, Sauter B, Roy P, Silverstein RL, et al. Immature dendritic cells phagocytose apoptotic cells via alphavbeta5 and CD36, and cross-present antigens to cytotoxic T lymphocytes. *J Exp Med*. (1998) 188:1359–68. doi: 10.1084/jem.188.7.1359.

122. Heath WR, Carbone FR. Cross-presentation, dendritic cells, tolerance and immunity. *Annu Rev Immunol*. (2001) 19:47–64. doi: 10.1146/annurev.immunol.19.1.47.

123. Palucka K, Banchereau J. Cancer immunotherapy via dendritic cells. *Nat Rev Cancer*. (2012) 12:265–77. doi: 10.1038/nrc3258.

124. Cavanagh LL, Bonasio R, Mazo IB, Halin C, Cheng G, van der Velden AWM, et al. Activation of bone marrow-resident memory T cells by circulating, antigen-bearing dendritic cells. *Nat Immunol*. (2005) 6:1029–37. doi: 10.1038/ni1249.

125. Capietto AH, Faccio R. Immune regulation of bone metastasis. *Bonekey Rep*. (2014) 3:600. doi: 10.1038/bonekey.2014.95.

126. Magidey-Klein K, Cooper TJ, Kveler K, Normand R, Zhang T, Timaner M, et al. IL-6 contributes to metastatic switch via the differentiation of monocytic-dendritic progenitors into prometastatic immune cells. *J Immunother Cancer*. (2021) 9:e002856. doi: 10.1136/jitc-2021-002856.

127. Giorello MB, Matas A, Marenco P, Davies KM, Borzone FR, Calcagno M de L, et al. CD1a- and CD83-positive dendritic cells as prognostic markers of metastasis development in early breast cancer patients. *Breast Cancer*. (2021) 28:1328–39. doi: 10.1007/s12282-021-01270-9.

128. Sawant A, Hensel JA, Chanda D, Harris BA, Siegal GP, Maheshwari A, et al. Depletion of plasmacytoid dendritic cells inhibits tumor growth and prevents bone metastasis of breast cancer cells. *J Immunol*. (2012) 189:4258–65. doi: 10.4049/jimmunol.1101855.

129. Lu T, Zhang Z, Bi Z, Lan T, Zeng H, Liu Y, et al. TFAM deficiency in dendritic cells leads to mitochondrial dysfunction and enhanced antitumor immunity through cGAS-STING pathway. *J Immunother Cancer*. (2023) 11:e005430. doi: 10.1136/jitc-2022-005430.

130. Correale P, Micheli L, Vecchio MT, Sabatino M, Petrioli R, Pozzessere D, et al. A parathyroid-hormone-related-protein (PTH-rP)-specific cytotoxic T cell response induced by in *vitro* stimulation of tumour-infiltrating lymphocytes derived from prostate cancer metastases, with epitope peptide-loaded autologous dendritic cells and low-dose IL-2. *Br J Cancer*. (2001) 85:1722–30. doi: 10.1054/bjoc.2001.2136.

131. Imai K, Minamiya Y, Koyota S, Ito M, Saito H, Sato Y, et al. Inhibition of dendritic cell migration by transforming growth factor-β1 increases tumor-draining lymph node metastasis. *J Exp Clin Cancer Res*. (2012) 31:3. doi: 10.1186/1756-9966-31-3.

132. Anderson DM, Maraskovsky E, Billingsley WL, Dougall WC, Tometsko ME, Roux ER, et al. A homologue of the TNF receptor and its ligand enhance T-cell growth and dendritic-cell function. *Nature*. (1997) 390:175–9. doi: 10.1038/36593.

133. Dougall WC, Glaccum M, Charrier K, Rohrbach K, Brasel K, De Smedt T, et al. RANK is essential for osteoclast and lymph node development. *Genes Dev*. (1999) 13:2412–24. doi: 10.1101/gad.13.18.2412.

134. Josien R, Li HL, Ingulli E, Sarma S, Wong BR, Vologodskaia M, et al. TRANCE, a tumor necrosis factor family member, enhances the longevity and adjuvant properties of dendritic cells in vivo. *J Exp Med*. (2000) 191:495–502. doi: 10.1084/jem.191.3.495.

135. Totsuka T, Kanai T, Nemoto Y, Tomita T, Okamoto R, Tsuchiya K, et al. RANK-RANKL signaling pathway is critically involved in the function of CD4+CD25+ regulatory T cells in chronic colitis. *J Immunol*. (2009) 182:6079–87. doi: 10.4049/jimmunol.0711823.

136. Demoulin SA, Somja J, Duray A, Guénin S, Roncarati P, Delvenne PO, et al. Cervical (pre)neoplastic microenvironment promotes the emergence of tolerogenic dendritic cells via RANKL secretion. *Oncoimmunology*. (2015) 4:e1008334. doi: 10.1080/2162402X.2015.1008334.

137. Ahern E, Harjunpää H, Barkauskas D, Allen S, Takeda K, Yagita H, et al. Co-administration of RANKL and CTLA4 antibodies enhances lymphocyte-mediated antitumor immunity in mice. *Clin Cancer Res*. (2017) 23:5789–801. doi: 10.1158/1078-0432.CCR-17-0606.

138. Esposito M, Kang Y. Targeting tumor-stromal interactions in bone metastasis. *Pharmacol Ther*. (2014) 141:222–33. doi: 10.1016/j.pharmthera.2013.10.006.

139. Thiede MA, Smock SL, Petersen DN, Grasser WA, Thompson DD, Nishimoto SK. Presence of messenger ribonucleic acid encoding osteocalcin, a marker of bone turnover, in bone marrow megakaryocytes and peripheral blood platelets. *Endocrinology*. (1994) 135:929–37. doi: 10.1210/endo.135.3.8070388.

140. Kelm RJ, Hair GA, Mann KG, Grant BW. Characterization of human osteoblast and megakaryocyte-derived osteonectin (SPARC). *Blood*. (1992) 80:3112–9. doi: 10.1182/blood.V80.12.3112.bloodjournal80123112.

141. Breton-Gorius J, Clezardin P, Guichard J, Debili N, Malaval L, Vainchenker W, et al. Localization of platelet osteonectin at the internal face of the alpha-granule membranes in platelets and megakaryocytes. *Blood*. (1992) 79:936–41. doi: 10.1182/blood.V79.4.936.bloodjournal794936.

142. Chenu C, Delmas PD. Platelets contribute to circulating levels of bone sialoprotein in human. *J Bone Miner Res*. (1992) 7:47–54. doi: 10.1002/jbmr.5650070108.

143. Kacena MA, Nelson T, Clough ME, Lee SK, Lorenzo JA, Gundberg CM, et al. Megakaryocyte-mediated inhibition of osteoclast development. *Bone*. (2006) 39:991–9. doi: 10.1016/j.bone.2006.05.004.

144. Li X, Koh AJ, Wang Z, Soki FN, Park SI, Pienta KJ, et al. Inhibitory effects of megakaryocytic cells in prostate cancer skeletal metastasis. *J Bone Miner Res*. (2011) 26:125–34. doi: 10.1002/jbmr.204.

145. Previdi S, Maroni P, Matteucci E, Broggini M, Bendinelli P, Desiderio MA. Interaction between human-breast cancer metastasis and bone microenvironment through activated hepatocyte growth factor/Met and beta-catenin/Wnt pathways. *Eur J Cancer*. (2010) 46:1679–91. doi: 10.1016/j.ejca.2010.02.036.

146. Jackson W, Sosnoski DM, Ohanessian SE, Chandler P, Mobley A, Meisel KD, et al. Role of megakaryocytes in breast cancer metastasis to bone. *Cancer Res*. (2017) 77:1942–54. doi: 10.1158/0008-5472.CAN-16-1084.

147. Capparello A, Maurizi A, Veeriah V, Teti A. Reprint of: The Great Beauty of the osteoclast. *Arch Biochem Biophys*. (2014) 561:13–21. doi: 10.1016/j.abb.2014.08.009.

148. Boyle WJ, Simonet WS, Lacey DL. Osteoclast differentiation and activation. *Nature*. (2003) 423:337–42. doi: 10.1038/nature01658.

149. Buenrostro D, Mulcrone PL, Owens P, Sterling JA. The bone microenvironment: a fertile soil for tumor growth. *Curr Osteoporos Rep*. (2016) 14:151–8. doi: 10.1007/s11914-016-0315-2.

150. Bendre MS, Gaddy-Kurten D, Mon-Foote T, Akel NS, Skinner RA, Nicholas RW, et al. Expression of interleukin 8 and not parathyroid hormone-related protein by human breast cancer cells correlates with bone metastasis in vivo. *Cancer Res*. (2002) 62:5571–9.

151. Boucharaba A, Serre CM, Grès S, Saulnier-Blache JS, Bordet JC, Guglielmi J, et al. Platelet-derived lysophosphatidic acid supports the progression of osteolytic bone metastases in breast cancer. *J Clin Invest*. (2004) 114:1714–25. doi: 10.1172/JCI22123.

152. Guise TA, Yin JJ, Taylor SD, Kumagai Y, Dallas M, Boyce BF, et al. Evidence for a causal role of parathyroid hormone-related protein in the pathogenesis of human breast cancer-mediated osteolysis. *J Clin Invest*. (1996) 98:1544–9. doi: 10.1172/JCI118947.

153. Ouellet V, Tiedemann K, Mourskaia A, Fong JE, Tran-Thanh D, Amir E, et al. CCN3 impairs osteoblast and stimulates osteoclast differentiation to favor breast cancer metastasis to bone. *Am J Pathol*. (2011) 178:2377–88. doi: 10.1016/j.ajpath.2011.01.033.

154. Thomas RJ, Guise TA, Yin JJ, Elliott J, Horwood NJ, Martin TJ, et al. Breast cancer cells interact with osteoblasts to support osteoclast formation. *Endocrinology*. (1999) 140:4451–8. doi: 10.1210/en.140.10.4451.

155. Weilbaecher KN, Guise TA, McCauley LK. Cancer to bone: a fatal attraction. *Nat Rev Cancer*. (2011) 11:411–25. doi: 10.1038/nrc3055.

156. Welm AL, Sneddon JB, Taylor C, Nuyten DSA, van de Vijver MJ, Hasegawa BH, et al. The macrophage-stimulating protein pathway promotes metastasis in a mouse model for breast cancer and predicts poor prognosis in humans. *Proc Natl Acad Sci U S A*. (2007) 104:7570–5. doi: 10.1073/pnas.0702095104.

157. Walsh MC, Choi Y. Biology of the RANKL-RANK-OPG system in immunity, bone, and beyond. *Front Immunol*. (2014) 5:511. doi: 10.3389/fimmu.2014.00511.

158. Miao D, He B, Jiang Y, Kobayashi T, Sorocéanu MA, Zhao J, et al. Osteoblast-derived PTHrP is a potent endogenous bone anabolic agent that modifies the therapeutic efficacy of administered PTH 1-34. *J Clin Invest*. (2005) 115:2402–11. doi: 10.1172/JCI24918.

159. Ma Q, Liang M, Wu Y, Dou C, Xu J, Dong S, et al. Small extracellular vesicles deliver osteolytic effectors and mediate cancer-induced osteolysis in bone metastatic niche. *J Extracell Vesicles*. (2021) 10:e12068. doi: 10.1002/jev2.12068.

160. Mulholland BS, Forwood MR, Morrison NA. Monocyte chemoattractant protein-1 (MCP-1/CCL2) drives activation of bone remodelling and skeletal metastasis. *Curr Osteoporos Rep*. (2019) 17:538–47. doi: 10.1007/s11914-019-00545-7.

161. Wu K, Feng J, Lyu F, Xing F, Sharma S, Liu Y, et al. Exosomal miR-19a and IBSP cooperate to induce osteolytic bone metastasis of estrogen receptor-positive breast cancer. *Nat Commun*. (2021) 12:5196. doi: 10.1038/s41467-021-25473-y.

162. Yue Z, Niu X, Yuan Z, Qin Q, Jiang W, He L, et al. RSPO2 and RANKL signal through LGR4 to regulate osteoclastic premetastatic niche formation and bone metastasis. *J Clin Invest*. (2022) 132:e144579. doi: 10.1172/JCI144579.

163. Mourskaia AA, Amir E, Dong Z, Tiedemann K, Cory S, Omeroglu A, et al. ABCC5 supports osteoclast formation and promotes breast cancer metastasis to bone. *Breast Cancer Res*. (2012) 14:R149. doi: 10.1186/bcr3361.

164. Chen J, Xu W, Song K, Da LT, Zhang X, Lin M, et al. Legumain inhibitor prevents breast cancer bone metastasis by attenuating osteoclast differentiation and function. *Bone*. (2023) 169:116680. doi: 10.1016/j.bone.2023.116680.

165. Li L, Ameri AH, Wang S, Jansson KH, Casey OM, Yang Q, et al. EGR1 regulates angiogenic and osteoclastogenic factors in prostate cancer and promotes metastasis. *Oncogene*. (2019) 38:6241–55. doi: 10.1038/s41388-019-0873-8.

166. He Y, Luo W, Liu Y, Wang Y, Ma C, Wu Q, et al. IL-20RB mediates tumoral response to osteoclastic niches and promotes bone metastasis of lung cancer. *J Clin Invest*. (2022) 132:e157917. doi: 10.1172/JCI157917.

167. Nakajima K, Kho DH, Yanagawa T, Harazono Y, Hogan V, Chen W, et al. Galectin-3 cleavage alters bone remodeling: different outcomes in breast and prostate cancer skeletal metastasis. *Cancer Res*. (2016) 76:1391–402. doi: 10.1158/0008-5472.CAN-15-1793.

168. Uluçkan O, Becker SN, Deng H, Zou W, Prior JL, Piwnica-Worms D, et al. CD47 regulates bone mass and tumor metastasis to bone. *Cancer Res*. (2009) 69:3196–204. doi: 10.1158/0008-5472.CAN-08-3358.

169. Cai WL, Huang WD, Li B, Chen TR, Li ZX, Zhao CL, et al. microRNA-124 inhibits bone metastasis of breast cancer by repressing Interleukin-11. *Mol Cancer*. (2018) 17:9. doi: 10.1186/s12943-017-0746-0.

170. Yu L, Sui B, Fan W, Lei L, Zhou L, Yang L, et al. Exosomes derived from osteogenic tumor activate osteoclast differentiation and concurrently inhibit osteogenesis by transferring COL1A1-targeting miRNA-92a-1-5p. *J Extracell Vesicles*. (2021) 10:e12056. doi: 10.1002/jev2.12056.

171. Urabe F, Kosaka N, Yamamoto Y, Ito K, Otsuka K, Soekmadji C, et al. Metastatic prostate cancer-derived extracellular vesicles facilitate osteoclastogenesis by transferring the CDCP1 protein. *J Extracell Vesicles*. (2023) 12:e12312. doi: 10.1002/jev2.12312.

172. Zhang S, Liao X, Chen S, Qian W, Li M, Xu Y, et al. Large oncosome-loaded VAPA promotes bone-tropic metastasis of hepatocellular carcinoma via formation of osteoclastic pre-metastatic niche. *Adv Sci (Weinh)*. (2022) 9:e2201974. doi: 10.1002/advs.202201974.

173. Verbruggen ASK, McNamara LM. Mechanoregulation may drive osteolysis during bone metastasis: A finite element analysis of the mechanical environment within bone tissue during bone metastasis and osteolytic resorption. *J Mech Behav BioMed Mater*. (2023) 138:105662. doi: 10.1016/j.jmbbm.2023.105662.

174. Li X, Liang Y, Lian C, Peng F, Xiao Y, He Y, et al. CST6 protein and peptides inhibit breast cancer bone metastasis by suppressing CTSB activity and osteoclastogenesis. *Theranostics*. (2021) 11:9821–32. doi: 10.7150/thno.62187.

175. Kong D, Ye C, Zhang C, Sun X, Wang F, Chen R, et al. Procoxacin bidirectionally inhibits osteoblastic and osteoclastic activity in bone and suppresses bone metastasis of prostate cancer. *J Exp Clin Cancer Res*. (2023) 42:45. doi: 10.1186/s13046-023-02610-7.

176. de Castro LF, Michel Z, Pan K, Taylor J, Szymczuk V, Paravastu S, et al. Safety and efficacy of denosumab for fibrous dysplasia of bone. *N Engl J Med*. (2023) 388:766–8. doi: 10.1056/NEJMc2214862.

177. Omata D, Munakata L, Maruyama K, Suzuki R. Ultrasound and microbubble-mediated drug delivery and immunotherapy. *J Med Ultrason*. (2001). doi: 10.1007/s10396-022-01201-x

178. Petitdemange C, Becquart P, Wauquier N, Béziat V, Debré P, Leroy EM, et al. Unconventional repertoire profile is imprinted during acute chikungunya infection for natural killer cells polarization toward cytotoxicity. *PLoS Pathog*. (2011) 7:e1002268. doi: 10.1371/journal.ppat.1002268.

179. Nishikawa H, Koyama S. Mechanisms of regulatory T cell infiltration in tumors: implications for innovative immune precision therapies. *J Immunother Cancer*. (2021) 9:e002591. doi: 10.1136/jitc-2021-002591.

180. Wang K, Donnelly CR, Jiang C, Liao Y, Luo X, Tao X, et al. STING suppresses bone cancer pain via immune and neuronal modulation. *Nat Commun*. (2021) 12:4558. doi: 10.1038/s41467-021-24867-2.

181. Ducy P, Schinke T, Karsenty G. The osteoblast: a sophisticated fibroblast under central surveillance. *Science*. (2000) 289:1501–4. doi: 10.1126/science.289.5484.1501.

182. Zunich SM, Valdovinos M, Douglas T, Walterhouse D, Iannaccone P, Lamm MLG. Osteoblast-secreted collagen upregulates paracrine Sonic hedgehog signaling by prostate cancer cells and enhances osteoblast differentiation. *Mol Cancer*. (2012) 11:30. doi: 10.1186/1476-4598-11-30.

183. Jin JK, Dayyani F, Gallick GE. Steps in prostate cancer progression that lead to bone metastasis. *Int J Cancer*. (2011) 128:2545–61. doi: 10.1002/ijc.26024.

184. Chen PC, Liu SC, Lin TH, Lin LW, Wu HC, Tai HC, et al. Prostate cancer-secreted CCN3 uses the GSK3β and β-catenin pathways to enhance osteogenic factor levels in osteoblasts. *Environ Toxicol*. (2021) 36:425–32. doi: 10.1002/tox.23048.

185. Devignes CS, Aslan Y, Brenot A, Devillers A, Schepers K, Fabre S, et al. HIF signaling in osteoblast-lineage cells promotes systemic breast cancer growth and metastasis in mice. *Proc Natl Acad Sci U S A*. (2018) 115:E992–1001. doi: 10.1073/pnas.1718009115.

186. Moon HH, Clines KL, O'Day PJ, Al-Barghouthi BM, Farber EA, Farber CR, et al. Osteoblasts generate testosterone from DHEA and activate androgen signaling in prostate cancer cells. *J Bone Miner Res*. (2021) 36:1566–79. doi: 10.1002/jbmr.4313.

187. Wu JB, Yin L, Shi C, Li Q, Duan P, Huang JM, et al. MAOA-dependent activation of shh-IL6-RANKL signaling network promotes prostate cancer metastasis by engaging tumor-stromal cell interactions. *Cancer Cell*. (2017) 31:368–82. doi: 10.1016/j.ccell.2017.02.003.

188. Kan C, Vargas G, Pape FL, Clézardin P. Cancer cell colonisation in the bone microenvironment. *Int J Mol Sci*. (2016) 17:1674. doi: 10.3390/ijms17101674.

189. Li Z, Xiao J, Wu X, Li W, Yang Z, Xie J, et al. Plumbagin inhibits breast tumor bone metastasis and osteolysis by modulating the tumor-bone microenvironment. *Curr Mol Med*. (2012) 12:967–81. doi: 10.2174/156652412802480871.

190. Lambert AW, Pattabiraman DR, Weinberg RA. Emerging biological principles of metastasis. *Cell*. (2017) 168:670–91. doi: 10.1016/j.cell.2016.11.037.

191. Badia-Ramentol J, Linares J, Gómez-Llonin A, Calon A. Minimal residual disease, metastasis and immunity. *Biomolecules*. (2021) 11:130. doi: 10.3390/biom11020130.

192. Risson E, Nobre AR, Maguer-Satta V, Aguirre-Ghiso JA. The current paradigm and challenges ahead for the dormancy of disseminated tumor cells. *Nat Cancer*. (2020) 1:672–80. doi: 10.1038/s43018-020-0088-5.

193. Shiozawa Y, Pedersen EA, Havens AM, Jung Y, Mishra A, Joseph J, et al. Human prostate cancer metastases target the hematopoietic stem cell niche to establish footholds in mouse bone marrow. *J Clin Invest*. (2011) 121:1298–312. doi: 10.1172/JCI43414.

194. Sosa MS, Bragado P, Aguirre-Ghiso JA. Mechanisms of disseminated cancer cell dormancy: an awakening field. *Nat Rev Cancer*. (2014) 14:611–22. doi: 10.1038/nrc3793.

195. Oskarsson T, Batlle E, Massagué J. Metastatic stem cells: sources, niches, and vital pathways. *Cell Stem Cell*. (2014) 14:306–21. doi: 10.1016/j.stem.2014.02.002.

196. Braun S, Vogl FD, Naume B, Janni W, Osborne MP, Coombes RC, et al. A pooled analysis of bone marrow micrometastasis in breast cancer. *N Engl J Med*. (2005) 353:793–802. doi: 10.1056/NEJMoa050434.

197. Melchior SW, Corey E, Ellis WJ, Ross AA, Layton TJ, Oswin MM, et al. Early tumor cell dissemination in patients with clinically localized carcinoma of the prostate. *Clin Cancer Res*. (1997) 3:249–56.

198. Price TT, Burness ML, Sivan A, Warner MJ, Cheng R, Lee CH, et al. Dormant breast cancer micrometastases reside in specific bone marrow niches that regulate their transit to and from bone. *Sci Transl Med*. (2016) 8:340ra73. doi: 10.1126/scitranslmed.aad4059.

199. Sun YX, Schneider A, Jung Y, Wang J, Dai J, Wang J, et al. Skeletal localization and neutralization of the SDF-1(CXCL12)/CXCR4 axis blocks prostate cancer metastasis and growth in osseous sites in vivo. *J Bone Miner Res*. (2005) 20:318–29. doi: 10.1359/JBMR.041109.

200. Taichman RS, Patel LR, Bedenis R, Wang J, Weidner S, Schumann T, et al. GAS6 receptor status is associated with dormancy and bone metastatic tumor formation. *PloS One*. (2013) 8:e61873. doi: 10.1371/journal.pone.0061873.

201. Fujisaki J, Wu J, Carlson AL, Silberstein L, Putheti P, Larocca R, et al. *In vivo* imaging of Treg cells providing immune privilege to the haematopoietic stem-cell niche. *Nature*. (2011) 474:216–9. doi: 10.1038/nature10160.

202. Reinstein ZZ, Pamarthy S, Sagar V, Costa R, Abdulkadir SA, Giles FJ, et al. Overcoming immunosuppression in bone metastases. *Crit Rev Oncol Hematol*. (2017) 117:114–27. doi: 10.1016/j.critrevonc.2017.05.004.

203. Ahmadzadeh M, Johnson LA, Heemskerk B, Wunderlich JR, Dudley ME, White DE, et al. Tumor antigen-specific CD8 T cells infiltrating the tumor express high levels of PD-1 and are functionally impaired. *Blood*. (2009) 114:1537–44. doi: 10.1182/blood-2008-12-195792.

204. Fourcade J, Sun Z, Benallaoua M, Guillaume P, Luescher IF, Sander C, et al. Upregulation of Tim-3 and PD-1 expression is associated with tumor antigen-specific CD8+ T cell dysfunction in melanoma patients. *J Exp Med*. (2010) 207:2175–86. doi: 10.1084/jem.20100637.

205. Seidel JA, Otsuka A, Kabashima K. Anti-PD-1 and anti-CTLA-4 therapies in cancer: mechanisms of action, efficacy, and limitations. *Front Oncol*. (2018) 8:86. doi: 10.3389/fonc.2018.00086.

206. Wen Y, Tang F, Tu C, Hornicek F, Duan Z, Min L. Immune checkpoints in osteosarcoma: Recent advances and therapeutic potential. *Cancer Lett*. (2022) 547:215887. doi: 10.1016/j.canlet.2022.215887.

207. Agata Y, Kawasaki A, Nishimura H, Ishida Y, Tsubata T, Yagita H, et al. Expression of the PD-1 antigen on the surface of stimulated mouse T and B lymphocytes. *Int Immunol*. (1996) 8:765–72. doi: 10.1093/intimm/8.5.765.

208. Ishida M, Iwai Y, Tanaka Y, Okazaki T, Freeman GJ, Minato N, et al. Differential expression of PD-L1 and PD-L2, ligands for an inhibitory receptor PD-1, in the cells of lymphohematopoietic tissues. *Immunol Lett*. (2002) 84:57–62. doi: 10.1016/S0165-2478(02)00142-6.

209. Mizuno R, Sugiura D, Shimizu K, Maruhashi T, Watada M, Okazaki IM, et al. PD-1 primarily targets TCR signal in the inhibition of functional T cell activation. *Front Immunol*. (2019) 10:630. doi: 10.3389/fimmu.2019.00630.

210. Parry RV, Chemnitz JM, Frauwirth KA, Lanfranco AR, Braunstein I, Kobayashi SV, et al. CTLA-4 and PD-1 receptors inhibit T-cell activation by distinct mechanisms. *Mol Cell Biol*. (2005) 25:9543–53. doi: 10.1128/MCB.25.21.9543-9553.2005.

211. Joseph GJ, Johnson DB, Johnson RW. Immune checkpoint inhibitors in bone metastasis: Clinical challenges, toxicities, and mechanisms. *J Bone Oncol*. (2023) 43:100505. doi: 10.1016/j.jbo.2023.100505.

212. Pham F, Belkaid S, Maillet D, Confavreux CB, Dalle S, Péron J. Impact of bone metastases on patients with renal cell carcinoma or melanoma treated with combotherapy ipilimumab plus nivolumab. *Biomedicines*. (2022) 10:2758. doi: 10.3390/biomedicines10112758.

213. Desai K, Brown L, Wei W, Tucker M, Kao C, Kinsey E, et al. A multi-institutional, retrospective analysis of patients with metastatic renal cell carcinoma to bone treated with combination ipilimumab and nivolumab. *Target Oncol*. (2021) 16:633–42. doi: 10.1007/s11523-021-00832-3.

214. Landi L, D'Incà F, Gelibter A, Chiari R, Grossi F, Delmonte A, et al. Bone metastases and immunotherapy in patients with advanced non-small-cell lung cancer. *J Immunother Cancer*. (2019) 7:316. doi: 10.1186/s40425-019-0793-8.

215. Zhu YJ, Chang XS, Zhou R, Chen YD, Ma HC, Xiao ZZ, et al. Bone metastasis attenuates efficacy of immune checkpoint inhibitors and displays "cold" immune characteristics in Non-small cell lung cancer. *Lung Cancer*. (2022) 166:189–96. doi: 10.1016/j.lungcan.2022.03.006.

216. Wang K, Gu Y, Liao Y, Bang S, Donnelly CR, Chen O, et al. PD-1 blockade inhibits osteoclast formation and murine bone cancer pain. *J Clin Invest*. (2020) 130:3603–20. doi: 10.1172/JCI133334.

217. Dahlberg CIM, Sarhan D, Chrobok M, Duru AD, Alici E. Natural killer cell-based therapies targeting cancer: possible strategies to gain and sustain anti-tumor activity. *Front Immunol*. (2015) 6:605. doi: 10.3389/fimmu.2015.00605.

218. Xavier KB. Bacterial interspecies quorum sensing in the mammalian gut microbiota. *C. R Biologies*. (2018) 341:300. doi: 10.1016/j.crvi.2018.03.006

219. Cannarile MA, Weisser M, Jacob W, Jegg AM, Ries CH, Rüttinger D. Colony-stimulating factor 1 receptor (CSF1R) inhibitors in cancer therapy. *J Immunother Cancer*. (2017) 5:53. doi: 10.1186/s40425-017-0257-y.

220. Kitamura T, Qian BZ, Soong D, Cassetta L, Noy R, Sugano G, et al. CCL2-induced chemokine cascade promotes breast cancer metastasis by enhancing retention of metastasis-associated macrophages. *J Exp Med*. (2015) 212:1043–59. doi: 10.1084/jem.20141836.

221. Mantovani A, Marchesi F, Malesci A, Laghi L, Allavena P. Tumour-associated macrophages as treatment targets in oncology. *Nat Rev Clin Oncol*. (2017) 14:399–416. doi: 10.1038/nrclinonc.2016.217.

222. Zhang J, Pang Y, Xie T, Zhu L. CXCR4 antagonism in combination with IDO1 inhibition weakens immune suppression and inhibits tumor growth in mouse breast cancer bone metastases. *Onco Targets Ther*. (2019) 12:4985–92. doi: 10.2147/OTT.

223. Johansson M, Giger FA, Fielding T, Houart C. Dkk1 controls cell-cell interaction through regulation of non-nuclear β-catenin pools. *Dev Cell*. (2019) 51:775–786.e3. doi: 10.1016/j.devcel.2019.10.026.

224. Müller P, Martin K, Theurich S, von Bergwelt-Baildon M, Zippelius A. Cancer chemotherapy agents target intratumoral dendritic cells to potentiate antitumor immunity. *Oncoimmunology*. (2014) 3:e954460. doi: 10.4161/21624011.2014.954460.

225. MaChado FC, Girola N, Maia VSC, Bergami-Santos PC, Morais AS, Azevedo RA, et al. Immunomodulatory protective effects of rb9 cyclic-peptide in a metastatic melanoma setting and the involvement of dendritic cells. *Front Immunol*. (2019) 10:3122. doi: 10.3389/fimmu.2019.03122.

226. Mittal D, Vijayan D, Putz EM, Aguilera AR, Markey KA, Straube J, et al. Interleukin-12 from CD103+ Batf3-dependent dendritic cells required for NK-cell suppression of metastasis. *Cancer Immunol Res*. (2017) 5:1098–108. doi: 10.1158/2326-6066.CIR-17-0341.

227. Zhou Y, Slone N, Chrisikos TT, Kyrysyuk O, Babcock RL, Medik YB, et al. Vaccine efficacy against primary and metastatic cancer with in *vitro*-generated CD103+ conventional dendritic cells. *J Immunother Cancer*. (2020) 8:e000474. doi: 10.1136/jitc-2019-000474

Increased circulating polymorphonuclear myeloid-derived suppressor cells are associated with prognosis of metastatic castration-resistant prostate cancer

Takuro Kobayashi[1,2], Masayoshi Nagata[1], Tsuyoshi Hachiya[2], Haruhiko Wakita[1], Yoshihiro Ikehata[1,2], Keiji Takahashi[1], Toshiyuki China[1], Fumitaka Shimizu[1], Jun Lu[1], Yiming Jin[1], Yan Lu[1], Hisamitsu Ide[1] and Shigeo Horie[1,2]*

[1]Department of Urology, Graduate School of Medicine, Juntendo University, Tokyo, Japan,
[2]Department of Advanced Informatics for Genetic Diseases, Graduate School of Medicine, Juntendo University, Tokyo, Japan

Introduction: Myeloid-derived suppressor cell (MDSC) exhibits immunosuppressive functions and affects cancer progression, but its relationship with prostate cancer remains unclear. We elucidated the association of polymorphonuclear MDSC (PMN-MDSC) and monocytic MDSC (M-MDSC) levels of the total peripheral blood mononuclear cells (PBMCs) with prostate cancer progression and evaluated their roles as prognostic indicators.

Methods: We enrolled 115 patients with non-metastatic hormone-sensitive prostate cancer (nmHSPC, n = 62), metastatic hormone-sensitive prostate cancer (mHSPC, n = 23), and metastatic castration-resistant prostate cancer (mCRPC, n = 30). Subsequently, the proportions of MDSCs in each disease progression were compared. Log-rank tests and multivariate Cox regression analyses were performed to ascertain the associations of overall survival.

Results: The patients with mCRPC had significantly higher PMN-MDSC percentage than those with nmHSPC and mHSPC (P = 7.73 × 10⁻⁵ and 0.0014). Significantly elevated M-MDSC levels were observed in mCRPC patients aged <70 years (P = 0.016) and with a body mass index (BMI) <25 kg/ m² (P = 0.043). The high PMN-MDSC group had notably shorter median survival duration (159 days) than the low PMN-MDSC group (768 days, log-rank P = 0.018). In the multivariate analysis including age, BMI, and MDSC subset, PMN-MDSC was significantly associated with prognosis (hazard ratios, 3.48; 95% confidence interval: 1.05–11.56, P = 0.042).

Discussion: PMN-MDSC levels are significantly associated with mCRPC prognosis. Additionally, we highlight the remarkable associations of age and BMI with M-MDSC levels in mCRPC, offering novel insights into MDSC dynamics in prostate cancer progression.

1 Introduction

Prostate cancer is the second most frequently diagnosed cancer and the fifth leading cause of cancer-related mortality worldwide. The incidence of prostate cancer was estimated to range from 1 to 4 million cases per year in 2020 and is projected to nearly double to between 2 to 9 million cases annually by 2040 (1). The number of deaths due to prostate cancer was 375,000 in 2020 and is estimated to increase by 85%, reaching nearly 700,000 by 2040 (1). Prostate cancer is a predominantly diagnosed cancer in 112 countries and is the primary cause of cancer death in 48 countries (2). The incidence and mortality rates of prostate cancer are positively associated with advancing age, with 66 years being the average age at diagnosis (3). Androgen deprivation therapy (ADT) is the primary treatment for cancer with advanced stages, but its effectiveness wanes over time. Many patients progress to castration-resistant prostate cancer (CRPC) within 2–3 years, which considerably worsens their prognosis (4, 5).

Recent insights into prostate cancer progression have spotlighted the role of myeloid-derived suppressor cells (MDSCs) within the tumor microenvironment (TME). MDSCs are a heterogeneous group of immature myeloid cells that exhibit immunosuppressive functions affecting various immune cells, and humans have two primary MDSC subtypes, which are as follows: polymorphonuclear MDSC (PMN-MDSC) and monocytic MDSC (M-MDSC) (6, 7). These cells, by expanding and activating within the TME, create an immunosuppressive environment that promotes cancer development by undermining innate and adaptive immune responses (8). In humans, MDSCs produce immunosuppressive cytokines, including TGF-β, IL-10, arginase 1, PGE2 (9, 10), stimulating regulatory T cells (11). High MDSC concentrations have been linked to unfavorable outcomes in various cancers (12–14). The microenvironment of prostate cancer varies

due to the differences in hormone sensitivity; however, not all aspects have been fully elucidated (15). Therefore, clarifying the contribution of MDSCs is crucial for understanding the mechanism behind the acquisition of castration resistance in prostate cancer.

Several human studies on prostate cancer and MDSC subtypes have been conducted. A previous study reported elevated M-MDSC levels in patients with CRPC as compared with those in a healthy group (16). Another study on M-MDSC and prognosis in patients with CRPC reported that increased M-MDSC was associated with a poor prognosis (17). A previous survival analysis involving mCRPC patients showed that patients without elevated M-MDSC level after treatment had prolonged overall survival (OS) (18). Contrarily, the PMN-MDSC levels in prostate cancer patients correlated with advanced cancer stages and predicted poorer outcomes (19). A recent study on mHSPC patients indicated that PMN-MDSC is a negative prognostic indicator, whereas M-MDSC seemed to have no significant impact (20). Notably, no detailed studies have examined the background factors associated with MDSC subtype levels by classifying the prostate cancer patients according to hormone sensitivity and metastasis. Moreover, research comparing the prognostic value of the two MDSC subtypes in mCRPC patients is lacking. A recent meta-analysis explored the prognostic impact of circulating MDSC levels in patients with prostate cancer, and reported that those with high circulating MDSC levels had poorer prognosis as compared to those with lower MDSC levels (21). However, notable inconsistencies exist in defining the cutoff value across studies, with some studies employing methods such as median or mean while others use techniques such as Cox regression. This lack of standardization complicates the effective comparison of results among studies. Furthermore, as some studies did not identify the MDSC subtypes while others focused solely on M-MDSCs or PMN-MDSC, the absence of MDSC subtypes identification remains as a challenge (16–19, 21, 22). This inconsistency in reporting hampers the comprehensive understanding of the roles and impacts of MDSC.

The present research aimed to assess the association between MDSC subtypes and prostate cancer progression, considering hormone sensitivity and metastasis. Additionally, we also sought to evaluate the association of MDSC subtypes with prostate cancer prognosis.

Abbreviations: ADT, Androgen deprivation therapy; AUC, Area under the curve; BMI, Body mass index; CI, Confidence intervals; CRPC, Castration-resistant prostate cancer; HR, Hazard ratios; MDSC, Myeloid-derived suppressor cell; OS, Overall survival; PBMC, Peripheral blood mononuclear cells; PSA, Prostate specific antigen; ROS, Reactive oxygen species.

2 Materials and methods

2.1 Patients and data collection

Patients with prostate cancer who provided consent to participate in this study from August 2019 and March 2023 at Juntendo University (Tokyo, Japan) were included. Patients with normalized prostate specific antigen (PSA) levels after 3 months of ADT with a GnRH antagonist (degarelix) or untreated patients were diagnosed with mHSPC and included in the study. CRPC was defined by a castrate serum testosterone level of <50 ng/dl or 1.7 nmol/l, along with either three consecutive PSA increases occurring at least 1 week apart resulting in at least two ≥50% increases over the nadir, with a PSA level of ≥2.0 ng/ml, or the appearance of new lesions on radiologic imaging (23). The patients who lacked prostate cancer activity and MDSC data and those with nmCRPC were excluded from the analysis.

For each patient, data on their age and body mass index (BMI), presented as mean ± standard deviation, were gathered. Given the nonparametric nature of the initial PSA (iPSA) levels, they were expressed as medians along with their respective ranges. For subsequent analysis, the patients were categorized into two groups with age of 70 years as the cutoff, BMI of 25 kg/m^2 as the cutoff, and iPSA of 20 ng/mL as the cutoff. Additionally, we used the Gleason scoring system to assess the invasiveness of prostate cancer, classifying the patients into two groups based on scores of ≤7 and ≥8.

The assessment of the presence of metastases encompassed various sites, including bone, distant lymph nodes, and lung/liver/other sites during blood collection. Additionally, each patient's treatment history, other than ADT, prior to blood sampling was recorded. This included a variety of treatments, including radical prostatectomy; radiation therapy [radium-223 and intensity modulated radiation therapy (IMRT)], heavy particle radiation, and postoperative salvage; androgen receptor axis targeted therapy (enzalutamide, abiraterone, apalutamide, and darolutamide); and chemotherapy, including docetaxel and cabazitaxel.

The study was conducted in accordance with the Declaration of Helsinki, and approved by the Institutional Review Board of the Juntendo University Institutional Review Board (protocol code: M19–0158 and H20–0187, date of approval: Nov. 1, 2019 and Sep. 11, 2020). Written informed consent was obtained from the patients to publish this paper.

2.2 MDSC measurement

MDSCs were detected from fresh peripheral blood mononuclear cells (PBMC), isolated from peripheral blood by density gradient centrifugation using Histopaque®-1077 (Sigma-Aldrich, Missouri, United States). PMN-MDSCs are particularly sensitive to cryopreservation; thus, the assays of MDSC were performed using fresh samples immediately on the day of sample collection (24, 25). Altogether, 1.0×10^6 single cells were suspended in 100-μl PBS and incubated with a FcR blocking reagent (Biolegend, California, United States) for 15 minutes at a room temperature, followed by an appropriate concentration of fluorescent-conjugated antibody in 100-μl PBS for 15 minutes at 4°C. PMN-MDSC and M-MDSC were characterized as HLA-DR$^{low/-}$ CD33$^+$ CD15$^+$ CD14$^-$ and HLA-DR$^{low/-}$ CD33$^+$ CD15$^-$ CD14$^+$ as a percentage of live cells in the total PBMC, respectively. The fluorochrome-labeled antibodies used for detecting cell surface antigens were CD14-PerCP-Cy5.5, CD15-APC-Cy7, CD33-PE-Cy7, and HLA-DR-PE-Texas Red (Biolegend, California, United States). The labeled cells were washed twice and resuspended in 500-μL buffer with DAPI (1 μg/mL). FACS data were acquired using the BD® LSR II Flow Cytometer (BD Biosciences, California, United States) with BD FACSDiva™ software and analyzed using Flowjo software (Tree Star Incs, Oregon, United States). The gating strategy for MDSC is presented in Figure 1.

2.3 Statistical analysis

The missing values were handled by excluding cases with any missing data in our analysis. This approach resulted in the use of a
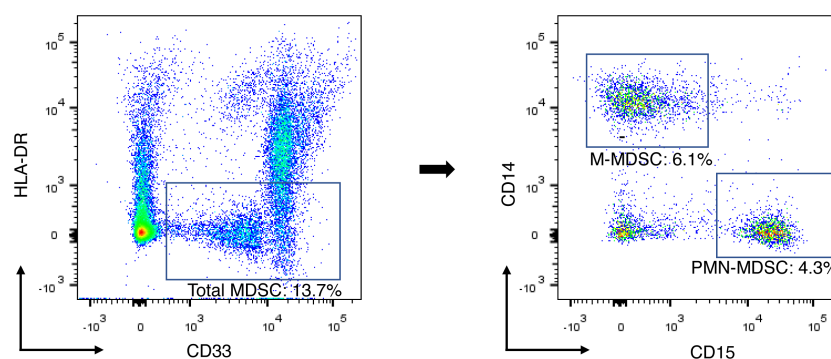
FIGURE 1
Gating strategy for identification of MDSC subsets and example of flow cytometry data. Total-MDSC, PMN-MDSC, and M-MDSC were characterized as HLA-DR$^{low/-}$ CD33$^+$, HLA-DR$^{low/-}$ CD33$^+$ CD15$^+$ CD14$^-$, and HLA-DR$^{low/-}$ CD33$^+$ CD15$^-$ CD14$^+$, respectively. Each population of the MDSC subsets was presented as a percentage of the total PBMCs. M-MDSC, monocytic myeloid-derived suppressor cell; PBMC, peripheral blood mononuclear cell; PMN-MDSC, polymorphonuclear myeloid-derived suppressor cell.

complete-case dataset for all statistical analyses. The proportions of M-MDSC and PMN-MDSC, which are MDSC subtypes, were treated as nonparametric data. We compared these proportions using Mann–Whitney's U test to explore their relationship with the patients' characteristics, including hormone sensitivity and cancer metastasis. This analysis aimed to understand relation of the M-MDSC and PMN-MDSC levels with cancer progression, particularly in the context of hormone sensitivity and metastasis. For prognostic association analysis, M-MDSC and PMN-MDSC values were divided into two groups using the Youden index (sensitivity + specificity − 1): M-MDSC$_{low/high}$ and PMN-MDSC$_{low/high}$.

The Kaplan–Meier method was used to assess OS for all patients. Log-rank tests were used to compare the survival curves by prostate cancer progression and MDSC level. Additionally, hazard ratios (HRs) were estimated using the Cox proportional hazards model, with all confidence intervals (CI) at the 95% level. In addition to the univariate analysis, multiple models were created to adjust for potential confounders. In Model 1, age was treated as a category and adjusted for. Model 2 was adjusted for BMI as a category in addition to Model 1. Model 3 was further adjusted for the presence of bone metastases and chemotherapy effects, in addition to model 2. For further sensitivity analysis, Model 3 was adjusted for potential confounding between M-MDSC and PMN-MDSC.

For all analyses, a two-tailed P value of <0.05 was considered statistically significant. When comparing three groups, a corrected P value accounting for multiple comparisons (P = 0.05/3) was deemed statistically significant. All statistical analyses were performed using the R language, version 4.3.0 (R Foundation for Statistical Computing, Vienna, Austria).

3 Results

3.1 Patient characteristics

During the study period, 119 prostate cancer patients were assessed (Figure 2). One patient could not be evaluated due to indeterminate disease status, two were unable to provide MDSC data, and one patient with non-metastatic CRPC was excluded due to insufficient data for analysis. After applying the exclusion criteria, the final patient cohort comprised of 115 individuals, who were
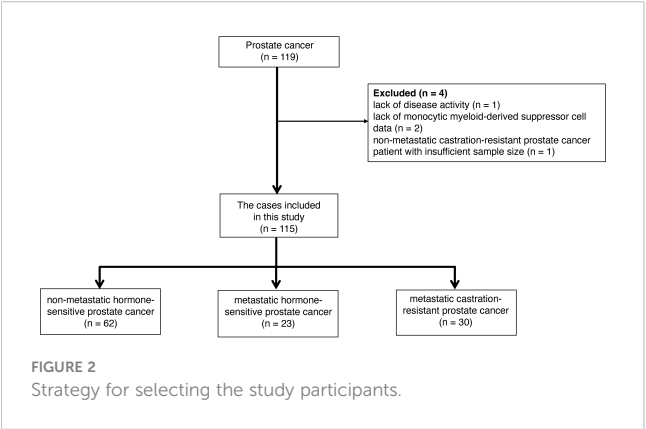
TABLE 1   Patients' baseline characteristics.

Variables	nmHSPC (n = 62)	mHSPC (n = 23)	mCRPC (n = 30)
Age, years, mean ± SD	70.1 ± 7.7	70.2 ± 6.7	70.8 ± 9.4
<70, n(%)	28 (45.2)	7 (30.4)	11 (36.7)
≥70, n(%)	34 (54.8)	16 (69.6)	19
BMI, kg/m², mean ± SD	24.1 ± 3.1	23.9 ± 3.5	22.2 ± 2.2
<25, n (%)	44 (71.0)	7 (30.4)	24 (80.0)
≥25, n (%)	18 (29.0)	16 (69.6)	5 (20.0)
iPSA, ng/mL, median(range)	8.8 (3.4–57.1)	107.4 (8.6–3025.0)	53.0 (2.8–9556.8)
<20, n(%)	53 (85.5)	3 (13.0)	11 (36.7)
≥20, n(%)	8 (12.9)	19 (82.6)	18 (60.0)
Gleason score			
<8, n(%)	43 (69.4)	2 (8.7)	7 (23.3)
≥8, n(%)	19 (30.6)	21 (91.3)	22 (73.3)
Metastatic sites			
Bone, n (%)	–	21 (91.3)	26 (86.7)
Distant lymph nodes, n (%)	–	6 (26.1)	11 (36.7)
Lung/Liver/Others, n (%)	–	9 (39.1)	10 (33.3)
Prior additional treatments to ADT			
Radical prostatectomy, n (%)	0 (0.0)	0 (0.0)	8 (26.7)
Radiation, n (%)	1 (1.6)	1 (4.3)	14 (46.7)
ARAT, n (%)	0 (0.0)	2 (8.7)	25 (83.3)
Chemotherapy, n (%)	0 (0.0)	0 (0.0)	12 (40.0)
None, n (%)	61 (98.4)	16 (69.6)	0 (0.0)

ADT, androgen deprivation therapy; ARAT, Androgen Receptor Axis Targeted; BMI, Body Mass Index; SD, standard deviation; iPSA, initial prostate specific antigen; mCRPC, metastatic castration-resistant prostate cancer; mHSPC, metastatic hormone-sensitive prostate cancer; nmHSPC, non-metastatic hormone-sensitive prostate cancer; SD, standard deviation.

categorized in non-metastatic hormone-sensitive prostate cancer (nmHSPC, n = 62), metastatic hormone-sensitive prostate cancer (mHSPC, n = 23), and metastatic castration-resistant prostate cancer (mCRPC, n = 30) groups. The detailed demographic and clinical characteristics of these patients are presented in Table 1.

3.2 MDSC levels and prostate cancer progression

We investigated the distribution of MDSC percentages in total PBMCs across different disease states. Notably, the median PMN-MDSC percentages were 0.50% (0.10%–4.73%) for nmHSPC, 0.59% (0.04%–12.50%) for mHSPC, and 1.24% (0.02%–14.40%) for mCRPC, revealing a significant increase in mCRPC (Figure 3A). These findings suggest that the MDSC levels may correlate with disease aggressiveness, particularly evident from the significant differences observed between nmHSPC and mCRPC (P = 7.73 × 10^{-5}) and between mHSPC and mCRPC (P = 0.0014).
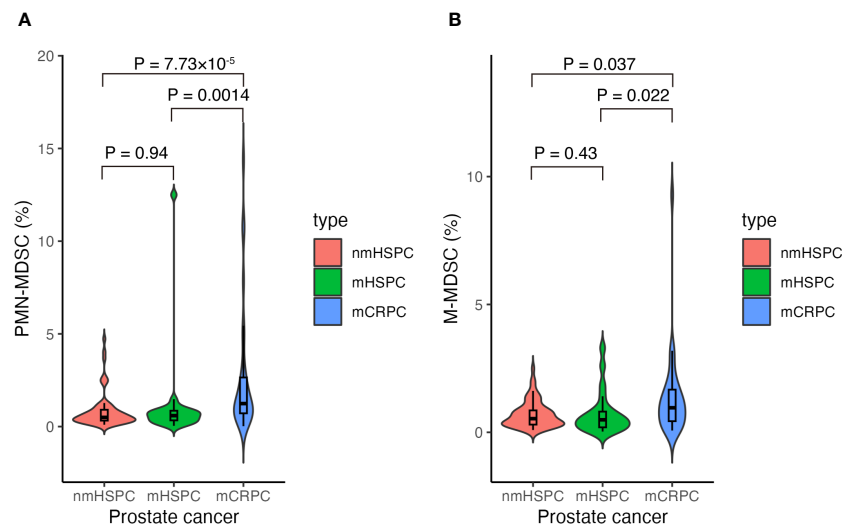
FIGURE 3
Violin and box plots of the percentage of MDSCs according to prostate cancer type. **(A)** PMN-MDSCs and prostate cancer. **(B)** M-MDSCs and prostate cancer. The x-axis shows prostate cancer disease status, whereas the y-axis shows the percentage of MDSCs in the total PBMCs. Differences were considered significant when p <0.05. mCRPC, metastatic castration-resistant prostate cancer; mHSPC, metastatic hormone-sensitive prostate cancer; nmHSPC, non-metastatic hormone-sensitive prostate cancer; M-MDSC, monocytic myeloid-derived suppressor cell; PBMC, peripheral blood mononuclear cell; PMN-MDSC, polymorphonuclear myeloid-derived suppressor cell.

The median values for M-MDSCs demonstrated an upward trend with disease progression; however, statistical significance was not maintained after adjusting for multiple testing (i.e., P > 0.05/3), highlighting the requirement for further investigation into their role across prostate cancer stages (Figure 3B).

3.3 Factors impacting the MDSC levels

Factors such as age, BMI, Gleason score, and iPSA were analyzed to understand their impact on MDSC percentages across the different prostate cancer stages (Figures 4A–D, 5A–D). The relationship between metastasis and MDSC was exclusively explored in the mHSPC and mCRPC groups (Figures 4E–G, 5E–G). Furthermore, the association between additional treatment history and MDSC was solely assessed within the mCRPC group (Figures 4H–K, 5H–K).

Within the mCRPC group, younger patients showed a significantly higher M-MDSC percentage, with those aged <70 years having a median value of 1.43% (0.23%–9.29%), as compared to 0.77% (0.07%–3.19%) for those aged ≥70 years (P = 0.016) (Figure 5A). Additionally, a higher BMI was correlated with increased M-MDSC levels, with median values of 0.83% (0.07%–9.29%) and 1.81% (0.90%–3.19%) for BMI of <25 and ≥25 kg/m², respectively (P = 0.043) (Figure 5B). These associations were not observed in the nmHSPC and mHSPC groups.

3.4 Survival outcomes and MDSC levels

The median survival durations for the nmHSPC and mHSPC group were 834 (71–994) and 732 (28–949) days, respectively. Conversely, the mCRPC group displayed a notably shorter median survival duration of 262 (10–1059) days. Throughout the observation period, no mortality events were noted in either the nmHSPC or mHSPC group. However, in the mCRPC group, 15 deaths were confirmed out of the 30 patients (Figure 6A). Given these observations, further analysis was undertaken, focusing on the PMN-MDSC and M-MDSC levels in the patients with mCRPC.

Using the Youden index to identify the optimal threshold for the area under the curve (AUC) of MDSC, the PMN-MDSC percentage of 2.135% showed a sensitivity of 86.7% and a specificity of 53.3% (Supplementary Figure 1). Conversely, the M-MDSC percentage of 1.365% presented a sensitivity of 46.7% and a specificity of 80.0% (Supplementary Figure 2).

For the PMN-MDSC subgroups, the median survival durations were 159 and 768 days for the PMN-MDSC$_{low}$ and PMN-MDSC$_{high}$ subgroups, respectively. A log-rank test indicated a significant difference in survival durations between these two subgroups (P = 0.018) (Figure 6B). However, no statistically significant (P = 0.11) difference in survival was observed between the M-MDSC$_{low}$ and M-MDSC$_{high}$ subgroups, which suggests that PMN-MDSC, but not M-MDSC, might be a more critical marker for poor prognosis among patients with mCRPC (Figure 6C).

3.5 Association between the subtypes based on the MDSC levels and prognosis

To assess the prognostic significance of MDSC subtypes in patients with prostate cancer, we utilized the Cox proportional hazards models and explored influence of different variables on the risk associated with high PMN-MDSC levels. Each model was defined and adjusted as follows: Model 1 was age-adjusted to provide a HR that isolates the effect of MDSC levels from the age
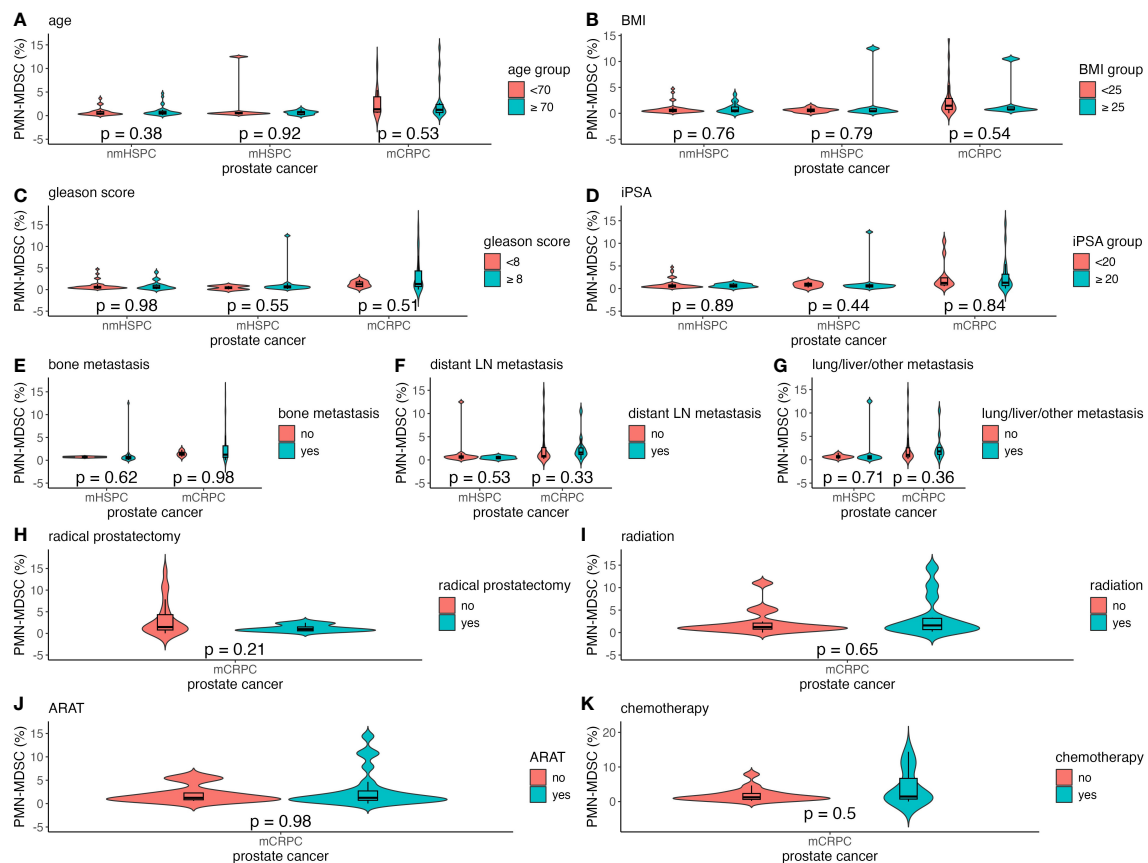
FIGURE 4
Violin and box plots of the percentage of PMN-MDSC by each factor in prostate cancer. **(A)** Age. **(B)** BMI. **(C)** Gleason score. **(D)** iPSA. **(E)** Bone metastases. **(F)** Distant lymph node metastases. **(G)** Lung/liver/other metastases. **(H)** Previous radical prostatectomy. **(I)** Previous radiation therapy. **(J)** Previous ARAT treatment. **(K)** Previous chemotherapy treatment. The x-axis indicates the comparison of prostate cancer disease status in the three groups, whereas the y-axis indicates the percentage of MDSCs in the total PBMCs. Differences were considered significant when p <0.05 within the respective figures. LN, lymph node; mCRPC, metastatic castration-resistant prostate cancer; mHSPC, metastatic hormone-sensitive prostate cancer; nmHSPC, non-metastatic hormone-sensitive prostate cancer; PBMC, peripheral blood mononuclear cell; PMN-MDSC, polymorphonuclear myeloid-derived suppressor cell.

factor; Model 2 extends this and includes adjustments for age and BMI that offers insights into impact of MDSC levels on the prognosis independent of these common confounders; and Model 3, our most comprehensive model, which incorporates adjustments for age, BMI, presence of bone metastases, and chemotherapy treatments. This model was designed to evaluate the influence of MDSC in the context of multiple clinically relevant factors.

Our findings suggest that patients with high PMN-MDSC levels consistently showed poorer outcomes across all models, which highlights the robustness of the prognostic value of PMN-MDSC. The results are presented in Table 2, which showed that the univariate HR for PMN-MDSC$_{high}$ patients was 3.41 (95% CI: 1.17–9.99, P = 0.025). The age-adjusted analysis (Model 1) yielded an HR of 3.64 (95% CI: 1.22–10.87, P = 0.021). In Model 2, adjusted for age and BMI, the HR was 4.62 (95% CI: 1.43–14.87, P = 0.010). Model 3, which further considered bone metastases and chemotherapy, showed an HR of 4.46 (95% CI: 1.34–14.85, P = 0.015).

Conversely, we observed a trend showing that higher M-MDSC levels might be associated with more favorable outcomes, although this finding was not statistically significant (Table 2). The univariate

HR was 0.37 (95% CI: 0.10–1.33, P = 0.13). The age-adjusted HR of Model 1 was 0.25 (95% CI: 0.06–1.00, P = 0.050). Model 2, which was adjusted for age and BMI, obtained an HR of 0.25 (95% CI: 0.06–1.02, P = 0.053). Model 3, which was further adjusted, showed an HR of 0.20 (95% CI: 0.04–0.99, P = 0.049).

To further investigate the potential of PMN-MDSC and M-MDSC as prognostic factors, a sensitivity analysis was conducted by incorporating both factors into Model 3 (Table 3). Higher PMN-MDSC levels were significantly associated with poorer outcomes, with an HR of 3.48 (95% CI: 1.05–11.56, P = 0.042). Contrarily, M-MDSC was not associated with prognosis (HR, 0.24; 95% CI: 0.04–1.41, P = 0.11). Additionally, we performed an analysis to examine the interaction between PMN-MDSC and M-MDSC (Table 4), which revealed no significant interaction between the two factors (P = 0.50).

4 Discussion

Our study examined the relationship between MDSCs and prostate cancer progression, focusing specifically on mCRPC. We
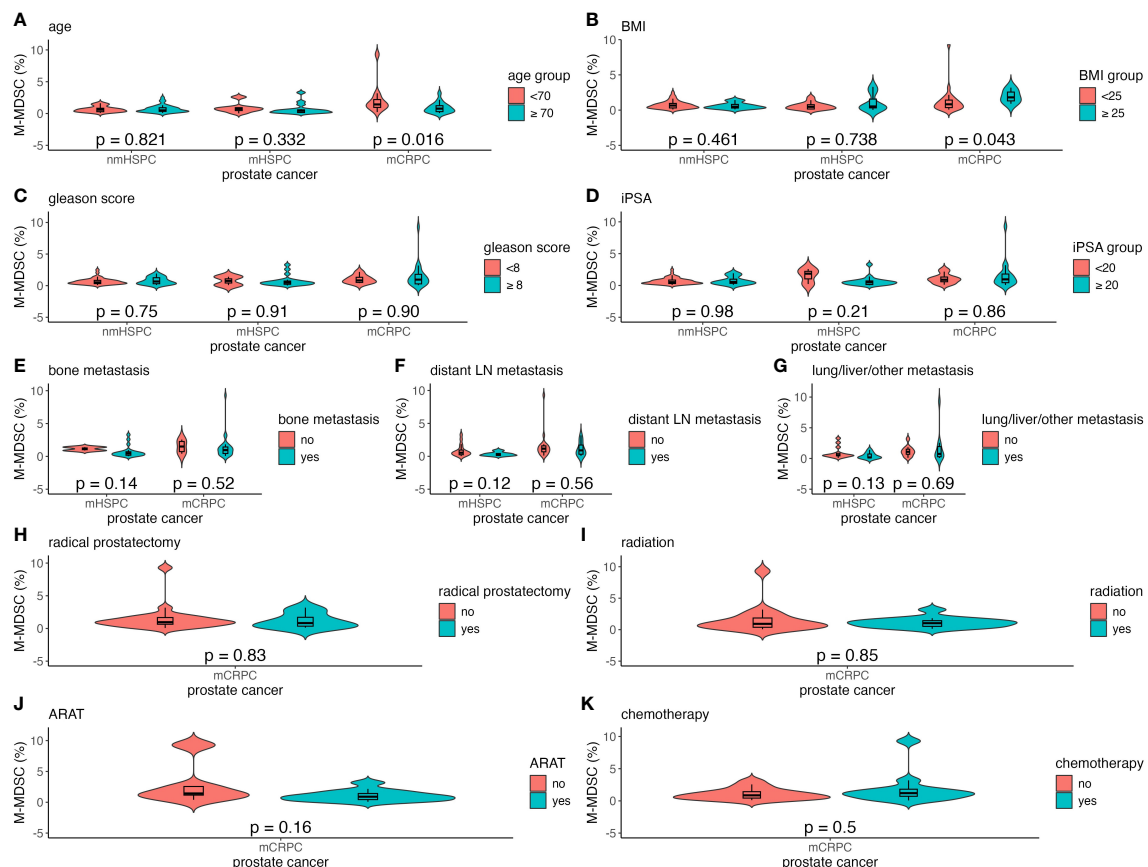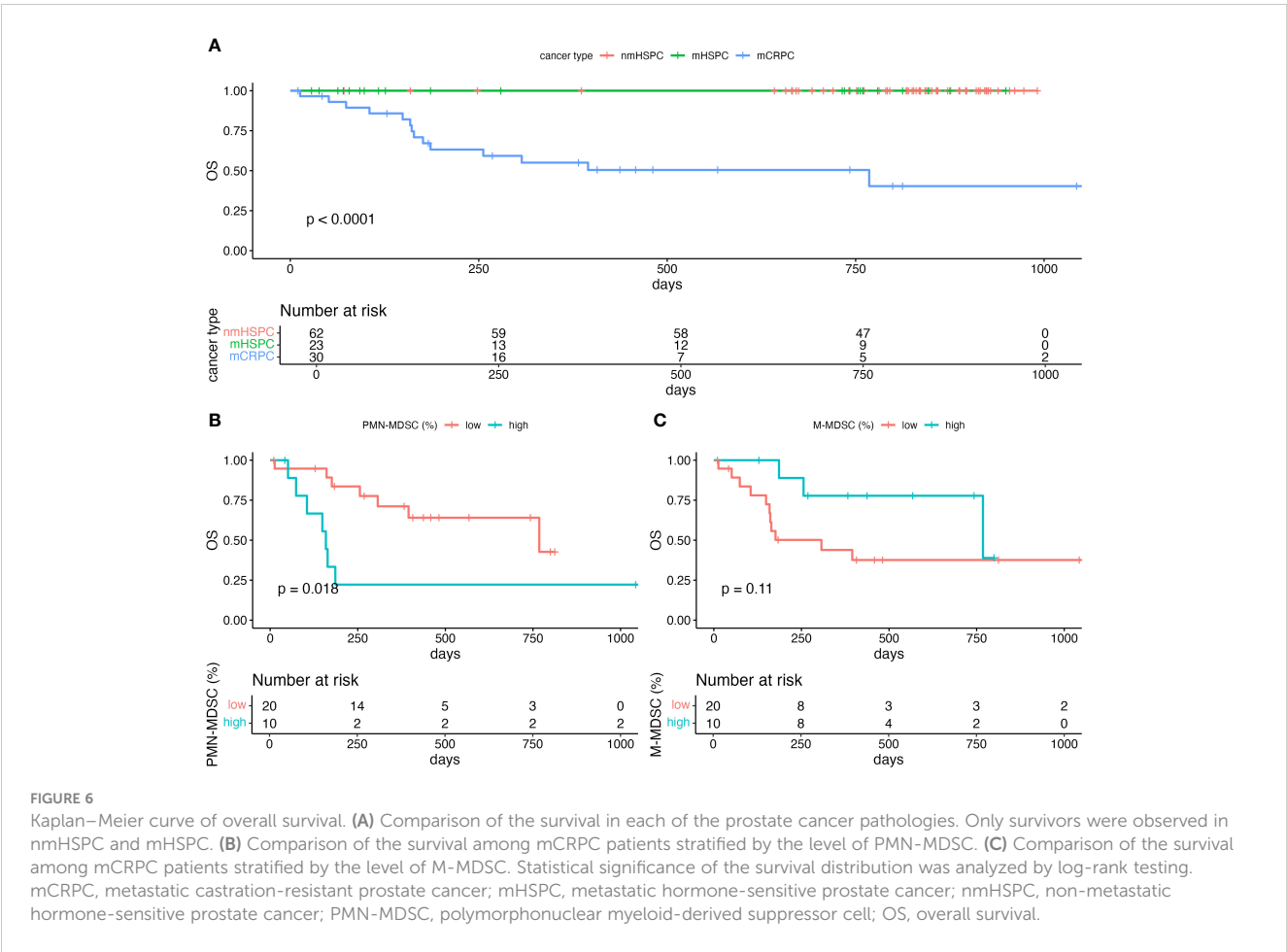
FIGURE 5
Violin and box plots of the percentage of M-MDSC by each factor in prostate cancer. **(A)** Age. **(B)** BMI. **(C)** Gleason score. **(D)** iPSA. **(E)** Bone metastases. **(F)** Distant lymph node metastases. **(G)** Lung/liver/other metastases. **(H)** Previous radical prostatectomy. **(I)** Previous radiation therapy. **(J)** Previous ARAT treatment. **(K)** Previous chemotherapy treatment. The x-axis indicates the comparison of prostate cancer disease status in the three groups, whereas the y-axis indicates the percentage of MDSCs in PBMCs. Differences were considered significant when p <0.05 within the respective figures. LN, lymph node; mCRPC, metastatic castration-resistant prostate cancer; mHSPC, metastatic hormone-sensitive prostate cancer; nmHSPC, non-metastatic hormone-sensitive prostate cancer; M-MDSC, monocytic myeloid-derived suppressor cell; PBMC, peripheral blood mononuclear cell.

found correlations between age, BMI, and M-MDSC levels in these patients; specifically, younger individuals and those with a higher BMI showed increased M-MDSC levels. In comparison to nmHSPC and mHSPC, the mCRPC was significantly increased in the PMN-MDSC. Additionally, to the best of our knowledge, this is the first report to identify an association between elevated PMN-MDSC levels and unfavorable outcomes in patients with mCRPC, highlighting the critical importance of MDSC measurement.

Aging has been recognized as a multifaceted process characterized by an increased accumulation of proinflammatory cytokines, concomitant with alterations in the composition and functionality of various immune cell types across the adaptive and innate immune spectra (26). The total MDSCs with age has been reported as a potential contributor to immunological abnormalities and pathologies observed in the elderly individuals (27). Verschoor et al. observed a significant increase in the frequency of total MDSCs and PMN-MDSCs in the elderly as compared to that observed in younger adults (28). Another study indicated that, although the total MDSC levels were higher in elderly individuals than in younger patients, the M-MDSC levels were significantly

higher in the younger group, partially aligning with the findings of our study (29). This could imply that robust immune responses, perhaps more reactive to tumor antigens, might drive the compensatory upregulation of M-MDSCs as a mechanism to mitigate excessive inflammation in younger patients. Alternatively, the aggressive nature of tumors in younger individuals could directly and more profoundly stimulate M-MDSC expansion, reflecting a dynamic and aggressive tumor–immune interaction.

We observed elevated M-MDSC levels among the mCRPC patients with a higher BMI. Interestingly, this correlation was not evident with PMN-MDSC. This observation aligns with findings from previous studies that reported an association between increased BMI and higher M-MDSC levels, even in individuals without metabolic abnormalities (30). M-MDSCs were found to be expanded in obese/overweight Chinese men; however, the cohort size was very small, consisting of only eight normal controls and eight obese/overweight patients (30). In another study involving 27 normal-weight, 23 overweight, and 60 obese individuals, obese individuals were found to have higher M-MDSC levels (31).

FIGURE 6
Kaplan−Meier curve of overall survival. **(A)** Comparison of the survival in each of the prostate cancer pathologies. Only survivors were observed in nmHSPC and mHSPC. **(B)** Comparison of the survival among mCRPC patients stratified by the level of PMN-MDSC. **(C)** Comparison of the survival among mCRPC patients stratified by the level of M-MDSC. Statistical significance of the survival distribution was analyzed by log-rank testing. mCRPC, metastatic castration-resistant prostate cancer; mHSPC, metastatic hormone-sensitive prostate cancer; nmHSPC, non-metastatic hormone-sensitive prostate cancer; PMN-MDSC, polymorphonuclear myeloid-derived suppressor cell; OS, overall survival.

Evidence from mouse studies suggests that obesity-induced inflammation prompts macrophages to produce IL-6, resulting in the elevation of MDSC levels characterized by CD45^{+}, CD11b^{+}, Ly6G, and Ly6C^{+} markers [32]. Additionally, hypoxic environments within tumors lead to IL-6 overexpression, specifically in malignant cells, resulting in the expansion of

TABLE 2 Prognostic factor analysis of MDSCs using univariate and multivariate Cox regression models.

Subsets of MDSC	Model	HR (95%CI)	P value
PMN-MDSC	univariate	3.41 (1.17–9.99)	0.025
	Model 1	3.64 (1.22–10.87)	0.021
	Model 2	4.62 (1.43–14.87)	0.01
	Model 3	4.46 (1.34–14.85)	0.015
M-MDSC	univariate	0.37 (0.10–1.33)	0.13
	Model 1	0.25 (0.06–1.00)	0.05
	Model 2	0.25 (0.06–1.02)	0.053
	Model 3	0.20 (0.04–0.99)	0.049

Model 1: adjusted with age group, Model 2: adjusted with age group and BMI group, Model 3: adjusted with age group, BMI group, chemotherapy and bone metastasis. CI, confidence interval; HR, hazard ratio; M-MDSC, monocytic myeloid-derived suppressor cell; PMN-MDSC, polymorphonuclear myeloid-derived suppressor cell.

MDSCs expressed as Gr1^{+}/CD11b^{+} in tumors [33]. Adipose tissue, which is a characteristic of obesity, is known to foster chronic inflammation, potentially inducing an overproduction of leptin. This leptin overproduction can possibly stimulate the accumulation of PMN-MDSC and M-MDSC in the bloodstream and solid tumors [34]. These obesity-induced PMN-MDSCs and M-MDSCs are implicated in suppressing tumor-reactive T cells and obstructing the entry of activated T cells into the TME, thereby promoting tumor proliferation. Furthermore, obesity in adulthood has been linked with worse outcomes among patients with prostate cancer, increasing their risk of developing advanced-stage disease, higher rates of recurrence, and greater cancer-specific mortality rates after diagnosis [35]. A comprehensive meta-analysis has shown a 15% increase in the risk of fatal prostate cancer and 20% increase in prostate cancer-specific mortality for every 5-kg/m² increase in BMI [36]. These findings suggest that the influence of obesity on prostate cancer prognosis may be mediated partly by its effect on the M-MDSC levels and function, further complicating the interplay between metabolic health and cancer progression.

Our findings indicate that the increase in the PMN-MDSC levels is more closely associated with the acquisition of hormonal resistance than with the presence or absence of metastasis. This insight advances beyond the findings a previous study, which primarily reported a link between PMN-MDSC levels and prostate cancer stage [19]. Although the mechanisms underlying

TABLE 3 Sensitivity analysis of the association between prognosis and MDSCs using multivariate Cox proportional hazards models.

Variables	HR (95%CI)	P value
PMN-MDSC	3.48 (1.05–11.56)	0.042
M-MDSC	0.24 (0.04–1.41)	0.11
Age	0.36 (0.07–1.74)	0.20
BMI	0.35 (0.05–2.62)	0.30
Bone metastasis	6.05 (0.47–78.59)	0.17
chemotherapy	3.25 (0.63–16.93)	0.16

BMI, Body Mass Index; CI, confidence interval; HR, hazard ratio; M-MDSC, monocytic myeloid-derived suppressor cell; PMN-MDSC, polymorphonuclear myeloid-derived suppressor cell.

CRPC are not yet fully understood, PMN-MDSCs are known to be an important subset of immune cells that invade the CRPC microenvironment (37). Additionally, PMN-MDSC-derived exosomes increase the level of a molecule called circMID1 in prostate cancer cells via its specific protein (37). This elevation triggers a series of molecular interactions that contribute to CRPC progression. Another mechanism is that mCRPC have different genomic sequences and AR signaling pathway alterations as compared to HSPCs (38–41). These differences may suggest a unique response of mCRPC patients to immune changes associated with aging and BMI as compared to those with hormone-sensitive prostate cancer.

The most significant outcome of this research is the identification of an association between PMN-MDSC levels and prognosis in patients with mCRPC, supported by robust statistical evidence. Contrarily, decreased M-MDSC levels showed a potential association with an adverse outcome. This dynamic is potentially rooted in the differentiation of M-MDSC to PMN-MDSC, a process believed to be driven by an epigenetic change involving histone deacetylase 2 (HDAC-2) acting on the retinoblastoma gene (Rb1) (42). HDAC overexpression in prostate cancer, which is crucial for functional androgen receptor signaling (43), suggests their influential role in PMN-MDSC and M-MDSC dynamics within mCRPC. Our study aligns with emerging research highlighting MDSC's critical role in prostate cancer progression. Specifically, MDSC-mediated IL-23 production bolsters

TABLE 4 Multivariate Cox proportional hazards model including the interaction between PMN-MDSC and M-MDSC.

Variables	HR (95%CI)	P value
PMN-MDSC	4.50 (1.08–18.65)	0.038
M-MDSC	0.31 (0.05–2.07)	0.23
PMN-MDSC * M-MDSC	0.34 (0.02–7.56)	0.50
Age	0.32 (0.06–1.58)	0.16
BMI	0.25 (0.03–2.20)	0.21
Bone metastasis	8.26 (0.54–126.30)	0.13
Chemotherapy	4.22 (0.72–24.78)	0.11

BMI, Body Mass Index; CI, confidence interval; HR, hazard ratio; M-MDSC, monocytic myeloid-derived suppressor cell; PMN-MDSC, polymorphonuclear myeloid-derived suppressor cell.

castration resistance by preserving AR signaling (44). The possibility that mCRPC patients with low M-MDSCs is associated with a worse prognosis suggests that the proportion of M-MDSCs in the total PBMC population may be relatively reduced because of progressive differentiation into PMN-MDSCs in the castration-resistant state. However, this association between M-MDSC and prognosis was not statistically significance in our analysis. Additionally, the sensitivity analysis did not reveal any interaction between PMN-MDSC and M-MDSC. Consequently, a future study involving a larger sample size may be required to elucidate the dynamics more comprehensively between M-MDSC and PMN-MDSC.

M-MDSCs are characterized by their high suppressive activity, primarily through nitric oxide (NO) production via the inducible nitric oxide synthase (iNOS) (45–47). Contrarily, PMN-MDSCs exert their immunosuppressive effects through different pathways, primarily involving reactive oxygen species (ROS) and peroxynitrite (PNT) productions, mediated by enzymes like nox2 and endothelial NO synthase (nos3) (48). The association of elevated PMN-MDSC levels with poorer outcomes among mCRPC patients underscores the evolving and complex interplay of these cell types in cancer immunology and progression. A previous study identified significant infiltration of PMN-MDSCs, particularly in the stromal compartments of primary and metastatic prostate cancers, with a greater infiltration noted in the stromal areas of the metastatic sites than in the primary tumors (49). These findings underscore the role of the stroma as a significant reservoir for PMN-MDSCs, supporting their involvement in promoting vascularization, immune evasion, and possibly metastatic progression of prostate cancer. In mCRPCs, where patients often exhibit advanced disease characterized by high tumor burden and immune evasion, circulating PMN-MDSCs may serve as a herald of heightened immunosuppressive activity within tumors. The infiltration patterns described in the previous study suggest that these cells, once recruited to the tumor stroma, contribute significantly to the creation of an immunosuppressive niche that protects tumor cells from immune surveillance and facilitates tumor growth and metastasis (49).

Our study addresses several critical gaps identified in the current MDSC research in prostate cancer, particularly mCRPC. Although previous studies have highlighted significant limitations due to model fidelity, immune system discrepancies between species, technical challenges in MDSC profiling, and biological heterogeneity of prostate cancer, our research implemented robust methodologies to overcome these challenges and provide meaningful insights into the role of MDSCs in mCRPC progression (50). Additionally, recognizing the technical issues, including the impact of cryopreservation on MDSC phenotyping and functional assays, our study strictly utilized fresh blood samples, which were processed within 4 hours of collection (24). This approach ensures the reliability of our study findings related to MDSC phenotypes and functions, addressing the concerns raised about the potential biases introduced by sample handling and preservation. As previous studies have reported the need for more homogeneous patient groups, this study carefully selected participants based on well-defined criteria of disease state, from nmHSPC and mHSPC to mCRPC. This stratification allows for a meticulous understanding of MDSC dynamics across different

stages of prostate cancer progression, enhancing the generalizability of our findings within each specific context.

However, our study presents several limitations. First, the causative relationship between elevated MDSC levels in mCRPC patients, as compared to mHSPC patients, remains unclear. Our analysis was constrained due to the limited number of included mHSPC patients who transitioned to mCRPC within our study duration. Second, mCRPC patients have undergone various treatment lines, making it impossible to standardize the baseline. Therefore, although we adjusted for confounding factors through a multivariate analysis, further research is necessary to determine the appropriate timing for MDSC measurement. Third, sample size determination in our study was based on consecutive inclusion within a predefined time frame rather than being calculated explicitly for statistical power. Thus, the absence of random sampling or randomization may introduce a selection bias, potentially impacting the validity and reliability of our findings. Additionally, the role of M-MDSCs in prostate cancer progression and prognosis is also complex. Despite observing a trend wherein higher M-MDSC levels might be associated with more favorable outcomes, these findings were not statistically significant; hence, it should be interpreted with caution. This highlights a potential limitation in the predictive value of M-MDSCs within our study cohort and underscores the need for further investigation in the future to clarify their biological impact and clinical utility in different stages of prostate cancer. Such studies could help in establishing the potential of M-MDSC levels as a reliable biomarker for determining prognosis or reflecting other underlying biological processes in the tumor microenvironment.

In conclusion, our study illuminates an association between PMN-MDSC levels and prognosis in patients with mCRPC and underscores the higher proportion of MDSCs in those with mCRPC than those with mHSPC. Further validation is required to see if the association can be replicated in other institutions and populations.

Data availability statement

The raw data supporting the conclusions of this article will be made available by the authors, without undue reservation.

Ethics statement

The studies involving humans were approved by the Juntendo University Institutional Review Board (protocol code: M19-0158 and H20-0187, date of approval: Nov. 1, 2019 and Sep. 11, 2020). The studies were conducted in accordance with the local legislation and institutional requirements. The participants provided their written informed consent to participate in this study.

Author contributions

TK: Writing – original draft, Conceptualization, Formal analysis, Funding acquisition, Methodology, Software,

Visualization, Writing – review & editing. MN: Conceptualization, Supervision, Writing – review & editing. TH: Investigation, Writing – review & editing. HW: Data curation, Investigation, Resources, Writing – review & editing. YI: Data curation, Formal analysis, Software, Validation, Writing – review & editing. KT: Data curation, Writing – review & editing. JL: Resources, Writing – review & editing. YJ: Resources, Writing – review & editing. YL: Formal analysis, Methodology, Resources, Software, Writing – review & editing. TC: Writing – review & editing. FS: Writing – review & editing, Supervision. HI: Supervision, Writing – review & editing. SH: Supervision, Writing – review & editing.

Funding

Acknowledgments

Conflict of interest

The authors declare that the research was conducted in the absence of any commercial or financial relationships that could be construed as a potential conflict of interest.

Publisher's note

All claims expressed in this article are solely those of the authors and do not necessarily represent those of their affiliated organizations, or those of the publisher, the editors and the reviewers. Any product that may be evaluated in this article, or claim that may be made by its manufacturer, is not guaranteed or endorsed by the publisher.

Supplementary material

The Supplementary Material for this article can be found online at: https://www.frontiersin.org/articles/10.3389/fimmu.2024.1372771/full#supplementary-material

References

1. James ND, Tannock I, N'Dow J, Feng F, Gillessen S, Ali SA, et al. The lancet commission on prostate cancer: planning for the surge in cases. *Lancet*. (2024) 403:1683–722. doi: 10.1016/S0140–6736(24)00651–2

2. Sung H, Ferlay J, Siegel RL, Laversanne M, Soerjomataram I, Jemal A, et al. Global cancer statistics 2020: globocan estimates of incidence and mortality worldwide for 36 cancers in 185 countries. *CA Cancer J Clin*. (2021) 71:209–49. doi: 10.3322/caac.21660

3. Rawla P. Epidemiology of prostate cancer. *World J Oncol*. (2019) 10:63–89. doi: 10.14740/wjon1191

4. Harris WP, Mostaghel EA, Nelson PS, Montgomery B. Androgen deprivation therapy: progress in understanding mechanisms of resistance and optimizing androgen depletion. *Nat Clin Pract Urol*. (2009) 6:76–85. doi: 10.1038/ncpuro1296

5. Marques RB, Dits NF, Erkens-Schulze S, van Weerden WM, Jenster G. Bypass mechanisms of the androgen receptor pathway in therapy-resistant prostate cancer cell models. *PloS One*. (2010) 5:e13500. doi: 10.1371/journal.pone.0013500

6. Gabrilovich DI, Nagaraj S. Myeloid-derived suppressor cells as regulators of the immune system. *Nat Rev Immunol*. (2009) 9:162–74. doi: 10.1038/nri2506

7. Movahedi K, Guilliams M, Van den Bossche J, Van den Bergh R, Gysemans C, Beschin A, et al. Identification of discrete tumor-induced myeloid-derived suppressor cell subpopulations with distinct T cell-suppressive activity. *Blood*. (2008) 111:4233–44. doi: 10.1182/blood-2007–07-099226

8. Kumar V, Patel S, Tcyganov E, Gabrilovich DI. The nature of myeloid-derived suppressor cells in the tumor microenvironment. *Trends Immunol*. (2016) 37:208–20. doi: 10.1016/j.it.2016.01.004

9. Filipazzi P, Valenti R, Huber V, Pilla L, Canese P, Iero M, et al. Identification of a new subset of myeloid suppressor cells in peripheral blood of melanoma patients with modulation by a granulocyte-macrophage colony-stimulation factor-based antitumor vaccine. *J Clin Oncol*. (2007) 25:2546–53. doi: 10.1200/jco.2006.08.5829

10. Obermajer N, Muthuswamy R, Lesnock J, Edwards RP, Kalinski P. Positive feedback between pge2 and cox2 redirects the differentiation of human dendritic cells toward stable myeloid-derived suppressor cells. *Blood*. (2011) 118:5498–505. doi: 10.1182/blood-2011–07-365825

11. Walter S, Weinschenk T, Stenzl A, Zdrojowy R, Pluzanska A, Szczylik C, et al. Multipeptide immune response to cancer vaccine ima901 after single-dose cyclophosphamide associates with longer patient survival. *Nat Med*. (2012) 18:1254–61. doi: 10.1038/nm.2883

12. Solito S, Falisi E, Diaz-Montero CM, Doni A, Pinton L, Rosato A, et al. A human promyelocytic-like population is responsible for the immune suppression mediated by myeloid-derived suppressor cells. *Blood*. (2011) 118:2254–65. doi: 10.1182/blood-2010–12-325753

13. Yang Z, Guo J, Weng L, Tang W, Jin S, Ma W. Myeloid-derived suppressor cells—New and exciting players in lung cancer. *J Hematol Oncol*. (2020) 13:10. doi: 10.1186/s13045–020-0843–1

14. Hao Z, Li R, Wang Y, Li S, Hong Z, Han Z. Landscape of myeloid-derived suppressor cell in tumor immunotherapy. *biomark Res*. (2021) 9:77. doi: 10.1186/s40364–021-00333–5

15. Yuen KCY, Tran B, Gibbs P, Anton A, Mariathasan S, Sandhu SK, et al. The tumor immune microenvironment differs between metastatic castrate resistant prostate cancer (Crpc) and hormone sensitive prostate cancer (Hspc). *J Clin Oncol*. (2019) 37:251. doi: 10.1200/JCO.2019.37.7_suppl.251

16. Idorn M, Kollgaard T, Kongsted P, Sengelov L, Thor Straten P. Correlation between frequencies of blood monocytic myeloid-derived suppressor cells, regulatory T cells and negative prognostic markers in patients with castration-resistant metastatic prostate cancer. *Cancer Immunol Immunother*. (2014) 63:1177–87. doi: 10.1007/s00262–014-1591–2

17. Santegoets SJ, Stam AG, Lougheed SM, Gall H, Jooss K, Sacks N, et al. Myeloid derived suppressor and dendritic cell subsets are related to clinical outcome in prostate cancer patients treated with prostate gvax and ipilimumab. *J Immunother Cancer*. (2014) 2:31. doi: 10.1186/s40425–014-0031–3

18. Koga N, Moriya F, Waki K, Yamada A, Itoh K, Noguchi M. Immunological efficacy of herbal medicines in prostate cancer patients treated by personalized peptide vaccine. *Cancer Sci*. (2017) 108:2326–32. doi: 10.1111/cas.13397

19. Chi N, Tan Z, Ma K, Bao L, Yun Z. Increased circulating myeloid-derived suppressor cells correlate with cancer stages, interleukin-8 and -6 in prostate cancer. *Int J Clin Exp Med*. (2014) 7:3181–92.

20. Kohada Y, Kuromoto A, Takeda K, Iwamura H, Atobe Y, Ito J, et al. Circulating pmn-mdsc level positively correlates with a poor prognosis in patients with metastatic hormone-sensitive prostate cancer. *Front Urol*. (2022) 2:967480. doi: 10.3389/fruro.2022.967480

21. Bronte G, Conteduca V, Landriscina M, Procopio AD. Circulating myeloid-derived suppressor cells and survival in prostate cancer patients: systematic review and meta-analysis. *Prostate Cancer Prostatic Dis*. (2023) 26:41–6. doi: 10.1038/s41391–022-00615–5

22. Karzai F, VanderWeele D, Madan RA, Owens H, Cordes LM, Hankin A, et al. Activity of durvalumab plus olaparib in metastatic castration-resistant prostate cancer in men with and without DNA damage repair mutations. *J Immunother Cancer*. (2018) 6:141. doi: 10.1186/s40425–018-0463–2

23. Cornford P, Bellmunt J, Bolla M, Briers E, De Santis M, Gross T, et al. Eau-estro-siog guidelines on prostate cancer. Part ii: treatment of relapsing, metastatic, and castration-resistant prostate cancer. *Eur Urol*. (2017) 71:630–42. doi: 10.1016/j.eururo.2016.08.002

24. Kotsakis A, Harasymczuk M, Schilling B, Georgoulias V, Argiris A, Whiteside TL. Myeloid-derived suppressor cell measurements in fresh and cryopreserved blood samples. *J Immunol Methods*. (2012) 381:14–22. doi: 10.1016/j.jim.2012.04.004

25. Trellakis S, Bruderek K, Hutte J, Elian M, Hoffmann TK, Lang S, et al. Granulocytic myeloid-derived suppressor cells are cryosensitive and their frequency does not correlate with serum concentrations of colony-stimulating factors in head and neck cancer. *Innate Immun*. (2013) 19:328–36. doi: 10.1177/1753425912463618

26. Rybtsova N, Berezina TN, Rybtsov S. Molecular markers of blood cell populations can help estimate aging of the immune system. *Int J Mol Sci*. (2023) 24:5708. doi: 10.3390/ijms24065708

27. Bueno V, Sant'Anna OA, Lord JM. Ageing and myeloid-derived suppressor cells: possible involvement in immunosenescence and age-related disease. *Age (Dordr)*. (2014) 36:9729. doi: 10.1007/s11357-014-9729-x

28. Verschoor CP, Johnstone J, Millar J, Dorrington MG, Habibagahi M, Lelic A, et al. Blood cd33(+)Hla-dr(-) myeloid-derived suppressor cells are increased with age and a history of cancer. *J Leukoc Biol*. (2013) 93:633–7. doi: 10.1189/jlb.0912461

29. Alves AS, Ishimura ME, Duarte YAO, Bueno V. Parameters of the immune system and vitamin D levels in old individuals. *Front Immunol*. (2018) 9:1122. doi: 10.3389/fimmu.2018.01122

30. Bao Y, Mo J, Ruan L, Li G. Increased monocytic cd14(+)Hladrlow/- myeloid-derived suppressor cells in obesity. *Mol Med Rep*. (2015) 11:2322–8. doi: 10.3892/mmr.2014.2927

31. Friedrich K, Sommer M, Strobel S, Thrum S, Bluher M, Wagner U, et al. Perturbation of the monocyte compartment in human obesity. *Front Immunol*. (2019) 10:1874. doi: 10.3389/fimmu.2019.01874

32. Hayashi T, Fujita K, Nojima S, Hayashi Y, Nakano K, Ishizuya Y, et al. High-fat diet-induced inflammation accelerates prostate cancer growth via il6 signaling. *Clin Cancer Res*. (2018) 24:4309–18. doi: 10.1158/1078–0432.CCR-18–0106

33. Hong J, Tobin NP, Rundqvist H, Li T, Lavergne M, Garcia-Ibanez Y, et al. Role of tumor pericytes in the recruitment of myeloid-derived suppressor cells. *J Natl Cancer Inst*. (2015) 107. doi: 10.1093/jnci/djv209

34. Ostrand-Rosenberg S. Myeloid derived-suppressor cells: their role in cancer and obesity. *Curr Opin Immunol*. (2018) 51:68–75. doi: 10.1016/j.coi.2018.03.007

35. Wilson KM, Giovannucci EL, Mucci LA. Lifestyle and dietary factors in the prevention of lethal prostate cancer. *Asian J Androl*. (2012) 14:365–74. doi: 10.1038/aja.2011.142

36. Cao Y, Ma J. Body mass index, prostate cancer-specific mortality, and biochemical recurrence: A systematic review and meta-analysis. *Cancer Prev Res (Phila)*. (2011) 4:486–501. doi: 10.1158/1940–6207.Capr-10–0229

37. Gao F, Xu Q, Tang Z, Zhang N, Huang Y, Li Z, et al. Exosomes derived from myeloid-derived suppressor cells facilitate castration-resistant prostate cancer progression via S100a9/circmid1/mir-506–3p/mid1. *J Transl Med*. (2022) 20:346. doi: 10.1186/s12967–022-03494–5

38. Castro E, Goh C, Olmos D, Saunders E, Leongamornlert D, Tymrakiewicz M, et al. Germline brca mutations are associated with higher risk of nodal involvement, distant metastasis, and poor survival outcomes in prostate cancer. *J Clin Oncol*. (2013) 31:1748–57. doi: 10.1200/jco.2012.43.1882

39. Robinson D, Van Allen EM, Wu YM, Schultz N, Lonigro RJ, Mosquera JM, et al. Integrative clinical genomics of advanced prostate cancer. *Cell*. (2015) 162:454. doi: 10.1016/j.cell.2015.06.053

40. Cancer Genome Atlas Research, N. The molecular taxonomy of primary prostate cancer. *Cell*. (2015) 163:1011–25. doi: 10.1016/j.cell.2015.10.025

41. Penning TM. Mechanisms of drug resistance that target the androgen axis in castration resistant prostate cancer (Crpc). *J Steroid Biochem Mol Biol*. (2015) 153:105–13. doi: 10.1016/j.jsbmb.2015.05.010

42. Youn JI, Kumar V, Collazo M, Nefedova Y, Condamine T, Cheng P, et al. Epigenetic silencing of retinoblastoma gene regulates pathologic differentiation of myeloid cells in cancer. *Nat Immunol*. (2013) 14:211–20. doi: 10.1038/ni.2526

43. Coulter JB, Easwaran H. Combining ezh2 and hdac inhibitors to target castration-resistant prostate cancers. *PloS Biol*. (2023) 21:e3002081. doi: 10.1371/journal.pbio.3002081

44. Calcinotto A, Spataro C, Zagato E, Di Mitri D, Gil V, Crespo M, et al. Il-23 secreted by myeloid cells drives castration-resistant prostate cancer. *Nature*. (2018) 559:363–9. doi: 10.1038/s41586–018-0266–0

45. Cuenca AG, Delano MJ, Kelly-Scumpia KM, Moreno C, Scumpia PO, Laface DM, et al. A paradoxical role for myeloid-derived suppressor cells in sepsis and trauma. *Mol Med*. (2011) 17:281–92. doi: 10.2119/molmed.2010.00178

46. Dolcetti L, Peranzoni E, Ugel S, Marigo I, Fernandez Gomez A, Mesa C, et al. Hierarchy of immunosuppressive strength among myeloid-derived suppressor cell subsets is determined by gm-csf. *Eur J Immunol*. (2010) 40:22–35. doi: 10.1002/eji.200939903

47. Haverkamp JM, Smith AM, Weinlich R, Dillon CP, Qualls JE, Neale G, et al. Myeloid-derived suppressor activity is mediated by monocytic lineages maintained by

continuous inhibition of extrinsic and intrinsic death pathways. *Immunity*. (2014) 41:947–59. doi: 10.1016/j.immuni.2014.10.020

48. Raber PL, Thevenot P, Sierra R, Wyczechowska D, Halle D, Ramirez ME, et al. Subpopulations of myeloid-derived suppressor cells impair T cell responses through independent nitric oxide-related pathways. *Int J Cancer*. (2014) 134:2853–64. doi: 10.1002/ijc.28622

49. Wen J, Huang G, Liu S, Wan J, Wang X, Zhu Y, et al. Polymorphonuclear mdscs are enriched in the stroma and expanded in metastases of prostate cancer. *J Pathol Clin Res*. (2020) 6:171–7. doi: 10.1002/cjp2.160

50. Koinis F, Xagara A, Chantzara E, Leontopoulou V, Aidarinis C, Kotsakis A. Myeloid-derived suppressor cells in prostate cancer: present knowledge and future perspectives. *Cells*. (2021) 11:20. doi: 10.3390/cells11010020

Regulatory and memory T lymphocytes infiltrating prostate tumors predict long term clinical outcomes

Oscar Eduardo Molina[1,2], Hélène LaRue[1,2], David Simonyan[3], Hélène Hovington[1,2], Benjamin Vittrant[1,2], Bernard Têtu[1,2,4], Vincent Fradet[1,2,5], Louis Lacombe[1,2,5], Alain Bergeron[1,2,5] and Yves Fradet[1,2,5]*

[1]Axe oncologie, Centre de recherche du CHU de Québec-Université Laval, Québec, QC, Canada, [2]Centre de recherche sur le cancer de l'Université Laval, Québec, QC, Canada, [3]Plateforme de recherche clinique et évaluative, Centre de recherche du CHU de Québec-Université Laval, Québec, QC, Canada, [4]Département de pathologie, CHU de Québec-Université Laval, Québec, QC, Canada, [5]Département de chirurgie, Université Laval, Québec, QC, Canada

Introduction: The localization, density but mostly the phenotype of tumor infiltrating lymphocytes (TIL) provide important information on the initial interaction between the host immune system and the tumor. Our objective was to assess the prognostic significance of T (CD3$^+$), T regulatory (T$_{reg}$) (FoxP3$^+$) and T memory (T$_{mem}$) (CD45RO$^+$) infiltrating lymphocytes and of genes associated with TIL in prostate cancer (PCa).

Methods: Immunohistochemistry (IHC) was used to assess the infiltration of CD3$^+$, FoxP3$^+$ and CD45RO$^+$ cells in the tumor area, tumor margin and adjacent normal-like epithelium of a series of 98 PCa samples with long clinical follow-up. Expression of a panel of 31 TIL-associated genes was analyzed by Taqman Low-Density Array (TLDA) technology in another series of 50 tumors with long clinical follow-up. Kaplan-Meier and Cox proportional hazards regression analyses were performed to determine association of these markers with biochemical recurrence (BCR), need for definitive androgen deprivation therapy (ADT) or lethal PCa.

Results: TIL subtypes were present at different densities in the tumor, tumor margin and adjacent normal-like epithelium, but their density and phenotype in the tumor area were the most predictive of clinical outcomes. In multivariate analyses, a high density of T$_{reg}$ (high FoxP3$^+$/CD3$^+$ cell ratio) predicted a higher risk for need of definitive ADT (HR=7.69, p=0.001) and lethal PCa (HR=4.37, p=0.04). Conversely, a high density of T$_{mem}$ (high CD45RO$^+$/CD3$^+$ cell ratio) predicted a reduced risk of lethal PCa (HR=0.06, p=0.04). TLDA analyses showed that a high expression of FoxP3 was associated with a higher risk of lethal PCa (HR=5.26, p=0.02). Expression of CTLA-4, PD-1, TIM-3 and LAG-3 were correlated with that of FoxP3. Amongst these, only a high expression of TIM-3 was associated with a significant higher risk for definitive ADT in univariate Cox regression analysis (HR=3.11, p=0.01).

Conclusion: These results show that the proportion of T_{reg} and T_{mem} found within the tumor area is a strong and independent predictor of late systemic progression of PCa. Our results also suggest that inhibition of TIM-3 might be a potential approach to counter the immunosuppressive functions of T_{reg} in order to improve the anti-tumor immune response against PCa.

1 Introduction

Prostate cancer (PCa) remains the second most commonly diagnosed cancer and the fifth cause of cancer death among men worldwide despite PCa screening and early effective treatments (1, 2). This may be due in part to the late systemic recurrences occurring after years of apparent PCa control in aging men who live longer, thanks to reduced competing cause of mortality. The management of PCa is challenging because this cancer is a highly heterogeneous disease (3, 4). Therapeutic options will vary considerably for patients with low-risk indolent PCa and those with high-risk life-threatening PCa. One major challenge lies in the adequate risk stratification to help select the most appropriate therapeutic strategy and avoid under or overtreatment (5). So far, the stratification of risk is based on clinico-pathological factors such as tumor grade (Gleason score) and stage (TNM), PSA level at diagnosis and presence of adverse pathological features at prostatectomy (6, 7). However, the risk of recurrence and progression and the response to treatments vary significantly between patients with otherwise similar clinico-pathological characteristics. Therefore, new biomarkers are needed to refine the prognostication and improve the management of PCa (8). Moreover, the most common endpoint of biomarker studies in PCa has been biochemical recurrence (BCR), but few studies have been able to relate biomarkers with long-term outcomes such as metastasis and mortality by PCa. It is even more challenging to identify biomarkers in the primary PCa that could lead to potential early interventions to reduce late PCa mortality.

The influence of the tumor microenvironment (TME) on the development and progression of cancer has gained greater interest during the last decade (9). The TME influences cancer evolution through diverse mechanisms including tumor differentiation, stimulation of angiogenesis and promotion of immune evasion

(10–12) Tumor-infiltrating lymphocytes (TIL) participate in the host defense against tumor cells but their antitumor activity is greatly hampered by the immunosuppressive factors found within the TME which favors immune evasion (13). Several studies have shown that the density, phenotype and localization of TIL are associated with clinical outcomes in various types of solid cancers and that their detailed analysis can provide important prognostic information (14, 15). The prognostic potential of TIL has been notably well demonstrated in colorectal cancers (CRC). Studies by Galon et al. have shown that TIL could predict better than TNM disease-free survival and overall survival of CRC patients (16, 17). These studies led to the development of the "Immunoscore" to complement the current TNM in order to better predict the risk of recurrence and even response to therapy of CRC patients (18–20).

While the prognostic potential of TIL has been well established in CRC and some other solid cancers, the study of the relationship between TIL and the clinical outcomes of PCa has provided inconsistent results (21–33). These inconsistencies may be due in part to differences in study designs, to various subtypes of TIL studied and their localization within the specimen and to the different methodologies used to measure them. The types of patients' cohorts and the length of their follow-up are also very important parameters to assess the clinical relevance of the findings. The most recent immunohistochemical (IHC) studies have focused on regulatory T (T_{reg}) cells using antibodies against the transcription factor FoxP3, the most specific biomarker of the T_{reg} cells. These studies showed an association between FoxP3$^+$ TIL and higher risk of BCR or death from PCa (25, 31, 34). However, very few studies have characterized the infiltration of prostate tumors by CD45RO$^+$ cells. CD45RO is a marker of central and effector memory T (T_{mem}) cells and is therefore associated with an effective immune response. In CRC, the combined analysis of CD45RO$^+$ T_{mem} cells and CD8$^+$ T cells in specific tumor areas helped predict cancer recurrence and patients' survival (17).

To further characterize the intra-tumoral immune response against PCa and assess the potential prognostic value of TIL, we analyzed the infiltration of CD3$^+$, FoxP3$^+$ and CD45RO$^+$ cells in the tumor core, tumor margin and the adjacent normal-like epithelium area in radical prostatectomy specimens from 98 PCa patients at increased risk of recurrence and with very mature long-term clinical

follow-up. We also analyzed the expression of 31 genes associated with TIL by qRT-PCR using TaqMan® Low Density Array (TLDA) technology in another set of 50 similar patients with fresh frozen radical prostatectomy. The combined results show that the balance between T_{mem} and T_{reg} infiltrating cells within the cancer is a strong independent predictor of systemic cancer progression and lethality by PCa. They also identify the immune checkpoint TIM-3 as a potential target to reverse T_{reg} dominant immunosuppression in PCa.
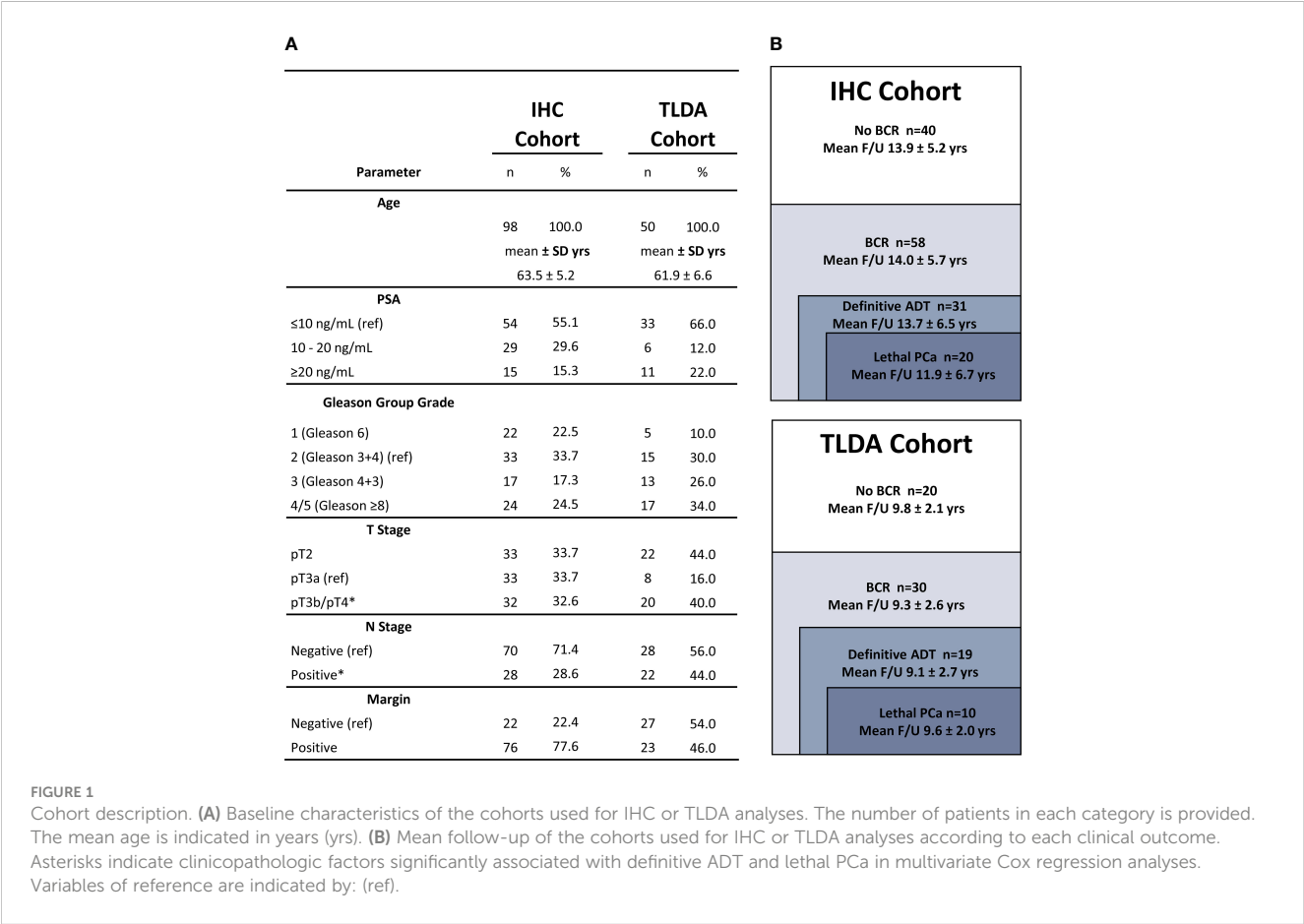
2 Results

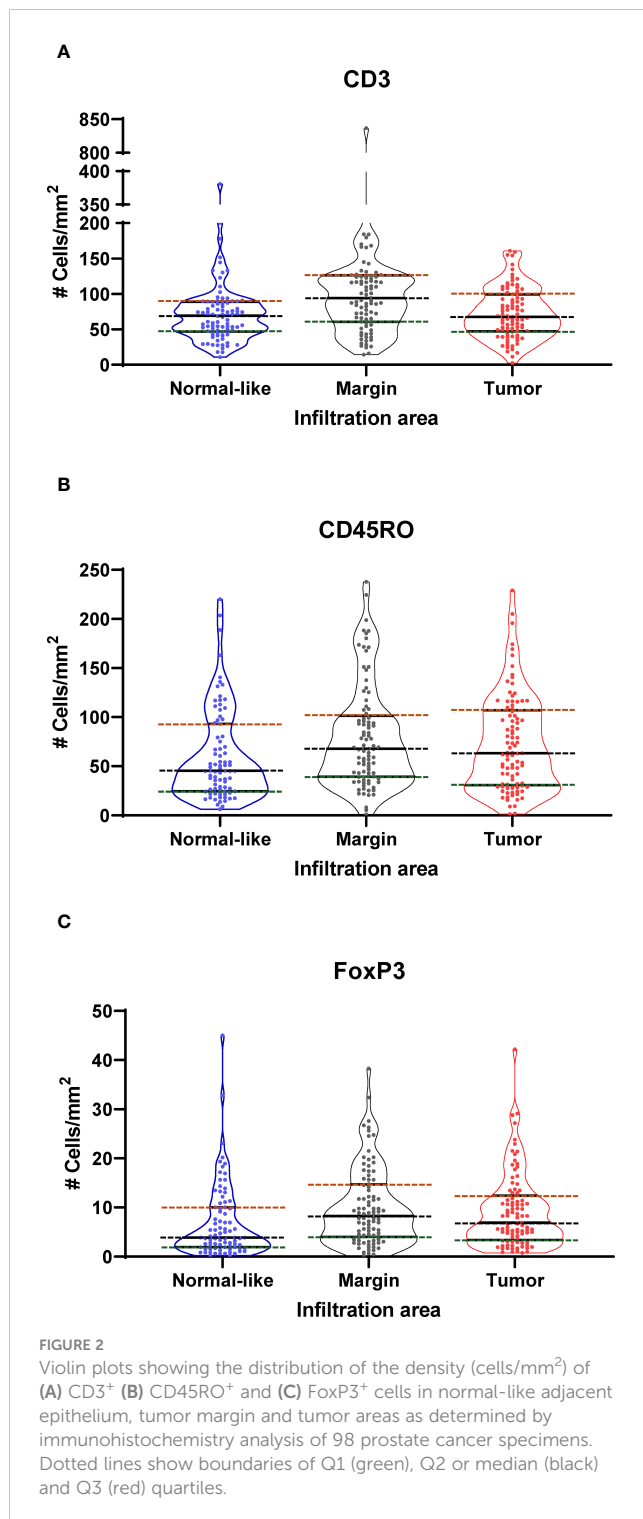## 2.1 Immunohistochemistry analyses

2.1.1 Cohort description

The infiltration by CD3$^+$, CD45RO$^+$ and FoxP3$^+$ lymphocytes was analyzed in a series of 98 prostatectomy specimen of PCa patients at increased risk of recurrence and progression and with a very long clinical follow-up (median of 15.5 years; mean of 14.0 years). Figure 1 shows the baseline characteristics of this cohort (IHC cohort). The long clinical follow-up of these tumors allows for a more accurate association of the markers with late clinical events. These events were defined as occurrence of a BCR, the need for continuous androgen-deprivation therapy (ADT) and lethal cancer defined as having a metastatic disease and/or castration-resistant

PCa (CRPC) and/or death from PCa. Multivariate Cox regression analyses were performed to assess the association between the age, PSA levels, Gleason Group Grade categories, stage categories and presence or not of positive surgical margins with each of the clinical endpoints. Supplementary Table S1 shows that pT3b/pT4 and lymph node invasion were independent predictors of definitive ADT and lethal PCa. Moreover, in this cohort, from the 98 patients, 58 experienced BCR at a median time of 6 years: 31 progressed to continuous ADT and 20 to lethal PCa. Of the other 27 BCR patients who did not progress to ADT or lethal PCa, 21 responded to salvage radiotherapy and 6 received short-term intermittent ADT.

2.1.2 Immunohistochemistry scoring

The number of positive cells per mm^2 was determined in the tumor area, at the tumor margin and in the adjacent normal-like epithelium (Supplementary Figure S1). Positive cells in tertiary lymphoid aggregates were not considered in the analysis. The evaluation of the infiltration in the tumor and the margin areas showed that the highest density of these positive cells was found at the tumor margin. A qualitative description of the infiltration for each type of positive cells is provided in Supplementary Data. The distribution of cell densities for each TIL subtype, in each compartment and for each patient is represented in Figure 2 with bars separating the data into quartiles. Examples of the staining obtained with the antibodies against CD3, CD45RO and FoxP3 are shown in Supplementary Figure S2.

A

Parameter	IHC Cohort n	IHC Cohort %	TLDA Cohort n	TLDA Cohort %
Age				
	98	100.0	50	100.0
	mean ± SD yrs		mean ± SD yrs	
	63.5 ± 5.2		61.9 ± 6.6	
PSA				
≤10 ng/mL (ref)	54	55.1	33	66.0
10 - 20 ng/mL	29	29.6	6	12.0
≥20 ng/mL	15	15.3	11	22.0
Gleason Group Grade				
1 (Gleason 6)	22	22.5	5	10.0
2 (Gleason 3+4) (ref)	33	33.7	15	30.0
3 (Gleason 4+3)	17	17.3	13	26.0
4/5 (Gleason ≥8)	24	24.5	17	34.0
T Stage				
pT2	33	33.7	22	44.0
pT3a (ref)	33	33.7	8	16.0
pT3b/pT4*	32	32.6	20	40.0
N Stage				
Negative (ref)	70	71.4	28	56.0
Positive*	28	28.6	22	44.0
Margin				
Negative (ref)	22	22.4	27	54.0
Positive	76	77.6	23	46.0

B

IHC Cohort

No BCR n=40
Mean F/U 13.9 ± 5.2 yrs

BCR n=58
Mean F/U 14.0 ± 5.7 yrs

Definitive ADT n=31
Mean F/U 13.7 ± 6.5 yrs

Lethal PCa n=20
Mean F/U 11.9 ± 6.7 yrs

TLDA Cohort

No BCR n=20
Mean F/U 9.8 ± 2.1 yrs

BCR n=30
Mean F/U 9.3 ± 2.6 yrs

Definitive ADT n=19
Mean F/U 9.1 ± 2.7 yrs

Lethal PCa n=10
Mean F/U 9.6 ± 2.0 yrs

FIGURE 1
Cohort description. **(A)** Baseline characteristics of the cohorts used for IHC or TLDA analyses. The number of patients in each category is provided. The mean age is indicated in years (yrs). **(B)** Mean follow-up of the cohorts used for IHC or TLDA analyses according to each clinical outcome. Asterisks indicate clinicopathologic factors significantly associated with definitive ADT and lethal PCa in multivariate Cox regression analyses. Variables of reference are indicated by: (ref).

FIGURE 2
Violin plots showing the distribution of the density (cells/mm²) of
(A) CD3⁺ **(B)** CD45RO⁺ and **(C)** FoxP3⁺ cells in normal-like adjacent
epithelium, tumor margin and tumor areas as determined by
immunohistochemistry analysis of 98 prostate cancer specimens.
Dotted lines show boundaries of Q1 (green), Q2 or median (black)
and Q3 (red) quartiles.

2.1.3 Association with clinical outcomes

Kaplan-Meier analyses were performed to determine the
association between the levels of infiltration by each type of
immune cells in each of the three compartments and the clinical
outcomes. Kaplan-Meier analyses were performed with data
categorized into quartiles and dichotomized as the lowest quartile
vs the three other quartiles (Q1, *i.e.* low infiltration *vs* Q2-Q4) or as
the highest quartile *vs* the three other quartiles (Q4, *i.e.* high

infiltration *vs* Q1-Q3). Ratios between markers were determined
for each compartment. The ratios were divided into quartiles to be
analyzed by Kaplan-Meier curves and in multivariate proportional
hazards Cox regression analyses. The ratios of FoxP3⁺ and
CD45RO⁺ cells over the CD3⁺ cells in the tumor area as well as
the ratios of FoxP3⁺ over the CD45RO⁺ cells in the tumor area were
significantly associated with clinical outcomes.

Some examples of the Kaplan-Meier curves comparing the
levels of the ratio of FoxP3⁺/CD45RO⁺ cells categorized as
quartiles or dichotomized as Q1 *vs* Q2-Q4 or Q1-Q3 *vs* Q4 and
of the ratio of CD45RO⁺/CD3⁺ cells categorized as quartiles or
dichotomized as Q4 *vs* Q1-Q3 or Q1-Q3 *vs* Q4 for their association
with outcomes are presented in Figures 3A–H. Figure 3B shows
that a low ratio (Q1) of FoxP3⁺/CD45RO⁺ cells was associated with
a longer survival without the need for definitive ADT (log-rank
p=0.017) while Figure 3F shows that a high ratio (Q4) of FoxP3⁺/
CD45RO⁺ cells predicts a shorter time to BCR (log-rank=0.003). At
the opposite a low ratio (Q1) of CD45RO⁺/CD3⁺ is associated with
a shorter BCR-free survival (Figure 3D, log-rank=0.024) while a
high ratio (Q4) of CD45RO⁺/CD3⁺ cells was associated with a
longer lethal PCa-free survival (Figure 3H, log-rank=0.022).

The association between the levels of these cell densities or the
ratios of the cell density and the clinical outcomes was further
studied using univariate and multivariate Cox regression analyses.
Univariate Cox models revealed several associations with outcomes
but since the objective was to assess the independent prognostic
value of TIL, only results from multivariate analyses are presented
here. While looking at the whole population of lymphocytes, we
found that high density of CD3⁺ in the adjacent normal-like
epithelium or at the margin was associated with a lower risk of
BCR (HR=0.45, p=0.04 and HR=0.36, p=0.03, respectively). On the
other hand, a low density of CD3⁺ cells in the tumor area was
associated with a higher risk of lethal PCa (HR=3.77, p=0.04).

The ratios of FoxP3⁺/CD3⁺, CD45RO⁺/CD3⁺ and the FoxP3⁺/
CD45RO⁺ provided several significant associations with the
outcomes (Supplementary Table S2). Interestingly, it was mostly
the ratio of the cell densities within the tumor area that were found
to be significantly associated with the clinical events. Figure 4 shows
in a forest plot the various HR values and corresponding p values
for the ratio of these cell populations that had the strongest
association with the outcomes. As presented, a high ratio of
FoxP3⁺/CD3⁺ cells was associated with higher risk (HR=7.69,
p=0.001) whereas at the opposite a low ratio of FoxP3⁺/CD3⁺
cells was associated with a lower risk (HR=0.10, p=0.006) of the
need for definitive ADT. Consistent with this result, a high ratio of
FoxP3⁺/CD3⁺ cells was also associated with a higher risk of lethal
PCa (HR=4.37, p=0.040). Also, a high ratio of FoxP3⁺/CD45RO⁺
cells was associated with a higher risk (HR=2.54, p=0.010) of BCR
whereas a low ratio was associated with a lower risk of needing
definitive ADT (HR=0.10, p=0.007) and also with a lower risk of
lethal PCa (HR=0.17, p=0.058), although the statistical significance
was not reached. Finally, a low ratio of CD45RO⁺/CD3⁺ cells was
associated with a higher risk (HR=2.18, p=0.017) of BCR whereas a
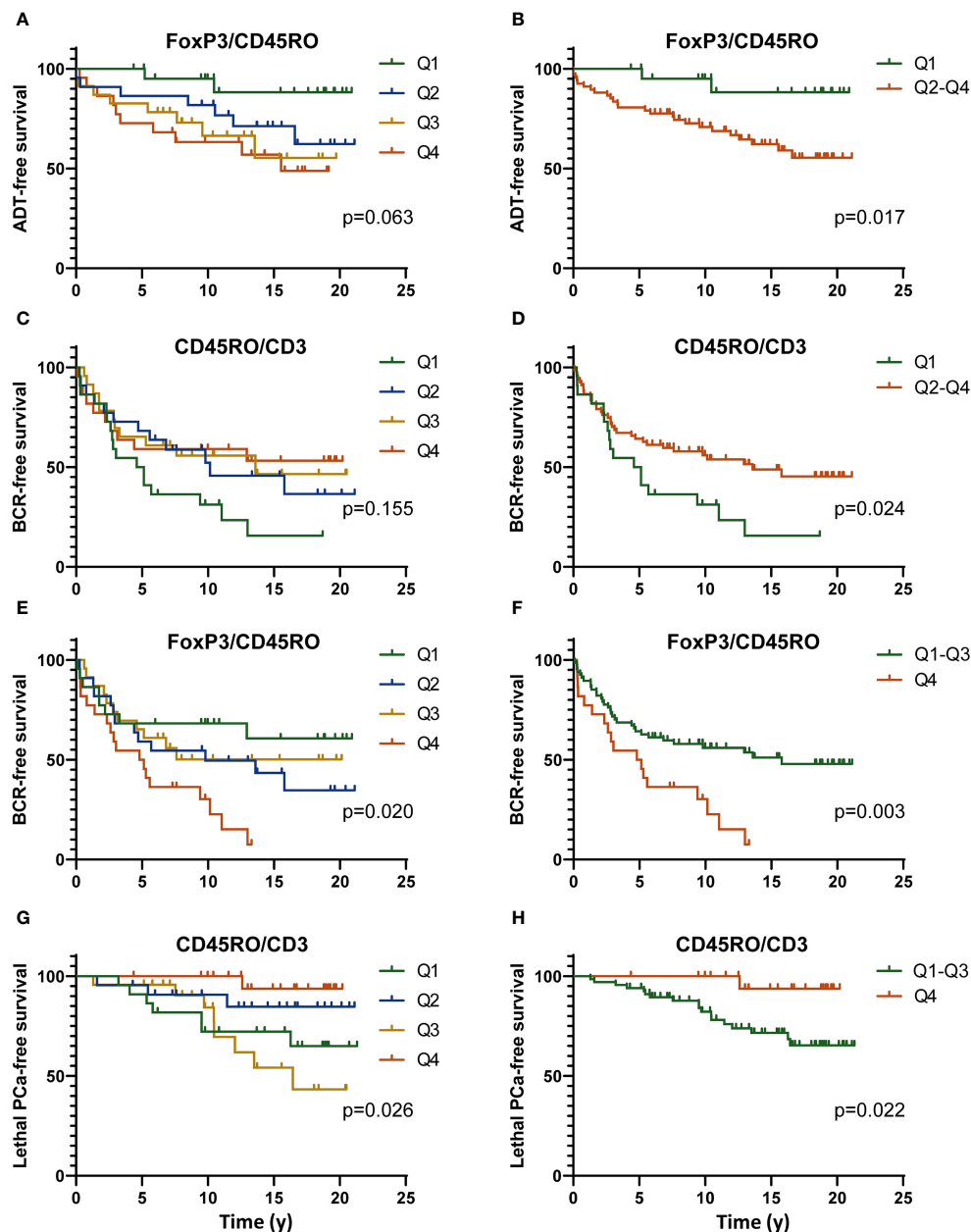high ratio was associated with a lower risk (HR=0.06, p=0.040) of
lethal PCa.

FIGURE 3

Kaplan-Meier curves showing the definitive ADT-free **(A, B)**, BCR-free **(C−F)** or lethal PCa-free survival according to the level of the ratio of the number of FoxP3$^+$/CD45RO$^+$ cells **(C−F)** or CD45RO$^+$/CD3$^+$ cells **(C, D, G, H)** categorized as quartiles (Q1 to Q4) **(A, C, E, G)** or dichotomized as to low value vs high (Q1 vs Q2-Q4) **(A−D)** or high value vs low (Q4 vs Q1-Q3) **(E−H)** of the ratios. All data are from the analysis of the infiltration of these immune cells in the tumor area only. The *p* value were estimated by the log-rank test.

## 2.2 Gene expression analyses

2.2.1 Cohort description

A total of 50 frozen radical prostatectomy specimens were available for the analysis of immune genes. These tumors were selected in order to have a representation of tumor and peri-tumor tissues including normal-like glands as we wanted to include in the analysis immune cells from the peri-tumor area since these might have important prognosis value. As for the IHC cohort, this cohort also contains a high proportion of tumors at higher risk of recurrence and progression and has a distribution of clinical

outcomes that is similar to that of the IHC cohort (Figure 1). Despite a shorter < 10 years mean follow-up, a similar proportion *i.e.* 30 out of 50 patients experienced BCR and 19 progressed to ADT of which 10 progressed to lethal PCa. Similarly, for the 11 BCR patients who did not progress to ADT or lethal PCa, 9 responded to salvage radiotherapy and 2 received short-term ADT.

2.2.2 FoxP3 is associated with lethal PCa

The RNA extracted from these tumors was tested using TLDA for the expression of 31 genes associated with T lymphocyte phenotypes and functions (Supplementary Table S3). The level of
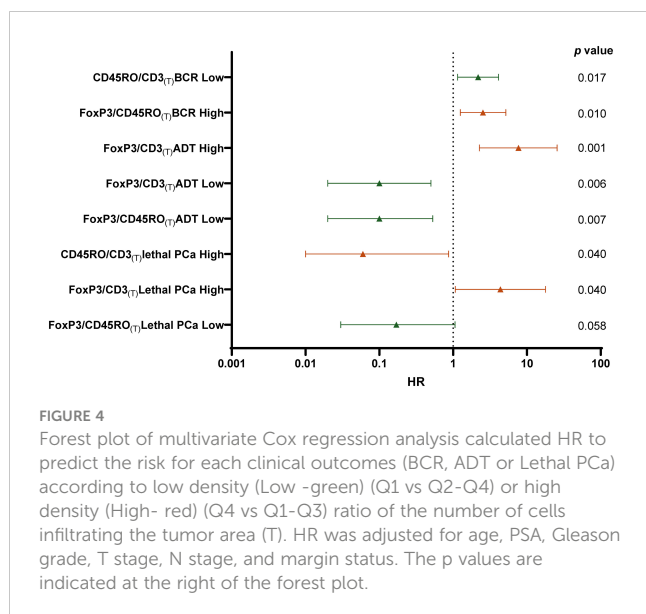
expression was normalized over the expression of two housekeeping genes, *i.e.* GUSB and PPIA.

Relative quantification values for each gene were categorized as tertiles (T1 to T3). Data dichotomized as high (T3) *vs* low (T1-T2) expression were analyzed in function of the clinical outcomes using the Kaplan-Meier estimator. This analysis revealed that very few genes were associated with the outcomes. Among these was FoxP3. Figure 5C shows that a high expression (T3) of FoxP3 was associated with a shorter lethal PCa-free survival (log-rank p=0.008). High *vs* low expression of FoxP3 was however not able to significantly predict the survival without ADT nor BCR although a clear separation of the curves can be observed (Figures 5A, B).

The association of high expression of FoxP3 with a higher risk of lethal PCa was also observed in univariate Cox regression analysis (HR=5.26, 95%CI=1.35-20.41, p=0.017). The expression of this gene was however not predictive of the survival without ADT or BCR (Supplementary Table S4).

2.2.3 Expression of FoxP3 gene correlates with that of CTLA-4

We performed a Pearson correlation with each gene of the T_{reg} and the immune checkpoint (ICP) pathway from our selected targets to determine which genes where the most strongly correlated with FoxP3. CTLA-4 was among the genes that were the most strongly correlated with FoxP3 ($r_p=0.759$, p<0.001). Since T_{reg} exert their immunosuppressive activity through secretions of cytokines such as TGFß1, IL-10 and IL-35, we also looked at the correlation of FoxP3 with the genes encoding these cytokines. As IL-35 is a cytokine that is part of the IL-12 cytokine family and is composed of two subunits, *i.e.* IL-12α and IL-27β chains, we only correlated FoxP3 with IL-12A as the gene encoding IL-27β was not in our panel. There was a significant correlation of FoxP3 expression with that of IL-10 ($r_p=0.550$, p <0.001), IL-12A ($r_p= 0.456$, p<0.001) and TGFß1 ($r_p=0.558$, p<0.001) (Figure 6).

In view of the importance of ICP in the function of TIL, and since we found a significant correlation between the expression of FoxP3 and CTLA-4, we further looked at the correlation between the expression of FoxP3 with the expression of other important ICP. LAG-3, ($r_p=0.513$, p <0.001), TIM-3 ($r_p= 0.441$, p<0.001) and PD-1 ($r_p=0.545$, p<0.001) were all found to be correlated with FoxP3 (Figure 6). In order to assess the correlation between the expression of these ICP and the outcomes, a hierarchical clustering was performed to define two molecular subgroups based on the expression of the 4 genes (low *vs* high expression) (Figure 7A). Kaplan-Meier survival curves were used to determine the association of these two groups with clinical outcomes. Results showed that tumors showing a high expression of these genes were associated with a shorter lethal PCa-free survival (log-rank p=0.029)(Figure 7D), but they were not significantly associated with survival without BCR nor ADT (Figures 7B, C). Kaplan-Meier analyses were also conducted with data from these genes taken individually (Figures 7E–J). Figure 7E shows that a high expression of CTLA-4 (T3) tended to be associated with a shorter BCR-free survival but the difference between the curves were not statistically significant. However, a high expression of TIM-3 (T3) was predictive of a shorter ADT-free survival (log-rank p=0.010) (Figure 7I) but not of BCR and lethal PCa-free survivals (Figures 7H, J). This association of TIM-3 with late clinical outcomes was also observed in Cox regression analysis as a high expression of TIM-3 (T3) was associated with higher risk of definitive ADT (HR=3.11 (1.25-7.69), p=0.014; Supplementary Table S4). High expression of LAG3 or PD-1 was not significantly associated with any of the outcomes in these analyses.
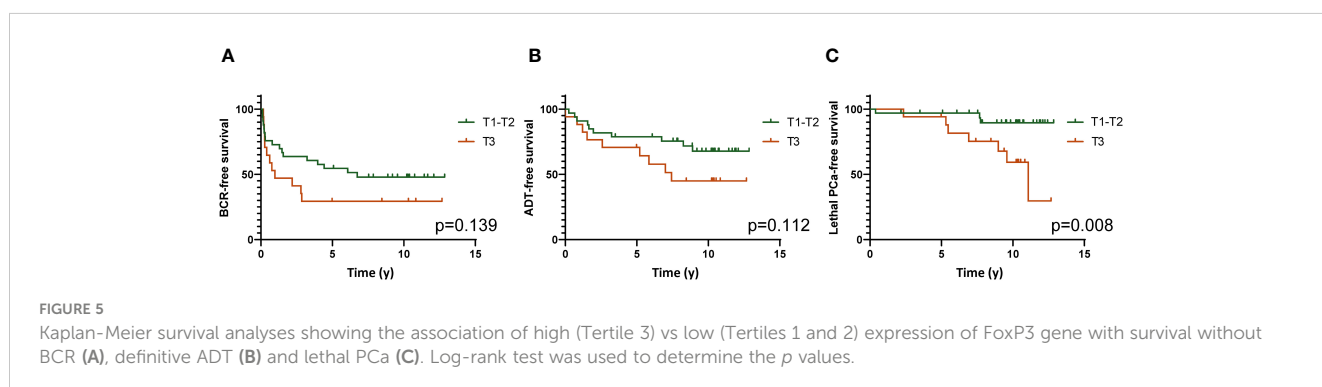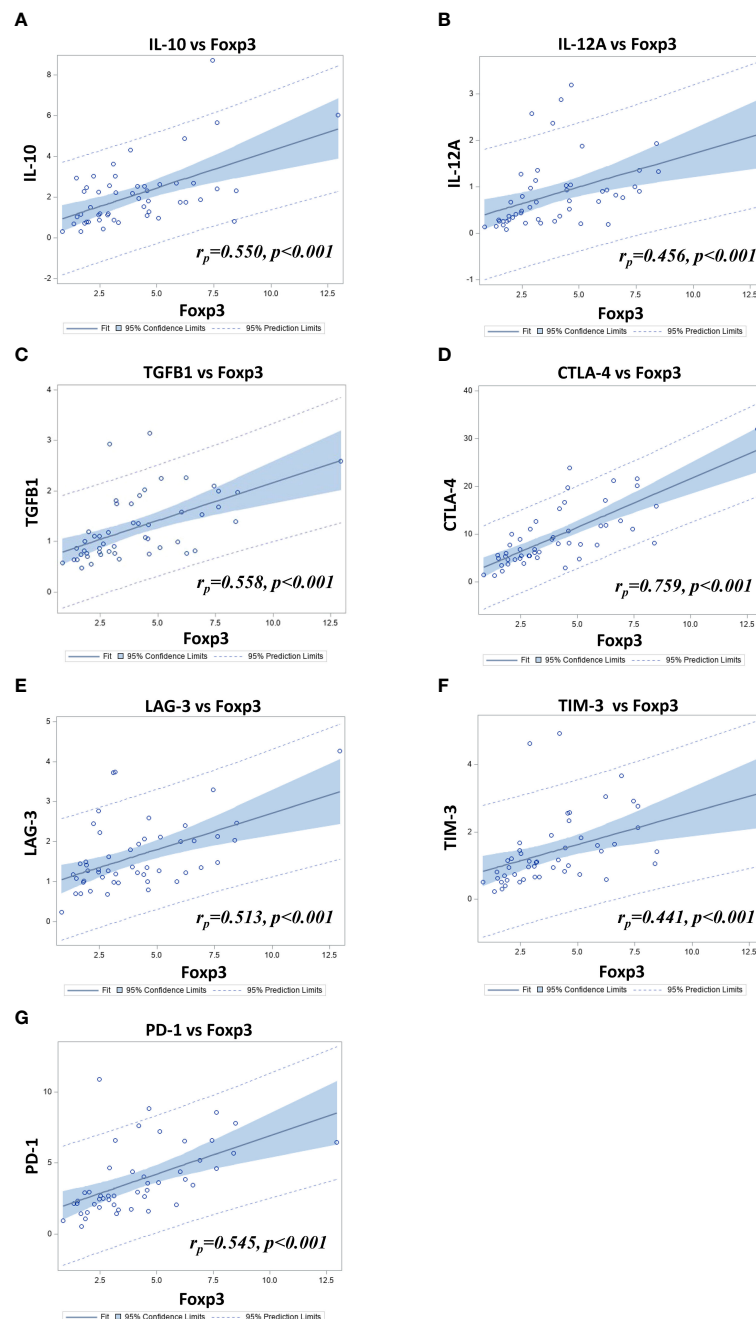
FIGURE 6

Scatter-plots combined with fit-plots for the Pearson correlation between FoxP3 and **(A)** IL-10 (IL10), **(B)** IL-12A (IL12A), **(C)** TGFβ1 (TGFB1) **(D)** CTLA-4 (CTLA4) **(E)** LAG-3 (LAG3) **(F)** TIM-3 (HAVCR2) and **(G)** PD-1 (PDCD1) relative gene expression in 50 PCa samples as determined by TLDA.

3 Discussion

T ($CD3^+$) and B ($CD20^+$) lymphocytes infiltrate prostate cancers, but it was previously shown that B lymphocytes are not associated with clinical outcomes (24). We thus deliberately omitted the analysis of B lymphocytes in this study. $CD3^+$ TIL are the effectors of the adaptative cellular immune response and therefore their number, phenotype and localization provide important information on the antitumor response specifically directed against tumor antigens and have been shown to predict clinical outcomes in many types of cancers (19, 35–37). Their presence reflects the immunogenicity of the tumor caused by the presence of either shared tumor antigens or mutated antigens. Although the mutational burden of most PCa is low compared to melanomas or lung cancers, some PCa show some high levels of TIL which might reflect some specific characteristics of these tumors (38, 39). It has been notably shown that tumor with deficient mismatch repair mechanisms are associated with a higher density of TIL due to the creation of neoepitopes resulting from the unrepaired DNA replication errors (40). Similarly, it was found that advanced PCa
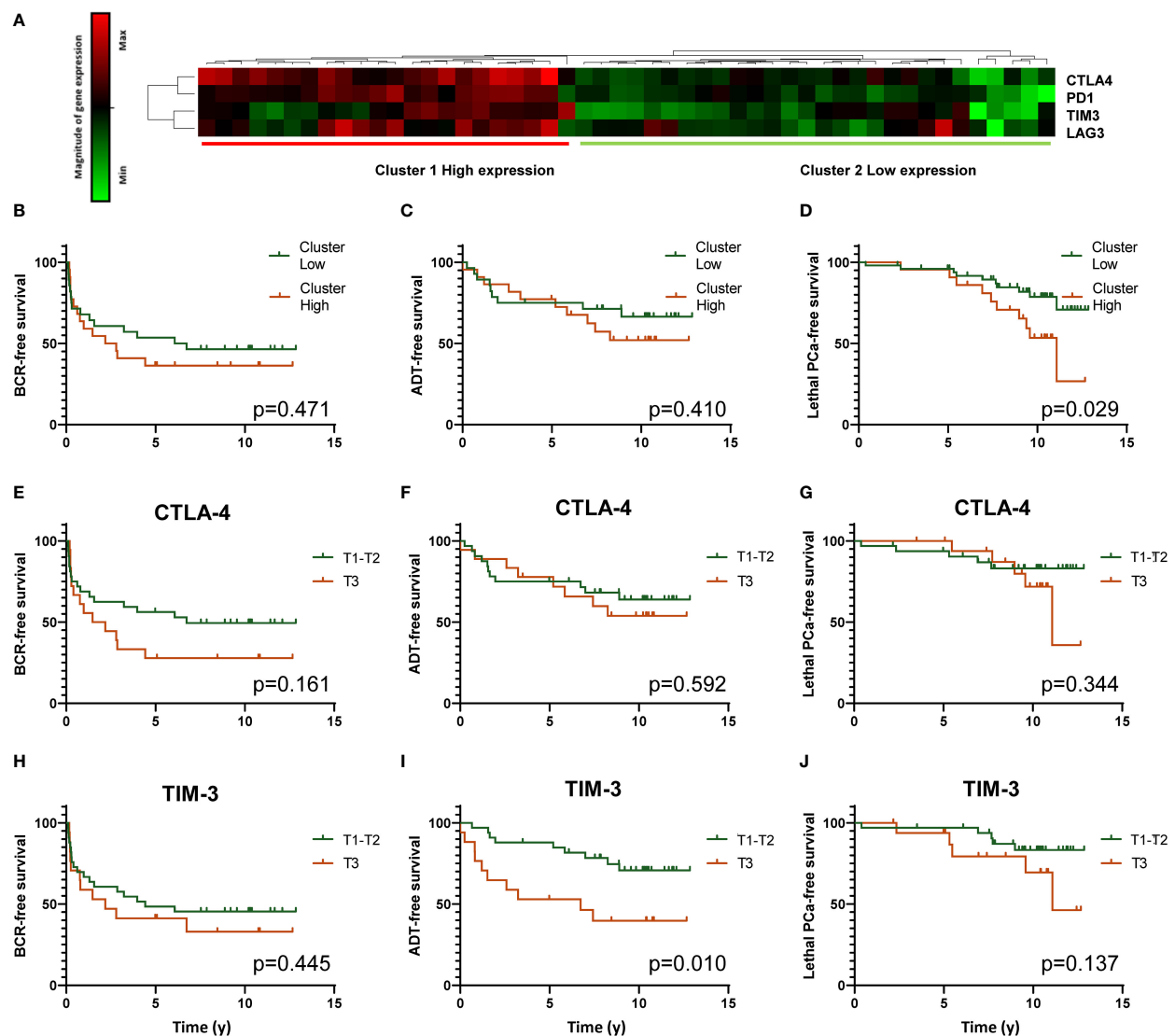
FIGURE 7

Analysis of CTLA-4 (CTLA4), PD-1 (PDCD1), TIM-3 (HAVCR2) and LAG-3 (LAG3) gene expression by TLDA. Heatmap resulting from the unsupervised hierarchical clustering of the expression of four ICP genes into two clusters corresponding to high and low expression of the genes is presented **(A)**. Gene expression determined by real time qPCR with Taqman probes is shown in the heatmap. Each horizontal row represents the same gene product and each vertical row, each patient. Magnitude of expression from high (red) to low (green) is indicated by the colored bar. Kaplan-Meier survival curves showing the association of high (red) and low (green) expression clusters with survival without BCR, definitive ADT and lethal PCa are presented in **(B–D)** panels, respectively. Other Kaplan-Meier analyses were performed to analyse the association between individual ICP gene expression and the three clinical outcomes. Panels **(E–G)**, **(H–J)** present these analyses for CTLA-4 and TIM-3, respectively. A high expression of TIM-3 is significantly associated with a shorter survival without definitive ADT. Log-rank test was used to determine the p value.

with inactivating CDK12 mutations, which affect the expression of genes involved in DNA damage response, had elevated neoantigen burden and were more infiltrated with T cells which even showed some clonal expansion (41, 42). Other characteristics were associated with a higher density of TIL in PCa. Vidotto et al. and Kaur et al. showed that tumors with loss of the PTEN tumor suppressor gene had higher density of FoxP3^{+} cells (33, 43). It was also found that higher TIL density was more frequent in ERG positive tumors (24, 33, 44). Hence, there is growing evidence of a relationship between genomic alterations and immune cell infiltration in PCa and thus the level of TIL subtypes may reflect distinct biological behaviors and prognoses.

In this study, we analyzed the infiltration of TIL by immunohistochemistry using CD3 as a marker to identify the entire T cell population, FoxP3 to identify the T_{reg} cells and CD45RO to identify T cells with a memory phenotype. We studied these T cell subtypes in three compartments of the tissue sections in order to assess whether the localization of these immune cells had a significant impact on the prognosis. Contrary to many other immunohistochemical studies that analyzed TIL using tissue microarrays (TMA) (22–25, 31, 33, 34) our study was performed on whole sections of FFPE tumors which allowed us to assess more accurately the number of TIL in the different tissue compartments. We showed that no matter the phenotype, the number of CD3^{+},

FoxP3$^+$ or CD45RO$^+$ cells was highly variable from one tumor to the other and these cells were on average more frequent at the tumor margin, although the difference was not statistically significant (Figure 2). This is consistent with another study reported by Yuan et al. which found that the majority of immune cells were found in the normal-like or pre-invasive tissue areas rather than in the tumor core (45). The higher density of immune cells at the tumor margin may reflects the properties of the tumor microenvironment making access to the tumor core more difficult. Such accumulation of immune cells outside the tumor core might provide important prognostic information. However, we found that it was the density of the T cells within the tumor area and not in the peritumor area (margin and adjacent normal-like areas) that was the most informative on the late clinical outcomes suggesting that T cells within the tumor core have a more important impact on the tumor evolution (Figure 4, Supplementary Table S2).

Our results showed that a high density of CD3$^+$ cells in the peritumor area was associated with a lower risk of BCR while a low density of these cells in the tumor area increased the risk of lethal PCa. This is in contrast with some studies that concluded that a higher TIL density was associated with poorer prognosis. For example, McArdle et al. performed a study in a cohort of 80 patients with PCa, in which they analyzed on whole tumor sections the infiltration of CD4$^+$ and CD8$^+$ lymphocytes within the tumor (including the cancer cell nests and surrounding stroma) but excluding any infiltration in the surrounding normal-like epithelium. The analysis revealed that a higher infiltration of CD4$^+$ T lymphocytes in the tumor was associated with a shorter PCa specific-free survival in both univariate (HR= 2.03, 95% CI=1.15–3.59, p=0.015) and multivariate (HR=2.29, 95% CI=1.25-4.22, p=0.008) analyses. Infiltration by CD8$^+$ T lymphocytes was however not predictive of PCa specific-free survival (21). A Norwegian study carried out on 535 primary PCa displayed on TMA, showed that in multivariate Cox regression analysis, a higher density of CD8$^+$ lymphocytes in both tumor epithelial and tumor stromal areas taken as one single value, was an independent negative prognostic factor for BCR-free survival (HR= 1.565, CI 95%= 1.132–2.165, p= 0.007). Also, when the infiltration of CD8$^+$ cells was assessed only in the tumor area, the association remained significant (HR=1.445, CI 95%1.028–2.032, p=0.032) (23). Flammiger et al. reported the analysis of a large TMA encompassing 3261 PCa samples. They found that both a low and high infiltration by CD3$^+$ lymphocytes were associated with a shorter BCR-free survival when compared with an intermediate level of infiltration in Kaplan-Meier analyses (p=0.019), a phenomenon known as the Goldilocks effect (24). This Goldilocks effect along with the study design including the characteristics of the tumor series, the choice of TMA *vs* whole sections to analyze the cell density in the different tumor compartments, the choice of the antibodies as well as the known heterogeneity of PCa could all contribute to generate variable results from one study to the other. Moreover, looking at the whole T lymphocyte population with markers such as CD3 or even CD4 and CD8 knowing that these cell populations are also heterogeneous as they contain subpopulations with anti-tumor, but also tumor-promoting phenotypes might not provide accurate prognosis. Looking at TIL corresponding to T cell

subpopulation with more define characteristics such as T$_{reg}$ and T$_{mem}$ is expected to provide more informative data.

We showed in this study that the ratio of immune cells within the tumor area have important independent prognostic values. We showed that low ratio of FoxP3$^+$/CD3$^+$ or of FoxP3$^+$/CD45RO$^+$ cell density was associated with a lower risk of definitive ADT. Consistent with the previous finding, to the opposite a high ratio of FoxP3$^+$/CD3$^+$ cell density was associated with a higher risk of definitive ADT or lethal PCa and a high ratio of FoxP3$^+$/CD45RO$^+$ was associated with a higher risk of BCR. Our results are in concordance with results of other studies looking at the prognostic value of T$_{reg}$. Davidsson et al. conducted a study using a TMA comprising tumor samples from 1367 men. The results inferred that neither infiltration of total CD4$^+$ cells nor of CD8$^+$ cells was associated with lethal PCa. However, a higher risk of lethal PCa was found when comparing the highest with the lowest quartile of FoxP3$^+$ cells (odds ratio=1.98; 95% CI= 1.15–3.40) (25). Likewise, an Italian study aiming to characterize TIL in tumor and peripheral stroma areas of tumors of 22 men treated by radical prostatectomy and salvage radiotherapy concluded that a low infiltration by CD45$^+$ and FoxP3$^+$ cells in the peripheral stroma was correlated to a prolonged BCR-free survival and a better overall survival. However, there was no correlation between the infiltration by CD3$^+$ and CD4$^+$ TIL and clinical outcomes. Higher risks of dying from prostate PCa was found when comparing the highest with the lowest quartiles of FoxP3$^+$ cells (odds ratio=1.98; 95% CI= 1.15–3.40) (26). Kaur et al. also found after analysis of the tumors of 144 African-American men an association between increased FoxP3$^+$ cell density and a higher risk of metastasis in multivariate analysis (HR=12.89 (1.59-104.40) p=0.02) (33). More recently, Andersen et al. analyzed the prognostic potential of different immune cells in two large cohorts of radical prostatectomy specimens available in TMA (34). They observed that T$_{reg}$ and M2 macrophages in stroma and epithelium, respectively, were adverse predictors of BCR in multivariate Cox regression analyses. A similar association of T$_{reg}$ with BCR was found at the mRNA level in a third cohort therefore thus further supporting the association of T$_{reg}$ with poorer prognosis (34). Using the same cohort as in this study, we recently reported the analysis of the prognostic value of the infiltration of tumors by macrophages and dendritic cells (DC) (46). We also found M2 macrophages were associated with a poorer prognosis. Indeed, a higher infiltration of CD163$^+$ M2 macrophages in the normal adjacent epithelium as well as a higher infiltration of CD209$^+$ immature DC at the tumor margin were associated with lethal PCa and BCR, respectively. Deeper analyses showed that the ratio of CD209$^+$ immature DC over CD83$^+$ mature DC was even more predictive of late adverse events, showing that the proportion of these immune cells must be taken into account to fully evaluate their prognostic value.

Our study also shows that CD45RO$^+$ cell density and the ratio of CD45RO$^+$/CD3$^+$ cells in the tumor area was associated with good prognosis since a high density of CD45RO$^+$ cells was associated with a lower risk of BCR and a high ratio of CD45RO$^+$/CD3$^+$ was associated with a lower risk of lethal PCa. To the contrary, a low ratio of CD45RO$^+$/CD3$^+$ density was associated with a higher risk of BCR. To our knowledge, our study appears to be the first to

determine the prognostic value of CD45RO$^+$ cells by immunohistochemistry in the microenvironment of PCa. There was one previous report of CD45RO$^+$ cell infiltration in normal prostate but not in tumors (47). The infiltration of tumors by CD45RO$^+$ cells was shown to be associated with clinical outcomes in various types of tumors (35, 48, 49). The independent prognostic value of CD45RO$^+$ cells highlighted by this study underscore the importance to include this biomarker in future studies looking at TIL in PCa. Our data also show that the balance between CD45RO$^+$ and FoxP3$^+$ cells in the tumor area has an important prognostic value.

Supporting the results of the immunohistochemistry study, we found that high expression of FoxP3 gene as measured using TLDA technology was associated with a shorter lethal PCa-free survival in Kaplan-Meier analyses (Figure 7) but also in univariate Cox regression analysis (Supplementary Table S4). Amongst the genes we studied, CTLA-4 was the one that was the most highly correlated to FoxP3. The high expression of CTLA-4 by effector T$_{reg}$ is well known and the use of anti-CTLA-4 is a relevant approach to kill T$_{reg}$ or at least attenuate their suppressive activity (50–52). Beside CTLA-4, effector T$_{reg}$ also express other ICP such as PD-1, TIM-3, LAG-3, GITR and OX40 that are also potential targets to modulate T$_{reg}$ functions (50–53). In our analysis of the TLDA results we found that high expression of CTLA-4, PD-1, TIM-3 and LAG-3 genes together was associated with a shorter lethal PCa-free survival consistent with the immunosuppressive action of these molecules on T cells. However, when taken separately CTLA-4, PD-1 and LAG-3 were not significantly associated with the clinical outcomes but a high expression of TIM-3 was significantly associated with a shorter definitive ADT-free survival (Figure 7). Inhibition of TIM-3 might be an approach to consider to counteract the immunosuppressive activity of FoxP3$^+$ cells in PCa as suggested by some authors (54–56).

This study has however some limitations. The first one concerns the technical approach. We used in this study a standard IHC technique in which each slide is stained with a single antibody against a marker specific to a cell population instead of performing a multiplex analysis for the simultaneous detection of different markers and corresponding cell populations on a single slide. We selected the standard IHC approach for practical reasons and to ease an eventual clinical application as this approach is still the most frequently used in clinical pathology laboratories. However, when the objective is to determine a ratio between cell populations, this approach is less adapted and tedious compared to the use of a multiplex assay. Moreover, the multiplex assay also have the advantage to detect various cell phenotypes i.e. cell expressing combinations of markers. For example, it was reported that some T$_{reg}$ cells may also express CD45RO (57–59). The use of a multiplex assay would allow to assess the prognostic value of the density of such double positive FoxP3$^+$CD45RO$^+$ cell population in addition of that of the single positive FoxP3$^+$ or CD45RO$^+$ cell populations. In this study, we could not detect this double positive cell population and so we don't know the frequency of these cells in the series of tumors we analyzed. But since the FoxP3$^+$ cell population is about 8 times less numerous than the CD45RO$^+$ cell population, the occurrence of some cells expressing both

markers is not expected to significantly modify the conclusion of the study. A second limitation of the study is the size of the cohorts. In several occasions, association with the outcomes did not reach statistical significance because of the limited size of the cohorts. The results of this study should be validated in larger cohorts.

In conclusion, we showed in this study that the infiltration of the tumor area by FoxP3$^+$ T$_{reg}$ and CD45RO$^+$ T$_{mem}$ cells are highly predictive of late clinical events when they are related to the CD3$^+$ cell population or related to one another using ratio of cell density. Using ratio of FoxP3$^+$ and CD45RO$^+$ over CD3$^+$ cell density or to one another is a way to normalize the frequency of these cells in the tissue which hopefully might offer more reproducible results. Our gene expression analysis by TLDA supported the association between a high expression of FoxP3 gene and a higher risk of lethal PCa. It also identified a correlation between a high TIM-3 gene expression with a higher risk for definitive ADT. These results let us to suggest that inhibition of TIM-3 might be a relevant approach to counter the immunosuppressive functions of T$_{reg}$ in order to improve the anti-tumor immune response against PCa.

4 Material and methods

4.1 Patient data and tissue samples

Two cohorts of patients treated by radical prostatectomy at CHU de Québec-Université Laval were used for this study (Figure 1). The first cohort (IHC cohort) was composed of 98 men treated between March 1996 and November 1998. This cohort is composed of men that had a least one factor that increased their chance to experience progression, i.e. an extraprostatic extension, a positive margin, a lymph node invasion or a high-grade tumor. For each participant, whole sections of a tissue block representative of the tumor but also containing normal-like adjacent epithelium were used for IHC analyses. The second cohort (TLDA cohort) was composed of 50 men who underwent radical prostatectomy between September 2004 and August 2009. Tumor tissues frozen in optimal cutting temperature (OCT) compound were available for this cohort and were used for the gene expression analysis using TLDA. Clinico-pathological data used include patient demographics, tumor, BCR, ADT, development of metastases and survival data. Time to lethal PCa was defined as either death from PCa and/or occurrence of metastasis and/or development of CRPC status. Further details on the definition of the clinical outcomes used in this study are presented in the Supplementary Material and Methods.

4.2 Immunohistochemistry

The most representative formalin-fixed and paraffin-embedded (FFPE) tumor block was cut to prepare consecutive 5 μm-thick sections which were dried overnight at 37°C. Sections were deparaffinized and heat-induced antigen retrieval was performed using a PT Link (Pre-Treatment Module for Tissue Specimens) with either citrate buffer pH 6.1 (Dako Code K8005: EnVision^{TM} FLEX,

Low pH) for CD3 and CD45RO or Tris/EDTA, pH 9 (Dako Code K8004: EnVision™ FLEX, High pH) for FoxP3. The immunodetection was performed using the IDetect Super Stain HRP-Polymer kit (ID labs, London, Ontario, Canada) after blockade of endogenous peroxidase activity by incubation in 3% peroxide solution for 10 min. Briefly, slides were incubated with Super block solution for 10 min to prevent non-specific background. Sections were then incubated overnight at room temperature with primary antibodies against CD3 (clone SP7, dilution 1/500, Abcam, Toronto, ON), CD45RO (clone UCHL-1, dil 1/6000, Abcam), and FoxP3 (clone 236A/E7, dil 1/600, Abcam). After washes, slides were incubated for 30 min with HRP-Polymer Conjugate. After 5 min of staining with DAB (3,3′-Diaminobenzidine), the slides were rinsed, counterstained with hematoxylin, dehydrated and mounted using MM 24 low viscosity mounting medium (Leica Microsystems, Durham, USA). Slides were digitalized using a Nanozoomer (Hamamatsu Photonics, Bidgewater NJ, USA) and visualized using the NDP.view2 software (Hamamatsu Photonics).

For each section, ten fields of view at 20x magnification (surface area of 0.460 mm^2) were randomly selected in the tumor, tumor margin and normal-like areas. The number of positive cells in each field of view was determined either manually by two trained observers (OEM and HL) or by a trained observer (OEM) and semi-automatically using the Calopix software (TRIBVN Healthcare, Châtillon, France). For each marker, 10% of the slides were randomly selected then reviewed and confirmed by a trained pathologist (BT).

4.3 Gene expression analysis

For these analyses, frozen tumor specimens were selected to ensure representation of normal-like tissues and tumor margins, so we selected specimens in which tumor area represented between 30 and 70% of the whole tissue. We also used, as control tissue for gene expression normalization, six normal prostate tissues from cadaver organ donors that had no PCa after pathology review. For each of the 50 eligible tumors, ten slides of 10 µm in thickness were used for RNA extraction. An H&E-stained section was prepared before and after the ten sections for RNA extraction to ensure that the tumor was present throughout the tissue depth. RNA extraction was performed on the ten frozen tumor sections using the Quick mirVana™ miRNA Isolation Kit from Ambion (ThermoFisher Scientific) in accordance with the manufacturer's instructions. Following extraction, DNA contamination was removed from the RNA samples using the Ambion DNAfree™ kit (ThermoFisher Scientific) in accordance with the manufacturer's instructions. The RNA was then reverse transcribed into first strand cDNA using the SuperScript® VILO™ Invitrogen system (Life technologies, Waltham, MA, USA). TaqMan® Array Micro Fluidic 384-Wells TLDA cards (Life technologies) were custom designed with pre-loaded gene-specific primer and probe sets for the analysis of 31 selected immune gene targets and two house-keeping genes for

mRNA normalization (Supplementary Table S3). Each cDNA sample, 300 ng at a concentration of 3 ng/µl were added to an equal volume of 2X TaqMan Universal PCR Master Mix (Thermo Scientific) and 100 µL of the sample-specific PCR mix was added to the fill reservoir on the TLDA card. The card was centrifuged twice for one minute at 1200 rpm and sealed using the TaqMan Array Micro Fluidic Card Sealer (Thermo Scientific). The amplification was performed in a StepOnePlus™, 7900HT Fast Real-Time PCR System (Applied Biosystems) using the following cycling conditions: 2 min at 50°C, 10 min at 94.5°C, 30 s at 97°C, 1 min at 59.7°C for 40 cycles. The mRNA expression levels were normalized to GUSB and PPIA (reference genes), and the expression values of immune gene expression were calculated using ΔΔCT method, as recommended by the manufacturer. Each tumor gene expression value was then reported as a fold change of the same gene mean value in normal prostates. This resulting value was used for statistical analysis.

4.4 Statistics

The characteristics of the patients in each cohort are summarized by means, standard deviation (± SD), frequency, and percentage. Time-to-event period for each outcome was calculated from the date of surgery to corresponding event date or to last follow-up date, for right censored cases. Univariate and multivariate Cox proportional hazards regression models were used to estimate the hazard ratio (HR) and HR adjusted for age, PSA, Gleason grade, T (tumor stage), N (nodal stage), and margin status. The assumption of proportional hazards was evaluated using the supreme test for all Cox regression models. Kaplan-Meier curves of markers categorized in either quartiles (or tertiles) and dichotomized by higher or lower quartiles (or tertiles) were used to estimate the association with clinical outcomes and the log-rank test was used to assess the differences between the curves. Pearson correlations (r_p) were used to estimate the correlation between gene expression targets. Statistical analyses were performed using SAS Statistical Software v.9.4 (SAS Institute, Cary, NC, USA), with a two-sided significance level set at p ≤ 0.05.

Data availability statement

The raw data supporting the conclusions of this article will be made available by the authors, without undue reservation.

Ethics statement

The studies involving humans were approved by Research ethics committee of the CHU de Québec-Université Laval. The studies were conducted in accordance with the local legislation and institutional requirements. The participants provided their written informed consent to participate in this study.

Author contributions

OM: Visualization, Validation, Methodology, Investigation, Formal analysis, Data curation, Conceptualization, Writing – review & editing, Writing – original draft. HL: Writing – review & editing, Supervision, Resources, Project administration, Methodology, Investigation, Funding acquisition, Formal analysis, Data curation, Conceptualization. DS: Writing – review & editing, Methodology, Formal analysis. HH: Writing – review & editing, Resources, Investigation. BV: Writing – review & editing, Investigation, Formal analysis. BT: Writing – review & editing, Investigation, Funding acquisition. VF: Writing – review & editing, Funding acquisition. LL: Writing – review & editing, Methodology, Funding acquisition, Conceptualization. AB: Writing – review & editing, Writing – original draft, Supervision, Resources, Funding acquisition. YF: Writing – review & editing, Writing – original draft, Supervision, Resources, Project administration, Methodology, Funding acquisition, Formal analysis, Conceptualization.

Funding

Acknowledgments

Conflict of interest

The authors declare that the research was conducted in the absence of any commercial or financial relationships that could be construed as a potential conflict of interest.

Publisher's note

All claims expressed in this article are solely those of the authors and do not necessarily represent those of their affiliated organizations, or those of the publisher, the editors and the reviewers. Any product that may be evaluated in this article, or claim that may be made by its manufacturer, is not guaranteed or endorsed by the publisher.

Supplementary material

The Supplementary Material for this article can be found online at: https://www.frontiersin.org/articles/10.3389/fimmu.2024.1372837/full#supplementary-material

SUPPLEMENTARY FIGURE 1
Example of a prostate cancer sample with delimitation of normal-like epithelium, tumor margin and tumor areas. For scoring of each slide after staining with the different antibodies, ten fields of view at 20x magnification (surface area of 0.460 mm^2) were randomly selected in the tumor (represented as red rectangles in the red-encircled zone), tumor margin (represented as black rectangles at the periphery of the tumor) and normal-like areas (represented as green rectangles in the green-encircled zones). The number of positive cells in each field of view was determined either manually by two trained observers or by a trained observer and semi-automatically using the Calopix software (TRIBVN Healthcare, Châtillon, France). Magnification 4X.

SUPPLEMENTARY FIGURE 2
Immunohistochemical analysis of the infiltration by T lymphocytes. **(A-J)** Examples of staining for CD3$^+$, CD45RO$^+$ and FOXP3$^+$ cells in normal-like adjacent epithelium, the tumor margin and in the tumor areas. Magnification 20X. Insert magnification equivalent to 40X. Scale bar = 200 μm. **(K)** The mean number of CD3$^+$, CD45RO$^+$, or FoxP3$^+$ cells $\pm$ SD per mm^2 infiltrating the adjacent normal-like adjacent epithelium, tumor margin and tumor areas is provided in the table. SD: Standard deviation.

SUPPLEMENTARY TABLE 1
Multivariate Cox regression analysis calculated HR according to the three clinical outcomes.

SUPPLEMENTARY TABLE 2
Multivariate Cox regression analysis calculated HR to predict the risk for each clinical outcomes according to low (Q1 *vs* Q2-Q4) or high (Q4 *vs* Q1-Q3) ratio of the number of cells infiltrating the various tissue compartments. HR was adjusted for age, PSA, Gleason grade, T stage, N stage, and margin status.

SUPPLEMENTARY TABLE 3
List of immune genes analyzed in TLDA experiment and their associated activity or pathway.

SUPPLEMENTARY TABLE 4
Univariate Cox regression analysis calculated HR to predict the risk for each clinical outcomes according to a high (T3 *vs* T1-T2) level of expression of FoxP3, CTLA-4 (CTLA4), TIM-3 (HAVCR2), LAG-3 (LAG3) and PD-1 (PDCD1) genes.

References

1. Bergengren O, Pekala KR, Matsoukas K, Fainberg J, Mungovan SF, Bratt O, et al. 2022 Update on prostate cancer epidemiology and risk factors-A systematic review. *Eur Urol*. (2023) 84:191–206. doi: 10.1016/j.eururo.2023.04.021

2. Wang L, Lu B, He M, Wang Y, Wang Z, Du L. Prostate cancer incidence and mortality: global status and temporal trends in 89 countries from 2000 to 2019. *Front Public Health*. (2022) 10:811044. doi: 10.3389/fpubh.2022.811044

3. Carm KT, Hoff AM, Bakken AC, Axcrona U, Axcrona K, Lothe RA, et al. Interfocal heterogeneity challenges the clinical usefulness of molecular classification of primary prostate cancer. *Sci Rep*. (2019) 9:13579. doi: 10.1038/s41598-019-49964-7

4. Lovf M, Zhao S, Axcrona U, Johannessen B, Bakken AC, Carm KT, et al. Multifocal primary prostate cancer exhibits high degree of genomic heterogeneity. *Eur Urol*. (2019) 75:498–505. doi: 10.1016/j.eururo.2018.08.009

5. Hanna B, Ranasinghe W, Lawrentschuk N. Risk stratification and avoiding overtreatment in localized prostate cancer. *Curr Opin Urol*. (2019) 29:612–9. doi: 10.1097/MOU.0000000000000672

6. Shore ND, Moul JW, Pienta KJ, Czernin J, King MT, Freedland SJ. Biochemical recurrence in patients with prostate cancer after primary definitive therapy: treatment based on risk stratification. *Prostate Cancer Prostat Dis*. (2023) 27:192–201. doi: 10.1038/s41391-023-00712-z

7. Sanda MG, Cadeddu JA, Kirkby E, Chen RC, Crispino T, Fontanarosa J, et al. Clinically localized prostate cancer: AUA/ASTRO/SUO guideline. Part I: risk stratification, shared decision making, and care options. *J Urol*. (2018) 199:683–90. doi: 10.1016/j.juro.2017.11.095

8. Counago F, Lopez-Campos F, Diaz-Gavela AA, Almagro E, Fenandez-Pascual E, Henriquez I, et al. Clinical applications of molecular biomarkers in prostate cancer. *Cancers (Basel)*. (2020) 12:1550. doi: 10.3390/cancers12061550

9. de Visser KE, Joyce JA. The evolving tumor microenvironment: From cancer initiation to metastatic outgrowth. *Cancer Cell*. (2023) 41:374–403. doi: 10.1016/j.ccell.2023.02.016

10. Labani-Motlagh A, Ashja-Mahdavi M, Loskog A. The tumor microenvironment: A milieu hindering and obstructing antitumor immune responses. *Front Immunol*. (2020) 11:940. doi: 10.3389/fimmu.2020.00940

11. Baghban R, Roshangar L, Jahanban-Esfahlan R, Seidi K, Ebrahimi-Kalan A, Jaymand M, et al. Tumor microenvironment complexity and therapeutic implications at a glance. *Cell Commun Signaling*. (2020) 18:59. doi: 10.1186/s12964-020-0530-4

12. Giraldo NA, Sanchez-Salas R, Peske JD, Vano Y, Becht E, Petitprez F, et al. The clinical role of the TME in solid cancer. *Br J Cancer*. (2019) 120:45–53. doi: 10.1038/s41416-018-0327-z

13. Hanahan D. Hallmarks of cancer: new dimensions. *Cancer Discovery*. (2022) 12:31–46. doi: 10.1158/2159-8290.CD-21-1059

14. Hendry S, Salgado R, Gevaert T, Russell PA, John T, Thapa B, et al. Assessing tumor-infiltrating lymphocytes in solid tumors: A practical review for pathologists and proposal for a standardized method from the international immuno-oncology biomarkers working group: part 2: TILs in melanoma, gastrointestinal tract carcinomas, non-small cell lung carcinoma and mesothelioma, endometrial and ovarian carcinomas, squamous cell carcinoma of the head and neck, genitourinary carcinomas, and primary brain tumors. *Adv Anat Pathol*. (2017) 24:311–35. doi: 10.1097/PAP.0000000000000161

15. Badalamenti G, Fanale D, Incorvaia L, Barraco N, Listi A, Maragliano R, et al. Role of tumor-infiltrating lymphocytes in patients with solid tumors: Can a drop dig a stone? *Cell Immunol*. (2019) 343:103753. doi: 10.1016/j.cellimm.2018.01.013

16. Galon J, Costes A, Sanchez-Cabo F, Kirilovsky A, Mlecnik B, Lagorce-Pages C, et al. Type, density, and location of immune cells within human colorectal tumors predict clinical outcome. *Science*. (2006) 313:1960–4. doi: 10.1126/science.1129139

17. Pages F, Kirilovsky A, Mlecnik B, Asslaber M, Tosolini M, Bindea G, et al. *In situ* cytotoxic and memory T cells predict outcome in patients with early-stage colorectal cancer. *J Clin Oncol*. (2009) 27:5944–51. doi: 10.1200/JCO.2008.19.6147

18. Marliot F, Pages F, Galon J. Usefulness and robustness of Immunoscore for personalized management of cancer patients. *Oncoimmunology*. (2020) 9:1832324. doi: 10.1080/2162402X.2020.1832324

19. Pagès F, Mlecnik B, Marliot F, Bindea G, Ou F-S, Bifulco C, et al. International validation of the consensus Immunoscore for the classification of colon cancer: a prognostic and accuracy study. *Lancet*. (2018) 391:2128–39. doi: 10.1016/S0140-6736(18)30789-X

20. Mlecnik B, Lugli A, Bindea G, Marliot F, Bifulco C, Lee JJ, et al. Multicenter international study of the consensus immunoscore for the prediction of relapse and survival in early-stage colon cancer. *Cancers (Basel)*. (2023) 15. doi: 10.3390/cancers15020418

21. McArdle PA, Canna K, McMillan DC, McNicol AM, Campbell R, Underwood MA. The relationship between T-lymphocyte subset infiltration and survival in patients with prostate cancer. *Br J Cancer*. (2004) 91:541–3. doi: 10.1038/sj.bjc.6601943

22. Karja V, Aaltomaa S, Lipponen P, Isotalo T, Talja M, Mokka R. Tumour-infiltrating lymphocytes: A prognostic factor of PSA-free survival in patients with local prostate carcinoma treated by radical prostatectomy. *Anticancer Res*. (2005) 25:4435–8.

23. Ness N, Andersen S, Valkov A, Nordby Y, Donnem T, Al-Saad S, et al. Infiltration of CD8+ lymphocytes is an independent prognostic factor of biochemical failure-free survival in prostate cancer. *Prostate*. (2014) 74:1452–61. doi: 10.1002/pros.22862

24. Flammiger A, Bayer F, Cirugeda-Kuhnert A, Huland H, Tennstedt P, Simon R, et al. Intratumoral T but not B lymphocytes are related to clinical outcome in prostate cancer. *APMIS*. (2012) 120:901–8. doi: 10.1111/j.1600-0463.2012.02924.x

25. Davidsson S, Ohlson A-L, Andersson S-O, Fall K, Meisner A, Fiorentino M, et al. CD4 helper T cells, CD8 cytotoxic T cells, and FOXP3+ regulatory T cells with respect to lethal prostate cancer. *Modern Pathol*. (2013) 26:448–55. doi: 10.1038/modpathol.2012.164

26. Nardone V, Botta C, Caraglia M, Martino EC, Ambrosio MR, Carfagno T, et al. Tumor infiltrating T lymphocytes expressing FoxP3, CCR7 or PD-1 predict the outcome of prostate cancer patients subjected to salvage radiotherapy after biochemical relapse. *Cancer Biol Ther*. (2016) 17:1213–20. doi: 10.1080/15384047.2016.1235666

27. Petitprez F, Fossati N, Vano Y, Freschi M, Becht E, Luciano R, et al. PD-L1 expression and CD8(+) T-cell infiltrate are associated with clinical progression in patients with node-positive prostate cancer. *Eur Urol Focus*. (2019) 5:192–6. doi: 10.1016/j.euf.2017.05.013

28. Mo RJ, Han ZD, Liang YK, Ye JH, Wu SL, Lin SX, et al. Expression of PD-L1 in tumor-associated nerves correlates with reduced CD8(+) tumor-associated lymphocytes and poor prognosis in prostate cancer. *Int J Cancer*. (2019) 144:3099–110. doi: 10.1002/ijc.32061

29. Vicier C, Ravi P, Kwak L, Werner L, Huang Y, Evan C, et al. Association between CD8 and PD-L1 expression and outcomes after radical prostatectomy for localized prostate cancer. *Prostate*. (2021) 81:50–7. doi: 10.1002/pros.24079

30. Yang Y, Attwood K, Bshara W, Mohler JL, Guru K, Xu B, et al. High intratumoral CD8(+) T-cell infiltration is associated with improved survival in prostate cancer patients undergoing radical prostatectomy. *Prostate*. (2021) 81:20–8. doi: 10.1002/pros.24068

31. Flammiger A, Weisbach L, Huland H, Tennstedt P, Simon R, Minner S, et al. High tissue density of FOXP3+ T cells is associated with clinical outcome in prostate cancer. *Eur J Cancer*. (2013) 49:1273–9. doi: 10.1016/j.ejca.2012.11.035

32. Leclerc BG, Charlebois R, Chouinard G, Allard B, Pommey S, Saad F, et al. CD73 expression is an independent prognostic factor in prostate cancer. *Clin Cancer Res*. (2016) 22:158–66. doi: 10.1158/1078-0432.CCR-15-1181

33. Kaur HB, Guedes LB, Lu J, Maldonado L, Reitz L, Barber JR, et al. Association of tumor-infiltrating T-cell density with molecular subtype, racial ancestry and clinical outcomes in prostate cancer. *Mod Pathol*. (2018) 31:1539–52. doi: 10.1038/s41379-018-0083-x

34. Andersen LB, Norgaard M, Rasmussen M, Fredsoe J, Borre M, Ulhoi BP, et al. Immune cell analyses of the tumor microenvironment in prostate cancer highlight infiltrating regulatory T cells and macrophages as adverse prognostic factors. *J Pathol*. (2021) 255:155–65. doi: 10.1002/path.5757

35. Ahmadvand S, Faghih Z, Montazer M, Safaei A, Mokhtari M, Jafari P, et al. Importance of CD45RO+ tumor-infiltrating lymphocytes in post-operative survival of breast cancer patients. *Cell Oncol (Dordr)*. (2019) 42:343–56. doi: 10.1007/s13402-019-00430-6

36. Angell HK, Bruni D, Barrett JC, Herbst R, Galon J. The immunoscore: colon cancer and beyond. *Clin Cancer Res*. (2020) 26:332–9. doi: 10.1158/1078-0432.CCR-18-1851

37. Vihervuori H, Autere TA, Repo H, Kurki S, Kallio L, Lintunen MM, et al. Tumor-infiltrating lymphocytes and CD8(+) T cells predict survival of triple-negative breast cancer. *J Cancer Res Clin Oncol*. (2019) 145:3105–14. doi: 10.1007/s00432-019-03036-5

38. Bodor JN, Boumber Y, Borghaei H. Biomarkers for immune checkpoint inhibition in non-small cell lung cancer (NSCLC). *Cancer*. (2020) 126:260–70. doi: 10.1002/cncr.32468

39. Fraser M, Sabelnykova VY, Yamaguchi TN, Heisler LE, Livingstone J, Huang V, et al. Genomic hallmarks of localized, non-indolent prostate cancer. *Nature*. (2017) 541:359–64. doi: 10.1038/nature20788

40. Guedes LB, Antonarakis ES, Schweizer MT, Mirkheshti N, Almutairi F, Park JC, et al. MSH2 loss in primary prostate cancer. *Clin Cancer Res*. (2017) 23:6863–74. doi: 10.1158/1078-0432.CCR-17-0955

41. Wu YM, Cieslik M, Lonigro RJ, Vats P, Reimers MA, Cao X, et al. Inactivation of CDK12 delineates a distinct immunogenic class of advanced prostate cancer. *Cell*. (2018) 173:1770–82 e14. doi: 10.1016/j.cell.2018.04.034

42. Lotan TL, Antonarakis ES. CDK12 deficiency and the immune microenvironment in prostate cancer. *Clin Cancer Res*. (2020). doi: 10.1158/1078-0432.CCR-20-3877

43. Vidotto T, Saggioro FP, Jamaspishvili T, Chesca DL, Picanco de Albuquerque CG, Reis RB, et al. PTEN-deficient prostate cancer is associated with an immunosuppressive tumor microenvironment mediated by increased expression of IDO1 and infiltrating FoxP3+ T regulatory cells. *Prostate*. (2019) 79:969–79. doi: 10.1002/pros.23808

44. Vos JH, van den Ingh TS, van Mil FN. Non-exfoliative canine cytology: the value of fine needle aspiration and scraping cytology. *Vet Q*. (1989) 11:222–31. doi: 10.1080/01652176.1989.9694228

45. Yuan H, Hsiao Y-H, Zhang Y, Wang J, Yin C, Shen R, et al. Destructive impact of T-lymphocytes, NK and Mast cells on basal cell layers: implications for tumor invasion. *BMC Cancer*. (2013) 13:258–. doi: 10.1186/1471-2407-13-258

46. Molina OE, LaRue H, Simonyan D, Hovington H, Tetu B, Fradet V, et al. High infiltration of CD209(+) dendritic cells and CD163(+) macrophages in the peritumor area of prostate cancer is predictive of late adverse outcomes. *Front Immunol*. (2023) 14:1205266. doi: 10.3389/fimmu.2023.1205266

47. Bostwick DG, de la Roza G, Dundore P, Corica FA, Iczkowski KA. Intraepithelial and stromal lymphocytes in the normal human prostate. *Prostate*. (2003) 55:187–93. doi: 10.1002/pros.10224

48. Malka D, Lievre A, Andre T, Taieb J, Ducreux M, Bibeau F. Immune scores in colorectal cancer: Where are we? *Eur J Cancer*. (2020) 140:105–18. doi: 10.1016/j.ejca.2020.08.024

49. Huang Z, Xie N, Liu H, Wan Y, Zhu Y, Zhang M, et al. The prognostic role of tumour-infiltrating lymphocytes in oral squamous cell carcinoma: A meta-analysis. *J Oral Pathol Med*. (2019) 48:788–98. doi: 10.1111/jop.12927

50. Tanaka A, Sakaguchi S. Regulatory T cells in cancer immunotherapy. *Cell Res*. (2017) 27:109–18. doi: 10.1038/cr.2016.151

51. Shitara K, Nishikawa H. Regulatory T cells: a potential target in cancer immunotherapy. *Ann N Y Acad Sci*. (2018) 1417:104–15. doi: 10.1111/nyas.13625

52. Ngiow SF, Young A. Re-education of the tumor microenvironment with targeted therapies and immunotherapies. *Front Immunol*. (2020) 11:1633. doi: 10.3389/fimmu.2020.01633

53. Fujio K, Yamamoto K, Okamura T. Overview of LAG-3-expressing, IL-10-producing regulatory T cells. *Curr Top Microbiol Immunol*. (2017) 410:29–45. doi: 10.1007/82_2017_59

54. Das M, Zhu C, Kuchroo VK. Tim-3 and its role in regulating anti-tumor immunity. *Immunol Rev*. (2017) 276:97–111. doi: 10.1111/imr.12520

55. Jafari S, Molavi O, Kahroba H, Hejazi MS, Maleki-Dizaji N, Barghi S, et al. Clinical application of immune checkpoints in targeted immunotherapy of prostate cancer. *Cell Mol Life Sci*. (2020) 77:3693–710. doi: 10.1007/s00018-020-03459-1

56. Piao Y, Jin X. Analysis of Tim-3 as a therapeutic target in prostate cancer. *Tumour Biol*. (2017) 39:1010428317716628. doi: 10.1177/1010428317716628

57. Sakaguchi S, Miyara M, Costantino CM, Hafler DA. FOXP3+ regulatory T cells in the human immune system. *Nat Rev Immunol*. (2010) 10:490–500. doi: 10.1038/nri2785

58. Kwiecien I, Rutkowska E, Sokolowski R, Bednarek J, Raniszewska A, Jahnz-Rozyk K, et al. Effector memory T cells and CD45RO+ Regulatory T cells in metastatic vs. Non-metastatic lymph nodes in lung cancer patients. *Front Immunol*. (2022) 13:864497. doi: 10.3389/fimmu.2022.864497

59. Booth NJ, McQuaid AJ, Sobande T, Kissane S, Agius E, Jackson SE, et al. Different proliferative potential and migratory characteristics of human CD4+ regulatory T cells that express either CD45RA or CD45RO. *J Immunol*. (2010) 184:4317–26. doi: 10.4049/jimmunol.0903781

Inhibition of insulin-like growth factors increases production of CXCL9/10 by macrophages and fibroblasts and facilitates CD8+ cytotoxic T cell recruitment to pancreatic tumours

Patrick Freeman[1], Gaia Bellomo[1], Lucy Ireland[1],
Maidinaimu Abudula[1], Teifion Luckett[1], Michael Oberst[2],
Ruth Stafferton[1], Paula Ghaneh[1], Chris Halloran[1],
Michael C. Schmid[1] and Ainhoa Mielgo[1*]

[1]Department of Molecular and Clinical Cancer Medicine, University of Liverpool, Liverpool,
United Kingdom, [2]Department of Oncology Research, AstraZeneca, One Medimmune Way,
Gaithersburg, MD, United States

Pancreatic ductal adenocarcinoma (PDAC) is a highly lethal malignancy with an
urgent unmet clinical need for new therapies. Using a combination of *in vitro*
assays and *in vivo* preclinical models we demonstrate that therapeutic inhibition
of the IGF signalling axis promotes the accumulation of CD8+ cytotoxic T cells
within the tumour microenvironment of PDAC tumours. Mechanistically, we
show that IGF blockade promotes macrophage and fibroblast production of the
chemokines CXCL9 and CXCL10 to facilitate CD8+ T cell recruitment and
trafficking towards the PDAC tumour. Exploring this pathway further, we show
that IGF inhibition leads to increased STAT1 transcriptional activity, correlating
with a downregulation of the AKT/STAT3 signalling axis, in turn promoting *Cxcl9*
and *Cxcl10* gene transcription. Using patient derived tumour explants, we also
demonstrate that our findings translate into the human setting. PDAC tumours
are frequently described as "immunologically cold", therefore bolstering CD8+ T
cell recruitment to PDAC tumours through IGF inhibition may serve to improve
the efficacy of immune checkpoint inhibitors which rely on the presence of CD8+
T cells in tumours.

1 Introduction

Pancreatic ductal adenocarcinoma (PDAC), accounting for > 85% of all pancreatic cancers (1), is a devastating disease with current treatment outcomes remaining notoriously poor and current treatment modalities lagging far behind those of other solid malignancies. PDAC is currently the 5th leading cause of cancer-related death in the UK and is projected to become the second leading cause of cancer death within the next decade, having already surpassed breast cancer in the United States (2). Late diagnosis, early (and high) rates of metastasis and therapeutic resistance (3, 4) are all key driving factors for disease lethality, with only 11% of patients achieving a 5-year survival (5). As such, PDAC poses a major public health concern, and greater emphasis needs to be made on delineating the complex pathophysiology underpinning this deadly disease and developing new therapeutic interventions.

A defining hallmark of PDAC, and one of the major contributing factors for therapeutic resistance, is the complex nature of its tumour microenvironment (TME) which has been explored by us and others (3, 6–11). The TME is a complex environment in which various non-cancerous cell populations co-exist, co-evolve and interact with tumour cells, having a profound impact on cancer progression (12). PDAC has been described as "immunologically cold", with tumours generally displaying very limited numbers of cytotoxic CD8+ T cells (13). Compounding this, the pancreatic TME is highly infiltrated by a variety of immunosuppressive cells, including: "M2-like" tumour-associated macrophages (TAMs); cancer-associated fibroblasts (CAFs) and regulatory T cells (Tregs) (14–17). Collectively, these cells work in concert to mitigate the function of cytotoxic CD8+ T cells through the secretion of a host of immunosuppressive factors, resulting in a poor anti-tumour immune response (12, 18). Additionally, immune/stromal derived factors and the characteristically dense desmoplastic reaction of PDAC serve to impede CD8+ accumulation within the pancreatic TME (6, 19–23). With CD8+ T cells being the backbone of emerging immunotherapeutic strategies such as immune checkpoint inhibitors (ICIs) and cancer treatment vaccines, their low abundance within the pancreatic TME can explain the overall lack of success of these therapeutic modalities in the treatment of PDAC (24–28). Indeed, retrospective analysis of surgically resected specimens displays that a greater abundance of CD8+ T cells alongside high levels of tumour-specific antigens within the TME confers a survival advantage in PDAC patients (29). Any therapy that is able to bolster the accumulation of CD8+ T cells within the TME of pancreatic tumours therefore has the potential to improve anti-tumour immunity.

Previous work published by our group and others shows an important role for the IGF signalling pathway in promoting cancer progression and resistance to therapies in a multitude of human malignancies, including PDAC, triple-negative breast cancer (TNBC), colorectal, bladder and ovarian cancer (3, 30–33). Importantly, we previously found that IGF signalling through stromal components including tumour associated macrophages (TAMs) and cancer associated fibroblasts (CAFs) contributes to chemoresistance in the context of both PDAC and TNBC, with

blockade of the IGF signalling pathway sensitising these tumours to gemcitabine and paclitaxel respectively (3, 30). Since IGF signalling is known to influence tumour progression through extrinsic mechanisms via the tumour microenvironment (TME) (34–37), we sought to further characterise changes in the PDAC TME upon blockade of the IGF signalling axis. In addition to this, evidence suggests an emerging immunomodulatory role of the IGF signalling axis, which has been subject of a recent review by Pellegrino et al. (38).

In the present article we show that therapeutic inhibition of the IGF signalling axis leads to an increased accumulation of CD8+ cytotoxic T cells within orthotopic PDAC tumours. Mechanistically, using a combination of in vitro assays, an in vivo preclinical model of PDAC and patient-derived tumour explants, we provide evidence that inhibition of IGF signalling promotes TAM/CAF production of the T cell chemokines CXCL9 and CXCL10 leading to an increase in CD8+ T cell recruitment and trafficking towards the pancreatic TME.

2 Materials and methods

2.1 Generation of primary KPC-derived pancreatic cancer cells

The murine pancreatic cancer cells KPC FC1242 were generated in the Tuveson lab (Cold Spring Harbor Laboratory, New York, USA), isolated from PDAC tumour tissues obtained from LSL-KrasG12D; LSL-Trp53R172H; Pdx1-Cre mice of a pure C57BL/6 background as described previously (39). FC1242luc/zsGreen cells were generated using pHIV Luc-zsGreen lentiviral infection. FC1242luc/zsGreen were cultured in DMEM supplemented with 10% FBS, 1% penicillin/streptomycin, at 37°C, 5% CO2 incubator.

2.2 Cell lines

Jurkat human T lymphocyte cells were cultured in in RPMI 1640 Medium supplemented with 10% FBS and 1% penicillin/streptomycin, at 37°C, 5% CO2 incubator. Jurkat cells were switched to DMEM, high glucose, GlutaMAX medium (Gibco, 10569010) with 10% FBS and 1% penicillin/streptomycin, at 37°C, 5% CO2 incubator for 24 hours prior to use in chemotaxis assays. All cells were routinely tested negative for the presence of Mycoplasma contamination.

2.3 Mice

6-8 weeks old female C57BL/6 mice were purchased from Charles River. All animal experiments were performed in accordance with current UK legislation under an approved project license PPL P16F36770 (M.C. Schmid). Mice were housed under specific pathogen-free conditions at the Biomedical Science Unit at the University of Liverpool.

2.4 Syngeneic orthotopic pancreatic cancer models

1 x 10⁶ primary KPC^luc/zsGreen (zsGreen) cells (FC1242^luc/zsGreen) isolated from a pure C57Bl/6 background were implanted in 30 µL of Matrigel (VWR, 734-0269) into the pancreas of immunocompetent syngeneic C57Bl/6 six-to 8-week-old female mice, and tumours were established for two weeks before beginning treatment. Mice were administered intraperitoneally either IgG2 control antibody (BioXcell, BE0301) (60 mg/kg), or IGF-blocking antibody (MEDI-573) (60 mg/kg), kindly provided by Medimmune (AstraZeneca) at days 14, 17 and 21 post-implantation before harvesting and formalin fixation of both tumours and mesenteric lymph nodes, or collagenase digestion of tumours and subsequent CyTOF analysis at day 22. In a subsequent model, tumours were established as described above and mice administered a single intraperitoneal dose of IgG2 control antibody or IGF blocking antibody at day 23, before tumour harvesting and collagenase digestion and subsequent FACS analysis at day 25 post-implantation.

2.5 Analysis and quantification of immune cells in orthotopic PDAC tumours by mass cytometry

Single-cell suspensions from murine pancreatic tumours were prepared by mechanical and enzymatic disruption in Hank's Balanced Salt Solution (Gibco, 24020091) with 1 mg/mL Collagenase P (Roche, 11213865001) as described (6, 9). Cells were centrifuged for 5 min at 1500 rpm, resuspended in HBSS and filtered through a 500 µm polypropylene mesh (Spectrum Laboratories). Cell suspensions were resuspended in 1mL 0.05% trypsin and incubated at 37°C, for 5 minutes. Suspensions were further enriched for immune cells by density gradient centrifugation using Histopaque-1083 (Sigma Aldrich) at 400x g for 30 minutes at room temperature without brakes. The cloudy band/interface containing the cells plus the bottom layer was transferred into new tube and gently washed with PBS. After one wash with PBS, the cell suspension was washed in double-deionised water (ddH2O; ≥ 18Ω)/Maxpar cell staining buffer (1:2 dilution). The pellet was resuspended in 1 ml of Maxpar cell staining buffer and cells were stained with Cell-ID ^195-Cisplatin (Fluidigm) viability marker in Maxpar PBS (Fluidigm) for 5 min. Cells were washed with Maxpar cell staining buffer, blocked with Fc Block (BD Pharmingen, Clone 2.4G2) on ice for 10 min and metal-conjugated antibody cocktail added and incubated for 40 min at 4°C. See Supplementary Table 1 for list of metal-conjugated antibodies. Antibodies were used at the concentrations recommended by the manufacturer. Cells were then washed twice in cell staining buffer and stained with 125 µM Intercalator ^191Ir (Fluidigm) diluted 1:2,000 in Maxpar fix and perm buffer (Fluidigm) overnight at 4°C. Cells were then washed twice in Maxpar cell staining buffer followed by two washes in 18Ω distilled water (Fluidigm) and resuspended in 0.1X EQTM Four

Element Calibration Beads (Fluidigm) prior acquisition on the Helios CyTOF system (Fluidigm). Samples were acquired at a rate of <500 events/sec. All generated FCS files were normalized and EQ beads standard (40). Data analysis was performed using Cytobank software (mrc.cytobank.org, v6.3 and v7.0, Beckman Coulter); manual gating was used to remove debris, identify single cells (^191Ir+) and to distinguish between dead cells (^195Pt+). Spanning-tree progression analysis for density-normalised events (SPADE) was performed on the data for mapping high dimensional relationships. Viable CD45⁺ singlets selected by manual gating were used for SPADE unsupervised clustering using equal sampling. Manual gating was then performed on the SPADE map created to determine cell population percentages.

2.6 Fluorescence activated cell sorting

Single-cell suspensions from murine pancreatic tumours were prepared by mechanical and enzymatic disruption as described above. Cells were filtered through a 70 µm cell strainer (Miltenyi) and resuspended in 0.5% BSA/PBS. Cells were blocked for 10 minutes on ice with purified rat anti-mouse CD16/CD32 (Mouse BD Fc Block^TM, BD biosciences, 553142) and then stained with Sytox® blue viability marker (Invitrogen, S34857) and conjugated antibodies against anti-CD45-PE-Cy7 (1:100, Biolegend, clone 30-F11, 103114) and anti-F480-APC (1:100, Biolegend, clone BM8, 123116). Cells were incubated with antibodies for 45 min in the dark on ice and fluorescence activated cell sorting (FACS) was carried out using FACS Aria IIIu (BD Biosciences). Cells were sorted directly in RLT buffer + β-mercaptoethanol according to the manufacturer's instruction for RNA isolation (Qiagen).

2.7 Generation of primary bone marrow derived macrophages, primary pancreatic fibroblasts, macrophage and fibroblasts conditioned media

Primary murine bone marrow derived macrophages (BMDMs) were generated by flushing the bone marrow from the femur and tibia of C57BL/6 mice followed by incubation for 5 days in DMEM containing 10% FBS and 10 ng/mL murine M-CSF (PeproTech, AF-315-02) as described (3). Primary pancreatic stellate cells were isolated from C57BL/6 mice pancreas by density gradient centrifugation, and were activated into fibroblasts by culturing them on uncoated plastic dishes in Iscove's Modified Dulbecco's Medium (IMDM) containing 10% FBS and 1% L-glutamine (Sigma Aldrich, G7513). Conditioned media was generated from both BMDMs and fibroblasts by culturing cells in serum free DMEM and IMDM respectively for 24 to 48 hours. For chemotaxis assays fibroblast conditioned media was generated from fibroblasts cultured in serum free RPMI 1640 medium. Supernatants were harvested and filtered using 0.22 µm filter and stored at 4°C until use.

2.8 siRNA knockdown of primary pancreatic fibroblasts

1×10^5 primary pancreatic fibroblasts were treated in 6 well plates with either 5 µM scrambled control siRNA (Dharmacon, D-001810-10-05), or 5 µM ON-TARGETplus siRNA against *Igf1r* (Dharmacon, L-056843-00-0005) or against *Insr* (Dharmacon, L-043748-00-0005), or a combination of both *Igf1r* and *Insr* (double knockdown). Transfection was achieved using 3.5 µl of DharmaFECT 2 transfection reagent (Dharmacon, T-2002-01) per well according to manufacturer's instructions.

2.9 *In vitro* T cell activation assay

Primary murine splenocytes were isolated from spleens of C57BL/6 mice as described previously (6). Dissected spleens were dissociated in MAC buffer and passed through a 70 µm cell strainer to obtain a single-cell suspension. Cells were centrifuged (300 × g), and red blood cells were lysed using 1× Red blood lysis buffer (Biolegend). Obtained splenocytes were cultured in either primary pancreatic fibroblast conditioned media in which fibroblasts had been treated with either IgG control antibody (100 µg/ml) or IGF-blocking antibody (100 µg/ml). As a positive and negative control separate splenocytes were cultured in serum free RPMI 1640 medium with or without Dynabeads Mouse T activator CD3/CD28 (Thermofisher, 11452D). Cells were plated in 96-well plates and incubated at 37°C for 24 hours. Subsequently, Brefeldin A (eBioscience; 1:100) was added to the cells for 5 hours. Cells were then harvested, stained with LIVE/DEAD™ Fixable Aqua Stain (1:1000, Invitrogen, L34957 before subsequent fixation and permeabilisation using FIX & PERM™ Cell Permeabilization Kit (Invitrogen). Fixed cells were then incubated with conjugated antibodies against anti-CD8-PerCP/Cyanine5.5 (1:100 Biolegend; clone 53-6.7) and IFNγ-PE (1:100, Biolegend; clone XMG1.2) for 45 minutes prior to flow cytometric analysis on a FACS Canto II (BD bioscience) instrument.

2.10 Human studies

Human studies using primary tissue samples were approved by the National Research Ethics (NRES) Service Committee North West – Greater Manchester REC15/NW/0477 and REC19/NW/0298. All samples included in the analysis were histologically confirmed as PDAC by an independent team of histopathologists at the Royal Liverpool University Hospital NHS Trust. All individuals provided informed consent for tissue donations on approved institutional protocols.

2.11 Precision cut tumour slicing and *ex vivo* culture

Precision cut tumour slicing (PCTS) was performed on fresh primary PDAC specimens following a protocol adapted from (7, 41, 42). Briefly, 0.5 cm samples of primary PDAC tissues were embedded in 3% UltraPureLMP Agarose (Invitrogen) dissolved in PBS, onto specimen small dishes. Sectioning was performed using Leica vibrating blade microtome VT1200 S (Leica), using stainless steel razor blades (Personal Medical) under buffered conditions with ice-cold HBSS containing 25 mM glucose (Merck), at the following adjustable settings: knife angle: 15°; sectioning speed: 0.4–1 mm/s; oscillation amplitude: 3 mm; step size: 250 µm; retract: 10 µm; continuous stroke. The first slice was immediately fixed in formalin as a day 0 and embedded in paraffin. Slices were cultured on inserts (0.4 µm pore size, 30 mm diameter, Millicell®, Millipore, PICM0RG50) placed inside 6 well plates containing 1.1 ml DMEM, high glucose, GlutaMAX (Gibco, 10569010) with 10% FBS and 1% Penicillin/Streptomycin with an additional 150 µl of media being added on top of slices. Inserts were coated with 250 µl of collagen gel consisting of 3 mg/ml rat tail collagen type 1 (Merck, C3867-1VL), 0.025 N NaOH in PBS. Slices were cultured for 24 hours at 37°C, 5% CO2 before media was replaced and slices were treated with either IgG control antibody (100 µg/ml) or IGF-blocking antibody (100 µg/ml) for a further 72 hours of culture at the same conditions. Treated slices were fixed in formalin and embedded in paraffin prior to downstream immunohistochemical and immunofluorescent analysis. Conditioned media from treated slices was filtered at 0.22 µm and stored at -20°C until use.

2.12 Chemotaxis assays

In the mouse model experiment primary murine CD8$^+$ T cells were obtained from the spleen of C57BL/6 mice using the murine CD8a$^+$ T Cell Isolation Kit (Miltenyi, 130-104-075) according to manufacturer's instructions. 1×10^6 CD8$^+$ T cells were added in serum free RPMI into 5 µm transwell inserts (Corning) and allowed to migrate into the bottom chamber of the 24- well plate for 15 hours. The bottom chamber was loaded with fibroblast conditioned media whereby primary murine fibroblasts had been cultured in fibroblast conditioned media treated with either IgG control antibody (100 µg/ml) or IGF-blocking antibody (100 µg/ml) for 48 hours. CD8$^+$ T cells were treated with or without the CXCR3 antagonist SCH 546738 (10 nM, MedChemExpress), normal goat IgG control (1 µg/ml, R&D Systems, AB-108-C) or Human/Mouse IGF-I R/IGF1R Antibody (1 µg/ml, R&D Systems, AF-305-SP) and their migration towards anti-IGF treated fibroblast conditioned media measured after 15 hours. As a positive and negative control, the bottom chamber was loaded with serum free RPMI +/- recombinant murine CXCL9 (1000 ng/ml, Peprotech).

In the human model experiment, 1×10^6 Jurkat cells were added in DMEM, high glucose, GlutaMAX media into upper chamber of 5 µm inserts and their migration towards conditioned media generated from PCTS *ex vivo* human PDAC slices treated with either IgG control antibody (100 µg/ml) or IGF-blocking antibody (100 µg/ml) measured after 15 hours. For both experiments and all treatments, both the top and bottom chamber was supplemented with recombinant murine IL-2 (50 U/ml, Peprotech). Migrated cells were recovered from the lower chamber and counted by using a haemocytometer.

2.13 RT–qPCR

Total RNA purification was performed with the RNeasy Kit (Qiagen), and cDNA was generated using the M-MLV Reverse Transcriptase kit (Invitrogen). 500 ng of total RNA was used to generate cDNA. qPCR was performed using 5 x HOT FIREPol EvaGreen qPCR Mix Plus (ROX; Solis Biodyne) on an AriaMx Real-Time PCR (qPCR) Instrument (Agilent). Three-step amplification was performed (95°C for 15 seconds, 60°C for 20 seconds, and 72°C for 30 seconds) for 45 cycles. Relative expression levels were normalized to Gapdh expression according to the formula: $2^{\wedge -(Ct\ gene\ of\ interest\ -\ Ct\ Gapdh)}$. Fold increase in expression levels was calculated by the comparative Ct method: $2^{\wedge (-ddCt)}$. The control used to apply $2^{\wedge (-ddCt)}$ was either the IgG control antibody treatment or the scrambled siRNA control as applicable. The following QuantiTect Primers Assays (Qiagen) were used to assess mRNA levels: Mm-Gapdh (Mm_Gapdh_3_SG; QT01658692), Mm-IL10 (Mm_ IL10_1_SG; QT00106169), Mm-Tgfb1 (Mm_Tgfb1_1_SG; QT00145250), Mm-IL6 (Mm_Il6_1_SG QuantiTect; QT00098875), Mm-Tnf (Mm_Tnf_1_SG; QT00104006), Mm-Cxcl10 (Mm_Cxcl10_1_SG; QT00093436), Mm-Cxcl12 (Mm_Cxcl12_va.1_SG), Mm-Arginase (Mm_Arg1_1_SG; QT00134288), Mm-Col1a1 (Mm_Col1a1_1_SG; QT00162204), Mm-Col1a2 (Mm_Col1a2_1_SG; QT01055572), Mm-Fn1 (Mm-Fn1_1_SG; QT00135758), Mm-Stat1 (Mm-Stat1_1_SG; QT00162183), Mm-Insr (Mm-Insr_vb.1_SG; QT01540854), Mm-Igf1r (Mm-Igf1r_1_SG; QT00155351). Mm-Cxcl9 (Mm-Cxcl9_Fw CAGCTCTGCCATGAAGTCCG; Mm-Cxcl9_Rev TCCTTATCACTAGGGTTCCTCG), Mm-Icam1 (Mm-Icam1_Fw GAGCTCGAGAGTGGACCCAA; Mm-Icam1_Rev TCTCAGCTCCACACTCTCCG), Mm-Irf1 (Mm-Irf1_Fw CGGGCATCTTTCGCTTCGT; Mm-Irf1_Rev AGGGTCTCATCCGCATTCGAG), Mm-Oas2 (Mm-Oas2_Fw CAGGAGGGATCTTGTGGCAGG; Mm_Oas2_Rev TGCCAGATCACTCCAGAAGCG) were purchased from Merck.

2.14 Immunohistochemistry analysis

Deparaffinization and antigen retrieval were performed using an automated DAKO PT-link. Paraffin-embedded human and mouse PDAC tissues were immunostained using the DAKO envision system-HRP. 4 μm tissue sections were incubated overnight at 4°C with the following primary antibodies: CD3 (Abcam, SP7 clone, ab16669, 1:100, high pH antigen retrieval); CD4 (Abcam, ab183685, 1:500, high pH antigen retrieval); αSMA (Abcam, ab5694, 1:200 high pH antigen retrieval), CXCL10 (Invitrogen, 10H11L3 clone, 701225, 1:100, low pH antigen retrieval); Ki67 (Abcam, ab15580, 1:1000, low pH antigen retrieval); CC3 (Cell Signaling Technology, #9661, 1:200, high pH antigen retrieval); phospho-Insulin/IGF1 receptors (R&D, AF2507, 1:50 high pH antigen retrieval). Secondary HRP-conjugated antibodies were incubated for 30 minutes at room temperature. Staining was developed using diaminobenzidine and counterstained with haematoxylin.

2.15 Immunofluorescent analysis

For immunofluorescence staining, 4 μm tissue sections were permeabilised by 0.1% TritonX-100 (Sigma Aldrich) for 2 min at room temperature. Unspecific bindings were prevented by using PBS + 10% donkey serum for 1 hour at room temperature. Tissue sections were incubated overnight at 4°C with the following antibodies: CD8a (eBioscience, 53-6.7 clone, 14-0081-82, 1:50); CD8 (Dako, C8/144B clone, M7103, 1:100), Granzyme B (Abcam, ab4059, 1:100); PD-1 (Abcam, ab214421, 1:500); Ki67 (Abcam, ab15580, 1:1000); CC3 (Cell Signaling Technology, #9661, 1:200); CD4 (Invitrogen, 14-9766-80, 4SM95 clone, 1:50); FoxP3 (Cell Signaling Technology, #12653, 1:100); F4/80 (Biolegend, BM8 clone, 123101 1:50); F4/80 (Cell Signaling Technology, #70076, 1:100), CD206 (Abcam, ab64693, 1:1000); MHC II (Novus Biologicals, NBP1-43312, 1:100); CXCL9 (R&D Systems, AF-492-NA, 1:50); phospho-Stat3 (Tyr705) (Cell Signaling Technology, #4093, 1:100); phospho-Stat1 (Tyr701) (Cell Signaling Technology, #9167, 1:300); PDGFRβ (R&D Systems, AF1042, 1:50); αSMA (Abcam, ab5694, 1:200). The following day, sections were washed with PBS and incubated with 5 mg/ml 4′,6-diamidino-2-phenylindole (DAPI) and fluorescently labelled secondary antibodies for 2 hrs at room temperature: Donkey anti rat AF488 (Abcam, ab150149, 1:300); Donkey anti-rat AF647 (Abcam, ab150155, 1:300); Donkey anti-rabbit AF488 (Biolegend, 406416, 1:300); Donkey anti-rabbit AF594 (Biolegend, 406418 1:300); Donkey anti-goat AF488 (Abcam, ab150129, 1:300); Donkey anti-goat AF594 (Abcam, ab150132, 1:300); Donkey anti-mouse AF488 (Abcam, ab150105, 1:300). Sections were mounted onto coverslips using Dako Fluorescent mounting medium (Agilent). Slides were imaged using Axio Observer Light Microscope with the Apotome.2 (Zeiss). Positive cells were counted manually (using 5-10 field of view per sample) whereas cell nuclei counting was automated using QuPath (v0.2.3).

2.16 Immunocytochemistry analysis

Primary pancreatic fibroblasts were grown on cover slips and fixed with 4% paraformaldehyde in PBS (VWR, ALFAJ19943.K2) for 10 min at room temperature with gentle agitation. Cells were washed gently with PBS and permeabilised by 0.1% TritonX-100 (Sigma Aldrich) for 2 min at room temperature. Cells were blocked in 2% BSA/PBS for 30 min at room temperature with gentle agitation before subsequent incubation overnight at 4°C with primary antibody against anti-STAT1 (Cell Signaling Technology, #9172, 1:100). The following day, cells were washed with PBS and incubated with 5mg/ml 4′,6-diamidino-2-phenylindole (DAPI) and Donkey anti-rabbit AF594 (Biolegend, 406418 1:300) for 2 hr room temperature. Following incubation cells were washed with PBS and mounted onto microscope slides with Dako Fluorescent mounting medium (Agilent). Slides were imaged using Axio Observer Light Microscope with the Apotome.2 (Zeiss) with the total STAT1$^+$ and total cell nuclei quantified using QuPath (v0.2.3) software.

2.17 Immunoblotting

Primary pancreatic fibroblasts or primary BMDMs were lysed in 62.5 mM Tris-HCl pH 6.8, 10% glycerol, 2% SDS, 1% β-mercaptoethanol) supplemented with complete protease inhibitor mixture (Sigma), phosphatase inhibitor cocktail (Invitrogen), 1 mM phenylmethylsulfonyl fluoride and 0.2 mM sodium orthovanadate. Following sonication and clarification, protein concentration was determined using Pierce Protein BCA Assay Kit – Reducing Agent Compatible (Thermo Fisher) according to manufacturer's instructions. 30 µg of cell lysates were loaded and ran on 10% SDS-PAGE gels. Conditioned media generated from PCTS *ex vivo* human PDAC slices was concentrated using SrataClean Resin (Agilent), loaded and ran on 15% SDS-PAGE gels. After protein transfer using the Trans-blot Turbo Transfer System (Bio-rad), PVDF membranes were blocked in 5% BSA-TBST for 1 hr and blotted overnight at 4 ˚C with the following primary antibodies: anti-IGF1R (R&D Systems, AF305-NA, 1:1000); anti-Insulin receptor (Abcam, ab137747,1:1000); anti-phospho-AKT (Ser473) (Cell Signaling Technology, #4060, 1:1000); anti-AKT (Cell Signaling Technology, #9272, 1:1000); anti-phospho-Stat3 (Tyr705) (Cell Signaling Technology, #4093, 1:1000); anti-STAT3 (Cell Signaling Technology, #4094, 1:1000), anti-GAPDH (Sigma, G9545, 1:10,000); anti-CXCL9 (R&D Systems, AF392, 1:2000), anti-tubulin (Sigma, T6199, 1:10,000); followed by HRP-conjugated secondary antibodies for 2 hours at room temperature. Protein bands were visualised using Pierce ECL Western Blotting Substrate (Thermo Fisher) on a ChemiDoc MP (Bio-rad) imaging system.

2.18 Picrosirius red staining

Paraffin-embedded human and mouse PDAC samples were dewaxed and hydrated using a graded ethanol series. Tissue sections were then treated with 0.2% phosphomolybdic acid and subsequently stained with 0.1% Sirius Red F3B (Direct Red 80; Sigma Aldrich) in saturated picric acid solution for 90 minutes at room temperature. Tissues were then rinsed twice in acidified water (0.5% glacial acetic acid; Sigma Aldrich) before and after the staining with 0.033% fast green FCF (Sigma Aldrich). Finally, tissues were dehydrated in three changes of 100% ethanol, cleared in xylene, and mounted. Picrosirius red staining was quantified using Image J software.

Quantification of collagen deposition by primary pancreatic fibroblasts was measured following a protocol adapted from (43). Following 72 hours of culture with IgG control antibody (100 µg/ml) or IGF-blocking antibody (100 µg/ml), primary pancreatic fibroblasts were fixed *in situ* with 70% ice cold ethanol and transferred to -80°C for 30 min. Cells were subsequently stained with 0.1% Sirius Red F3B (Direct Red 80; Sigma Aldrich) in saturated picric acid solution and incubated overnight at 4°C with gentle agitation. Unbound dye was washed away with distilled water and fixed cells were subsequently treated with 1 M NaOH at room temperature for 10 min with gentle agitation. 100 µl of dissolved collagen-dye complex was transferred in duplicate to a 96 well microplate and absorbance measured at 490 nm on a Varioskan Flash Spectral Scanning Multimode Reader (Thermo Fisher Scientific). A standard curve was constructed by drying known

concentrations of rat-tail collagen type I (Merck, C3867-1VL), on the surface of tissue culture plastic before staining, dissolving and quantification as described above.

2.19 Statistical analysis

Statistical significance (analysed with GraphPad Prism v8 software) was determined using two-tailed unpaired Student's t tests when comparing differences between two experimental groups for parametric data or Mann-Whitney U test for non-parametric data. Unless otherwise stated, one-way ANOVA with Dunnett's multiple comparisons test was used for all experiments with more than two groups. For Figures 4J and 4K two-way ANOVA with Dunnett's multiple comparisons test was performed. For Figure 5B and Supplementary Figure 5A one sample t test with a theoretical mean of 1 was performed. For Figure 5G and Supplementary Figure 1F two-way ANOVA with Bonferroni's multiple comparisons test was performed. A P-value < 0.05 was considered statistically significant and P values are indicated in the figures using asterisks: *P<0.05; **P<0.01; ***P<0.001; ****P<0.0001; ns denotes not significant.

3 Results

3.1 IGF blockade leads to an increase in cytotoxic T cell accumulation in pancreatic tumours.

Mice bearing established orthotopic PDAC tumours were treated with either IgG2 control antibody or IGF-blocking antibody (MEDI-573). In line with previous work in our lab and others (3, 44), treatment with IGF-blocking antibody alone only led to a modest decrease in tumour weight (Figure 1A). However, further analysis of these tumours through immunohistochemistry revealed a significant increase in the number of tumour infiltrating lymphocytes (TILs) upon IGF blockade as determined by the percentage of CD3^{+} T cells (Figures 1B, C). Further characterisation of these TILs by immunohistochemistry and immunofluorescent analysis revealed no significant difference in the number of CD4^{+} T cells (Supplementary Figures S1A, B) but a significant difference in the number of CD8^{+} cytotoxic T cells upon IGF blockade (Figures 1D, E). Of note, the number of regulatory T cells (Tregs; CD4^{+} FoxP3^{+}) remained unchanged by IGF inhibition (Supplementary Figures S1C, D). Corroborating these results, the overall increase in CD8^{+} T cells in tumours treated with IGF-blocking antibody was also observed in whole tumour digests using CyTOF mass cytometry (Supplementary Figures S1E, F). Despite the overall increase in CD8^{+} T cells within PDAC tumours upon IGF blockade, the proportion of CD8^{+} T cells concomitantly expressing granzyme B, a marker of T cell functional activity, remains low after IGF blockade (Figures 1F, G). Additionally, the fraction of CD8^{+} T cells which are positive for the inhibitory immune checkpoint PD-1 and the activation marker CD69 is unaffected by IGF blockade (Figures 1H, I; Supplementary Figures S1E, F), suggesting that while their overall numbers increase, these CD8^{+} T cells remain functionally inactive (45). Corroborating this, the

proportion of CD8$^+$ PD1$^+$ T cells among all CD8$^+$ T cells remains unaffected by IGF blockade (Supplementary Figure S1G).

Taken together, these data show that IGF blockade leads to an increase in CD8$^+$ accumulation within primary pancreatic tumours. Despite this overall increase in CD8$^+$ T cells within the tumour, the resulting decrease in tumour size upon treatment with anti-IGF antibody is modest, which can be explained at least in part by the fact that these T cells remain functionally inactive.

3.2 IGF blockade does not affect CD8$^+$ T cell priming, survival or proliferation within the PDAC TME

The cancer immunity (CI) cycle proposed by Chen and Mellman (and recently updated (46) describes the series of stepwise events necessary for an effective anti-tumour immune response, beginning with the release of cancer neoantigens and
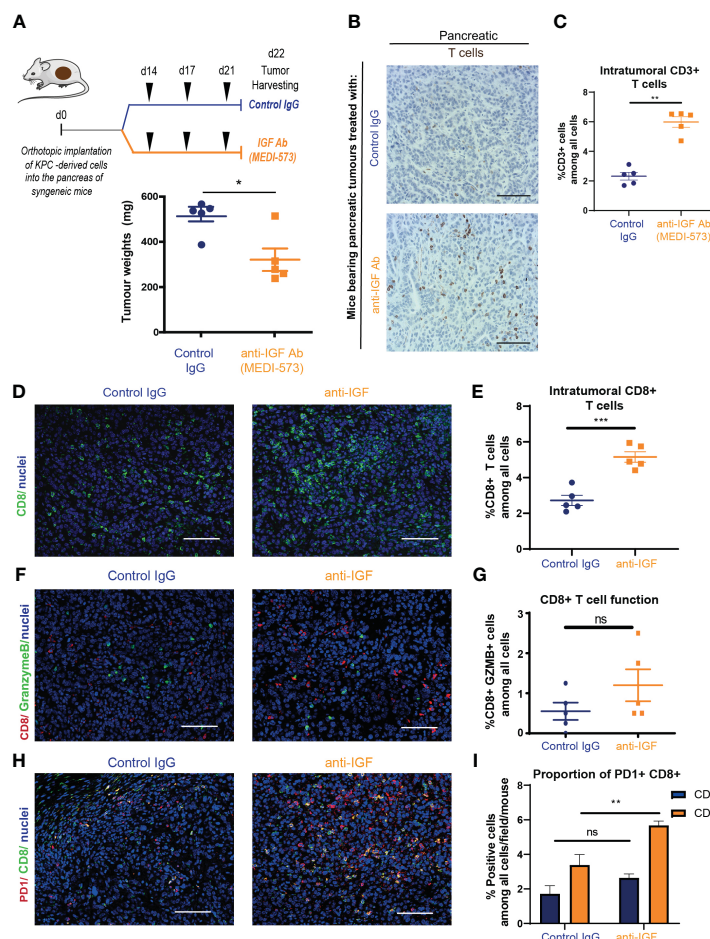

FIGURE 1

IGF blockade leads to an increase in cytotoxic T cell accumulation in pancreatic tumours **(A)** Top, *LSL-Kras$^{G12D/+}$;LSL-Trp53$^{R172H/+}$;Pdx-1-Cre* (KPC) derived FC1242 cells were orthotopically implanted into the pancreas tail of syngeneic C57BL-6J recipient mice. Mice were treated by intraperitoneal injection with either IgG2 control antibody (60 mg/kg) or IGF-blocking antibody MEDI-573 (60 mg/kg) at days 14, 17 and 21 post implantation. Pancreatic tumours were harvested at day 22 post implantation. Below, tumour weights at harvest for both treatment groups (n = 5 mice per treatment group), *P ≤ 0.05 using Mann-Whitney U test. **(B)** Immunohistochemical staining of CD3$^+$ T cells in formalin fixed paraffin embedded tissues from orthotopic murine PDAC tumours treated with IgG2 control antibody or IGF-blocking antibody MEDI-573. Scale bar; 50 μm. **(C)** Quantification of CD3 staining. Data displayed as total CD3+ T cells among all cells. A total of 5-8 fields of view counted/mouse tumour, n = 5 mice per treatment group, *P ≤ 0.05 using Mann-Whitney U test. **(D)** Immunofluorescent staining of CD8 (green), and nuclei (blue) in formalin fixed paraffin embedded tissues from orthotopic murine PDAC tumours treated with IgG2 (control) antibody or IGF blocking antibody MEDI-573. Scale bar 50 μm. **(E)** Quantification of CD8 staining. Data displayed as total CD8$^+$ T cells among all cells. A total of 5-8 fields of view counted/ mouse tumour, n = 5 mice per treatment group, ***P ≤ 0.001 using unpaired t test. **(F)** Immunofluorescent staining of CD8 (red), granzyme B (green) and nuclei (blue) in formalin fixed paraffin embedded tissues from orthotopic murine PDAC tumours treated with IgG2 (control) antibody or IGF blocking antibody MEDI-573. Scale bar 50 μm. **(G)** Quantification of functionally active CD8$^+$ T cells in IgG control treated and anti-IGF treated orthotopic murine pancreatic tumours. Data displayed as percentage of CD8$^+$/GranzymeB$^+$ cells among all cells. A total of 5-8 fields of view counted/mouse tumour, n= 5 mice per treatment group, ns; P > 0.05 using Mann-Whitney U test. **(H)** Immunofluorescent staining of CD8 (green), PD1 (red) and nuclei (blue) in formalin fixed paraffin embedded tissues from orthotopic murine PDAC tumours treated with IgG2 (control) antibody or IGF blocking antibody MEDI-573. Scale bar 50 μm. **(I)** Quantification of PD1$^+$ CD8$^+$ T cells in IgG control treated and anti-IGF treated orthotopic murine pancreatic tumours. Data displayed as either percentage of CD8$^+$ T cells among all cells or PD1$^+$/CD8$^+$ T cells among all cells. A total of 5-8 fields of view counted/mouse tumour, n= 5 mice per treatment group, ns; P > 0.05, **P ≤ 0.01 using Mann-Whitney U test.

culminating with the targeted CD8^{+} cytotoxic T cell mediated destruction of tumour cells. In order for CD8^{+} T cells to accumulate within the tumour, they must first be primed/ activated in the tumour draining lymph node. Following this they must effectively traffic towards the tumour bed, infiltrate into the tumour and stroma, and survive within the hypoxic, immunosuppressive conditions of the TME maintaining their effector states and function (46). We therefore hypothesised that aberrant IGF signalling affects one/or multiple steps in this cycle to impede T cell accumulation within the pancreatic TME.

Immunofluorescent analysis of tumour draining mesenteric lymph nodes from mice bearing orthotopic PDAC tumours (Figure 2A) revealed no differences in the numbers of CD8^{+} T cells upon treatment with IGF blocking antibody (Figures 2B, C). In addition, no differences in the proportion of proliferative (Ki67^{+}) or functionally active (Granzyme B^{+}) CD8^{+} T cells were observed, suggesting that IGF blockade is unlikely to affect T cell priming (Figures 2B, D). Following this we sought to further characterise the CD8^{+} T cells present within primary PDAC tumours following anti-IGF treatment. Again, no differences in CD8^{+} T cell proliferation were detected (Figures 2E, F) and additionally, no differences in their survival (cleaved caspase 3^{+}) (Figures 2E, G) were observed upon IGF blockade.

Collectively, these data show that IGF blockade is unlikely to affect CD8^{+} T cells priming, does not affect CD8^{+} T cell survival or proliferation within the PDAC TME and that their increased accumulation in tumours must be attributed to other factors affecting different steps of the CI cycle.

3.3 IGF blockade promotes the production of T cell chemoattractants CXCL9 and CXCL10 by TAMs and CAFs

TAMs and CAFs remain two of the most abundant non-cancerous cell populations within the PDAC tumour microenvironment and both cell populations play a pleiotropic role in regulating CD8^{+} T cell accumulation within solid tumours via multiple mechanisms (20, 47–49). In addition to this, previously published work from our group demonstrated that TAMs and CAFs are the main extracellular source of IGF ligands within both the pancreatic and TNBC TME (3, 30). In addition, both primary murine macrophages and primary murine fibroblasts express IGF-1R and Insulin receptor (Supplementary Figures S2A, B) potentially indicative of an autocrine signalling axis. In accordance, immunohistochemical and immunofluorescent analysis of murine orthotopic PDAC tumours reveals overall changes on TAM and CAF populations when mice are treated with IGF-blocking antibody. Here we demonstrate an increase in αSMA[+] CAFs upon IGF blockade (Figures 3A, B). With regard to TAMs, no changes in total F4/80[+] TAM numbers are observed (Figures 3C, D), yet we demonstrate an increase in MHCII[+] F480^{+} macrophages, that have been described as a immunostimulatory population of TAMs (50, 51), upon IGF blockade (Figures 3D, F). No changes in CD206^{+} TAMs (Figures 3E, G) are observed upon IGF blockade.

Given the role of IGF signalling in the TAM and CAF cell populations and the observed changes in these two cell populations upon IGF blockade, as well as the concomitant increases in CD8^{+} T cells within pancreatic tumours, we hypothesised that aberrant IGF signalling in TAMs and/or CAFs negatively regulates the accumulation of CD8^{+} T cells within pancreatic tumours through TAM and/or CAF derived factors.

To test this hypothesis, we isolated both TAMs (CD45^{+}/F4/80^{+} cells) and non-immune stromal cells (CD45^{-}/zsGreen^{-}) using FACS from established orthotopic PDAC tumours that had been treated with either IgG2 control antibody or IGF-blocking antibody (Figure 3H). We then analysed the transcriptional expression of a panel of cytokines and chemokines known to regulate T cell survival, function or chemoattraction including: *Il10, Tgfb, Il6, Tnfa, Cxcl9, Cxcl10* and *Cxcl12* (52–64); and extracellular matrix (ECM) components including: *Col1a1, Col1a2* and *Fn1* in CAFs known to affect T cell infiltration into the tumour milieu (6, 20, 65–67)), in response to treatment with IGF-blocking antibody.

Measuring this panel of transcriptional markers by RT-qPCR revealed significant decreases in TAM expression of *Il6* (Figure 3I) upon IGF blockade. Interestingly CAF expression of both *Col1a1* and *Col1a2* is significantly decreased upon treatment with IGF-blocking antibody (Figure 3J). Furthermore, borderline significant increases in expression are observed for *Cxcl9* in TAMs (Figure 3I) and *Cxcl10* in CAFs (Figure 3J) upon IGF blockade. An increase in T cell chemokines could serve to facilitate CD8^{+} T cell accumulation into the PDAC TME through increased trafficking/recruitment towards the tumour.

We then sought to corroborate these findings *in vitro* utilising both primary murine macrophages and primary murine fibroblasts isolated from the bone marrow and pancreata of wild type C57BL/ 6J mice respectively (Supplementary Figure S2C). Any changes observed both *in vitro* and *in vivo* are likely to be the result of a direct mechanistic effect of blocking IGF signalling on the cell types in question as opposed to a potentially indirect change mediated through the multitude of interacting cells within the TME.

No significant changes were observed in transcriptional levels of *Il6* in either BMDMs or fibroblasts upon IGF blockade (Supplementary Figure S2D, E). A small but statistically significant increase was observed in *Il10* expression in BMDMs (Supplementary Figure S2D), as well as an increase in *Col1a2* expression in fibroblasts upon IGF blockade (Supplementary Figure S2E). Interestingly, and in accordance with our *in vivo* findings, we observed a statistically significant increase in the transcriptional expression of both *Cxcl9* and *Cxcl10* in the case of both BMDMs (Supplementary Figure S2D) and fibroblasts (Supplementary Figure S2E) upon IGF blockade. Supporting this, a statistically significant increase in both *Cxcl9* (Figure 3K) and *Cxcl10* (Figure 3L) was observed upon genetic ablation of the IGF signalling pathway through simultaneous siRNA knockdown of both *Igf1r* and *Insr* in primary murine fibroblasts. IGF ligands can elicit signal transduction through both the IGF-1R and insulin receptor (68, 69), with the IGF-blocking antibody MEDI-573 inhibiting this signalling pathway through scavenging of IGF1/2 ligands. Therefore, targeted genetic ablation of *Igf1r* and *Insr* serves as a surrogate for our pharmacological inhibition of IGF signalling,

with statistically significant knockdowns for both these genes being observed upon siRNA treatment (Supplementary Figure S2F, G). Given that pharmacological blockade of IGF signalling elicited a reduction in *Il6 in vivo* which was not recapitulated *in vitro*, this discrepancy led to further analysis of primary murine fibroblasts, revealing no changes in *Il6* transcription upon genetic abrogation of IGF signalling (Supplementary Figure S2H).

To our knowledge, this direct increase in CD8+ T cell chemokines, *Cxcl9* and *Cxcl10* in response to IGF blockade has not been previously reported in any cell type. Significantly, our results demonstrate that this increase is conserved across both primary murine BMDMs and fibroblasts, and translates into preclinical models of PDAC *in vivo*. Further strengthening these data, immunohistochemical and immunofluorescent analysis
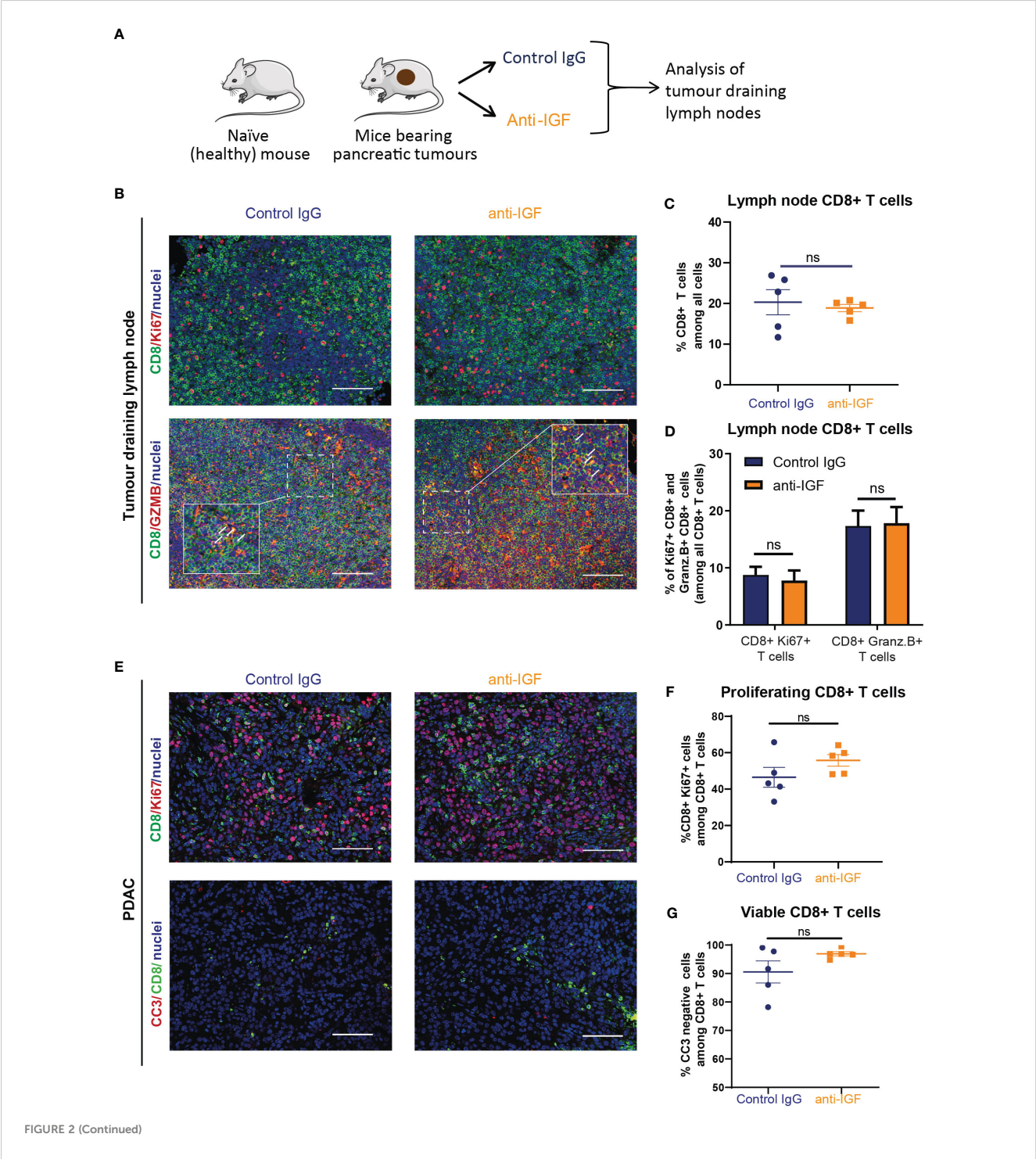

FIGURE 2 (Continued)

FIGURE 2 (Continued)

IGF blockade does not affect CD8$^+$ T cell priming, survival or proliferation within the PDAC TME. **(A)** *LSL-Kras$^{G12D/+}$;LSL-Trp53$^{R172H/+}$;Pdx-1-Cre* (KPC) derived FC1242 cells were orthotopically implanted into the pancreas tail of syngeneic C57BL-6J recipient mice. Mice were treated by intraperitoneal injection with either IgG2 control antibody (60 mg/kg) or IGF-blocking antibody MEDI-573 (60 mg/kg) at days 14, 17 and 21 post implantation. Mesenteric lymph nodes were harvested at day 22 post implantation. **(B)** Top, immunofluorescent staining of CD8 (green), Ki67 (red) and nuclei (blue) in formalin fixed paraffin embedded mesenteric lymph nodes from mice bearing orthotopic PDAC tumours treated with IgG2 (control) antibody or IGF blocking antibody MEDI-573. Scale bar 50 μm. Below, immunofluorescent staining of CD8 (green), Granzyme B (red) and nuclei (blue) in formalin fixed paraffin embedded mesenteric lymph nodes from mice bearing orthotopic PDAC tumours treated with IgG2 (control) antibody or IGF blocking antibody MEDI-573. Scale bar 50 μm. **(C)** Quantification of CD8 staining in mesenteric lymph nodes. Data displayed as total CD8$^+$ T cells among all cells. A total of 3 fields of view counted/mouse lymph node, n = 5 mice per treatment group, ns; P > 0.05 using Mann-Whitney U test. **(D)** Quantification of Ki67+/CD8+ T cells and Granzyme B+/CD8+ T cells in mesenteric lymph nodes in IgG control treated and anti-IGF treated mice bearing orthotopic pancreatic tumours. Data displayed as percentage of Ki67$^+$/CD8$^+$ T cells and Granzyme B$^+$/CD8$^+$ T cells among all CD8$^+$ T cells. A total of 3 fields of view counted/mouse tumour, n= 5 mice per treatment group, ns; P > 0.05 using Mann-Whitney U test. **(E)** Top, immunofluorescent staining of CD8 (green), Ki67 (red) and nuclei (blue) in formalin fixed paraffin embedded tissues from orthotopic murine PDAC tumours treated with IgG2 (control) antibody or IGF blocking antibody MEDI-573. Bottom, Immunofluorescent staining of CD8 (green), cleaved caspase 3 (red) and nuclei (blue) in formalin fixed paraffin embedded tissues from orthotopic murine PDAC tumours treated with IgG2 (control) antibody or IGF blocking antibody MEDI-573. Scale bar 50 μm. **(F)** Quantification of proliferating CD8$^+$ T cells in IgG control treated and anti-IGF treated orthotopic murine pancreatic tumours. Data displayed as percentage of CD8$^+$/Ki67$^+$ cells among all CD8+ T cells. **(G)** Quantification of viable CD8$^+$ T cells in IgG control treated and anti-IGF treated orthotopic murine pancreatic tumours. Data displayed as percentage of CD8$^+$/CC3- cells among all CD8$^+$ T cells. A total of 5-8 fields of view counted/mouse tumour, n= 5 mice per treatment group, ns; P > 0.05 using Mann-Whitney U test.

revealed an overall significant increase in the levels of CXCL9 and CXCL10 (Figures 3M–O) within the TME of mouse PDAC tumours upon IGF blockade.

We next sought to explore whether these observed increases in the T cell chemokines CXCL9 and CXCL10 upon IGF blockade could incur an increase in CD8$^+$ T cell migration at a more functional level. To model this, we designed an *in vitro* chemotaxis assay in which the migration of primary murine CD8$^+$ T cells towards fibroblast conditioned media was measured, whereby primary murine fibroblasts had been treated with fibroblast conditioned media and either IgG control antibody (100 μg/ml) or IGF-blocking antibody (100 μg/ml) (Figure 3P). CD8$^+$ T cells preferentially migrated towards fibroblast conditioned media following IGF blockade (Figure 3Q) in accordance with transcriptional increases in *Cxcl9* and *Cxcl10* in these fibroblasts (Figures 3R, S). In addition to this, pretreatment of CD8$^+$ T cells with the CXCR3 antagonist SCH 546738 (10 nM) significantly abrogated their migration towards anti-IGF treated fibroblast conditioned media (Figure 3Q). Additionally, blockade of IGF-1R on CD8$^+$ T cells had no effect on their migration towards anti-IGF treated fibroblast conditioned media (Supplementary Figure S2I), suggesting that the increase in migration is not due to IGF signalling on CD8$^+$ T cells themselves. As a positive control we demonstrate a significant increase in CD8$^+$ T cell migration towards RPMI upon the addition of recombinant CXCL9 (1000 ng/ml) (Supplementary Figure S2J).

Furthermore, flow cytometric analysis of CD8$^+$ T cells cultured in fibroblast conditioned media revealed no differences in CD8$^+$ T cell viability (CD8$^+$ Amycan$^-$) or functional status (CD8$^+$ IFN-γ$^+$) regardless of fibroblast treatment (Supplementary Figure S3A, B), supporting our *in vivo* findings that IGF blockade does not affect CD8$^+$ survival or function within the PDAC TME. As a positive control we demonstrate a significant increase in CD8$^+$ T cell activation upon stimulation with CD3/CD28 Dynabeads (Supplementary Figures S3C, D).

Taken together these results highlight a novel role for IGF in regulating the production of the T cell chemokines CXCL9 and CXCL10 by TAMs and CAFs. These data suggest that IGF blockade promotes CD8$^+$ T cell accumulation within the PDAC TME at least

in part through increased T cell recruitment/trafficking towards the tumour in a stroma-derived CXCL9/CXCL10 chemokine-dependent manner.

3.4 IGF blockade reverses phosphorylation of STAT3 in TAMs and CAFs whilst promoting STAT1 transcription of *Cxcl9* and *Cxcl10*

Having demonstrated a clear role of the IGF signalling axis in regulating the expression of the T cell chemokines CXCL9 and CXCL10 in both macrophages and fibroblasts, we investigated this pathway further to gain greater mechanistic insight.

The transcription of *Cxcl9* and *Cxcl10* is a tightly regulated process. Canonically, this occurs under the control of the transcription factor STAT1 following activation of the IFN gamma receptor and subsequent phosphorylation of STAT1 (70–72). It is well established that activation of the IGF signalling pathway promotes the phosphorylation and activation of the downstream effector AKT via the IRS1/2/PI3K/PDK1 cascade (3, 73, 74). Downstream of this, AKT activation promotes the phosphorylation and activation of STAT3 (75), with STAT3 having a pleiotropic role in oncogenesis, via cancer cell intrinsic and extrinsic mechanisms through promotion of an immunosuppressive TME in multiple cancer settings (76–80). Moreover, several studies highlight a role for IGF signalling in promoting immunosuppression via STAT3 activation, regulating this through multiple signalling cascades including JAK1/RACK1/STAT3, as well as the aforementioned PI3K/PDK1/AKT/STAT3 (81–83). Furthermore, AKT phosphorylation can indirectly activate STAT3 via mTOR or PKM2 activation (84–87). Critically, there is mounting evidence to show that STAT3 inhibits the activation and/or nuclear translocation of STAT1 via multiple reported mechanisms (88–91).

We therefore hypothesised that inhibition of the IGF signalling pathway in macrophages and fibroblasts would inhibit the

phosphorylation of STAT3. The inhibition of pSTAT3 would in turn attenuate STAT3 repression of STAT1 – ultimately facilitating the transcriptional increases in *Cxcl9* and *Cxcl10* that we observe both *in vitro* and *in vivo* upon IGF blockade (Figures 3I–O; Supplementary Figures S2D, E).

In line with this hypothesis, immunofluorescent analysis of murine orthotopic PDAC tumours revealed an overall decrease in the expression of pSTAT3[Tyr705] in both TAMs (F480[+]/pSTAT3^{+} cells) (Figures 4A, B) and CAFs (αSMA[+]/STAT3^{+} cells)

(Figures 4D, E) upon IGF blockade. In turn, this marked reduction in pSTAT3 activity corresponded with an increased expression of pSTAT1[Tyr701] in both cell types (Figures 4A, C, D, F).

Following this we designed further *in vitro* assays to assess whether IGF blockade inhibited the phosphorylation of STAT3 in either primary murine fibroblasts or BMDMs (Figure 4G). Fibroblasts or BMDMs were treated respectively with either fibroblast or BMDM conditioned media (known to contain secretory IGF ligands (3)). We found that IGF blockade inhibits
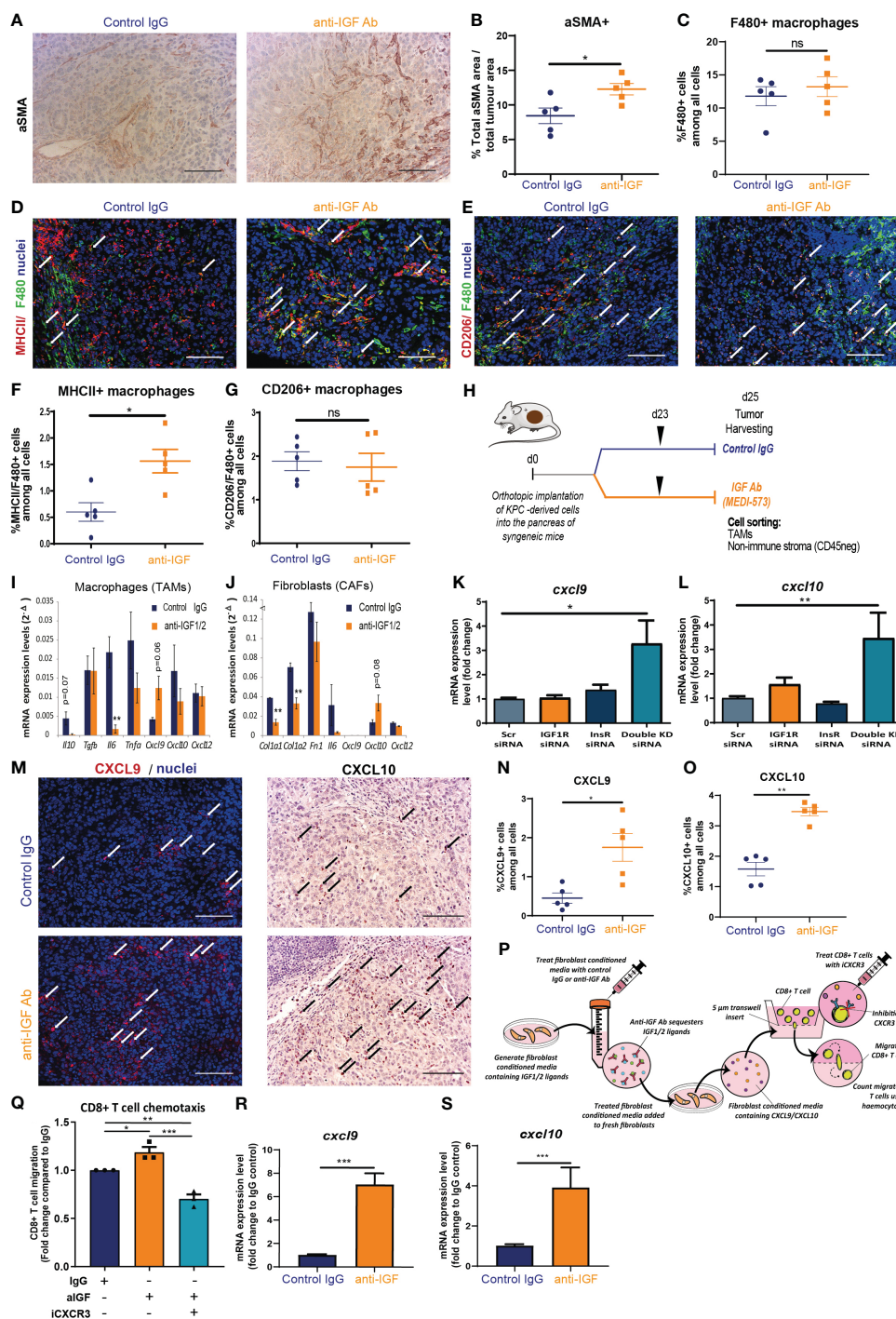

FIGURE 3 (Continued)

FIGURE 3 (Continued)

TAM and CAF derived chemokines CXCL9 and CXCL10 facilitate CD8$^+$ T cell recruitment to PDAC tumours upon IGF blockade. **(A)** Immunohistochemical staining of αSMA in formalin fixed paraffin embedded tissues from orthotopic murine PDAC tumours treated with IgG2 control antibody or IGF-blocking antibody MEDI-573. Scale bar; 50 μm. **(B)** Quantification of αSMA staining. Data displayed as total αSMA$^+$ area/ total tumour area. A total of 5-8 fields of view counted/mouse tumour, n = 5 mice per treatment group, *P $\leq$ 0.05 using Mann-Whitney U test. **(C)** Quantification of F480 staining. Data displayed as % F480$^+$ cells among all cells. A total of 5-8 fields of view counted/mouse tumour, n = 5 mice per treatment group, ns; P > 0.05 using Mann-Whitney U test. **(D)** Immunofluorescent staining of F480 (green), MHCII (red) and nuclei (blue) in formalin fixed paraffin embedded tissues from orthotopic murine PDAC tumours treated with IgG2 (control) antibody or IGF blocking antibody MEDI-573. Scale bar 50 μm. White arrows denote cells which are positive for both F480 and MHCII. **(E)** Immunofluorescent staining of F480 (green), CD206 (red) and nuclei (blue) in formalin fixed paraffin embedded tissues from orthotopic murine PDAC tumours treated with IgG2 (control) antibody or IGF blocking antibody MEDI-573. Scale bar 50 μm. White arrows denote cells which are positive for both F480 and CD206. **(F)** Quantification of MHCII$^+$/F480$^+$ macrophages in IgG control treated and anti-IGF treated orthotopic murine pancreatic tumours. Data displayed as percentage of MHCII$^+$/F480$^+$ cells among all cells. A total of 5-8 fields of view counted/mouse tumour, n= 5 mice per treatment group, * P $\leq$ 0.05 using Mann-Whitney U test. **(G)** Quantification of CD206$^+$/F480$^+$ macrophages in IgG control treated and anti-IGF treated orthotopic murine pancreatic tumours. Data displayed as percentage of CD206$^+$/F480$^+$ cells among all cells. A total of 5-8 fields of view counted/mouse tumour, n= 5 mice per treatment group, ns; P > 0.05 using Mann-Whitney U test. **(H)** *LSL-Kras$^{G12D/+}$;LSL-Trp53$^{R172H/+}$;Pdx-1-Cre* (KPC) derived FC1242 cells were orthotopically implanted into the pancreas of syngeneic recipient (C57BL/6J) mice. Mice were treated with IgG2 control antibody or IGF-blocking antibody MEDI-573 at days 23. Tumours were harvested and digested at day 25 post implantation with TAMs (CD45$^+$/F4/80$^+$ cells) and non-immune stromal cells (CD45$^-$/zsGreen^{-a}) being sorted by flow cytometry and subsequently subjected to transcriptional analysis. **(I)** Quantification of *Il10, Tgfb, IL6, Tnfa, Cxcl9, Cxcl10* AND *Cxcl12* mRNA expression levels in zsGreen$^-$/CD45$^+$/F4/80$^+$ tumour associated macrophages isolated from murine PDAC tumours treated with IgG2 control antibody or IGF-blocking antibody MEDI-573 (n=3). **P $\leq$ 0.01 using unpaired t tests **(J)** Quantification of *Col1a1, Col1a2, Fn1, Il6, Cxcl9, Cxcl10* and *Cxcl12* mRNA expression levels in zsGreen$^-$/CD45$^-$ stromal fibroblasts isolated from murine PDAC tumours treated with IgG2 control antibody or IGF-blocking antibody MEDI-573 (n=3). **P $\leq$ 0.01 using unpaired t tests. **(K)** Quantification of *Cxcl9* and **(L)** *Cxcl10* mRNA expression levels in primary murine fibroblasts isolated from the pancreata of wild-type C57BL/6J mice and treated with scrambled control siRNA (5 μM) *Igfr1* siRNA (5 μM) *Igf1r* (5 μM) or a combination of both *Igf1r* and *Insr* siRNAs (5 μM). Expression data displayed as fold change compared to scrambled control siRNA treatment *, *P* $\leq$ 0.05; **P $\leq$ 0.01 using one-way ANOVA with Tukey's multiple comparisons *post hoc* test. **(M)** Left, Immunofluorescent staining of CXCL9 (red) and nuclei (blue) in formalin fixed paraffin embedded tissues from orthotopic murine PDAC tumours treated with IgG2 (control) antibody or IGF blocking antibody MEDI-573. White arrows denote CXCL9$^+$ cells. Right, Immunohistochemical staining of CXCL10 in formalin fixed paraffin embedded tissues from orthotopic murine PDAC tumours treated with IgG2 control antibody or IGF-blocking antibody MEDI-573. Black arrows denote CXCL10$^+$ cells. Scale bar 50 μm. **(N)** Quantification of CXCL9$^+$ cells in IgG control treated and anti-IGF treated orthotopic murine pancreatic tumours. Data displayed as percentage of CXCL9$^+$ cells among all cells. A total of 5-8 fields of view counted/mouse tumour, n= 5 mice per treatment group, *P $\leq$ 0.05 using Mann-Whitney U test. **(O)** Quantification of CXCL10$^+$ cells in IgG control treated and anti-IGF treated orthotopic murine pancreatic tumours. Data displayed as percentage of CXCL10$^+$ cells among all cells. A total of 5-8 fields of view counted/mouse tumour, n= 5 mice per treatment group, **P $\leq$ 0.01 using Mann-Whitney U test. **(P)** Summary schematic for CD8$^+$ T cell chemotaxis assay. Fibroblast conditioned media was generated from primary murine fibroblasts isolated from the pancreata of wild-type C57BL/6J mice and treated with IgG control antibody (100 μg/ml) or IGF-blocking antibody MEDI-573 (100 μg/ml). Fresh primary murine fibroblasts were cultured in treated fibroblast conditioned media for 48 hours and conditioned media collected for use in CD8$^+$ T cell chemotaxis assays. Migration of primary murine CD8$^+$ T cells through a 5 μm transwell insert towards fibroblast conditioned media was measured after 15 hours using a haemocytometer. CD8$^+$ T cells were treated with or without the CXCR3 antagonist SCH 546738 (10 nM) before inclusion in migration assay. **(Q)** Data are presented as the number of migratory T cells as a fold change compared to the IgG control treated fibroblast conditioned media AFTER 15 hr. n=3, *P $\leq$ 0.05, **P $\leq$ 0.01, ***P $\leq$ 0.001 using one-way ANOVA with Tukey's multiple comparisons test. **(R)** Quantification of *Cxcl9* and **(S)** *Cxcl10* mRNA expression levels in primary murine fibroblasts isolated from the pancreata of wild-type C57BL/6J mice and treated with IgG control antibody (100 μg/ml) or IGF-blocking antibody MEDI-573 (100 μg/ml) for 24 hours. Expression data displayed as fold change compared to IgG control treatment. n=3, ***P $\leq$ 0.001 using Mann-Whitney U test.

phosphorylation of STAT3 in both macrophages and fibroblasts (Figures 4H, I). Concomitantly, IGF blockade also inhibited the phosphorylation of the upstream effector AKT (Figures 4H, I), in accordance with our previous work (3) and others (34).

Critically, alongside the inhibition of STAT3 phosphorylation we also observed statistically significant increases in *Stat1* gene induction in primary murine fibroblasts after 6 hours following anti-IGF treatment (Figure 4J), with this induction even exceeding that of fibroblasts treated with IFN-γ, a direct activator of the IFNGR/JAK/STAT1 signalling pathway (92–94). Moreover, both the indirect induction of fibroblast *Stat1* transcription through IGF blockade as well as direct induction with IFN-γ, correlated with an increased transcription of known STAT1-regulated genes *Icam1*, *Irf1* and *Oas2* (95), (Figure 4K), indicating an increased level of STAT1 functional activity. Finally, this increased transcriptional expression of *Stat1* upon IGF blockade correlated with an increased protein expression of STAT1 when analysing fibroblasts by immunocytochemistry (Figure 4L).

Taken together, these data provide mechanistic insight into how inhibition of IGF signalling in macrophages and fibroblasts leads to

an inhibition of the AKT/STAT3 signalling axis, subsequent activation of STAT1 and expression of CXCL9 and CXCL10 with the dephosphorylation of STAT3 correlating with an increased expression and transcriptional activity of STAT1.

3.5 IGF blockade leads to increased CD8$^+$ T cell recruitment towards human PDAC tumours

Having demonstrated that blocking IGF signalling increases the recruitment/trafficking of CD8$^+$ T cells towards the PDAC TME via CXCL9/10 in both *in vitro* assays and in a mouse PDAC model, we aimed to validate these findings in a PDAC patient-derived *ex-vivo* model. Precision cut tumour slice (PCTS) models have been developed to allow researchers to culture fresh patient tumour tissue *ex vivo* and assess experimental drug regimens as a means of bridging the translational gap between *in vitro* and preclinical experimental findings into a more clinically relevant model of the human disease. A further advantage of the PCTS technique over
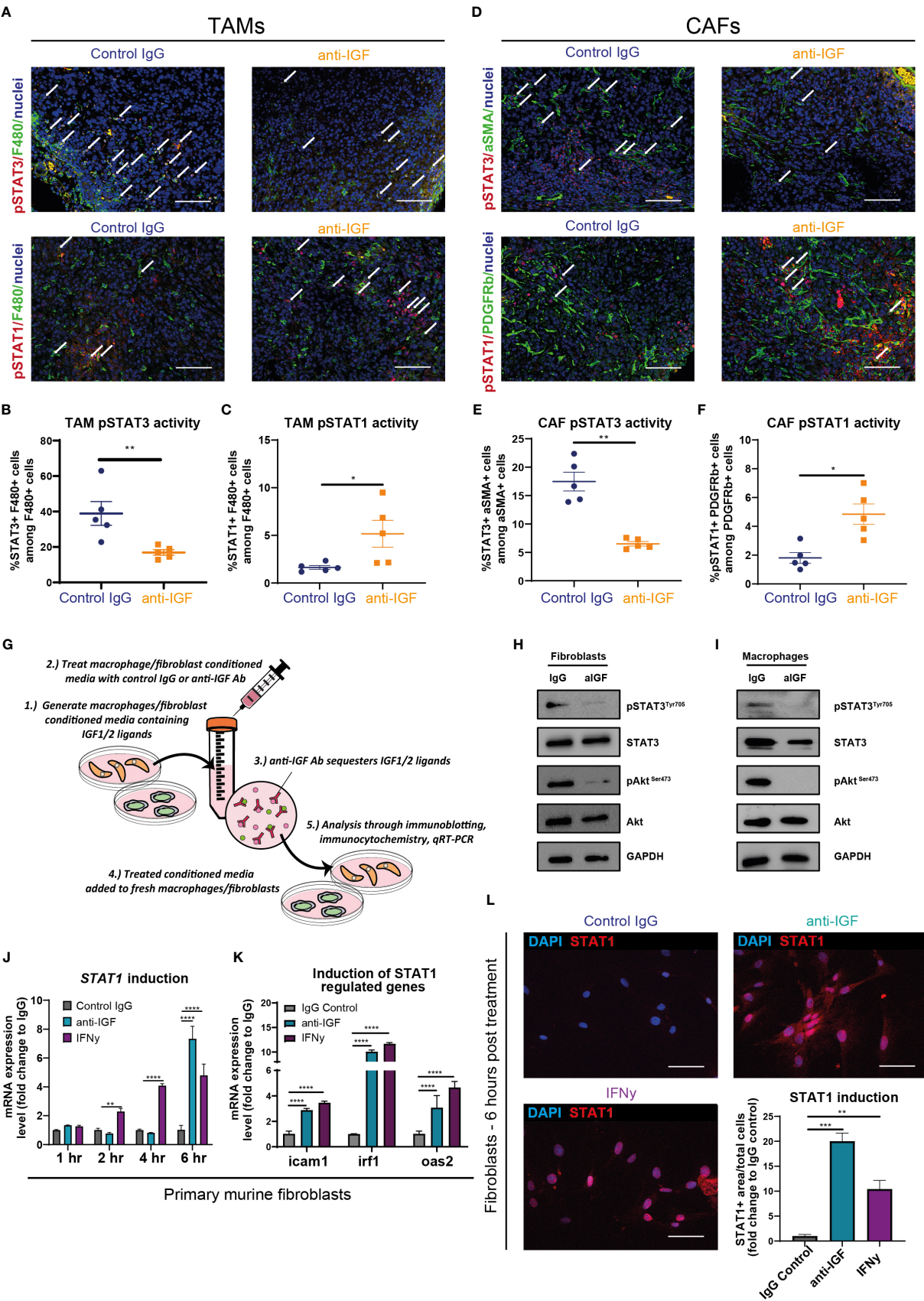
FIGURE 4 (Continued)

FIGURE 4 (Continued)

IGF blockade reverses phosphorylation of STAT3 in TAMs and CAFs to facilitate STAT1 induction of *Cxcl9* and *Cxcl10* genes **(A)** Top, immunofluorescent staining of F480 (green), pSTAT3 (red) and nuclei (blue) in formalin fixed paraffin embedded tissues from orthotopic murine PDAC tumours treated with IgG2 (control) antibody or IGF blocking antibody MEDI-573. Bottom, immunofluorescent staining of F480 (green), pSTAT1(red) and nuclei (blue) in formalin fixed paraffin embedded tissues from orthotopic murine PDAC tumours treated with IgG2 (control) antibody or IGF blocking antibody MEDI-573. Scale bar 50 μm. **(B)** Quantification of the number of F480$^+$ macrophages displaying active pSTAT3 signalling in IgG control treated and anti-IGF treated orthotopic murine pancreatic tumours. Data displayed as percentage of pSTAT3$^+$/F480$^+$ macrophages among all F480$^+$ macrophages. **(C)** Quantification of the number of F480$^+$ macrophages displaying active pSTAT1 signalling in IgG control treated and anti-IGF treated orthotopic murine pancreatic tumours. Data displayed as percentage of pSTAT1$^+$/F480$^+$ macrophages among all F480$^+$ macrophages. A total of 5-8 fields of view counted/mouse tumour, n= 5 mice per treatment group, *P $\leq$ 0.05, **P $\leq$ 0.01 using Mann-Whitney U test. **(D)** Top, immunofluorescent staining of αSMA (green), pSTAT3 (red) and nuclei (blue) in formalin fixed paraffin embedded tissues from orthotopic murine PDAC tumours treated with IgG2 (control) antibody or IGF blocking antibody MEDI-573. Bottom, immunofluorescent staining of PDGFRβ (green), pSTAT1 (red) and nuclei (blue) in formalin fixed paraffin embedded tissues from orthotopic murine PDAC tumours treated IgG2 (control) antibody or IGF blocking antibody MEDI-573. Scale bar 50 μm. **(E)** Quantification of the number of αSMA$^+$ fibroblasts displaying active pSTAT3 signalling in IgG control treated and anti-IGF treated orthotopic murine pancreatic tumours. Data displayed as percentage of pSTAT3$^+$/αSMA$^+$ fibroblasts among all αSMA$^+$ fibroblasts. **(F)** Quantification of the number of PDGFRβ$^+$ fibroblasts displaying active pSTAT1 signalling in IgG control treated and anti-IGF treated orthotopic murine pancreatic tumours. Data displayed as percentage of pSTAT1$^+$/PDGFRβ$^+$ fibroblasts among all PDGFRβ$^+$ fibroblasts. A total of 5-8 fields of view counted/mouse tumour, n= 5 mice per treatment group, *P $\leq$ 0.05, **P $\leq$ 0.01 using Mann-Whitney U test. **(G)** Schematic to display experimental design of mechanistic study assessing the role of STAT signalling in controlling response to IGF blockade in BMDMS/Fibroblasts. **(H)** Immunoblotting analysis of primary murine fibroblasts and **(I)** primary murine bone-marrow derived macrophages in response to IGF blockade. Whole cell lysates were probed for both total and phosphorylated AKT, total and phosphorylated STAT3 as well as GAPDH loading control. **(J)** Quantification of *Stat1* mRNA expression levels in primary murine fibroblasts and treated with fibroblast conditioned media supplemented with either IgG control antibody (100 μg/ml), IGF-blocking antibody MEDI-573 (100 μg/ml) or recombinant IFNγ (50 ng/ml) for 1, 2, 4 or 6 hrs. n=3, **P $\leq$ 0.01, ****P $\leq$ 0.0001 using two-way ANOVA with Dunnett's multiple comparisons test. **(K)** Quantification of *Icam1*, *Irf1* and *Oas2* mRNA expression levels in primary murine fibroblasts and treated with fibroblast conditioned media supplemented with either IgG control antibody (100 μg/ml), IGF-blocking antibody MEDI-573 (100 μg/ml) or recombinant IFNγ (50 ng/ml) for 6 hrs. n=3, ****P $\leq$ 0.0001 using two-way ANOVA with Dunnett's multiple comparisons test. **(L)** Immunocytochemistry staining of STAT1 (red) and nuclei (blue) in primary murine fibroblasts and treated with fibroblast conditioned media supplemented with either IgG control antibody (100 μg/ml), IGF-blocking antibody MEDI-573 (100 μg/ml) or recombinant IFNγ (50 ng/ml) for 6 hrs. Bottom right, quantification of STAT1$^+$ area/total cell number in IgG control, anti-IGF and IFNγ treated fibroblasts. Data displayed as fold change compared to IgG control treatment. n=3, **P $\leq$ 0.01,***P $\leq$ 0.001 using one-way ANOVA with Bonferroni's multiple comparisons test.

other widely accepted methods of primary tissue culture, for example patient derived organoid/spheroid models is that we are able to preserve the spatial localisation of the various interacting cell types of the PDAC TME (41).

Figure 5A describes the workflow for each primary PDAC sample using a protocol adapted from (41) and (42). Before proceeding with any downstream analysis, the viability of each PCTS tissue was assessed by immunohistochemistry (cleaved caspase 3 and Ki67) (Supplementary Figure S4A). In addition, we confirmed successful inhibition of pIGF-1R/InsR signalling within slices treated with IGF-blocking antibody as a further quality control (Supplementary Figure S4A). We also confirmed the presence of both αSMA expressing fibroblasts and CD206 expressing macrophages within the TME of all PCTS tissues (Supplementary Figures S4B, C), which are the known top producers of IGF ligands (3) and our proposed source of extracellular CXCL9/10 upon IGF blockade.

Recapitulating our *in vitro* and *in vivo* findings, we observed a modest but statistically significant increase in the expression of extracellular CXCL9 when analysing the conditioned media of PDAC patients-derived PCTS upon IGF blockade (Figure 5B). Moreover, we found that human Jurkat T cells migrate preferentially towards PCTS conditioned media in which the primary PDAC slices were treated with IGF-blocking antibody (Figures 5C, D), consolidating our *in vitro* findings utilising primary murine fibroblast conditioned media (Figure 3Q).

Following this, immunofluorescent analysis was used to assess the overall number and status of CD8$^+$ T cells within the PCTS tissue upon IGF blockade. In accordance with our *in vivo* findings, IGF blockade does not affect the overall survival of CD8$^+$ T cells

within the PCTS tissue, observing similarly decreased numbers of CD8$^+$ T cells within control IgG and IGF-blocking antibody-treated slices after 3 days when compared to day 0 control slices (Figures 5E, H). In addition, there was no difference in CD8$^+$ expression of cleaved caspase 3 or Ki67 within PCTS tissue after IGF blockade (Figures 5F, G, I). Of note, we also observe a statistically significant decrease in the expression of collagen within PCTS tissue upon IGF blockade, as analysed by picrosirius red staining (Figures 5J, K). This is in accordance with our *in vivo* findings at the transcriptional level in CAFs (Figure 3J) and *in vitro* data at the protein level assessing collagen deposition by primary murine fibroblasts (Supplementary Figures S5A, B). Supporting this we also observe a tendency towards a decrease collagen deposition *in vivo*, but these data did not achieve statistical significance (Supplementary Figures S5C, D).

4 Discussion

Previously reported findings from our group and others demonstrate that stromal-derived IGFs can support tumour progression in multiple cancer types. TAM/CAF derived IGFs promote tumour cell chemoresistance to gemcitabine and paclitaxel in the case of pancreatic cancer, and TNBC respectively (3, 30). Similarly, CAF derived IGF-1 promotes cisplatin resistance in bladder cancer (33) as well as the tyrosine kinase inhibitor gefitinib in non-small cell lung cancer (NSCLC) (36). In addition, CAF-derived IGF-1 stimulates tumour cell invasion and lung metastasis in orthotopic models of breast cancer through activation of the RhoA/ROCK/p-MLC pathway (35) and TAM-derived IGFs promotes cancer cell-
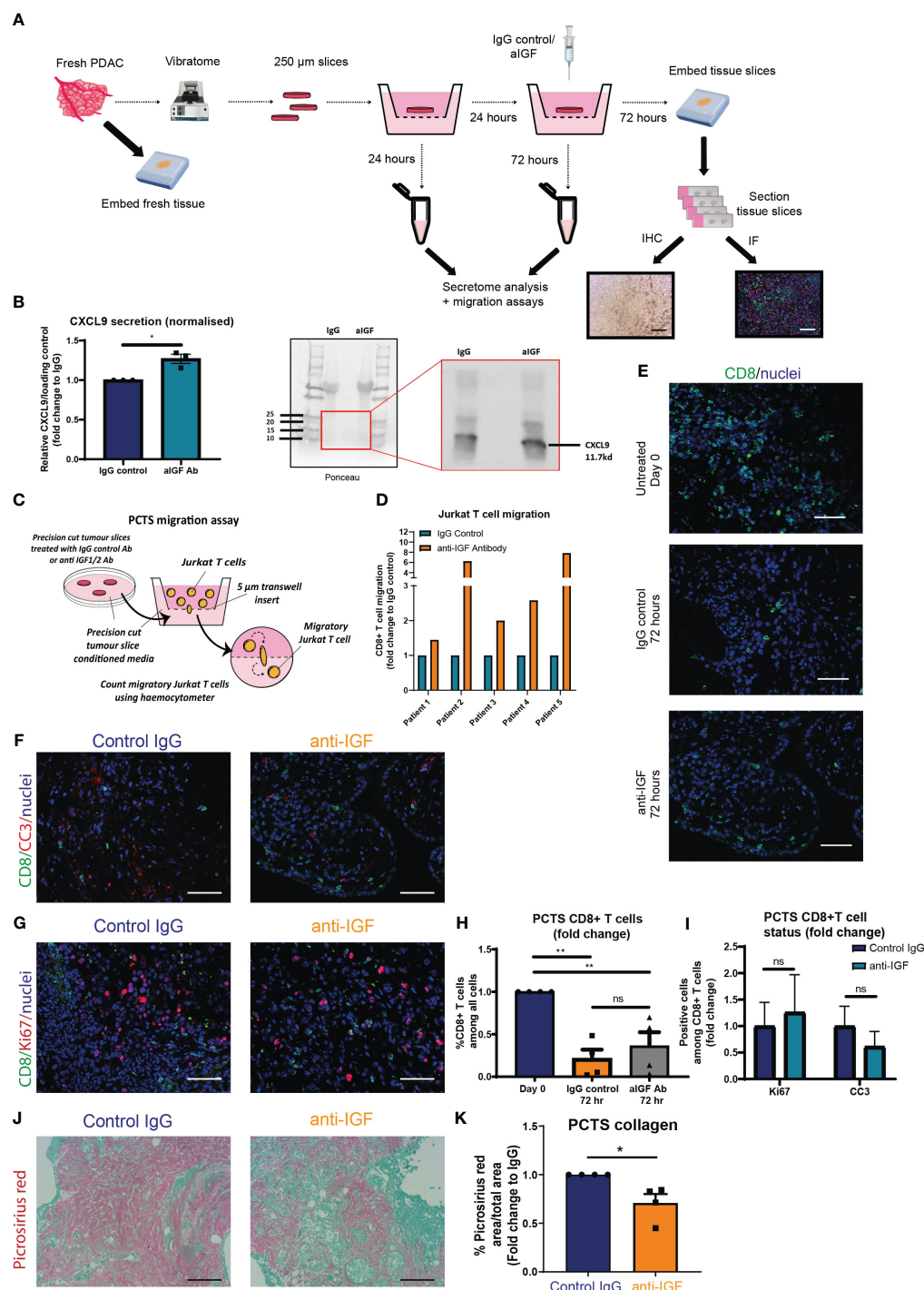
FIGURE 5 (Continued)

stemness and invasiveness in *in vitro* models of thyroid cancer (37). As such, extrinsic stromal IGF signalling plays a pleiotropic role in promoting tumour progression in a multitude of cancers and through influencing multiple cancer hallmarks.

The data presented herein describe an emerging immunomodulatory role for the IGF signalling pathway in regulating the recruitment of CD8^{+} T cells to the PDAC TME. In strong accordance with these findings, Hashimoto et al. demonstrated an increased accumulation of CD8^{+} T cells within the TME of PDAC liver metastases upon IGF blockade using

intrasplenic models of PDAC liver metastasis (44). Moreover, the authors demonstrate a marked reduction in liver metastasis and prolonged survival with concomitant inhibition of the PD1/PD-L1 signalling axis, providing strong rationale for a combinatory approach that simultaneously targets the TME when designing immunotherapeutic treatment regimens.

Interestingly, these authors also observe an increase in CD8^{+} functional activity within the TME upon inhibition of IGF signalling, demonstrating an increased protein level of IFN-γ and

FIGURE 5 (Continued)

IGF blockade leads to increased CD8^{+} T cell recruitment towards human PDAC conditioned media utilising the precision cut tumour slice model **(A)** Schematic detailing the workflow for each fresh PDAC sample and generation of 250 µm precision cut tumour slices. **(B)** Left, densitometry data displaying expression of CXCL9 in conditioned media of PCTS tissue treated with IgG2 (control) antibody or IGF blocking antibody MEDI-573 for 72 hours, analysed by immunoblotting. Data displayed as fold change compared to the IgG2 control antibody of CXCL9/Ponceau loading control. n=3, *P $\leq$ 0.05 using one-sample t test. Right, representative immunoblotting analysis of PCTS CM, using ponceau as loading control. **(C)** Migration of Jurkat T cells through a 5 µm transwell insert towards PCTS conditioned media was measured after 15 hours using a haemocytometer. Conditioned media was generated from PCTS samples treated with IgG control antibody (100 µg/ml) or IGF-blocking antibody MEDI-573 (100 µg/ml) for 72 hours. **(D)** Data are presented separately for each patient displaying the number of migratory Jurkat T cells as a fold change compared to the IgG control treated PCTS conditioned media AFTER 15 hr. n=5. **(E)** Immunofluorescent staining of CD8 (green) and nuclei (blue) in formalin fixed paraffin embedded tissues from day 0 control PCTS samples, or PCTS samples treated with IgG2 (control) antibody or IGF blocking antibody MEDI-573 for 72 hours. Scale bar 50 µm. **(F)** Immunofluorescent staining of CD8 (green), cleaved caspase 3 (red) and nuclei (blue) in formalin fixed paraffin embedded tissues from PCTS samples treated with IgG2 (control) antibody or IGF blocking antibody MEDI-573 for 72 hours. Scale bar 50 µm. **(G)** Immunofluorescent staining of CD8 (green), ki67 (red) and nuclei (blue) in formalin fixed paraffin embedded tissues from PCTS samples treated with IgG2 (control) antibody or IGF blocking antibody MEDI-573 for 72 hours. Scale bar 50 µm. **(H)** Quantification of CD8^{+} T cells in Day 0 control, IgG control treated and anti-IGF treated PCTS samples. Data displayed as fold change of CD8^{+} T cells among all cells compared to day 0 control slices. A total of 3-4 fields of view counted/slice, n= 4 slices per treatment group, ns; P > 0.05, **P $\leq$ 0.01 one-way ANOVA Bonferroni's multiple comparison *post hoc* test. **(I)** Quantification of CC3^{+} CD8^{+} T cells and Ki67^{+} CD8^{+} T cells in IgG control treated and anti-IGF treated PCTS samples. Data displayed as fold change of either CC3^{+} CD8^{+} T cells or Ki67^{+} CD8^{+} among all CD8^{+} T cells compared to IgG control treatment. A total of 3-4 fields of view counted/slice, n= 6 slices per treatment group, ns; P > 0.05 using two-way ANOVA with Bonferroni's multiple comparisons test. **(J)** Picrosirius red staining of collagen fibres in formalin fixed paraffin embedded tissues from PCTS samples treated with IgG2 (control) antibody (top) or IGF blocking antibody MEDI-573 (bottom) for 72 hours. **(K)** Quantification of picrosirius red staining in PCTS samples. Data displayed as fold change in picrosirius red area over total area stained compared to IgG control treatment. n=4, *P $\leq$ 0.05 using one-sample t test.

transcriptional increases in *GZMB* encoding the serine protease Granzyme B (44). This is in direct contrast to our *in vivo* findings where we observe no changes in CD8^{+} T cell survival (cleaved caspase 3), proliferation (Ki67) or function (CD69, Granzyme B) in response to IGF blockade. In support of this *in vivo* data we also observe no differences in CD8^{+} T cell survival (cleaved caspase 3) or function (IFN-γ) *in vitro* when T cells are grown in IGF-inhibited fibroblast conditioned media. This discrepancy likely owes to the inherently vastly differing TMEs of both the PDAC liver metastatic site and the primary PDAC site (96, 97).

Building on these findings our study explores the effects of IGF blockade on the TME at a more mechanistic level providing convincing data to show that inhibition of the IGF signalling axis promotes CD8^{+} T cell recruitment to PDAC tumours, at least in part through increased CXCL9/10 production by tumour associated macrophages and fibroblasts (Figure 6). IGF blockade inhibits
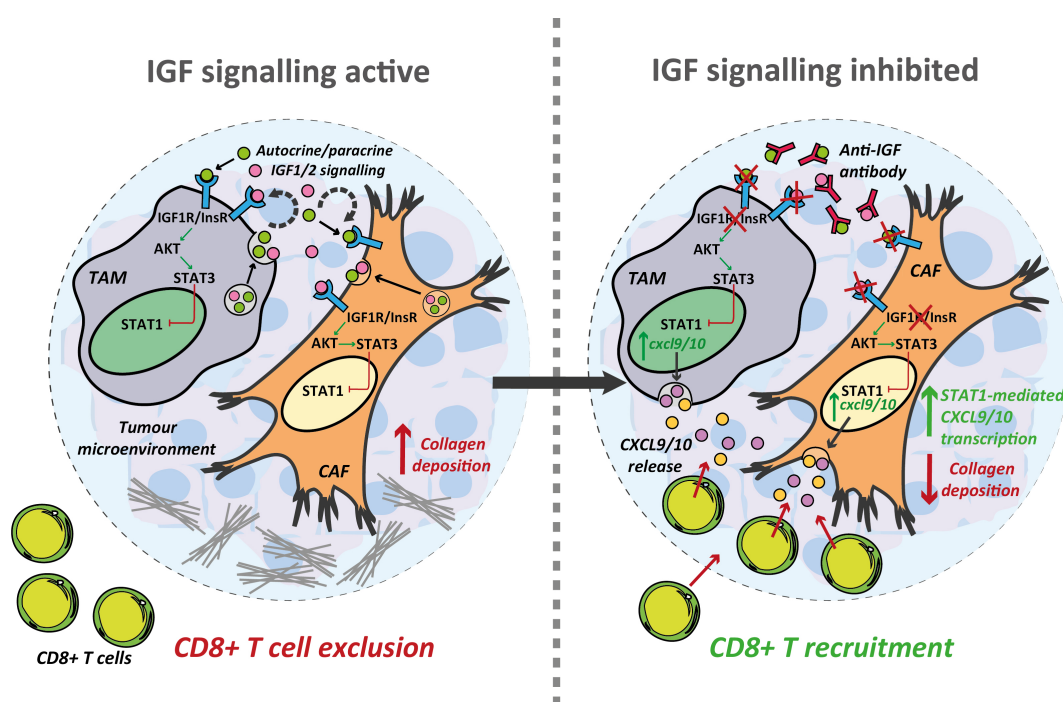

FIGURE 6

Inhibition of the IGF signalling axis facilitates T cell recruitment towards the PDAC TME. Summary schematic detailing the proposed mechanism through which IGF blockade facilitates CD8^{+} T cell recruitment towards the PDAC TME. IGF blockade inhibits STAT3 signalling in both TAMs and CAFs driving STAT1 mediated transcription of the T cell chemokines *Cxcl9/10*. Concomitantly, IGF blockade leads to a reduction in collagen deposition which may further facilitate CD8^{+} T cell infiltration into and through the PDAC TME.

phosphorylation/activation of STAT3, which attenuates pSTAT3 repression of STAT1, increasing its transcriptional activity and thereby inducing the expression of both *Cxcl9* and *Cxcl10*. In addition, we provide evidence to show that IGF blockade inhibits CAF collagen deposition, potentially facilitating CD8^{+} T cell infiltration into the PDAC TME (Figure 6).

In support of our findings, a recent study by Shang et al. has shown that inhibition of TRIB3 signalling increases CD8^{+} T cell accumulation in colorectal tumours in a similar STAT3/STAT1/CXCL10 dependent mechanism (71). The authors had previously demonstrated a role of TRIB3 in promoting STAT3 phosphorylation/activation in NSCLC (98), with targeted therapeutic degradation of TRIB3 promoting STAT1 protein stability and resultant *Cxcl10* transcription (71). This ultimately led to an increase in CD8^{+} T cell accumulation within colorectal tumours and potentiated the effects of PD-1 based immune checkpoint inhibition. With the majority of colorectal cancer patients displaying "immunologically cold" tumours and poor response to ICIs (99), this represents an exciting therapeutic angle: turning "cold" tumours "hot" through increased recruitment of CD8^{+} T cells provides a platform to increase efficacy of ICIs in the context of cancers which have traditionally shown limited response such as colorectal carcinoma and PDAC.

Indeed, the link between CXCR3 ligands, including both CXCL9 and CXCL10 in promoting anti-tumour immunity is becoming increasingly recognised, with their expression correlating with improved patient responses and sensitisation to immune checkpoint blockade in pan-cancer studies (60, 100, 101). Additionally, the role of CXCL9-expressing TAMs in the recruitment and positioning of functional CD8^{+} cytotoxic T cells has been shown to be increasingly important in orchestrating an effective anti-tumour response, and has been the focus of a recent review by Marcovecchio et al. (102). Furthermore, a recent study redefines macrophage polarity on the basis of their expression of *CXCL9* and *SPP1*, as opposed to traditional "M1" and "M2" markers, with this signature displaying prognostic significance across multiple cancer types (103).

The clinical relevance of our study is strengthened by incorporating a human *ex vivo* model of PDAC which we employ to faithfully reproduce both our *in vitro* and *in vivo* findings. However, since IGF blockade alone provides only limited efficacy, future studies should evaluate the therapeutic potential of combining IGF inhibition with ICI and chemotherapy. Given that ~50% of CD8^{+} T cells remain positive for PD-1 after IGF blockade, despite their increased intra-tumoral accumulation, a concomitant inhibition of the PD-1/PD-L1 signalling axis alongside anti-IGF treatment and chemotherapy would be a logical combinatory approach to be explored in future studies. In addition, a recent study evaluating melanoma tumours utilising multiplexed imaging mass cytometry with RNAscope *in situ* hybridisation revealed that *Cxcl9* and *Cxcl10* rich milieus also contain high densities of LAG3^{+} CD8^{+} (104). Whilst the expression of the exhaustion marker LAG3^{+} was not evaluated in the present study, this could represent another logical target of combinatory anti-IGF and ICI treatment. Given that aberrant IGF signalling is implicated in a multitude of solid malignancies, further studies should also see if this immunomodulatory role in regulating CD8^{+} T cell recruitment to tumours is conserved across multiple cancer types. Additionally, the decreases in fibroblast collagen deposition *in vitro* as well as the

decreases in CAF *Col1a1* and *Col1a2* upon IGF blockade are recapitulated in our *ex vivo* culture of primary patient PDAC tissues. This could suggest an additional role for IGF signalling in regulating ECM proteins within the TME, with IGF blockade potentially facilitating CD8^{+} T cell infiltration through a decrease in collagen deposition, which should be further explored by future studies.

Overall, inhibition of the IGF signalling axis promotes TAM and CAF production of CXCL9/10 to facilitate CD8^{+} T cell recruitment to PDAC tumours. The development of strategies to enhance T cell trafficking towards the tumour is fundamental to improving therapeutic response to immunotherapy (105).

Data availability statement

The original contributions presented in the study are included in the article/Supplementary Material. Further inquiries can be directed to the corresponding author.

Ethics statement

Author contributions

PF: Data curation, Formal analysis, Investigation, Methodology, Validation, Visualization, Writing – original draft, Writing – review & editing. GB: Formal analysis, Investigation, Validation, Writing – review & editing. LI: Formal analysis, Investigation, Methodology, Writing – review & editing. MA: Investigation, Methodology, Writing – review & editing. TL: Investigation, Methodology, Writing – review & editing. MO: Resources, Writing – review & editing, Methodology. RS: Resources, Writing – review & editing. PG: Resources, Writing – review & editing. CH: Resources, Writing – review & editing. MS: Investigation, Resources, Writing – review & editing. AM: Conceptualization, Funding acquisition, Investigation, Project administration, Resources, Supervision, Visualization, Writing – original draft, Writing – review & editing.

Funding

studies were supported by grants from North West Cancer Research and Wellcome Trust (102521/Z/13/Z) for AM, Cancer Research UK (A25607, A26978), Medical Research Council (MR/P018920/1) for MS. We also give thanks to the generous funding of the Roaf family for supporting this project.

Acknowledgments

Conflict of interest

Author MO was employed by AstraZeneca.

The remaining authors declare that the research was conducted in the absence of any commercial or financial relationships that could be construed as a potential conflict of interest.

Publisher's note

All claims expressed in this article are solely those of the authors and do not necessarily represent those of their affiliated organizations, or those of the publisher, the editors and the reviewers. Any product that may be evaluated in this article, or claim that may be made by its manufacturer, is not guaranteed or endorsed by the publisher.

Supplementary material

The Supplementary Material for this article can be found online at: https://www.frontiersin.org/articles/10.3389/fimmu.2024.1382538/full#supplementary-material

References

1. Li D, Xie K, Wolff R, Abbruzzese JL. Pancreatic cancer. *Lancet*. (2004) 363:1049–57. doi: 10.1016/S0140-6736(04)15841-8

2. Rahib L, Smith BD, Aizenberg R, Rosenzweig AB, Fleshman JM, Matrisian LM. Projecting cancer incidence and deaths to 2030: the unexpected burden of thyroid, liver, and pancreas cancers in the United States. *Cancer Res*. (2014) 74:2913–21. doi: 10.1158/0008-5472.CAN-14-0155

3. Ireland L, Santos A, Ahmed MS, Rainer C, Nielsen SR, Quaranta V, et al. Chemoresistance in pancreatic cancer is driven by stroma-derived insulin-like growth factors. *Cancer Res*. (2016) 76:6851–63. doi: 10.1158/0008-5472.CAN-16-1201

4. Royal RE, Levy C, Turner K, Mathur A, Hughes M, Kammula US, et al. Phase 2 trial of single agent Ipilimumab (anti-CTLA-4) for locally advanced or metastatic pancreatic adenocarcinoma. *J Immunother (Hagerstown Md: 1997)*. (2010) 33:828. doi: 10.1097/CJI.0b013e3181eec14c

5. Siegel RL, Miller KD, Fuchs HE, Jemal A. Cancer statistics, 2022. *CA: A Cancer J Clin*. (2022) 72:7–33. doi: 10.3322/caac.21708

6. Quaranta V, Rainer C, Nielsen SR, Raymant ML, Ahmed MS, Engle DD, et al. Macrophage-derived granulin drives resistance to immune checkpoint inhibition in metastatic pancreatic cancer. *Cancer Res*. (2018) 78:4253–69. doi: 10.1158/0008-5472.CAN-17-3876

7. Bellomo G, Rainer C, Quaranta V, Astuti Y, Raymant M, Boyd E, et al. Chemotherapy-induced infiltration of neutrophils promotes pancreatic cancer metastasis via Gas6/AXL signalling axis. *Gut*. (2022) 71:2284–99. doi: 10.1136/gutjnl-2021-325272

8. Ireland L, Luckett T, Schmid MC, Mielgo A. Blockade of stromal gas6 alters cancer cell plasticity, activates NK cells, and inhibits pancreatic cancer metastasis. *Front Immunol*. (2020) 11:297. doi: 10.3389/fimmu.2020.00297

9. Nielsen SR, Quaranta V, Linford A, Emeagi P, Rainer C, Santos A, et al. Macrophage-secreted granulin supports pancreatic cancer metastasis by inducing liver fibrosis. *Nat Cell Biol*. (2016) 18:549–60. doi: 10.1038/ncb3340

10. Zhang Y, Velez-Delgado A, Mathew E, Li D, Mendez FM, Flannagan K, et al. Myeloid cells are required for PD-1/PD-L1 checkpoint activation and the establishment of an immunosuppressive environment in pancreatic cancer. *Gut*. (2017) 66:124–36. doi: 10.1136/gutjnl-2016-312078

11. Nywening TM, Belt BA, Cullinan DR, Panni RZ, Han BJ, Sanford DE, et al. Targeting both tumour-associated CXCR2(+) neutrophils and CCR2(+) macrophages disrupts myeloid recruitment and improves chemotherapeutic responses in pancreatic ductal adenocarcinoma. *Gut*. (2018) 67:1112–23. doi: 10.1136/gutjnl-2017-313738

12. Uzunparmak B, Sahin IH. Pancreatic cancer microenvironment: a current dilemma. *Clin Transl Med*. (2019) 8:2. doi: 10.1186/s40169-019-0221-1

13. Ullman NA, Burchard PR, Dunne RF, Linehan DC. Immunologic strategies in pancreatic cancer: making cold tumors hot. *J Clin Oncol*. (2022) 40:2789–805. doi: 10.1200/JCO.21.02616

14. Balachandran VP, Beatty GL, Dougan SK. Broadening the impact of immunotherapy to pancreatic cancer: challenges and opportunities. *Gastroenterology*. (2019) 156:2056–72. doi: 10.1053/j.gastro.2018.12.038

15. Clark CE, Hingorani SR, Mick R, Combs C, Tuveson DA, Vonderheide RH. Dynamics of the immune reaction to pancreatic cancer from inception to invasion. *Cancer Res*. (2007) 67:9518–27. doi: 10.1158/0008-5472.CAN-07-0175

16. Zhu Y, Herndon JM, Sojka DK, Kim K-W, Knolhoff BL, Zuo C, et al. Tissue-resident macrophages in pancreatic ductal adenocarcinoma originate from embryonic hematopoiesis and promote tumor progression. *Immunity*. (2017) 47:323–38.e6. doi: 10.1016/j.immuni.2017.07.014

17. Siret C, Collignon A, Silvy F, Robert S, Cheyrol T, André P, et al. Deciphering the crosstalk between myeloid-derived suppressor cells and regulatory T cells in pancreatic ductal adenocarcinoma. *Front Immunol*. (2020) 10:3070. doi: 10.3389/fimmu.2019.03070

18. Karamitopoulou E. Tumour microenvironment of pancreatic cancer: immune landscape is dictated by molecular and histopathological features. *Br J Cancer*. (2019) 121:5–14. doi: 10.1038/s41416-019-0479-5

19. Ene-Obong A, Clear AJ, Watt J, Wang J, Fatah R, Riches JC, et al. Activated pancreatic stellate cells sequester CD8+ T cells to reduce their infiltration of the juxtatumoral compartment of pancreatic ductal adenocarcinoma. *Gastroenterology*. (2013) 145:1121–32. doi: 10.1053/j.gastro.2013.07.025

20. Salmon H, Franciszkiewicz K, Damotte D, Dieu-Nosjean M-C, Validire P, Trautmann A, et al. Matrix architecture defines the preferential localization and migration of T cells into the stroma of human lung tumors. *J Clin Invest*. (2012) 122:899–910. doi: 10.1172/JCI45817

21. Gorchs L, Fernandez Moro C, Bankhead P, Kern KP, Sadeak I, Meng Q, et al. Human pancreatic carcinoma-associated fibroblasts promote expression of co-inhibitory markers on CD4(+) and CD8(+) T-cells. *Front Immunol*. (2019) 10:847. doi: 10.3389/fimmu.2019.00847

22. de Lourdes Mora-García M, García-Rocha R, Morales-Ramírez O, Montesinos JJ, Weiss-Steider B, Hernández-Montes J, et al. Mesenchymal stromal cells derived from cervical cancer produce high amounts of adenosine to suppress cytotoxic T lymphocyte functions. *J Trans Med*. (2016) 14:1–14. doi: 10.1186/s12967-016-1057-8

23. Freeman P, Mielgo A. Cancer-associated fibroblast mediated inhibition of CD8+ Cytotoxic T cell accumulation in tumours: mechanisms and therapeutic opportunities. *Cancers (Basel)*. (2020) 12:2687. doi: 10.3390/cancers12092687

24. O'Reilly EM, Oh D-Y, Dhani N, Renouf DJ, Lee MA, Sun W, et al. Durvalumab with or without tremelimumab for patients with metastatic pancreatic ductal adenocarcinoma: a phase 2 randomized clinical trial. *JAMA Oncol*. (2019) 5:1431–8. doi: 10.1001/jamaoncol.2019.1588

25. Nywening TM, Wang-Gillam A, Sanford DE, Belt BA, Panni RZ, Cusworth BM, et al. Targeting tumour-associated macrophages with CCR2 inhibition in combination with FOLFIRINOX in patients with borderline resectable and locally advanced pancreatic cancer: a single-centre, open-label, dose-finding, non-randomised, phase 1b trial. *Lancet Oncol*. (2016) 17:651–62. doi: 10.1016/S1470-2045(16)00078-4

26. Le DT, Picozzi VJ, Ko AH, Wainberg ZA, Kindler H, Wang-Gillam A, et al. Results from a phase IIb, randomized, multicenter study of GVAX pancreas and CRS-207 compared with chemotherapy in adults with previously treated metastatic pancreatic adenocarcinoma (ECLIPSE study). *Clin Cancer Res*. (2019) 25:5493–502. doi: 10.1158/1078-0432.CCR-18-2992

27. Joyce JA, Fearon DT. T cell exclusion, immune privilege, and the tumor microenvironment. *Science*. (2015) 348:74–80. doi: 10.1126/science.aaa6204

28. Upadhrasta S, Zheng L. Strategies in developing immunotherapy for pancreatic cancer: recognizing and correcting multiple immune "defects" in the tumor microenvironment. *J Clin Med*. (2019) 8:1472. doi: 10.3390/jcm8091472

29. Balachandran VP, Łuksza M, Zhao JN, Makarov V, Moral JA, Remark R, et al. Identification of unique neoantigen qualities in long-term survivors of pancreatic cancer. *Nature*. (2017) 551:512–6. doi: 10.1038/nature24462

30. Ireland L, Santos A, Campbell F, Figueiredo C, Hammond D, Ellies LG, et al. Blockade of insulin-like growth factors increases efficacy of paclitaxel in metastatic breast cancer. *Oncogene*. (2018) 37:2022–36. doi: 10.1038/s41388-017-0115-x

31. Yao C, Su L, Shan J, Zhu C, Liu L, Liu C, et al. IGF/STAT3/NANOG/Slug signaling axis simultaneously controls epithelial-mesenchymal transition and stemness maintenance in colorectal cancer. *Stem Cells*. (2016) 34:820–31. doi: 10.1002/stem.2320

32. Alemi Yahya M, Meisel Sharon S, Hantisteanu S, Hallak M, Werner H, Bruchim I. The proliferative effect of dendritic cells in ovarian cancer and the relationship with the Igf signaling pathway. *Harefuah*. (2019) 158:30–4.

33. Long X, Xiong W, Zeng X, Qi L, Cai Y, Mo M, et al. Cancer-associated fibroblasts promote cisplatin resistance in bladder cancer cells by increasing IGF-1/ERbeta/Bcl-2 signalling. *Cell Death Dis*. (2019) 10:375. doi: 10.1038/s41419-019-1581-6

34. Sanchez-Lopez E, Flashner-Abramson E, Shalapour S, Zhong Z, Taniguchi K, Levitzki A, et al. Targeting colorectal cancer via its microenvironment by inhibiting IGF-1 receptor-insulin receptor substrate and STAT3 signaling. *Oncogene*. (2016) 35:2634–44. doi: 10.1038/onc.2015.326

35. Daubriac J, Han S, Grahovac J, Smith E, Hosein A, Buchanan M, et al. The crosstalk between breast carcinoma-associated fibroblasts and cancer cells promotes RhoA-dependent invasion via IGF-1 and PAI-1. *Oncotarget*. (2018) 9:10375–87. doi: 10.18632/oncotarget.v9i12

36. Yi Y, Zeng S, Wang Z, Wu M, Ma Y, Ye X, et al. Cancer-associated fibroblasts promote epithelial-mesenchymal transition and EGFR-TKI resistance of non-small cell lung cancers via HGF/IGF-1/ANXA2 signaling. *Biochim Biophys Acta Mol Basis Dis*. (2018) 1864:793–803. doi: 10.1016/j.bbadis.2017.12.021

37. Lv J, Liu C, Chen FK, Feng ZP, Jia L, Liu PJ, et al. M2–like tumour–associated macrophage–secreted IGF promotes thyroid cancer stemness and metastasis by activating the PI3K/AKT/mTOR pathway. *Mol Med Rep*. (2021) 24:604. doi: 10.3892/mmr

38. Pellegrino M, Secli V, D'Amico S, Petrilli LL, Caforio M, Folgiero V, et al. Manipulating the tumor immune microenvironment to improve cancer immunotherapy: IGF1R, a promising target. *Front Immunol*. (2024) 15. doi: 10.3389/fimmu.2024.1356321

39. Hingorani SR, Wang L, Multani AS, Combs C, Deramaudt TB, Hruban RH, et al. Trp53R172H and KrasG12D cooperate to promote chromosomal instability and widely metastatic pancreatic ductal adenocarcinoma in mice. *Cancer Cell*. (2005) 7:469–83. doi: 10.1016/j.ccr.2005.04.023

40. Finck R, Simonds EF, Jager A, Krishnaswamy S, Sachs K, Fantl W, et al. Normalization of mass cytometry data with bead standards. *Cytometry A*. (2013) 83:483–94. doi: 10.1002/cyto.a.22271

41. Misra S, Moro CF, Del Chiaro M, Pouso S, Sebestyén A, Löhr M, et al. *Ex vivo* organotypic culture system of precision-cut slices of human pancreatic ductal adenocarcinoma. *Sci Rep*. (2019) 9:2133. doi: 10.1038/s41598-019-38603-w

42. Jiang X, Seo YD, Chang JH, Coveler A, Nigjeh EN, Pan S, et al. Long-lived pancreatic ductal adenocarcinoma slice cultures enable precise study of the immune microenvironment. *Oncoimmunology*. (2017) 6:e1333210. doi: 10.1080/2162402X.2017.1333210

43. Jones RR, Castelletto V, Connon CJ, Hamley IW. Collagen stimulating effect of peptide amphiphile C16–KTTKS on human fibroblasts. *Mol Pharmaceutics*. (2013) 10:1063–9. doi: 10.1021/mp300549d

44. Hashimoto M, Konda JD, Perrino S, Celia Fernandez M, Lowy AM, Brodt P. Targeting the IGF-axis potentiates immunotherapy for pancreatic ductal adenocarcinoma liver metastases by altering the immunosuppressive microenvironment. *Mol Cancer Ther*. (2021) 20:2469–82. doi: 10.1158/1535-7163.MCT-20-0144

45. Raskov H, Orhan A, Christensen JP, Gögenur I. Cytotoxic CD8+ T cells in cancer and cancer immunotherapy. *Br J Cancer*. (2021) 124:359–67. doi: 10.1038/s41416-020-01048-4

46. Mellman I, Chen DS, Powles T, Turley SJ. The cancer-immunity cycle: Indication, genotype, and immunotype. *Immunity*. (2023) 56:2188–205. doi: 10.1016/j.immuni.2023.09.011

47. Petty AJ, Li A, Wang X, Dai R, Heyman B, Hsu D, et al. Hedgehog signaling promotes tumor-associated macrophage polarization to suppress intratumoral CD8+ T cell recruitment. *J Clin Invest*. (2019) 129:5151–62. doi: 10.1172/JCI128644

48. Feig C, Jones JO, Kraman M, Wells RJ, Deonarine A, Chan DS, et al. Targeting CXCL12 from FAP-expressing carcinoma-associated fibroblasts synergizes with anti-PD-L1 immunotherapy in pancreatic cancer. *Proc Natl Acad Sci USA*. (2013) 110:20212–7. doi: 10.1073/pnas.1320318110

49. Peranzoni E, Lemoine J, Vimeux L, Feuillet V, Barrin S, Kantari-Mimoun C, et al. Macrophages impede CD8 T cells from reaching tumor cells and limit the efficacy of anti-PD-1 treatment. *Proc Natl Acad Sci USA*. (2018) 115:E4041–e50. doi: 10.1073/pnas.1720948115

50. Wang B, Li Q, Qin L, Zhao S, Wang J, Chen X. Transition of tumor-associated macrophages from MHC class II(hi) to MHC class II(low) mediates tumor progression in mice. *BMC Immunol*. (2011) 12:43. doi: 10.1186/1471-2172-12-43

51. Boutilier AJ, Elsawa SF. Macrophage polarization states in the tumor microenvironment. *Int J Mol Sci*. (2021) 22:6995. doi: 10.3390/ijms22136995

52. Matsuzaki J, Gnjatic S, Mhawech-Fauceglia P, Beck A, Miller A, Tsuji T, et al. Tumor-infiltrating NY-ESO-1–specific CD8+ T cells are negatively regulated by LAG-3 and PD-1 in human ovarian cancer. *Proc Natl Acad Sci*. (2010) 107:7875–80. doi: 10.1073/pnas.1003345107

53. Ruffell B, Chang-Strachan D, Chan V, Rosenbusch A, Ho CM, Pryer N, et al. Macrophage IL-10 blocks CD8+ T cell-dependent responses to chemotherapy by suppressing IL-12 expression in intratumoral dendritic cells. *Cancer Cell*. (2014) 26:623–37. doi: 10.1016/j.ccell.2014.09.006

54. Li L, Ma Y, Xu Y. Follicular regulatory T cells infiltrated the ovarian carcinoma and resulted in CD8 T cell dysfunction dependent on IL-10 pathway. *Int Immunopharmacol*. (2019) 68:81–7. doi: 10.1016/j.intimp.2018.12.051

55. Chen X, Wang L, Li P, Song M, Qin G, Gao Q, et al. Dual TGF-β and PD-1 blockade synergistically enhances MAGE-A3-specific CD8+ T cell response in esophageal squamous cell carcinoma. *Int J Cancer*. (2018) 143:2561–74. doi: 10.1002/ijc.31730

56. Mace TA, Ameen Z, Collins A, Wojcik S, Mair M, Young GS, et al. Pancreatic cancer-associated stellate cells promote differentiation of myeloid-derived suppressor cells in a STAT3-dependent manner. *Cancer Res*. (2013) 73:3007–18. doi: 10.1158/0008-5472.CAN-12-4601

57. Mace TA, Shakya R, Pitarresi JR, Swanson B, McQuinn CW, Loftus S, et al. IL-6 and PD-L1 antibody blockade combination therapy reduces tumour progression in murine models of pancreatic cancer. *Gut*. (2018) 67:320–32. doi: 10.1136/gutjnl-2016-311585

58. Flint TR, Janowitz T, Connell CM, Roberts EW, Denton AE, Coll AP, et al. Tumor-induced IL-6 reprograms host metabolism to suppress anti-tumor immunity. *Cell Metab*. (2016) 24:672–84. doi: 10.1016/j.cmet.2016.10.010

59. Bertrand F, Rochotte J, Colacios C, Montfort A, Andrieu-Abadie N, Levade T, et al. Targeting TNF alpha as a novel strategy to enhance CD8(+) T cell-dependent immune response in melanoma? *Oncoimmunology*. (2016) 5:e1068495. doi: 10.1080/2162402X.2015.1068495

60. Tokunaga R, Zhang W, Naseem M, Puccini A, Berger MD, Soni S, et al. CXCL9, CXCL10, CXCL11/CXCR3 axis for immune activation - A target for novel cancer therapy. *Cancer Treat Rev*. (2018) 63:40–7. doi: 10.1016/j.ctrv.2017.11.007

61. Nagarsheth N, Wicha MS, Zou W. Chemokines in the cancer microenvironment and their relevance in cancer immunotherapy. *Nat Rev Immunol*. (2017) 17:559–72. doi: 10.1038/nri.2017.49

62. Dangaj D, Bruand M, Grimm AJ, Ronet C, Barras D, Duttagupta PA, et al. Cooperation between constitutive and inducible chemokines enables T cell engraftment and immune attack in solid tumors. *Cancer Cell*. (2019) 35:885–900.e10. doi: 10.1016/j.ccell.2019.05.004

63. Zboralski D, Hoehlig K, Eulberg D, Frömming A, Vater A. Increasing tumor-infiltrating T cells through inhibition of CXCL12 with NOX-A12 synergizes with PD-1 blockade. *Cancer Immunol Res*. (2017) 5:950–6. doi: 10.1158/2326-6066.CIR-16-0303

64. Seo YD, Jiang X, Sullivan KM, Jalikis FG, Smythe KS, Abbasi A, et al. Mobilization of CD8(+) T cells via CXCR4 blockade facilitates PD-1 checkpoint therapy in human pancreatic cancer. *Clin Cancer Res*. (2019) 25:3934–45. doi: 10.1158/1078-0432.CCR-19-0081

65. Nicolas-Boluda A, Vaquero J, Vimeux L, Guilbert T, Barrin S, Kantari-Mimoun C, et al. Tumor stiffening reversion through collagen crosslinking inhibition improves T cell migration and anti-PD-1 treatment. *eLife*. (2021) 10:e58688. doi: 10.7554/eLife.58688.sa2

66. Peng DH, Rodriguez BL, Diao L, Chen L, Wang J, Byers LA, et al. Collagen promotes anti-PD-1/PD-L1 resistance in cancer through LAIR1-dependent CD8(+) T cell exhaustion. *Nat Commun*. (2020) 11:4520. doi: 10.1038/s41467-020-18298-8

67. Espinosa-Carrasco G, Le Saout C, Fontanaud P, Michau A, Mollard P, Hernandez J, et al. Integrin β1 optimizes diabetogenic T cell migration and function in the pancreas. *Front Immunol*. (2018) 9:1156. doi: 10.3389/fimmu.2018.01156

68. Pollak M. The insulin and insulin-like growth factor receptor family in neoplasia: an update. *Nat Rev Cancer*. (2012) 12:159–69. doi: 10.1038/nrc3215

69. Belfiore A, Frasca F, Pandini G, Sciacca L, Vigneri R. Insulin receptor isoforms and insulin receptor/insulin-like growth factor receptor hybrids in physiology and disease. *Endocrine Rev*. (2009) 30:586–623. doi: 10.1210/er.2008-0047

70. Moore F, Naamane N, Colli ML, Bouckenooghe T, Ortis F, Gurzov EN, et al. STAT1 is a master regulator of pancreatic {beta}-cell apoptosis and islet inflammation. *J Biol Chem*. (2011) 286:929–41. doi: 10.1074/jbc.M110.162131

71. Shang S, Yang YW, Chen F, Yu L, Shen SH, Li K, et al. TRIB3 reduces CD8(+) T cell infiltration and induces immune evasion by repressing the STAT1-CXCL10 axis in colorectal cancer. *Sci Transl Med*. (2022) 14:eabf0992. doi: 10.1126/scitranslmed.abf0992

72. Huang B, Wang W, Li Q, Wang Z, Yan B, Zhang Z, et al. Osteoblasts secrete Cxcl9 to regulate angiogenesis in bone. *Nat Commun*. (2016) 7:13885. doi: 10.1038/ncomms13885

73. Zheng WH, Quirion R. Insulin-like growth factor-1 (IGF-1) induces the activation/phosphorylation of Akt kinase and cAMP response element-binding protein (CREB) by activating different signaling pathways in PC12 cells. *BMC Neurosci*. (2006) 7:51. doi: 10.1186/1471-2202-7-51

74. Schiaffino S, Mammucari C. Regulation of skeletal muscle growth by the IGF1-Akt/PKB pathway: insights from genetic models. *Skeletal Muscle*. (2011) 1:4. doi: 10.1186/2044-5040-1-4

75. Abdelhamed S, Ogura K, Yokoyama S, Saiki I, Hayakawa Y. AKT-STAT3 pathway as a downstream target of EGFR signaling to regulate PD-L1 expression on NSCLC cells. *J Cancer*. (2016) 7:1579–86. doi: 10.7150/jca.14713

76. Wang T, Niu G, Kortylewski M, Burdelya L, Shain K, Zhang S, et al. Regulation of the innate and adaptive immune responses by Stat-3 signaling in tumor cells. *Nat Med*. (2004) 10:48–54. doi: 10.1038/nm976

77. Cheng F, Wang H-W, Cuenca A, Huang M, Ghansah T, Brayer J, et al. A critical role for Stat3 signaling in immune tolerance. *Immunity*. (2003) 19:425–36. doi: 10.1016/S1074-7613(03)00232-2

78. Zou S, Tong Q, Liu B, Huang W, Tian Y, Fu X. Targeting STAT3 in cancer immunotherapy. *Mol Cancer*. (2020) 19:145. doi: 10.1186/s12943-020-01258-7

79. Jones LM, Broz ML, Ranger JJ, Ozcelik J, Ahn R, Zuo D, et al. STAT3 establishes an immunosuppressive microenvironment during the early stages of breast carcinogenesis to promote tumor growth and metastasis. *Cancer Res*. (2016) 76:1416–28. doi: 10.1158/0008-5472.CAN-15-2770

80. Tolomeo M, Cascio A. The multifaced role of STAT3 in cancer and its implication for anticancer therapy. *Int J Mol Sci*. (2021) 22:630. doi: 10.3390/ijms22020603

81. Salminen A, Kaarniranta K, Kauppinen A. Insulin/IGF-1 signaling promotes immunosuppression via the STAT3 pathway: impact on the aging process and age-related diseases. *Inflammation Res*. (2021) 70:1043–61. doi: 10.1007/s00011-021-01498-3

82. Zhang W, Zong CS, Hermanto U, Lopez-Bergami P, Ronai Z, Wang L-H. RACK1 recruits STAT3 specifically to insulin and insulin-like growth factor 1 receptors for activation, which is important for regulating anchorage-independent growth. *Mol Cell Biol*. (2006) 26:413–24. doi: 10.1128/MCB.26.2.413-424.2006

83. Kiely PA, Sant A, O'Connor R. RACK1 is an insulin-like growth factor 1 (IGF-1) receptor-interacting protein that can regulate IGF-1-mediated Akt activation and protection from cell death. *J Biol Chem*. (2002) 277:22581–9. doi: 10.1074/jbc.M201758200

84. Saxton RA, Sabatini DM. mTOR signaling in growth, metabolism, and disease. *Cell*. (2017) 168:960–76. doi: 10.1016/j.cell.2017.02.004

85. Dodd KM, Yang J, Shen MH, Sampson JR, Tee AR. mTORC1 drives HIF-1α and VEGF-A signalling via multiple mechanisms involving 4E-BP1, S6K1 and STAT3. *Oncogene*. (2015) 34:2239–50. doi: 10.1038/onc.2014.164

86. Gao X, Wang H, Yang JJ, Liu X, Liu Z-R. Pyruvate kinase M2 regulates gene transcription by acting as a protein kinase. *Mol Cell*. (2012) 45:598–609. doi: 10.1016/j.molcel.2012.01.001

87. Salani B, Ravera S, Amaro A, Salis A, Passalacqua M, Millo E, et al. IGF1 regulates PKM2 function through Akt phosphorylation. *Cell Cycle*. (2015) 14:1559–67. doi: 10.1080/15384101.2015.1026490

88. Lu L, Zhu F, Zhang M, Li Y, Drennan AC, Kimpara S, et al. Gene regulation and suppression of type I interferon signaling by STAT3 in diffuse large B cell lymphoma. *Proc Natl Acad Sci USA*. (2018) 115:E498–e505. doi: 10.1073/pnas.1715118115

89. Wang H, Yuan M, Wang S, Zhang L, Zhang R, Zou X, et al. STAT3 regulates the type I IFN-mediated antiviral response by interfering with the nuclear entry of STAT1. *Int J Mol Sci*. (2019) 20:4870. doi: 10.3390/ijms20194870

90. Ho HH, Ivashkiv LB. Role of STAT3 in type I interferon responses: negative regulation of STAT1-dependent inflammatory gene activation. *J Biol Chem*. (2006) 281:14111–8. doi: 10.1074/jbc.M511797200

91. Tsai M-H, Lee C-K. STAT3 cooperates with phospholipid scramblase 2 to suppress type I interferon response. *Front Immunol*. (2018) 9:1886. doi: 10.3389/fimmu.2018.01886

92. Lehtonen A, Matikainen S, Julkunen I. Interferons up-regulate STAT1, STAT2, and IRF family transcription factor gene expression in human peripheral blood mononuclear cells and macrophages. *J Immunol*. (1997) 159:794–803. doi: 10.4049/jimmunol.159.2.794

93. Krause CD, He W, Kotenko S, Pestka S. Modulation of the activation of Stat1 by the interferon-γ receptor complex. *Cell Res*. (2006) 16:113–23. doi: 10.1038/sj.cr.7310015

94. Michalska A, Blaszczyk K, Wesoly J. Bluyssen HAR. A positive feedback amplifier circuit that regulates interferon (IFN)-stimulated gene expression and controls type I and type II IFN responses. *Front Immunol*. (2018) 9. doi: 10.3389/fimmu.2018.01135

95. Sekrecka A, Kluzek K, Sekrecki M, Boroujeni ME, Hassani S, Yamauchi S, et al. Time-dependent recruitment of GAF, ISGF3 and IRF1 complexes shapes IFNα and IFNγ-activated transcriptional responses and explains mechanistic and functional overlap. *Cell Mol Life Sci*. (2023) 80:187. doi: 10.1007/s00018-023-04830-8

96. Lin W, Noel P, Borazanci EH, Lee J, Amini A, Han IW, et al. Single-cell transcriptome analysis of tumor and stromal compartments of pancreatic ductal adenocarcinoma primary tumors and metastatic lesions. *Genome Med*. (2020) 12:80. doi: 10.1186/s13073-020-00776-9

97. Yang D, Moniruzzaman R, Wang H, Wang H, Chen Y. Cross-dataset single-cell analysis identifies temporal alterations in cell populations of primary pancreatic tumor and liver metastasis. *Cancers*. (2023) 15:2396. doi: 10.3390/cancers15082396

98. Yu J-J, Zhou D-D, Yang X-X, Cui B, Tan F-W, Wang J, et al. TRIB3-EGFR interaction promotes lung cancer progression and defines a therapeutic target. *Nat Commun*. (2020) 11:3660. doi: 10.1038/s41467-020-17385-0

99. Liu JL, Yang M, Bai JG, Liu Z, Wang XS. "Cold" colorectal cancer faces a bottleneck in immunotherapy. *World J Gastrointest Oncol*. (2023) 15:240–50. doi: 10.4251/wjgo.v15.i2.240

100. Litchfield K, Reading JL, Puttick C, Thakkar K, Abbosh C, Bentham R, et al. Meta-analysis of tumor- and T cell-intrinsic mechanisms of sensitization to checkpoint inhibition. *Cell*. (2021) 184:596–614.e14. doi: 10.1016/j.cell.2021.01.002

101. Reschke R, Gajewski TF. CXCL9 and CXCL10 bring the heat to tumors. *Sci Immunol*. (2022) 7:eabq6509. doi: 10.1126/sciimmunol.abq6509

102. Marcovecchio PM, Thomas G, Salek-Ardakani S. CXCL9-expressing tumor-associated macrophages: new players in the fight against cancer. *J Immunother Cancer*. (2021) 9. doi: 10.1136/jitc-2020-002045

103. Bill R, Wirapati P, Messemaker M, Roh W, Zitti B, Duval F, et al. CXCL9:SPP1 macrophage polarity identifies a network of cellular programs that control human cancers. *Science*. (2023) 381:515–24. doi: 10.1126/science.ade2292

104. Hoch T, Schulz D, Eling N, Gómez JM, Levesque MP, Bodenmiller B. Multiplexed imaging mass cytometry of the chemokine milieus in melanoma characterizes features of the response to immunotherapy. *Sci Immunol*. (2022) 7: eabk1692. doi: 10.1126/sciimmunol.abk1692

105. Galon J, Bruni D. Approaches to treat immune hot, altered and cold tumours with combination immunotherapies. *Nat Rev Drug Discovery*. (2019) 18:197–218. doi: 10.1038/s41573-018-0007-y

Check for updates

Unlocking the tumor-immune microenvironment in osteosarcoma: insights into the immune landscape and mechanisms

Santhasiri Orrapin[1†], Sutpirat Moonmuang[1,2†],
Sasimol Udomruk[1,3], Petlada Yongpitakwattana[1],
Dumnoensun Pruksakorn[1,3,4] and Parunya Chaiyawat[1,3*]

[1]Center of Multidisciplinary Technology for Advanced Medicine (CMUTEAM), Faculty of Medicine,
Chiang Mai University, Chiang Mai, Thailand, [2]Office of Research Administration, Chiang Mai
University, Chiang Mai, Thailand, [3]Musculoskeletal Science and Translational Research (MSTR) Center,
Faculty of Medicine, Chiang Mai University, Chiang Mai, Thailand, [4]Department of Orthopedics,
Faculty of Medicine, Chiang Mai University, Chiang Mai, Thailand

Osteosarcoma has a unique tumor microenvironment (TME), which is characterized as a complex microenvironment comprising of bone cells, immune cells, stromal cells, and heterogeneous vascular structures. These elements are intricately embedded in a mineralized extracellular matrix, setting it apart from other primary TMEs. In a state of normal physiological function, these cell types collaborate in a coordinated manner to maintain the homeostasis of the bone and hematopoietic systems. However, in the pathological condition, i.e., neoplastic malignancies, the tumor-immune microenvironment (TIME) has been shown to promote cancer cells proliferation, migration, apoptosis and drug resistance, as well as immune escape. The intricate and dynamic system of the TIME in osteosarcoma involves crucial roles played by various infiltrating cells, the complement system, and exosomes. This complexity is closely associated with tumor cells evading immune surveillance, experiencing uncontrolled proliferation, and facilitating metastasis. In this review, we elucidate the intricate interplay between diverse cell populations in the osteosarcoma TIME, each contributing uniquely to tumor progression. From chondroblastic and osteoblastic osteosarcoma cells to osteoclasts, stromal cells, and various myeloid and lymphoid cell subsets, the comprehensive single-cell analysis provides a detailed roadmap of the complex osteosarcoma ecosystem. Furthermore, we summarize the mutations, epigenetic mechanisms, and extracellular vesicles that dictate the immunologic landscape and modulate the TIME of osteosarcoma. The perspectives of the clinical implementation of immunotherapy and therapeutic approaches for targeting immune cells are also intensively discussed.

1 Introduction

Osteosarcoma is the most common malignant bone tumor, primarily affecting children and adolescents. It is a highly aggressive tumor that commonly results in patient mortality due to metastasis (1). However, this therapeutic approach is limited by metastatic or relapsing osteosarcoma as the current regimen is not entirely curable. Approximate 5-year survival rates are greater than 78% for localized disease, whereas it drops to 20-25% in those who develop chemotherapeutic resistance, metastasis, and recurrence (2–5). Despite therapeutic efforts, there has been minimal improvement in effective treatment options and clinical outcomes for individuals affected by osteosarcoma (6, 7). This challenge arises from multifactorial molecular mechanisms likely involved in drug targets and the development of resistance (8). Consequently, there is an urgent need to consider new therapeutic strategies to effectively eliminate osteosarcoma, especially in the case of metastatic osteosarcoma, and circumvent resistance.

The use of cancer immunotherapy in conjunction with traditional osteosarcoma management has aimed to improve the quality-of-life outcomes in osteosarcoma patients. Strategies involving macrophage modulation, dendritic vaccination, activation of immune-modulating cytokines, immune checkpoint blockade, adoptive cell therapy [such as chimeric antigen receptors (CARs) and T lymphocyte receptors (TCRs)], and combinational immunotherapy have become a focal point in tumor (9, 10). The tumor-immune microenvironment (TIME) plays significant roles in determining the efficacy of cancer immunotherapy (11). This complex ecosystem consists of various components, including malignant cells, endothelial cells, tumor-infiltrating immune cells, and stromal cells, each serving distinct functions. For instance, the types, activity, and quantities of immune cells within the TIME significantly influence the response to cancer immunotherapy. Cytokines and chemokines in the TIME modulate immune cell recruitment, activation, and suppression. Tumor-derived exosomes can carry immunosuppressive molecules that inhibit immune responses. Metabolites produced in TIME can impair immune cell function, support the growth and dissemination of osteosarcoma cells, and contribute to the emergence of drug resistance.

The presented data emphasize the need to study the immune system within the biology of osteosarcoma and gain an understanding of its comprehensive effects, potentially contributing to the successful implementation of novel immunotherapy. In this review, we summarize the immunological landscape existing within osteosarcoma tissue tumors, exploring specific hallmarks modulating the TIME and their clinical implications. We present a future perspective and outlook for novel immunotherapeutic strategies in osteosarcoma, considering the current knowledge centered around the immune microenvironment.

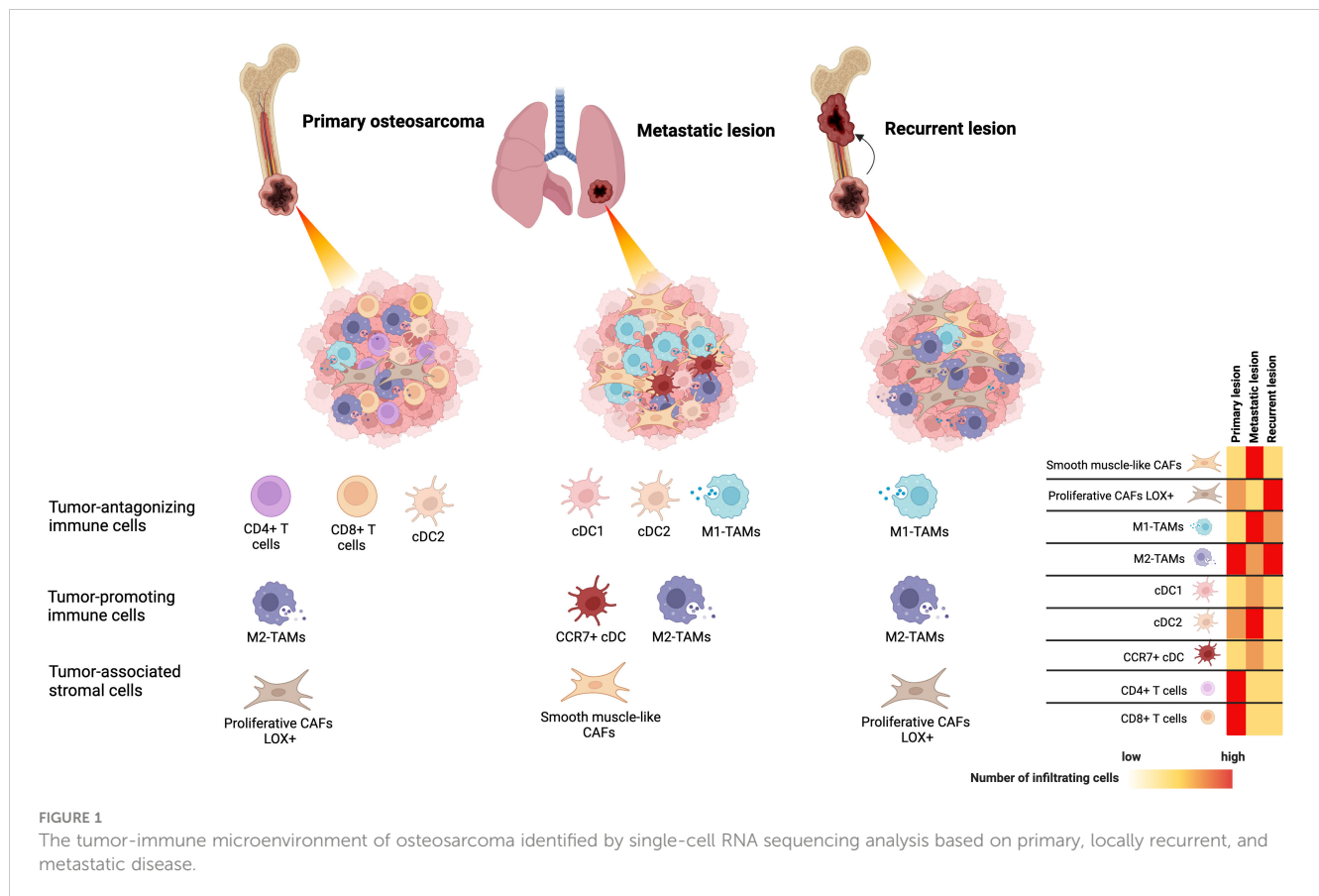# 2 The immune landscape and tumor-immune microenvironment of osteosarcoma

Osteosarcomas are malignant tumors that develop in the long bones of the limbs, including the femur, tibia, and humerus, and have special molecular and biological characteristics (12). Bone contains a highly specialized immune milieu and immune signaling pathways that are crucial for bone homeostasis. The immune microenvironment within osteosarcoma predominantly consists of T lymphocytes and macrophages, with additional subgroups such as B lymphocytes and mast cells also present. Osteosarcoma has an immunosuppressive TIME characterized by low T-cell infiltration. Overall, osteosarcoma samples have intermediate median immune infiltration scores (ESTIMATE) compared with melanoma and lung cancer, which have high ESTIMATE scores and respond well to immune checkpoint inhibitors (ICIs). Studies of the ICGC and TARGET cohorts show that 10–15% of osteosarcoma samples have high immune infiltration with high ESTIMATE scores. However, osteosarcoma cases with a T-cell presence exhibit low T-cell receptor productive clonality and low activity. T-cell activity reaches a maximum of 0.3 in comparison with normal skin (0.15), with a lack of T-cell clonal diversity and low T-cell clonotypes (<100).

The association between the TIME and clinical outcomes of osteosarcoma has been widely studied through the analysis of gene expression profiles in immune cells, immunohistochemical examination of archived samples, and single-cell RNA sequencing analysis of osteosarcoma tissues. In osteosarcoma, tumor antagonizing immune cells, particularly activated CD4+ T cells, activated CD8+ T cells, central memory CD4+ and CD8+ T cells, M1 macrophages, natural killer (NK) cells, and tumor-associated neutrophils (TANs) are detected at relatively lower levels in patients with shorter survival rates (13–17). B cells, with controversial roles in cancer, are found at lower levels in patients with poor prognoses (13, 18). Among these infiltrating immune cells, the levels and characteristics of macrophages and T cells are significantly related to key events in the poor prognosis of osteosarcoma, including metastasis and chemoresistance. Decreased M1 macrophage infiltration is observed in metastatic lesions of osteosarcoma and is significantly related to worse overall survival and disease-free survival (19, 20). Increased infiltration of CD4+ T cells, follicular helper (Tfh) cells, and CD8+ T cells is found in patients who respond well to chemotherapeutic treatment (21, 22). Higher levels of memory activated CD4+ T-cell infiltration are associated with better survival outcomes (23). The TIMEs of osteosarcoma are summarized in Figure 1.

2.1 Monocytes and tumor-associated macrophages

Monocytes play a crucial role in the TIME, acting as a link between the innate and adaptive immune systems during cancer development (24). They exhibit diverse functions in both pro-tumoral and anti-tumoral immunity, such as phagocytosis, lymphocyte recruitment, angiogenesis, and differentiation into TAMs and monocyte-derived dendritic cells (DCs). Two subtypes of monocytes, classical (CD14+CD16-) and non-classical (CD14-CD16+), show distinct functions in osteosarcoma. In primary osteosarcoma tissues, classical (CD14+D16-) monocytes with an overexpression of VCAN and S100A8/9/12 exhibit pro-

FIGURE 1

The tumor-immune microenvironment of osteosarcoma identified by single-cell RNA sequencing analysis based on primary, locally recurrent, and metastatic disease.

inflammatory functions, whereas the non-classical (CD14-D16+) monocytes with high levels of *CDKN1C, LILRB2, TGAL*, and *CX3CR1* expression exhibit the anti-inflammatory effects (25).

The phenotypes of TAMs are linked to clinical outcomes in osteosarcoma. TAMs expressing CD14 or CD163 are associated with improved overall survival and metastasis-free survival in multiple osteosarcoma cohorts (25). However, the relationship between increased CD68+ TAMs and clinical prognosis in osteosarcoma patients is controversial. Elevated CD68+ TAMs are linked with either better overall survival or poorer (26) 5-year event-free survival (25). Interestingly, TAMs expressing both CCL18 and CD68 are correlated with lung metastasis and a worse prognosis (27).

TAMs in osteosarcoma consist of a heterogeneity of subpopulations, classified as anti-tumor M1-prolarized macrophages and pro-tumor M2-prolarized macrophages. TAMs infiltrate massively into osteosarcoma tissues and specific subpopulations are involved in a wide range of tumor progression pathways. Primary osteosarcoma tissues consist of high infiltration M2-prolarized TAMs. Liu et al. classified TAMs in treatment-naïve osteosarcoma based on the expression of *FABP5, NR4A3, TXNIP, IFIT1, MCM5, and MKI67* (25). They found that TXNIP+ TAMs exhibited M2 polarization with a high expression of M2 markers (*MERTK, MRC1, STAB1*, and *CD163*), whereas IFIT1+ TAMs displayed M1 polarization, regulated by STAT1 and characterized by an increased expression of IFN signaling and proinflammatory genes (*CCL2, CCL3, CCL4, CXCL9, CXCL10,* and *TNF*). M1-TAMs interacted with Tregs and exhausted CD8+ T cells through ligand

receptors like LGALS9, PDCD1LG, CD274, and SP1. Zhou et al. also identified a high proportion of M2-like TAMs (*CD163, MRC1, MS4A4*, and *MAF*) in primary osteosarcoma patients receiving chemotherapy (28).

Hybrid TAM phenotypes also exist, indicating the plastic nature of TAMs in the TIME of osteosarcoma. Liu et al. found that NR4A3 + cells, identified as M2-TAMs in primary naïve osteosarcoma lesions, express both M1 and M2 phenotypes simultaneously (25). By inferring cellular trajectory, it was found that these NR4A3+ TAMs originate from FABP+ TAMs, forming a branched structure into M1 (IFIT1+ cluster) or M2-TAMs (NR4A3+ and TXNIP+ cluster). Lipid metabolism plays a role in regulating the M1/M2 polarization switch through multiple cellular pathways. The lipogenic phenotype of TAMs may serve as a metabolic hallmark influencing tumorigenesis and cancer progression in primary osteosarcoma. Correspondingly, genes associated with lipid metabolism are reported to correlate with the TIME and prognosis in osteosarcoma patients (29). The presence of immune cells with a high lipid metabolic profile is associated with poor prognoses in osteosarcoma patients (30).

2.1.1 The roles of TAMs in chemoresistant and immunosuppressive mechanisms of osteosarcoma

Activated TAMs, particularly under neoadjuvant treatment, decrease the sensitivity of osteosarcoma cells to drugs by inhibiting tumor apoptosis and promoting cell survival (31). This

effect is attributed to the secretion of IL1β by TAMs, which leads to the upregulation of IL1R1 and IL1RAP expression in osteosarcoma cells (Figure 2). IL1β treatment has been shown to reduce the sensitivity of osteosarcoma cells to chemotherapeutic agents in animal studies. Interestingly, IL1β secretion is triggered by the cascade signals from neoadjuvant treatment, promoting the assembly of inflammasomes in TAMs and activating the caspase pathway that induces the secretion of IL1β. Furthermore, TAMs are among the main immune cells expressing PD-L1 in the TME (32). The PD-1-PD-L1 signaling pathway is well-known for its impact on T-cell exhaustion and the reduction of T-cell function. ICIs, such as PD-1 or PD-L1 inhibitors, are the mainstay of immunotherapy in cancer treatment. The expression of PD-L1 and M2 polarization of TAMs are induced by MerTK-mediated efferocytosis, a critical macrophage function involved in clearing apoptotic bodies (Figure 2) (32). Blocking the MerTK-mediated efferocytosis
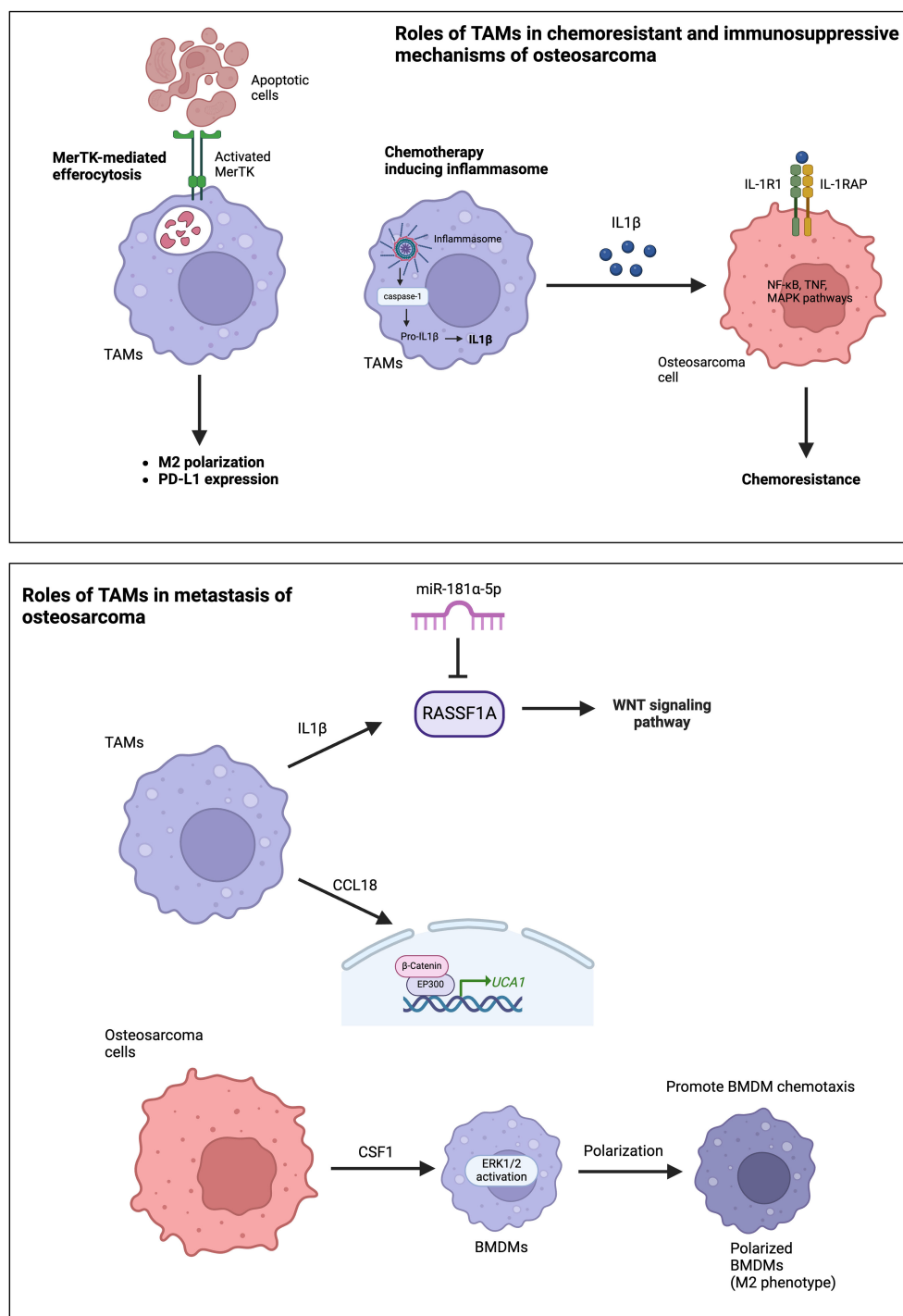

FIGURE 2
Roles of TAMs in chemoresistance, immunosuppressive mechanisms, and the metastasis of osteosarcoma.

pathway significantly suppresses osteosarcoma progression and immune tolerance. Therefore, inhibiting MerTK could be an effective approach to enhance osteosarcoma immunotherapy. Another immunosuppressive mechanism of TAMs involves the role of CD163+ M2-polarized TAMs in T cell exhaustion (33). CD163+ M2-polarized TAMs secrete immunosuppressive cytokines, such as IL-10 and TGF-β, which inhibit T-cell activation and proliferation, leading to T-cell exhaustion. Furthermore, CD163+ M2-polarized TAMs can express PD-L1, which induces an exhausted T-cell phenotype characterized by reduced cytokine production and proliferative capacity. Han et al. reported high levels of the exhausted T-cell subset in osteosarcoma, TIM-3+ PD-1+ T cells, correlated with the frequencies of CD163+ M2-polarized TAMs and tumor IL-10 concentration (33). Depletion of CD163+ M2-TAMs effectively increased T-cell proliferation and the production of proinflammatory cytokines.

The presence of CD163+ TAMs has been reported in various types of solid cancers with similar effects on the induction of T-cell exhaustion. In colorectal cancers, a high expression of CD163 on PD-L1 positive TAMs results in increased CD4+ lymphocyte infiltration, which contributes to upregulate PD-1 expression and the mediated PD-1/PD-L1 axis (34). In melanoma, CD163+ TAMs inhibited the recruitment of antitumor CD8+ T cells by suppressing the accumulation of Ly6C+, Nr4a1^{neg} monocytes (MNs) and CD11c^{hi} inflammatory TAMs (iTAMs). Upon depletion of CD163+ TAMs, there was a rapid mobilization of Ly6C+, Nr4a1^{neg} MNs, leading to an increased presence of CD11c^{hi} iTAMs. These iTAMs, in conjunction with CD4+ T cells, provoked the recruitment and activation of antitumor CD8+ T cells (35).

2.1.2 The roles of TAMs in angiogenesis

Angiogenesis is a crucial mechanism enabling cancer cells to survive and metastasize to distant organs. In osteosarcoma, it has been observed that IL-34 can promote M2 macrophage polarization of osteosarcoma TAMs and induce angiogenesis (36). The association of angio-TAMs, characterized by high expression levels of angiogenic markers, has been identified in pre-chemotherapy biopsies from primary osteosarcoma lesions with and without metastasis (37). The frequency of angio-TAMs demonstrates a significant correlation with the malignant phenotype of osteosarcoma, with genes associated with angio-TAMs involved in biological processes linked to the malignant progression of tumors (38). Consistent with previous findings, the analysis of multiple datasets indicates that as the expression pattern of angiogenesis genes increases, the malignant degree of osteosarcoma also increases (39). Interestingly, a comprehensive quantification of the angiogenesis state may accurately differentiate prognosis, metastasis, and the therapeutic response for osteosarcoma patients.

2.1.3 The roles of TAMs in the metastasis of osteosarcoma

The roles of TAMs in osteosarcoma metastasis primarily occur through the production and secretion of various cytokines and chemokines. The frequency of TAMs is higher in metastatic lesions than in corresponding primary lesions (40, 41). TAM-derived molecules, such as IL-1β and C-C motif chemokine ligand 18 (CCL18), significantly promote osteosarcoma metastasis (41). IL-1β secreted by M2-TAMs supports osteosarcoma metastasis via the RASSF1A-Wnt pathway (41). RASSF1A is a direct target of miR-181α-5p. Therefore, the RASSF1A-Wnt pathway could be targeted by miR-181α-5p and affected by nuclear factor-kappa B (NF-κB). CCL18 secreted from TAMs promotes osteosarcoma cell proliferation and migration via the EP300-UCA1-Wnt-β-catenin pathway (Figure 2) (27). CCL18 levels increased in the osteosarcoma tissues and serum of patients associated with lung metastasis. Furthermore, TAMs promote osteosarcoma cell metastasis through the stimulation of the epithelial-mesenchymal transition (EMT) of osteosarcoma cells via activation of the COX-2-STAT3 axis (40). The inhibition of COX-2 suppresses the metastasis of osteosarcoma cells in both *in vitro* and *in vivo* studies. Osteosarcoma cells also secrete colony-stimulating factor-1 (CSF1), which can stimulate ERK1/2 phosphorylation in bone marrow-derived macrophages (BMDMs), polarize BMDMs toward an M2 (TAM-like) phenotype, and promote BMDM chemotaxis (Figure 2) (42).

Osteosarcoma cells and TAMs communicate through the secretion of exosomes. Osteosarcoma cells increases the polarization of M2 TAMs, and exosomal miR-221-3p, secreted from M2-TAMs, further exacerbates the proliferation, migration, and invasion of osteosarcoma cells (43). Notably, SOCS3 is a target of miR-221-3p. The upregulation of miR-221-3p decreases SOC3 levels and activates the JAK2-STAT3 pathway. In addition, exosomes secreted from the osteosarcoma cell line can induce M2 polarizations of TAMs through the regulation of the expression of T-cell immunoglobulin and mucin domain (Tim) family proteins, particularly Tim-3, which promotes the migration, invasion, epithelial-mesenchymal transition (EMT), and lung metastasis of osteosarcoma cells (44).

2.2 Dendritic cells

DCs serve as efficient antigen-presenting cells and play a crucial role in orchestrating T-cell-mediated antitumor responses. DCs account for less than 5% of the total tumor-infiltrating myeloid cells in the TIME of osteosarcoma. A subcluster of DCs in osteosarcoma has been reported for their anti-tumor functions. Conventional DCs (cDCs) in primary osteosarcoma can be classified into two subsets: cDC1 (CLEC9A+ and XCR1+) and cDC2 (CD1c+, CLEC10A+, and FCER1A+) (25). Both subsets are widely recognized as key orchestrators of immune responses to cancer. Further characterization of four DC subclusters based on CD14/CD163, cDC1, cDC2, and CCR7 marker positivity demonstrates a higher number of cDC2 found in the TME of metastatic lung lesions than in primary and recurrent osteosarcoma (28). Furthermore, the CCR7+ DC subset specializes in directing DC mobilization to lymphoid organs and exhibits increased migratory speed, potentially indicating a close association with the metastatic potential of osteosarcoma (28). The chemokine receptor CCR7, expressed by cDCs, increases their migratory abilities from peripheral tissues to lymphoid organs, where these cells can elicit T-cell activation (45). Additionally, CCR7 employs

distinct signaling pathways (such as PI3K-Akt, MAPKs, and RhoA) downstream to regulate the biased functionality of DCs, chemotaxis, controlling migratory speed, cytoarchitecture, and endocytosis (46). CCR7 and its ligand might be the key players that are closely related to metastatic sites and their axis regulates local anti-tumor activity as a means of controlling immune cell trafficking to tumors.

An analysis of a single-cell atlas of osteosarcoma and myeloid cells revealed that mature immunoregulatory dendritic cells (mregDCs), which are abundant in osteosarcoma samples, play a significant role in suppressing antitumor immunity in osteosarcoma (47). The mregDCs, expressing CCR7, LAMP3, and CD83, interact with Tregs through CD274-PDCD1 and PVR-TIGIT signaling, as well as their physical juxtaposition. The role of mregDCs in recruiting Treg cells, leading to an immunosuppressive microenvironment, has been observed in various cancer types (48). Studies in other cancers have demonstrated that mregDCs exert immunosuppressive functions by promoting the migration of Treg into the TME and interact with Treg through CCR4 binding and the CXCL9/10-CXCR3 axis, among other mechanisms.

2.3 Tumor infiltrating lymphocytes

The heterogeneity of TILs clearly suggests their role in shaping and controlling interactive networks with other cells in the TIME. Phenotypic studies and the quantification of TIL subsets have demonstrated the immune system's capacity, implying their involvement in modulating cancer progression and predicting responses to immunotherapies. scRNA-seq analysis of osteosarcoma tissues revealed that CD4-/CD8- (double negative; DN) T cells were one of the major types of lymphocytes, frequently observed in TILs of primary and advanced osteosarcoma tissues (25, 28). Cheng et al. also indicated that DN-TILs occupy the initial position in the trajectory plot and differentiate into CD4+ T cells and regulatory T cells (Tregs) (49).

2.3.1 Effector T cells

Accumulative evidence emphasizes the predominant infiltration of exhausted CD8+ T cells in primary osteosarcoma tissues. Metastatic and recurrent osteosarcoma lesions exhibit a lower proportion of CD4+ and CD8+ TILs than primary lesions (28). In naïve primary osteosarcoma, the CD8+ T-cell subcluster is highly observed among tumor-TILs, further characterized based on the relative expression levels of cytotoxic-associated genes and regulatory factors. The C1_CD8+ subcluster represented naïve CD8+ T cells, displaying a high expression of JUND and FOSB, and a low expression of cytotoxicity genes (*GZMK*, *GZMA*, *GZMB*, and *PRF1*). The C2_CD8+ subcluster exhibited T-cell exhaustion signatures, expressing immune checkpoint-related genes (*PDCD1*, *CTLA4*, *LAG3*, *TIGIT*, and *HAVCR2*), CXCL13 chemokine, and tissue-resident genes (*ITGAE* and *ITGA1*). This dysfunctional subpopulation was also evident in advanced osteosarcoma lesions, marked by an elevated expression of T-cell exhausted inhibitory receptors (TIGIT and LAG3) (28). Finally, the

C3_CD8+ subcluster represented cytotoxic T lymphocytes, characterized by the expression of CD69 and co-stimulatory genes, along with the TNF signaling pathways. Additionally, CD4+ TILs were uniquely observed by relatively high expression levels of cytotoxic GZMA and co-stimulatory molecules, including TNFRSF14, TNFRSF25, and ICOS5 (28). This concomitant expression suggests their ability to stimulate the cytotoxic activities of neighboring T cells.

2.3.2 Regulatory T-cells

In the TIME, Tregs play a critical role in the evasion of immunological surveillance and reducing responses to immunotherapy. Intratumoral Tregs impair effector T-cell functions by producing the inhibitory cytokines IL-10 and IL-35, delivering bioactive TGF-β and inducing the apoptosis of effector T cells by depleting IL-2 via high-affinity IL-2Ra (CD25) (50). Indirect suppressive mechanisms involve the elimination of antigen-MHCII and CD80-CD86 through TCR and CTLA-4-mediated transendocytosis and trogocytosis events (50). The reverse signaling of CTLA-4 can induce the activation of the indoleamine 2,3-dioxygenase activity of APC to suppress the function of effector T cell (51). The study of the heterogeneity and immunosuppressive function of Tregs in naïve primary osteosarcoma demonstrated greater Treg infiltration than in normal bone, with a positive expression of *FOXP3*, *CD4*, *CTLA-4*, and *TIGIT* in Tregs (49). The abundant expression of *TIGIT* in Tregs is consistent with a previous study that identified *TIGIT* as widely present in various TIL subsets but most abundant in the Tregs of osteosarcoma (28). Interestingly, hallmark pathways involved in tumorigenesis and progression, such as oxidative phosphorylation, angiogenesis, and the mTORC1 pathway, were highly activated in Tregs from osteosarcoma tissues (49).

2.3.3 B cells

Although only a very small proportion of B cells resided in the TIME, scRNA-seq analysis revealed unique heterogeneity in primary osteosarcoma lesions (25). Liu et al. explored five subsets of the B-cell population and a diversity of naïve, memory B cells, and plasma cells were observed. The naïve CD27- B cell was identified as follicular B cells expressing MS4A1 and CD79A/B, the phenotypic subtypes that mostly found lymphoid follicles of tertiary lymphoid structures (TLSs) of osteosarcoma tumor. Importantly, the naïve B-cell cluster also exhibited IGHD (IgD) and IGHM (IgM) characteristics. This unique phenotype has a migratory ability to undergo germinal centers. On the other hand, memory B-cell clusters that were identified as antibody secretory cells (expressing MZB1 and SDC1/CD138) showed an elevated relative expression of IGHG3 (IgG) but low IGHD and IGHM. The activated IgG memory B cells preferentially differentiate to a plasma cell fate. Additionally, plasma cells were identified with the high expression levels of immunoglobulin heavy chains, IGHG1, IGHG2, IGHA1 (IgA), and IGHA2. This subcluster was committed to mature plasma cells due to the expression of transcription factor PRDM1/Blimp1 (52).

2.3.4 Natural killer cells

NK cells are a class of innate lymphoid cells that are recognized as non-specific cytotoxic immune cells. They possess the ability to control tumor growth and metastasis without requiring prior activation or sensitization (53). NK cells can eliminate cancer cells through complex mechanisms: releasing cytotoxic granules containing perforin, granzymes, and granulysin; generating cytokines (such as IFN-γ and TNF-α) to activate antitumor immunity; and death ligands, such as Fas ligand (FasL) and TNF-related apoptosis-inducing ligand (TRAIL) (54).

In osteosarcoma, NK cells were identified as a common TIL subset that could be classified into two subclusters based on their NK cell marker expression (NKG7 and GNLY) (28). One subcluster, expressing the T-cell markers CD3D and CD8A, was classified as NK T cells. These cells showed activation and a strong expression of *GZMB*, *GZMA*, and *IFN-γ*, indicating tumor cytotoxicity in osteosarcoma. The other subcluster, classified as NK cells, had only a small fraction expressing *GZMB*, *IFN-γ*, and *PRF1*, suggesting a non-activated state in osteosarcoma lesions (28).

2.4 Myeloid-derived suppressor cells

Myeloid-derived suppressor cells (MDSCs) are immune cells derived from the myeloid lineage that play a crucial role in the TME by suppressing the immune response and promoting tumor growth. MDSCs originate from bone marrow and consist of immature myeloid cells that fail to develop into mature cells, eventually differentiating into polymorphonuclear-MDSCs or monocytic-MDSCs. In osteosarcoma, MDSCs have been reported to heavily infiltrate the TME (55). The accumulated MDSCs within the TME suppress T-cell-mediated immune responses through the high expression of IL-18 and CXCL12 (55, 56). Furthermore, scRNA-seq analysis of six treatment-naïve osteosarcoma tumors, combined with a dataset of 22,035 cells from six osteosarcoma tumors, demonstrated that MDSCs were among the most abundant in the immunosuppressive milieu, as evidenced by MDSC hallmark genes (*VCAN*, *CLEC4E*, and *CSF3R*) (57).

2.5 Chondroblastic osteosarcoma cells

Chondroblastic cells have a valuable role in chondroblast-type osteosarcoma and are predominantly found in chondroid matrix production with variable cellularity. Four clusters of chondroblastic osteosarcoma derived from primary, recurrent, and lung metastasis were characterized based on the high expression levels of *ACAN*, *COL2A1*, and *SOX9* and their distinctive gene expression pattern (28). Among the chondroblastic osteosarcoma cells, the proliferating malignant chondroblastic osteosarcoma was identified by the expression of the gene-regulating tumor cell cycle, including *TOP2A*, *PCNA*, *TYMS*, and *MKI67*. On the other hand, two subclusters were hypertrophic chondroblastic cells that elevated the expression of the *MEF2C*, *PTH1R*, and *IHH* genes. Gene expression involving the IL-2-STAT5, Hedgehog, and Notch pathways was higher in heterotypic subcluster I, whereas the IL-6-

JAK-STAT-mediated inflammatory pathway was highly expressed in heterotypic subcluster II. Finally, the last subcluster was described as trans-differentiated cells in which the osteoblastic differentiation genes, such as *RUNX2*, *SPP1*, and *COL1A*, were highly expressed. Gou et al. revealed two subclusters of chondroblastic cell populations, namely Osteosarcoma_3 and Osteosarcoma_8, for which the later subcluster was implicated in tumor invasiveness. Several genes associated with metastasis, such as *COL6A1*, *COL6A3*, and *MIF*, were found to be highly expressed, and gene enrichment analysis showed that the PI3K-AKT pathway was highly activated.

2.6 Osteoblastic osteosarcoma cells

Traditionally, osteosarcomas are mostly derived from osteoblasts. It is well known that osteoblasts participate in new bone formation during the bone remodeling process. Many studies demonstrated that osteoblastic cells are shown to be important players in the development of osteosarcoma. The comprehensively analyzed single-cell dataset of treatment-naïve osteosarcoma represented cancer cell subpopulations based on their divergent phenotypes in primary tissues (25, 58). Liu et al. investigated five osteoblastic osteosarcoma clusters (C1-C5) that differentially expressed the genes corresponding to multifaceted physiological traits, including inflammatory markers, cell-cycle proliferation, cell metabolism associated with carbohydrate transmembrane transporter activity and glucose catabolic processes, extracellular matrix regulation, and ossification (25) Remarkably, osteoblastic-C1 and C5 displayed the most malignant stage by showing an increased expression of genes associated with a poor prognosis. With the same single-cell dataset, Zeng et al. found that the specific clusters of osteogenic cancer stem cell (CSC)-like tumor cells had a chemoresistant-related expression profile annotated by bulk RNA results (58). These subclusters bridged between tumor and non-tumor cells by stimulating several growth factors to promote themselves into a proliferative stage. For osteosarcoma patients receiving chemotherapy, the transcriptional heterogeneity of malignant osteosarcoma cells showed six subclusters belonging to osteoblastic lineages in primary, recurrent, and lung metastatic lesions (28). Osteoblastic-C1 and -C2 typically expressed proliferation markers with the cell cycle-regulated transcripts of S phase genes (C1: *PCNA*, *TYMS*, and *RRM2*) and G2/M phase genes (C2: *UBE2C* and *HMGB2*). Osteoblastic-C3 was functional in angiogenesis and the IFN-α and IFN-γ signaling pathways, whereas C4 was involved in MYC and oxidative phosphorylation. Osteoblastic-C5, enriched in the TGF-β, P53, KRAS, and hypoxia pathways, and C6 displayed a significant increase of myogenesis and inflammatory responses as well as immune rejection signaling pathways (58). These subclusters bridged between tumor and non-tumor cells by stimulating several growth factors to promote themselves into a proliferative stage.

Transcriptomic profiling of osteoblastic osteosarcoma cells demonstrated a higher activation of oxidative phosphorylation, reactive oxygen species, mTORC1, hypoxia signaling pathways, and MYC gene targets in lung metastases than primary and recurrent

tissues. Likewise, the hypoxia, TNF-α, TGF-β, IL2-STAT5, and mTORC1 pathways were functionally enriched in recurrent lesions. These signaling pathways may contribute to osteosarcoma chemotherapeutic resistance and tumor relapse.

2.7 Osteoclasts

In addition to osteoblasts, osteoclasts play a crucial role in the pathogenesis of osteosarcoma by mediated osteolysis. Osteoclasts are unique multinucleated cells responsible for the resorption of bone during bone homeostasis (59). Osteoclasts dysfunction is associated with osteosarcoma pathology by which their elevated osteoclast activity contributes to sustained proliferation and survival (60). Through scRNA-seq analysis, four clusters of osteoclasts were dissected in naïve primary osteosarcoma tissues, where progenitor and mature cells were two major subclusters and hypofunctional and non-functional osteoclasts were minor subclasses (25). According to the specific gene expression, myeloid markers (*CD74*, *CD14*, *HLA-DRA*, and *MKI67*) were highly expressed in progenitor cells but decreased in mature osteoclasts. Trajectory analysis showed that the minor osteoclast subpopulations were located at a terminal position in pseudo-time where the expression levels of osteoclast markers were decreased. Cellular interaction analysis suggested that the differentiation of osteoclasts was regulated by osteoblastic cells through the TNFSF11-TNFRSF11A interaction. Osteoclasts have been classified into three major types of progenitor, immature, and mature osteoclasts in advanced osteosarcoma (28). Progenitor osteoclasts could differentiate into mature osteoclasts and exhibited a hyperproliferative phenotype due to the high expression of TOP2A. Immature osteoclasts were positive for osteoclast and myeloid markers, whereas mature osteoclasts had high osteoclast marker expression levels compared with progenitor cells. The distribution of osteoclast clusters was respective to the progressive stage of osteosarcoma. Interestingly, osteoclast infiltrations were relatively lower in lung metastases and recurrent lesions than in primary lesions. The tissue-specific accumulation suggested a significant burden of osteoclasts in the TIME of advanced osteosarcoma.

2.8 Tumor-associated stromal cells

2.8.1 Stromal mesenchymal stem cell

The diversity of MSC populations were identified based on the markers CD10, CD90, and CXCL12 by Zhou et al. Clustering analysis revealed three MSC subsets through the differential expression of feature genes involved in metastasis and the following mesenchymal progenitors: NT5E+-MSCs, WISP2+ -MSC, and CLEC11A+-MSC clusters. NT5E+-MSCs was shown to stimulate angiogenesis and metastasis, whereas WISP2+-MSCs and CLEC11A+-MSCs were associated with the promotion of metastasis and differentiation of mesenchymal progenitors into mature osteoblasts, respectively (28). Systematically cell mapping by scRNA-seq analysis revealed the stem-like population in chemotherapy-resistant osteosarcoma having stem cell marker CD117, MYC oncogene, epigenetic

regulator JMJD3, and angiogenesis marker VEGFR2. Interestingly, the JMJD3+/VEGFR2+ subset concomitantly expressed stem cell markers CD117, indicating its stem cell quiescence. By using pseudo-time ordering analysis, it was shown that the JMJD3-VEGFR2 positive subset expressing CD117 potentially differentiated toward chondrocyte-like or fibroblast-like cell lineages. This suggested the stem-like/progenitor cells were involved in the hierarchy of therapy-resistant osteosarcoma. Based on this evidence, immunofluorescence staining of chemo-resistant osteosarcoma lesions was further confirmed by the high level of JMJD3+/VEGFR2+, and double positive cells were observed in the those tissue samples (61). The inhibition of VEGFR2 and JMJD3 synergistically impeded osteosarcoma cell propagation and tumor growth.

2.8.2 Cancer-associated fibroblasts

Within the TIME of treatment-naïve osteosarcoma tissue samples, CAFs contribute to the malignant phenotype of osteosarcoma cells by stimulating the proliferation and invasion of osteosarcoma cells (25). Based on the expression of the common CAF gene signature, CAFs formed the distinct subclusters by which each of them were involved in (1) tumor angiogenesis and invasion (MMP9 and MCAM) (2), osteoblast proliferation development and ossification, and (3) cell cycle and cell proliferation. Notably, these CAFs exhibited heterogeneous gene expression promoting angiogenetic behavior through ligand-receptor mediating angiogenic signaling pathways. scRNA-seq analysis by Zhou et al. also found diverse CAF clusters isolated from advanced osteosarcoma lesions, which showed remarkably high levels of the fibroblast markers decorin (DCN) and lumican (LUM) (28). CAF clusters were sub-categorized into (1) COL14A1+ ACTA2+ matrix fibroblasts, (2) smooth muscle-like fibroblasts (increased expression of DES along with the downregulation of ACTA2 and COL14A1), and (3) a myofibroblast cluster (a high level of MYL9, LUM, and ACTA2 expression alongside no expression of COL14A1 and DES) that exhibited strong osteoblast marker expression (IBSP and SPP1), suggesting their function as an osteoblast-like phenotype. These findings implied that most CAF subpopulations were seemingly dysfunctional in advanced osteosarcoma, where they lack the common functionality genes inherited in the fibroblast. COL14A1+ matrix fibroblasts and myofibroblast phenotypes were predominantly found in primary and recurrent osteosarcomas, whereas smooth muscle-like fibroblasts were foremost in metastatic lesions. Previously, it was noted that the expression of ACTA2 was associated with distant metastasis in lung adenocarcinoma (62) and the clinical response to the ICI of gastric cancer patients (63). Therefore, ACTA2 expression in CAF might be a favorable target for osteosarcoma management as a prognostic biomarker and/or therapeutic target. Furthermore, the scRNA-seq datasets of naïve (GSE162454) and advanced (GSE152048) osteosarcomas were compared by Huang et al. Across the different tissue sample types, CAF populations of recurrent lesions had a higher infiltration level than primary and lung metastatic samples. In this respect, the pathway enrichment analysis revealed that the EMT pathway was increasingly activated in the particular CAFs, with a high expression level of lysyl oxidase

(*LOX*) genes. *LOX* expressed by CAFs was associated with immune infiltration levels and EMT state, which in turn contributed to a poor prognosis. Further experiments demonstrated that the upregulated *LOX* promoted tumor progression, metastasis, and poor overall survival in different tumors (64–66). Therefore, the reconstructed analysis suggested *LOX* as a promising therapeutic target for recurrent osteosarcoma.

3 Cell-cell communication in the TIME of osteosarcoma

Within the complex environment of osteosarcoma, intercellular communication among different cell types plays significant roles in tumor development and immunosuprression. During osteosarcoma development, osteosarcoma cells directly influence osteoclasts by secreting various signaling molecules that shift osteoclast activity toward disrupting bone, thereby promoting the onset of osteosarcoma (Figure 3A). These mechanisms include the activation of osteoclast through TNFSF11-TNFRSF11A interaction triggered by TNSF1 secreted from osteoblastic osteosarcoma clusters (25, 67). TNFSF functions in the bone induce osteolysis and the differentiation of progenitor cells into

mature osteoclasts. Additionally, the interaction of VEGFA produced by osteoblastic osteosarcoma cells and CAFs can stimulate endothelial cell proliferation through VEGF receptor (VEGFR) binding, leading to a new vascular formation that supports osteosarcoma cell survival (68).

Osteosarcoma cells also play important roles in immunosuppression within the TME, mainly through the inhibition of T-cell functions and the induction of macrophage polarizarion. In this context, the immunoregulatory NECTIN2-TIGIT interaction between osteosarcoma and CD8+ T cells induces TIGIT-mediated T-cell suppression by impairing CD8+ T-cell proliferation and activation (69). This interaction possibly exerted immunosuppressive activity by blocking co-stimulatory signaling via the counterpart CD226, which typically modulates anti-tumor immunity and inflammatory responses (70). Additionally, a paracrine loop of CSF1 secreted from osteosarcoma cells in the tumor niche continuously activates M2-TAM, leading to the differentiation and polarization of macrophages (71, 72), as well as aggravates tumorigenesis (73).

Other important cells known for their chemoresistant phenotypes, osteogenic CSCs, exhibit significant roles in intercellular communication within the TIME of chemo-naïve osteosarcoma tissues (Figure 3B) (58). Osteogenic CSC clusters
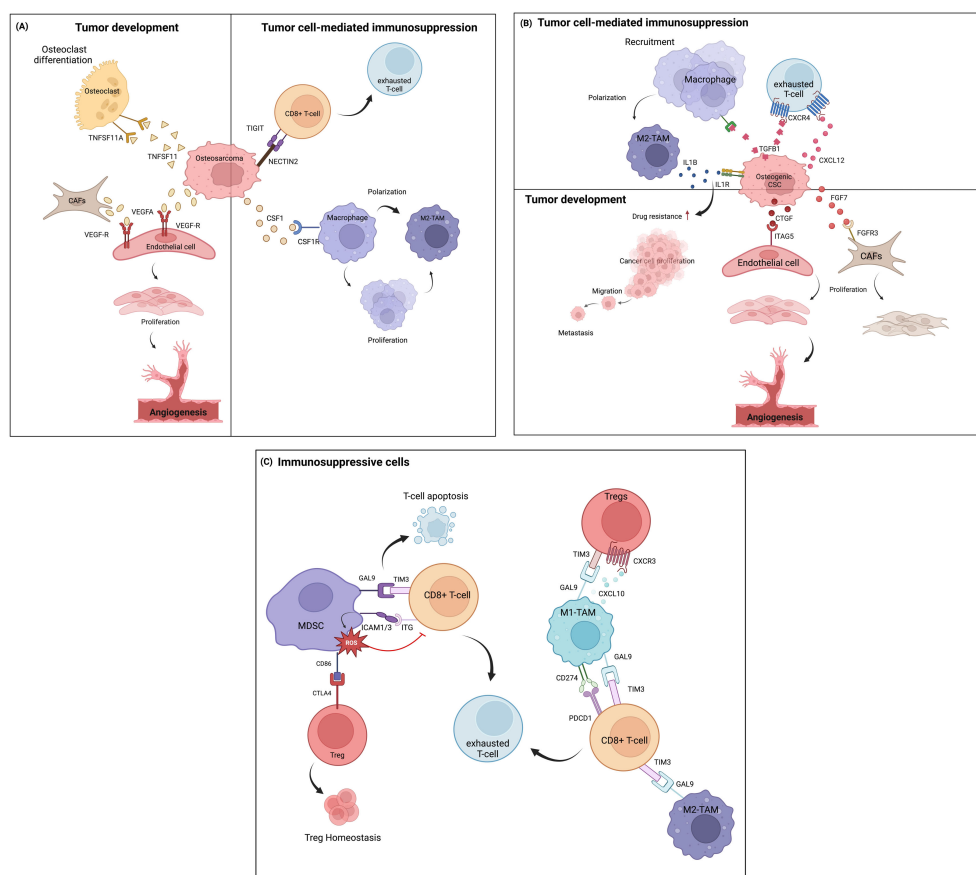

FIGURE 3
Cell-cell communication in the TIME of osteosarcoma, based on ligand-receptor interactions at the single-cell level. (A) Communication between osteosarcoma cells and other immune cells and other cell types in the TME. (B) Intercellular communication among osteogenic CSCs and other cells. (C) Communication involving immunosuppressive cells.

release growth factors (FGF and CTGF) that induce CAF growth and vascular endothelial formation by binding to their receptors. CAF clusters can express various cytokines and factors that stimulate vascularization and trigger angiogenesis (74). These signal transductions further induce therapeutic resistance and tumor progression (75, 76). TGFβ-1 secreted by osteogenic CSCs is involved in the regulation of immune cell function through TGFβ signaling effects by inducing monocyte recruitment and activating them into the M2-TAM state (77). Moreover, TGF-β and CXCL12 often orchestrate cancer progression by depleting the T-cell response through the TGFβ1-CXCR4 or CXCL12-CXCR4 axes (78, 79). Osteogenic CSCs also facilitate TAM-mediated IL-1β production. IL-1β release can lead to the transcription of signaling pathways previously found to promote chemoresistance in osteosarcoma (31) and initiate a pro-tumoral response contributing to metastasis (80, 81). These M2-TAM populations, in turn, definitely support tumor progression.

Apart from the tumor cells, the TIME of osteosarcoma presents a wide range of immune cell types that largely contribute to immunosuppressive milieus (Figure 3C). Myeloid cells constitute the highest proportion of cells in tumor tissues. MDSCs play an important role in cellular network regulation by suppressing T-cell-mediated immune responses, which are relevant to the clinical outcome of cancer (82). MDSC signaling to exhausted T cells and Tregs has been investigated in the TIME of osteosarcoma (83). It was shown that the strong interaction between the GAL9 ligand and its receptor TIM3 on T cells promotes the apoptosis of CD4+ and CD8+ TILs (84, 85). Similarly, highly expressed ICAM1/3 in MDSCs, which bind with ITG receptors (ITGB2, IL2RG, and ITGAL) expressed on T cells, contributes to the ROS-dependent inhibition of T-cell activation. This suppressive activity depends on CD11b-dependent physical contact via cell-cell contact-dependent mechanisms (86, 87). MDSCs have also been shown to indirectly suppress T-cell activation by inducing regulatory T cells. In the osteosarcoma TIME, this occurs through the interaction of CD86 molecules on MDSCs, which serve as ligands for CTLA4 on Tregs. The CTLA4-CD80/CD86 signal is a well-known ICI pathway, in which high-affinity binding limits the further activation of effector T cells, thereby maintaining the suppressive function of Tregs. Previous studies reported that CTLA4-CD80/CD86 signaling maintains homeostatic proliferation and a regulatory phenotype of Tregs, and anti-CTLA4 blockade treatment provides a reversible effect (88, 89).

On the one hand, ligand-receptor interactions were also identified between TAMs and subsets of T cells. Both M1- and M2-TAM phenotypes participate in T-cell inhibitory signaling by regulating Tregs and inducing CD8+ T-cell exhaustion through chemokine (CXCL9-CXCL10 signaling through CXCR3) and T-cell immune checkpoint (GAL9-TIM3 and CD274-PDCD1 signaling) pathways. These signaling pathways are crucial suppressors of the cytotoxic immune response. Blockade of the GAL9-TIM3 and CD274-PDCD1 pathways reinvigorates exhausted T cells and has shown favorable therapeutic efficacy in various malignancies (90–93).

4 Mechanisms modulating the tumor-immune microenvironment in osteosarcoma

In recent years, there has been growing focus on the TIME as a potential therapeutic target in osteosarcoma. Understanding the mechanisms influencing the TIME in osteosarcoma (Table 1) is crucial for comprehending tumorigenesis, evolution, progression, and metastasis. This knowledge provides valuable insights for developing novel therapeutic approaches, including molecularly targeted therapies and innovative immuno-oncology strategies, by elucidating the mechanisms that modulate the TIME in osteosarcoma.

4.1 Mutations

The point mutation burden of osteosarcoma is approximately 1.5 per Mb (100), giving it the greatest mutation burden among pediatric solid tumors but intermediate overall and much lower than other type of cancers such as melanoma or non-small cell lung cancer. Recent investigations involving whole-genome sequencing (WGS) and molecular profiling in osteosarcoma have revealed substantial occurrences of structural changes in chromosomes, such as rearrangements due to chromothripsis (ranging from 20% to 89%), along with the presence of mutation clusters termed kataegis (found in 50% to 85% of cases). These phenomena contribute significantly to osteosarcoma heterogeneity but are associated with limited recurrent alterations that can be clinically targeted (100–102). The association of osteosarcoma mutational profiles and the TIME includes clusters of immune cells ranging from low to high levels of immune infiltrate. High immune infiltrate is associated with an enrichment of tumor-intrinsic immunosuppressive pathways, indicating the increased expression of signals that inhibit T-cell activation (PD-L1, CTLA4, and IFN-γ) and the IDO1 molecule involved in immunosuppressive cell recruitment (95). Conversely, low immune infiltrate is associated with a greater number of deleted genes, *TP53* being among the top-hit loss genes (95). This observation aligns with recent studies indicating that high levels of genome aneuploidy in cancer are associated with lower levels of immune-related markers (103, 104). Furthermore, the study demonstrates a significant negative correlation between the expression levels of poly(ADP-ribose) polymerase 2 (*PARP2)* and immune infiltrate in osteosarcoma samples (95).

4.2 Epigenetics

Hypermethylation in promoter regions can epigenetically silence tumor suppressor genes during oncogenesis. Simultaneously, abnormal DNA methylation in non-promoter regions significantly contributes to intratumoral diversity. Deyao S et al. identified three immune methylation patterns (IMPs) that can be used to construct a signature scoring model based on six genes (*MYC, COL13A1, UHRF2, MT1A, ACTB,* and *GBP1*) to predict osteosarcoma prognosis (99). High-IMP_Risk patients

TABLE 1 Studies of the alteration of the genomic and epigenetic modulation of the tumor-immune microenvironment in osteosarcoma.

Genomic alterations		
Study	Population	Findings
Pires, S.F et al. (94)	• 28 Brazilian treatment-naïve osteosarcoma individuals •	• 445 potentially deleterious SNVs/indels and 1,176 copy number alterations (CNAs). *TP53* was the most frequently altered gene. • A protein-protein network enrichment revealed biological pathways associated with immune response and bone development.
Wu, CC et al. (95)	• 48 pediatric and adult patients with high-grade osteosarcoma •	• The median immune infiltrate level in high-grade osteosarcoma with poor-risk and adverse survival outcome was lower than other cancer types, with concomitant low T-cell receptor clonalities. • High immune infiltrate represents an enrichment of tumor-intrinsic immunosuppressive pathways • Low immune infiltrate showed a high number of deleted genes and negatively correlated with *PARP2* expression levels
Xie, L et al. (96)	• 12 high-grade osteosarcoma patients with initial bone metastasis and 26 patients with initial pulmonary metastasis	• Initial bone metastasis group carried more single-nucleotide variations. • Initial pulmonary metastasis exhibited structural variants. • Initial bone metastasis group exhibited better immunogenicity in the tumor microenvironment.
Liu, R et al. (97)	• Normalized sequencing datasets of osteosarcoma from Gene Expression Omnibus (GEO), GSE126209 • 11 expression datasets of osteosarcoma tissues and the 11 datasets of normal adjacent tissues	• Osteosarcoma disease-related immune cell populations, mainly Mast cells activated were enriched in osteosarcoma tissue. • Nine genes with varying levels of immune cell infiltration were associated with osteosarcoma, four of which, including *SORBS2*, *BAIAP2L2*, *SNAPC3*, and *ZDHHC21*, had a greater disease-free survival probability than the high abundance group.
Epigenetic alterations		
Study	Population	Findings
Mills, LJ et al. (98)	• 24 treatment-naïve osteosarcoma individuals	• Low abundance of stromal and immune cells in human osteosarcoma samples were predicted by a custom signature file for CIBERSORT. • Most methylation clusters showed positive correlations with mesenchymal stromal cells and were less influenced by immune cell abundance.
Shi, D et al. (99)	• Multi-omics data for osteosarcoma patients from the Therapeutically Applicable Research to Generate Effective Treatments (TARGET) and Gene Expression Omnibus (GEO) databases	• Three immune methylation patterns (IMPs) of osteosarcoma patients were cluster based on methylation levels of CpG sites related to immunologic gene sets. • Six gene signatures (*MYC*, *COL13A1*, *UHRF2*, *MT1A*, *ACTB*, and *GBP1*) were constructed to predict osteosarcoma prognosis. • Osteosarcoma patients in the high-IMP Risk group had higher infiltrations of potential immunosuppressive cells, higher infiltrations of naïve CD4 + T cells, and lower infiltrations of activated NK cells, potentially leading to an immunosuppressive TME status and a poor response to ICI therapy.

exhibited aggressive features, with activated MYC targets and tumorigenesis-related pathways, whereas low-IMP_Risk patients showed intense immune responses. High-IMP_Risk patients might have a stronger immunosuppressive microenvironment, potentially limiting the efficacy of immunotherapy. Additionally, high-IMP_Risk patients displayed genetic amplifications in oncogenes, including MYC and MCL1, that might be potential therapeutic targets for osteosarcoma treatment.

N6-methyladenosine (m6A) is a prevalent RNA modification crucial for regulating gene expression. Dysregulation of m6A, often observed in cancer, can alter mRNA stability, splicing, and translation, leading to oncogenic changes in gene expression patterns (105). In osteosarcoma, m6A plays multifaceted roles in the TME. It affects metabolic dysregulation by regulating glycolysis, influencing glucose uptake, lactate production, and ATP levels through interactions with circ-CTNNB1 and RBM15 (106).

Additionally, m6A-associated non-coding RNAs (ncRNAs) influence the TIME in osteosarcoma, affecting various immune cell populations that potentially impact tumor initiation and progression (107, 108). Yikang et al. demonstrated that TNS1 antisense RNA 1 (TNS1-AS1) and TFPI2 divergent transcript (TFPI2-DT) expressions were positively correlated with the levels of memory B cells and naïve B cells in osteosarcoma. Their findings also revealed a correlation between the expression of various long non-coding RNAs (lncRNAs) and the levels of immune cells that might be involved with the immunosuppressive microenvironment. Their findings also revealed a correlation between the expression of various long lnRNAs and the levels of immune cells that might be involved with the immunosuppressive microenvironment. For instance, LINC00910 expression showed a negative association with CD8+ T cells, and LINC00538 had a positive correlation with resting dendritic cells but a negative correlation with activated dendritic cells (107). Furthermore, the m6A-related lncRNAs had prognostic significance: lncRNAs in cluster 1 were associated with lower survival rates than those in cluster 2, which was notably enriched with immune plasma cells (108).

4.3 Extracellular vesicles

Extracellular vesicles (EVs), released by tumor cells, are membranous structures containing proteins, nucleic acids, and other biomolecules. These EVs facilitate intercellular communication within the TIME and with distant cells. Their role in cancer progression involves the modulation of cellular processes, the promotion of angiogenesis, immune evasion, and the creation of a supportive milieu conductive to tumor advancement (109–111). In osteosarcoma, EVs play a crucial role in reprogramming various cell types, especially MSCs, within the TIME (112). The osteosarcoma-derived EVs increase the angiogenic activities of endothelial cells, induce macrophage dedifferentiation, and increase the number of osteoclast-like cells and CAFs in both local and metastatic sites (113, 114). Furthermore, these EVs can induce a tumor-like phenotype in non-transformed cells, indicating their involvement in oncogenic transformation (115). Osteosarcoma EVs have been shown to promote epigenetic changes in MSCs, which are highly susceptible to EV-mediated transformation (112). As MSCs are considered potential cells of origin for osteosarcoma (116), their reprogramming by osteosarcoma EVs might be an early event in osteosarcoma development. Baglio et al. elucidated that membrane-associated TGF-β was highly observed in exosomes derived from highly metastatic osteosarcoma. Once internalized by MSCs, it induced the proinflammatory cytokine IL-6, thereby promoting pro-metastatic and pro-tumorigenic phenotypes in vivo (117). This finding highlights the significant role of exosomal proteins in the development and progression of osteosarcoma.

Tumor EVs carrying tumor-specific antigens (TSAs) and major histocompatibility complex (MHC) can act as decoys or directly activate T cells, with improved antigen presentation when interacting with mature dendritic cells (DCs). This underscores the complex mechanisms employed by EVs in immune evasion and modulation within the osteosarcoma microenvironment. The downregulation of MHC molecules and TSAs poses a significant challenge in osteosarcoma treatment by hindering the immune system's ability to recognize and target cancer cells (118–120). Tumor EVs carrying TSAs serve as decoys, redirecting anti-tumor immunity away from cancer cells. These EVs can be taken up by immune and non-immune cells, potentially disrupting the immune response. Interestingly, EVs containing TSA-MHC complexes can directly activate T cells, and their effectiveness in antigen presentation is significantly increased when attached to the surface of mature DCs (119, 120).

5 Therapeutic perspectives

A deepening understanding of the biological characteristics of osteosarcoma and rapid advancements in understanding the osteosarcoma-TIME have accelerated the development of immunotherapies. Promising monotherapy or combination approaches involving tumor vaccines, ICIs, immunomodulators, and genetically modified T cells, aim to increase treatment efficacy while minimizing side effects, offering hope for improved outcomes. The immune cocktail therapy, which combines various immunotherapeutic strategies, has shown promise in modulating the cancer-immunity cycle for more effective osteosarcoma treatment. We summarize the ongoing or planned clinical experiments exploring these strategies in Table 2.

Although immunotherapy holds potential for treating osteosarcoma, its efficacy is currently limited by insufficient T-cell infiltration and an immunosuppressive TME (121). Oncolytic viruses have demonstrated potential in overcoming resistance to PD-1 blockade by increasing CD8+ T-cell infiltration (122). Additionally, angiotensin inhibitors have been proposed to mitigate extracellular matrix sclerosis, thereby improving tumor responsiveness to checkpoint immunotherapy in solid tumors (123). Biodegradable nanoparticles may function as adjuvants, targeting specific sites and eliciting inflammatory chemokines within the TIME, consequently promoting T-cell infiltration (124, 125).

6 Conclusion

Overall, the modulation of the TIME in osteosarcoma involves a complex interplay between genomic, immunologic, and epigenetic mechanisms, as well as intercellular communication among different cell types in the TME. Understanding these intricacies at

TABLE 2 Ongoing or planned clinical trials of immunotherapies for osteosarcoma.

Approach	Clinical settings	Phase	NCT number	Status
PD-1 inhibitor + CTLA-4 inhibitor	Recurrent/refractory	I+II	NCT02304458	Completed
HER-2 inhibitor + chemotherapy	Newly diagnosed/recurrent	II	NCT04616560	Suspended
B7-H3 CAR T cells	Recurrent/refractory solid tumors including osteosarcoma	I	NCT04483778	Active, not recruiting
GD2 CAR-modified VZV-specific T cells + fludarabine + cyclophosphamide	Recurrent/refractory	I	NCT01953900	Active, not recruiting
TCRαβ+/CD19+ depleted haploidentical HSCT + zoledronate	Relapsed with pulmonary or bone metastases	I	NCT02508038	Recruiting
TIL T cells + PD-1 inhibitor + CTLA-4 inhibitor	Recurrent/refractory	II	NCT03449108	Active, not recruiting

the single-cell level and within the spatial landscape of the TME is crucial for developing novel therapeutic strategies, including targeted therapies and immunotherapies, to improve outcomes in osteosarcoma treatment.

Author contributions

SO: Conceptualization, Writing – original draft, Writing – review & editing. SM: Conceptualization, Writing – original draft, Writing – review & editing. SU: Writing – review & editing. PY: Writing – review & editing. DP: Writing – review & editing. PC: Conceptualization, Supervision, Writing – original draft, Writing – review & editing.

Funding

Acknowledgments

Conflict of interest

The authors declare that the research was conducted in the absence of any commercial or financial relationships that could be construed as a potential conflict of interest.

Publisher's note

All claims expressed in this article are solely those of the authors and do not necessarily represent those of their affiliated organizations, or those of the publisher, the editors and the reviewers. Any product that may be evaluated in this article, or claim that may be made by its manufacturer, is not guaranteed or endorsed by the publisher.

References

1. Casali PG, Bielack S, Abecassis N, Aro HT, Bauer S, Biagini R, et al. Bone sarcomas: ESMO–PaedCan–EURACAN Clinical Practice Guidelines for diagnosis, treatment and follow-up. *Ann Oncol*. (2018) 29:iv79–95. doi: 10.1093/annonc/mdy310

2. Gaspar N, Occean BV, Pacquement H, Bompas E, Bouvier C, Brisse HJ, et al. Results of methotrexate-etoposide-ifosfamide based regimen (M-EI) in osteosarcoma patients included in the French OS2006/sarcome-09 study. *Eur J Cancer*. (2018) 88:57–66. doi: 10.1016/j.ejca.2017.09.036

3. Heare T, Hensley MA, Dell'Orfano S. Bone tumors: osteosarcoma and Ewing's sarcoma. *Curr Opin Pediatr*. (2009) 21:365–72. doi: 10.1097/MOP.0b013e32832b1111

4. Moore DD, Luu HH. Osteosarcoma. *Cancer Treat Res*. (2014) 162:65–92. doi: 10.1007/978-3-319-07323-1_4

5. Kempf-Bielack B, Bielack SS, Jürgens H, Branscheid D, Berdel WE, Exner GU, et al. Osteosarcoma relapse after combined modality therapy: an analysis of unselected patients in the Cooperative Osteosarcoma Study Group (COSS). *J Clin Oncol*. (2005) 23:559–68. doi: 10.1200/JCO.2005.04.063

6. Harris MA, Hawkins CJ. Recent and ongoing research into metastatic osteosarcoma treatments. *Int J Mol Sci*. (2022) 23. doi: 10.3390/ijms23073817

7. Meazza C, Scanagatta P. Metastatic osteosarcoma: a challenging multidisciplinary treatment. *Expert Rev Anticancer Ther*. (2016) 16:543–56. doi: 10.1586/14737140.2016.1168697

8. He H, Ni J, Huang J. Molecular mechanisms of chemoresistance in osteosarcoma (Review). *Oncol Lett*. (2014) 7:1352–62. doi: 10.3892/ol.2014.1935

9. Miwa S, Shirai T, Yamamoto N, Hayashi K, Takeuchi A, Igarashi K, et al. Current and emerging targets in immunotherapy for osteosarcoma. *J Oncol*. (2019) 2019:7035045. doi: 10.1155/2019/7035045

10. Smrke A, Tam YB, Anderson PM, Jones RL, Huang PH. The perplexing role of immuno-oncology drugs in osteosarcoma. *J Bone Oncol*. (2021) 31:100400. doi: 10.1016/j.jbo.2021.100400

11. Wang Q, Shao X, Zhang Y, Zhu M, Wang FXC, Mu J, et al. Role of tumor microenvironment in cancer progression and therapeutic strategy. *Cancer Med*. (2023) 12:11149–65. doi: 10.1002/cam4.5698

12. Simpson E, Brown HL. Understanding osteosarcomas. *JAAPA*. (2018) 31:15–9. doi: 10.1097/01.JAA.0000541477.24116.8d

13. Wu C, Gong S, Duan Y, Deng C, Kallendrusch S, Berninghausen L, et al. A tumor microenvironment-based prognostic index for osteosarcoma. *J BioMed Sci*. (2023) 30:23. doi: 10.1186/s12929-023-00917-3

14. Yang M, Cao Y, Wang Z, Zhang T, Hua Y, Cai Z. Identification of two immune subtypes in osteosarcoma based on immune gene sets. *Int Immunopharmacol*. (2021) 96:107799. doi: 10.1016/j.intimp.2021.107799

15. Casanova JM, Almeida JS, Reith JD, Sousa LM, Fonseca R, Freitas-Tavares P, et al. Tumor-infiltrating lymphocytes and cancer markers in osteosarcoma: influence on patient survival. *Cancers (Basel)*. (2021) 13. doi: 10.3390/cancers13236075

16. Chen Y, Zhao B, Wang X. Tumor infiltrating immune cells (TIICs) as a biomarker for prognosis benefits in patients with osteosarcoma. *BMC Cancer*. (2020) 20:1022. doi: 10.1186/s12885-020-07536-3

17. Yang X, Zhang W, Xu P. NK cell and macrophages confer prognosis and reflect immune status in osteosarcoma. *J Cell Biochem*. (2019) 120:8792–7. doi: 10.1002/jcb.28167

18. Li GQ, Wang YK, Zhou H, Jin LG, Wang CY, Albahde M, et al. Application of immune infiltration signature and machine learning model in the differential diagnosis and prognosis of bone-related Malignancies. *Front Cell Dev Biol*. (2021) 9:630355. doi: 10.3389/fcell.2021.630355

19. Wang Z, Wu H, Chen Y, Chen H, Yuan W, Wang X. The heterogeneity of infiltrating macrophages in metastatic osteosarcoma and its correlation with immunotherapy. *J Oncol*. (2021) 2021:4836292. doi: 10.1155/2021/4836292

20. Liang T, Chen J, Xu G, Zhang Z, Xue J, Zeng H, et al. TYROBP, TLR4 and ITGAM regulated macrophages polarization and immune checkpoints expression in osteosarcoma. *Sci Rep*. (2021) 11:19315. doi: 10.1038/s41598-021-98637-x

21. Song YJ, Xu Y, Zhu X, Fu J, Deng C, Chen H, et al. Immune landscape of the tumor microenvironment identifies prognostic gene signature CD4/CD68/CSF1R in osteosarcoma. *Front Oncol*. (2020) 10:1198. doi: 10.3389/fonc.2020.01198

22. He L, Yang H, Huang J. The tumor immune microenvironment and immune-related signature predict the chemotherapy response in patients with osteosarcoma. *BMC Cancer*. (2021) 21:581. doi: 10.1186/s12885-021-08328-z

23. Tan J, Feng X, Wu H, Yang B, Shi M, Xie C, et al. Characterization of the tumor microenvironment in osteosarcoma identifies prognostic- and immunotherapy-relevant gene signatures. *J Immunol Res*. (2022) 2022:6568278. doi: 10.1155/2022/6568278

24. Olingy CE, Dinh HQ, Hedrick CC. Monocyte heterogeneity and functions in cancer. *J Leukocyte Biol*. (2019) 106:309–22. doi: 10.1002/JLB.4RI0818-311R

25. Liu Y, Feng W, Dai Y, Bao M, Yuan Z, He M, et al. Single-cell transcriptomics reveals the complexity of the tumor microenvironment of treatment-naive osteosarcoma. *Front Oncol*. (2021) 11:709210. doi: 10.3389/fonc.2021.709210

26. Buddingh EP, Kuijjer ML, Duim RA, Burger H, Agelopoulos K, Myklebost O, et al. Tumor-infiltrating macrophages are associated with metastasis suppression in high-grade osteosarcoma: a rationale for treatment with macrophage activating agents. *Clin Cancer Res.* (2011) 17:2110–9. doi: 10.1158/1078-0432.CCR-10-2047

27. Su Y, Zhou Y, Sun YJ, Wang YL, Yin JY, Huang YJ, et al. Macrophage-derived CCL18 promotes osteosarcoma proliferation and migration by upregulating the expression of UCA1. *J Mol Med (Berl).* (2019) 97:49–61. doi: 10.1007/s00109-018-1711-0

28. Zhou Y, Yang D, Yang Q, Lv X, Huang W, Zhou Z, et al. Single-cell RNA landscape of intratumoral heterogeneity and immunosuppressive microenvironment in advanced osteosarcoma. *Nat Commun.* (2020) 11:6322. doi: 10.1038/s41467-020-20059-6

29. Qian H, Lei T, Hu Y, Lei P. Expression of lipid-metabolism genes is correlated with immune microenvironment and predicts prognosis in osteosarcoma. *Front Cell Dev Biol.* (2021) 9:673827. doi: 10.3389/fcell.2021.673827

30. Li Z, Jin C, Lu X, Zhang Y, Zhang Y, Wen J, et al. Studying the mechanism underlying lipid metabolism in osteosarcoma based on transcriptomic RNA sequencing and single-cell data. *J Gene Med.* (2023) 25:e3491. doi: 10.1002/jgm.3491

31. Liang X, Guo W, Ren T, Huang Y, Sun K, Zhang H, et al. Macrophages reduce the sensitivity of osteosarcoma to neoadjuvant chemotherapy drugs by secreting Interleukin-1 beta. *Cancer Lett.* (2020) 480:4–14. doi: 10.1016/j.canlet.2020.03.019

32. Lin J, Xu A, Jin J, Zhang M, Lou J, Qian C, et al. MerTK-mediated efferocytosis promotes immune tolerance and tumor progression in osteosarcoma through enhancing M2 polarization and PD-L1 expression. *Oncoimmunology.* (2022) 11:2024941. doi: 10.1080/2162402X.2021.2024941

33. Han Q, Shi H, Liu F. CD163(+) M2-type tumor-associated macrophage support the suppression of tumor-infiltrating T cells in osteosarcoma. *Int Immunopharmacol.* (2016) 34:101–6. doi: 10.1016/j.intimp.2016.01.023

34. Cantero-Cid R, Casas-Martin J, Hernandez-Jimenez E, Cubillos-Zapata C, Varela-Serrano A, Avendano-Ortiz J, et al. PD-L1/PD-1 crosstalk in colorectal cancer: are we targeting the right cells? *BMC Cancer.* (2018) 18:945. doi: 10.1186/s12885-018-4853-0

35. Etzerodt A, Tsalkitzi K, Maniecki M, Damsky W, Delfini M, Baudoin E, et al. Specific targeting of CD163(+) TAMs mobilizes inflammatory monocytes and promotes T cell-mediated tumor regression. *J Exp Med.* (2019) 216:2394–411. doi: 10.1084/jem.20182124

36. Segaliny AI, Mohamadi A, Dizier B, Lokajczyk A, Brion R, Lanel R, et al. Interleukin-34 promotes tumor progression and metastatic process in osteosarcoma through induction of angiogenesis and macrophage recruitment. *Int J Cancer.* (2015) 137:73–85. doi: 10.1002/ijc.29376

37. Ma R-Y, Black A, Qian B-Z. Macrophage diversity in cancer revisited in the era of single-cell omics. *Trends Immunol.* (2022) 43:546–63. doi: 10.1016/j.it.2022.04.008

38. Yi C, Li Z, Zhao Q, Gong D, Zhao S, Chen Z, et al. Single-cell RNA sequencing pro-angiogenic macrophage profiles reveal novel prognostic biomarkers and therapeutic targets for osteosarcoma. *Biochem Genet.* (2023) 62:1325-46. doi: 10.1007/s10528-023-10483-w

39. Liao Z, Li M, Wen G, Wang K, Yao D, Chen E, et al. Comprehensive analysis of angiogenesis pattern and related immune landscape for individual treatment in osteosarcoma. *NPJ Precis Oncol.* (2023) 7:62. doi: 10.1038/s41698-023-00415-7

40. Han Y, Guo W, Ren T, Huang Y, Wang S, Liu K, et al. Tumor-associated macrophages promote lung metastasis and induce epithelial-mesenchymal transition in osteosarcoma by activating the COX-2/STAT3 axis. *Cancer Lett.* (2019) 440-441:116–25. doi: 10.1016/j.canlet.2018.10.011

41. Han ZP, Liu DB, Wu LQ, Li Q, Wang ZG, Zang XF. IL-1beta secreted by macrophage M2 promotes metastasis of osteosarcoma via NF-kappaB/miR-181alpha-5p/RASSF1A/Wnt pathway. *Transl Cancer Res.* (2020) 9:2721–33. doi: 10.21037/tcr

42. Fujiwara T, Yakoub MA, Chandler A, Christ AB, Yang G, Ouerfelli O, et al. CSF1/CSF1R signaling inhibitor pexidartinib (PLX3397) reprograms tumor-associated macrophages and stimulates T-cell infiltration in the sarcoma microenvironment. *Mol Cancer Ther.* (2021) 20:1388–99. doi: 10.1158/1535-7163.MCT-20-0591

43. Liu W, Long Q, Zhang W, Zeng D, Hu B, Liu S, et al. miRNA-221-3p derived from M2-polarized tumor-associated macrophage exosomes aggravates the growth and metastasis of osteosarcoma through SOCS3/JAK2/STAT3 axis. *Aging (Albany NY).* (2021) 13:19760–75. doi: 10.18632/aging.v13i15

44. Cheng Z, Wang L, Wu C, Huang L, Ruan Y, Xue W. Tumor-derived exosomes induced M2 macrophage polarization and promoted the metastasis of osteosarcoma cells through tim-3. *Arch Med Res.* (2021) 52:200–10. doi: 10.1016/j.arcmed.2020.10.018

45. Brandum EP, Jørgensen AS, Rosenkilde MM, Hjortø GM. Dendritic cells and CCR7 expression: an important factor for autoimmune diseases, chronic inflammation, and cancer. *Int J Mol Sci.* (2021) 22. doi: 10.3390/ijms22158340

46. Rodríguez-Fernández JL, Criado-García O. The chemokine receptor CCR7 uses distinct signaling modules with biased functionality to regulate dendritic cells. *Front Immunol.* (2020) 11:528. doi: 10.3389/fimmu.2020.00528

47. Liu W, Hu H, Shao Z, Lv X, Zhang Z, Deng X, et al. Characterizing the tumor microenvironment at the single-cell level reveals a novel immune evasion mechanism in osteosarcoma. *Bone Res.* (2023) 11:4. doi: 10.1038/s41413-022-00237-6

48. Li J, Zhou J, Huang H, Jiang J, Zhang T, Ni C. Mature dendritic cells enriched in immunoregulatory molecules (mregDCs): A novel population in the tumour microenvironment and immunotherapy target. *Clin Transl Med.* (2023) 13:e1199. doi: 10.1002/ctm2.1199

49. Cheng D, Zhang Z, Mi Z, Tao W, Liu D, Fu J, et al. Deciphering the heterogeneity and immunosuppressive function of regulatory T cells in osteosarcoma using single-cell RNA transcriptome. *Comput Biol Med.* (2023) 165:107417. doi: 10.1016/j.compbiomed.2023.107417

50. McRitchie BR, Akkaya B. Exhaust the exhausters: Targeting regulatory T cells in the tumor microenvironment. *Front Immunol.* (2022) 13:940052. doi: 10.3389/fimmu.2022.940052

51. Tie Y, Tang F, Wei YQ, Wei XW. Immunosuppressive cells in cancer: mechanisms and potential therapeutic targets. *J Hematol Oncol.* (2022) 15:61. doi: 10.1186/s13045-022-01282-8

52. Tellier J, Shi W, Minnich M, Liao Y, Crawford S, Smyth GK, et al. Blimp-1 controls plasma cell function through the regulation of immunoglobulin secretion and the unfolded protein response. *Nat Immunol.* (2016) 17:323–30. doi: 10.1038/ni.3348

53. Maskalenko NA, Zhigarev D, Campbell KS. Harnessing natural killer cells for cancer immunotherapy: dispatching the first responders. *Nat Rev Drug Discovery.* (2022) 21:559–77. doi: 10.1038/s41573-022-00413-7

54. Ramirez-Labrada A, Pesini C, Santiago L, Hidalgo S, Calvo-Perez A, Onate C, et al. All about (NK cell-mediated) death in two acts and an unexpected encore: initiation, execution and activation of adaptive immunity. *Front Immunol.* (2022) 13:896228. doi: 10.3389/fimmu.2022.896228

55. Jiang K, Li J, Zhang J, Wang L, Zhang Q, Ge J, et al. SDF-1/CXCR4 axis facilitates myeloid-derived suppressor cells accumulation in osteosarcoma microenvironment and blunts the response to anti-PD-1 therapy. *Int Immunopharmacol.* (2019) 75:105818. doi: 10.1016/j.intimp.2019.105818

56. Guan Y, Zhang R, Peng Z, Dong D, Wei G, Wang Y. Inhibition of IL-18-mediated myeloid derived suppressor cell accumulation enhances anti-PD1 efficacy against osteosarcoma cancer. *J Bone Oncol.* (2017) 9:59–64. doi: 10.1016/j.jbo.2017.10.002

57. Taylor AM, Sheng J, Ng PKS, Harder JM, Kumar P, Ahn JY, et al. Immunosuppressive tumor microenvironment of osteosarcoma [Preprint]. (2024). Available at: https://www.biorxiv.org/content/10.1101/2023.11.01.565008v3 (Accessed July 17, 2024).

58. Zeng Z, Li W, Zhang D, Zhang C, Jiang X, Guo R, et al. Development of a chemoresistant risk scoring model for prechemotherapy osteosarcoma using single-cell sequencing. *Front Oncol.* (2022) 12:893282. doi: 10.3389/fonc.2022.893282

59. Corre I, Verrecchia F, Crenn V, Redini F, Trichet V. The osteosarcoma microenvironment: A complex but targetable ecosystem. *Cells.* (2020) 9:976. doi: 10.3390/cells9040976

60. Lamoureux Fo, Richard P, Wittrant Y, Battaglia Sv, Pilet P, Trichet Vr, et al. Therapeutic relevance of osteoprotegerin gene therapy in osteosarcoma: blockade of the vicious cycle between tumor cell proliferation and bone resorption. *Cancer Res.* (2007) 67:7308–18. doi: 10.1158/0008-5472.CAN-06-4130

61. Wang L, Huang X, You X, Yi T, Lu B, Liu J, et al. Nanoparticle enhanced combination therapy for stem-like progenitors defined by single-cell transcriptomics in chemotherapy-resistant osteosarcoma. *Signal Transduction Targeted Ther.* (2020) 5:196. doi: 10.1038/s41392-020-00248-x

62. Lee HW, Park YM, Lee SJ, Cho HJ, Kim D-H, Lee J-I, et al. Alpha-smooth muscle actin (ACTA2) is required for metastatic potential of human lung adenocarcinoma. *Clin Cancer Res.* (2013) 19:5879–89. doi: 10.1158/1078-0432.CCR-13-1181

63. Park S, Karalis JD, Hong C, Clemenceau JR, Porembka MR, Kim I-H, et al. ACTA2 expression predicts survival and is associated with response to immune checkpoint inhibitors in gastric cancer. *Clin Cancer Res.* (2023) 29:1077–85. doi: 10.1158/1078-0432.CCR-22-1897

64. Zhu J, Luo C, Zhao J, Zhu X, Lin K, Bu F, et al. Expression of LOX suggests poor prognosis in gastric cancer. *Front Med (Lausanne).* (2021) 8:718986. doi: 10.3389/fmed.2021.718986

65. Saatci O, Kaymak A, Raza U, Ersan PG, Akbulut O, Banister CE, et al. Targeting lysyl oxidase (LOX) overcomes chemotherapy resistance in triple negative breast cancer. *Nat Commun.* (2020) 11:2416. doi: 10.1038/s41467-020-16199-4

66. Wu M, Min C, Wang X, Yu Z, Kirsch KH, Trackman PC, et al. Repression of BCL2 by the tumor suppressor activity of the lysyl oxidase propeptide inhibits transformed phenotype of lung and pancreatic cancer cells. *Cancer Res.* (2007) 67:6278–85. doi: 10.1158/0008-5472.CAN-07-0776

67. Gao YM, Pei Y, Zhao FF, Wang L. Osteoclasts in osteosarcoma: mechanisms, interactions, and therapeutic prospects. *Cancer Manag Res.* (2023) 15:1323–37. doi: 10.2147/CMAR.S431213

68. Yang J, Yang D, Sun Y, Sun B, Wang G, Trent JC, et al. Genetic amplification of the vascular endothelial growth factor (VEGF) pathway genes, including VEGFA, in human osteosarcoma. *Cancer.* (2011) 117:4925–38. doi: 10.1002/cncr.26116

69. Ge Z, Peppelenbosch MP, Sprengers D, Kwekkeboom J. TIGIT, the next step towards successful combination immune checkpoint therapy in cancer. *Front Immunol.* (2021) 12. doi: 10.3389/fimmu.2021.699895

70. Yeo J, Ko M, Lee D-H, Park Y, Jin H-s. TIGIT/CD226 axis regulates anti-tumor immunity. *Pharmaceuticals*. (2021) 14:200. doi: 10.3390/ph14030200

71. Cannarile MA, Weisser M, Jacob W, Jegg A-M, Ries CH, Rüttinger D. Colony-stimulating factor 1 receptor (CSF1R) inhibitors in cancer therapy. *J ImmunoTherapy Cancer*. (2017) 5:53. doi: 10.1186/s40425-017-0257-y

72. Hume DA, MacDonald KPA. Therapeutic applications of macrophage colony-stimulating factor-1 (CSF-1) and antagonists of CSF-1 receptor (CSF-1R) signaling. *Blood*. (2012) 119:1810–20. doi: 10.1182/blood-2011-09-379214

73. Azhar Z, Grose RP, Raza A, Raza Z. In silico targeting of colony-stimulating factor-1 receptor: delineating immunotherapy in cancer. *Explor Target Antitumor Ther*. (2023) 4:727–42. doi: 10.37349/etat

74. Sarkar M, Nguyen T, Gundre E, Ogunlusi O, El-Sobky M, Giri B, et al. Cancer-associated fibroblasts: The chief architect in the tumor microenvironment. *Front Cell Dev Biol*. (2023) 11. doi: 10.3389/fcell.2023.1089068

75. Feng B, Wu J, Shen B, Jiang F, Feng J. Cancer-associated fibroblasts and resistance to anticancer therapies: status, mechanisms, and countermeasures. *Cancer Cell Int*. (2022) 22:166. doi: 10.1186/s12935-022-02599-7

76. Chen Z, Zhang N, Chu HY, Yu Y, Zhang Z-K, Zhang G, et al. Connective tissue growth factor: from molecular understandings to drug discovery. *Front Cell Dev Biol*. (2020) 8. doi: 10.3389/fcell.2020.593269

77. Maldonado LAG, Nascimento CR, Rodrigues Fernandes NA, Silva ALP, D'Silva NJ, Rossa C. Influence of tumor cell-derived TGF-β on macrophage phenotype and macrophage-mediated tumor cell invasion. *Int J Biochem Cell Biol*. (2022) 153:106330. doi: 10.1016/j.biocel.2022.106330

78. Cantelli G, Crosas-Molist E, Georgouli M, Sanz-Moreno V. TGFB-induced transcription in cancer. *Semin Cancer Biol*. (2017) 42:60–9. doi: 10.1016/j.semcancer.2016.08.009

79. Anastasiadou DP, Quesnel A, Duran CL, Filippou PS, Karagiannis GS. An emerging paradigm of CXCL12 involvement in the metastatic cascade. *Cytokine Growth Factor Rev*. (2024) 75:12–30. doi: 10.1016/j.cytogfr.2023.10.003

80. Han Z-P, Liu D-B, Wu L-Q, Li Q, Wang Z-G, Zang X-F. IL-1β secreted by macrophage M2 promotes metastasis of osteosarcoma via NF-κB/miR-181α-5p/RASSF1A/Wnt pathway. *Trans Cancer Res*. (2020) 9:2721–33. doi: 10.21037/tcr

81. Rébé C, Ghiringhelli F. Interleukin-1β and cancer. *Cancers (Basel)*. (2020) 12. doi: 10.3390/cancers12071791

82. Li Y, He H, Jihu R, Zhou J, Zeng R, Yan H. Novel characterization of myeloid-derived suppressor cells in tumor microenvironment. *Front Cell Dev Biol*. (2021) 9:698532. doi: 10.3389/fcell.2021.698532

83. Taylor AM, Shing Ng PK, Harder JM, Kumar P, Dzis AM, Jillette NL, et al. Immunosuppressive tumor microenvironment of osteosarcoma. *bioRxiv*. (2023) 2023:565008. doi: 10.1101/2023.11.01.565008

84. Kang CW, Dutta A, Chang LY, Mahalingam J, Lin YC, Chiang JM, et al. Apoptosis of tumor infiltrating effector TIM-3+CD8+ T cells in colon cancer. *Sci Rep*. (2015) 5:15659. doi: 10.1038/srep15659

85. Yang R, Sun L, Li C-F, Wang Y-H, Yao J, Li H, et al. Galectin-9 interacts with PD-1 and TIM-3 to regulate T cell death and is a target for cancer immunotherapy. *Nat Commun*. (2021) 12:832. doi: 10.1038/s41467-021-21099-2

86. Aarts CEM, Hiemstra IH, Béguin EP, Hoogendijk AJ, Bouchmal S, van Houdt M, et al. Activated neutrophils exert myeloid-derived suppressor cell activity damaging T cells beyond repair. *Blood Advances*. (2019) 3:3562–74. doi: 10.1182/bloodadvances.2019031609

87. Law AMK, Valdes-Mora F, Gallego-Ortega D. Myeloid-derived suppressor cells as a therapeutic target for cancer. *Cells*. (2020) 9. doi: 10.3390/cells9030561

88. Panda AK, Kim Y-H, Shevach EM. Control of memory phenotype T lymphocyte homeostasis: role of costimulation. *J Immunol*. (2022) 208:851–60. doi: 10.4049/jimmunol.2100653

89. Halliday N, Williams C, Kennedy A, Waters E, Pesenacker AM, Soskic B, et al. CD86 is a selective CD28 ligand supporting FoxP3+ Regulatory T cell homeostasis in the presence of high levels of CTLA-4. *Front Immunol*. (2020) 11:600000. doi: 10.3389/fimmu.2020.600000

90. Elomaa H, Ahtiainen M, Väyrynen SA, Ogino S, Nowak JA, Lau MC, et al. Spatially resolved multimarker evaluation of CD274 (PD-L1)/PDCD1 (PD-1) immune checkpoint expression and macrophage polarisation in colorectal cancer. *Br J Cancer*. (2023) 128:2104–15. doi: 10.1038/s41416-023-02238-6

91. Lv Y, Ma X, Ma Y, Du Y, Feng J. A new emerging target in cancer immunotherapy: Galectin-9 (LGALS9). *Genes Diseases*. (2023) 10:2366–82. doi: 10.1016/j.gendis.2022.05.020

92. Sauer N, Janicka N, Szlasa W, Skinderowicz B, Kołodzińska K, Dwernicka W, et al. TIM-3 as a promising target for cancer immunotherapy in a wide range of tumors. *Cancer Immunology Immunother*. (2023) 72:3405–25. doi: 10.1007/s00262-023-03516-1

93. Sun Q, Hong Z, Zhang C, Wang L, Han Z, Ma D. Immune checkpoint therapy for solid tumours: clinical dilemmas and future trends. *Signal Transduction Targeted Ther*. (2023) 8:320. doi: 10.1038/s41392-023-01522-4

94. Pires SF, Barros JS, Costa SSD, Carmo GBD, Scliar MO, Lengert AVH, et al. Analysis of the mutational landscape of osteosarcomas identifies genes related to metastasis and prognosis and disrupted biological pathways of immune response and bone development. *Int J Mol Sci*. (2023) 24. doi: 10.3390/ijms241310463

95. Wu CC, Beird HC, Andrew Livingston J, Advani S, Mitra A, Cao S, et al. Immuno-genomic landscape of osteosarcoma. *Nat Commun*. (2020) 11:1008. doi: 10.1038/s41467-020-14646-w

96. Xie L, Cai Z, Lu H, Meng F, Zhang X, Luo K, et al. Distinct genomic features between osteosarcomas firstly metastasing to bone and to lung. *Heliyon*. (2023) 9: e15527. doi: 10.1016/j.heliyon.2023.e15527

97. Liu R, Hu Y, Liu T, Wang Y. Profiles of immune cell infiltration and immune-related genes in the tumor microenvironment of osteosarcoma cancer. *BMC Cancer*. (2021) 21:1345. doi: 10.1186/s12885-021-09042-6

98. Mills LJ, Scott MC, Shah P, Cunanan AR, Deshpande A, Auch B, et al. Comparative analysis of genome-wide DNA methylation identifies patterns that associate with conserved transcriptional programs in osteosarcoma. *Bone*. (2022) 158:115716. doi: 10.1016/j.bone.2020.115716

99. Shi D, Mu S, Pu F, Liu J, Zhong B, Hu B, et al. Integrative analysis of immune-related multi-omics profiles identifies distinct prognosis and tumor microenvironment patterns in osteosarcoma. *Mol Oncol*. (2022) 16:2174–94. doi: 10.1002/1878-0261.13160

100. Chen X, Bahrami A, Pappo A, Easton J, Dalton J, Hedlund E, et al. Recurrent somatic structural variations contribute to tumorigenesis in pediatric osteosarcoma. *Cell Rep*. (2014) 7:104–12. doi: 10.1016/j.celrep.2014.03.003

101. Behjati S, Tarpey PS, Haase K, Ye H, Young MD, Alexandrov LB, et al. Recurrent mutation of IGF signalling genes and distinct patterns of genomic rearrangement in osteosarcoma. *Nat Commun*. (2017) 8:15936. doi: 10.1038/ncomms15936

102. Perry JA, Kiezun A, Tonzi P, Van Allen EM, Carter SL, Baca SC, et al. Complementary genomic approaches highlight the PI3K/mTOR pathway as a common vulnerability in osteosarcoma. *Proc Natl Acad Sci U.S.A*. (2014) 111:E5564–73. doi: 10.1073/pnas.1419260111

103. Davoli T, Uno H, Wooten EC, Elledge SJ. Tumor aneuploidy correlates with markers of immune evasion and with reduced response to immunotherapy. *Science*. (2017) 355. doi: 10.1126/science.aaf8399

104. Roh W, Chen PL, Reuben A, Spencer CN, Prieto PA, Miller JP, et al. Integrated molecular analysis of tumor biopsies on sequential CTLA-4 and PD-1 blockade reveals markers of response and resistance. *Sci Transl Med*. (2017) 9. doi: 10.1126/scitranslmed.aah3560

105. Zhang Y, Xu Y, Bao Y, Luo Y, Qiu G, He M, et al. N6-methyladenosine (m6A) modification in osteosarcoma: expression, function and interaction with noncoding RNAs - an updated review. *Epigenetics*. (2023) 18:2260213. doi: 10.1080/15592294.2023.2260213

106. Yang F, Liu Y, Xiao J, Li B, Chen Y, Hu A, et al. Circ-CTNNB1 drives aerobic glycolysis and osteosarcoma progression via m6A modification through interacting with RBM15. *Cell Prolif*. (2023) 56:e13344. doi: 10.1111/cpr.13344

107. Bi Y, Meng D, Wan M, Xu N, Xu Y, Yuan K, et al. m6A-related lncRNAs predict overall survival of patients and regulate the tumor immune microenvironment in osteosarcoma. *Comput Intell Neurosci*. (2022) 2022:9315283. doi: 10.1155/2022/9315283

108. Wu Z, Zhang X, Chen D, Li Z, Wu X, Wang J, et al. N6-methyladenosine-related LncRNAs are potential remodeling indicators in the tumor microenvironment and prognostic markers in osteosarcoma. *Front Immunol*. (2021) 12:806189. doi: 10.3389/fimmu.2021.806189

109. Wortzel I, Dror S, Kenific CM, Lyden D. Exosome-mediated metastasis: communication from a distance. *Dev Cell*. (2019) 49:347–60. doi: 10.1016/j.devcel.2019.04.011

110. Pegtel DM, Gould SJ. Exosomes. *Annu Rev Biochem*. (2019) 88:487–514. doi: 10.1146/annurev-biochem-013118-111902

111. Mathieu M, Martin-Jaular L, Lavieu G, Thery C. Specificities of secretion and uptake of exosomes and other extracellular vesicles for cell-to-cell communication. *Nat Cell Biol*. (2019) 21:9–17. doi: 10.1038/s41556-018-0250-9

112. Mannerstrom B, Kornilov R, Abu-Shahba AG, Chowdhury IM, Sinha S, Seppanen-Kaijansinkko R, et al. Epigenetic alterations in mesenchymal stem cells by osteosarcoma-derived extracellular vesicles. *Epigenetics*. (2019) 14:352–64. doi: 10.1080/15592294.2019.1585517

113. Raimondi L, De Luca A, Gallo A, Costa V, Russelli G, Cuscino N, et al. Osteosarcoma cell-derived exosomes affect tumor microenvironment by specific packaging of microRNAs. *Carcinogenesis*. (2020) 41:666–77. doi: 10.1093/carcin/bgz130

114. Mazumdar A, Urdinez J, Boro A, Migliavacca J, Arlt MJE, Muff R, et al. Osteosarcoma-derived extracellular vesicles induce lung fibroblast reprogramming. *Int J Mol Sci*. (2020) 21. doi: 10.3390/ijms21155451

115. Urciuoli E, Giorda E, Scarsella M, Petrini S, Peruzzi B. Osteosarcoma-derived extracellular vesicles induce a tumor-like phenotype in normal recipient cells. *J Cell Physiol*. (2018) 233:6158–72. doi: 10.1002/jcp.26464

116. Sarhadi VK, Daddali R, Seppanen-Kaijansinkko R. Mesenchymal stem cells and extracellular vesicles in osteosarcoma pathogenesis and therapy. *Int J Mol Sci*. (2021) 22. doi: 10.3390/ijms222011035

117. Baglio SR, Lagerweij T, Perez-Lanzon M, Ho XD, Leveille N, Melo SA, et al. Blocking tumor-educated MSC paracrine activity halts osteosarcoma progression. *Clin Cancer Res*. (2017) 23:3721–33. doi: 10.1158/1078-0432.CCR-16-2726

118. Evdokimova V, Gassmann H, Radvanyi L, Burdach SEG. Current state of immunotherapy and mechanisms of immune evasion in ewing sarcoma and osteosarcoma. *Cancers (Basel)*. (2022) 15. doi: 10.3390/cancers15010272

119. Zeng F, Morelli AE. Extracellular vesicle-mediated MHC cross-dressing in immune homeostasis, transplantation, infectious diseases, and cancer. *Semin Immunopathol*. (2018) 40:477–90. doi: 10.1007/s00281-018-0679-8

120. Robbins PD, Morelli AE. Regulation of immune responses by extracellular vesicles. *Nat Rev Immunol*. (2014) 14:195–208. doi: 10.1038/nri3622

121. Balta E, Wabnitz GH, Samstag Y. Hijacked immune cells in the tumor microenvironment: molecular mechanisms of immunosuppression and cues to improve T cell-based immunotherapy of solid tumors. *Int J Mol Sci*. (2021) 22. doi: 10.3390/ijms22115736

122. Ribas A, Dummer R, Puzanov I, VanderWalde A, Andtbacka RHI, Michielin O, et al. Oncolytic virotherapy promotes intratumoral T cell infiltration and improves anti-PD-1 immunotherapy. *Cell*. (2017) 170:1109–19.e10. doi: 10.1016/j.cell.2017.08.027

123. Xie G, Cheng T, Lin J, Zhang L, Zheng J, Liu Y, et al. Local angiotensin II contributes to tumor resistance to checkpoint immunotherapy. *J Immunother Cancer*. (2018) 6:88. doi: 10.1186/s40425-018-0401-3

124. Di Gioacchino M, Petrarca C, Gatta A, Scarano G, Farinelli A, Della Valle L, et al. Nanoparticle-based immunotherapy: state of the art and future perspectives. *Expert Rev Clin Immunol*. (2020) 16:513–25. doi: 10.1080/1744666X.2020.1762572

125. Ma Q, Zhou D, DeLyria ES, Wen X, Lu W, Thapa P, et al. Synthetic poly(L-glutamic acid)-conjugated CpG exhibits antitumor efficacy with increased retention in tumor and draining lymph nodes after intratumoral injection in a mouse model of melanoma. *J Immunother*. (2017) 40:11–20. doi: 10.1097/CJI.0000000000000145

Frontiers in
Immunology

Explores novel approaches and diagnoses to treat immune disorders.

The official journal of the International Union of Immunological Societies (IUIS) and the most cited in its field, leading the way for research across basic, translational and clinical immunology.

Discover the latest Research Topics

See more →

Frontiers

Avenue du Tribunal-Fédéral 34
1005 Lausanne, Switzerland
frontiersin.org

Contact us

+41 (0)21 510 17 00
frontiersin.org/about/contact

frontiers

Frontiers in
Immunology